

DOE/NASA/0329-1
NASA CR-179531
DDA R01-ADECD-NAS

1N-85
109761
4708

**Adiabatic Diesel Engine
Component Development
Program-Phase I
Interim Report
Reference Engine For
On-Highway Applications**

Nabil S. Hakim
Detroit Diesel Allison

April 1986

(NASA-CR-179531) ADIABATIC DIESEL ENGINE
COMPONENT DEVELOPMENT: REFERENCE ENGINE FOR
ON-HIGHWAY APPLICATIONS Interim Report, 1
May 1985 - 30 Apr. 1986 (Detroit Diesel
Allison) 470 p Avail: NTIS HC A20/HF A01 G3/85

N88-12428

Unclas
0109761

Prepared for
NATIONAL AERONAUTICS AND SPACE ADMINISTRATION
Lewis Research Center
Under Contract DEN 3-329

for
**U.S. DEPARTMENT OF ENERGY
Conservation and Renewable Energy
Office of Vehicle and Engine R&D**

**Adiabatic Diesel Engine
Component Development
Program—Phase I
Interim Report
Reference Engine For
On-Highway Applications**

Nabil S. Hakim
Detroit Diesel Allison

April 1986

Prepared for
National Aeronautics and Space Administration
Lewis Research Center
Cleveland, Ohio 44135
Under Contract DEN 3-329

for
U.S. DEPARTMENT OF ENERGY
Conservation and Renewable Energy
Office of Vehicle and Engine R&D
Washington, D.C. 20545
Under Interagency Agreement DE-AI01-86CE50162

1. Report No. CR-179531		2. Government Accession No.		3. Recipient's Catalog No.	
4. Title and Subtitle ADIABATIC DIESEL ENGINE COMPONENT DEVELOPMENT - Reference Engine for On-highway Applications			5. Report Date April, 1986		
			6. Performing Organization Code		
7. Author(s) Nabil S. Hakim			8. Performing Organization Report No. R01-ADECD-NAS		
			10. Work Unit No.		
9. Performing Organization Name and Address Detroit Diesel Allison 13400 W. Outer Drive Detroit, MI 48239			11. Contract or Grant No. DEN3-329		
			13. Type of Report and Period Covered Phase I Interim Report May 1, 1985 - April 30, 1986		
12. Sponsoring Agency Name and Address U.S. Department of Energy Office of Vehicle and Engine R & D Washington, D.C. 20585			14. Sponsoring Agency Code DOE/NASA/0329-1		
			15. Supplementary Notes Interim Report. Prepared under Interagency Agreement DE-A101-86CE50162. Project Manager, Howard Yacobucci, Propulsion System Division, NASA Lewis Research Center, Cleveland, Ohio, 44135.		
16. Abstract The main objectives of Phase I of the Advanced (Adiabatic) Diesel Engine Component Development program were to select an Advanced low heat rejection Diesel Reference Engine [ADRE], and to carry out ADRE systems analysis and design. The ADRE concept selection consisted of: 1) rated point performance optimization, 2) study of various exhaust energy recovery scenarios, 3) components, systems and engine configuration studies, and 4) life cycle cost estimates of the ADRE economic worth. The resulting ADRE design proposed a reciprocator with many advanced features for the 1995 technology demonstration time frame. These included ceramic air gap insulated hot section structural components, high temperature tribology treatments, nonmechanical (camless) valve actuation system, and elimination of the cylinder head gasket. ADRE system analysis and design resulted in more definition of the engine systems. These systems include: 1) electro-hydraulic valve actuation, 2) electronic common rail injection system, 3) engine electronic control, 4) power transfer for accessory drives and exhaust energy recovery systems, and 5) truck installation. Tribology and performance assessments were also carried out. Finite element and probability of survival analyses were undertaken for the ceramic low heat rejection component.					
17. Key Words (Suggested by Author(s)) Low Heat Rejection, Tribology, Engine Performance, Emission, On-Highway, Diesel, Truck, Ceramic			18. Distribution Statement Unclassified-Unlimited STAR Category 85 DOE Category UC-96		
19. Security Classif. (of this report) Unclassified		20. Security Classif. (of this page) Unclassified		21. No. of pages	22. Price*

FORWARD

This report covers the state-of-the-art review, selection, design and analysis of an advanced reference heavy-duty diesel engine for truck applications. The study was Phase I of the Adiabatic Diesel Engine Component Development [ADECD] program, which is sponsored by the US Department of Energy and technically managed by NASA Lewis Research Center. The author acknowledges the technical support and direction provided by the DOE Program Manager, Mr. John Fairbanks, and the NASA Project Manager, Mr. Howard Yacobucci.

The reported work is the contribution of many persons of the Detroit Diesel technical staff. The author acknowledges these contributions and expresses his sincere gratitude to each individual. Integral Technologies Incorporated, SKF Tribonetics and Thermo Electron Corporation were subcontractors on this phase of the ADECD program. The final subcontractor reports are provided as appendices to this report.

TABLE OF CONTENTS

	Page
Executive Summary	1
Section I - Introduction	14
Section II - Adiabatic Diesel Reference Engine Concept Selection.	18
II.1 - Performance Assessment	21
II.1.1 - Methodology	22
II.1.2 - Preliminary Optimization	24
II.1.3 - Detailed Optimization	30
II.1.4 - Fuel Economy	38
II.1.5 - Performance Assessment Conclusions	38
II.1.6 - References	41
II.2 - Candidate Design Configurations	63
II.2.1 - Low Heat Rejection Concepts	64
II.2.2 - Bearing and Lubrication Concepts	81
II.2.3 - References	86
II.3 - Exhaust Energy Recovery Systems	116
II.3.1 - Systems Survey	116
II.3.2 - Bottoming Cycle Systems.	121
II.3.3 - Bottoming System Selection	126
II.3.4 - Conclusions.	128
II.3.5 - References	129
II.4 - Life Cycle Cost Evaluation	142
II.4-1 - Candidate Configurations Analyzed	145
II.4.2 - LCC Model	147
II.4.3 - Evaluation Strategy	158
II.4.4 - Life Cycle Cost Results.	160
II.4.5 - Summary and Conclusions.	164

TABLE OF CONTENTS (Continued)

	Page
II.4.6 - References	167
II.5 - The Adiabatic Diesel Reference Engine	180
Section III - ADRE System Analysis and Design	183
III.1 - Main Design Features	184
III.2 - Performance Analysis	200
III.2.1 - Performance Maps.	200
III.2.2 - Performance Advantages of Variable Valve Events	201
III.3 - Valve and Valve Actuation Systems	204
III.3.1 - Valve Dynamics.	204
III.3.2 - Non-Mechanical Valve Actuation Concepts	209
III.3.3 - Ceramic Valve Structural Analysis	216
III.4 - Fuel Injection System	233
III.4.1 - Common Rail Fuel Injection Concept.	233
III.5 - Electronic Control System	244
III.6 - Power Transfer Systems	246
III.7 - Roller Bearing Design	255
III.8 - Solid Lubrication Tribology	276
III.9 - Additional Component and Concept Analyses	286
III.9.1 - Piston Assembly	286
III.9.2 - Firedeck and Cylinder Head.	295
III.9.3 - Crankshaft Related Analysis	303
Section IV - Planned Future Work.	305
Appendix A - SKF Subcontract Final Report	A
Appendix B - Integral Technologies Inc. Subcontract Final Report.	B-1
Appendix C - Thermo Electron Subcontract Final Report	C-1
Appendix D - Acronym Definition	D-1

LIST OF TABLES

		Page
Table II.1-1	- Basic Parameters and Their Levels - Preliminary Study. . .	43
Table II.1-2	- Pertinent Engine Simulation Data	44
Table II.1-3	- Emissions and Structural (Thermomechanical) Loading Constraints.	45
Table II.1-4	- Parametric Combinations for Best Fuel Economy at Various Peak Pressures, A/F and Strokes.	46
Table II.1-5	- Statistically Predicted Versus Directly Calculated Values of Selected Variables	47
Table II.1-6	- Parameters and Levels - Detailed Study	48
Table II.2-1	- Assessment of Insulation Methods	88
Table II.2-2	- Piston Design Considerations	90
Table II.2-3	- LHR Piston Concepts	91
Table II.2-4	- Salient Features of "Ringless" Piston Design	92
Table II.2-5	- Cylinder Liner Design Considerations	92
Table II.2-6	- Generic Material Treatments for Liner Tribology.	93
Table II.3-1	- Price Estimates for Alternate Power Cycles	130
Table II.3-2	- Maintenance and Repair Costs, Estimates for Alternative Power Cycles	131
Table II.3-3	- ADE Bottoming Cycle Performance Comparison	132
Table II.4-1	- Price Model "Parts List" with Quantities Shown for State-of-the-Art In-Line 6-Cylinder Diesel Engine.	168
Table II.4-2	- WHUS Power Contributions for Engine Pricing.	169
Table II.4-3	- Prices of Exhaust Energy Recovery Systems.	170
Table II.4-4	- Parameters of the LCC Model, with Typical Values	171
Table II.4-5	- Parameter Levels for Extreme Circumstances	172
Table III.7-1	- Task 1 Selected ADRE Bearing	269

LIST OF FIGURES

		Page
Figure 1	- Engine Block and Power Assembly Cross Section	4
Figure 2	- Cylinder Head Cross Section	5
Figure 3	- Layout of Overhead Components	6
Figure 4	- Accessory Drives	7
Figure 5	- Exhaust Energy Recovery Power Drive	8
Figure 6	- Truck Installation - Side View	9
Figure 7	- Truck Installation - Rear View	10
Figure 8	- Cylinder Head and Firedeck - Isotherms and Thermal Stress Contours	11
Figure 9	- In Situ Solid Lubricant System.	12
Figure 10	- Continuously Replenishing Lubricant Delivery System . .	13
Figure I.1	- Phase I Strategy Plan	17
Figure II.1-1	- Schematic of the LHRE-EERS System Simulation	49
Figure II.1-2	- Significant Parameters Affecting the Fuel Economy and Their Percentage Contribution Preliminary Study	50
Figure II.1-3	- Significant Parameters Affecting Peak Firing Pressure and Their Percentage Contribution- Preliminary Study.	51
Figure II.1-4	- Significant Parameters Affecting A/F and Their Percentage Contribution Preliminary Study.	52
Figure II.1-5	- Significant Parameters Affecting BMEP and Their Percentage Contribution-Preliminary Study.	53
Figure II.1-6	- Best Fuel Economy Predictions-Preliminary Study.	54
Figure II.1-7	- Significant Parameters Affecting the Fuel Economy and Their Percentage Contribution-Detailed Study	55
Figure II.1-8	- Effect of Liner Insulation on Volumetric Efficiency and Fuel Economy	56
Figure II.1-9	- Significant Parameters Affecting A/F and Their Percentage Contribution-Detailed Study	57

LIST OF FIGURES (Continued)

	Page
Figure II.1-10 - Significant Parameters Affecting Peak Firing Pressure and Their Percentage Contribution-Detailed Study	58
Figure II.1-11 - Significant Parameters Affecting BMEP and Their Percentage Contribution-Detailed Study	59
Figure II.1-12 - Best Fuel Economy Predictions for Various LHRE-EER Systems at Different Insulation Levels, and at Baseline Friction	60
Figure II.1-13 - Best Fuel Economy at Various Friction and Insulation Levels - LHRE with Turbocompounding and Bottoming System	61
Figure II.1-14 - Percent Gain in Fuel Economy as a Function of Degree of Insulation and Exhaust Energy Recovery Scenarios	62
Figure II.2-1[A] ADE Configuration Selection Methodology.	94
Figure II.2-1[B] Mechanical Design Evaluation Procedure - Engine Configuration Studies From Component Studies	95
Figure II.2-2 - DDA's 6.2L LHR Trunk Style Aluminum Piston	96
Figure II.2-3 - View of the Conventional Crosshead Piston	97
Figure II.2-4 - Hollow Particle Thermal Barrier Coating	98
Figure II.2-5 - Typical Crosshead Air Gap LHR Piston	99
Figure II.2-6 - Ringless Piston Design Concept	100
Figure II.2-7 - Leakage and Power Loss as a Function of Radial Clearance for a Ringless Piston.	101
Figure II.2-8 - Firedeck with Retaining Ring	102
Figure II.2-9 - Direct Press-Fit Firedeck Design	103
Figure II.2-10 - Individual Pot Head Concept.	104
Figure II.2-11 - Shielded Exhaust Valve (From Reference 12)	105
Figure II.2-12 - Brazed Ceramic/Metal Valve Concepts.	106
Figure II.2-13 - Floating Valve Guide Concept	107
Figure II.2-14 - DDA's Series 92 Cylinder Head with Insertable Shield	108

LIST OF FIGURES (Continued)

	Page
Figure II.2-15 - DDA's Series 60 Cylinder Head with Direct Press-Fit Shield	109
Figure II.2-16 - Cost Estimates for a Silicon Nitride Piston Cap.	110
Figure II.2-17 - Insulation Treatment Screening Process	111
Figure II.2-18 - Technical Risk vs Insulation Level for Different Piston Insulation Treatments	112
Figure II.2-19 - Relative Cost vs Insulation Level for Different Piston Insulation Treatments	113
Figure II.2-20 - Technical Risk vs Insulation Level for Cylinder Head Without Watercooling.	114
Figure II.2-21 - Relative Cost vs Insulation Level for Cylinder Head Without Watercooling.	115
Figure II.3-1 - Various Exhaust Energy Recovery Systems.	133
Figure II.3-2 - Diesel/Steam System Schematic.	134
Figure II.3-3 - Diesel/RC-1 Organic System Schematic	135
Figure II.3-4 - Schematic of an Organic Rankine RC-1 Cycle with Internal Heat Regeneration and Two Power Turbines.	136
Figure II.3-5 - Organic Rankine Bottoming System with Heat Regeneration. Single Power Turbine	137
Figure II.3-6 - Organic Rankine Bottoming System with Heat Regeneration. Two Stage Turbocharging.	137
Figure II.3-7 - Specific Fuel Consumption for Various Diesel Alternative Power Cycle Combination.	138
Figure II.3-8 - Sensitivity of Alternative Power Cycle Performance to Diesel Exhaust Temperature.	139
Figure II.3-9 - Temperature-Entropy Diagram for Rankine Bottoming Cycle.	140
Figure II.3-10 - Recommended Organic Rankine Bottoming System. [Turbocompounding and Regeneration are Optional Features].	141
Figure II.4-1 - Comparison of First-Year Maintenance Costs of a Particular Engine to Those of the Population of the Same Engine.	173

LIST OF FIGURES (Continued)

	Page
Figure II.4-2 - LCC Distribution Resulting from Uncertainty of Parameter Values in Full Factorial Analysis.	174
Figure II.4-3 - Percent LCC Difference (Max. LHRE Benefit Scenario) Between Leading LHRE Candidates in Each Risk Level and SOA. Positive Value Indicates Superiority of Configuration Relative to SOA	175
Figure II.4-4 - Breakdown of LCC in Mean and Max. LHRE Benefit Scenarios.	176
Figure II.4-5 - Sensitivity of LCC to Interest Rate.	177
Figure II.4-6 - Cost Relative to Turbocharged SOA Engine of Several Alternate Engine Configurations in Max. LHRE Benefit Scenario	178
Figure II.4-7 - Contribution of Parameters to LCC Variation in HR2 Engine	179
Figure II.5-1 - The Selected ADRE Reciprocator Concept	182
Figure III.1-1 - Engine Block and Power Assembly - Longitudinal Cross Section.	187
Figure III.1-2 - A Cylinder Cross Section - Rolling Element Bearing Treatments	188
Figure III.1-3 - Cylinder Head Cross Section.	189
Figure III.1-4 - Bolt Pattern for the Gasketless Design	190
Figure III.1-5 - Layout of Overhead Components.	191
Figure III.1-6 - Exhaust Energy Recovery Power Transfer System.	192
Figure III.1-7 - Accessory Drives	193
Figure III.1-8 - ADRE Package Size Comparison - Front View.	194
Figure III.1-9 - ADRE Package Size Comparison - Side View	195
Figure III.1-10- Truck Installation - Side View	196
Figure III.1-11- Truck Installation - Front View.	197
Figure III.1-12- Truck Installation - Top View.	198
Figure III.1-13- Truck Installation - Rear View	199

LIST OF FIGURES (Continued)

	Page
Figure III.2-1 - ADRE Performance Map	203
Figure III.3-1 - Monolithic Ceramic Valve	217
Figure III.3-2 - Performance-Based Air Flow Recommendation.	218
Figure III.3-3 - Performance-Based Intake Valve Displacement.	219
Figure III.3-4 - Performance-Based Exhaust Valve Displacement	219
Figure III.3-5 - 8° X 42° Exhaust Event	220
Figure III.3-6 - Air Flow per Valve for the 8° X 42° Exhaust Event.	220
Figure III.3-7 - Air Flow per Cylinder for the 8° X 42° Exhaust Event	221
Figure III.3-8 - Velocity Profile for the 8° X 42° Exhaust Valve Event.	221
Figure III.3-9 - Acceleration Profile for the 8° X 42° Exhaust Valve.	222
Figure III.3-10- Inertia Force on Each Exhaust Valve.	222
Figure III.3-11- Pressure Force on Each Exhaust Valve	223
Figure III.3-12- Required Actuation Force Profile for the 8° X 42° Exhaust Valve at 1800 r/min Engine Speed	223
Figure III.3-13- Power Required to Actuate Each Exhaust Valve for the 8° X 42° Valve Event at 1800 r/min Engine Speed.	224
Figure III.3-14- Power Required to Actuate the Exhaust Valves of the ADRE for the 8° X 42° Valve Event at 1800 r/min Engine Speed	224
Figure III.3-15- Power Required to Actuate the Exhaust Valves of the ADRE for the 28° X 50° Valve Event at 1800 r/min Engine Speed	225
Figure III.3-16- Power Required to Actuate the ADRE Intake and Exhaust Valves for the 28° X 50° Valve Event at 1800 r/min Engine Speed.	225
Figure III.3-17- Total Ideal Power Requirements for the ADRE Valve System	226
Figure III.3-18- Electromagnetic Valve Actuation System - Side View	227
Figure III.3-19- Electromagnetic Valve Actuation System - Top View.	228
Figure III.3-20- Hydraulic Valve Actuation System - Side View	229

LIST OF FIGURES (Continued)

	Page
Figure III.3-21- Hydraulic Valve Actuation System - Top View.	230
Figure III.3-22- Finite Element Heat Transfer Analysis of the ADRE Exhaust Valve.	231
Figure III.3-23- Structural Finite Element Analysis of the ADRE Exhaust Valve.	232
Figure III.4-1 - Single Piston Fuel Injector Concept.	236
Figure III.4-2 - Start of Injection Event for Single Piston Injector. . .	237
Figure III.4-3 - End of Injection Event for Single Piston Injector. . . .	238
Figure III.4-4 - Kinetics of the Fuel Injection Events for the Single Piston Injector	239
Figure III.4-5 - Double Piston Fuel Injector Concept.	240
Figure III.4-6 - Kinetics of the Fuel Injection Events for the Double Piston Injectors.	241
Figure III.4-7 - High Pressure Fuel Pump.	242
Figure III.4-8 - Insulation Provisions for the Injector	243
Figure III.5-1 - ADRE Electronic Control System	245
Figure III.6-1 - Exhaust Energy Recovery Gear Train	252
Figure III.6-2 - Accessory Drive System	253
Figure III.6-3 - Three-reduction Gear System for Exhaust Energy Recovery Power Input	254
Figure III.7-1 - Main Bearing Design Chart.	270
Figure III.7-2 - Rod Bearing Design Chart	271
Figure III.7-3 - Cross-Section Illustrating Main, Rod, and Thrust Bearings.	272
Figure III.7-4 - Preliminary ADRE Piston Bearing Design Concept	273
Figure III.7-5 - Relative Piston Pin Bearing Load Capacity as a Function of Roller Size.	274
Figure III.7-6 - Final ADRE Piston Pin Bearing Design	275
Figure III.8-1 - Solid Lubricant Supplying System Proposal.	278

LIST OF FIGURES (Continued)

	Page
Figure III.8-2 - Solid Lubricant Supplying System Proposal.	279
Figure III.8-3 - Solid Lubricant Supplying System Proposal.	280
Figure III.8-4 - Solid Lubricant Supplying System Proposal.	281
Figure III.8-5 - Solid Lubricant Supplying System Proposal.	282
Figure III.8-6 - Solid Lubricant Supplying System Proposal.	283
Figure III.8-7 - Solid Lubricant Supplying System Proposal.	284
Figure III.8-8 - Solid Lubricant Supplying System Proposal.	285
Figure III.9-1 - ADRE Piston - Pertinent Dimensions	292
Figure III.9-2 - Axisymmetric FEM of ADRE Piston.	293
Figure III.9-3 - Typical Piston FEA Output.	294
Figure III.9-4 - Sample Cylinder Head and Firedeck Analysis	300
Figure III.9-5 - Finite Element Model for the Gasketless Seal Study . . .	301
Figure III.9-6 - Typical Gasketless Seal Joint Pressure Distribution. . .	302
Figure III.9-7 - Remaining Unbalance of the ADRE Crankshaft	304

EXECUTIVE SUMMARY

The Adiabatic Diesel Engine Component Development [ADECD] Program is a multiple phase effort to develop and demonstrate the critical technology needed to advance the heavy-duty adiabatic diesel engine concept for the line-haul truck market. The main objectives of Phase I of the ADECD Program were to select an advanced low heat rejection Adiabatic Diesel Reference Engine [ADRE], and to carry out ADRE systems analysis and design. This is Phase I Interim Report.

The ADRE concept selection consisted of four distinct studies:

- 1) Rated point performance optimization.
- 2) Components, systems, and engine configuration studies.
- 3) Study of various exhaust energy recovery scenarios.
- 4) Life cycle cost estimates of the ADRE economic worth.

The ADRE design proposed a reciprocator with many advanced features for the 1995 technology demonstration time frame. These included ceramic air gap insulated hot section structural components, high temperature solid lubrication treatments, nonmechanical valve actuation system, no engine coolant, air to air charge cooling, heat-isolated intake manifold, metal air gap insulated exhaust manifold and turbocharger plumbing, and elimination of the cylinder head gasket. Assessment of the complete elimination of the liquid lubricant from the engine was to be pursued further.

Detailed ADRE system analysis and design resulted in the ADRE concepts shown in the cross sections of Figures 1 and 2. An electro-hydraulic valve actuation system and an electronic common rail injection system were conceptualized and are shown in Figure 3. The power transfer systems for the accessory drives, and the exhaust energy recovery systems are shown in Figures 4 and 5, respectively. The ADRE package size compares favorably with the current state-of-the-art engines. Typical truck installation drawings are shown in Figures 6 and 7.

The predicted ADRE performance map shows a possible minimum bsfc of 150.5 g/kW.h. The performance analysis also included assessment of possible improvements in performance that may result from the flexibility of variable valve events. This included examination of the effect of the change in valve opening and closing rate, pressure compounding, and alternate reciprocator-bottomer power transfer scenarios.

The proposed engine control strategy is based on the Detroit Diesel Electronic Control [DDEC] system. It offers integrated control of fuel injection, valve actuation, and lubricant injection systems.

Finite element and probability of survival analyses were undertaken for the ceramic low heat rejection component concepts in order to ensure adequate life expectancy. A sample result is shown in Figure 8 for the cylinder head and firedeck thermal stresses. Other finite element analyses included the study of the gasketless head/liner sealing interface and main bearing caps. Rolling bearings were designed with the goal of reducing the bearing friction by fifty percent over current values.

The solid lubrication assessment included surveying the state-of-the-art, generation of conceptual in situ, and continuously replenishing lubricant delivery systems. Figures 9 and 10 show two such conceptual approaches. The Phase I tribology assessment concluded that liquid lubricant should be used at least

for the components outside the ADRE hot section. Both liquid and non-liquid high temperature tribology approaches were recommended for future hot section investigations.

Figure 1: Engine Block and Power Assembly Cross Section

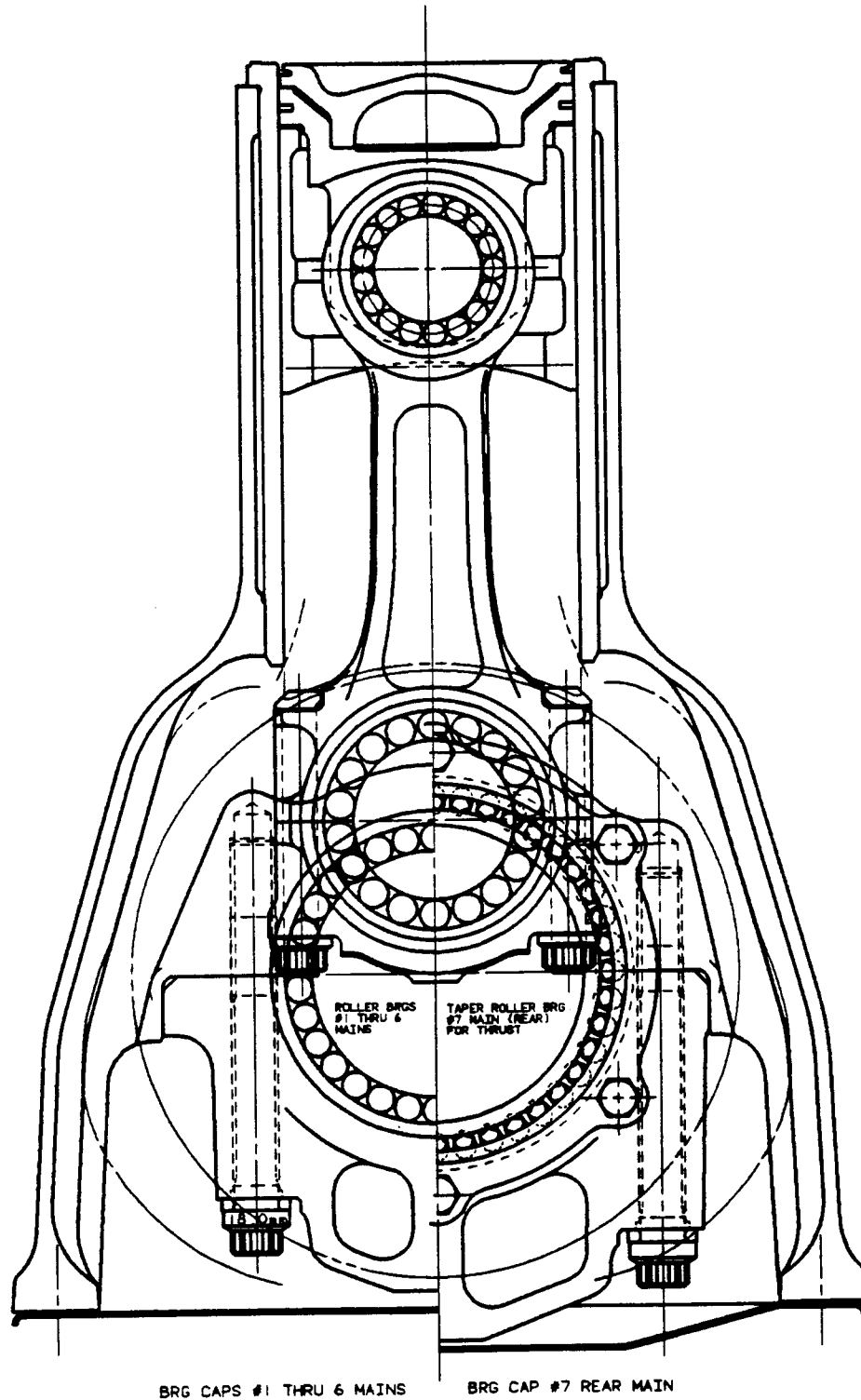
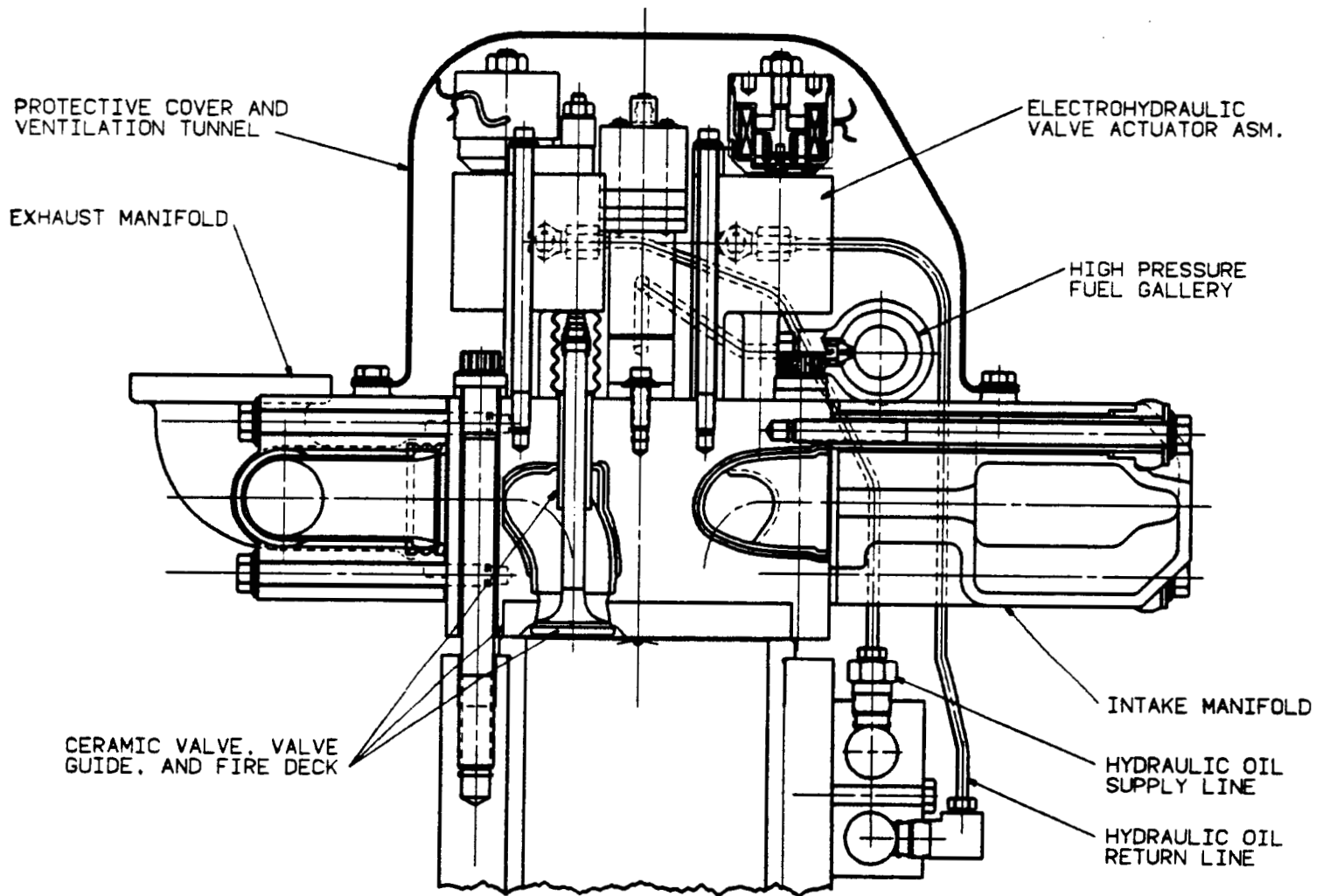
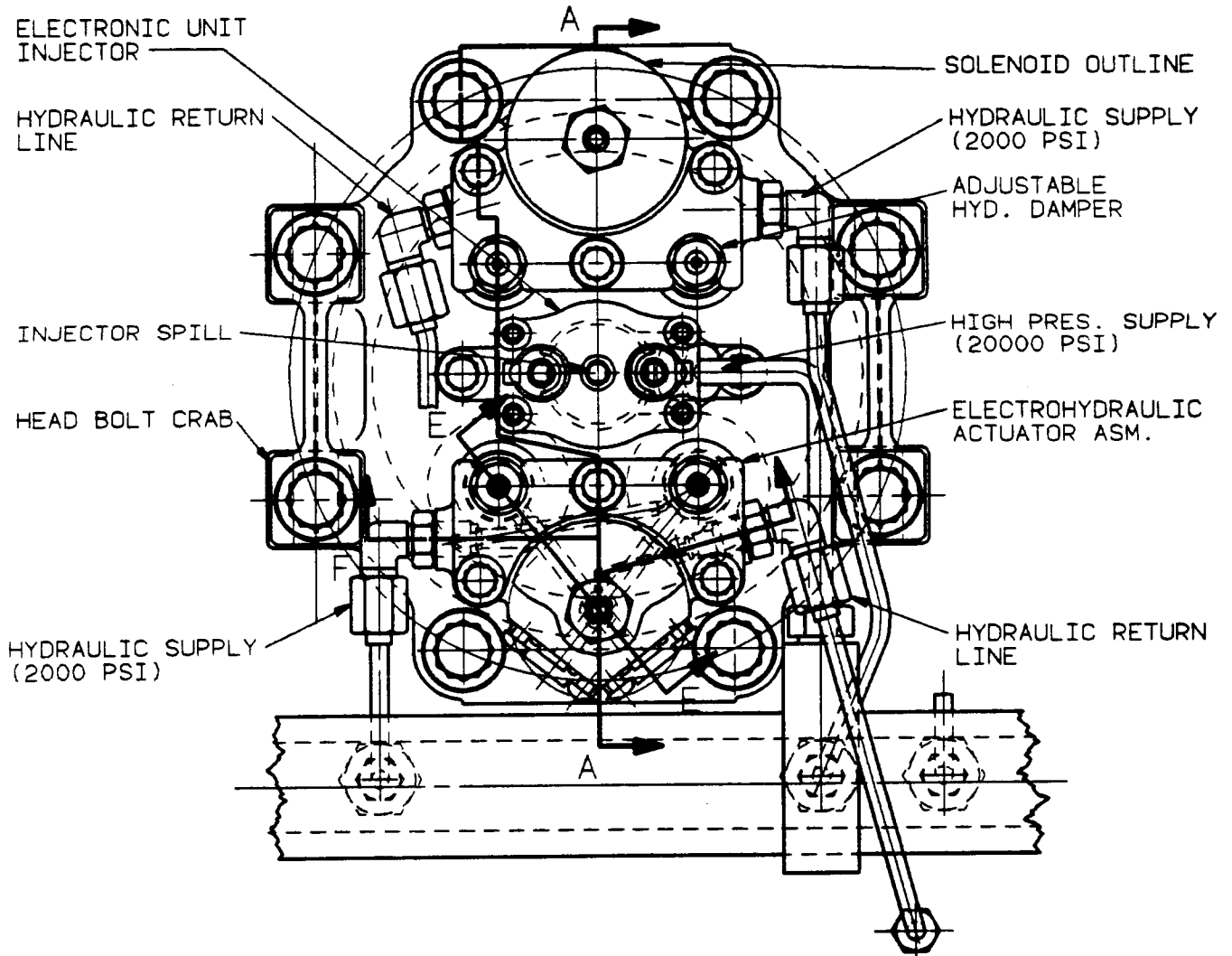


Figure 2: Cylinder Head Cross Section



**Figure 3: Layout of Overhead Components
(Cylinder Head Injector - Valve Acuator Arrangement)**



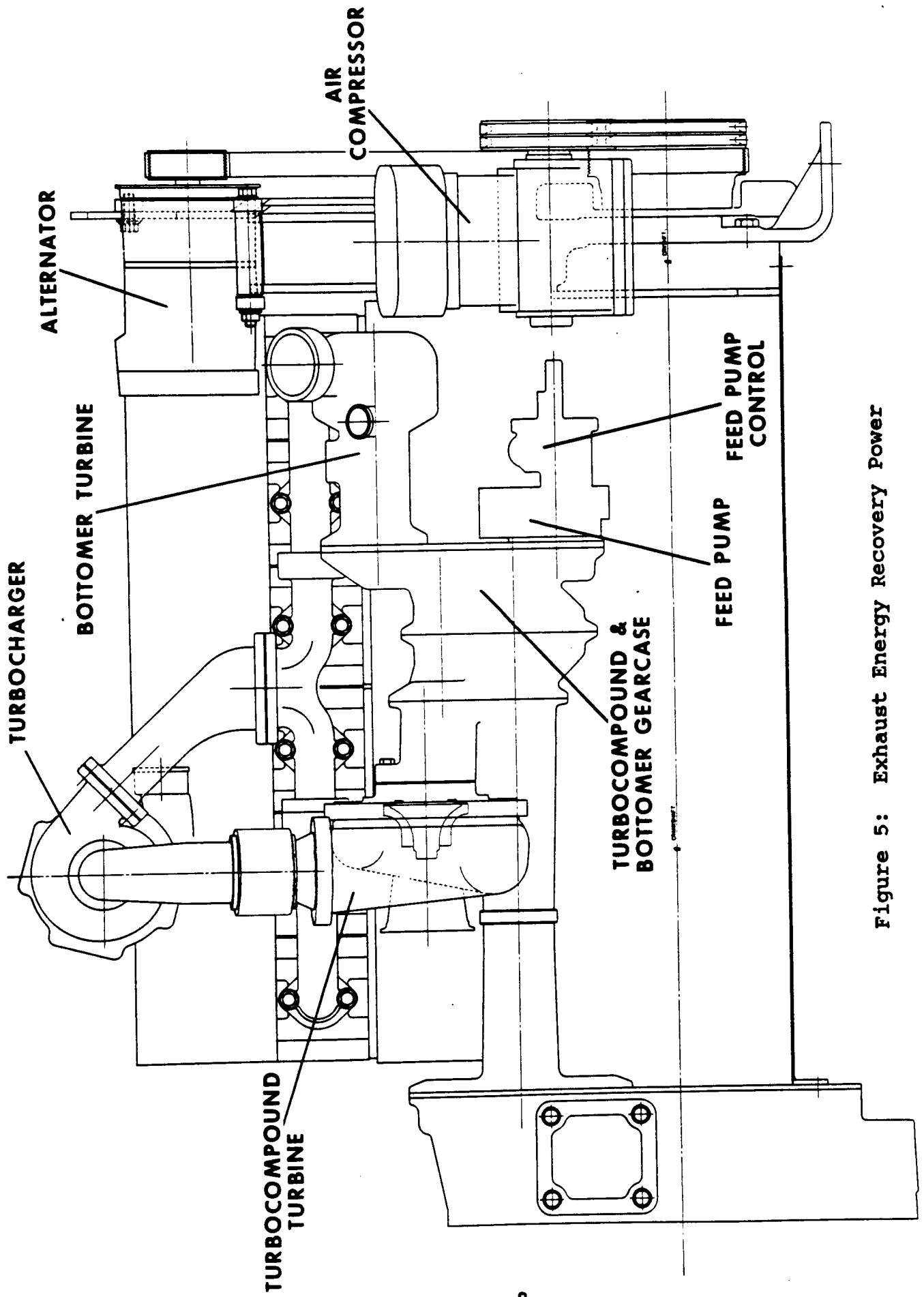


Figure 5: Exhaust Energy Recovery Power

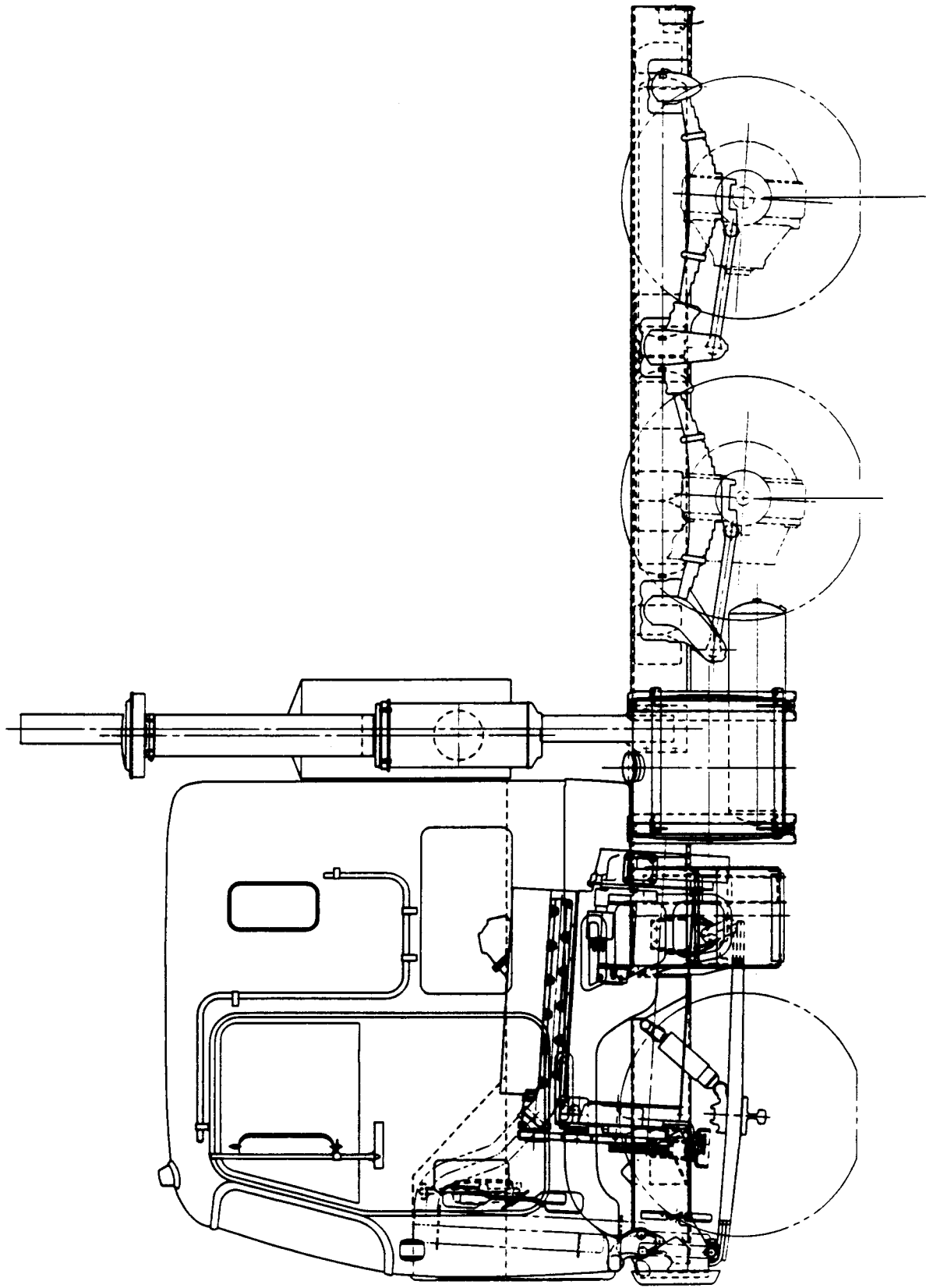
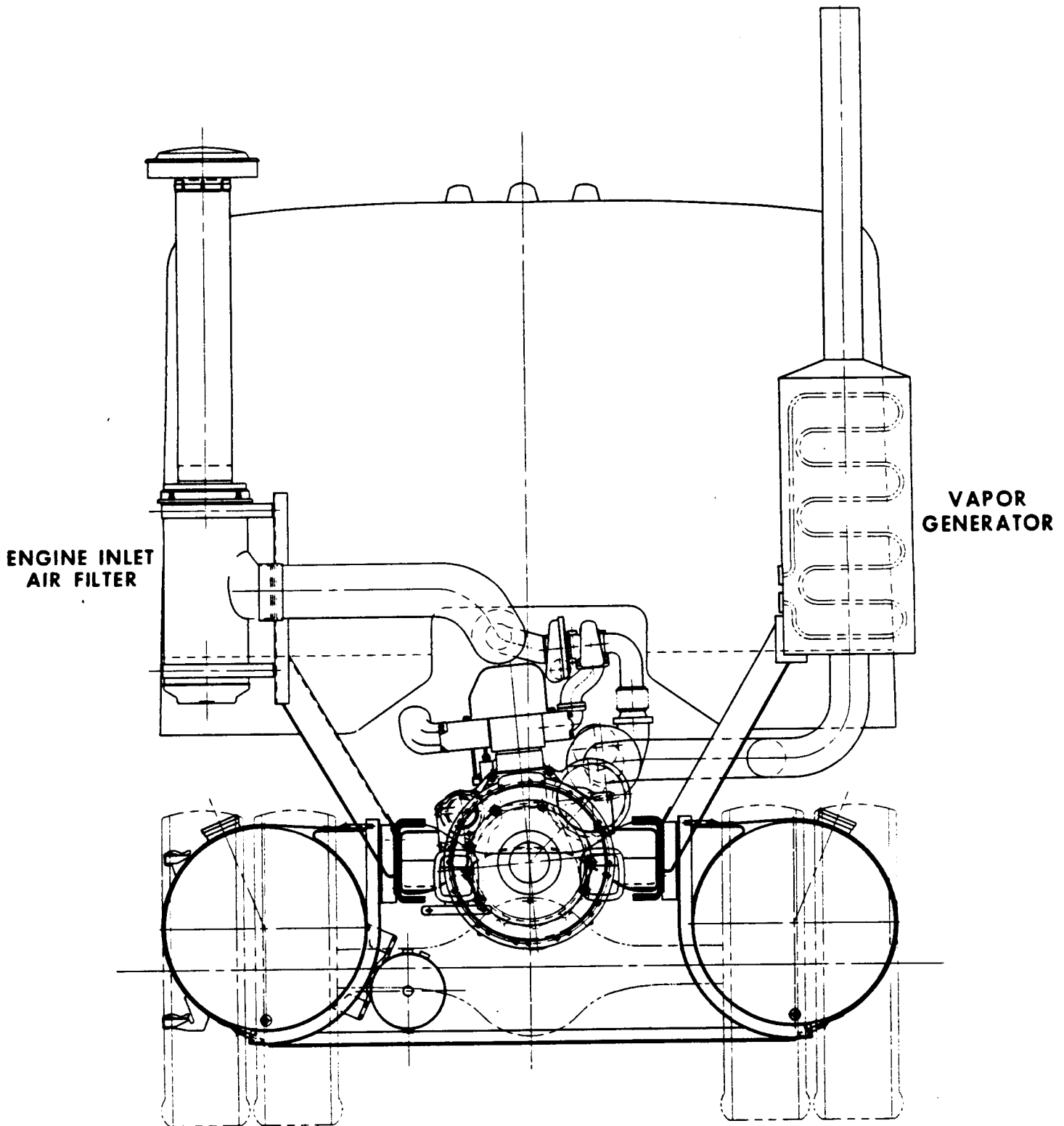


Figure 6: Truck Installation - Side View

Figure 7: Truck Installation - Rear View



- P.O.S. > 0.9995 at full load
- 70% INSULATION
- DESIGN IS FEASIBLE

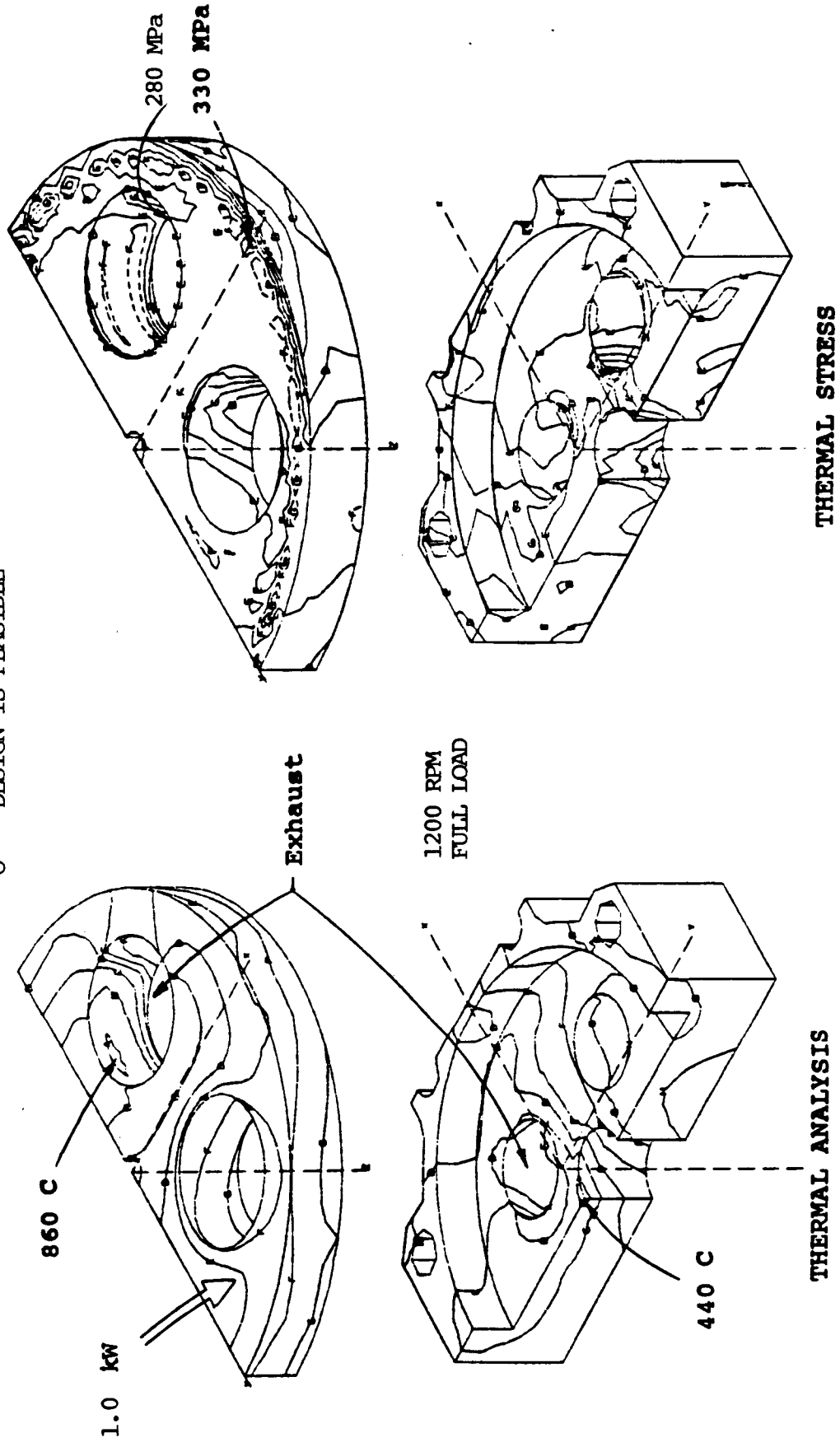


Figure 8: Cylinder Head and Firedeck -
(Isotherms and Thermal Stress Contours)

Figure 9: In-Situ Solid Lubricant Systems

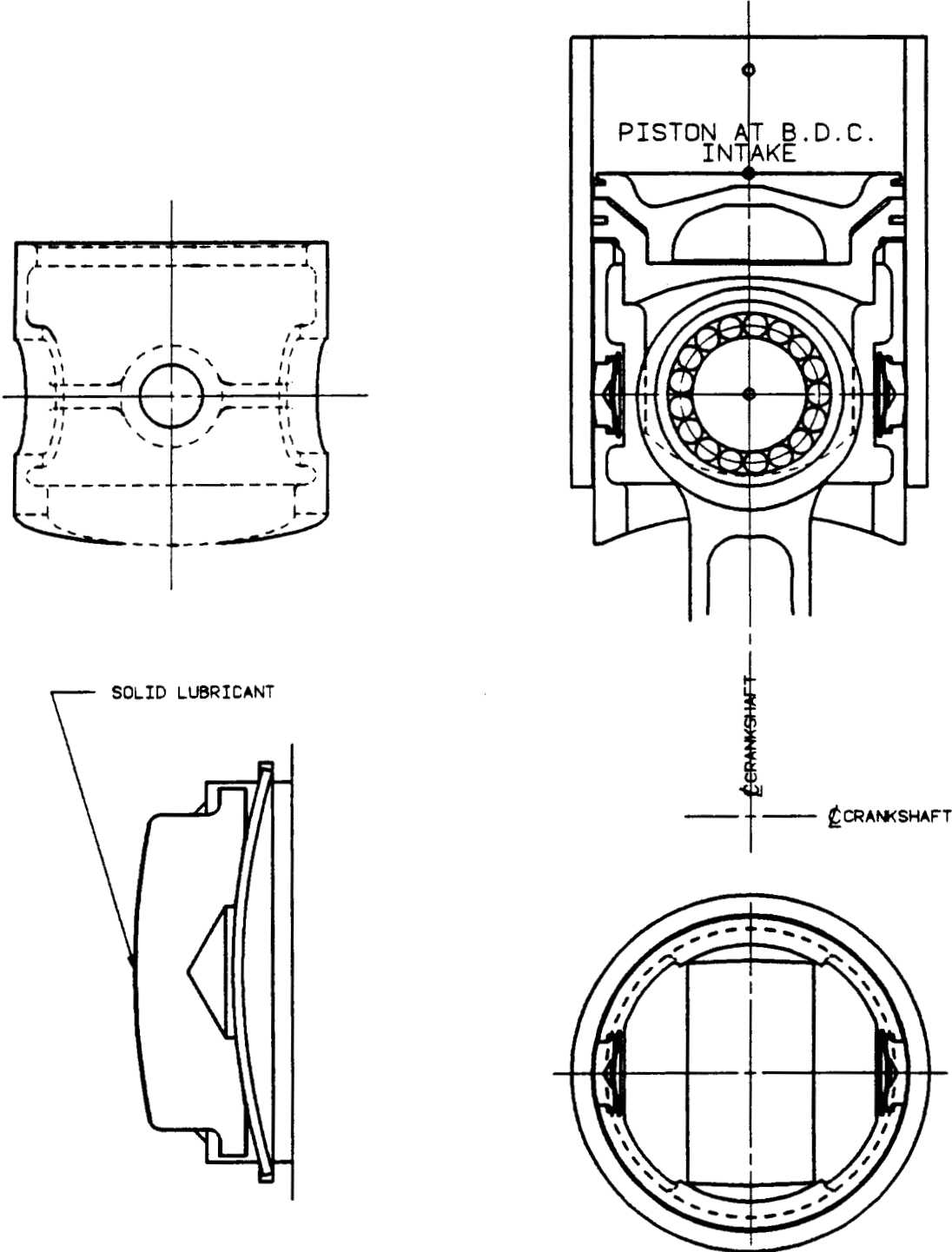
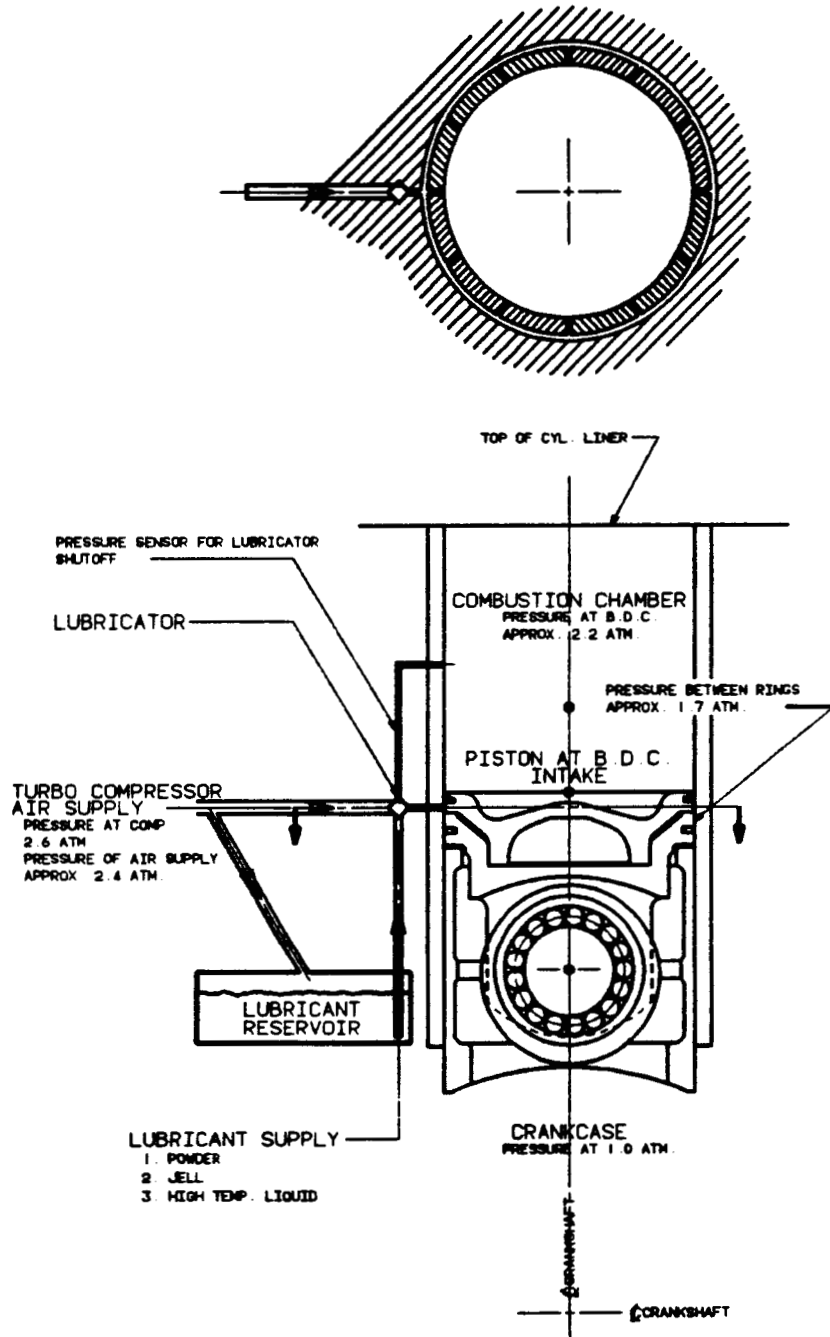


Figure 10: Continuously Replenishing Lubricant Delivery System



INTRODUCTION

The use of petroleum base fuels by the line haul heavy-duty trucks has been significant and is increasing annually. A highly insulated, uncooled diesel engine with exhaust energy recovery has the potential for vastly improved thermal efficiency, lighter weight, and longer life. Structural, material, and tribological problems must be overcome to bring this technology to the marketplace. With the future supply of fuels for the transportation industry uncertain and the importance to the movement of goods, improving the efficiency of the diesel engine as the prime mover is of utmost importance.

The primary objective of this multi-phase Adiabatic Diesel Engine Component Development [ADECD] program is to develop and demonstrate the critical technology needed to advance the heavy-duty adiabatic diesel engine concept for the line haul, heavy truck market. The work in this program is being sponsored by the Department of Energy and the technical direction is being provided by the NASA Lewis Research Center. This document is the Phase I interim report, which describes the work performed by Detroit Diesel Allison Division of General Motors and its subcontractors. This phase included studies of advanced low heat rejection and other synergistic concepts in order to select a reference engine. Further, the reference engine analysis and design were carried out.

The specific objectives of Phase I were to:

- o Evaluate the work done to date, particularly, available prior and present government funded research and development and paper studies.

- o Integrate the most promising concepts into a reference engine design.
- o Optimize the reference engine design relative to fuel consumption and initial and life cycle cost.
- o Demonstrate the feasibility and economic worth.
- o Identify the most critical areas which will need further research and development.

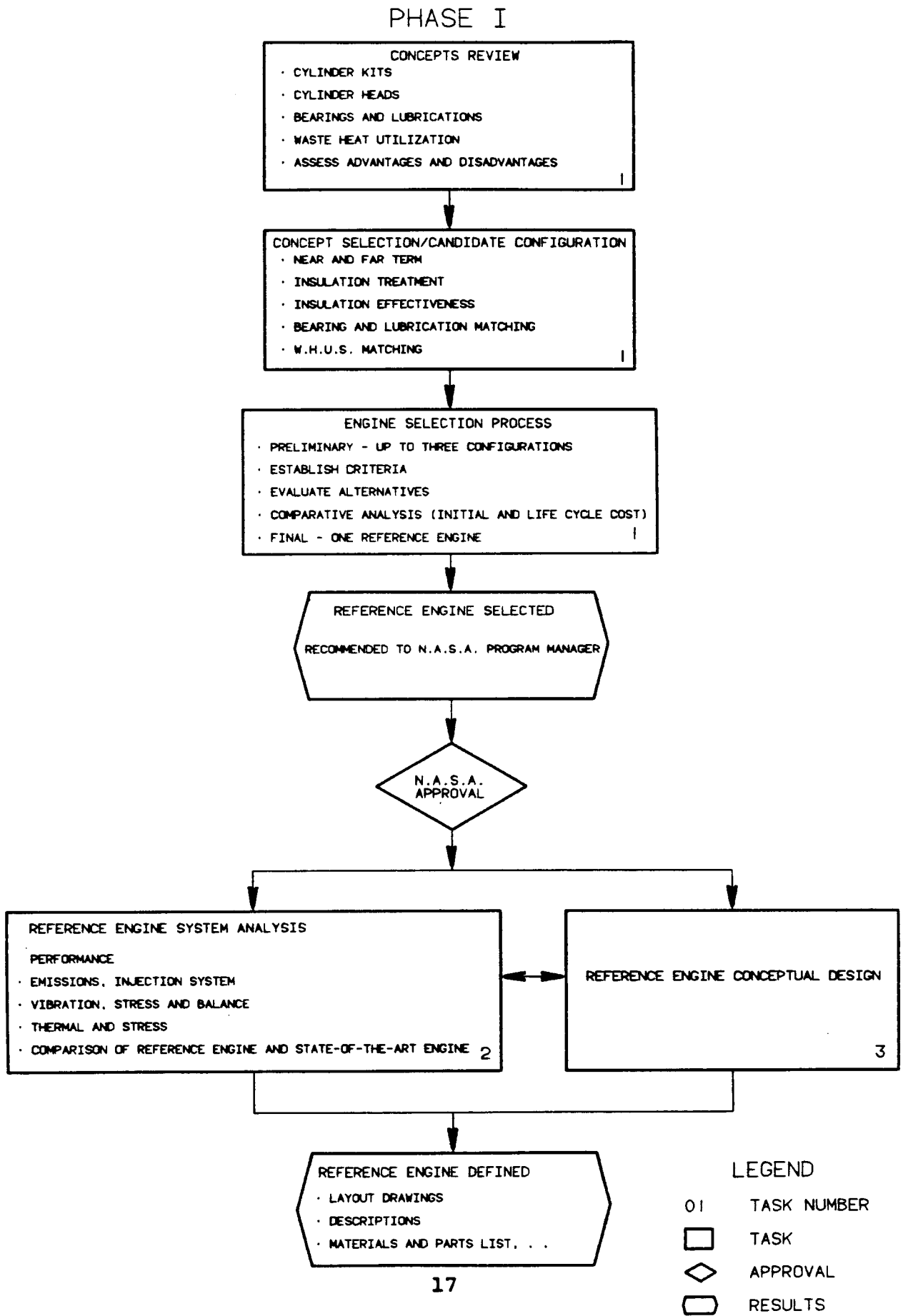
The program's Phase 1 strategy plan, Figure I.1, shows the three main tasks. These are Concept Selection, Reference Engine System Analysis, and Reference Engine System Design. During Task 1, some 47 advanced engine component concepts were identified and characterized according to technical risk for potential readiness for production development in 1995. These concepts were combined according to experience and design practice into six candidate reference engines; two "moderate risk," two "intermediate risk," and two "high risk." In order to examine the full benefit of the adiabatic diesel engine, several exhaust energy recovery scenarios were developed. These included turbocharging, turbocompounding, organic or steam Rankine cycles, and combinations thereof. Evaluation with a life cycle cost model was also developed as part of the Task 1 effort.

Task 1 culminated in the selection of one of the high risk candidates as the reference engine. The combination of turbocompounding and organic Rankine cycle system was the selected exhaust energy recovery system.

In Tasks 2 and 3, the concept of the reference engine was translated into a viable "first cut" engine design through a broad scope of analytical work on key systems and components. In particular, the stresses and heat transfer in the piston, cylinder head, and valves were analyzed through finite element models.

Valve and piston dynamics were analyzed in order to predict critical forces and velocities. System analyses were conducted for the fuel injection, valve actuation, crankshaft, power transfer, and exhaust energy recovery systems. Roller bearing performance and durability were analyzed, both in-house and by a subcontractor. Detailed packaging studies were conducted to ensure compatibility with a typical cab-over-engine tractor. Engine performance simulation was performed, both in-house and by a subcontractor. Engine control system specifications were developed to optimize performance with the advanced actuation systems.

Figure I.1: Phase I Strategy Plan



II

ADIABATIC DIESEL REFERENCE ENGINE CONCEPT SELECTION

The Adiabatic Diesel Reference Engine [ADRE] concept selection resulted in a reciprocator with many advanced features for the 1995 technology demonstration time frame. The end result of this effort was the selection of an advanced technology high risk ADRE concept.

The features of the selected ADRE included monolithic ceramic air gap insulated hot section structural components, high temperature solid lubrication treatments throughout, with no liquid lubrication, non-mechanical valve actuation system, no engine coolant, metal air gap insulated exhaust manifold and turbocharger plumbing, and the elimination of the cylinder head gasket. More assessment of the complete elimination of the liquid lubricant from the engine was to be pursued during the system analysis and design tasks, which will be reported in Section III of this report. The selected ADRE has turbocompounding and organic Rankine bottoming systems. The strategy of this task consisted of four distinct studies:

- 1) Optimization of rated point performance.
- 2) Examination of reciprocator concepts
- 3) Study of various exhaust energy recovery scenarios.
- 4) Life cycle cost estimates of the ADRE economic worth.

PERFORMANCE

The performance assessment was based on a statistically designed analytical modeling scheme, in connection with the cycle

simulation programs. The constraints for the rated point optimization were emissions, reciprocator thermal and mechanical loading, and a 224 kW total system brake power. Insulation levels, post reciprocator exhaust energy recovery options, and friction reduction levels were analyzed. This study resulted in a quantitative determination of the percentage contributions of the major influential parameters on fuel economy, peak firing pressure, and air/fuel ratio. Moreover, bsfc levels for all considered reciprocator and exhaust energy recovery configurations were determined, and optimum parameters for the proposed ADRE concept were selected. It was further determined that liner insulation is a deterrent to the ADRE concept.

RECIPROCATOR CONCEPTS

Review of the current state-of-the-art component concepts, as well as generation of new concepts, was undertaken, resulting in candidate design configurations. These concepts were qualitatively ranked with respect to risk, cost, benefits, serviceability, design synergy, material requirements, and ease of manufacture. ADRE configurations were then formulated by classifying these concepts into three risk levels: moderate, intermediate, and high.

Reciprocator insulation concepts included consideration of thermal barrier coatings, air gaps, and low conductivity ceramic insulation techniques of hot section components. The air gap approach can use either an all metal or monolithic ceramic/metallic multi-piece approach. Achievable insulation levels, risk, cost and component risk/benefit, and cost/benefit ratios were evaluated. Advanced journal/elastohydrodynamic and rolling element bearing concepts were considered for reduced friction. Liquid, grease, and/or solid lubrication were also examined.

The common elements for all the ADRE reciprocator configurations considered for the final ADRE selection included heat isolated intake manifold, metallic air gap insulated exhaust

manifold and turbocharger tubes, ceramic valve seats, guides, cam rollers, cast in place exhaust and intake port shields, with no engine water cooling. In addition, the moderate risk ADRE reciprocator configurations called for thin coatings, liquid lubrication, and relatively conventional tribological environments. The intermediate risk configurations used the metallic air gap insulation approach, liquid lubrication, and advanced liquid lubricated tribological interfaces. The high risk configurations called for monolithic ceramic air gap insulation, solid lubrication, and solid film lubrication tribology.

EXHAUST ENERGY RECOVERY

Turbocompounding, several bottoming systems, and combinations of both were assessed. Turbocompounding was the most recommended approach. Additional recovery via an organic Rankine bottoming cycle could be attractive.

LIFE CYCLE COST

An estimation of the economic worth of the ADRE was undertaken. The life cycle cost approach accounted for initial cost, fuel usage, and maintenance. All possible combinations of various reciprocator-exhaust energy recovery systems under study were analyzed. It was concluded that the ADRE concept has potential advantage, making it feasible for technology demonstration by 1995 and commercial development in the 2000 time frame.

II.1 PERFORMANCE ASSESSMENT

The Low Heat Rejection Engine [LHRE] has been under study for applications in the military [1,2], for passenger cars [3,4], and for the heavy-duty truck market. Many related studies have been reported [5,6]. Recent investigations included analytical studies on the performance of the LHRE [7,8]. Review of the work done to date revealed a need for an integrated system optimization assessment for the potential performance characteristics of the LHRE.

One of the objectives of the ADECD program was the selection of a low heat rejection reference engine that is optimized relative to fuel consumption. This would be an element in assessing the feasibility and economic worth of the LHRE. A performance analysis methodology was conceived to carry out the fuel consumption optimization, with the primary constraint being the future emissions for on-highway trucks.

A two-step, partial factorial orthogonal scheme was used for this performance optimization study. The basic approach for this scheme is a statistical technique known as the "Taguchi method" [9,10]. Optimum fuel economy for various insulation and friction reduction levels of uncooled, emission limited LHRE with likely EER scenarios was predicted. The results were compared to experimentally validated predictions for a state-of-the-art engine. Thus, incremental potential benefits for the LHRE were quantified. The major influential parameters on fuel economy, emissions, and engine thermomechanical loading were identified. Sensitivity analysis was used to determine the percentage contribution of individual influential parameters.

II.1.1 METHODOLOGY

OPTIMIZATION APPROACH

The so-called Taguchi method is an approach for systematic application of the factorial statistics [9,10]. The method minimizes the required number of runs to achieve a certain confidence level, for experimental or computer simulation analyses. It is especially effective when there are a large number of parameters and many levels of variation of parameters to be analyzed. It should be noted that the best possible parametric combination, as determined by a Taguchi analysis, is a piece-wise or discrete optimum, within the considered ranges. More details are available in the cited references.

Underlying the approach is the design of a two-dimensional orthogonal array [OA]. The first step is to identify the likely influential parameters, the range, and the discrete number of levels to be considered for each of these parameters. Additionally, parameter interactions, i.e., possible significant higher order effects, should be considered. Next, an appropriate OA should be selected. Individual parameters and interactions are assigned to some or all of the columns of the OA. This assignment is not arbitrary, but is systematically determined using a linear graph or a triangular table [9]. Remaining columns of an OA, if any, are "error terms." An error term is a statistically determined quantity that shows the lumped effects of many less influential factors, higher order and/or confounded interactions. For a well-designed scheme, the effect of the error terms should prove to have a very small contribution to the variations of interest.

Each row in an OA defines the parameters and their specified levels for an experimental or simulation run. The number of rows, i.e., the number of runs to be executed, defines the designated order of the OA. Individual column contributions to the total

possible variation of the dependent variable are determined via the analysis of variance of the results. The application of the Taguchi method to the LHRE performance optimization and the detailed design of the two orthogonal arrays used in this study have been reported [11].

ENGINE SIMULATION

The other element of the methodology is the engine system simulation. The DDA engine system simulation program used for this study has a modified combustion model based on the Whitehouse and Way formulations [12]. Burning rates are predicted based on validated in-house experimental data. The in-cylinder heat transfer is calculated using Woschni's model [13]. Combustion zone wall surface temperatures can either be specified as input boundary data or calculated, based on a simplified one-dimensional heat transfer network. Cylinder processes and turbomachinery calculations are executed at predetermined engine crank angle intervals. Figure II.1-1 is a schematic of the simulated engine system.

The scope of the analysis for this study called for the use of the turbomachinery operating point efficiencies. No component maps were needed or even available at this stage. In fact, the hardware was yet to be selected, based upon the resulting optimum parametric combination at the rated operating point and on further considerations of part load performance.

Two optimization studies were undertaken. The preliminary study used a limited size OA array with few operating variables. The second study was more elaborate and considered more influential parameters. Its design was based on the results of the preliminary optimization, and it utilized a higher order OA.

II.1.2 PRELIMINARY OPTIMIZATION

PARAMETERS, OA AND VARIABLES

The preliminary performance optimization study investigated the effects of six influential parameters. These are the compression ratio, compressor pressure ratio, beginning of injection [BOI], stroke, turbocompound pressure ratio, and insulation level. It was further decided to consider three levels for each parameter, in order to establish the trend and linearity behavior of their effects. These parameters and the selected levels are shown in Table II.1-1. The values shown in the table for the first level were intended to simulate the lowest degree of insulation. This would result from draining the coolant of a typical state-of-the-art [SOA] engine, without any additional insulation treatments. The remainder of the engine simulation input data for this study is summarized in Table II.1-2, which gives basic configuration, boundary data, fuel injection, and valve events, and turbomachinery efficiencies. This optimization phase was carried out considering a 130 mm cylinder bore and total system power of 223.7 kW (300 BHP). Finally, it was desired at this stage to determine the degree of interaction or the interdependence among three pairs of these parameters:

- 1) Engine compression ratio and compressor pressure ratio.
- 2) Engine compression ratio and BOI.
- 3) Compressor pressure ratio and BOI.

In addition to the data and parameters of Tables II.1-1 and II.1-2, considerations for emissions and engine thermomechanical loading imposed more constraints. The fuel economy trends were to be determined, subject to limitations listed in Table II.1-3.

A 3-level parameter has two degrees of freedom, and an interaction of two parameters has four degrees of freedom. The resulting total number of degrees of freedom for this study was 24. An L-27 OA was most suitable for this analysis. This two dimensional OA is 27 X 13. Twelve of the thirteen columns were assigned to parameters and interactions, leaving one column as an error term. Each of the twenty-seven rows of the OA specified the combination of above-mentioned parameter levels for a computer simulation run.

ANALYSIS OF RESULTS

The ultimate objective was to determine the parametric combinations for the best fuel economy, taking into account all the previously mentioned constraints. The variables considered were fuel input per cycle, peak firing pressure, air/fuel ratio [A/F], and reciprocator brake mean effective pressure [BMEP]. The parametric combinations for the best fuel economy were obtained at three different peak pressure and BMEP levels and two different A/F values at 1800 r/min.

Heat transfer rates from the piston, head, and liner surfaces were monitored. Further, the mean, variation, variance and percent contribution of each influential parameter were calculated for the dependent variables. Except for insulation levels, which were discrete, linear interpolation was used between levels for a given parametric effect on an optimization variable. Very limited extrapolations were also justified since, in this study, most of the effects were clearly linear.

Emissions Considerations - The peak firing, adiabatic, and in-cylinder surface temperatures were maintained below certain maxima imposed by limiting the NO_x emission to 5 gm/BHP-hr. Their values were based on currently classified, experimentally validated empirical correlations. The temperature limits were maintained through the control of the BOI. In this study, the BOI was maintained at 12 degrees BTDC, which met the above-mentioned temperature constraints.

Diesel engine smoke limit is mainly a function of the minimum A/F at the peak torque speed. Based on this, and considering an acceptable engine torque rise, the rated speed minimum A/F was selected. Considering a SOA fixed geometry turbine, the A/F must be at least 30:1 at rated speed to obtain a torque rise of 25-30 percent, at a reasonable peak torque speed and without exceeding the acceptable smoke limit. Increasing the torque rise to the 30-35 percent range would require a minimum A/F of about 32:1 at rated speed. These values are based upon current experience and previous analytical studies.

Particulates emission was not a concern in these studies. A particulate trap downstream from the LHRE is proposed to meet the prevailing 1995 particulates emission standards. This treatment would be the same perceived for a conventionally cooled SOA engine

Fuel/Cycle - For a fixed system power of 223.7 kW, the fuel/cycle represents the fuel economy or the bsfc. The significant parameters affecting the fuel/cycle are:

- o compression ratio,
- o stroke,
- o turbocompound pressure ratio, and
- o insulation.

The average fuel/cycle change for all levels of variation of each of these significant parameters is graphically displayed in Figure II.1-2. The results show that the best fuel economy or the lowest fuel/cycle would result from the highest compression ratio, lowest stroke, highest turbocompound turbine pressure ratio, and highest insulation level. It is important to note the percentage contribution of each of the parameters to the likely improvement in bsfc. Within the scope of this study, 90.1 percent of the likely change in the bsfc can be attributed to these four parameters.

Before deriving a final conclusion, however, results for other variables and constraints should be analyzed and taken into account.

Peak Firing Pressure - The peak firing pressure is a function of:

- o reciprocator compression ratio,
- o compressor pressure ratio, and
- o BOI.

These account for 96.3 percent of the total likely change in the peak firing pressure, as shown in Figure II.1-3. Note that the compression ratio is an influential parameter for both bsfc and peak firing pressure. For a given peak pressure limit, it is apparent that the lowest compressor pressure ratio combined with the highest reciprocator compression ratio would result in the best possible fuel economy.

Air/Fuel - The A/F is a strong function of:

- o compressor pressure ratio,
- o turbocompound pressure ratio, and
- o stroke.

These contribute 97 percent of the predicted change in A/F, as graphically displayed in Figure II.1-4. Note that the turbocompound pressure ratio and stroke are also influential parameters on bsfc.

BMEP - The engine system simulation was executed at constant power output and fixed bore. Hence, the reciprocator BMEP could be changed only by the change in:

- o turbocompound pressure ratio, and
- o stroke.

These two parameters accounted for 99.8 percent of the BMEP variation, as shown in Figure II.1-5.

Optimization Rationale - Choice of values for all influential parameters was made based on collective assessment of the above results. The maximum insulation level for this preliminary optimization study was 48 percent, when compared to the baseline SOA water cooled engine. This maximum insulation level was the most beneficial to fuel consumption, while piston and cylinder head temperatures were still within reasonable range. Hence, the maximum insulation was chosen as the optimum level. It should be noted that this study simulated a conventionally cooled liner, in order to examine potential compromises between fuel economy and the tribological integrity of the cylinder liner/piston ring interface.

The turbocompound turbine pressure ratio was chosen to be 1.5:1, as a compromise between bsfc gains and smoke limit restrictions. The curve in Figure II.1-2 shows the negligible gain in bsfc when this ratio was increased from 1.5 to 2.0. Note also that an increased turbine pressure ratio would result in an increase in pumping power losses.

The BOI was also fixed at 12 degrees BTDC to limit the peak firing pressure, and the NO_x emission as explained above. The mean A/F was then fixed at 30:1 and 32:1 to simulate two different torque rise characteristics for each stroke (effectively BMEP). Using analysis of variance, the compressor pressure ratio was calculated from the OA simulation results. The compression ratio was then calculated for the three different peak pressure levels.

The best fuel economy was calculated for the various peak pressure, stroke (BMEP), and A/F (torque rise) levels. The results are graphically shown in Figure II.1-6 for 30:1 and 32:1 A/F.

Table II.1-4 lists the combinations of parameters for the best fuel economy. Note that these values are statistically predicted, based on the expected value of the mean effect on fuel economy and the analysis of variance.

Validation - To validate the results of the parametric effects analysis, a confirmation run is essential [10]. This analytical step examines whether the initially perceived influential parameters and interactions between parameters are indeed the most significant. It can also identify any numerical or procedural errors resulting during the execution of the analysis. A confidence interval was calculated for each predicted value, and two confirmation runs were executed. Table II.1-5 shows the comparison of the statistically predicted values of the variables and those calculated from a confirmation run using the engine system simulation program. Predictions for most variables are within the confidence intervals. Deviations within a one-half percent of the confidence intervals can result from interpolation, extrapolation, and/or nonlinear effects. Because of the excellent agreement, the statistical analysis can be used to predict the effects on parameters within the validity range of the engine simulation model.

It is noted that this study did not predict the absolute optimum point for all influential parameters. Rather, it was considered a preliminary investigation leading to the more elaborate study, with new levels of variation and additional parameters. The detailed optimization study would then lead to the identification of optimized sets of parameters, which would be the basis for LHRE engine selection.

II.1.3 DETAILED OPTIMIZATION

PARAMETERS, OA AND VARIABLES

The detailed optimization can be viewed as a refinement to the preliminary study. A higher order array was necessary to incorporate further enhancements. Since the basic methodology has already been explained, the remainder of this section will address only the additional enhancements considered for the detailed study.

The parameters to be optimized and their levels of variation are shown in Table II.1-6. These selections were based on the results already available and prior experience with conventional and LHR engine characteristics. No interactions were considered because the preliminary optimization showed that they have no significant contribution. Based on the parameters of Table II.1-6, an L-36 OA was chosen for the study. This array is unique because all interactions are distributed equally among all columns, and it is most applicable to a situation where interactions are known to be insignificant.

Bottoming System - To simulate the additional power output of a waste heat utilization bottoming system, the Carnot cycle efficiency equation was used. The simulation considered the additional work recovery to be a fractional multiplier of the work of a Carnot machine operating between the two temperature limits of the bottoming system. The source temperature used was the inlet temperature to the bottoming system, while the sink temperature was considered constant at 422°K for all operating points. This scheme predicted the same organic Rankine bottoming cycle work output as that reported in Reference 14. In the case of a steam Rankine bottoming cycle, a simple correlation was inappropriate, due to the non-linearity introduced by the high latent heat of vaporization. To be expressed as a fractional multiplier, the work output derived from a steam Rankine bottoming system was first calculated using the information in Reference 14.

The fractional multiplier of the waste heat utilization system was considered as an influential parameter in the optimization study. It is referred to as the bottoming cycle effectiveness.

Friction - The engine system mechanical friction model was used as an influential parameter with three levels of variation. Level 1 simulated the SOA baseline engine friction values, while levels 2 and 3 represented further improvements in the overall engine mechanical efficiency. The cylinder kit friction and auxiliaries power consumption were considered as two separate categories of the baseline friction. Essentially, the latter simulated mechanical power losses or demands of the engine bearings, gear train, overhead mechanism and pumps.

Level 2 considered a friction reduction level that would be equivalent to fifty percent of the auxiliaries power. Level 3 assumed an overall friction reduction level of fifty percent. This third level is believed to be rather ambitious for the 10 years technology demonstration time frame. The three friction levels in Table II.1-6 are, hence, described by the following values:

$$FMEP_{total,i} = FMEP_{aux,i} + FMEP_{cyl\ kit,i}$$

where

FMEP = friction mean effective pressure
i = index for friction parameter
level in the orthogonal array
= 1 for baseline friction

and

$$FMEP_{aux,2} = .50 \times FMEP_{aux,1}$$

$$FMEP_{aux,3} = .50 \times FMEP_{aux,1}$$

$$FMEP_{\text{cyl kit},2} = FMEP_{\text{cyl kit},1}$$

$$FMEP_{\text{cyl kit},3} = .50 \times FMEP_{\text{cyl kit},1}$$

Insulation - In the preliminary study, the combustion chamber components' physical and thermal characteristics were the input parameters, while temperatures and component heat transfer rates were predicted by the simulation. Higher insulation levels were simulated by increased thermal resistance. Further, all the components, i.e., piston, cylinder head, and cylinder liner had the same characteristics.

In the detailed study, it was decided to separate the cylinder liner insulation treatment from the two other components. This was prompted by the desire to keep the liner surface temperature as low as possible, without sacrificing the likely performance gains. A lower liner surface temperature is extremely desirable for tribological reasons, which is believed to be a limiting factor in the development of the LHRE. Additional positive factors for maintaining lower liner temperatures relate to design synergy, blow-by control, and volumetric efficiency.

To facilitate interpolation of the statistical data, component temperatures, rather than the physical and thermal characteristics, were used as the input parameters. They were assumed to be constant throughout the cycle. The piston and cylinder head surface temperature was an influential parameter in the optimization study. It had three levels of variation from 555°K simulating the first insulation level, to 1111 °K simulating the third level. The liner surface temperature was an independent influential parameter and varied from 422°K simulating the first insulation level, to 667°K simulating the third level. It is noted that level 1 simulated the conditions for a water cooled SOA engine. Experimental validation data was available for this case, and was used to enhance the confidence in the simulation predictions.

ANALYSIS OF RESULTS

As before, the best parametric combinations for the optimum fuel economy under the emission constraints were to be determined. The OA output variables analyzed were fuel/cycle, A/F, peak firing pressure, BMEP, peak firing temperature, adiabatic flame temperature, exhaust temperature, total cylinder heat transfer, and component heat transfer rates. Pertinent findings are presented in the remainder of this section.

It should be noted that the results of the statistical analysis are dependent upon the selected influential parameters, their values, and the difference in magnitude among their levels. For example, the compression ratio was varied between 14:1 and 18:1 in the first study, and was found to have a best value of 18:1. Thus, it was decided to examine the effect of variation of the compression ratio in the neighborhood of 18:1 for the detailed study. This examined range proved no further significant influence on the performance and, moreover, showed that a value of about 18:1 is indeed optimum for the compression ratio.

To explain further, another example is considered. The insulation level was changed between 34 and 48 percent in the preliminary study. These values and the range of variation in the insulation level proved to have an effect of 8.9 percent on the likely change in fuel economy. In the detailed study, on the other hand, the insulation level of the piston and the cylinder head was changed between 0 and 100 percent. The results of this study showed that this variation in insulation would contribute 13.45 percent to the total possible change in the fuel economy. This was influenced not only by the above-mentioned change in insulation values, but also by the other refinements and additional variables considered. Similar rationale applies when considering other influential parameters or dependent variables.

Emissions Considerations - The NO_x emission, as mentioned earlier, is a strong function of the maximum temperatures. The BOI

was a major factor that influenced these temperatures. In this study, It was found that BOI at 10 degrees BTDC would maintain the desired temperature limits and, hence, was adopted to meet the NO_x emission constraint.

Considering a variable area turbocharger turbine as feasible for the 1995 technology demonstration time frame specified for this study, the acceptable A/F was determined to be at least 28 at the rated full load operating point. This is in order to meet the smoke emission constraint at the peak torque operating point, as was explained in the earlier study when a higher A/F was adopted for the case of a fixed area turbine.

Fuel/Cycle - For the prescribed fixed system power, the most significant parameters on fuel consumption are:

- o bottoming cycle effectiveness,
- o insulation of piston and cylinder head,
- o turbocompound pressure ratio,
- o friction level, and
- o compressor pressure ratio.

Figure II.1-7 shows each of the significant parameters and their respective average fuel consumption values. These parameters contribute 79.3 percent to the likely change in bsfc. The last parameter accounted for in Figure II.1-7, the compressor pressure ratio, would contribute an average of 2.03 percent to the likely change in the bsfc. Each of the remaining influential parameters of Table II.1-6 would contribute less than 2 percent, leaving only a small percent for the statistical "error" term explained earlier. For example, the sum of the likely contribution of the speed, compression ratio, BOI, and liner temperature amounts to 6.1 percent. The results indicate that under the simulation

constraints, the best possible fuel economy would result from the highest bottoming cycle effectiveness, highest piston and cylinder head insulation, lowest reciprocator friction, and certain intermediate values for the turbocompound pressure ratio and the compressor pressure ratio.

The piston and cylinder head surface temperature graph in Figure II.1-7 shows that they have a lower effect on the fuel economy when their level of variation is changed from 2 to 3, compared to when it is changed from 1 to 2. This is also the case for the effect of friction reduction. The results clearly show the progressively decreasing marginal gains in the fuel economy as the piston and cylinder head insulations are increased or the engine friction is decreased. Another rather significant finding is that the cylinder liner insulation has no significant effect on the fuel economy. The cylinder liner insulation did reduce the cylinder heat transfer, but it also reduced the volumetric efficiency, as shown in Figure II.1-8. The two opposing effects seemed to net in no significant influence of liner insulation on fuel economy.

Figure II.1-7 also shows that the higher compressor pressure ratio or turbocompound turbine pressure ratio does not necessarily result in improved bsfc. The optimum value for the compressor pressure ratio is in the neighborhood of 2.6:1, and that of the turbocompound pressure ratio is close to 1.7:1. This indicates that the LHRE engine configuration under consideration does not require a multi-stage turbocharging scheme, or a relatively high pressure ratio power turbine.

Finally, it is noted that the most significant improvement in bsfc can be attributed to a waste heat utilization bottoming system. However, the practicality, in terms of economic assessment for commercial utilization of such a system for LHRE applications, is being reported separately [15]. When compared to the bottoming system in terms of their relative contribution to the bsfc improvements, the piston and head insulation, turbocompound pressure ratio, friction level and compressor pressure ratio

contribute 29.4, 21.3, 17.4 and 4.4 percent, respectively. It is obvious that other factors, in addition to the likely contribution to performance enhancements, affect the relative practical ranking of the influential parameters in real life. Initial price, maintenance cost, and customer acceptability are examples of such factors.

Air/Fuel - The significant parameters affecting the A/F are:

- o compressor pressure ratio,
- o cylinder bore,
- o engine speed,
- o stroke,
- o bottoming cycle effectiveness, and
- o turbocompound pressure ratio.

These contribute 97.2 percent of the predicted change in A/F, as shown graphically in Figure II.1-9. Note that the compressor pressure ratio, bottoming cycle effectiveness, and turbocompound pressure ratio are also influential parameters on the bsfc. The A/F increased with the increase in bore and stroke. This factor was an element in the selection of a bore and a stroke for the LHRE.

Peak Firing Pressure - The significant parameters affecting the peak firing pressure are:

- o compressor pressure ratio,
- o BOI,
- o compression ratio,

- o cylinder bore, and
- o engine speed.

These contribute 94.9 percent to the likely change in the peak firing pressure, as shown in Figure II.1-10. The optimized values for compressor pressure ratio, compression ratio, and engine speed are selected based on fuel economy considerations. The NO_x emission constraint dictated the BOI value. The peak firing pressure decreased as the the bore size increased.

BMEP - The factors affecting the reciprocator BMEP are:

- o cylinder bore,
- o engine speed,
- o turbocompound pressure ratio,
- o stroke, and
- o bottoming cycle effectiveness.

These contribute 97 percent of the predicted change in BMEP, as shown in Figure II.1-11. The turbocompound turbine pressure ratio, engine speed, and bottoming cycle effectiveness values were determined for the best fuel economy. The BMEP decreased linearly with the increase in bore and stroke.

Reciprocator Sizing - The bore and stroke still needed further examination. The range of acceptable bore/stroke ratios for heavy-duty engines has been investigated [16]. The value of 0.95 was selected for the LHRE. It is shown above in Figures II.1-10 and II.1-11 that a larger bore resulted in lower peak firing pressure and BMEP. However, a larger bore tends to increase the in-cylinder heat transfer rates. This is even more significant at part loads and speeds because heat rejection becomes progressively

a larger percentage of the fuel energy input. Therefore, a smaller bore is more advantageous for the lower loads and speeds. Another contributing factor to the bore size selection is the consideration of limiting minimum A/F. It is clear from Figure II.1-9 that the A/F decreased rapidly with smaller bore size. The 110 mm bore gave an A/F of 24 at the rated point, which is not an acceptable value. A bore of 120 mm and a stroke of 125 mm were selected as the most reasonable trade off between A/F, engine mechanical loading, and part load performance.

II.1.4 FUEL ECONOMY

The optimum fuel economy was calculated for all likely EER scenarios at the three system friction levels and three reciprocator insulation levels. The baseline was considered the SOA turbocharged conventionally cooled engine. Additional EER via turbocompounding and/or bottoming cycle were investigated. The bsfc values for all the EER scenarios and the three insulation levels are shown in Figure II.1-12. This figure gives the best fuel economy prediction for the first level or baseline of reciprocator friction. The effect of friction reduction is explained in Figure II.1-13, which shows the best possible bsfc at the three friction and insulation levels for a LHRE with turbocompounding and waste heat bottoming cycle. Finally, the percent gain in fuel economy as a function of the piston and cylinder head insulation for various LHRE-EER systems is graphically shown in Figure II.1-14.

II.1.5 PERFORMANCE ASSESSMENT CONCLUSIONS

1. A comparison between different engine configurations under a fixed set of boundary and operating conditions is not necessarily a valid assessment of an individual system's potential. Instead, each configuration should be individually

optimized. Comparative evaluations can then be carried out among the optimized configurations.

2. The percent contributions of individual influential parameters on pertinent variables have been determined. This identifies the parameters that are likely to have the most impact on a certain variable and predicts the expected level of change.
3. The analytical predictions are based on engine simulations which have been experimentally validated using conventional SOA engine data and limited uncooled LHRE data. Refinements can be expected as more advanced LHRE data becomes available.
4. Interactions between primary influential parameters, or higher order effects, have a minor impact on performance, emissions or engine mechanical loading.
5. Liner insulation is not recommended for the LHRE.
6. Piston and cylinder head insulation is beneficial. However, decreasing marginal bsfc gains from higher insulation levels, along with the associated increase in design challenges, can affect the practical insulation limits for these components. This limit can be less than the maximum insulation level that can be demonstrated under research environments.
7. Obviously, a reduction in an engine friction is a direct improvement in bsfc. However, this also has a decreasing marginal gain. Beyond a certain level, engine friction reduction can be limited by other practical considerations.
8. Insulation can improve the bsfc for all considered LHRE-EERS configurations. A conventionally cooled SOA engine can have 3.4 and 5.0 percent improvement in bsfc for an overall engine insulation level of 40-50 and 80-100 percent, respectively. Other configurations have similar levels of improvements.

These percentages are 4.0 and 5.8 for an advanced engine with turbocompounding and bottoming exhaust energy recovery systems, respectively.

9. Exhaust energy recovery via a turbocompound power turbine is beneficial for all engine insulation levels. The SOA conventionally cooled and the maximum insulated engines would gain 4.2 and 4.4 percent improvement in bsfc from turbocompounding, respectively.
10. Exhaust energy recovery via a bottoming system is also beneficial for all engine insulation levels. The SOA conventionally cooled and the maximum insulated engines would gain 9.3 and 9.8 percent improvement in bsfc, from a bottoming system, respectively.
11. The combined turbocompounding and bottoming system exhaust energy recovery can result in 13.5 and 14.2 percent bsfc improvement for the SOA conventionally cooled and maximum insulated engines, respectively.
12. The baseline for all the quantitative comparisons used is a SOA engine that has an operating point bsfc of 193.10 g/kW.h (.317 lb/bhp.hr). The operating point bsfc for a typical current production, heavy-duty diesel engine is higher than this figure.

II.1.6 REFERENCES

1. Bryzik, W., and Kamo, R., "TACOM/Cummins Adiabatic Engine Program," SAE Paper 830314, 1983.
2. Kamo, R., and Bryzik W., "Cummins/TACOM Advanced Adiabatic Engine," SAE Paper 840428, 1984.
3. Siegla, D., and Amann, C., "Exploratory Study of the Low-Heat-Rejection Diesel for Passenger-Car Application," SAE Paper 840435, 1984.
4. Edwards, J., "Ceramics and the Swing Beam 2 Stroke Diesel for the Automotive Engine," SAE Paper 830315, 1983.
5. Bryzik, W. and Kamo, R., Edit., The Adiabatic Diesel Engine, SAE Pub. SP-543, 1983.
6. Bryzik, W. and Kamo, R., Edit., Adiabatic Engines: Worldwide Review, SAE Pub. SP-571, 1984.
7. Morel, T., et al., "Methods for the Integrated Analysis of Heat Transfer, Component temperatures and Performance in Insulated Engines," proc. 22nd ATD-CCM, SAE Pub. P-155, pp 281-295, 1984.
8. Assanis, D., et al., "Computer Simulation of the Turbocompounded Diesel Engine System," proc. 22nd ATD-CCM, SAE Pub. No. P-155, pp 297-316, 1984.
9. Taguchi, G., Quality Engineering, Methodology and Application, American Supplier Institute, Romulus, Michigan, 1984.
10. Taguchi, G., and Wu, Y., Introduction to off-line Quality Control, Central Japan Quality Control Association, Nagaya, Japan, 1985.
11. Roslund, J., and Savliwala, M., "A Theoretical Engine Design Using a Taguchi Factorial," Quality Engineering Using Design of Experiments, Proc. 3rd Symp. Taguchi Meth., pp29-52, Am. Supp. Inst., Romulus, Michigan, 1985.
12. Whitehouse, N., and Way, R., "Rate of Heat Release in Diesel Engines and its Correlation with Fuel Injection Data," Proc. Inst. Mech. Engrs., vol. 184 Pt 3J, pp 17-27, 1969-70.
13. Woschni, G., "A Universally Applicable Equation for the Instantaneous Heat Transfer Coefficient in the Internal Combustion Engine," SAE Paper 670931, 1967.
14. Bailey, M., Comparative Evaluation of Three Alternative Power Cycles for Waste Heat Recovery from the Exhaust of Adiabatic Diesel Engines, NASA Pub. DoE/NASA/50194-43, 1985.

15. Petersen, D., "Life Cycle Cost Assessment of Future Low Heat Rejection Engines," SAE Paper 860444, 1986.
16. Mahle GMBH, Private Communications, unpublished material, 1985.

Table II.1-1: Basic Parameters and Their Levels - Preliminary Study

<u>PARAMETER</u>	<u>LEVEL 1</u>	<u>LEVEL 2</u>	<u>LEVEL 3</u>
COMPRESSION RATIO	14	16	18
COMPRESSOR PRESSURE RATIO	2.4	2.7	3.0
BOI ($^{\circ}$ BTDC)	12	16	20
STROKE (mm)	125	135	145
TURBOCOMPOUND PRESSURE RATIO	1.0	1.5	2.0
AVERAGE INSULATION ($\frac{1}{2}$ BASELINE COOLED)	34	41	48

Table II.1-2: Pertinent Engine Simulation Data

1. 6 CYLINDER, FOUR-STROKE RECIPROCATOR
2. 1800 r/min RATED OPERATING SPEED
3. 130 mm CYLINDER BORE
4. 223.7 kW TOTAL SYSTEM BRAKE POWER
5. 422°K AVERAGE CYLINDER BORE TEMPERATURE
6. 28 DEGREES (APPROX.) FUEL INJECTION DURATION
7. 115° ATDC EXHAUST VALVE OPENING
8. 392° ATDC EXHAUST VALVE CLOSING
9. 324° ATDC INTAKE VALVE OPENING
10. 587° ATDC INTAKE VALVE CLOSING
11. 311°K INLET CHARGE AIR TEMPERATURE
12. 80% TOTAL ADIABATIC COMPRESSOR EFFICIENCY
13. 80% TOTAL ADIA. TURBOCHARGER TURBINE EFFICIENCY
14. 85% TOTAL ADIA. TURBOCOMPOUND TURBINE EFFICIENCY
15. 93% MECH. TURBOCOMPOUND GEAR DRIVE EFFICIENCY
16. 95% EXHAUST MANIFOLD INSULATION EFFECTIVENESS
17. 1.7 kPa INLET RESTRICTION
18. 8.4 kPa INLET MANIFOLD AND AIR/AIR
AFTERCOOLER PRESSURE DROP
19. 16.9 kPa EXHAUST RESTRICTION (TO
ACCOMMODATE A BOTTOMING SYSTEM)

Table II.1-3: Emissions and Structural (Thermomechanical) Loading Constraints

<u>PARAMETER LEVEL</u>	<u>EMISSION</u>	<u>EFFECT ON LOADING</u>
MAXIMUM PEAK FIRING TEMPERATURE	NO _x	THERMAL
ADIABATIC FLAME TEMPERATURE	NO _x	
MAXIMUM WALL SURFACE TEMPERATURE	NO _x	THERMAL
MAXIMUM PEAK FIRING PRESSURE		MECHANICAL
MAXIMUM BMEP		MECHANICAL
MINIMUM A/F	SMOKE	

Table II.1-4: Parametric Combinations for Best Fuel Economy at Various Peak Pressures, A/F and Strokes

<u>PEAK FIRING PRESSURE (MPa)</u>	<u>A/F = 30</u>	<u>COMPRESSOR PRESSURE RATIO</u>	<u>COMPRESSION RATIO</u>
	<u>STROKE = 125 mm</u>		
13.8		2.60	16.15
15.2		2.60	17.35
16.5		2.60	18.54
	<u>STROKE = 135 mm</u>		
13.8		2.46	16.66
15.2		2.46	17.85
16.5		2.46	19.05
	<u>STROKE = 145 mm</u>		
13.8		2.33	17.15
15.2		2.33	18.35
16.5		2.33	19.54
	<u>A/F = 32</u>		
	<u>STROKE = 125 mm</u>		
13.8		2.76	15.52
15.2		2.76	16.72
16.5		2.76	17.94
	<u>STROKE = 135 mm</u>		
13.8		2.62	16.07
15.2		2.62	17.26
16.5		2.62	18.46
	<u>STROKE = 145 mm</u>		
13.8		2.49	16.57
15.2		2.49	17.76
16.5		2.49	18.95
TURBOCOMPOUND TURBINE PRESSURE RATIO = 1.5			
CONDUCTION RESISTANCE: LEVEL 3 (INSULATION LEVEL OF APPROX. 48%)			
BOI = 12° BTDC			

Table II.1-5: Statistically Predicted Versus Directly Calculated Values of Selected Variables

VARIABLE	STATISTICAL VALUE	COMPUTER SIMULATION
BSFC (g/kW.h)	175.2 ± 1.642	175.2
PEAK FIRING PRESSURE (MPa)	15.17 ± .352	15.37
BMEP (kPa)	1351 ± 6.89	1351
AIR/FUEL RATIO	30 ± 0.2	30.5
PEAK FIRING TEMPERATURE (°K)	1732 ± 18.7	1748
PISTON TEMP. (°K)	910 ± 7.4	941
HEAD TEMP. (°K)	1005 ± 6.8	1012
LINER TEMP. (°K)	426 ± .56	426
HEAT TRANSFER (%FUEL)	6.86 ± 0.2	6.63

Table II.1-6: Parameters and Levels - Detailed Study

<u>PARAMETER</u>	<u>LEVEL 1</u>	<u>LEVEL 2</u>	<u>LEVEL 3</u>
COMPRESSION RATIO	17	18	19
COMPRESSOR PRESSURE RATIO	2.0	2.6	3.2
BEGINNING OF INJECTION ($^{\circ}$ BTDC)	10	14	18
BORE (mm)	110	120	130
STROKE (mm)	115	125	135
TURBOCOMPOUND PRESSURE RATIO	1.0	1.7	2.4
BOTTOMING CYCLE EFF. ($\frac{1}{2}$ CARNOT)	0	14	28
INSUL. LEVEL (PISTON & CYL. HEAD) [*]	1	2	3
INSULATION LEVEL (LINER) [*]	1	2	3
INTAKE LOBE RETARD ($^{\circ}$ CA)	0	10	20
FRICTION MODEL [*]	1	2	3
ENGINE SPEED (r/min)	1600	1800	2000

^{*} See Text for Explanation of Respective Insulation and Friction Levels

Figure II.1-1: Schematic of the LHRE-EERS System Simulation

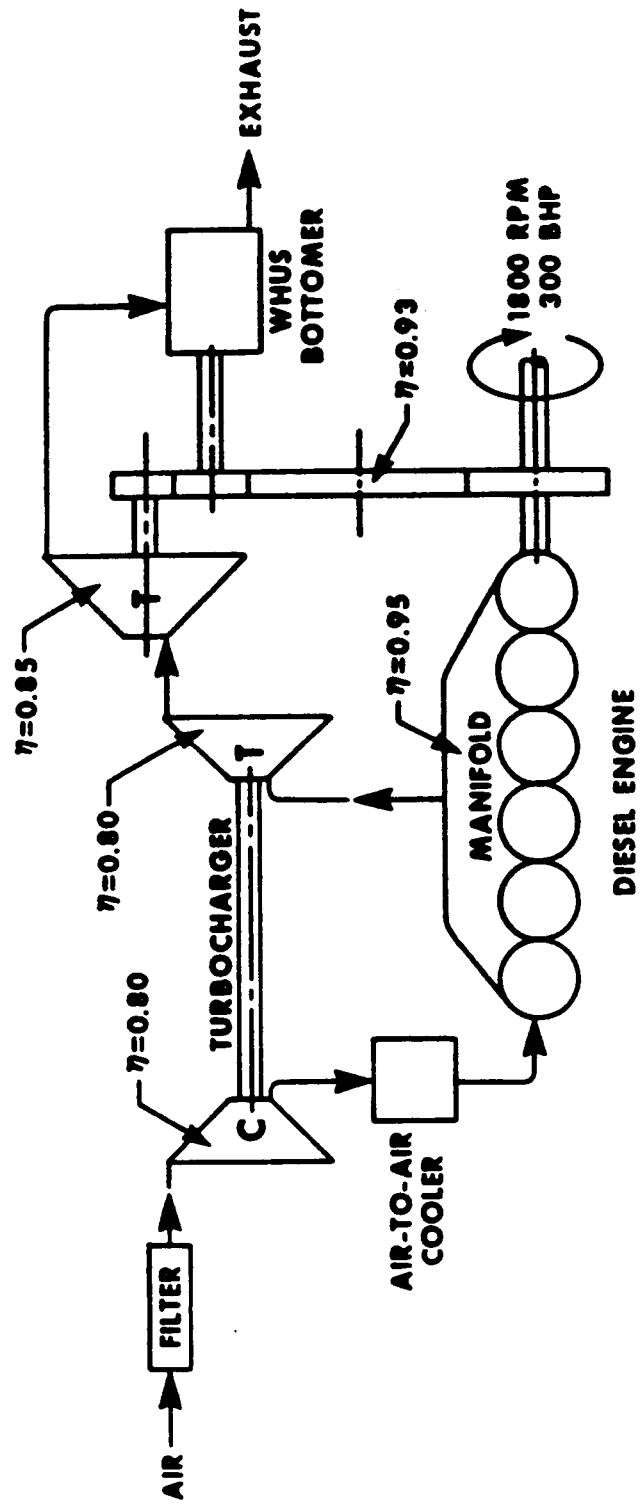


Figure II.1-2: Significant Parameters Affecting the Fuel Economy and Their Percentage Contribution Preliminary Study

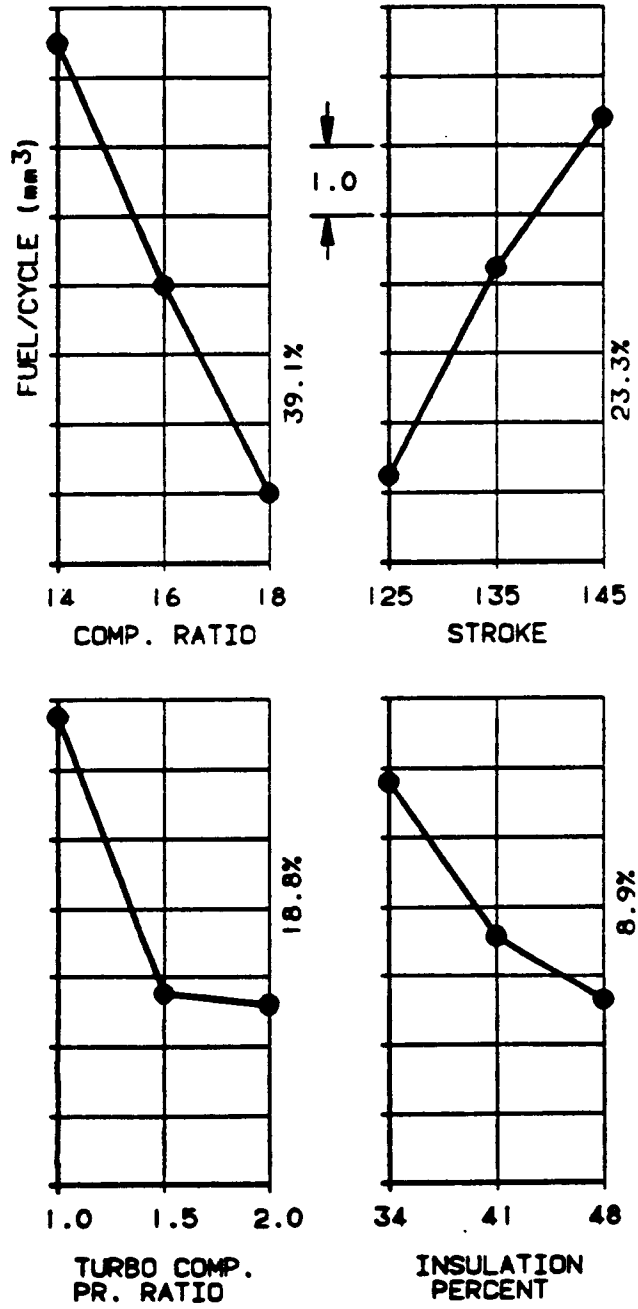


Figure II.1-3: Significant Parameters Affecting Peak Firing Pressure and Their Percentage Contribution- Preliminary Study

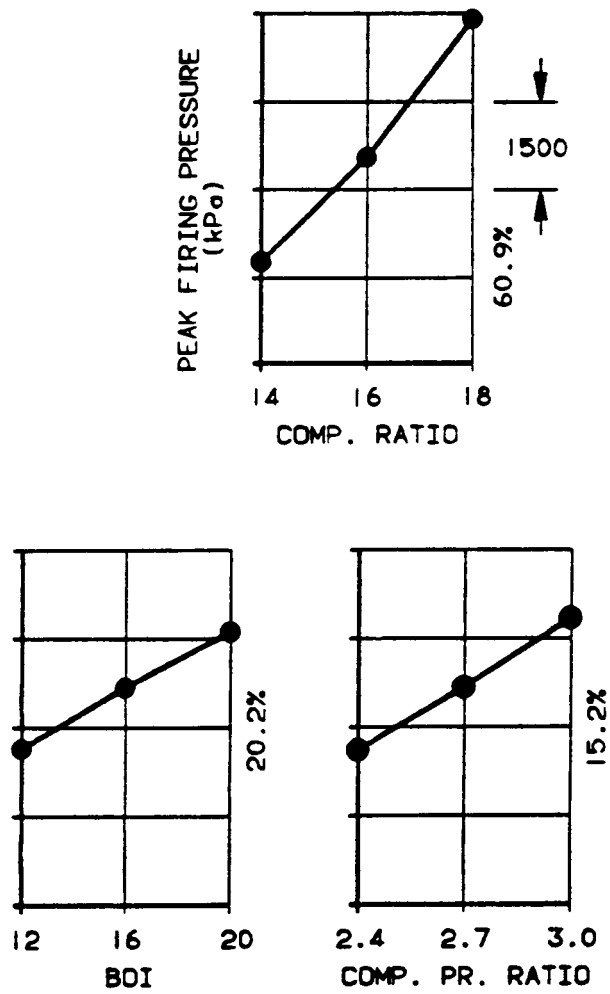


Figure II.1-4: Significant Parameters Affecting A/F and Their Percentage Contribution Preliminary Study

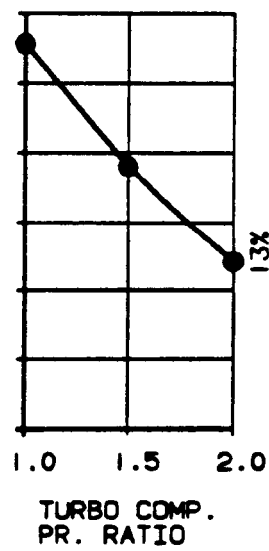
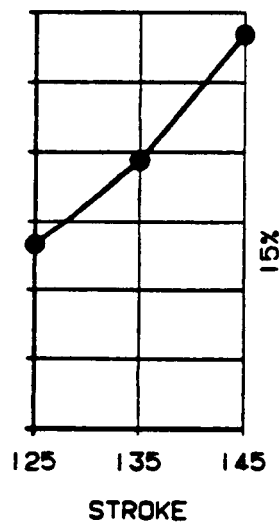
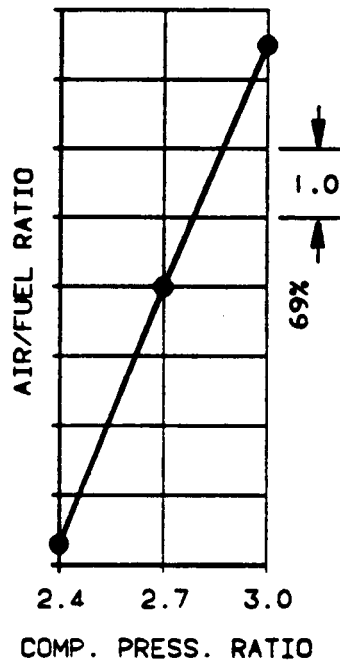


Figure II.1-5: Significant Parameters Affecting BMEP and Their Percentage Contribution-Preliminary Study

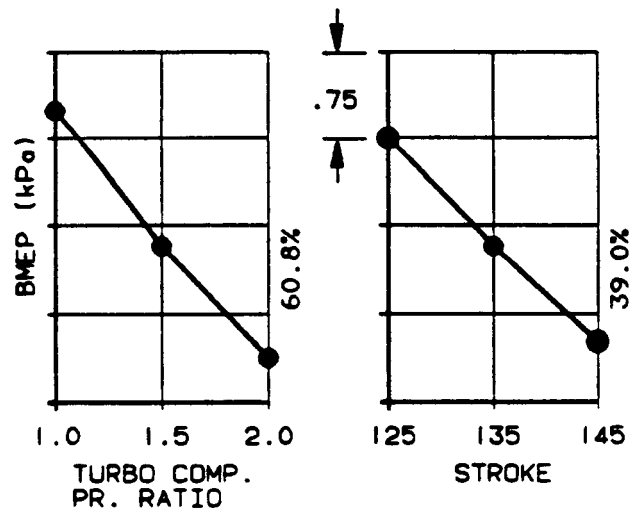


Figure II.1-6: Best Fuel Economy Predictions-Preliminary Study

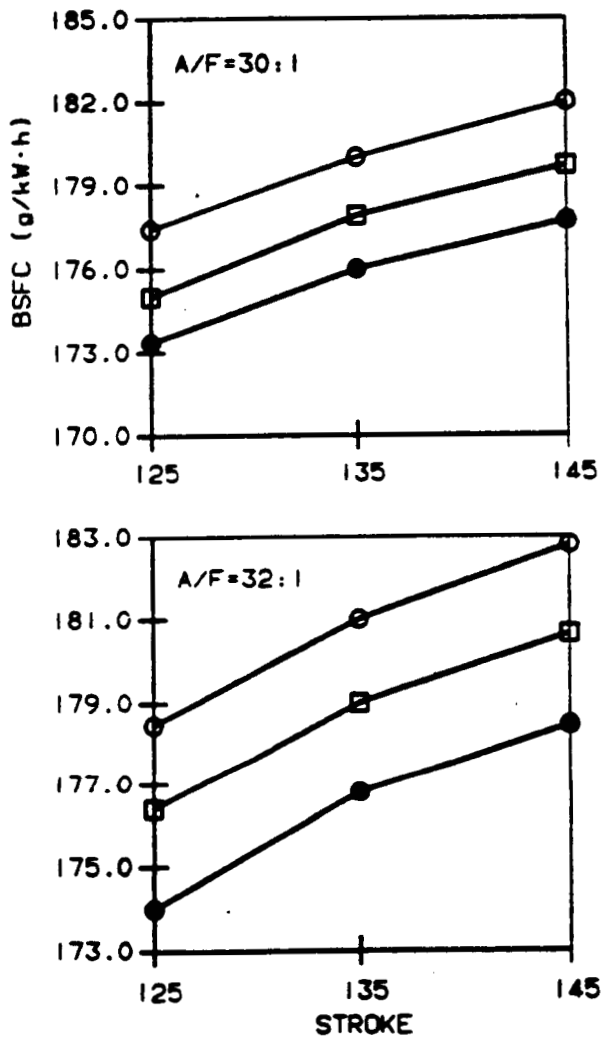


Figure II.1-7: Significant Parameters Affecting the Fuel Economy and Their Percentage Contribution-Detailed Study

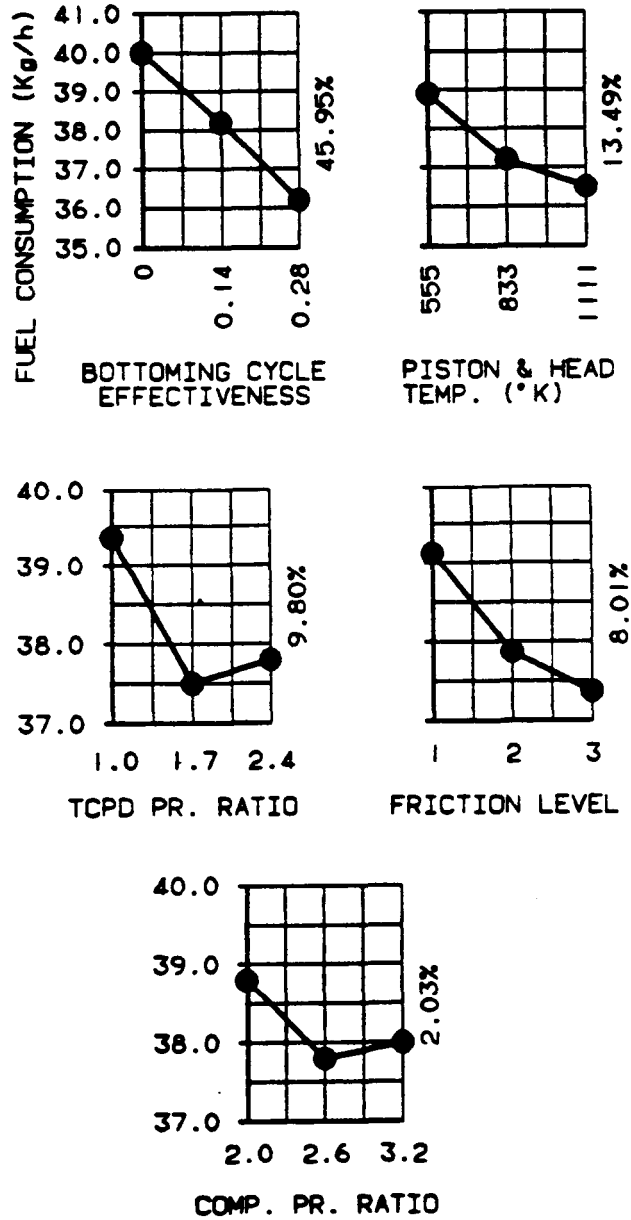


Figure II.1-8: Effect of Liner Insulation on Volumetric Efficiency and Fuel Economy.

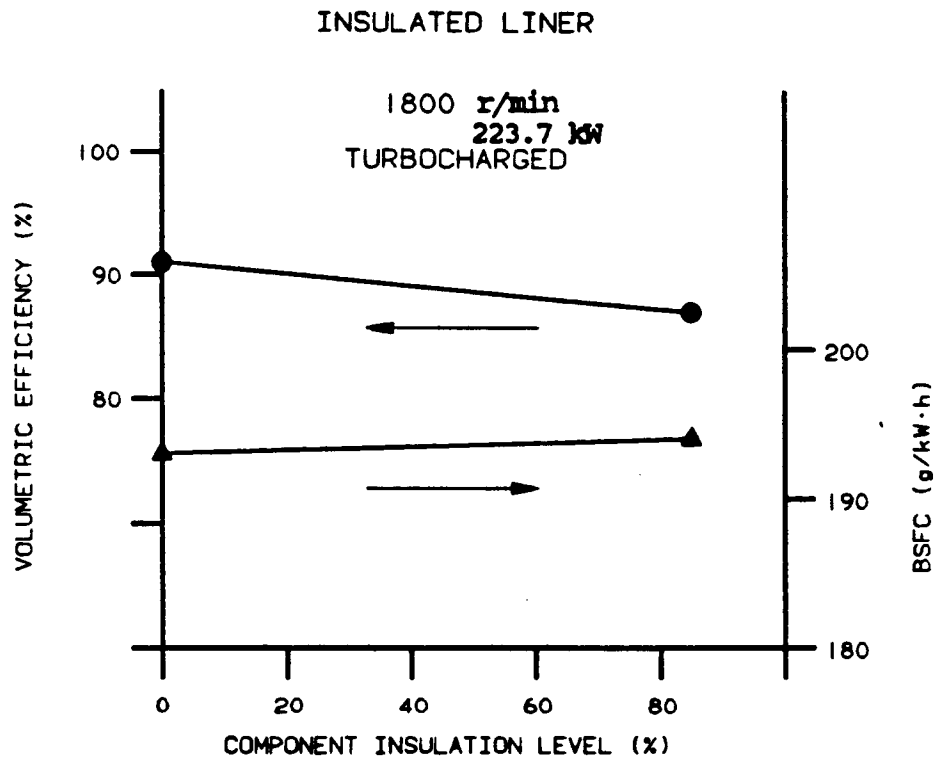


Figure II.1-9: Significant Parameters Affecting A/F and Their Percentage Contribution-Detailed Study

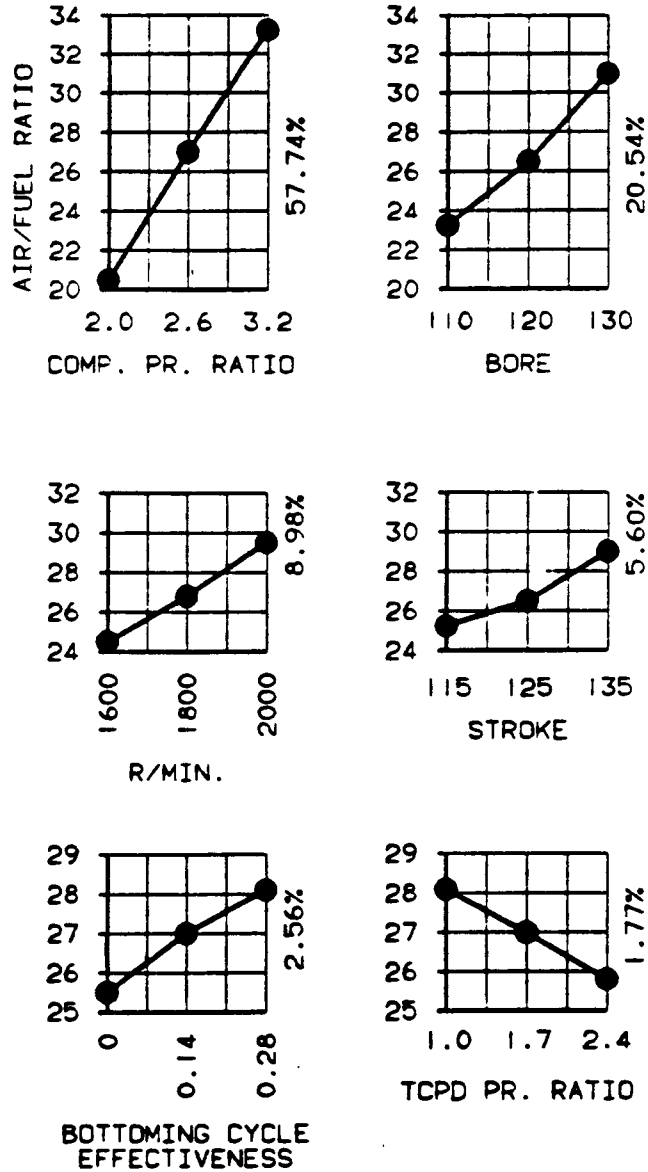


Figure II.1-10: Significant Parameters Affecting Peak Firing Pressure and Their Percentage Contribution- Detailed Study

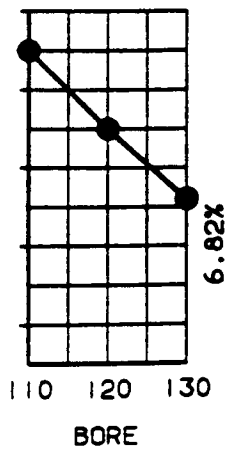
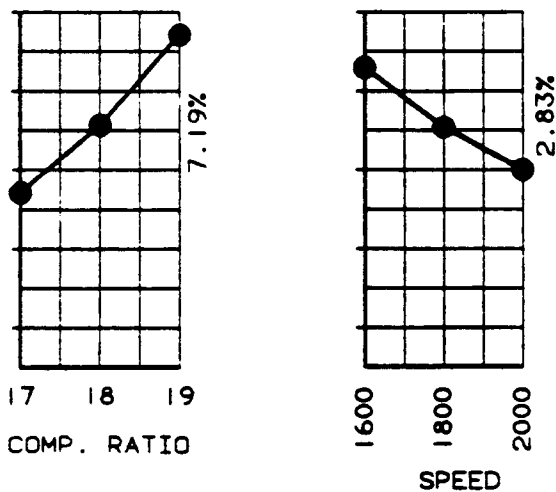
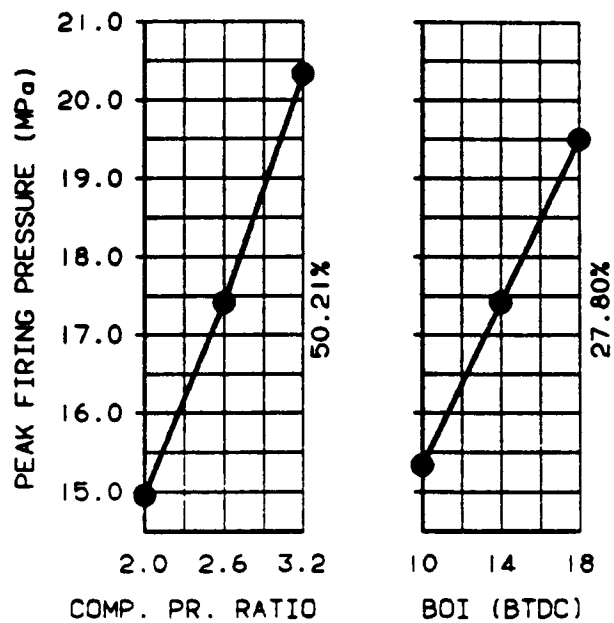


Figure II.1-11: Significant Parameters Affecting BMEP and Their Percentage Contribution-Detailed Study

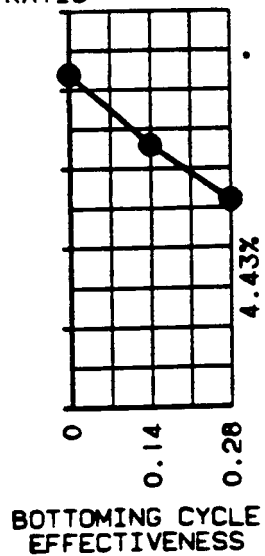
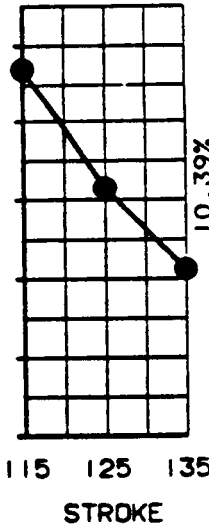
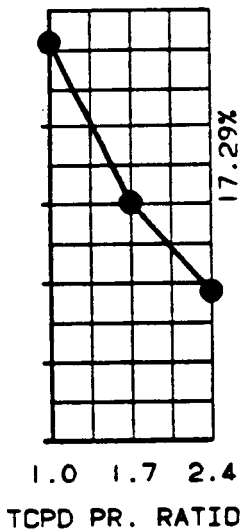
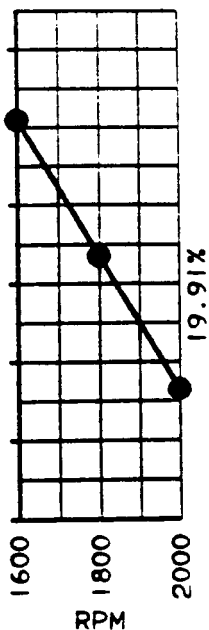
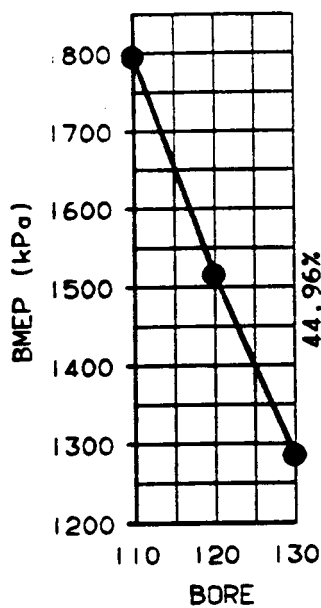


Figure II.1-12: Best Fuel Economy Predictions for Various LHRE-EER Systems at Different Insulation Levels, and at Baseline Friction

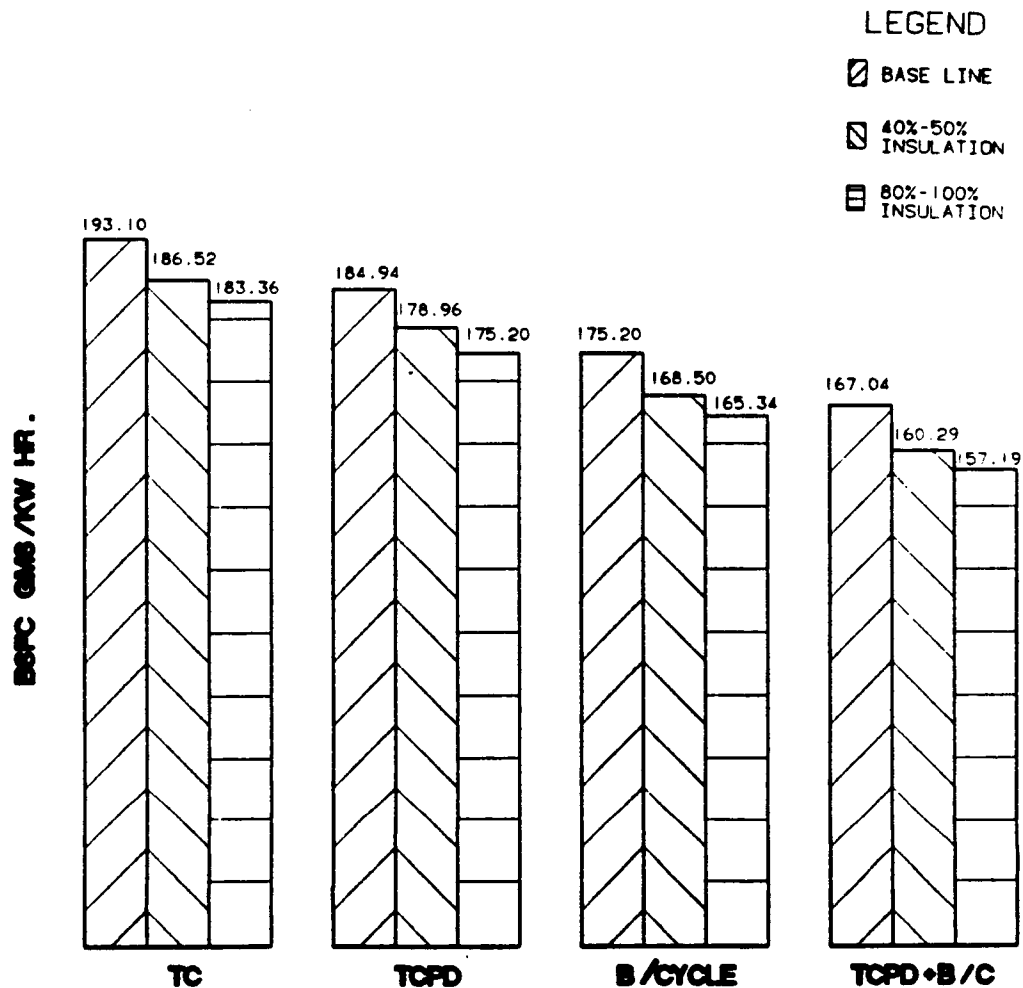
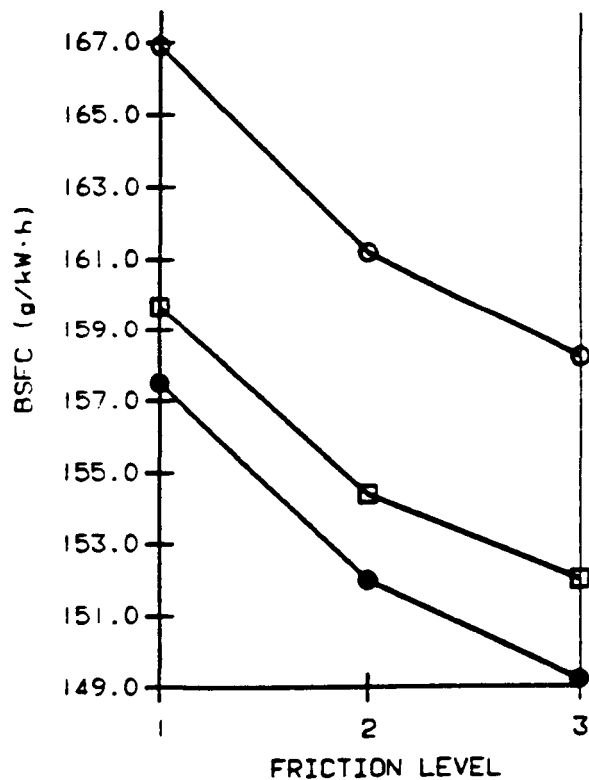


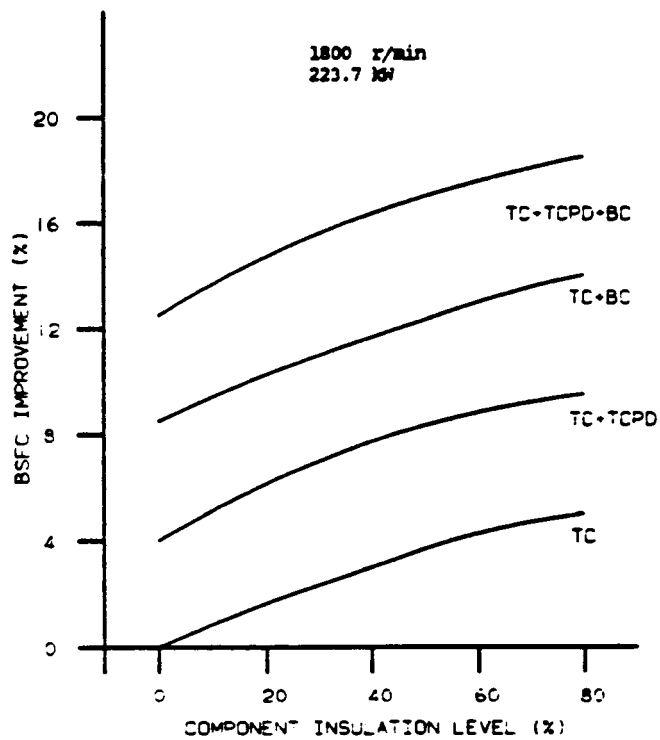
Figure II.1-13: Best Fuel Economy at Various Friction and Insulation Levels - LHRE with Turbocompounding and Bottoming System



- = INSULATION LEVEL 1 (BASELINE)
- = INSULATION LEVEL 2
- = INSULATION LEVEL 3

- 223.7 kW SYSTEM OUTPUT
- LHRE WITH TURBOCOMPOUNDING AND BOTTOMING SYSTEM

Figure II.1-14: Percent Gain in Fuel Economy as a Function of Degree of Insulation and Exhaust Energy Recovery Scenarios



II.2 CANDIDATE DESIGN CONFIGURATIONS

The mechanical design activity was divided into two major phases; component conceptual studies and engine integration with the most viable component designs. The full potential of the ADRE could better be realized through a complete engine redesign approach. Figure II.2 - 1 is a schematic representation of the adopted mechanical design evaluation procedure. First, component conceptual studies were undertaken. This was followed by integrating the successful component concepts into candidate engine configurations. In addition to insulation of the engine, design features resulting from the removal of the coolant system were evaluated. Reduced friction component scenarios were also investigated. The specific tribological environment of the ADRE required special concept evaluation.

Qualitative analysis of many different component concepts was accomplished by evaluation of the components with respect to fuel economy, design synergy, technical risk, initial cost, serviceability, manufacturability, material requirements, and weight. These concepts were then ranked in order of their perceived risk, cost, and potential impact on fuel economy. The averaged risk responses for various concepts were then divided into three levels ranging from moderate to high risk, for proof of concept technology demonstration by 1995. An engine configuration was deemed to have a risk level equal to that of its highest risk component.

After generation of several comparable risk engine configurations, ADRE cross sectional layout integration was undertaken. At this stage, certain groupings were found to be less advantageous and, hence, were eliminated. The final result of the design evaluation process was the development of six viable ADRE reciprocators, two in each risk level.

II.2.1 LOW HEAT REJECTION CONCEPTS

Based on experience and survey of the state-of-the-art, the methods of insulating the engine components were classified into air gaps, thermal barrier coatings and monolithic ceramics. A general assessment for each of these methods is given in Table II.2-1, and a classification by the risk level of these generic insulation strategies follows in the next section. Note that the air gap is a conceptual insulation treatment that, if used with metallic components, does not necessarily require new material developments. The other two insulation methods in the Table rely on new developments of low thermal conductivity materials. Ceramic composites is a new but rapidly developing technology that can very well influence the selection of the most viable insulation method for the year 1995 and beyond.

In-cylinder components exposed to high temperature and high pressure environments are the most critical LHR components. These include the cylinder kit and the cylinder head components. The conventional cylinder kit is composed of a piston, cylinder liner, and piston rings. A cylinder head concept can be viewed as a system composed of firedeck, valves, and other components affected by the severe LHR environment. Out-of-cylinder components include the ports, exhaust manifold and exhaust tubing. Basic insulation methodologies of various components are briefly reviewed, after the generic insulation classification by risk level is provided.

INSULATION CLASSIFICATION

Moderate Risk Concepts - Taking the coolant out of an engine is the single most effective measure to reduce heat loss from the working fluid to the combustion chamber walls. A simple steady state heat transfer model would predict that the insulation effectiveness can be as high as 93 percent. However, if the engine is still lubricated using a conventional lubrication system, the heat will be conducted to the lubricant. The practical overall

heat rejection level in this case would be approximately 45 percent. The resulting temperature distribution within the engine structure will be uneven, generating localized thermal stress of significant magnitudes.

A step further is the use of a thin thermal barrier coating. This coating sprayed on the firedeck, for example, can slightly lower the entire surface temperature level of the metal. Without water cooling, the firedeck metal surface temperature can be lowered by 30°C with 1 mm of ZrO₂ coating. This extra protection can be justified even though the temperature drop is only a small percent of the overall 700 to 800°C surface temperature. As for the piston, a .5 mm thin coating can be applied to a conventional piston, providing up to 15 percent insulation.

An uncooled cylinder liner can have a negative effect on the fuel economy, as explained earlier. In addition, higher temperature tribological issues remain to be a challenge. For the moderate risk level, an oil cooled liner was proposed. This would keep the top ring reversal at a temperature level below 350°C.

To accommodate the higher temperature at this insulation level, exhaust valve material would be upgraded to higher temperature alloys. It was suggested that both intake and exhaust ports be shielded. Valve seat inserts made of low thermal conductivity material would be used for the uncooled metal cylinder head. Valve guides can conceivably be made of ceramic for tribological reasons.

Intermediate Risk Concepts - The main path insulation in this risk category was via metal air gap insulating structural members. A piston design of this type can have an insulation level in the range of 50 percent. An air gap firedeck was recommended for the head concept, with possible insulation level in the range of 65 percent.

The cylinder liner would still be oil cooled and have a wear resistant coating. A ceramic valve or a ceramic valve head was recommended. The remaining hot section-related components, such as shields, guides, and manifold, are the same as the moderate risk package.

High Risk Concepts - Ceramics would be extensively used for the high risk configuration. A piston's ceramic cap could be attached on a base metal body. The insulation level can reach up to 70 percent, without oil cooling. An individual ceramic firedeck possesses the highest insulation level. Sealing and compliant joining techniques require further development. Other components essentially remain the same as the moderate risk package, with ceramics replacing metals in the higher temperature application areas.

INSULATED COMPONENT CONCEPTS

Piston Concepts - The cylinder kit components experience severe reversed reciprocating acceleration, as well as full gas pressure and thermal loading. They are required to slide relative to one another, with minimal friction and wear, while transmitting all of the developed power of the engine. A large portion of total in-cylinder heat transfer is through the piston because of the large heat transfer area and the high gas velocity near the piston surface.

Some design considerations for the piston are summarized in Table II.2-2. Factors such as these define several basic requirements for survival in such a critical component. These include being able to withstand high temperatures, having sufficient mechanical strength, and being tribologically compatible. Basic requirements of functional survival and the conditions of LHR operation help define the scope of design and material options. A more detailed definition of these constraints will be pursued in later phases of the program.

LHR piston development work to date has resulted in a wide variety of piston concepts. They can be categorized according to material combinations and design form. For instance, material candidates include: high temperature metal alloys, ceramic coated metals, monolithic ceramics, and composites. Perhaps more numerous than the candidate materials are the highly varied design forms. These range from trunk style to crosshead designs, with and without conventional type piston rings. A number of LHR piston concepts, tabulated in Table II.2-3, were considered for this review. Note that these concepts are typical applications of the three insulation methods mentioned earlier.

Trunk style aluminum pistons predominate the high speed, four-cycle diesel market. Numerous insulative treatments have been applied to them as reported in literature [1-5]. The application of thin ceramic coatings or cast-in-place sheet metal shields to the piston crown represent a rather straight-forward method.

A more aggressive concept is through composite construction. Here, the top of the piston is replaced by either a monolithic ceramic or metallic piece. An example of a DDA 6.2L composite piston utilizing a shrink fit cap is shown in Figure II.2-2. A view of a typical DDA crosshead piston is illustrated in Figure II.2-3. This design has demonstrated its merits in 4-stroke and 2-stroke production engines and is versatile relative to insulative treatments. One of the simplest insulative concepts is to change the base malleable iron dome material to one with improved mechanical properties and lower thermal conductivity at elevated temperatures. The addition of a .5 to 1.0 mm zirconia coating over the top of the piston profile can further help reduce metal temperatures and, to a limited extent, heat transfer through the dome. However, in order for thermal barrier coatings to be a viable insulation method, thicker, more reliable coatings are required. Under a DOE/NASA contract, General Motor's Allison Gas Turbine Division, in cooperation with Detroit Diesel, has undertaken an investigation on hollow particle, enhanced capability, thick coating systems [6]. This type of coating was

applied at thicknesses of 1.5 to 2.5 mm to the piston crown, as shown in Figure II.2-4, and has demonstrated its viability in limited DDA Series 60 single cylinder engine test runs. A more aggressive concept is the incorporation of an insulative air gap cavity. This design is shown in Figure II.2-5 and includes various material options for the piston cap.

A still higher risk proposal, that has been conceptually sketched, is the ringless piston concept shown in Figure II.2-6. This concept avoids some of the tribological concerns of other piston designs that depend on positive ring/liner/piston gas sealing under extreme environments. Simplified leakage and performance loss analyses, performed for a two-cycle version of the ringless piston concept, are shown in Figure II.2-7. For conceivable clearances up to .013 mm, the power loss due to leakage over a more conventional ringed piston could be held below five percent. Mechanical friction reduction features can possibly be designed into the ringless approach, which would offset power loss due to leakage. A few of the perceived salient features of this design approach have been outlined in Table II.2-4. Although some effort has been expended on the gas lubricated piston/ring concept, it is judged that this design is at a rather early stage of concept feasibility.

Prior to performing analysis and final concept selection, the number of candidates were to be narrowed, based upon past experience and the expectations for this program. Preliminary piston concepts selected include the following three designs, with variations in material treatments.

A candidate concept would likely be an all metal configuration, similar in form to that shown in Figure II.2-5. A Perlitic malleable iron body can be used to contain a D5-B Ni-Resist piston cap. A gap of 1.3 to 1.5 mm, formed between these two pieces, performs the majority of the insulating function. The thermal effectiveness of this approach, i.e., reduction in heat transfer relative to a baseline uninsulated piston, can reach 65

percent. Tribological concerns at the ring-to-liner interface in an uncooled engine still remain a challenge, especially for the top ring position.

A second candidate piston design concept is identical to the one just described, except that the finished piston receives a thin .5 to 1.0 mm ceramic coating. The intention here is to reduce metal temperatures and heat transfer through the piston. The concern introduced with this design is the long-term integrity of the ceramic coating. Spalling and inter-layer flaking of the plasma sprayed coatings have been observed. The problem of inconsistent coating durability is being addressed by many investigators. New materials and processing techniques have been introduced which have improved upon this problem to some extent. Continued development and improvements in this area promise to further enhance the long-term durability of the ceramic coatings by 1995.

A third, and perhaps a high technical risk concept suggested for this work, is the use of a monolithic ceramic piston bowl in an otherwise metallic air gap crosshead piston. Silicon nitride and partially stabilized zirconia have previously been investigated at DDA, using finite element and probability of survival analyses. Analytical results have been favorable, and limited experimental results have been encouraging. New 1995 type material developments can enhance the advantages of this design.

Liner Concepts - Any liner concept for the LHR engine must take into consideration certain key factors. These have been categorized in Table II.2-5. In the case of the liner, tribological concerns were handled preferentially to insulative treatments. Wear and friction of the ring/liner interface and its control are primary concerns in providing acceptable engine life. Although the ringless piston approach previously mentioned circumvents this problem, it was considered beyond the scope of the current phase of the program.

The generic material treatments for liner tribology optimization are outlined in Table II.2-6. To date, limited success in tests at DDA and outside has been mostly with thin, sol-gel applied ceramic coatings [7,8]. These ceramics have mainly been chromia and/or a combination of silica-chromia-alumina. Plasma sprayed zirconia coatings have also been tested, with and without sol-gel densification. Mechanically impregnated liners with various wear resistant coatings, and both monolithic and composite PSZ liners have been in various early phases of studies and developments. These concepts may provide more effective insulation than the thinner coatings, while at the same time address the tribological concerns under LHR engine conditions. It is noted that the concurrent performance assessment proved, later on, that liner insulation is not recommended. Another liner concept under consideration is one with the inclusion of ablative surface treatments. A solid lubricant, such as graphite, could be used to replenish the ring liner interface with a protective coating. Details of this concept must be resolved. Some of these liner concepts are being pursued by other organizations. Treatments of the liner outer surface for possible selective cooling was also considered.

Ring Concepts - As with the liner, wear and friction under the environmental extremes of the ADE operation are primary concerns for the piston rings. Ring concepts available for this program include ceramic coated and monolithic ceramic rings.

Uncooled engine development programs at DDA and elsewhere have considered hard moly, chrome carbide, alumina-titania, and chromia among other ring coatings. The concurrent ongoing coating deposition and base ring material work at TRW was also considered. A coating, applied to an appropriate high temperature metallic substrate, provides an option of ring concepts from which suitable candidates could be selected.

One more aggressive option is the monolithic ceramic piston ring. Partially stabilized zirconia I-shaped head land rings were

successfully run in limited Series 60 single cylinder engine tests. Alternate materials and forms include silicon nitride and conventional rectangular cross-sections. This approach avoids some of the problems of fully metallic or coated metallic rings, but the concept is not considered proven yet.

Cylinder Head Concepts - The cylinder head is treated as a system comprising the firedeck, valve, valve seat insert, valve guide, supporting structure, and ports for exhaust and intake.

Firedeck Concepts - The firedeck is the portion of the cylinder head that is exposed directly to the combustion gases. Most of the concepts addressed treated the firedeck as a separate piece. The firedeck appears in the literature with other names such as the head face plate, hot plate, and deck plate.

A conventional gray cast iron cylinder head can survive without water cooling under lighter engine fueling rates, if the local compressive yielding can be avoided. Several methods to combat the local excessive stress have been used in today's engines, such as individual heads for each cylinder, stress relief cut outs, or lateral saw slots between neighboring cylinders. However, to operate the engine without cooling requires not only material upgrade, but also major redesign.

Zirconia plasma coating has been a popular method to provide firedeck insulation. However, similar to the piston case, relatively thick coating is required to effect meaningful lower heat transfer. It has been proposed, however, to use thin coating, .7 mm, as a method for metal protection in light-duty passenger car diesel engines [5]. The method used in [6] consisted of a sintered wire mesh strain isolator that was brazed on the firedeck and then sprayed with zirconia. Although at short engine hours the system worked satisfactorily, long term durability still requires substantial development.

A firedeck made of a high temperature alloy has been fabricated and tested at DDA, primarily as an intermediate step leading to a ceramic firedeck development. With an air gap behind the plate, this design reduced the heat loss through the cylinder head by more than 50 percent. A ceramic firedeck requires additional design considerations in order to enhance the probability of survival. The retaining ring design, shown in Figure II.2-8, has been successfully used in single cylinder Series 60 engine tests. This not only holds the assembly in place, but also puts the plate in pre-compression, resulting in reduction of the operating tensile stress level. The interference fit can be tailored to provide an initial moment to counteract the thermal expansion resulting from axial temperature gradient during engine operation. The gas load is transferred from the firedeck to the retaining ring, and then via a zirconia support ring to the metal support structure. The support ring also creates an air gap for insulation purpose. A concern, common to all separate deck designs, is the sealing at the injector tip. Because of the use of a retaining ring, the center distance between neighboring cylinders will have to be increased. This can render this design unsuitable for a multi-cylinder engine.

A variation of the preceding design is shown in Figure II.2-9. Here, a ceramic firedeck is shrunk directly into a counterbore on the cylinder head. The air gap is a recess into the cylinder head casting, leaving bosses around the valve and injector holes as load transfer media. A special gasket is designed to seal the air gap. The majority of the gas load is transferred through the outer edge of the plate. This design allows the use of a conventional cylinder head with minimum changes, and the port shields can be inserted or cast into the head structure.

A pot head concept is shown in Figure II.2-10. An individual head is used for each cylinder. The ceramic firedeck is press fit or shrink fit into the pot head, which is bolted to the cylinder block. The transfer of the gas load is mainly through the outer edge. The bolt load transfer is also through the outer edge, to

the liner top, and then via liner flange to the block. Eventually, the inner pot shown here as a separate piece has to be integrated with the remainder of the engine structure.

A modification of the preceding design extends the outer edge of the firedeck downward to include the upper portion of the cylinder liner. This provides additional insulation of the upper liner, above top ring reversal. The merits of this variation will likely depend on the cost/benefit trade-off.

In general, an individual ceramic firedeck shrunk fit into a slab head is considered technically feasible. The individual pot head approach, if proven to have enough merits, can be examined as a long term concept.

Valve Concepts - Based on prior experience, Inconel 751 and Waspaloy can be considered for the uncooled cylinder head valve, with reasonable durability. The material limiting temperatures are 820°C (1500°F) and 870°C (1600°F), respectively. These temperatures are slightly above the preliminary projected exhaust valve temperatures for the ADRE. For heat transfer reduction, the three generic insulation treatments (air gap, thermal barrier coating and ceramics of lower conductivity) can be applied to the valve.

Thermal barrier coating on the exhaust valve head, face, and/or fillet area is the most widely used method to reduce the heat into the valve, or to lower the metal temperature [10,11]. However, significant benefits cannot be substantiated because of the already high heat flow resistance at the back face of the valve. In addition, from the durability standpoint, coating thickness is limited in order to maintain good adherence. Thus, the coating approach on the valve face has limited potential in blocking the heat into the combustion chamber. It can be considered a near-term measure to lower the metal temperature and, possibly, for tribological reasons. Coating can also be applied at the intake valve fillet location as a measure to improve the volumetric efficiency and emissions.

A case of using air gap as valve insulation is reported in [12]. As shown in Figure II.2-11, shields are welded onto the valve head and fillet to form air gaps. Theoretical analysis and actual measurements confirmed the insulation effectiveness of this concept. However, the long term durability is questionable since the weld may not withstand the thermal and mechanical loadings for a long period of time.

Using a partially stabilized zirconia disk that is brazed on the valve head has been reported [11]. This design failed at early engine test hours.

Monolithic valves made of partially stabilized zirconia and sialon have been tried in diesel engines [13]. Reported problem areas include the seat, fillet, and keeper groove locations. The failure at the seat is attributed mainly to the contact stress at impact and to the uneven seating. Fillet failure is tensile in nature, due to the bending loads induced by uneven seating. The highly concentrated contact stress, together with geometric and contact discontinuities at the upper keeper groove, cause early valve failure. A valve manufacturer has reportedly accumulated long test hours on a silicon nitride valve. Therefore, a monolithic valve is considered a viable approach for the uncooled cylinder head.

To alleviate the critical keeper groove problem, several composite designs made of a metal upper end and ceramic valve head have been conceived, as shown in Figure II.2-12. The brazed joint can be near the valve groove or near the valve head.

It was recommended that the intake and exhaust valve heads have a large radius of curvature at the fillets, to increase the strength and reduce gas flow losses. If the valve stem is made of metal, it should have some form of wear protection. Possible candidate materials and coatings include tungsten carbide, titanium nitride, titanium diboride, chromium carbide and chromium oxide.

For further assessment, the following concepts were recommended, by the risk level:

Moderate	Sil 10, .5 mm zirconia coating at fillet, wear coating at stem	Waspaloy, .75 mm zirconia coating at head face, wear coating at stem
Intermediate	Same as above	Composite, metal tip and PSZ head
High	Monolithic ceramic	Monolithic ceramic

Valve Seat Inserts - The valve seat is an essential heat transfer path in a water cooled engine, keeping the valves at an acceptable temperature level. In a DDA waterless engine program, a temperature drop of 10 to 15°C (18 to 27°F) was detected on the cylinder head, near the valve seat. If a conventional iron cylinder head is adopted for the reference engine, it is recommended that the seat be made of zirconia and pressed into the head. Alternatively, a ceramic firedeck will have the valve seat as an integral part.

Valve Guide Concepts - Tribological concerns should be treated preferentially to insulation for the valve guide. Conventional metal guides have been found unsuitable for the waterless engine. Wear rate is excessive due to poor lubrication and the increased eccentricity caused by uneven thermal expansion between interacting components. To combat this, concepts using different materials are pursued. Either a more forgiving elastic material or, conversely, a harder material concept can be proposed. An interference fitted zirconia valve guide, with proper valve/guide clearance and relief at the ends, is a viable choice of the latter option. If the engine is liquid lubricated, grooves normally machined on the inside diameter of conventional guides for oil retention purposes can conceivably be placed at the outside diameter of the valve stem. For such a concept, oil cooling may be needed to maintain a proper oil film and reduce wear.

To alleviate the eccentricity problem, a new design approach may be necessary. A floating valve guide concept was proposed, as shown in Figure II.2-13. This concept shows the spring seat and valve guide as an integral part, which is held down by the spring load. It would be externally cooled by an oil jacket if the engine is liquid lubricated. It can also be fuel cooled if the solid lubricated tribology concept is adopted for the reference engine. The floating valve guide concept may prove deficient in providing positive guidance to the valve motion.

A monolithic ceramic valve guide is recommended for the reference engine. It would be pressed or shrunk in place. Again, the use of ceramics for this component is for tribological reasons and not for insulation purposes.

Port Concepts - Substantial heat is lost through exhaust ports into the coolant in a conventional engine. Comparative tests conducted on 2-stroke and 4-stroke engines at the 300 BHP range indicated an increase of 35 to 50°C in turbine inlet temperature when an exhaust port shield was installed. Analysis also shows a volumetric efficiency loss of 2 to 4 percentage points occurring when the cylinder head is not water cooled. Further, the increase in inlet air temperature results in increased NO_x emissions. Therefore, insulation should be provided for both the exhaust and intake ports.

A port concept can be a porous metal wire mesh, cast directly into the cylinder head. At low thickness, the part rigidity is too low to sustain the casting loads. Thicker wire mesh is difficult to form and is costly. It was reported that the strength of the wire mesh port could be increased by dipping the port into ceramic slurry, sintering and then casting. The surface finish for minimum aerodynamic losses and insulation level of this port concept are questionable.

Ports made of low conductivity material, such as alumina titanate, may be cast into an iron head after wrapping with ceramic

felt or other compliant material. The purpose of the wrapping material is to cushion against thermal shock and to allow for differential shrink rates. Limited engine tests have proven that the design is viable. The concern is that the insulation level may not be sufficient unless a thick walled port is wrapped with relatively thick compliant insulation. This will likely result in a size that is too large to be accommodated within the space constraints of the reference engine.

DDA has had extensive experience with air gap insulation approach for the port shields. One such concept is a shield made of a stamping or investment casting and inserted into the cylinder head, as shown in Figures II.2-14 and -15. Laboratory engine tests showed that heat transfer was reduced by as much as 60 percent. This approach has the potential of gas leakage into the insulating air gap cavity. A cast-in-place shield concept would alleviate this problem and also enable the use of a more streamlined port shape. The challenge for the cast-in-place concept arises from coring the thin air gap behind the parts and the cleaning of the core sand after casting. A preformed air gap using double wall sheet metal is another viable concept which warrants further study. Applying a thermal barrier coating on the interior surface of a port is also a viable approach, but has limited insulation effectiveness.

For further assessment, the concepts were classified by the risk level. Moderate risk ports would be cast-in-place metal shield with air gap. Intermediate risk ports would be either cast-in-place double walled metal shield, or cast-in-place thick-walled ceramic shield. High risk ports would be cast-in-place ceramic shields with air gap.

INSULATION TECHNOLOGY ASSESSMENTS

Materials Forecast - This activity was undertaken to further enable the assessment of the likely technical and economical

feasibility for using advanced materials in the prescribed time frame for this program.

Economy - Cost projections for monolithic ceramic components were solicited using, as an example, a typical Detroit Diesel advanced ceramic piston cap design. Many advanced materials suppliers were unable to project the cost trends. However, Figure II.2-16 shows responses received from three domestic and foreign silicon nitride sources. The Figure shows that the projected cost range is several times higher than a current production piston assembly, but it is comparable to a cap made of high temperature metallic alloy. Cost reduction scenarios may further lower the projected ceramic component cost. The highly speculative nature of cost estimation for advanced materials is also apparent from the variations among different responses. It is also noticed that the general consensus is that structural ceramic components will be progressively less costly to produce in the future, as the industry matures and utilization increases.

Material Properties - The increase of toughness and the consistency of properties of manufactured ceramic components were identified as the primary goals to be realized by the year 1995. The limited data available from the survey indicated that the Weibull modulus can be increased to four times the current level in about five years time span. This would be achieved through advancements in the areas of powder preparation and manufacturing processes. The improvement in toughness will most likely be accomplished through the development of ceramic composite materials. One supplier's target is to raise the fracture toughness from the current range of $6 \text{ MPa}\cdot\text{m}^{1/2}$ to about $40 \text{ MPa}\cdot\text{m}^{1/2}$ in ten years. Note that, as a reference, the toughness of Inconel-751 is 75. The flexural strength is projected to gradually increase from about 800 MPa to 1200 MPa. With these targets, it is probably safe to assume that structural ceramic ADRE components can be a reality in the prescribed time frame.

Technical Risk and Cost - The insulation treatment screening process is graphically shown in Figure II.2-17. The risk and cost assessments are generally very challenging tasks. Undertaking these two tasks at the advanced concept stage, utilizing advanced materials and emerging technologies, is highly speculative in nature and adds more difficulty to the challenge. However, good qualitative assessments can be acquired by exploiting the available cumulative experience and expertise of workers in a specific discipline. Assessments for the LHR piston and head concepts are presented below. An evaluation update is recommended at a later phase as more relevant emerging technology and information become available.

Naturally, a higher insulation level leads to higher component surface temperatures. For a specific concept, increased surface temperatures generally result in lower reliability. On the other hand, technical risk denotes the degree of uncertainty with which a technology level can meet certain design requirements. Technical risk is closely associated with the level of development effort necessary to reach a development goal. Therefore, the technical risk involved in maintaining a constant reliability level for a specific concept increases with higher temperatures or insulation levels. The cost is taken as the manufacturing cost to have the component fabricated to a final usable form.

An assessment of the risk versus the insulation level for different piston insulation approaches is graphically depicted in Figure II.2-18. The curves in this figure are based upon Detroit Diesel experience with LHR pistons. Several design alternatives within the same general insulation treatment method had to be considered. The trends represented by these curves would still be valid for the ADRE piston case.

The risk potential of the thermal barrier coating concepts starts at no insulation, progressively becomes steeper, and has a limit at about 50 percent insulation. The metal air gap piston has relatively low risk at 30 percent insulation, which steeply curves

up at about 60 percent. This sharp increase in the risk level can be attributed to two reasons. First, the resulting higher surface temperature degrades the material strength. Secondly, the contact area in the heat transfer path has to be minimized to attain higher insulation, which compromises the load transfer capability of the component.

The relative cost versus insulation treatments of the piston concepts is shown in Figure II.2-19, based on a case study using Detroit Diesel's LHR crosshead state-of-the-art piston. The cost for a single piece ceramic piston has been estimated based on the overall mass and machining processes required for the final product. The curve for thermal barrier coating in Figure II.2-19 has a slight negative slope at the low insulation level, implying the possibility that a slight saving may be realized by using a lower grade of iron substrate. The TBC curve shows a steeper slope with increased insulation level, due to the increased processing time required to produce thicker coating and the likely quality problems of a thick TBC. The line has a bifurcation at about 30 percent insulation level, indicating an added cost increase if a strain isolator is needed. This added cost is graphically illustrated by the steep jump in the relative cost, as indicated by the dotted curve in Figure II.2-19.

The same logic applied above for the piston risk and cost assessments can be extended for the case of cylinder head concepts, as shown in Figures II.2-20 and -21. Of the five treatments considered, the first adopts a high temperature metal substitution for uncooled operation. The second treatment is a thermal barrier coating, where the head structure may or may not have a separate deck, depending on the temperature of the substrate. The third approach is a metal firedeck, separated from the rest of the cylinder head by an air gap, while the fourth is a similar design having a monolithic ceramic firedeck. The fifth is a ceramic pot head, with ports as an integral part of the firedeck. It is noted that merely draining the coolant from the cylinder head gives an insulation level of about 45 percent, which is the starting value for the curves in the two figures.

II.2.2 BEARING AND LUBRICATION CONCEPTS

Both advanced elastohydrodynamic journal bearings and rolling type bearing concepts were evaluated. Either bearing type can be viable for a liquid lubricated ADRE. On the other hand, a rolling type bearing is more feasible for a purely solid lubricated engine. Specific lubrication concepts for rolling element bearings include liquid, solid, and hybrid schemes.

It is pointed out that surface treatments of the components to minimize friction and wear can be considered as a subset of the lubrication scenarios. Preliminary analysis verified the potential suitability of both oil and grease lubrication for rolling bearing applications in the ADRE. Solid lubrication is an emerging technology that would be further examined in the remainder tasks of this phase of the program.

BEARING CONCEPTS

In the pursuit of improved fuel economy and higher engine output, lower friction bearings are being sought. The desire to operate the engine at the maximum possible temperature within the combustion chamber may ultimately require the elimination of oil from the high temperature interfaces. The best example of such a situation is the interface between the piston ring and the liner. As described earlier, this interface problem may be addressed by considering a ringless piston design, as well as by investigating high temperature monolithic ceramic piston rings, ceramic liner surfaces, and possibly some kind of a high temperature lubricant at the interface. In the case of bearings, however, the current state of technology developments appears to indicate a different philosophy. The bearing concepts examined include rolling element bearings with wet sump lubrication, rolling element bearings with alternate lubrication, reduced diameter journal bearings, and alternate journal bearings.

Rolling Element Bearings - The rolling bearing effort of this program was supported, in part, by a subcontract to SKF Industries, Inc. The SKF subcontract final report is enclosed here as Appendix A, which contains detailed information. Hence, it is sufficient to state here a brief summary of the findings, and the reader is referred to Appendix A for further details.

For the ADE, the friction savings of the rolling element bearings over the journal bearings in the crankshaft main, crank pin, and cam shaft bearing locations were evaluated. If conventional liquid (or grease) lubrication is designed into these locations, rolling element bearings can be designed under full film oil lubrication conditions. All metal, optimized bearing designs can evolve from the state-of-the-art rolling element bearing technology. Since the majority of bearing oil supply in today's engine is for cooling purposes, the rolling element bearings can reduce the oil demand because of significantly less friction generated heat. A design concept of this type may consider oil splash or packed grease types of lubrication. Replacement of one or more of the rolling element bearing components with monolithic ceramic parts was also considered.

The work performed by SKF included preliminary sizing studies for roller bearings at the main and crankpin locations. After examining the load cycles of crankpin bearings and the "worst" main bearing locations, several bearing designs were proposed. Each of these designs met or exceeded the 5000-hour durability goal typical of heavy-duty diesel engine bearings. The friction estimates pertaining to the rolling element bearing designs enabled life cycle cost comparisons between rolling element and journal bearings.

Analysis has verified the suitability of both oil and grease lubrication, with the latter possibly offering friction advantages. Preliminary analysis pertaining to the use of solid lubricants was also undertaken. Grease or solid lubricants offer the obvious advantage of elimination of pumping oil through the crankcase.

This decreases or eliminates oil pump work, thus adding further enhancement to fuel economy.

Journal Bearings - Because of their low cost and good serviceability, the life cycle cost goals of a commercial heavy-duty ADE may be better achieved by the use of properly designed elastohydrodynamic (EHD) journal bearings. The key to this is that insulation treatments should be effective enough to thermally segregate the crankcase and overhead regions from the combustion chamber area. Provided that ADE concepts for the hot areas of the engine do not preclude the necessary lubrication environment, journal bearings should be seriously considered as an alternative to rolling element bearings. If at all possible, high speed turbocharger bearings should also be conventionally lubricated. Optimizing bearing clearances and decreasing bearing diameters can help in reducing journal bearing friction. Recent advances in bearing analysis capabilities have coupled the oil film pressure distribution with the load/deformation response of the surrounding structure. This has suggested that, without affecting the load capacity, substantial reductions in journal bearing diameter can be made. This concept is just emerging and has not been fully assessed yet. However, it can permit bearing size reduction for decreased friction. Substantial reductions in journal diameter, the dominant geometric determinant of friction, may be possible through an advanced support structure (housing) design. Certain classical variations on the standard journal bearings, such as floating ring bearings, also have friction/size relations that are fairly well understood. Such designs can be pursued as additional options for minimum friction bearing concepts.

Crankshaft safety factor must also be considered in any downsizing of the main and pin journal diameters. High temperature ceramic journal bearing concepts can be an attractive alternative to the use of conventional soft interlay material. Transformation toughened zirconia sleeve bearing is a likely candidate, despite the rather scarce information available on the viability of ceramics for this application.

LUBRICATION CONCEPTS

Some of the Government and industry-sponsored low heat rejection engine programs suggest total elimination of liquid lubrication from the crankcase. Although it appears that liquid lubricant may still be necessary in the future for the commercial heavy-duty ADE, solid lubricated minimum friction bearing technology is being reviewed.

Solid lubrication at high temperatures, and with a wide operating temperature range, is the most limiting technology for ceramic or metallic rolling bearings. The sacrificial cage designs are simple in that they do not require a lubricant delivery system. A sacrificial cage also fits within a bearing envelope; hence, it offers the possibility of a smaller size bearing. One of the major reported disadvantages of the sacrificial cage approach is the limited cage life. A snap-in replaceable cage has been suggested for the crankpin and crankshaft bearings. Because the rolling element separator is continuously wearing to supply the necessary solid lubricant, the replaceable cage life would be limited to a few hundred hours at crankshaft speeds or no more than a few hours at turbocharger speeds. It has been reported that when testing this type of bearing, the dynamic motion becomes progressively unbalanced; thus, the wear rates accelerate, increasing the possibility of cage breakage, and leading to rapid failure [14,15]. It appears that the sacrificial cage solid lubricant approach still needs significant material developments and design innovations.

Powder (or vapor) lubrication is another solid lubrication concept that has been investigated and has shown some potential [15-20]. A very small supply of powder lubricant is delivered in an air or gas carrier in order to maintain surface separation between parts in relative motion. This appears to be an attractive system, especially since ceramic bearings are being considered as a concept. The carrier gas cools the bearing while the powder is responsible for lubrication. Issues to be addressed, however, are

the lubricant delivery system design and power demands, and possibly, emission concerns of the scavenged lubricating powder.

Another conceptual approach to external solid lubrication involves bringing a "stick" made of solid compacted lubricant in contact with the surface to be lubricated. Graphite brushes have been used for many decades as means of contact between the rotor and the winding of electric motors and alternators. The feasibility of such an approach for tribological application in the ADE has not been assessed yet, although it seems warranted. Replenishable or long lasting stick lubrication mechanisms can be incorporated in a non-conventional engine design when this concept is proven feasible.

Other technically aggressive systems that have been suggested include lubricating by controlled combustion products leakage into the bearings, or packing high temperature solid lubricant in a fashion similar to conventional grease-packed and sealed rolling bearings that are routinely produced and used for many applications, such as the automotive wheel bearings.

A summary of the bearing and lubrication concepts is given in Table II.2-7. Since an extensive component development is clearly beyond the scope of the current program, only a review of technologies is undertaken. It is suggested that minimum friction bearing technology for the ADE should be developed in an evolutionary approach.

II.2.3 REFERENCES

1. Wallace, F., et al., "Thermal Barrier Pistons and Their Effect on the Performance of Compound Diesel Engine Cycles," SAE Paper No. 830312.
2. Wilson, R., "Insulated Composite Piston From Perfect Circle," Diesel Progress North American, April 1984.
3. Schieber, G., and Sander, W., "Heavy Duty Pistons for Diesel Engines," Karl Schmidt GMBH, Kolloquium 1979.
4. Stang, J., "Designing Adiabatic Engine Components," SAE Paper No. 780069.
5. Fletcher-Jones, D., et al., "New Piston Features for Truck, Off-Highway and Industrial Diesel Engines," Third AE Technical Symposium, Paper No. 7, 1982.
6. Holtman, R., et al., "An Investigation of Enhanced Capability Thermal Barrier Coating Systems for Diesel Engine Components," DOE/NASA/0326-1, August 1984.
7. "Postfiring Impregnation of Refractories with Chromium Oxide," also other Kaman Sciences Corporation Technical Bulletins.
8. Carr, J., and Jones, J., "Post Densified Cr203 Coatings for Adiabatic Engine," SAE Paper No. 840432.
9. Sekhar, R., and Tozzi, L., "Advanced Automotive Diesel Assessment Program," DOE/NASA/0261-1, December 1983.
10. Scharnweber, D. H., et al, "Laboratory Evaluation of Ceramic Coatings for Diesel Exhaust Valves," Eaton Corporation, DOE Contract No. DE-AC03-79ET15320, November 1980.
11. Kamo, R., et al, "Development of an Adiabatic Diesel Engine," Contract NO. DAAK 30-77-C-0032, Report No. 12695, July 1981.
12. Worthen, R. P., and Tunnelcliffe, T. N., "Temperature Controlled Engine Valves," SAE 820501, 1982.
13. Asnani, M., and Kuonen, F., "Ceramic Valve and Seat Insert Performance in a Diesel Engine," SAE 850358, 1985.
14. Dayton, R. D., and Sheets, M. A., "Evaluation of Grooved Solid-Lubricated Bearings," AFAPL-TR-75-76, Feb. 1976.
15. Dill, J., Mechanical Technologies, Inc., Private Communications

II.2.3 REFERENCES (Continued)

16. Schlosser, A. L., "The Development of Lubricants for High-Speed Rolling Contact Bearings Operating Over the Range of Room Temperature to 1200 Degrees Fahrenheit," WADD TR-60-732, August 1962.
17. Wallerstein, S., "Development of Gas-Entrained Powder Lubricants for High Speed and High Temperature Operation of Spur Gears," AFAPL-TR-65-24, May 1965.
18. Wallerstein, S., "Application of a Powder Lubrication System to a Gas Turbine Engine," AFAPL-TR-65-43, Part I, September, 1965.
19. Wallerstein, S., "Application of a Powder Lubrication System to a Gas Turbine Engine," AFAPL-TR-65-43, Part II, December 1965.
20. Wallerstein, S., "Application of a Powder Lubrication System to a Gas Turbine Engine," AFAPL-TR-65-43, Part III, June 1967.

Table II.2-1: Assessment of Insulation Methods

A: Air Gap

Advantages:

- 0 Easier to analyze and design
- 0 Material property readily available
- 0 Good insulation, up to 65% effectiveness.

Disadvantages:

- 0 Multi-piece structure, leading to high machining cost
- 0 Likely higher expansion at high temperatures
- 0 High thermal stress if constraint is present
- 0 Air gap is difficult to seal

Overall Assessment:

- 0 Moderately aggressive approach
- 0 Meets insulation goal up to the 65% reduction
- 0 Mass producible in 1995 or earlier
- 0 Require low cost material with good machinability
- 0 Gap size optimization and sealing may require new technological developments

B: Thermal Barrier Coating

Advantages:

- 0 Applicable onto existing hardware with minimum modification
- 0 Flexible, can tailor coating composition for different application
- 0 Coating failure may not lead to catastrophe
- 0 Relatively moderate cost addition

Disadvantages:

- 0 Material properties unknown
- 0 Difficult to predict coating quality, failure mechanism and life
- 0 Thick coating required to meet insulation goal
- 0 Long term coating integrity unproven

Overall Assessment:

- 0 Near term solution to achieve up to 30% insulation
- 0 Consistent mass production methodology requires further basic developments
- 0 Unknown long term diesel engine's environmental and thermomechanical effects on coatings
- 0 In situ quality control has yet to be developed

Table II.2-1: Assessment of Insulation Methods (Cont'd . . .)

C: Monolithic Ceramic

Advantages:

- 0 Maintained high temperature strength
- 0 Abundant, non-strategic materials

Disadvantages:

- 0 Material property characterization difficult and not consistent
- 0 Too wide strength spread
- 0 Design methodology has yet to be developed
- 0 Fails catastrophically
- 0 High machining cost

Overall Assessment:

- 0 Feasible for uncooled engine with short durability goal in 5 years
- 0 Requires design innovations
- 0 Need to improve the toughness
- 0 Mass producible in Year 2000+
- 0 Consistent mass production methodology requires further basic developments
- 0 Unknown long term diesel engine's environmental and thermomechanical effects on material degradation

Table II.2-2: Piston Design Considerations

Major Considerations	Key Factors
Functional	Power Transfer Guiding Sealing Cooling
Performance	Combustion Friction Heat Transfer
Reliability & Durability	Material Selection Mechanical Stress Level Thermal Stress Level
Engine Package Size	Piston Dimensions
Manufacturing	Material Properties Design Complexity Dimensional Tolerances
Serviceability	Design Complexity

Table II.2-3: IHR Piston Concepts

Design Form \ Material Treatment	All Metal	Ceramic Coating	Monolithic Ceramic	
			Si ₃ N ₄	PSZ
Trunk		✓	✓	✓
Crosshead	✓	✓	✓	✓
Crosshead Air Gap	✓	✓	✓	✓
Ringless Crosshead	✓	✓	✓	✓

Table II.2-4: Salient Features of "Ringless" Piston Design

Salient features of "ringless" piston design

- Reduced mechanical friction, in-cylinder heat transfer and Oil Consumption
- Eliminate piston ring wear and reduce thermal stresses
- Decrease sensitivity to corrosive and abrasive materials
- For conditions of high temperature, marginal lubrication and high power output, simplified design could offer cost savings

Table II.2-5: Cylinder Liner Design Considerations

<u>Major Consideration</u>	<u>Key Factors</u>
Functional	Combustion Containment (sealing) Piston Guiding
Performance	Combustion Friction Heat Transfer Sealing
Reliability & Durability	Material Selection Mechanical Stress Level Thermal Stress Level Wear
Engine Package Size	Liner Dimensions Sealing Techniques
Manufacturing	Material Properties Geometric Complexity Dimensional Tolerance
Serviceability	Assembly Complexity

Table II.2-6: Generic Material Treatments for Liner Tribology

- Thin Coatings (Complete Overlay)
 - plasma spray
 - flame spray
 - Sol-gel
 - chemical vapor deposition
 - physical vapor deposition
- Mechanical Surface Treatments (Partial Overlay)
 - impregnation
- Ablative Surface Treatments
- Composite Assemblies
- Monolithic Structures

Figure II.2-1[A]: ADE Configuration Selection Methodology
 Mechanical Design Evaluation Procedure
 Component Concept Studies

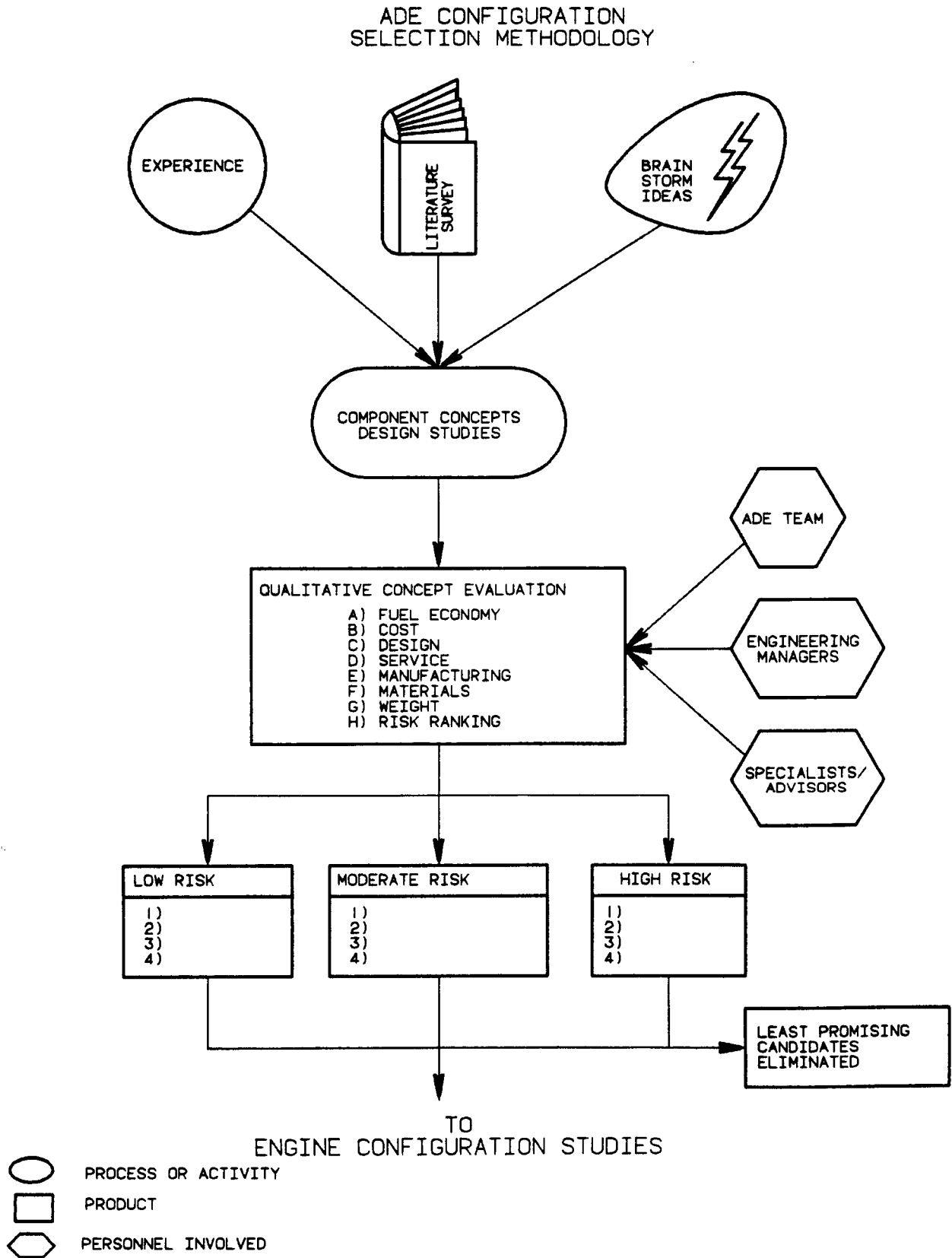


Figure II.2-1[B]: Mechanical Design Evaluation Procedure
 Engine Configuration Studies From
 Component Studies

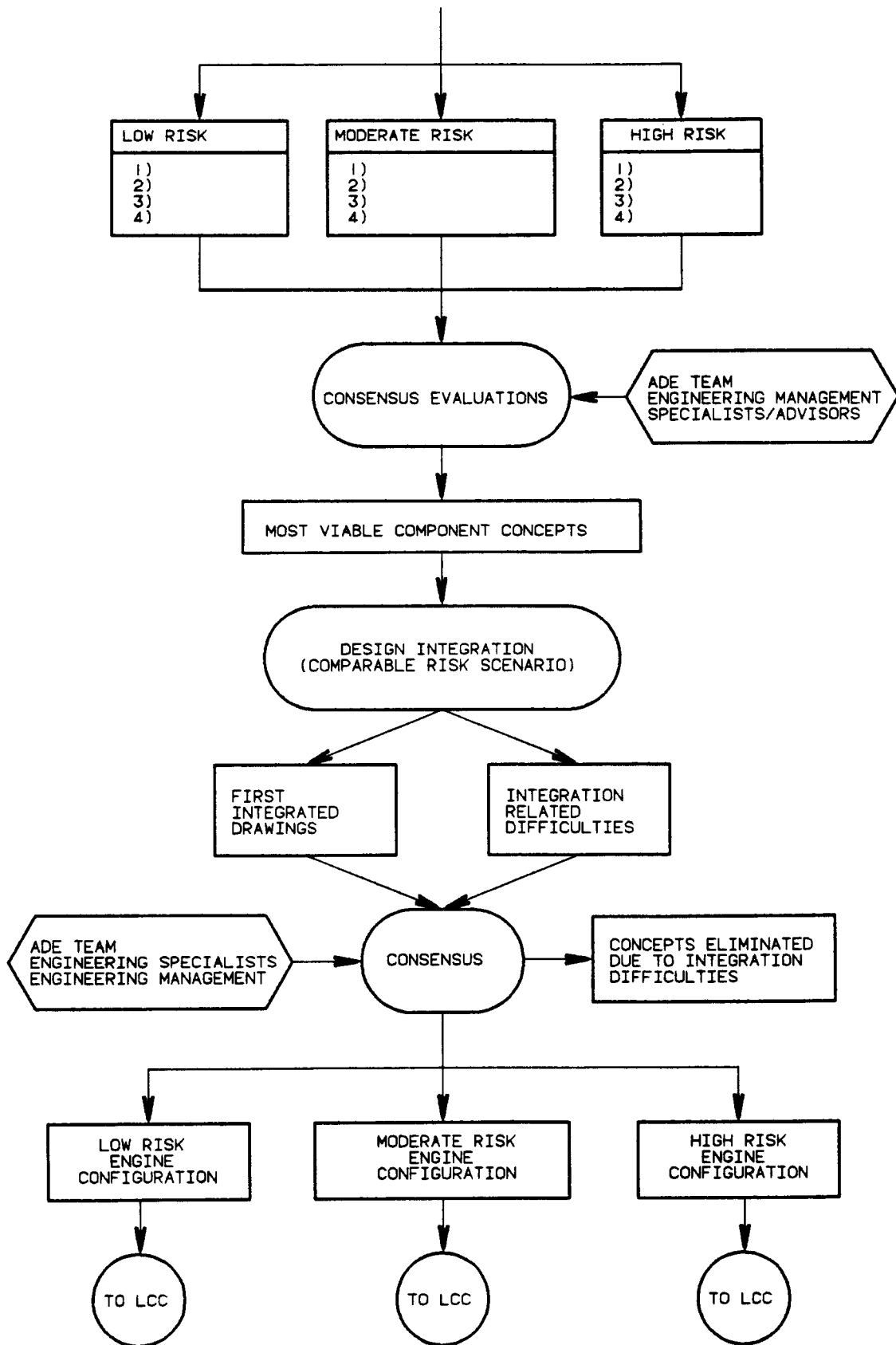


Figure II.2-2: DDA's 6.2L IHR Trunk Style Aluminum Piston

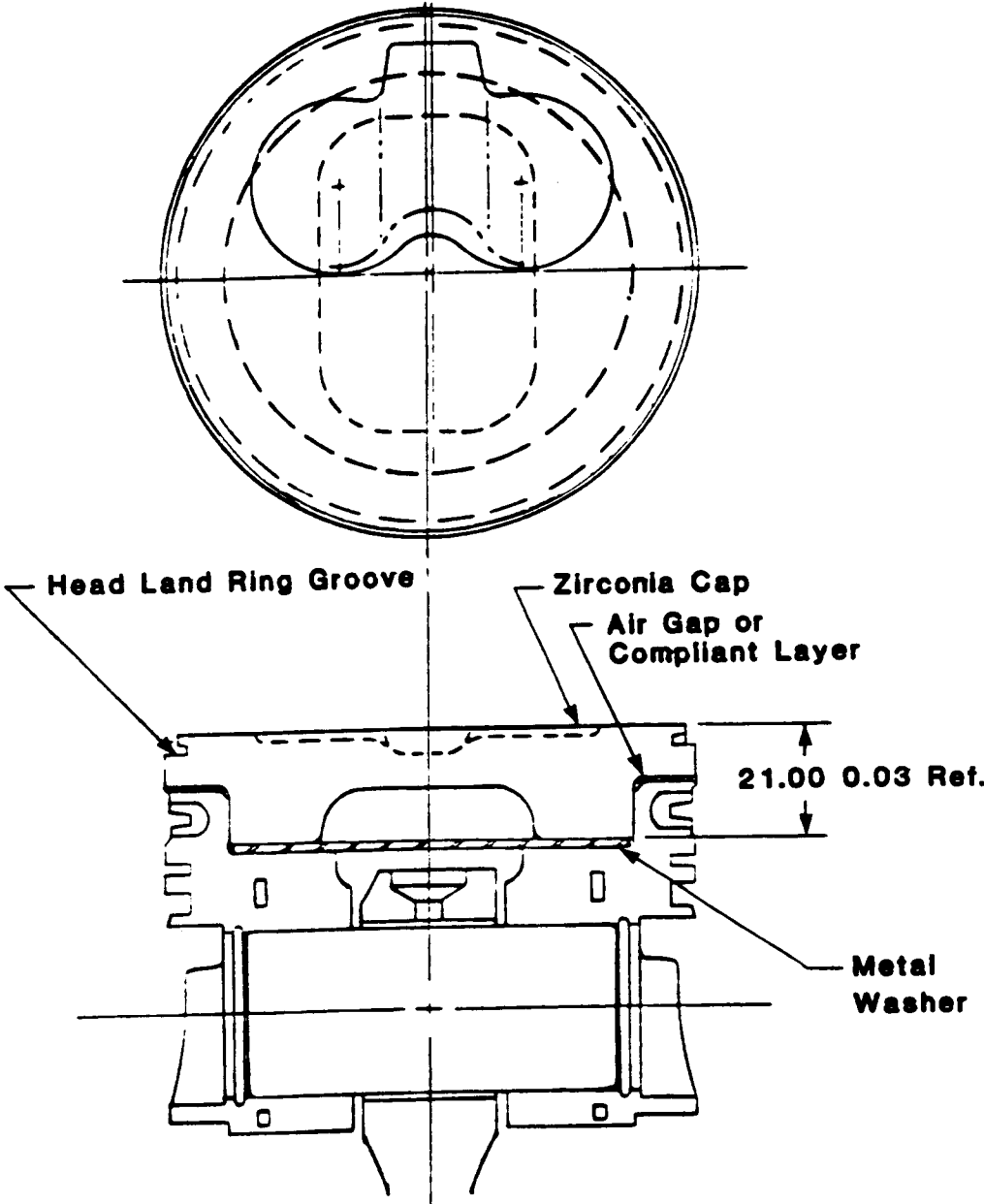


Figure II.2-3: View of the Conventional Crosshead Piston

ORIGINAL PAGE IS
OF POOR QUALITY

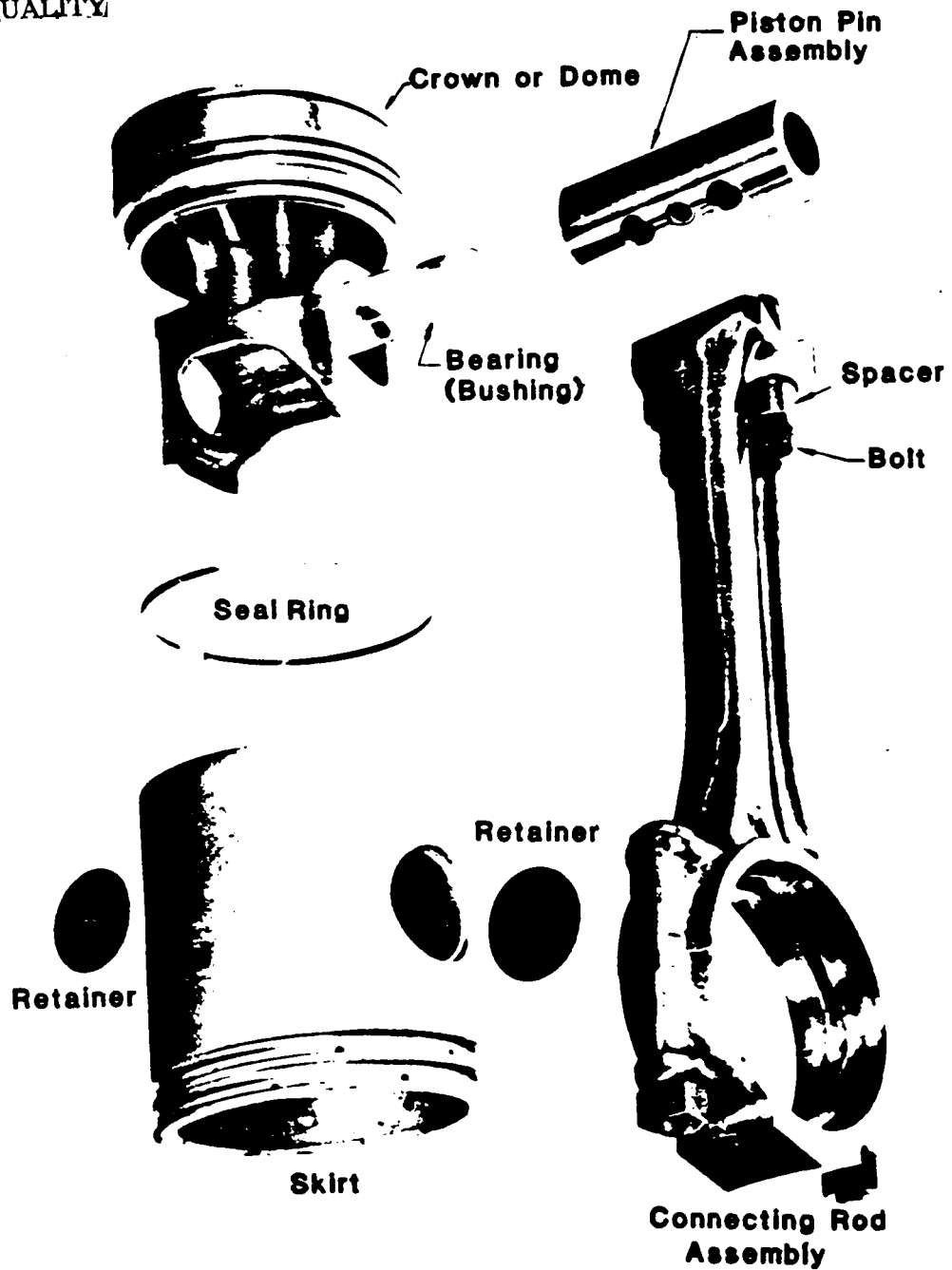


Figure II.2-4: Hollow Particle Thermal Barrier Coating

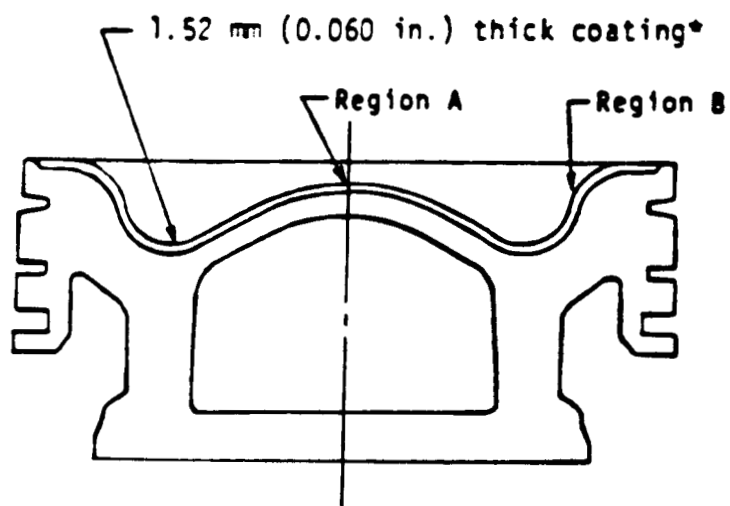


Figure II.2-5: Typical Crosshead Air-Gap IHR Piston

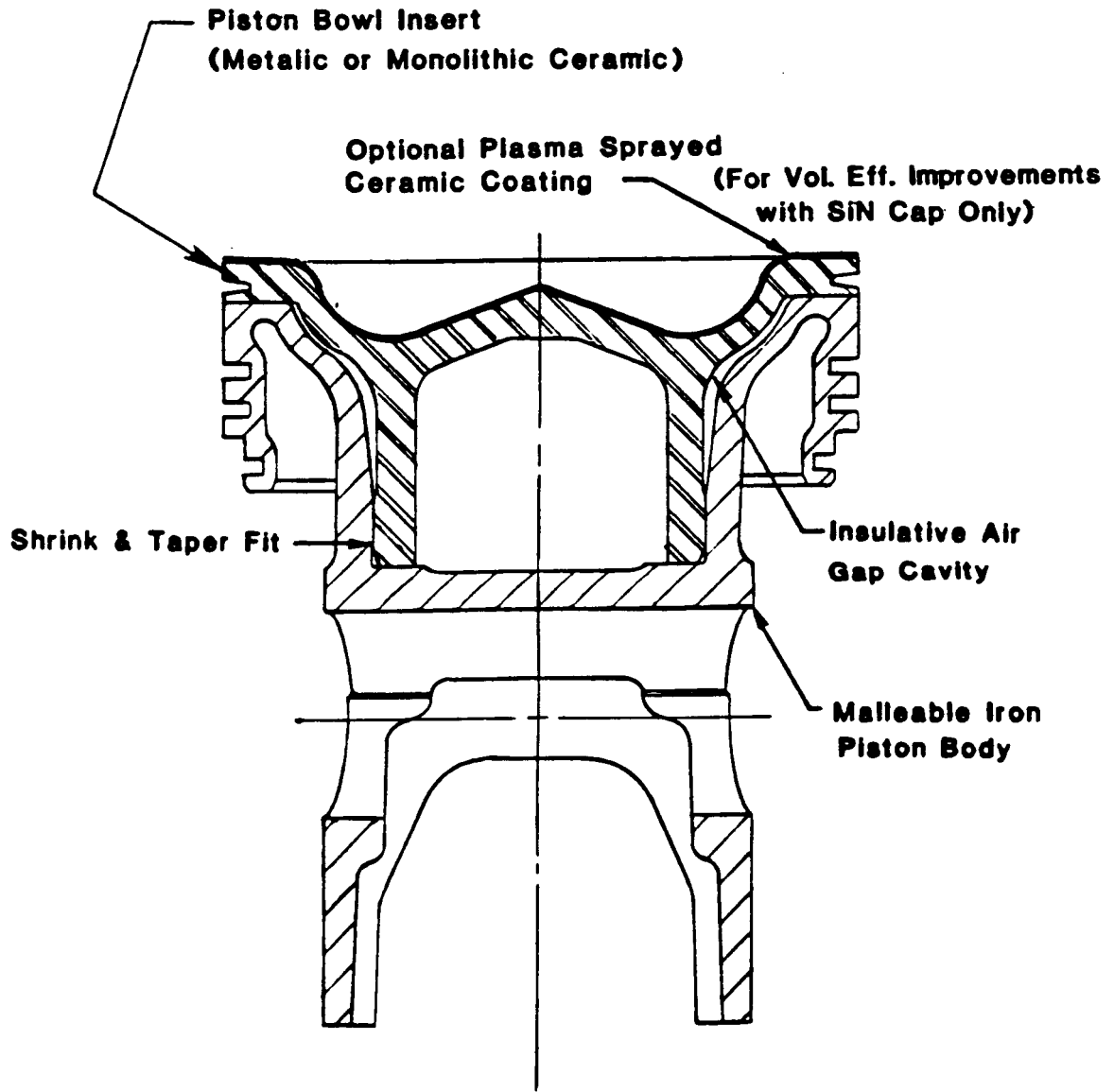


Figure II.2-6: Ringless Piston Design Concept

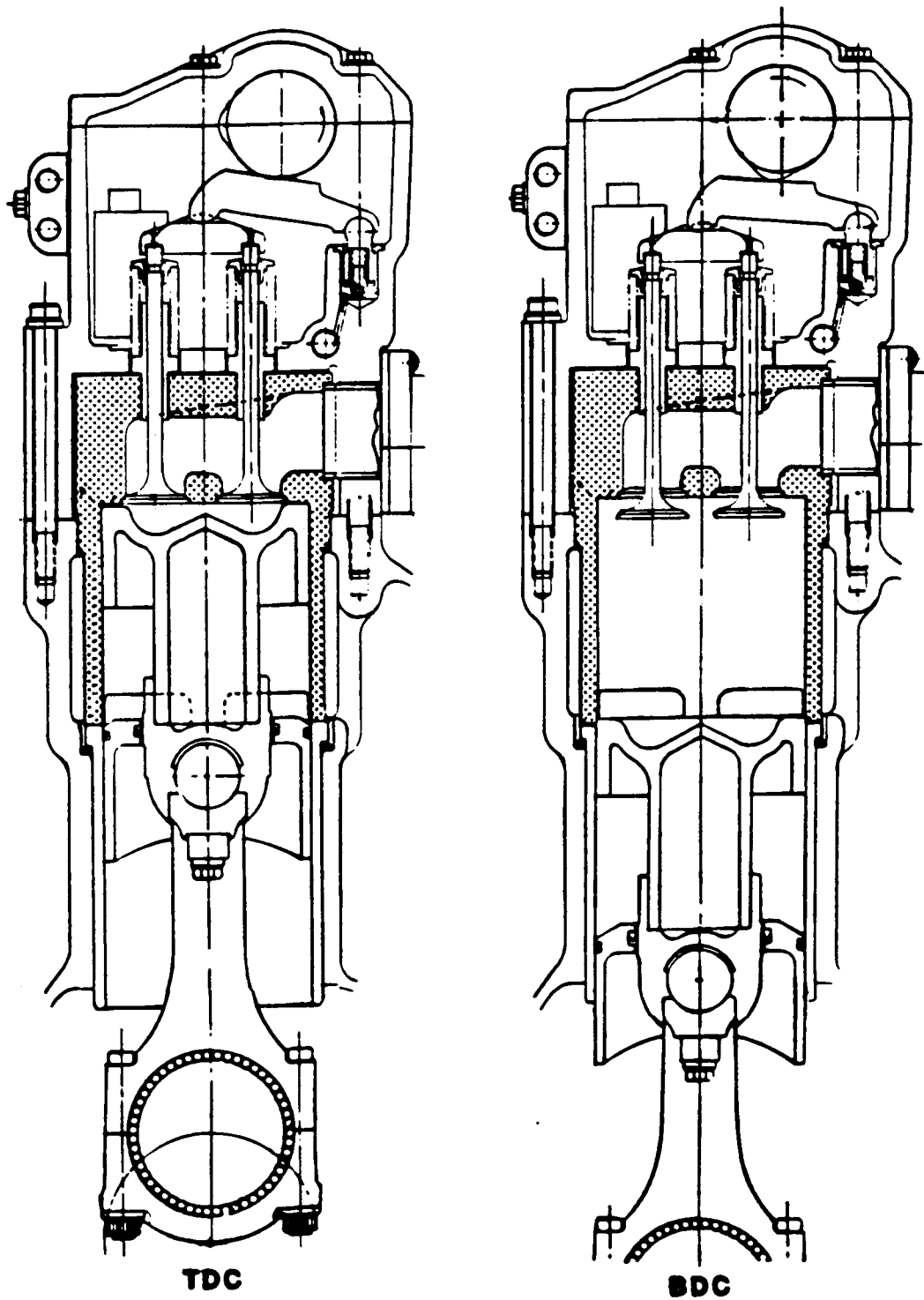


Figure II.2-7: Leakage and Power Loss as a Function of Radial Clearance for a Ringless Piston

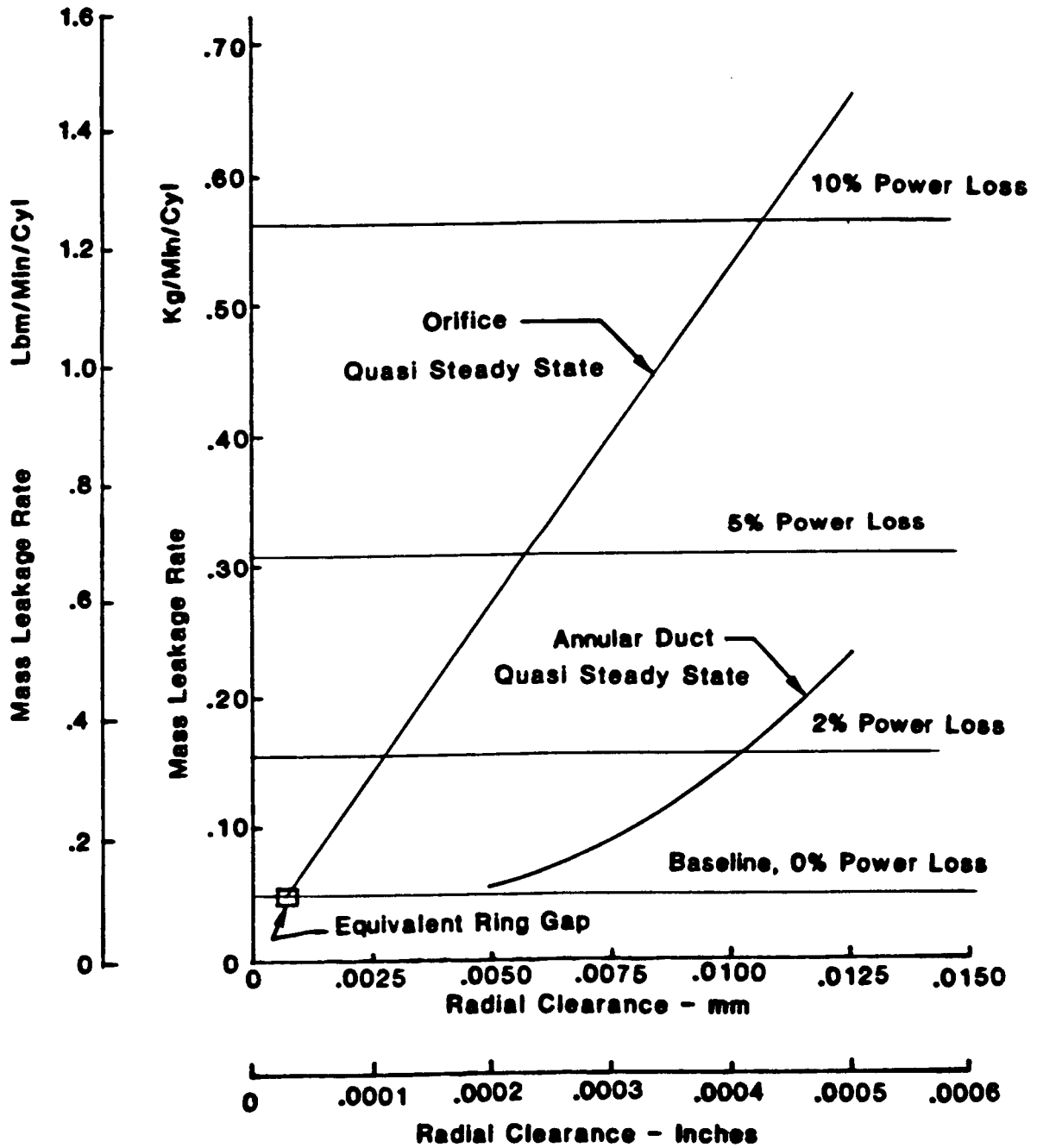


Figure II.2-8: Firedeck with Retaining Ring

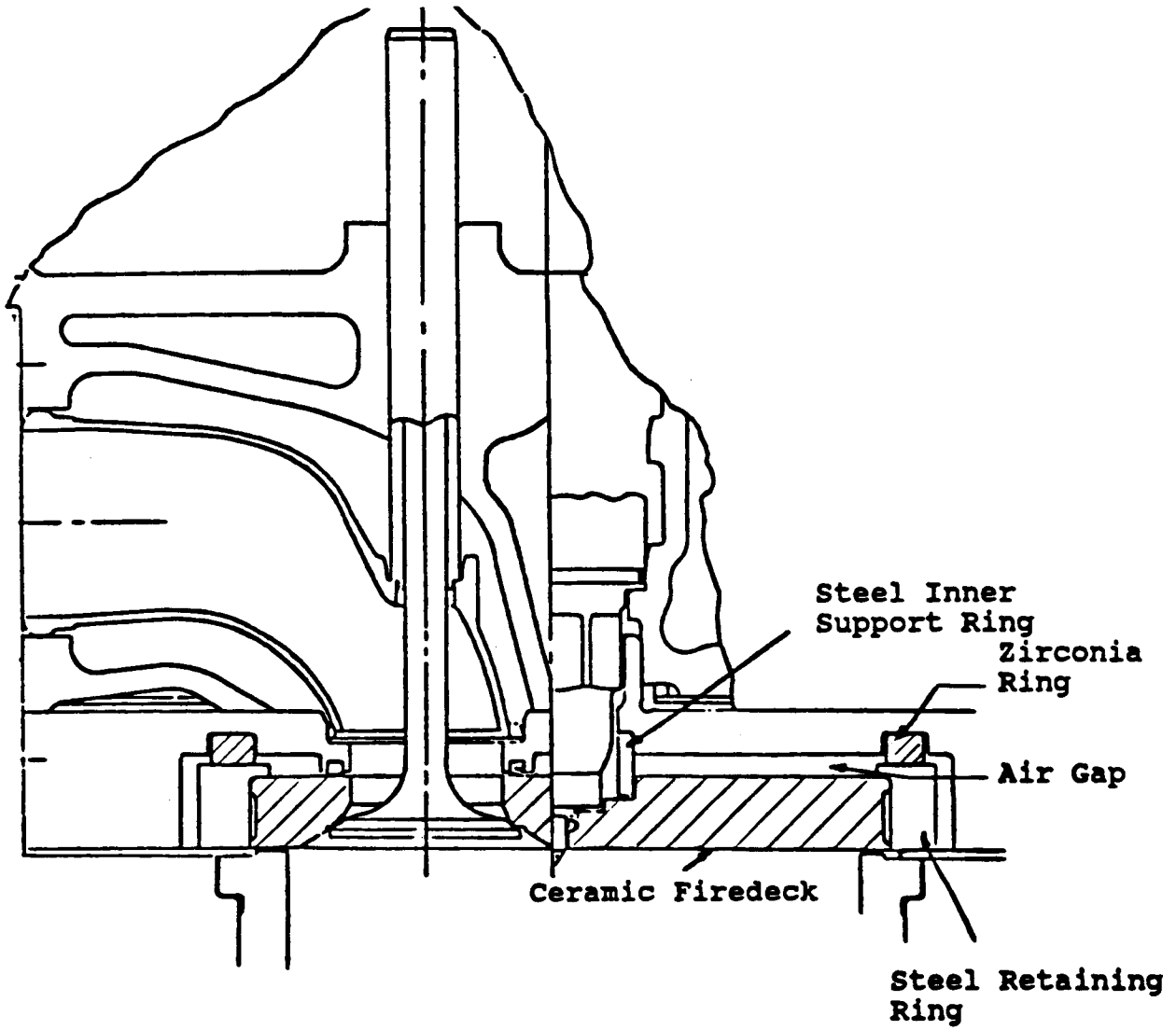


Figure II.2-9: Direct Press-Fit Firedeck Design

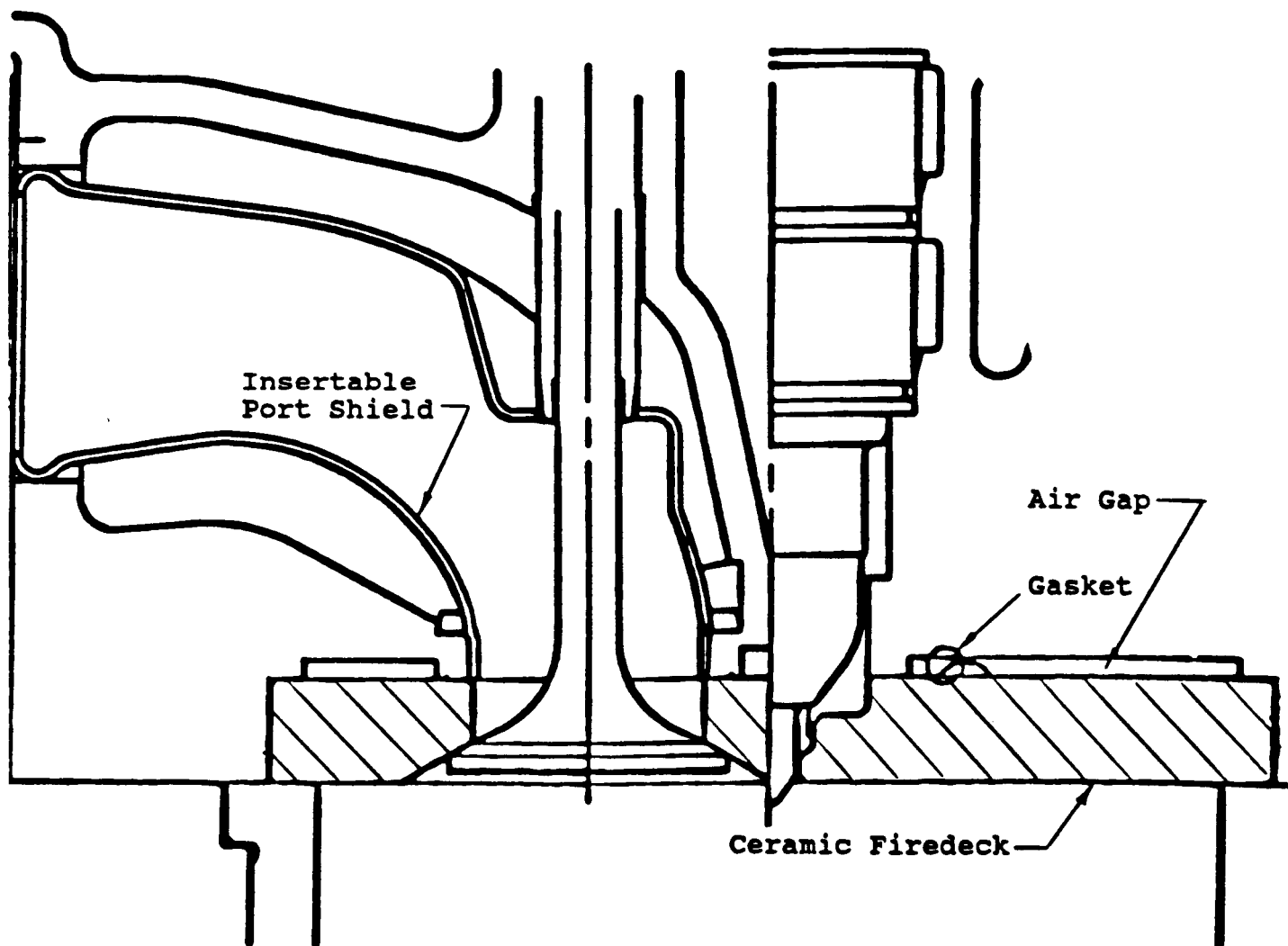


Figure II.2-10: Individual Pot Head Concept

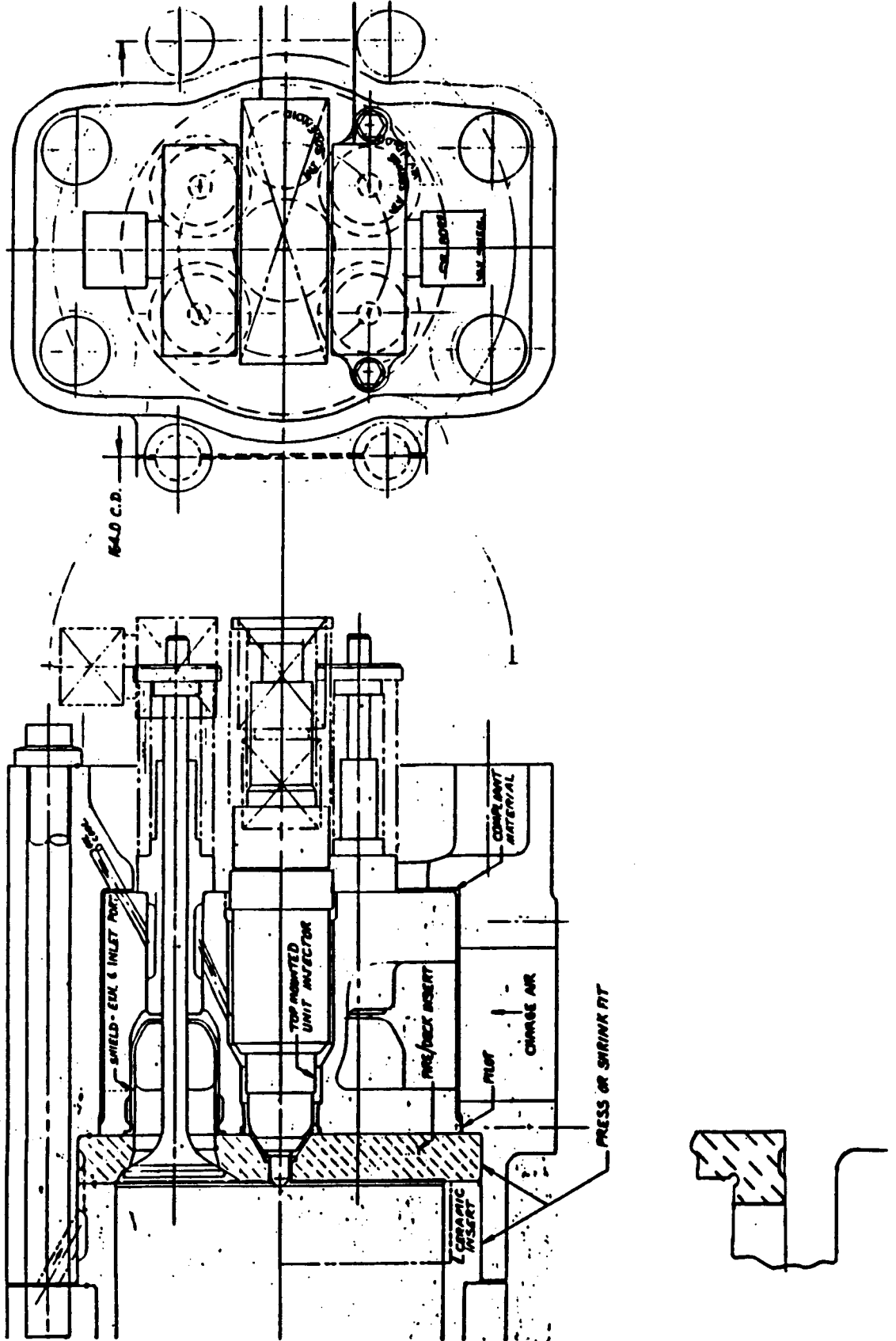


Figure II.2-11: Shielded Exhaust Valve (From Reference 12)

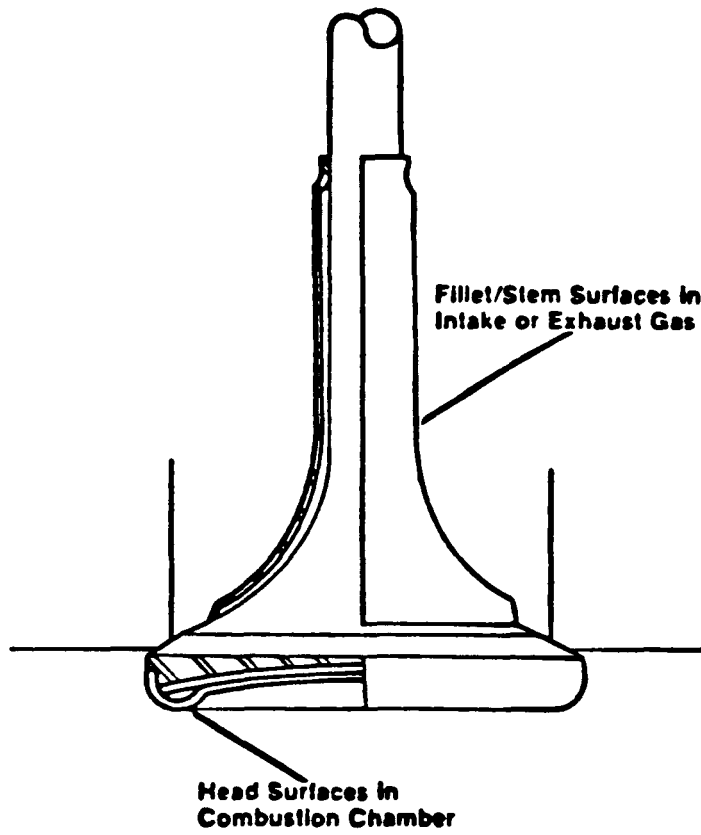
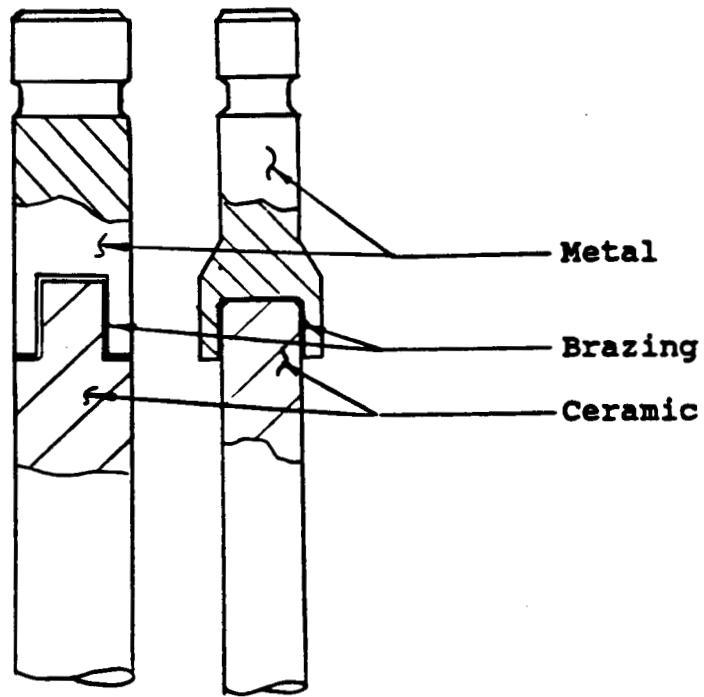
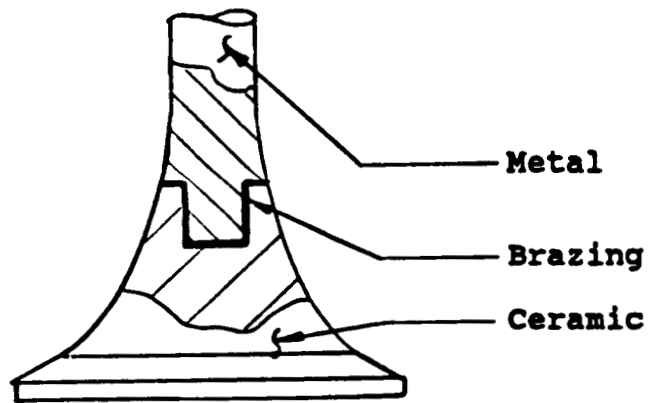


Figure II.2-12: Brazed Ceramic/Metal Valve Concepts



(a) Ceramic Stem



(b) Ceramic Valve Head

Figure II.2-13: Floating Valve Guide Concept

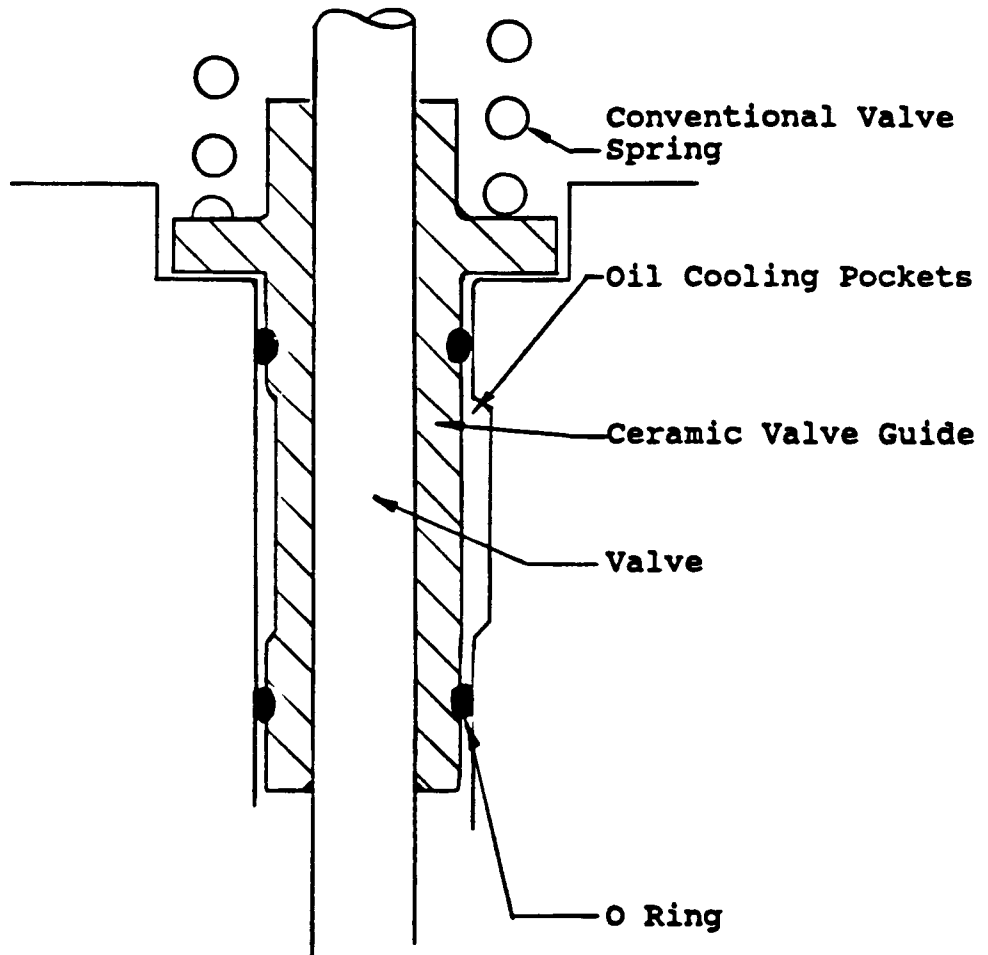


Figure II.2-14: DDA's Series 92 Cylinder Head with Insertable Shield

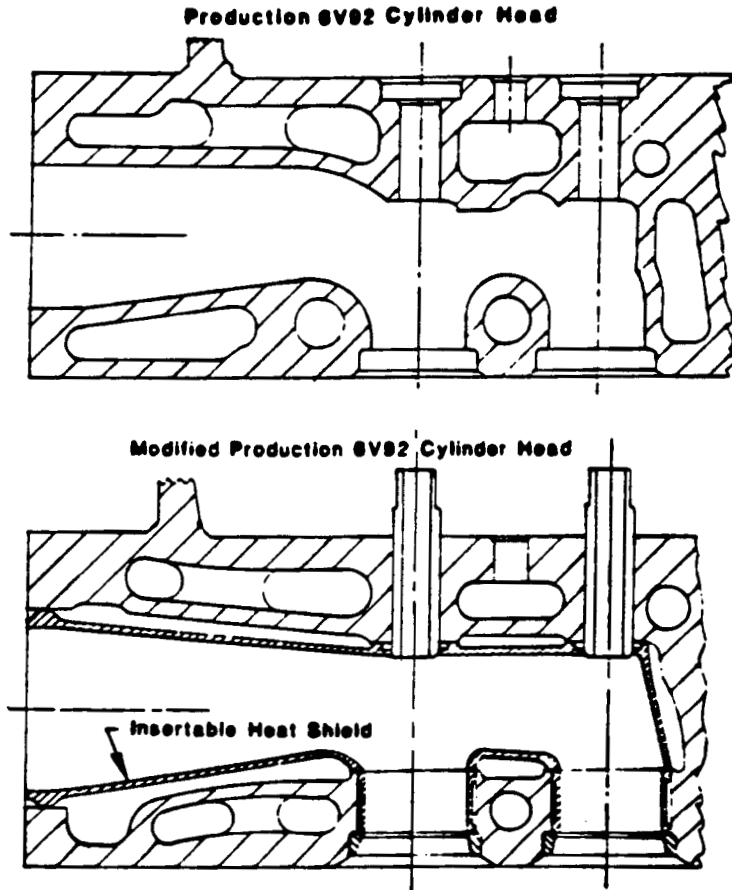


Figure II.2-15: DDA's Series 60 Cylinder Head with Direct Press-Fit Shield

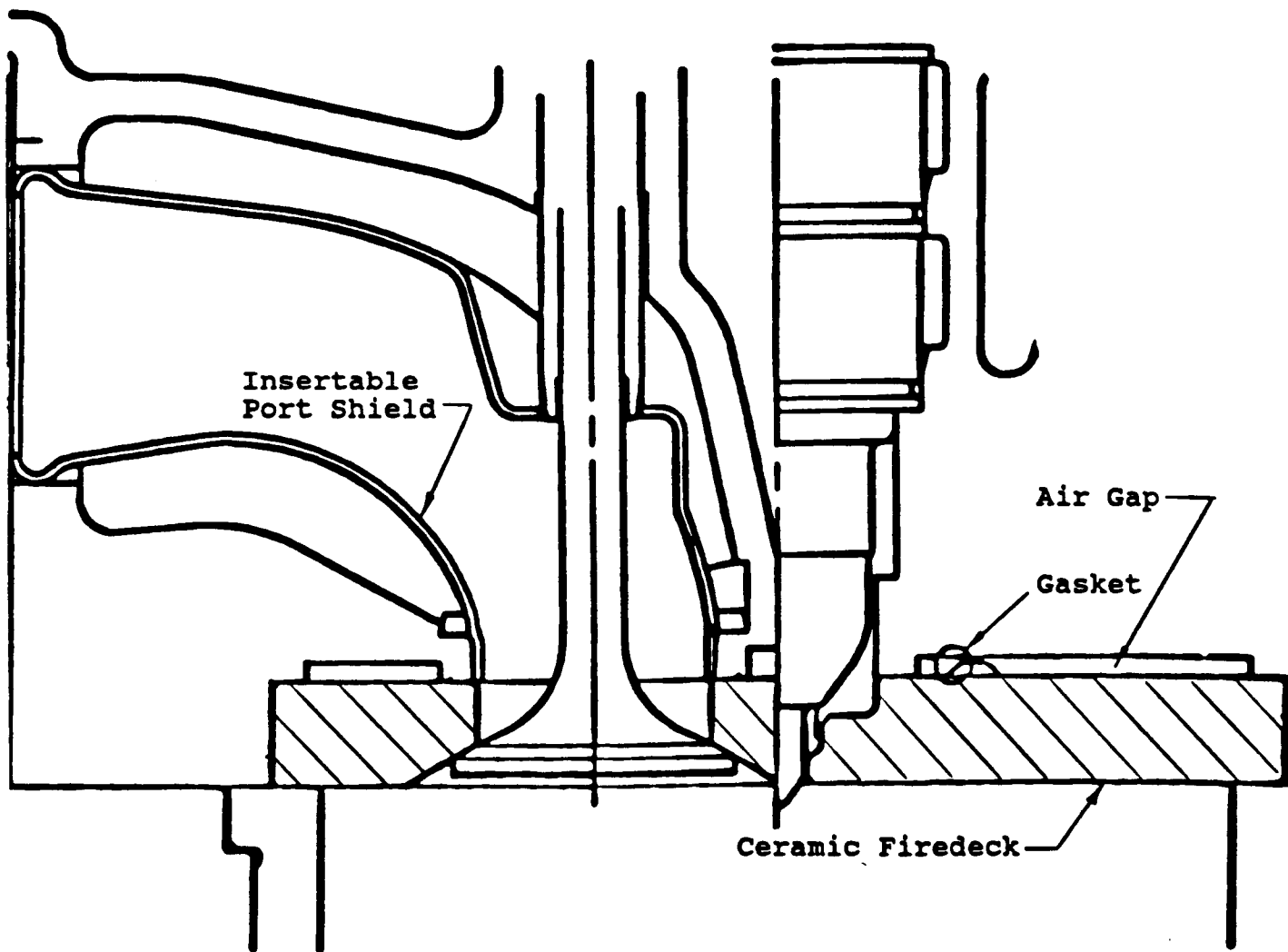


Figure II.2-16: Cost Estimates for a Silicon Nitride Piston Cap

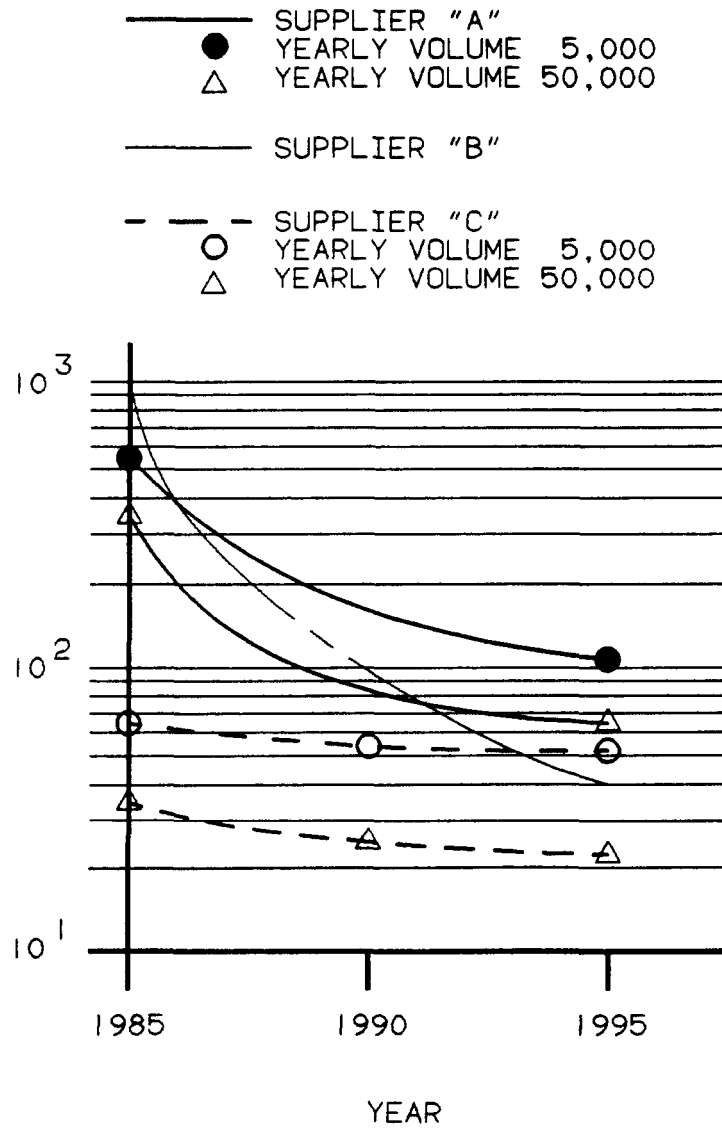


Figure II.2-17: Insulation Treatment Screening Process

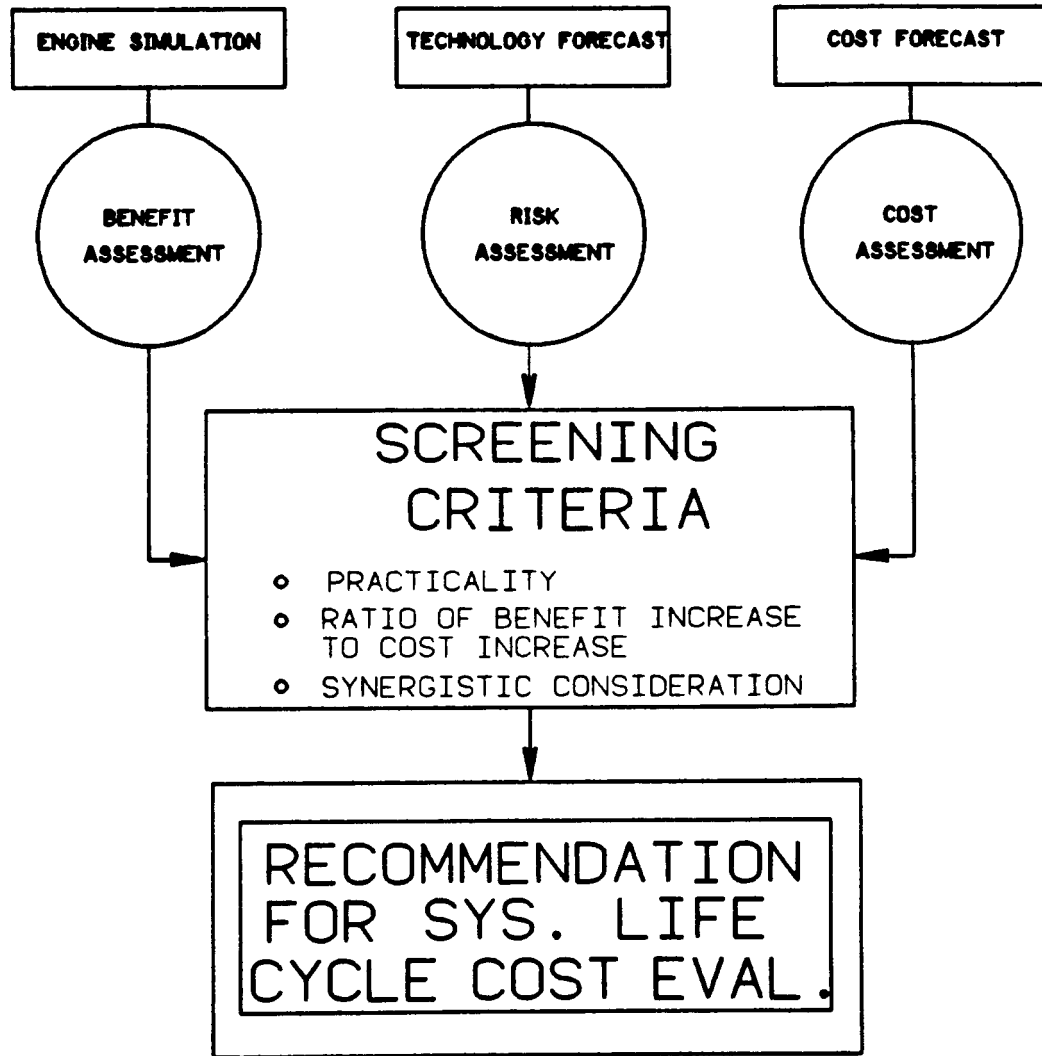


Figure II.2-18: Technical Risk vs Insulation Level for Different Piston Insulation Treatments

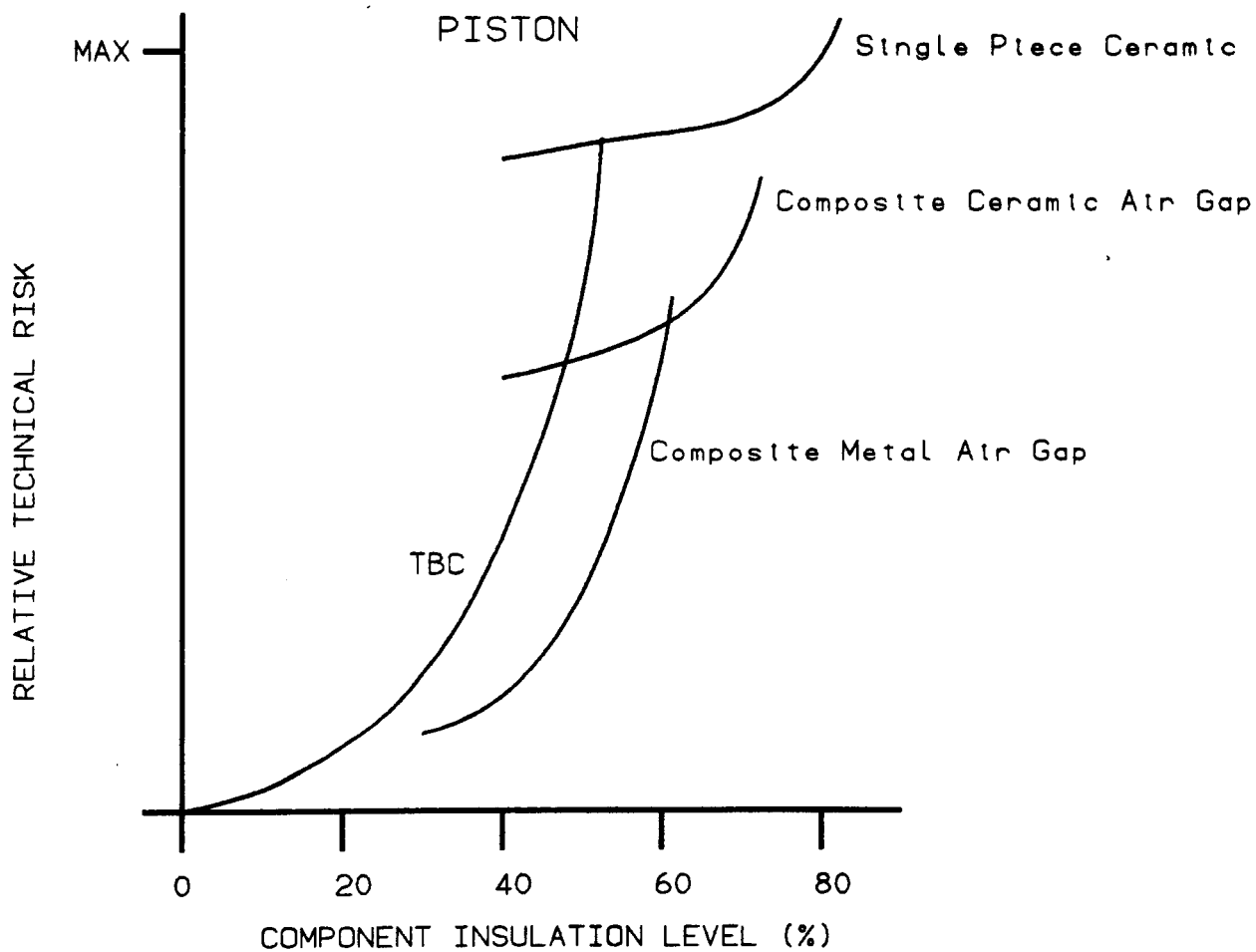
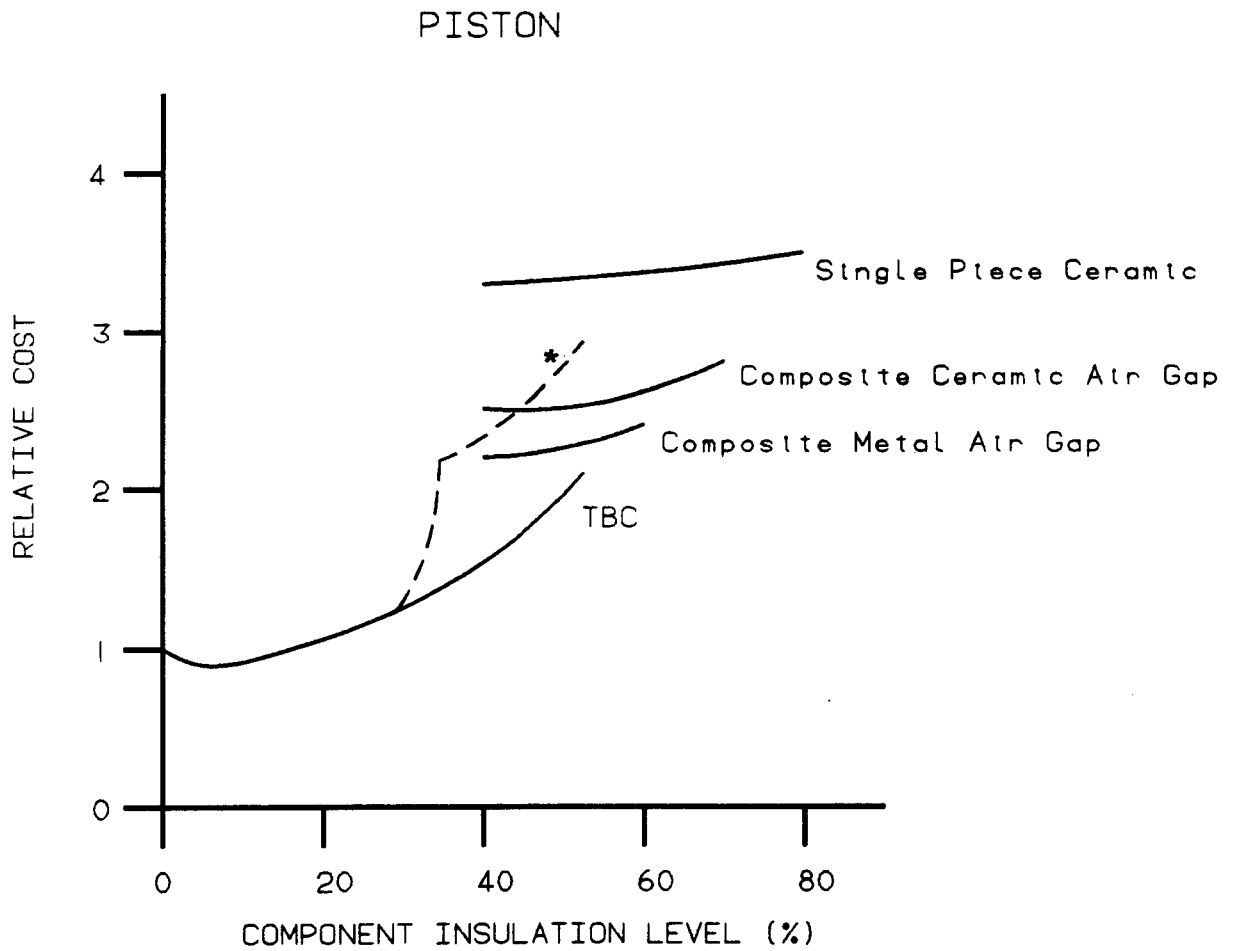


Figure II.2-19: Relative Cost vs Insulation Level for Different Piston Insulation Treatments



* TBC with strain isolator.

Figure II.2-20: Technical Risk vs Insulation Level for Cylinder Head Without Watercooling

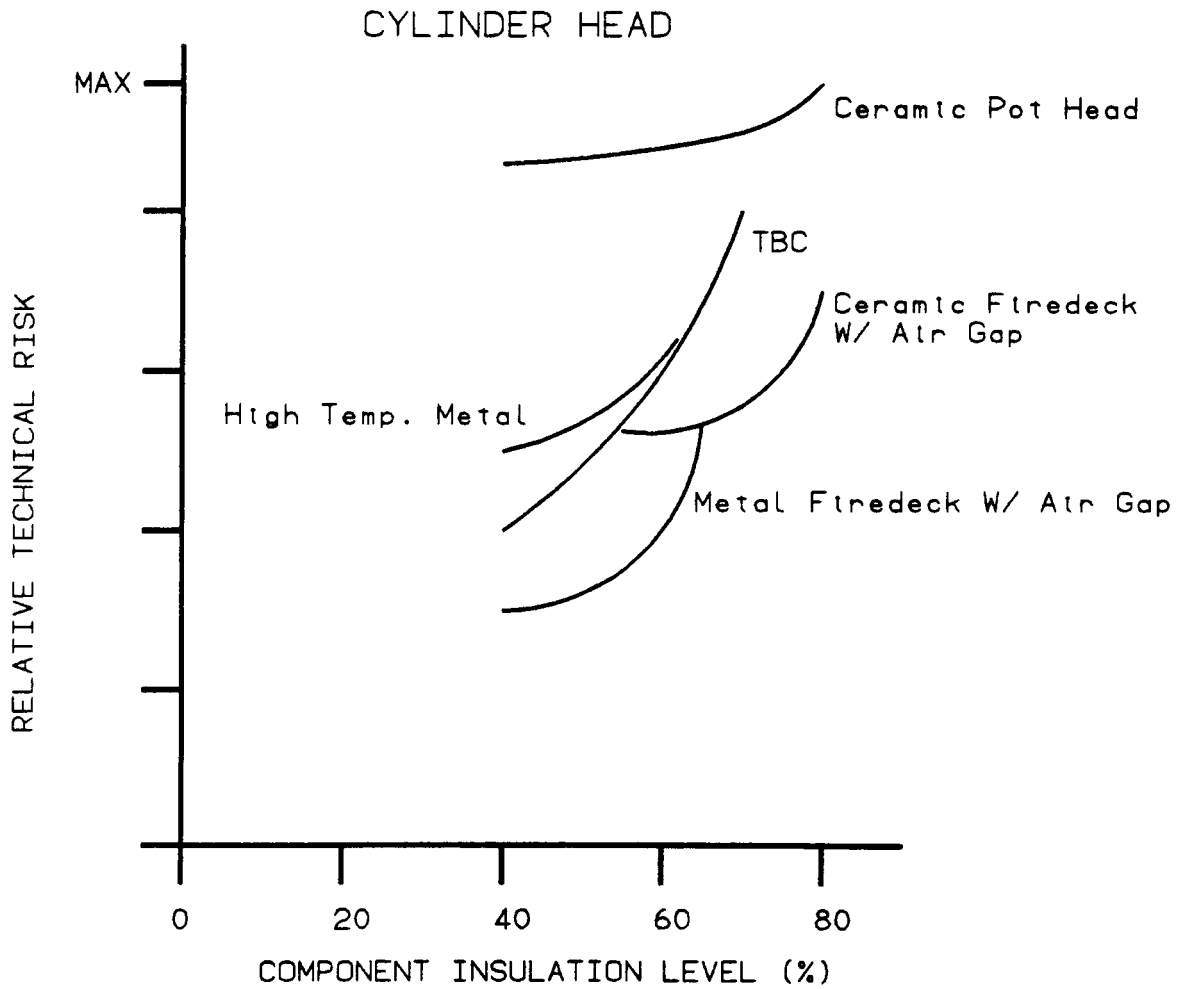
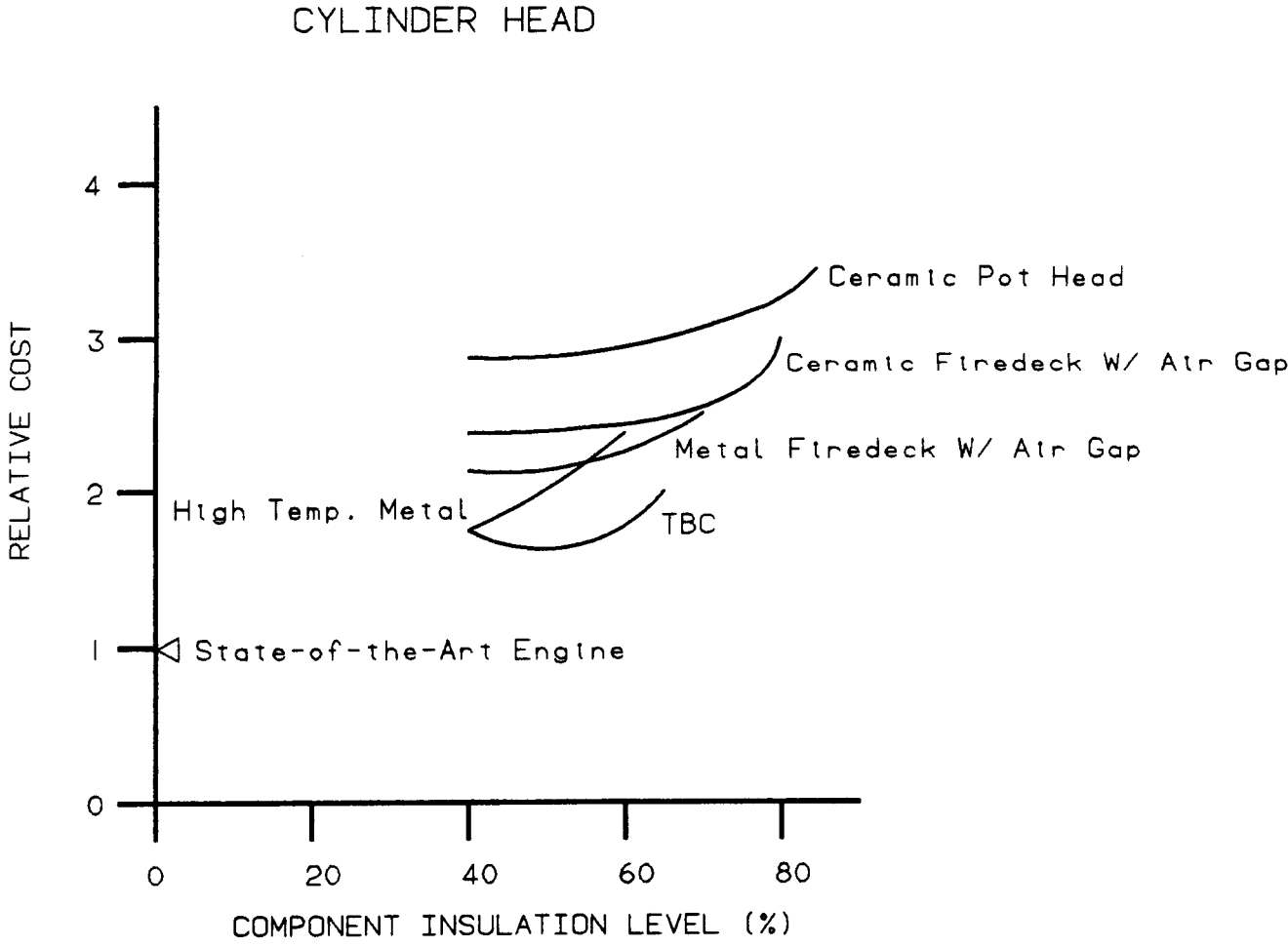


Figure II.2-21: Relative Cost vs Insulation Level for Cylinder Head Without Watercooling



II.3 EXHAUST ENERGY RECOVERY SYSTEMS

Diesel engine Exhaust Energy Recovery [EER] has been under development for many years, dating back to the first efforts involving the use of exhaust gas to power a compressor for boosting engines. Today, conventional turbocharging is a well-established technology for increasing the specific output of diesel engines. The energy balance of a turbocharged engine, however, shows that approximately one-third of the fuel energy input is lost in exhaust gases. A literature search and concept study of various EER systems were undertaken. Available DOE/NASA Contractor Technical Reports and several outside published technical papers were reviewed. A major portion of the information in this section is excerpted from these references.

In comparing the advantages and disadvantages of each of the systems, the preliminary evaluation should be based upon fuel economy, transient response, reliability/durability, cost/payback, compactness/packaging, ease of operation, etc. In connection with the definition of the LHRE configuration in terms of insulation levels and turbocompounding pressure ratio, this information can be used in selecting the most suitable EER system.

II.3.1 SYSTEMS SURVEY

TURBOCHARGING

Various turbocharging concepts, such as variable geometry, two-stage turbocharging, and compressor-to-turbine bleed have been investigated for improvement of turbocharger and engine match characteristics over the engine speed range. Improvement in turbocharger efficiency for reduced engine pumping power and

corresponding fuel consumption savings is a current and ongoing technology pursuit.

TURBOCOMPOUNDING

Turbocompounding is basically an extension of the turbocharging concept involving direct expansion of exhaust gases through a power turbine geared to the turbocharged engine. Some variations of this concept, including separately geared compressors and turbines, have also been examined. Since the fraction of exhaust energy recovered through this process depends upon the expansion ratio, it also increases pumping power loss due to higher engine back pressure. Thus, there is an optimum expansion ratio beyond which the pumping power exceeds the energy recovered by the power turbine.

This expansion ratio is affected by the efficiency of the turbomachinery components, as well as the energy available in the turbocharger exhaust, which in turn depends upon the low heat rejection effectiveness (adiabacity) of the engine. Due to the greater exhaust gas expansion, the final exhaust temperature of the turbocompound diesel engine is lower than a corresponding turbocharged diesel engine.

In an arrangement referred to as a "first-stage turbocompounded engine," the turbocharger would be mounted downstream of the power turbine. Claimed advantages of this system are improved throttle response, decreased temperature variation at power turbine inlet, and reduced effects of turbine exhaust gases on charge air temperature. Adding a burner before the power turbine is another modification.

In general, the fuel economy advantages due to turbocompounding are significantly reduced at part loads. Improvements in bsfc may be possible by using available step-down gear ratio or using a variable geometry turbine to maintain

compound power at part loads. These functionally improved concepts can have a significant effect on life cycle cost.

BOTTOMING CYCLES

Bottoming cycle concepts utilize diesel exhaust energy as a heat source with a secondary working fluid. They may operate in an open or closed cycle mode. Three basic types of systems, operating on the Brayton, Rankine, and Stirling cycles, respectively, have been considered as bottoming cycles for diesel engines, as shown schematically in Figure II.3-1. In each case, the exhaust temperature level is a key factor affecting the cycle parameters and resulting output. The working fluid and its thermal properties is another key factor which determines the performance of the system. The transfer of exhaust energy to a secondary fluid requires some form of heat exchanger, which can be bulky and subject to fouling by the exhaust gases.

In general, the bottoming cycles are more complex when compared to direct expansion turbocompound systems. On the other hand, due to the absence of direct expansion, the bottoming cycles do not significantly change the diesel cycle pressures or the engine pumping power loss. Thus, the performance of the basic turbocharged engine is not significantly affected by the addition of a bottoming cycle. The following paragraphs give the specific known performance characteristics and development stage for each of the bottoming cycles.

Rankine Bottoming Cycles - Organic Rankine bottoming cycles for a turbocharged diesel engine have been studied and demonstrated by Thermo Electron Corporation over the years. In this cycle, the working fluid properties must be matched to the heat source temperature for optimum system performance. A key fluid property is the boiling point relative to the exhaust heat source temperature. For a standard diesel exhaust temperature level, an organic working fluid, such as Fluorinol 85, has been

found to have suitable properties. At the higher temperatures expected from a LHRE, a different organic fluid or a water-steam system may be more appropriate.

Under a DOE/NASA contract, Thermo Electron Corporation has evaluated an organic Rankine bottoming cycle for the LHRE, using a high temperature organic fluid under the trade name of RC-1 [1]. Foster-Miller has studied a steam Rankine bottoming cycle for the same engine [2]. Basically, the two systems are similar, but the working fluid characteristics require different cycle pressures and must be matched to the available exhaust heat source. Different expansion systems have been proposed. These are a reciprocating system for the steam, and a turbine for the organic Rankine bottoming cycles.

- Organic systems yield better efficiency when coupled to a relatively lower temperature heat source because of the fluid's thermophysical properties.
- Organic systems have higher flow rates and, thus, turbine expanders in the anticipated 15 - 37 kW range can be used with increased efficiency.
- There is no potential damage to organic bottoming system components due to freezing. Freezing point temperatures for organic RC-1 and FL-85 are 231 K (-44°F) and 210 K (-82°F), respectively.
- Organic systems are more highly developed and available. No small steam bottoming cycles have been built for mobile diesels.

A major drawback associated with any Rankine system is the vapor generator fouling and its cleaning. Present systems accomplish cleaning through a built-in water spray manifold. The manifold can be connected to an external water supply to provide a method for washing the vapor generator core.

Although low temperature freezing may be a concern, some of the cited advantages of the steam Rankine bottoming cycle are:

- Unlike the candidate organic fluids, water is stable and does not decompose at diesel exhaust temperatures.
- System does not need emergency boiler bypass or other overheating protection devices.
- Soot fouling can be burnt out by running diesel exhaust for a few minutes with no water flow.
- Easier in-field service.

Brayton Bottoming Cycle - The Exhaust-driven Brayton bottoming system (BBS) represents an extension of the turbocompounding concept. United Technologies Research Center (UTRC) has studied BBS for a given adiabatic diesel engine under contract from DOE/NASA and concluded that a pressurized BBS (PBBS) is the preferred system. The engine exhaust gases in the PBBS are separated from the cycle working fluid (air) by the heat exchanger. Compressed air is heated before it expands in the turbine down to ambient pressure. The heat exchanger, however, could be a large component to achieve the desired effectiveness.

The UTRC analysis [3] indicates an optimum cycle pressure ratio of 5:1, a rotor speed of approximately 70,000-80,000 RPM, and a 40:1, two-stage speed reduction gear box. The cited advantages over a closed Rankine cycle are as follows:

- Open cycle, uses air as working fluid
- Turbomachine technology readily applicable
- Achievable faster cycle response

- Simpler hardware, smaller and likely lower weight

Stirling Bottoming Cycle - Cummins Engine Company, along with MTI, is studying a bottoming system based on the Stirling cycle for an adiabatic diesel engine, under a contract from DOE/NASA. The results of this study are pending. However, the performance logically depends upon the selection of a working fluid. The ideal fluid for the Stirling cycle is hydrogen. The sealing of fluid, as in the case of an organic Rankine bottoming cycle, is likely to be a serious development issue.

II.3.2 BOTTOMING CYCLE SYSTEMS

In addition to the information of the preceding section, a thorough comparative evaluation of steam Rankine, organic Rankine, and air Brayton cycle systems, designed for an adiabatic diesel long-haul truck, has recently been completed [4]. This information was used extensively as a guideline for the comparative analysis in this study and, for completeness, is briefly summarized in this section.

SYSTEM FEATURES

Steam Rankine Systems - The system is schematically illustrated in Figure II.3-2. A 14 percent improvement in fuel economy over the diesel core was estimated for optimized heat exchanger sizes. In the system, a condenser assembly replaced the conventional radiator, and the heat recovery steam generator replaced the truck muffler, with similar back pressure and muffling characteristics. The power module included a positive displacement expander and a feed water pump. The expander used was a two-cylinder piston device operating at engine speed through a chain drive to the flywheel drive gear. This chain drive replaces

a multistage gear box, which would be associated with reduction from high turbine speeds. Further, a piston expander avoids the inherent low efficiencies associated with small axial flow turbines, caused by the relatively significant tip clearance losses. In addition, working fluid, being water, exhibits a high specific enthalpy. Thus, the flow rate per unit power output is low, and the system is relatively more compact. A major drawback of the steam Rankine bottoming cycle system is the possible damage to system components due to freezing.

Organic Rankine Systems - For lower temperature systems, the organic fluid properties can offer a performance advantage over the water based system. The organic Rankine system was developed and studied under a DOE-sponsored Truck Bottoming Cycle Program. A considered organic fluid was Fluorinol-85, with a maximum fluid working temperature of 288°C (550°F). The heat source was 482°C (900°F) exhaust gases from a conventional water-cooled diesel. A highway fuel economy improvement of 12% over the diesel core was demonstrated. However, if higher exhaust gas temperatures are associated with the LHRE, organic fluids with higher working temperature capabilities would be required such as the "RC-1". Figure II.3-3 shows the schematic diagram of a simple RC-1 system, with flow conditions noted for operation with a turbocharged diesel. The RC-1 system has a significantly higher mass-flow rate and, hence, lower specific work in the expansion process. The system demonstrated a fuel economy improvement of 15 percent over the core diesel engine [1].

Figure II.3-4 shows a proposed alternate scheme, where the organic liquid flow is divided in two streams. The first part is vaporized in a compound power turbine exhaust heat-recovery heat-exchanger and then expanded in high temperature turbine #1. The second part of the fluid is directed to an enlarged regenerator for vaporization at a lower temperature by the superheated vapor, leaving the high temperature turbine, which then expands in low temperature turbine #2. Both turbines #1 and #2 are mounted on the same shaft with the turbocompounding (power) turbine. It is noted

that the addition of turbocompounding will further lower the exhaust temperature entering the bottomer, thereby reducing the temperature for the working fluid RC-1. This compound system will result in an overall improved performance, although the additional vapor generator, turbine stage, and increased controls for flow splits make the system rather complex and more costly.

Two additional concepts working on the organic Rankine bottoming cycle were considered. These concepts are illustrated schematically in Figures II.3-5 and 6. The EER turbine can either be coupled directly to the engine crankshaft, as represented by Figure II.3-5, or it can be used as an additional pressure boosting device shown in Figure II.3-6. However, performance optimization studies reported in Section II.1 have identified an optimum reciprocator compressor pressure ratio that requires only a simple, single stage compressor. Hence, increased reciprocator boosting via multi-stage compression of the charge air is not necessary.

Another modification to the basic system would be the incorporation of a regenerator between the working fluid leaving the bottomer turbine and that leaving the feed pump. The addition of this extra component can result in reduced condenser and vapor generator sizes, slightly improved thermal efficiency, and better vapor generator corrosion resistance. The drawbacks include the additional cost and system complications.

Air Brayton System - The Brayton system operates on an open cycle, with air as its working fluid. The system is free from problems associated with high pressure working fluid containment and sealing, as with the closed cycle steam or organic Rankine systems. Incorporation of a heat exchanger as part of the cycle distinguishes this system from the turbocompounding approach. The Brayton system can be either a sub-atmospheric or a pressurized system. The pressurized system demonstrated a modest 8 percent improvement in fuel economy over a core diesel. The added hardware of compressors and air-to-air intercooler or heat exchanger makes it less attractive, from a standpoint of high cost and economic payback.

SYSTEM LIFE CYCLE COST ASSESSMENT

The comparative evaluation in [4] included the bottoming systems performance, fuel economy, cost, and economic payback, when used for EER from the exhaust of an adiabatic diesel operating in a long-haul truck duty cycle. The evaluations were based on performance data resulting from various alternate power cycle configurations designed and developed under the DOE/NASA contracts, for consistent adiabatic diesel exhaust conditions.

Performance - Brake specific fuel consumption is a fundamental performance parameter which governs the vehicle fuel economy. Figure II.3.7 summarizes the bsfc results for various diesel/alternative power cycle combinations [4]. These results show a predicted 19 percent range of bsfc values between the baseline turbocharged (TC) diesel and the best diesel/alternative power cycle configuration: turbocompound (TCPD) with organic bottomer. The TCPD alone shows a 6 percent bsfc gain over the TC diesel.

Capital Cost - Initial capital investment on a system is one of the major factors in deciding its relative desirability. For fuel efficient diesels, the annual savings in fuel must compensate for any extra capital cost within some fraction of the vehicle's useful life. The purchase price of such engines/vehicles depends upon their production rate, as well as the pricing environment. The estimated capital cost of various alternative power cycle systems is tabulated in Table II.3-1, [4]. The basis of the data is a production rate of 10,000 units per year. The bottom line in the table gives the total price of the system. Although the incremental price difference between a TCPD and a steam Rankine system is \$4,070, the price difference for equal power level compound engine systems will be considerably lower due to the higher efficiency of the steam system.

Maintenance and Repair Cost - Inclusion of the alternative power cycle amounts to a rather significant subsystem addition to the diesel power plant, thereby adding extra maintenance and repair

burden. Table II.3-2 illustrates the maintenance and repair cost estimates developed in [4], based on a leveled annual payment for a lifetime maintenance and repair contract. Although the maintenance and repair price difference between the TCPD system and the steam Rankine system is \$1,150, as obtained directly with the data in Table II.3-2, this difference in price will be substantially lower when considered for the compound engine system at equal power level.

Economic Payback - The prospect of widespread implementation of any of the alternate power cycle systems is entirely dependent on the system ability to compete on an economic basis. The survey of heavy-duty trucking engine requirement indicates a desired payback time of 1.5 to two years [5]. A payback time for the TC/steam system of 4.7 years is calculated in [4], based on available data.

This result does not indicate that this system is economically attractive at current fuel prices. In fact, the payback calculations indicate that, at the current fuel price, none of the candidate alternative power cycle systems is economically attractive as a replacement for the TCPD aftercooled diesel engine.

GENERAL REMARKS

The bottoming cycle system is an attractive concept from the standpoint of both fuel economy and overall vehicle performance. However, the advantages of these systems are outweighed by capital cost and payback time associated with their implementation. Based on prior evaluations, the steam Rankine cycle exhibits the best opportunity of the bottoming cycle candidates for a reasonable payback period, within the parameters and constraints of the reported study [4]. It appears that an even more appealing package price could be achieved with further commitment to development and production of a bottoming cycle system on a widespread basis. On the other hand, practical experience with the organic Rankine cycle

systems and the organic working fluids has been reported [1]. This system can suit the current program to a greater extent with some modifications. A critical parameter in selecting among the Rankine systems is the temperature of the LHRE exhaust gases at the inlet to the bottoming system. This issue will be addressed in the next section.

Although considered beyond the scope of the current program, the idea of further utilization of the remaining exhaust gas thermal energy downstream from the bottomer is stated here. The LHRE will be an uncooled engine, which can result in the absence of the "coolant" used for in-cab heating. The exhaust gases at 395°K (250°F) can finally be used to heat the cab air via a gas-to-gas heat exchanger. Problems of such systems are not yet fully resolved. Other alternatives include EER power utilization in driving the engine accessories, e.g., cooling fan, air compressor, air conditioner compressor, etc., instead of the direct coupling to the crankshaft. These concepts, along with other EER schemes, require further exploration.

II.3.3 BOTTOMING SYSTEM SELECTION

Recent in-house simulation studies on a turbocharged aftercooled turbocompounded engine with various insulation levels, optimized for the ADECD program, indicate an exhaust gas temperature in the range of 673 to 738 K at the power turbine exit. The temperature at the power turbine inlet is in the range of 700 to 766 K. At this range of exhaust temperatures, an organic Rankine bottoming cycle working fluid is more effective in EER than a steam bottoming system.

WORKING FLUID SELECTION

The concurrent LHRE system simulation analyses was completed, predicting the exhaust gas temperatures for various risk or

insulation levels. Based on the performance analysis results, a more detailed analysis was carried out to further evaluate the three Rankine bottoming cycle systems, using RC-1, Fluorinol-85 (FL-85), and steam. The bottomer performance calculations were made for a LHRE, with and without turbocompounding, for the low, moderate, and high risk reciprocator systems. Some of the performance results are directly extracted from [4]. The calculated and derived results are summarized in Table II.3-3.

The results of Table II.3-3 indicate that for all the LHRE configurations and simulated exhaust conditions, the net output of the steam Rankine cycle is lower than the respective organic Rankine systems. The dependence of a Rankine bottoming cycle net output on the diesel exhaust temperature as the heat source was explained [4] and is shown in Figure II.3-8. The predicted LHRE exhaust temperature is in the range of 673-766 K (1212-1379^oR). In this low temperature range, the organic system outperforms the steam system because of its thermophysical properties.

For optimum performance of the bottoming cycle, the working fluid properties must be matched to the heat source temperature. Here, the saturation temperature of the working fluid becomes the key property, relative to the exhaust (source) temperature, as it determines the minimum temperature difference between the exhaust gas and working fluid. This minimum difference is known as the 'pinch temperature' difference and is illustrated in Figure II.3-9. For specific combinations of diesel exhaust and working fluid conditions, the pinch point effect imposes a minimum desirable stack temperature and, therefore, a maximum vapor generator heat recovery efficiency. Therefore, pinch temperature difference is a significant factor, impacting the vapor generator surface area requirements and corresponding size, weight, and cost. In fact, the steam Rankine system considered in [4] was designed for a significantly wider pinch temperature difference than the organic RC-1 system, with a compromise in heat-addition efficiency. The organic system vapor generator is about twice as large in size as the steam generator. The design stack temperature for the steam

Rankine cycle was 485 K (873^oR). If the pinch temperature difference was reduced to the level used for the organic cycle, it would have allowed the extraction of heat from the diesel exhaust down to the same organic system stack temperature of 448 K (807^oR). This additional heat recovery would boost the power of the steam cycle to be equal to that of the organic system, but only with a larger vapor generator size. It is concluded that for similar power performance under similar diesel exhaust/stack conditions, the vapor generators of either systems will be comparable in size. This should account for the majority of the differences in cost of the two bottoming systems, as reported earlier [4].

II.3.4 CONCLUSIONS

The organic Rankine bottoming system recommended for the Adiabatic Diesel Reference Engine is schematically illustrated in Figure II.3-10. The working fluid recommended is Fluorinol-85, based on economical considerations, for the predicted LHRE exhaust temperature range. For truck installation, the bottomer condenser can be configured similar and side-by-side to the air intake system. Alternatively, since an air-to-air charge radiator would be already mounted on the truck frontal area, a front mounted bottomer condenser is recommended at this time.

II.3.5 REFERENCES

1. DiNanno, L. R., DiBella, F. A., and Koplow, M.D.: An Rc-1 Organic Rankine Bottoming Cycle for an Adiabatic Diesel Engine, (TE4322-251-83, Thermo Electron Corporation, NASA Contract DEC3-302), NASA CR-168256, 1983.
2. Demler, R. L., Hug, H. A., Krepchin, I. P., Poulin, E. C., and Walker, D. H., "Steam Bottoming Cycle Study for Heavy Duty Transport," Proceedings of the Twenty-First Automotive Technology Development Contractors Coordination Meeting, Dearborn, Michigan, November 1983, pp. 149-154.
3. Khalifa, H. E., "Exhaust-Driven Brayton Bottoming Systems for Adiabatic Diesel Engines," UTRC, Proceedings of the Twenty-First Automotive Technology Development Contractors Coordination Meeting, Dearborn, Michigan, November 1983, pp. 141-148.
4. Bailey, M., "Comparative Evaluation of Three Alternative Power Cycles for Waste Heat Recovery from the Exhaust of Adiabatic Diesel Engines," DOE/NASA/50194-43, April 1985.
5. Strawhorn, L. W., and Suski, V.: Future Heavy Duty Trucking Engine Requirements, Proceedings of the Second Automotive Technology Development Contractor's Coordination Meeting, SAE P-155, pp. 233-260, 1985.

Table II.3-1: Price Estimates for Alternate Power Cycles

Power Cycle hardware	Turbo-compound	Brayton	Steam	Organic
Prime movers and speed reduction	\$2000 (1 wheel)	\$4273 (3 wheel)	\$2230 (2 cyl)	\$2664 (1 wheel)
Heat-recovery heat exchanger (heat transfer area)	NA	\$1586 (39 sqm)	\$1750 (19 sqm)	\$1750 (43 sqm)
Heat-rejection heat exchanger (heat transfer area)	NA	\$571 (39 sqm)	\$1060 (23 sqm)	\$1458 (39 sqm)
Controls and fluid inventory	NA	NA	\$1030	\$1034
Total estimated price	\$2000	\$6430	\$6070	\$8380

* Ref: Bailey, 1985

Table II.3-2: Maintenance and Repair Costs, Estimates for Alternative Power Cycles

Power Cycle hardware	Turbo-compound	Brayton	Steam	Organic
Prime movers and speed reduction	\$350 (1 wheel)	\$450 (3 wheel)	\$450 (2 cyl)	\$450 (1 wheel)
Heat-recovery heat exchanger	NA	\$200	\$400	\$400
Heat-rejection heat exchanger	NA	\$200	\$400	\$400
Controls and fluid inventory	NA	NA	\$250	\$350
Total estimated annual cost	\$350	\$850	\$1500	\$1600

* Ref: Bailey, 1985

Table II.3-3: ADE Bottoming Cycle Performance Comparison

WASTE HEAT UTILIZATION SYSTEMS

RECOMMENDED SYSTEM:

- o Performance predictions of various Rankine cycle systems

SYSTEM	ITEM	LOW RISK			MEDIUM RISK			HIGH RISK		
		ORC1	ORC	SRC	ORC1	ORC	SRC	ORCA	ORC	SRC
TC + TCPD+BC	Temp (K)	673			711			738		
	Net kW	21	20	8	24	22	12	26	25	15
TC + BC	Temp (K)	700			732			766		
	Net kW	23	21	11	25	24	15	28	27	18

TC = Turbocharged; TCPD = Turbocompounded; BC = Bottoming Cycle
 ORC1 = Organic Rankine Cycle (RC-1)
 ORC = Organic Rankine Cycle (FL-85)
 SRC = Steam Rankine Cycle

- o Organic Rankine cycle offers higher net horsepower in ADE temperature application range.

Figure II.3-1: Various Exhaust Energy Recovery Systems

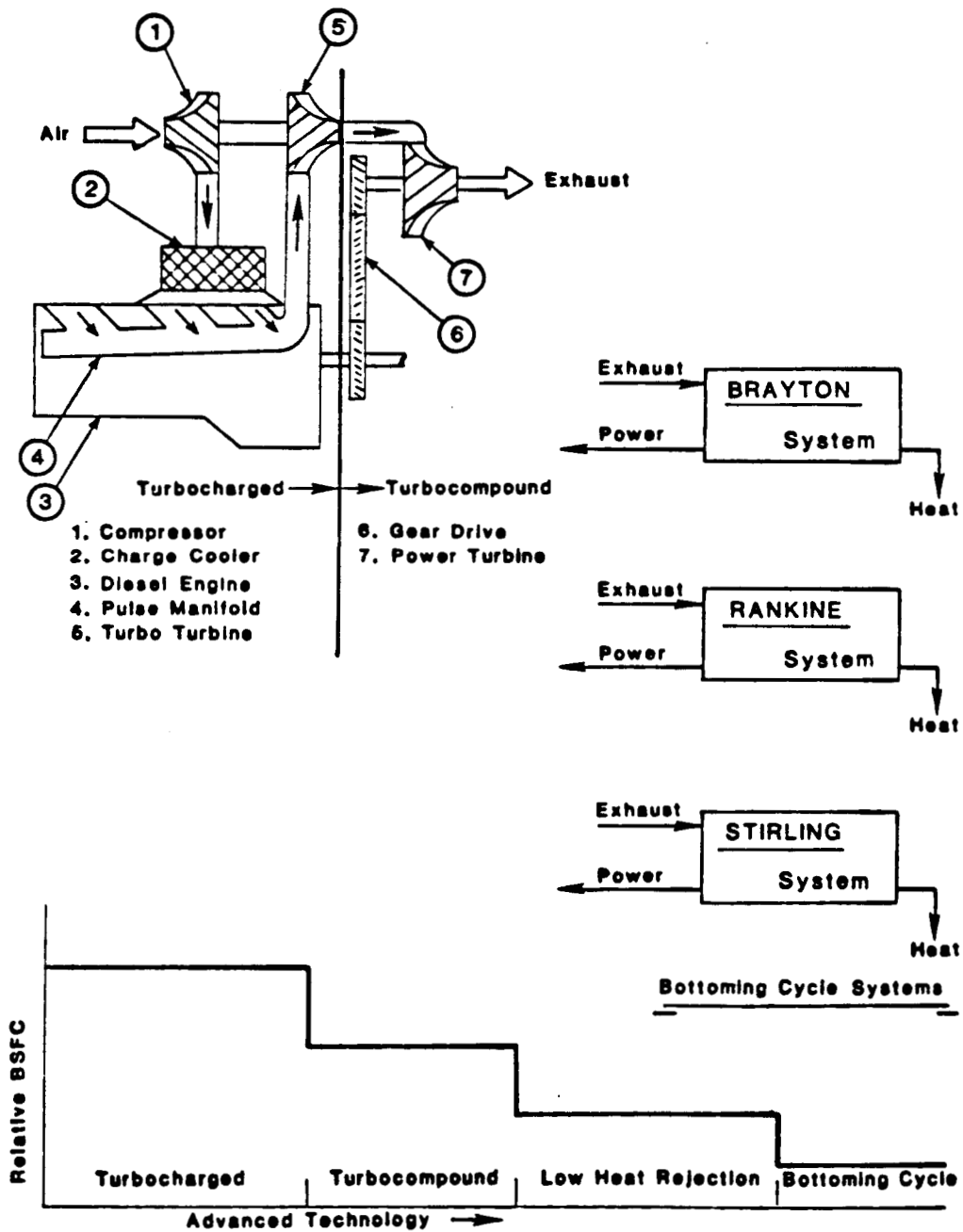


Figure II.3-2: Diesel/Steam System Schematic

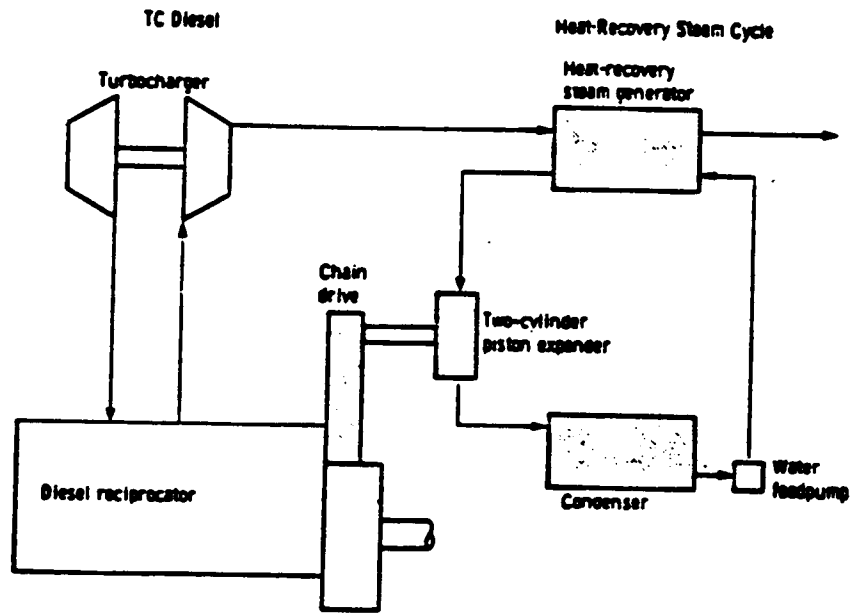


Figure II.3-3: Diesel/RC-1 Organic System Schematic

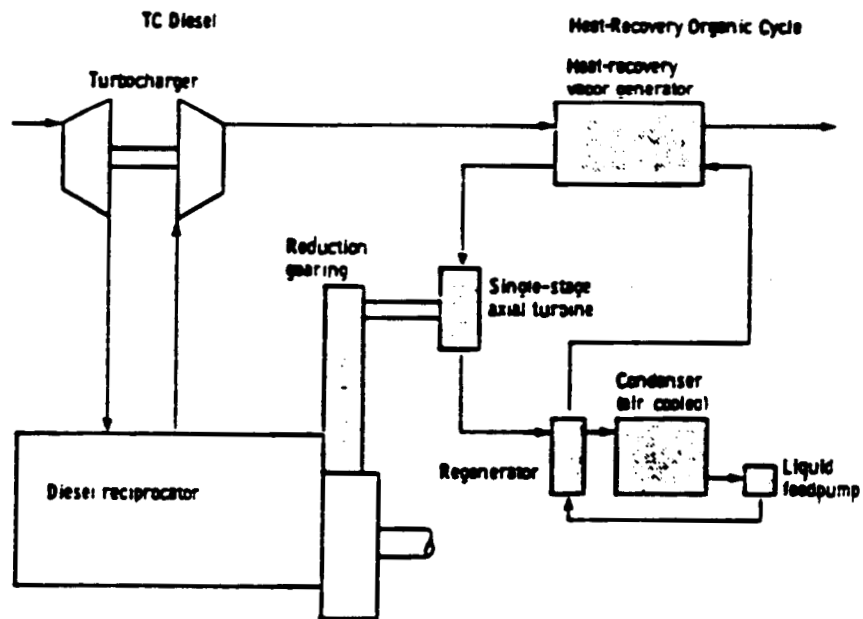


Figure II.3-4: Schematic of an Organic Rankine RC-1 Cycle with Internal Heat Regeneration and Two Power Turbines

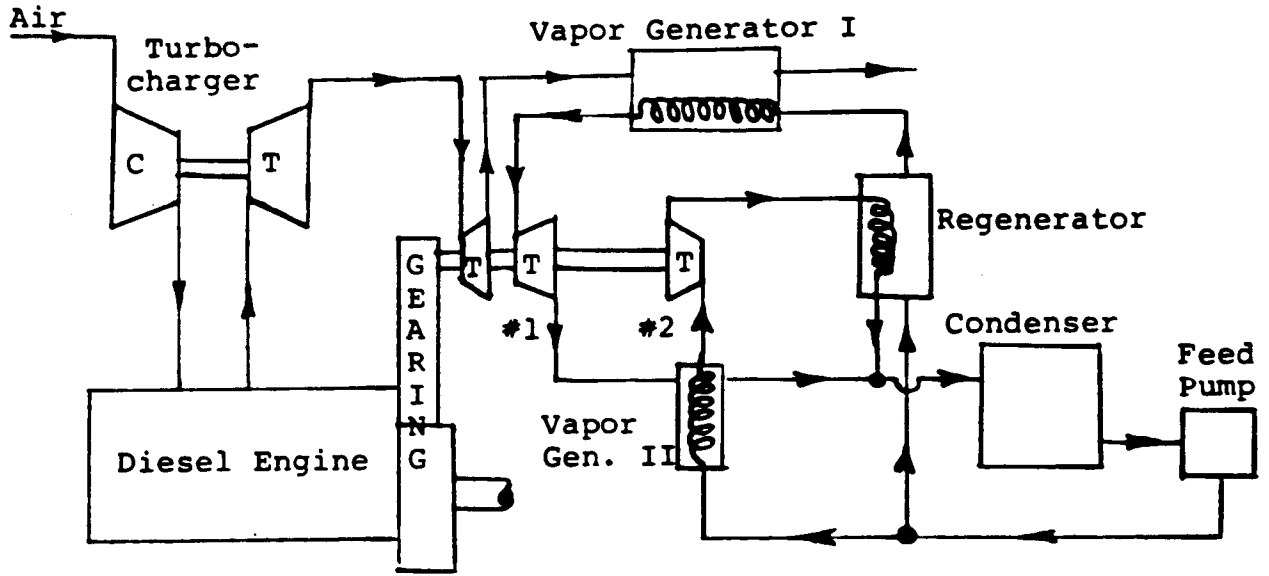


Figure II.3-5: Organic Rankine Bottoming System with Heat Regeneration. Single Power Turbine

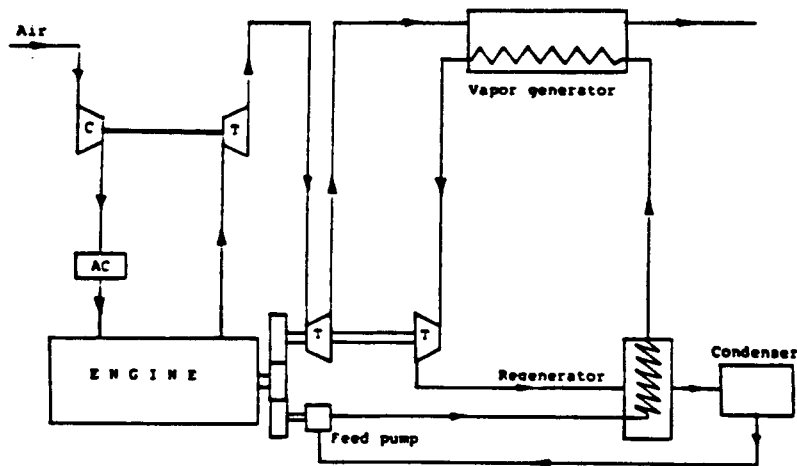


Figure II.3-6: Organic Rankine Bottoming System with Heat Regeneration. Two Stage Turbocharging

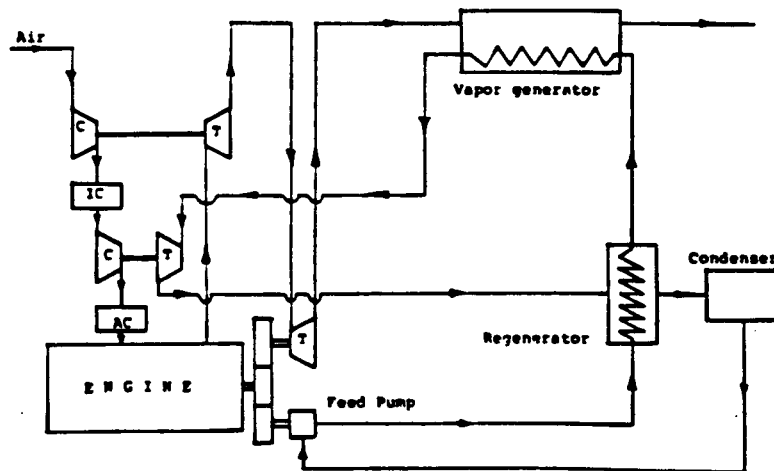


Figure II.3-7: Specific Fuel Consumption for Various Diesel Alternative Power Cycle Combination

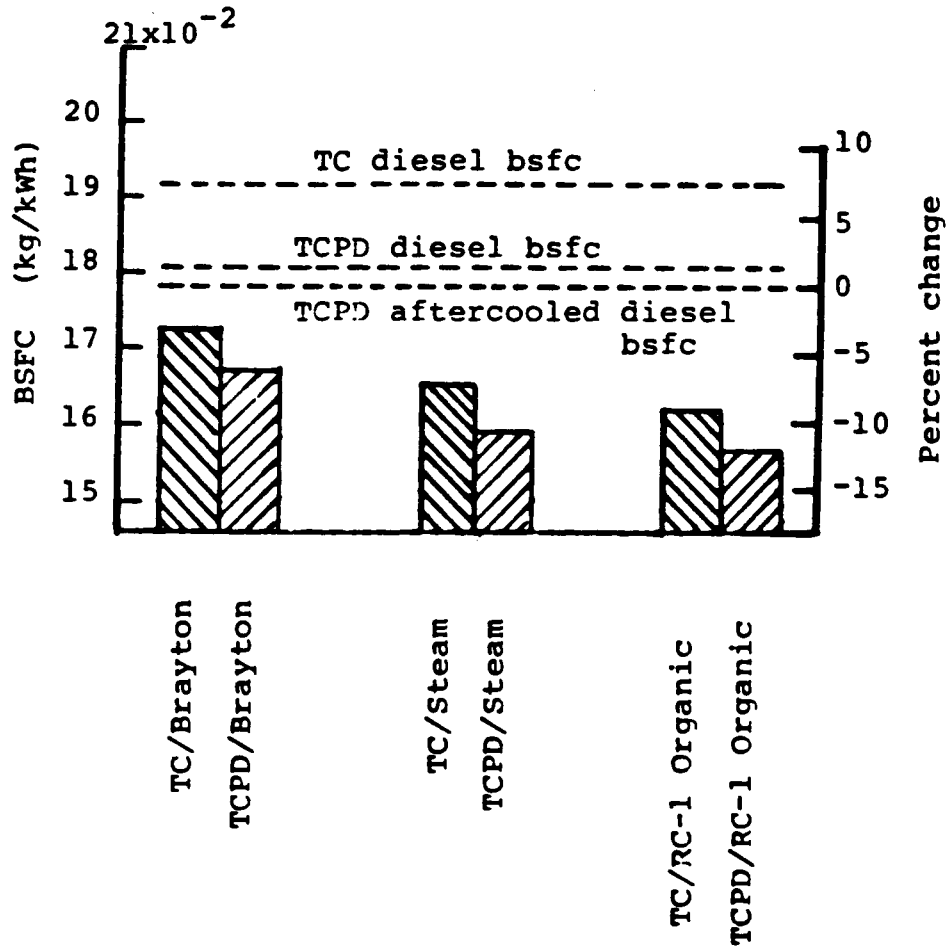


Figure II.3-8: Sensitivity of Alternative Power Cycle Performance to Diesel Exhaust Temperature

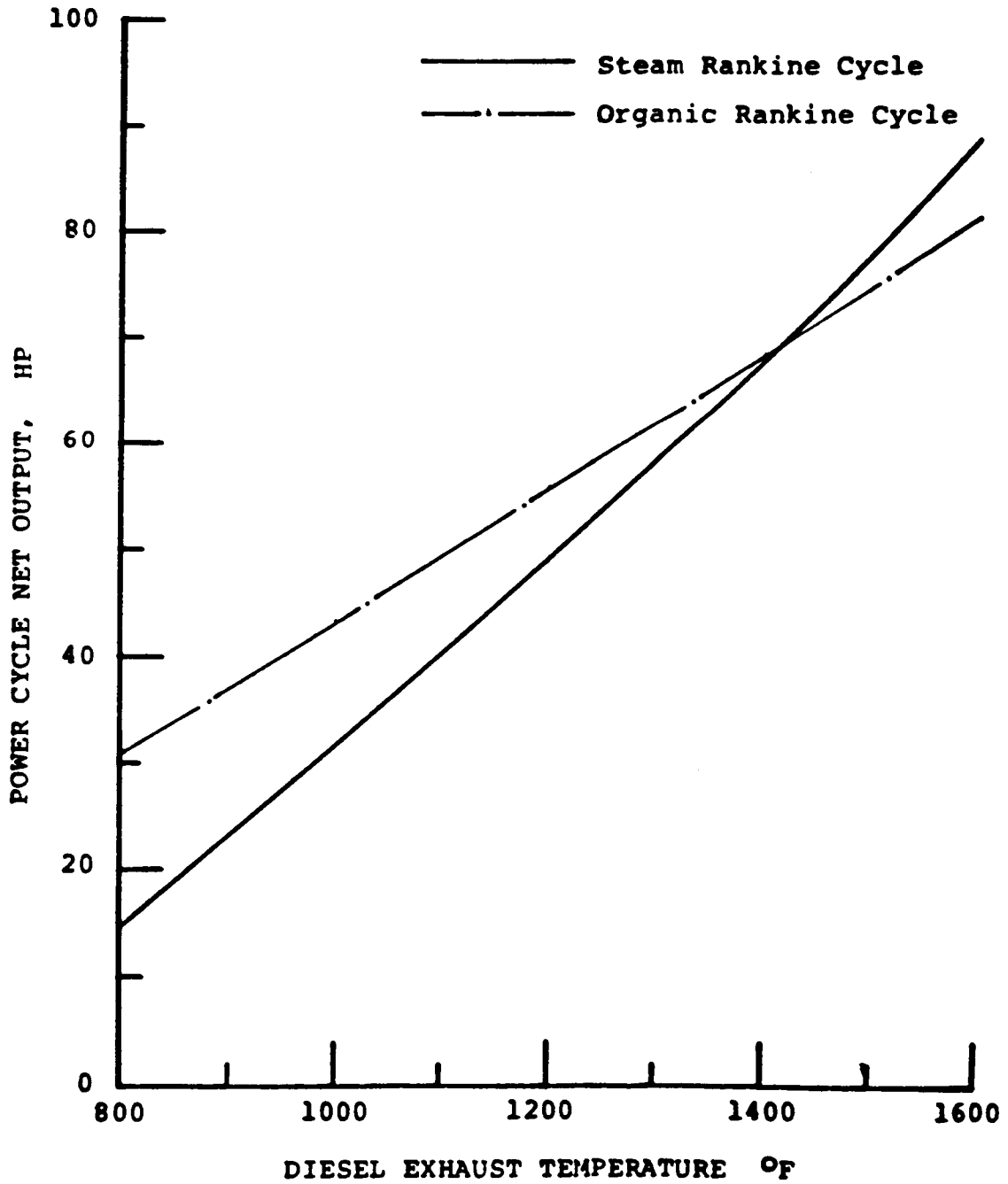


Figure II.3-9: Temperature-Entropy Diagram for Rankine Bottoming Cycle

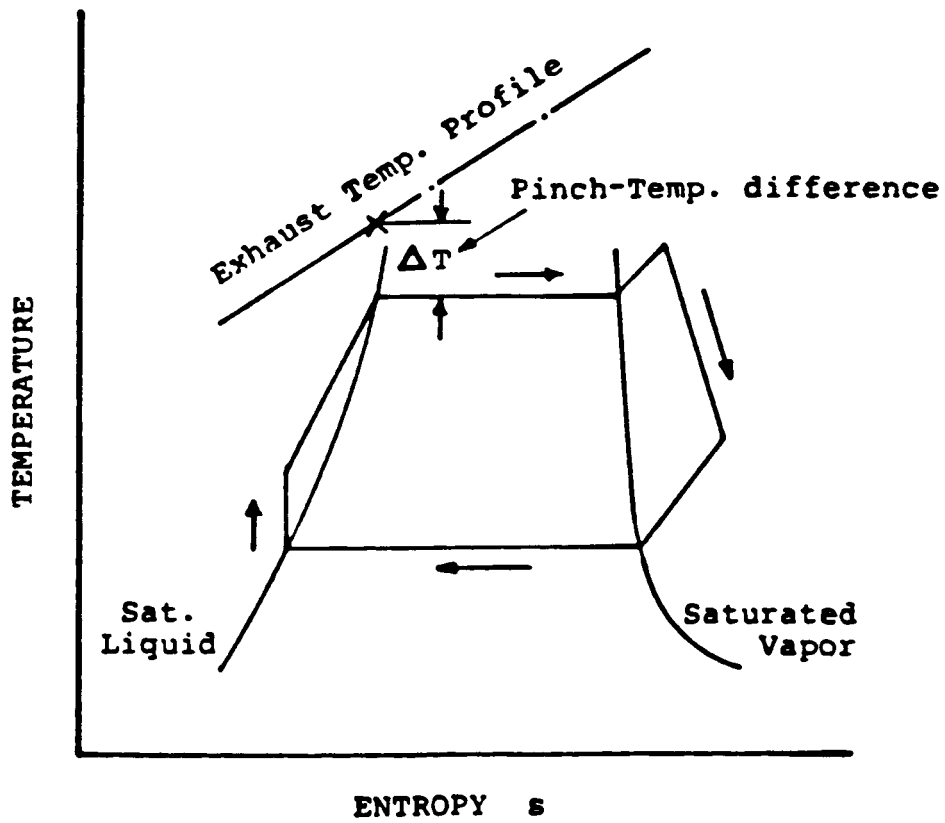
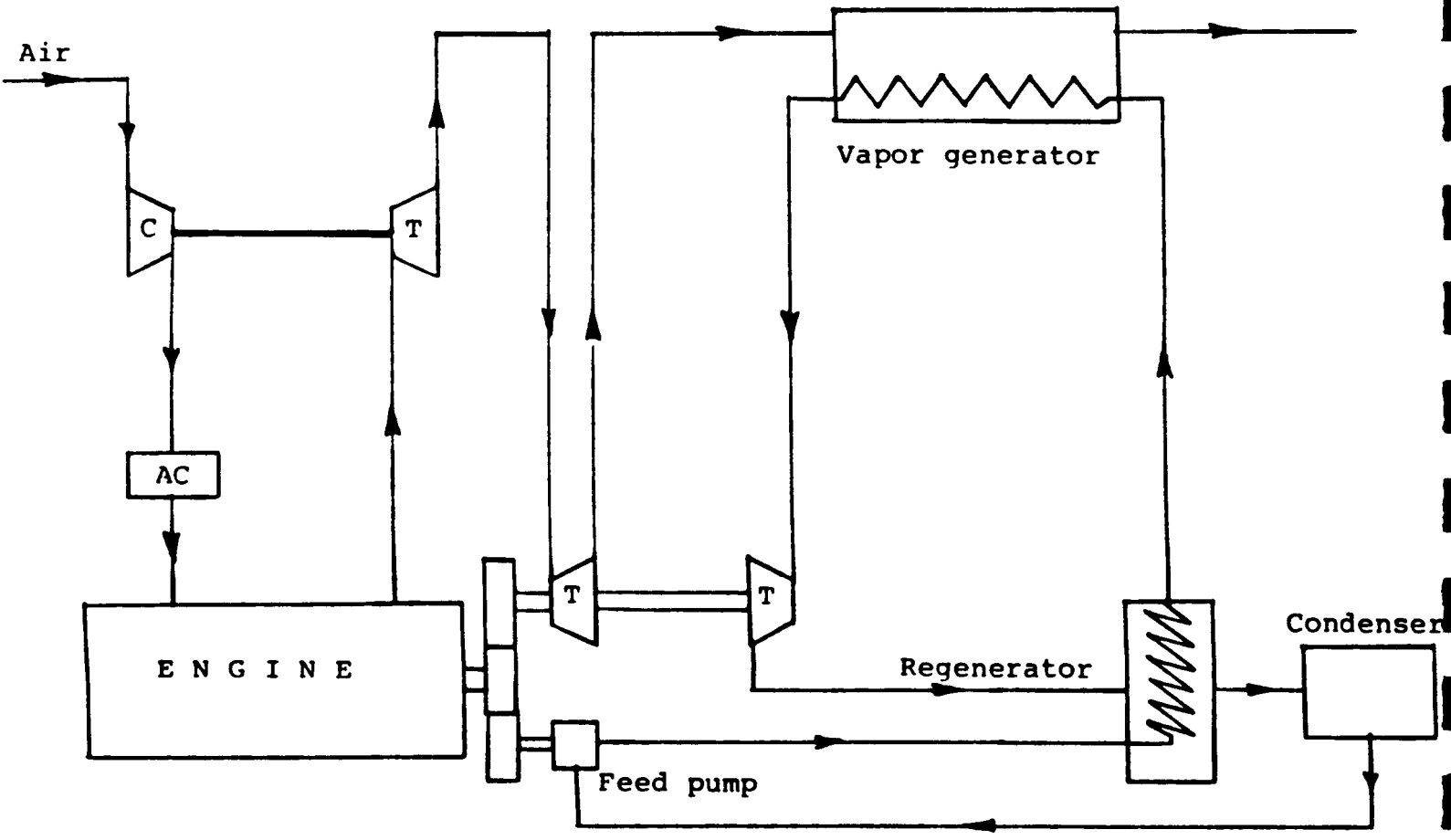


Figure II.3-10: Recommended Organic Rankine Bottoming System.
[Turbocompounding and Regeneration are Optional Features]



II.4 LIFE CYCLE COST EVALUATION

New diesel engine technology typically offers benefits of reduced fuel consumption, but not without the potential of some associated costs. These costs would come as a higher purchase price and, perhaps, higher maintenance cost. The method of selection of the best mix of new technology must, therefore, properly weigh benefits and cost.

The concept of life cycle cost has been, and continues to be, applied to planning and evaluation of various military hardware, and to such commercial tasks as establishing prices for service contracts. The latter application is used particularly in the heavy-duty diesel engine industry. For any commercial investment decisions, life cycle cost is an especially relevant rational criterion, since it identifies the ultimate cost/benefit performance of a possible decision. The approach to life cycle cost evaluation of the ADE involved three steps:

- 1) Synthesis of a number of engine candidate designs, each embodying different levels of technology,
- 2) Coupling each with a number of systems for utilizing exhaust gas energy
- 3) Evaluating each combination in terms of desirability

Life cycle cost is defined as the total of all costs associated with an article throughout its planned or useful life. Initial costs are combined with the present values of all costs which are predicted to occur later in the life cycle. For a commercial diesel engine, life cycle cost can accurately be represented by the sum of purchase price, fuel consumption, and maintenance.

Purchase price is established by the market for truck power plants of the given power output. Price variations may exist due to perceived life cycle benefits of some engines over others. Fuel consumption is normally estimated by vehicle/road cycle simulations, making use of complete engine performance maps and vehicle route characteristics. Maintenance cost is estimated by special Monte-Carlo simulations which are based on applicable data acquired from the field. These data include the frequency of failures in several different categories of severity, and the labor and parts costs incurred by failures in each severity level.

After some preliminary investigation, it was determined that these normal LCC approaches were unsuitable in several ways for the task of appraising a large number of conceptual designs that consist of substantially new technology. First, while the price of such an engine would still be primarily governed by demand in the marketplace, there would be additional concerns related to profitability of the new technology, so that current market prices could not be expected to apply if reductions in fuel consumption were one of the engine's features. Second, since the problem was to identify technological directions among a large number of alternatives, time and scope did not permit the establishment of complete performance maps for calculating fuel consumption. Lastly, no field data exist to support the ordinary sort of maintenance cost analysis, and engine reliability would have to be estimated from little more than proposed cross-sectional drawings.

In response to these shortcomings, a new life cycle cost model was developed for the purpose of evaluating the 40-plus candidate engine configurations that resulted from the early ADECD design work. This new model provides for:

- 1) Engine pricing in a manner consistent with the quality of available estimates of the costs of advanced-technology components and with the mandate of profitability.

- 2) Fuel consumption estimates based upon bsfc at rated conditions only.
- 3) Maintenance cost estimates based primarily on relevant economic variables and parameters, rather than failure mode effects and frequency analysis.

While the pricing and fuel consumption calculation methods are similar to those used in other work [1,2], the approach to maintenance cost estimation is believed to be new. The engine-related variables of the new model are limited to:

- 1) A parts count broken down into a number of pre-defined categories.
- 2) Bsfc at rated conditions.
- 3) The price of the exhaust energy recovery system (if any).

In addition, the new LCC model has explicit dependence on a number of parameters which largely transcend the particular characteristics of the engine(s) being evaluated and are more "environmental" in nature. This fact makes possible (indeed requires) LCC evaluation in what amounts to another level, in addition to that of the variables associated with each candidate engine. LCC evaluation must therefore be made according to a consistent strategy that accounts for variability in these parameters.

In the sections that follow, the details of the model and the strategy for its application are developed and discussed. For completeness, the design characteristics of the ADECD engine candidates are reiterated in general terms, and the application of the life cycle cost model to their assessment is discussed in detail.

II.4.1 CANDIDATE CONFIGURATIONS ANALYZED

The objective of LCC evaluation in the ADECD program was to select the best from among 42 different low heat rejection engine/exhaust energy recovery system configurations. These configurations were synthesized from a group of seven engines and six exhaust energy recovery concepts. Six of the engines were composed of selections from a group of 47 different advanced component concepts developed earlier in the work. The seventh engine was for comparison purposes: an advanced state-of-the-art (SOA) production engine.

Preliminary analysis based on a consensus of in-house experience led to each of the low heat rejection engines (LHRE's) having an in-line 6-cylinder configuration, but each incorporates a different type or level of advanced technology. All make use of charge air cooling, and all run without water cooling of components.

As reported earlier, with respect to the 1995 technology development, the engines were grouped in successively higher levels of technical risk. Three risk levels were defined: moderate, intermediate, and high. Moderate risk is to denote that the concept technology can probably be demonstrated successfully with reasonable research effort between now and 1995. Intermediate risk denotes that some rather challenging research is required for the same time frame. High risk denotes the necessity of major research and/or breakthrough(s) for successful development. The level of cylinder insulation increases with risk level, as does the level of friction reduction and other technical benefits. The engines' characteristics are briefly described as follows:

SOA Current state-of-art.

MR1 Moderate risk proposal 1. The main feature of the moderate risk engines is the use of ceramic coatings for cylinder insulation.

MR2 Moderate risk proposal 2. The same as MR1 except for the use of advanced mechanical components for friction reduction, in addition to the cylinder insulation treatments.

IR1 Intermediate risk proposal 1. The main features of the intermediate risk engines are: air gap insulation of high temperature metal cylinder surfaces, and the use of advanced mechanical components for friction reduction.

IR2 Intermediate risk proposal 2. The same as IR1 except for additional mechanical refinements.

HR1 High risk proposal 1. The main features of the high risk engines are the use of ceramic components with air gap insulation of the cylinders, and advanced mechanical technology for friction reduction.

HR2 High risk proposal 2. The same as HR1, except for a mechanism permitting refinement of part-load fuel economy over and above the level obtainable through digital injection control.

Six exhaust energy recovery scenarios were evaluated for each engine. These systems have been studied and compared extensively in [2], and extensive use of these results has been made in the present study. The exhaust energy recovery systems (EERS) were:

turbocharged only (TC)

...with turbocompounding (TC+TCPD)

...with an organic Rankine cycle system
(TC+ORCS)

...with a steam Rankine cycle system
(TC+STEAM)

...with turbocompounding and organic Rankine cycle systems (TC+TCPD+ORCS)

...with turbocompounding and steam Rankine cycle systems (TC+TCPD+STEAM)

II.4.2 LCC MODEL

For heavy-duty diesel engines, life cycle cost is accurately represented by the sum of purchase price, fuel costs, and maintenance costs. The LCC model consists of a separate sub-model for each of these components, and its details will be discussed accordingly. To a limited extent, the formulation of the sub-models has been tailored to the present application, but it is suggested that similar approaches may be applicable to many other types of LCC studies. It is noted that the model formulation used the old "U.S." customary engineering units. This section will report on this LCC model formulation with the results reported in S.I. units as appropriate.

PRICE

Each of the systems under consideration consist of an engine and an exhaust energy recovery system (EERS). Price estimates for the EERS are available [2], as these systems are current technology and are being developed for sale by their respective manufacturers. Since the engines are relatively advanced, a separate price model was devised for them.

Engine price has two contributing factors. The first of these is the customers' demand for engine power, and the second is the desire of the engine manufacturer to realize a profit. Profitability at the desired level would probably not be possible

with extra-cost technology except for the experience that engines can be sold at higher prices if their additional technology results in savings elsewhere for the customer. It is, therefore, expedient to configure the price model so as to enforce cost recovery and normal profit from all new technology. Then, if the resulting LCC is unchanged from the present state-of-the-art, there is no overall saving (nor overall loss) for the customer and, presumably, no impact on sales. If the LCC is lower than the current SOA, then the customer saves money and the manufacturer profits. If, on the other hand, the LCC is higher than the current SOA, the manufacturer must lower price to at least achieve LCC equality with the current SOA and risk that the engine may not be profitable to sell.

Given the add-on nature of the EERS price, the market for engine power, and the requirement of profitability, the price equation for the engine/EERS system was defined to be:

$$PR = P1 \times P2 + P3 \quad (1)$$

where P1 is a "technology scaling factor," P2 is a "power scaling factor," and P3 is the price of the EERS. Each of these is discussed separately below.

Technology Scaling Factor - The technology scaling component of the price model was constructed along the lines of some other concept-engine price models [1]. The basis of this model is a comprehensive parts list pertaining to a production engine: in the present case developed for a 223.7 kW [300 BHP] state-of-the-art diesel engine, and shown in Table II.4-1. Based on this type of list, the cost of an advanced engine can be estimated by appropriate multiplication of the known price of affected parts.

As illustrated in Table II.4-1, many individual parts are grouped into more meaningful sub-assemblies according to four primary criteria. For engines with radically different mechanisms, additions and deletions can be made from the list.

- 1) A sub-assembly should be a group of parts which have a single, unique function that is part of the generic diesel engine concept.
- 2) Further, the constituents are expected to be impacted by new technology in a manner which is separate and easily distinguished from that of other parts of the engine.
- 3) A sub-assembly may be subject to complete elimination in a low heat rejection engine.
- 4) Lastly, many parts which were not expected to be upgraded or eliminated were grouped for convenience.

In order to facilitate analysis, items in the list are divided into groups of roughly equivalent cost. Where detailed cost information for certain sub-systems is not available, this technique allows for estimation by analogy to other parts of similar size and complexity. Thus, the sub-assemblies are characterized by a number of relative cost categories. Components in the first category are deemed to have a unit cost, with components in each higher category having a successively higher ratio of cost to the unit. To obtain the unit cost of a standard part(s), one must determine the quantity of that part in the engine, multiply by the cost factor pertaining to its category, and divide the price of the standard engine by the total:

$$s = \frac{P_{SOA}}{\sum_{i=1}^7 N_i f_i} \quad (2)$$

Where N_i is the number of parts (sub-assemblies) which cost roughly f_i times the cost of a part in the first category. Whereas f_1 is, by definition, unity, the values of $f_1 - f_7$ will probably vary somewhat among manufacturers. Using a typical price for the

standard engine (P_{SOA}), with additions for a radiator and charge cooler, the unit cost(s) was found to be approximately \$10 for the example shown in Table II.4-1.

Relative to the standard engine, the LHRE candidates will, in general, contain two additional types of part in each cost category. These will be "special substitute" parts, for which technology already exists but which require high precision, special alloys, etc. Quantities of these are represented by symbols M_1, M_2, \dots, M_7 , according to whether they replace standard parts in categories 1 - 7, respectively. An additional cost unit multiplier, sp - a function of the maturity of the diesel engine application of these types of parts - is applied to these categories. In the same manner, "high technology substitute" parts, for which new technology is required, will be counted in categories L_1, L_2, \dots, L_7 , with an additional cost unit multiplier h . Also note, since the LHRE engines have no water systems, all water-related hardware would be deleted from their "parts list."

The technology scaling component of the price equation is thus defined as:

$$P_1 = \sum_{i=1}^7 (N_i + M_i * sp + L_i * h) * f_i * s \quad (3)$$

The N 's, M 's, and L 's constitute the variables of this component of the price model, and s , sp , and h the parameters. The variables can be determined rather objectively for each LHRE candidate, although some judgement may be required to determine whether certain LHRE components should be treated as "special" or "high tech." The treatment of the parameters has accommodated this uncertainty, as will be shown later.

While there are no fundamental assumptions required for this factor to accurately represent the price of a 223.7 kW [300 BHP] engine, it is apparent that its accuracy would increase with a

larger number of cost categories. In this case, the number of cost categories is consistent with the available information on the cost of parts embodying the new technologies within the scope of the ADECD program.

Scaling To Reciprocator Power - Since the objectives of this program specify the overall engine/EERS power to be at a fixed level, regardless of design, it is evident that the power rating required of the engine alone will vary according to the capabilities of individual EERS with which it is integrated.

The price of each engine is modified according to its power rating, which is, in turn, determined by the power added by the exhaust energy recovery system. The power output of each of the exhaust energy recovery systems depends, in turn, upon the level of cylinder insulation and, hence, roughly upon technical risk level, as shown in Table II.4-2.

Based on the data collected in [2], engine price should be scaled to power output through the .7 power of the ratio of engine power relative to a baseline. Thus, the power scaling component of the price model is defined to be:

$$P2 = [(BHP - EERSHP)/300]^{.7} \quad (4)$$

Recalling that the technology scaling component P1 is by definition the price of a 223.7 kW [300 BHP] engine, it can be seen that, in the context of the price model, P2 amounts to an automatic adjustment of the basic unit part price based on the part's capacity for power output manifested in such tangible properties as size and weight.

Exhaust Energy Recovery System Price - Prices for each of the exhaust energy recovery systems are taken from [2] and shown in Table II.4-3. Note that where turbocompounding is used in conjunction with another system, their prices are simply added.

FUEL CONSUMPTION MODEL

Of the three sub-models, the fuel consumption model is perhaps the most straightforward. Fundamental to it is the assumption justified by modeling experience and the findings in [2] that vehicle fuel consumption is approximately proportional to rated engine system BHP and bsfc, unit fuel price, vehicle speed, and life cycle distance driven for a given type of vehicle. The present value of the cost of fuel during the engine system's life cycle is thus given by:

$$\begin{aligned} \text{PVFC} = & \text{FCF} \times \text{bsfc} \times \text{BHP} \times \left(\frac{\text{D}}{12 \text{ VS}} \right) \\ & \times \left(\frac{\text{FCL}}{\text{FD}} \right) \times \text{PV} \end{aligned} \quad (5)$$

where bsfc and BHP are system rated fuel consumption and power, D is the distance driven per year during the life cycle, FD the density of fuel, FCL the unit volume price of fuel, and VS the average vehicle speed. FCF is the constant of proportionality, which represents average vehicle/route loading, and PV the present value of the monthly fuel payments throughout the life cycle:

$$\text{PV} = \left[\frac{(1+I)^{\text{LC}} - 1}{I(1+I)^{\text{LC}}} \right] \quad (6)$$

where I is the monthly rate of return on investment, and LC the duration of the life cycle in months.

Bsfc and power are considered the variables of this model, and FCF, FCL, LC, D, VS, and I the parameters. In practice, bsfc is, in turn, obtained from correlations with cylinder insulation effectiveness and is further scaled according to changes in friction losses relative to a baseline. The variables are rather easily evaluated within the scope of the overall ADECD work. While the evaluation and treatment of parameters will be discussed in detail later, it should be noted here again that the validity of

the model (viz, an appropriate value for FCF) is supported by substantial vehicle/route simulation experience.

MAINTENANCE COST MODEL

It was found that maintenance cost can be estimated rather easily by shifting from a fixed price view in which maintenance cost is dictated by fixed labor and parts prices given frequency and severity of failures, to a flexible price view in which the cost of maintenance is governed primarily by economic decision factors. These factors are: the price of a new engine, the amount recoverable from a "used" engine of given age if it is to be removed from service rather than fixed, rates of return on capital, and the expected improvement in maintenance cost available through engine replacement.

Before discussing the engine maintenance model, it is worth noting that this "supply side" maintenance cost scenario is indeed dominant in a variety of products such as calculators, small appliances, etc., whose purchase price is low enough that few individuals find the maintenance service market attractive enough to enter. Despite their less-than-perfect reliability, these items have no maintenance cost. Furthermore, in these instances, maintenance costs tend to be the highest for the most expensive products, despite the high reliability of these products relative to their lower-cost competition.

The basis of the engine maintenance cost model, then, is the assumption that maintenance cost can be no greater than the amount that would cause outright engine/vehicle replacement to be judged a better alternative. In particular, the model is of a "fix vs replace" decision to be made after the first twelve months of ownership of an engine, based on the comparison of maintenance costs experienced with that engine to those of other owners of the same engine. This situation is illustrated in Figure II.4-1. The population mean monthly maintenance cost (M) and its standard

deviation ($MF1 * M$) are as perceived by the owner of the engine in question. For a fleet owner, or for an environment in which maintenance costs for 12-month old engines are fairly well known, these figures would be good approximations.

Assuming that the engine in question has required one maintenance action in each of its first 12 months, the owner has a sample of monthly repair costs from which he can extract a sample mean (x). The first element of the model is that the owner will be caused to make a fix vs. replace decision if he perceives a statistically significant difference between his sample mean and the population mean. If we assume that, stated technically, the criterion is that there must be 90% confidence that the sample mean is greater than the population mean, then the ratio of sample to population means must be

$$x/M > MF2 = 1 + .37MF1 \quad (7)$$

if the monthly maintenance cost of the 12-month old population is normally distributed.

The ratio $MF2$ is an indicator of the probable improvement in monthly maintenance cost that would result from replacement of the engine in question. Whether this level of improvement is sufficient to make replacement economical depends on: the price of a new engine, the amount recoverable from the sale (or other use) of the old engine, rate of return on money, and length of the life cycle. Specifically, the cost of keeping the present engine would be the present value of all maintenance. The cost of replacing the engine would be the price of the new engine less the amount recovered from the old engine, plus the cost of maintaining the new engine. Mathematically, the present engine would be kept if:

$$M \leq \frac{P}{.37MF1} [1 - MF3(1-12/LC)]$$

$$x \frac{I(1+I)^{(LC-12)}}{(1+I)^{(LC-12)} - 1} \quad (8)$$

where P is the price of the new engine, MF3 is the fraction of the book value recoverable from the old engine, and the other terms are as defined in the fuel consumption model. Here we have assumed straight-line depreciation.

It is assumed that the maintenance cost is, indeed, such that the equality holds, so that the present value of the maintenance cost can be approximated by:

$$PVMC = M[(1+I)^{LC} - 1]/[I(1+I)^{LC}] \quad (9)$$

The only variable in this model is the engine price, P, which would, in turn, be as estimated by the price model. The treatment of parameters MF1, MF3, LC, and I will be discussed later.

Since this maintenance model may represent a new approach, it is worthwhile to note some features of its behavior. The trends caused by its own variables, relation to other models, and typical results have been examined. Equations (8) and (9) do predict the expected trends, and comparison with available data appears favorable.

For example, graphical and closed form correlations of annual maintenance cost to engine power are found in [5] for two presently available families of engines. These are:

$$M = 3320[(kW/239)^{1.14}] \quad (10a)$$

$$M = 3520[(kW/239)^{1.14}] \quad (10b)$$

for turbocharged (TC) and turbocharged and aftercooled (TC/A) engines, respectively. In Equations (10a) and (10b), M is the

annual cost of the service contract and kW is the power output of the engine in kilowatts.

Similar correlations between engine power and selling price have also been made [5], namely:

$$P = 14000[(kW/239)^{.7}] \quad (11a)$$

$$P = 14500[(kW/239)^{.7}] \quad (11b)$$

for the TC and TC/A engines, respectively. In Equations (11a) and (11b), P is the engine selling price.

Solving Equations (11a) and (11b) for power, in terms of price, and substituting into Equations (10a) and (10b), the following correlations between selling price and maintenance cost are obtained:

$$M = 3320[(P/14000)^{1.63}] \quad (12a)$$

$$M = 3520[(P/14500)^{1.63}] \quad (12b)$$

again, for TC and TC/A engines, respectively. While at first it may seem that Equations (12a) and (12b) represent two distinct families of maintenance cost, it can be seen from Equation (12a) (by multiplying and dividing the term in parentheses by 14500) that Equations (12a) and (12b) are identical. Thus, the data in [5] suggest that Equation (12b), or a function similar to it, predicts the maintenance cost of a heavy-duty diesel engine regardless of its design.

The discrepancy between Equations (8) and (12) is in the power index: unity, giving linear behavior in Equation (8), and 1.63 in Equation (12). Whereas Equation (8) has been derived from known premises, the set of control parameters that gives rise to the apparent 1.63 power index of Equation (12) is not easily identifiable. It is also unknown whether an extrapolation of

Equation (12) to the LHRE candidates under consideration is valid. Since a linear correlation is an appropriate first-cut approximation of any power index, especially between 1 and 2 over a sufficiently small interval, it is concluded that Equation (8) can appropriately model the maintenance - price relationship.

For example, a general study of the difference in maintenance cost prediction of Equation (12) vs. Equation (8) indicates the possibility of rather good agreement in the likely price range. Specifically, for engines priced between \$13000 and \$16000, the disagreement between the two models is at most +/- 6%, with a single choice of parameters for Equation (8). This analysis serves to reinforce confidence in the use of the linear model.

An example calculation illustrates the good agreement possible between Equation (8) and available data [2], as represented by Equation (12), for what seem to be reasonable values of the parameters. Specifically, the values $MF1 = .3$ (meaning that 68% of monthly maintenance expenditures fall within +/- 30% of the mean) and $MF3 = 1.1$ (meaning that the engine can be sold for 1.1 times current book value) are selected. Then, for an engine costing \$14,000 with a 6 year life cycle, Equation (8) predicts a monthly maintenance cost of \$233.80, or \$3341.23 per year, if prevailing interest rates are 1%/month. By Equation (12), the annual maintenance cost of an engine costing \$14,000 is estimated to be in the vicinity of \$3324.31 - the difference is less than 1%.

Lastly, the noted discrepancy between the two models arises only if the parameters of Equation (8) are assumed to be constants, or, at least, unrelated to price. Appropriate functional relationships between the parameters of Equation (8) and engine price would introduce non-linear behavior, possibly even the 1.63 power of Equation (12). The existence and nature of such functional relationships would be appropriate areas for further study.

II.4.3 EVALUATION STRATEGY

The approach chosen for LCC evaluation using the parametric model involves three key elements:

1. Assign high-confidence interval defined by upper and lower values for each model parameter.
2. Run a full factorial analysis with respect to model parameters for each engine/EERS configuration. This element requires, and is easily accomplished with, an appropriate computer code.
3. From resulting large number of scenarios or factorial set members, extract overall statistics and LCC for individual scenarios of significance to the LHRE.

Each of these tasks will be discussed in detail in the paragraphs that follow.

SELECTION OF PARAMETER RANGES

The 12 parameters arising from the price, fuel, and maintenance components of the LCC model are listed in Table II.4-4. As shown, they can be grouped merely for clarity according to their relevance to: diesel engine business / technology, trucking business / environment, life cycle, and "quality," the latter term having no precise definition in this context. These factors are characterized by two features: their relative independence from particular engine designs, as suggested by their designation as "parameters," and, in general, a degree of uncertainty as to their values.

Conceptually, the uncertainty associated with these parameters is dealt with rather easily. If values for all but one of the

parameters were known precisely, the remaining parameter could be represented by a "high" and a "low" value. The result would be "high" and "low" figures for life cycle cost. In practice, however, only a few of the parameters can be evaluated precisely, and these only because a particular choice may be inherent to the problem, as in the case of system BHP. By selecting high and low values for each of the parameters and evaluating LCC for each possible combination, an LCC distribution, such as the one shown in Figure II.4-2, is obtained.

In interpreting such a distribution, two points must be considered. First, it has been assumed that each of the parameters is independent of the others within the ranges specified. Second, the representation of uncertainty of the parameters by two extreme values, rather than by a more detailed distribution, is an approximation in itself. In fact, the LCC model is coded so as to accept up to 6 values for each parameter, but this feature is intended mainly to facilitate examination of the consequences of particular values.

The width of the LCC distribution is determined by the size of the range of values of each parameter. Therefore, the need for maximum resolution between the distributions of various engine candidates must be weighed against the need for confidence in the specified parameter ranges. The values shown in Table II.1-4 were selected to accurately reflect experience and judgement. Thus, the ranges shown are appropriately narrow.

FULL FACTORIAL ANALYSIS

A computer code was written to perform the LCC calculations with the model defined by Equations (1) - (9). This code is designed to run full factorial analyses for a group of engine candidates, given a set of parameter ranges, and accumulate appropriate statistics and points of interest in the results.

For each of the 42 engine-EERS configurations, a full factorial set of LCC evaluations was run with respect to the 12 model parameters. From this large set, four scenarios of interest were extracted. These are the mean LCC, minimum LCC, maximum LHRE benefit, and minimum LHRE benefit.

The maximum LHRE benefit scenario is defined as the set of parameter values that give most weight to the fuel economy of the engine, while at the same time minimizing the impact of new technology on the price of the engine. Conversely, the minimum LHRE benefit scenario is that which places most emphasis on the new-technology content of the engine and its implications for price, while simultaneously minimizing the importance of fuel economy improvements. The parameter values associated with the minimum LCC, maximum LHRE benefit, and minimum LHRE benefit scenarios are shown in Table II.4-5.

II.4.4 LIFE CYCLE COST RESULTS

The results of the full factorial analyses indicate that in all but the minimum LHRE benefit scenario, the HR2 engine is shown as an ingredient in the least costly configuration. In that case, the advantage is with the IR1 reciprocator, although the differences between reciprocators in this case are quite small.

In all but the maximum LHRE benefit scenario, turbocompounding, by itself, seems to be the most advantageous exhaust energy recovery treatment, and steam Rankine cycle, by itself, the poorest. In the maximum LHRE benefit scenario, the most advantageous treatment becomes turbocompounding and organic Rankine cycle system together. In this scenario, the steam Rankine cycle still leads to the highest life cycle costs.

In order to most effectively reduce the wealth of LCC data, candidates were first ranked within each risk level, namely MR1 vs.

MR2, IR1 vs. IR2, and HR1 vs. HR2. All further analyses are based only on the "winner" in each risk level. In performing this reduction, it was found that there is little apparent difference between proposals 1 and 2, in any combination with EERS, under any of the important scenarios. In general, then, the selection of one or the other is not critical from an LCC standpoint. Furthermore, in this study, the selection of an exhaust energy recovery system has little effect on the selection of an engine at a given risk level.

Since the "maximum LHRE benefit" scenario seems to be the most relevant to the ADECD program objectives, attention should be focused on the relative performance of the leading LHRE candidates. In this scenario, it was found that the more sophisticated of the candidates in each risk level - HR2, IR2, and MR2 - are the most desirable on the basis of LCC, so further analysis will concentrate on them. Figure II.4-3 is a graphical representation of the percent difference between the leading configurations in each risk level under the maximum LHRE benefit scenario. Note that for any given EERS configuration, the ranking of reciprocators is:

HR2 (best)
IR2
MR2
SOA

Conversely, for any choice of reciprocator, the ranking of EERS configurations is:

TC+TCPD+ORCS (best)
TC+TCPD
TC+ORCS
TC+TCPD+STEAM
TC
TC+STEAM

Note that the combination TC+STEAM is not as good as the current practice of turbocharging only.

LCC BREAKDOWN

The sources of the differences between the life cycle costs of the most advanced reciprocators (turbocharged only) are clarified through the breakdowns into price, fuel, and maintenance components shown in Figure II.4-4. In general, fuel cost is substantially higher than the other components, to the extent of usually being larger than the other two combined. It is this fact that makes LCC more sensitive to changes in fuel economy than to changes of similar relative proportion in price or maintenance. Relative to the mean, fuel cost is a much higher fraction of LCC in the maximum LHRE benefit scenario, and a much smaller fraction in the minimum LHRE benefit scenario.

SENSITIVITY OF LCC DIFFERENTIAL TO INTEREST RATE

The LCC model accounts for inflation implicitly through the "interest rate," or return on investment parameter. An explicit dependence would not be difficult, since evaluation of the impact of inflation on an interest rate is straightforward. Thus, the value of this parameter may be subject to the compound uncertainties of the engine owner's actual rate of return and of the rate of inflation. For this reason, it is worthwhile to briefly examine the impact of substantially lower rates of return on the LCC ranking of the various engine candidates. The LCC model does predict an increase in life cycle cost with decreases in interest rate, but the calculations made for the present set of candidate LHRE configurations show the impact of this dependence to be relatively small.

Specifically, with a decrease in interest rate, engine price remains unchanged, but the present values of fuel and maintenance costs increase. This suggests that as interest rates fall, LHRE engines will become even more attractive, relative to the current state-of-art. Analysis of the LCC results for sensitivity to interest rate shows that the growth in differential is very small,

however. Figure II.4-5 illustrates the effects of interest rate variation on life cycle cost by illustrating the high, mean, and low LCC's obtained at each value of interest rate. Results are shown for both the SOA and HR2 candidates, encompassing all six exhaust energy recovery schemes. As shown, the means vary by essentially the same amount with the same change in interest rate. Therefore, while consideration of a lower interest rate would cause an across-the-board increase in LCC, it would not lead to different conclusions as to the optimum LHRE configuration.

PAYBACK ANALYSIS

While life cycle cost is, per se, a complete measure of the quality of an investment alternative, payback analysis has some importance by way of providing not only an alternate view, but also as a means of assessing cost performance early in the life cycle, relative to LCC projections. Payback analysis consists of determination of the time required for the decrease in operating costs of one alternative relative to another to offset any attendant increase in purchase price.

Figure II.4-6 shows the payback analysis in terms of monthly cost relative to the current SOA, as applied to the leading LHRE candidates in the maximum LHRE benefit scenario. Note that all levels of insulation technology pay back in less than 5 months, as shown by the turbocharged-only configurations. Furthermore, adding the current technology of turbocompounding and ORCS to any of the reciprocators also pays back within two years, relative to the same reciprocator without exhaust energy recovery treatment. Combined, the insulated reciprocators with TC+TCPD+ORCS take longer to pay back, but their ultimate benefit is significantly greater. Indeed, the additional cost of TC+TCPD+ORCS on any of the reciprocators shown is recovered within two years.

SENSITIVITY OF LCC TO VARIATIONS IN PARAMETERS

The sensitivity of LCC to variations of parameter values is indicated in Figure II.4-7. This chart shows the relative contribution of each parameter in bringing LCC from the lowest to the highest possible value for the HR2 engine in both TC only and TC+TCPD+ORCS configurations. The relative contribution of a variation between low and high values of parameter p_i is defined to be:

$$C_i = \frac{\text{abs}(\text{Mean LCC}|_{p_i=\text{high}} - \text{Mean LCC}|_{p_i=\text{low}})}{(\text{Max LCC} - \text{Min LCC})}$$

Figure II.4-7 illustrates that, in the TC only configuration, the primary contribution comes from fuel-related parameters fuel cost, fuel usage constant, and distance driven per year, respectively. The next largest contribution comes from variation in the book value recovery factor. In the TC+TCPD+ORCS configuration, the variation in book value recovery factor makes a somewhat larger contribution than distance driven per year. This increased sensitivity is apparently due to the high price, hence, high maintenance cost of the HR2+TC+TCPD+ORCS system. If the book value recovery factor could be shown to be less variable and centered on a somewhat higher value, the LCC performance of the HR2 engine in the minimum LHRE benefit scenario could be expected to improve relative to the SOA, possibly to the point of showing a benefit even in this "worst case."

II.4.5 SUMMARY AND CONCLUSIONS

The LCC model developed for the ADECD program is simple, yet complete. Because its variables are relatively easy to determine for engines still at the concept stage, it is an effective tool for use in support of determination of design and technological direction.

The maintenance cost sub-model represents what is believed to be a new approach to the problem of maintenance cost estimation. The normal difficulties associated with identifying failure modes and estimating their frequency and criticality in the absence of applicable field data are thus avoided.

Uncertainty in the values of the model's parameters is dealt with by assigning high-confidence intervals, specified by high and low values, to each. Full or partial factorial analyses can then be made for each engine, with respect to the parameters and their high and low values. Investigation of possible functional relationships among the variables and parameters would be an appropriate future task.

The results of a full or partial factorial analysis include scenarios that are very favorable for LHRE's over the current SOA, as well as some that minimize the benefit of LHRE technology. The overall result, in the case of the ADECD candidate engines, is that the LHRE's are indeed attractive compared to the current SOA, and that the level of benefit increases as the technology becomes more advanced.

Specifically, from the foregoing discussion, the following conclusions can be made:

1. There is little difference in LCC between engine candidates in the same risk category. Thus, the selection of proposal 1 vs proposal 2 is not critical from an LCC standpoint. Also, it is apparent that cylinder insulation has greater impact on LCC than does reduction in friction by amounts envisioned in this study. HR2, IR2, MR2, and SOA are considered to be the leading engines based on their LCC performance in the maximum LHRE benefit scenario.
2. The ranking of engines between risk levels is the same for any given EERS configuration.

3. The leading LHRE/EERS alternatives all pay back within two years in the maximum LHRE benefit scenario. Also, the cost of TC+TCPD+ORCS on any of the leading engines, as well as the present SOA, is recovered within two years.
4. It is not necessary to simulate inflation rates lower than those encompassed by the present results.
5. The leading LHRE/EERS alternatives are of potential benefit to both customer and manufacturer in the maximum LHRE benefit scenario.

II.4.6 REFERENCES

1. Mechanical Technologies, Inc., "Automotive Stirling Engine Development Program," NASA Contract No. DEN 3-32.
2. Bailey, M., "Comparative Evaluation of Three Alternative Power Cycles for Waste Heat Recovery from the Exhaust of Adiabatic Diesel Engines," DOE/NASA/50194-43, April, 1985.

Table II.4-1: Price Model "Parts List" with Quantities Shown for State-of-the-Art In-Line 6-Cylinder Diesel Engine

<u>Category 1:</u> $f_1 =$ Unit Cost	N_1 --
main bearings	7
connecting rod bearings	6
piston pin bushings	6
camshaft bearings	7
exhaust port shields	6
intake port shields	0
valve assemblies	24
oil pressure regulator	1
thermostat	1
<u>Category 2:</u> $f_2 \times$ Unit Cost	
rocker assemblies	18
connecting rods & piston pins	6
oil inlet tube	1
oil fill assembly	1
fan	1
belts	1
hoses	1
crankshaft pulley	1
lifter brackets	2
<u>Category 3:</u> $f_3 \times$ Unit Cost	
pistons	6
liners	6
exhaust manifold	1
intake manifold	1
oil pump	1
water pump	1
fuel pump	1
oil filter assembly	1
rocker cover	1

Table II.4-1 (Cont'd): Price Model "Parts List" with Quantities Shown for State-of-the-Art In-Line 6-Cylinder Diesel Engine

Category 4: f_4 x Unit Cost

fuel injectors	6
oil cooler	1
oil pan	1
flywheel	1
vibration damper	1

Category 5: f_5 x Unit Cost

camshaft	1
----------	---

Category 6: f_6 x Unit Cost

cylinder head	1
turbocharger & plumbing	1
flywheel housing	1

Category 7: f_7 x Unit Cost

cylinder block	1
radiator	1
charge cooler	1
crankshaft	1
gears & case	1

Table II.4-2: WHUS Power Contributions for Engine Pricing

<u>WHUS</u>	<u>MODERATE RISK</u>	<u>INTERMEDIATE RISK</u>	<u>HIGH RISK</u>
TCPD	38 hp	38 hp	38 hp
ORCS	28.8	31.9	35.7
STEAM	14.5	19.7	24.8
TCPD+ORCS	66.8	69.9	73.7
TCPD+STEAM	52.5	57.7	62.8

Table II.4-3: Prices of Exhaust Energy Recovery Systems

<u>WHUS</u>	<u>PRICE (= P3)</u>
TC	\$0 (counted with engine)
TCPD	2000
ORCS	7380
STEAM	6070
TCPD+ORCS	8070
TCPD+STEAM	9380

Table II.4-4: Parameters of the LOC Model, with Typical Values

	<u>RANGE</u>
<u>Business/Technology</u>	
1. STANDARD PART PRICE (P)	\$8.60 - 10
2. MED.-TECH. COST MULT. (P)	1.4 - 1.8*
3. HIGH-TECH. COST MULT. (P)	2.2 - 2.9*
<u>Business/Environmental</u>	
4. FUEL COST (F)	\$1.10 - 1.70/gal
5. INTEREST RATE (F,M)	12 - 15 %/yr
<u>LIFE CYCLE</u>	
6. DURATION (F,M)	7 - 8 yr
7. AVE. VEHICLE SPEED (F)	55 mph
8. DISTANCE/YEAR (F)	80 - 100,000 mi
9. CYCLE FUEL USAGE CONST. (F)	.6 - .8
10. SYSTEM RATED POWER (P,F)	300 BHP
<u>"QUALITY"</u>	
11. MIHLY RPR STD DEV/MEAN (M)	.25 - .3
12. BOOK VAL RECOVERABILITY (M)	1.0 - 1.1

NOTES

- * Range may vary with engine design
- (P) Parameter of price model
- (F) Parameter of fuel consumption model
- (M) Parameter of maintenance cost model

Table II.4-5: Parameter Levels for Extreme Circumstances

	<u>Min.</u>	<u>Max.</u> LHRE <u>Ben.</u>	<u>Min.</u> LHRE <u>Ben.</u>
STD. PART UNIT COST	LOW	LOW	HIGH
MED.-TECH. COST MULT.	LOW	LOW	HIGH
HIGH-TECH COST MULT	LOW	LOW	HIGH
FUEL USAGE CONST.	LOW	HIGH	LOW
FUEL COST	LOW	HIGH	LOW
LC DURATION	HIGH	HIGH	LOW
DISTANCE/YEAR	LOW	HIGH	LOW
INTEREST RATE	HIGH	LOW	HIGH
BOOK VALUE RECOV.	HIGH	HIGH	LOW
MIHLY. MAINT. STD DEV/MEAN	HIGH	HIGH	LOW

Figure II.4-1: Comparison of First-Year Maintenance Costs of a Particular Engine to Those of the Population of the Same Engine

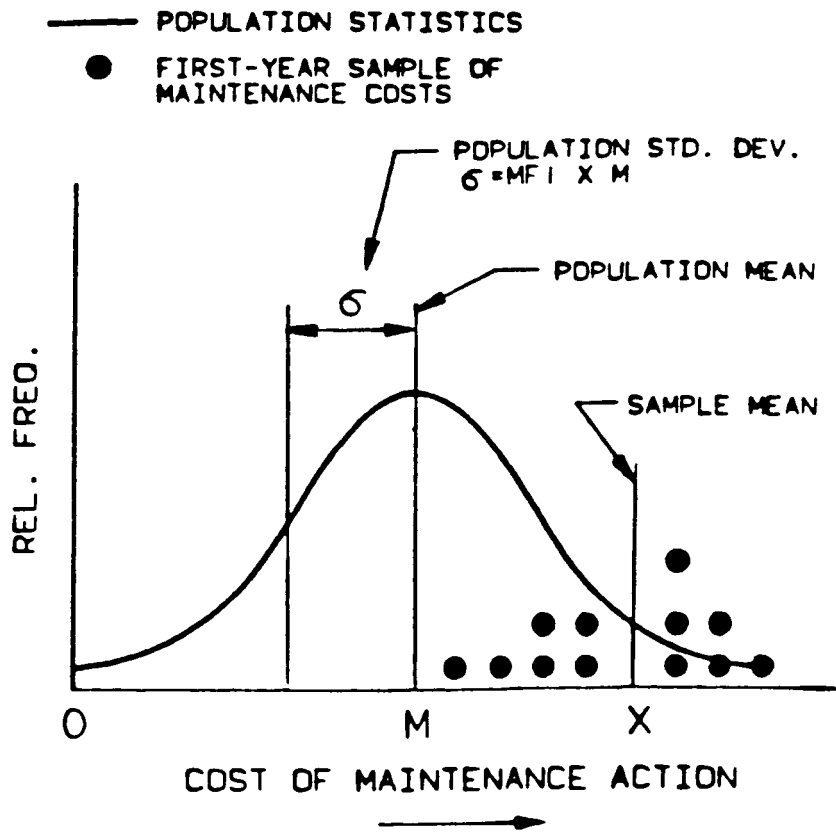


Figure II.4-2: LCC Distribution Resulting from Uncertainty of Parameter Values in Full Factorial Analysis

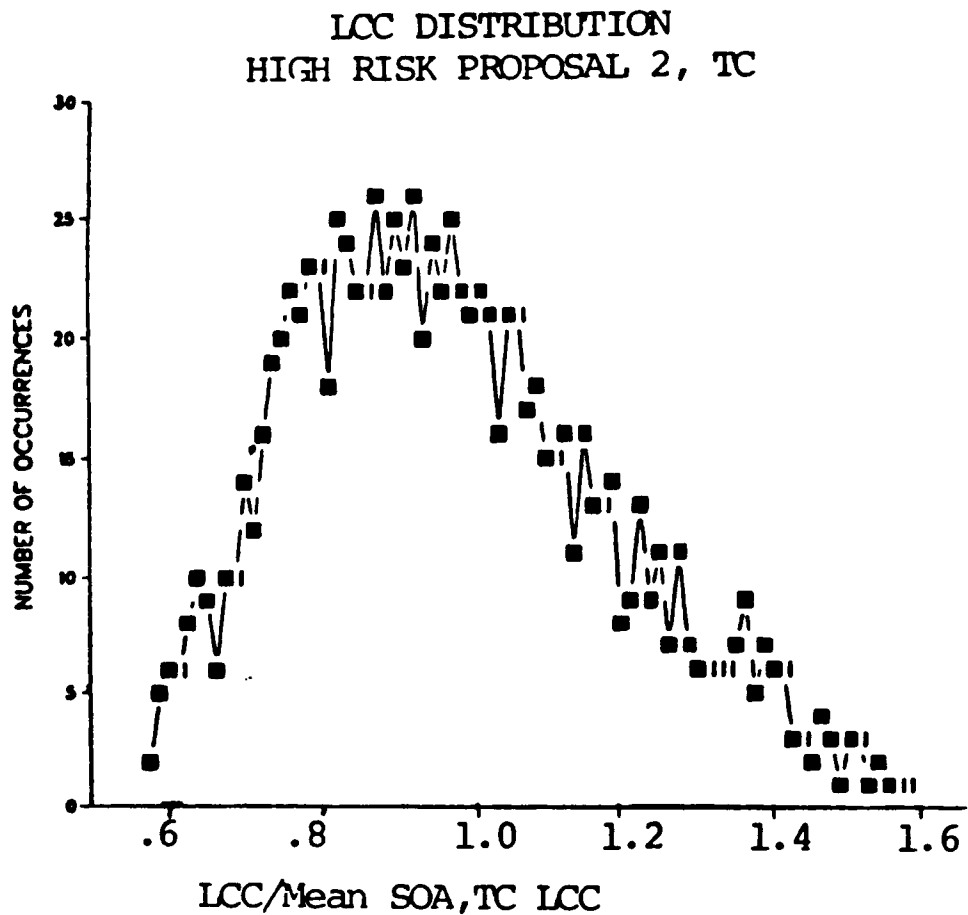


Figure II.4-3: Percent LOC Difference (Max. LHRE Benefit Scenario) Between Leading LHRE Candidates in Each Risk Level and SOA. Positive Value Indicates Superiority of Configuration Relative to SOA

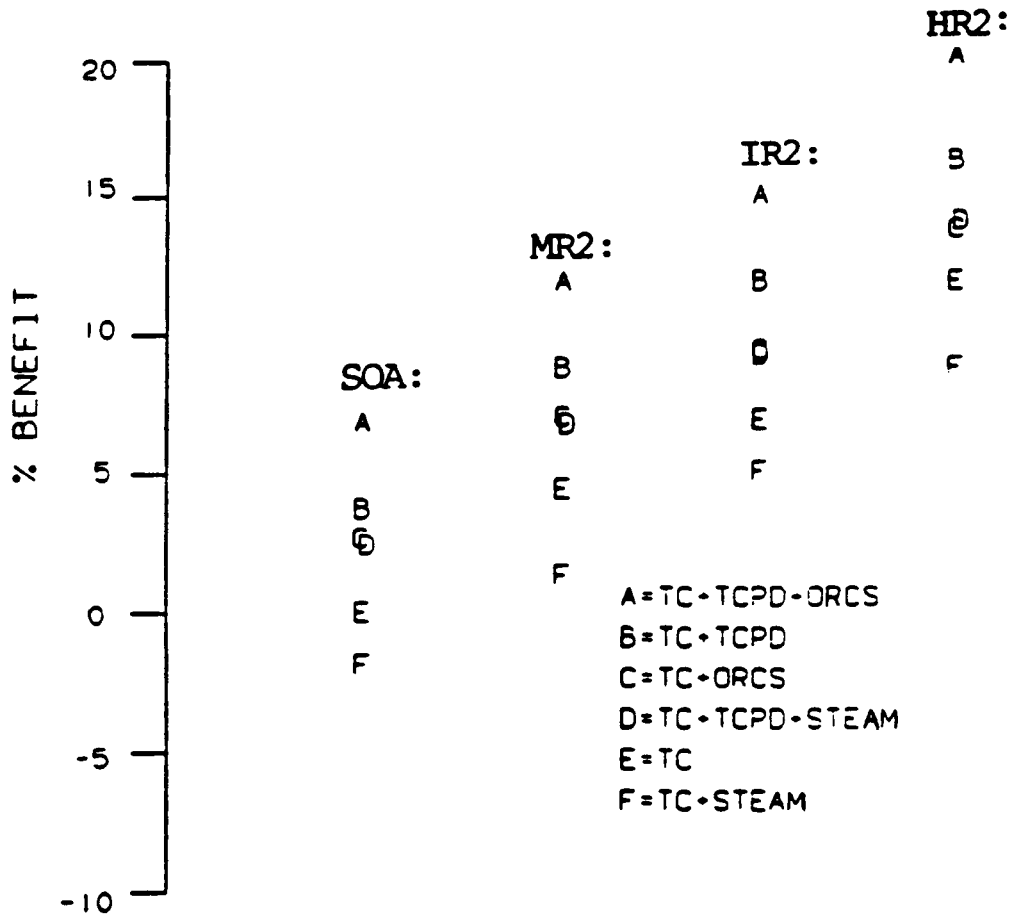


Figure II.4-4: Breakdown of LCC in Mean and Max. LHRE Benefit Scenarios

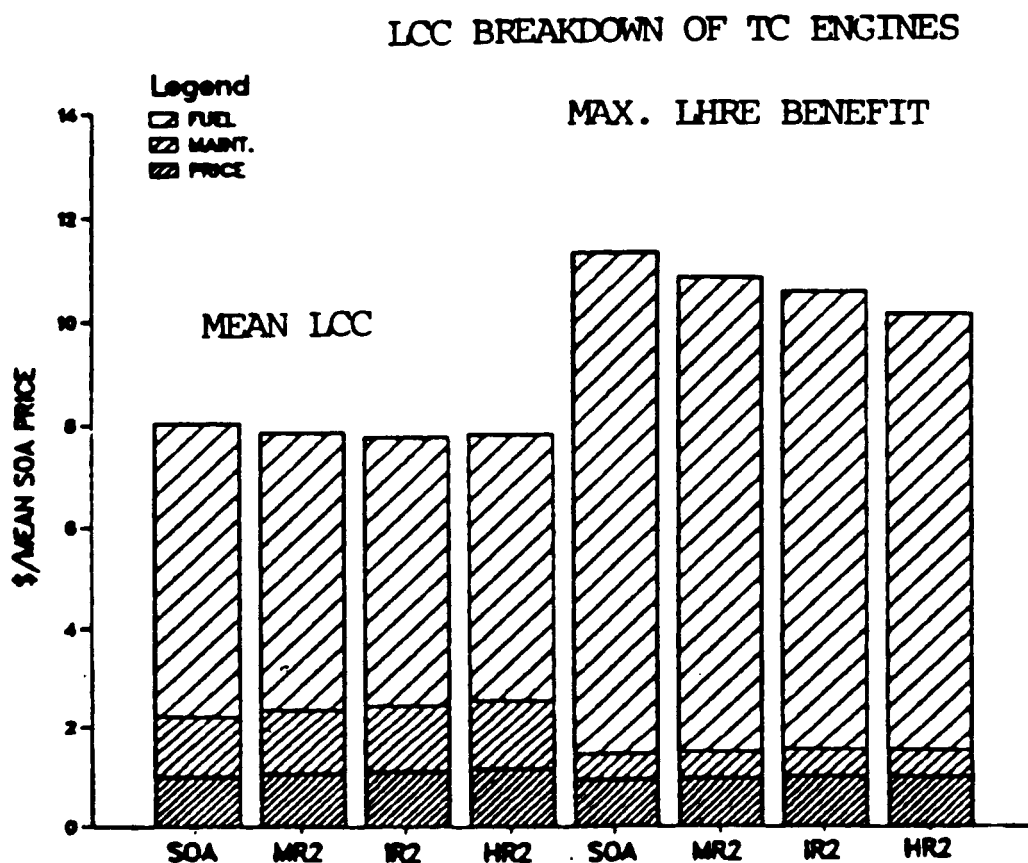


Figure II.4-5: Sensitivity of LCC to Interest Rate

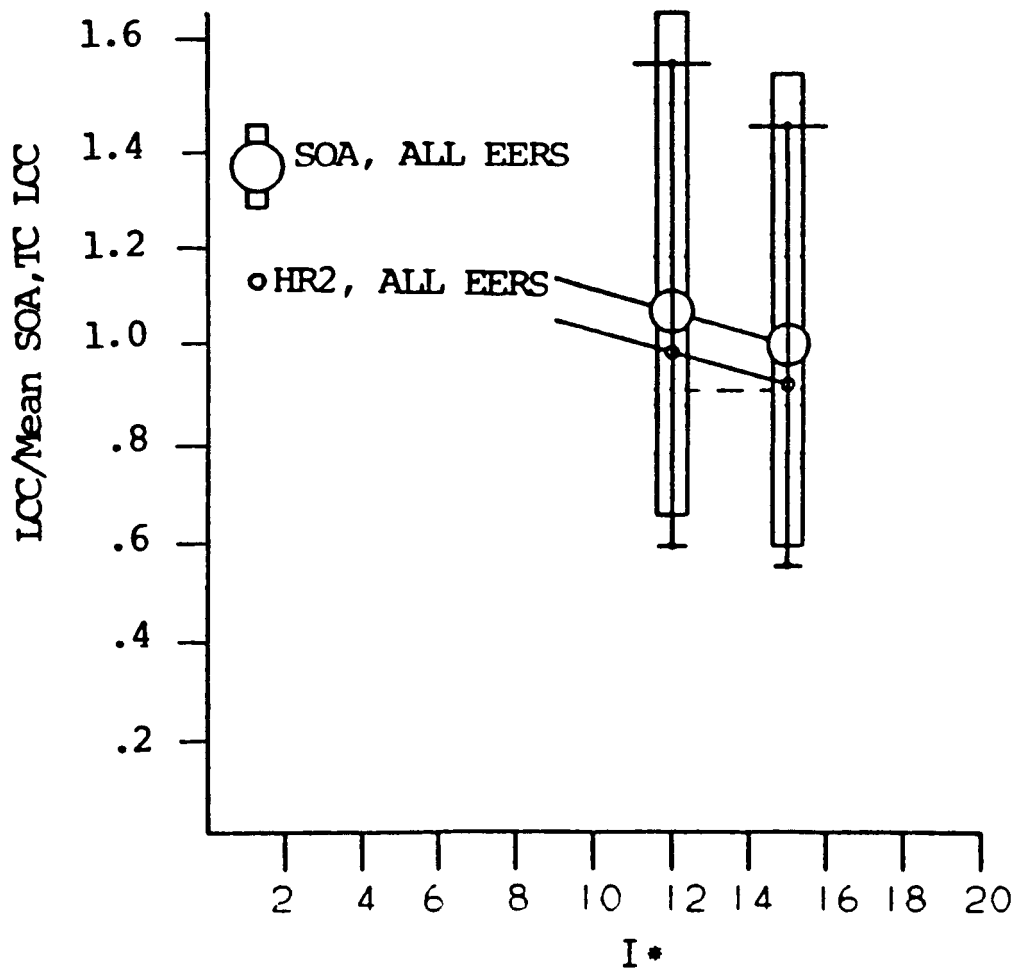


Figure II.4-6: Cost Relative to Turbocharged SOA Engine of Several Alternate Engine Configurations in Max. IHRE Benefit Scenario

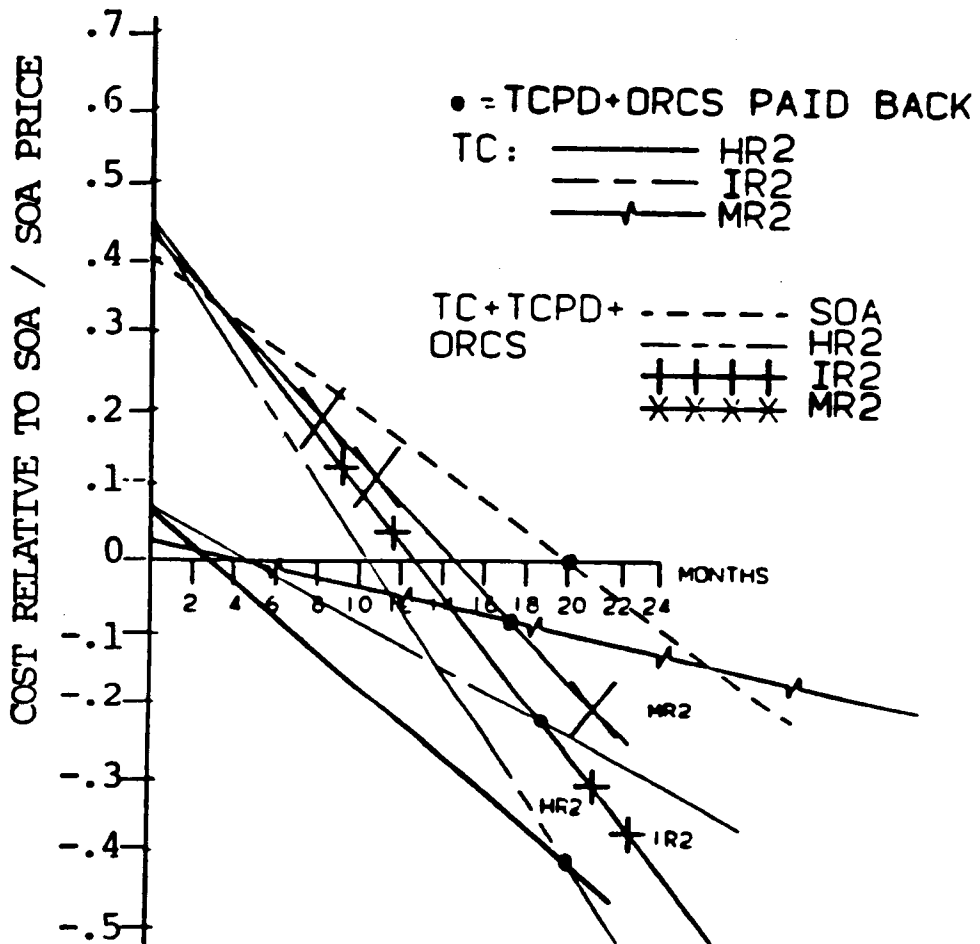
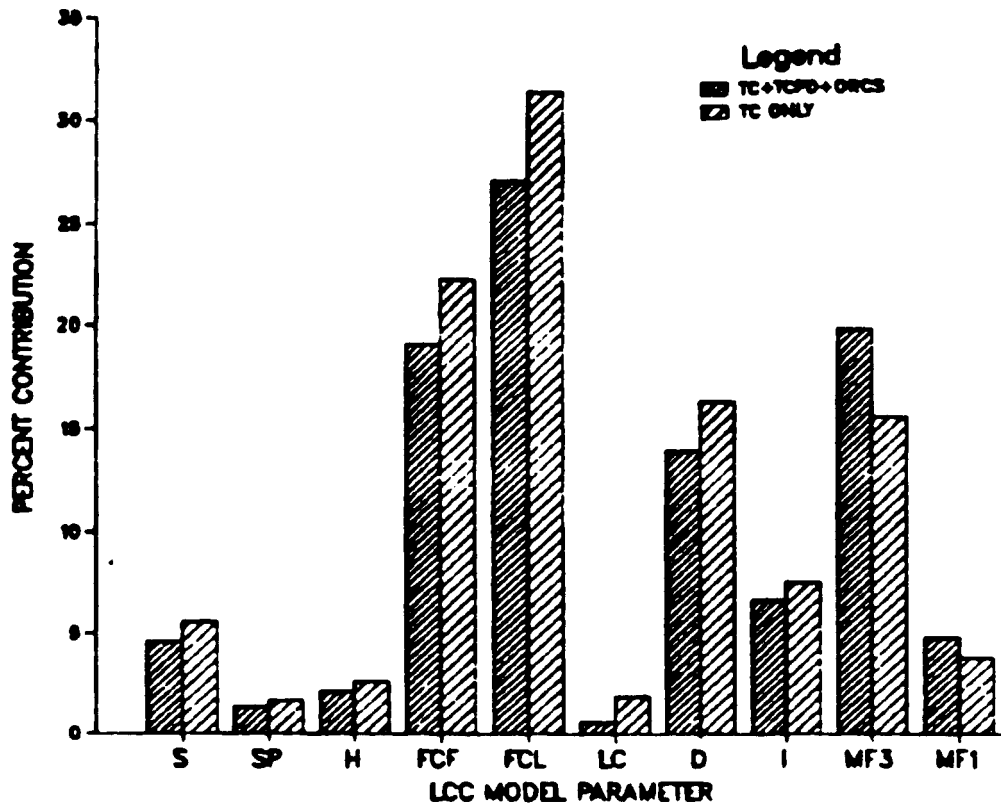


Figure II.4-7: Contribution of Parameters to LOC Variation in HR2 Engine



II.5 THE ADIABATIC DIESEL REFERENCE ENGINE

The end objective of this task of the program was to select the ADRE system configuration. The performance analysis suggested that more benefits can be obtained with increased insulation. The common elements for all the ADRE reciprocator configurations considered for the final analysis included:

- No engine water cooling.
- Air to air charge cooling.
- Heat isolated intake manifold.
- Metallic air gap insulated exhaust manifold and turbocharger tubes.
- Ceramic valve seats, guides, and cam rollers [if such components are utilized].
- Cast in place exhaust and intake port shields.

In addition, the moderate risk ADRE reciprocator configurations called for:

- Thin thermal barrier coatings.
- Liquid lubricated hot section interfaces and relatively conventional tribological environments.

The intermediate risk configurations suggested the use of:

- Metallic air gap insulation approach.

- Liquid lubrication and advanced liquid lubricated tribological interfaces.

The high risk configurations called for:

- Monolithic ceramic air gap insulation
- Solid lubrication and thin solid film lubrication tribology.

As explained earlier in Section II.4.1, a total of six reciprocator configurations were selected for the LCC analysis. Each risk category contained two candidate configurations. For maximum ADRE economic worth, a high risk concept was selected, providing maximum insulation. The solid lubricated concept was selected for further assessment during the remainder of this Phase of the program. The selected reciprocator is shown in Figure II.5-1.

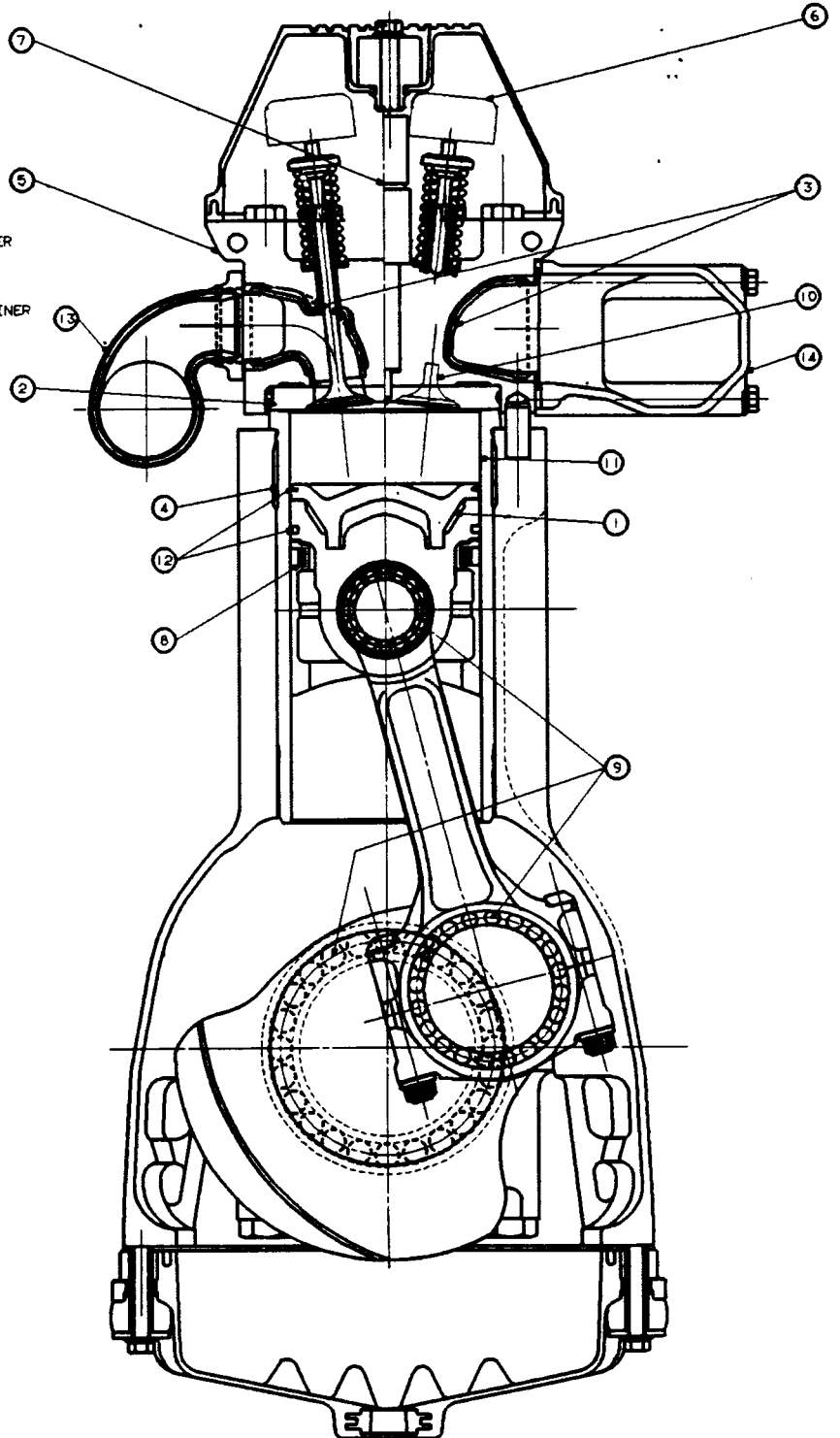
Turbocompounding was found to be the most recommended approach for EER. Additional recovery, via an organic Rankine bottoming cycle, was selected for the ADRE system analysis and design tasks in order to examine the likelihood of packaging a diesel engine with both turbocompounding and a bottomer for on-highway truck applications. LCC predictions also favored this package.

Figure II.5-1 The Selected ADRE Reciprocator Concept.

ORIGINAL PAGE IS
OF POOR QUALITY

HIGH RISK-PROPOSAL I

- 1 - CERAMIC AIR/GAP PISTON
- 2 - CERAMIC AIR/GAP FIREDECK
- 3 - CAST-IN CERAMIC AIR/GAP SHIELDS
- 4 - UNCOOLED LINER
- 5 - INDIVIDUAL HEADS PER CYLINDER
- 6 - HYDRAULIC OVERHEAD ACTUATORS
- 7 - HYDRAULIC INJECTION
- 8A - SOLID LUBRICANT PISTON RING/METALLIC EXPANDER
- 8B - SOLID LUBRICANT STICKS (ALTERNATE)
- 9 - SEALED ROLLER ELEMENT BEARINGS
- 10 - CERAMIC VALVES AND SHORT PORTS
- 11 - SOLID LUBRICANT TRIBOLOGICAL TREATMENT ON LINER
- 12 - CERAMIC HEADLAND RING AND A SECOND RING
- 13 - INSULATED EXHAUST MANIFOLD
- 14 - HEAT ISOLATED INTAKE MANIFOLD



III

ADRE SYSTEM ANALYSIS AND DESIGN

This section reports on the work done under Tasks 2 and 3 of Phase I of the ADECD program. For reporting purposes, the ADRE system analysis and design effort is subdivided into the following subsections:

- Main Design Features
- Performance Analysis
- Valve and Valve Actuation System
- Fuel Injection System
- Electronic Control System
- Component Analysis
- Tribology
- Exhaust Energy Recovery
- Power Transfer

III.1 MAIN DESIGN FEATURES

The main design features of the ADRE system are displayed in layout drawings of the reciprocator, overhead, power transfer, engine size envelope comparison, and truck installation. The remainder of this report will provide many of the design analyses that resulted in the final ADRE system design package. The design features are briefly described below, as a preview of the ADRE selected systems and components.

RECIPROCATOR

The reciprocator features are shown in Figures III.1-1 through III.1-4. The rolling element bearing treatment throughout the engine is represented in the longitudinal cross section of Figure III.1-1. This figure also shows the monolithic ceramic, air gap insulated piston concept. The fact that the ADRE reciprocator is solid lubricated is exemplified in the shallow crankcase cover that replaces a deep oil pan in the conventional engine.

More details of the rolling element bearing treatments for the crankshaft main, pin, and the piston pin bearings are displayed in Figure III.1-2. This figure also shows the relatively thin section between neighboring cylinders, due to the elimination of the water jacket. Hence, the cylinder block casting is significantly simplified, and the engine length is shorter.

Figure III.1-3 shows that the compression gasket is eliminated, with the monolithic ceramic firedeck clamped directly on the cylinder liner. The intake and exhaust portshields are cast-in-place monolithic ceramic, with an insulating air gap behind them. The figure also shows an electrohydraulic overhead mechanism concept. The rocker cover in the conventional engine is replaced with a "dust" cover for the electronic, camless and oil free overhead. Figure III.1-4 shows a symmetric eight bolt pattern for the gasketless design.

OVERHEAD

The overhead design is shown in Figures III.1-3 and -5. The top view of Figure III.1-5 shows details of the fuel lines for both the electronic injection and valve actuation systems. The valve actuation is proposed as a non-conventional, hydraulically actuated type. As such, it is continuously variable to optimize valve events for a specific engine operating condition. This system is electronically controlled by the ADRE central control system, which also controls the injection system.

POWER TRANSFER

Mechanical power transfer systems include the turbocompound and bottomer power transfer to the reciprocator crankshaft, as well as the engine accessory drives. Separate gear trains were selected for the bottomer and turbocompound units, as shown in Figure III.1-6. The selected location for power input to the crankshaft was the flywheel end of the reciprocator. Although, from a packaging viewpoint, a common gear train was preferred, complications arising from dynamic interaction and necessary controls precluded that approach.

Accessory drives for the Freon pump, power steering pump, and the bottomer feed pump utilize a common, serpentine belt drive, as shown in Figure III.1-7. The air compressor utilizes a separate belt drive, based on the analytical results which are reported in a later section.

SIZE ENVELOPE

The ADRE package size was compared to a state-of-the-art heavy-duty diesel engine that is designed specifically for on-highway application. The size comparison layouts are shown in Figures III.1-8 and -9. The figures show a rather favorable ADRE size envelope.

INSTALLATION

Installation of the engine system in a vehicle was conceptually carried out by the creation of layout drawings showing it in a typical cab-over-engine (a GM Astro) tractor. These drawings are shown in Figures III.1-10 through -13. The installation drawings demonstrated the feasibility of installing an ADRE reciprocator, with turbocompounding and bottoming EER systems, into the currently available engine space. In fact, it is likely that improvements can be made in the tractor aerodynamic drag for the case of ADRE system installation.

Figure III.1-1: Engine Block and Power Assembly - Longitudinal Cross Section

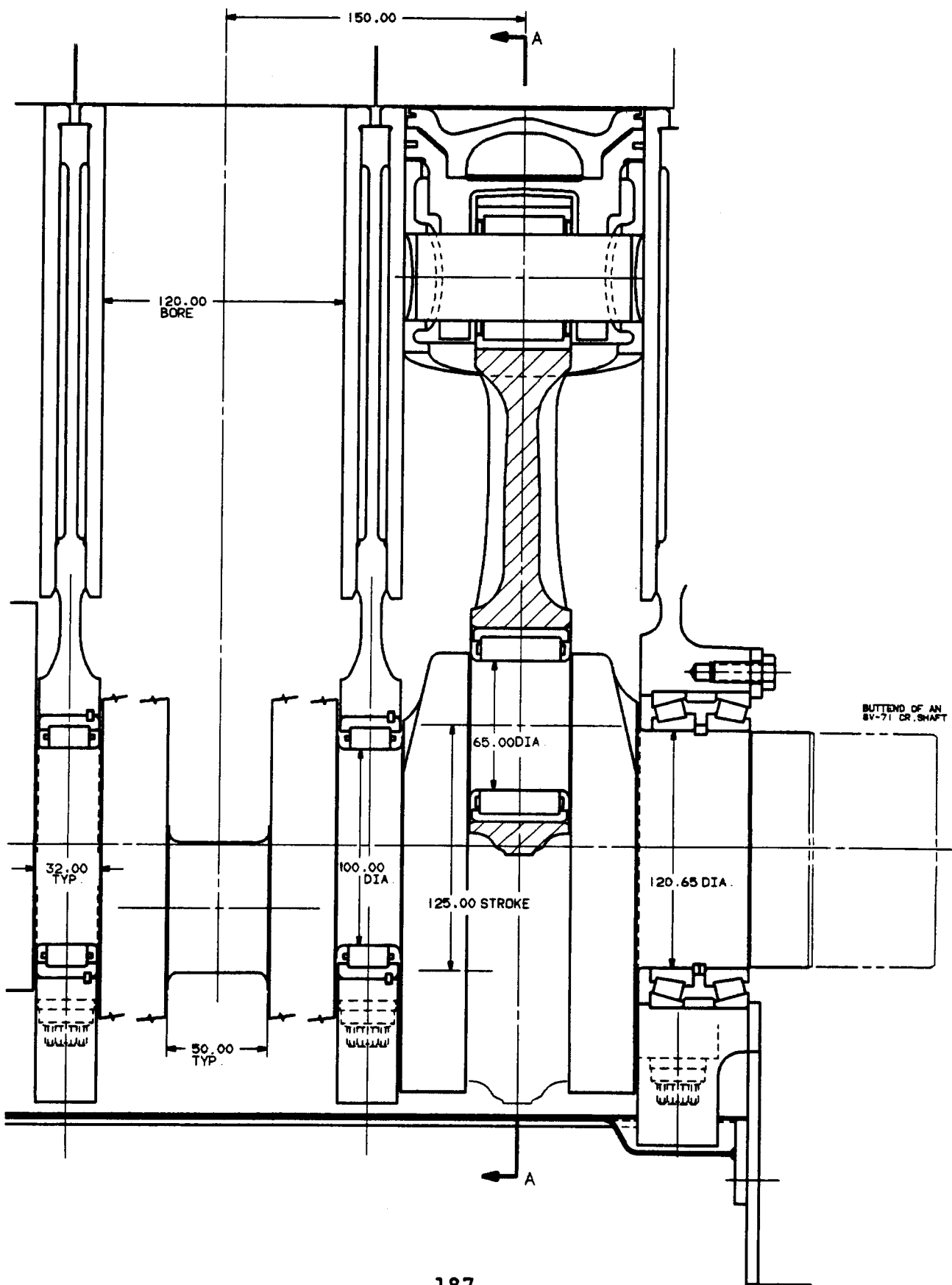


Figure III.1-2: A Cylinder Cross Section Showing More Details of the Rolling Element Bearing Treatments

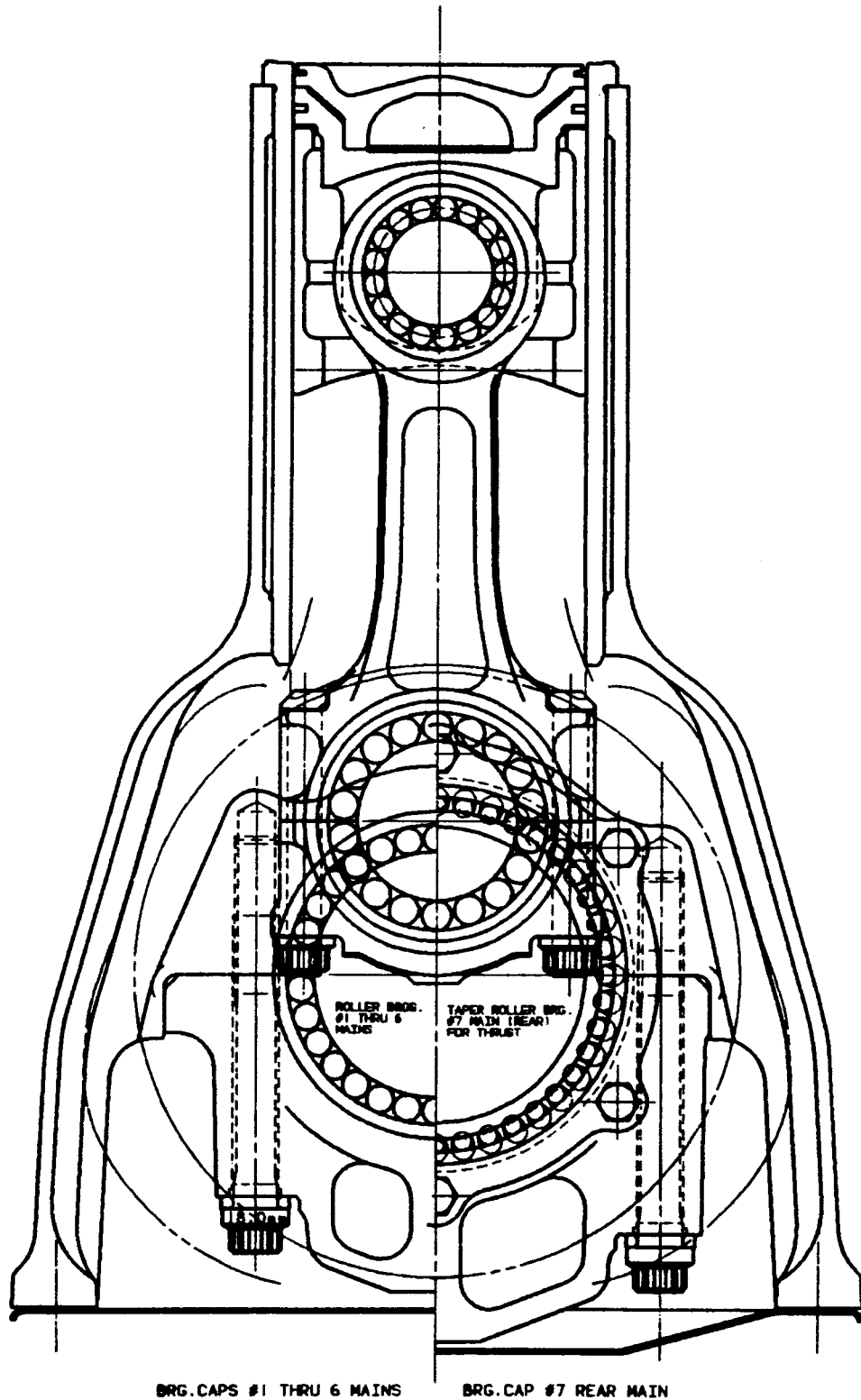


Figure III.1-3: Cylinder Head Cross Section

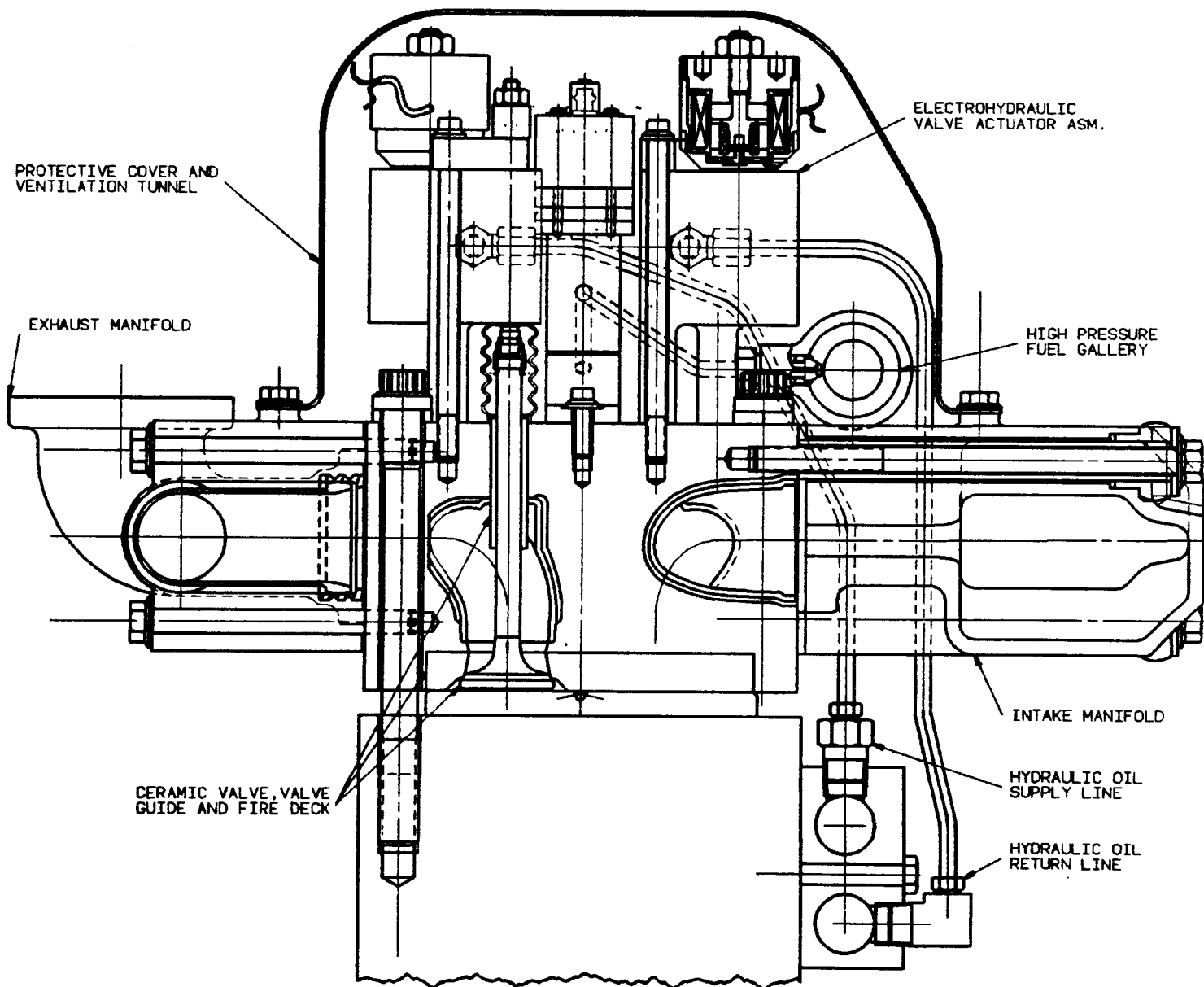
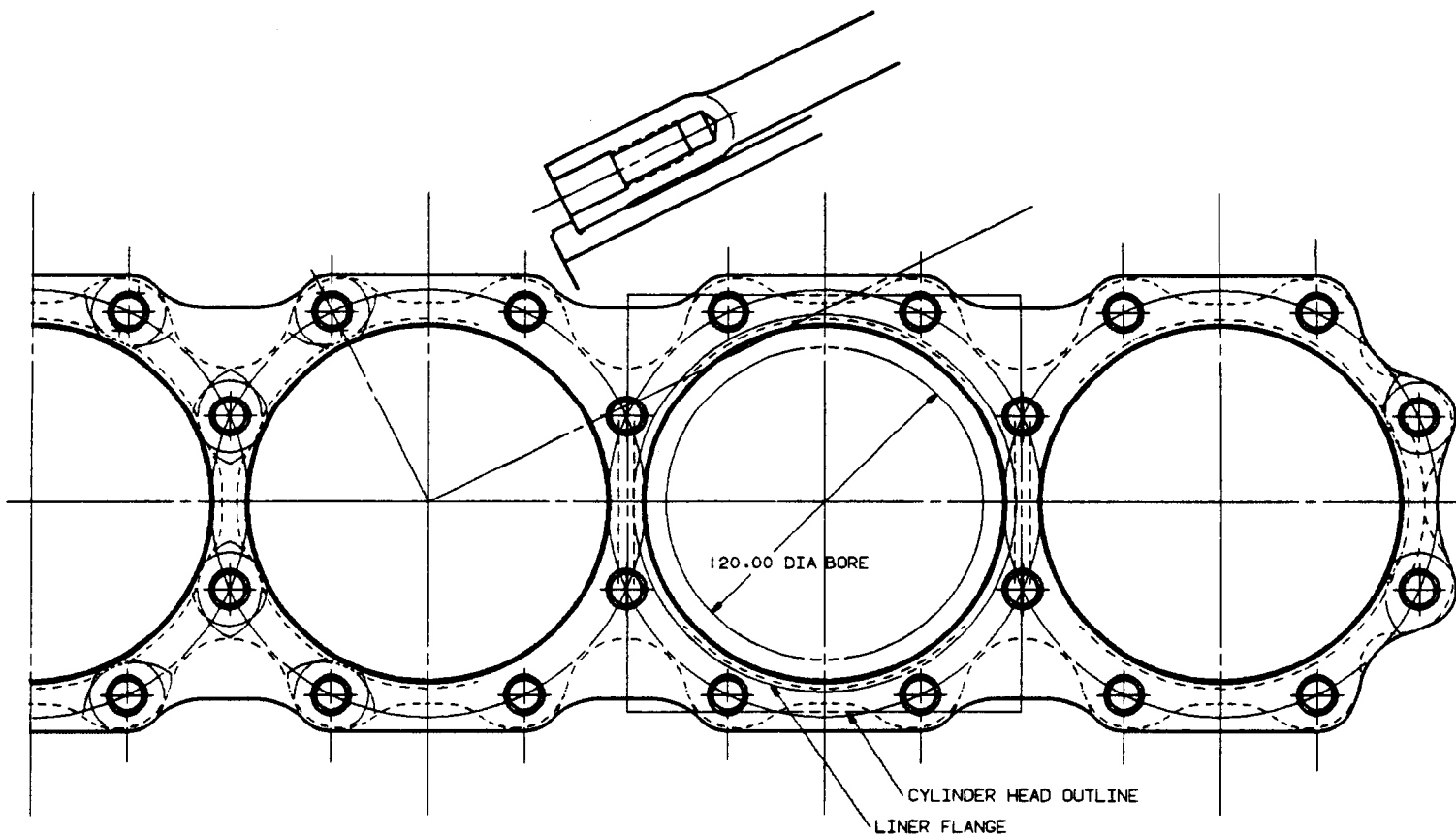


Figure III.1-4: Bolt Pattern For the Gasketless Design



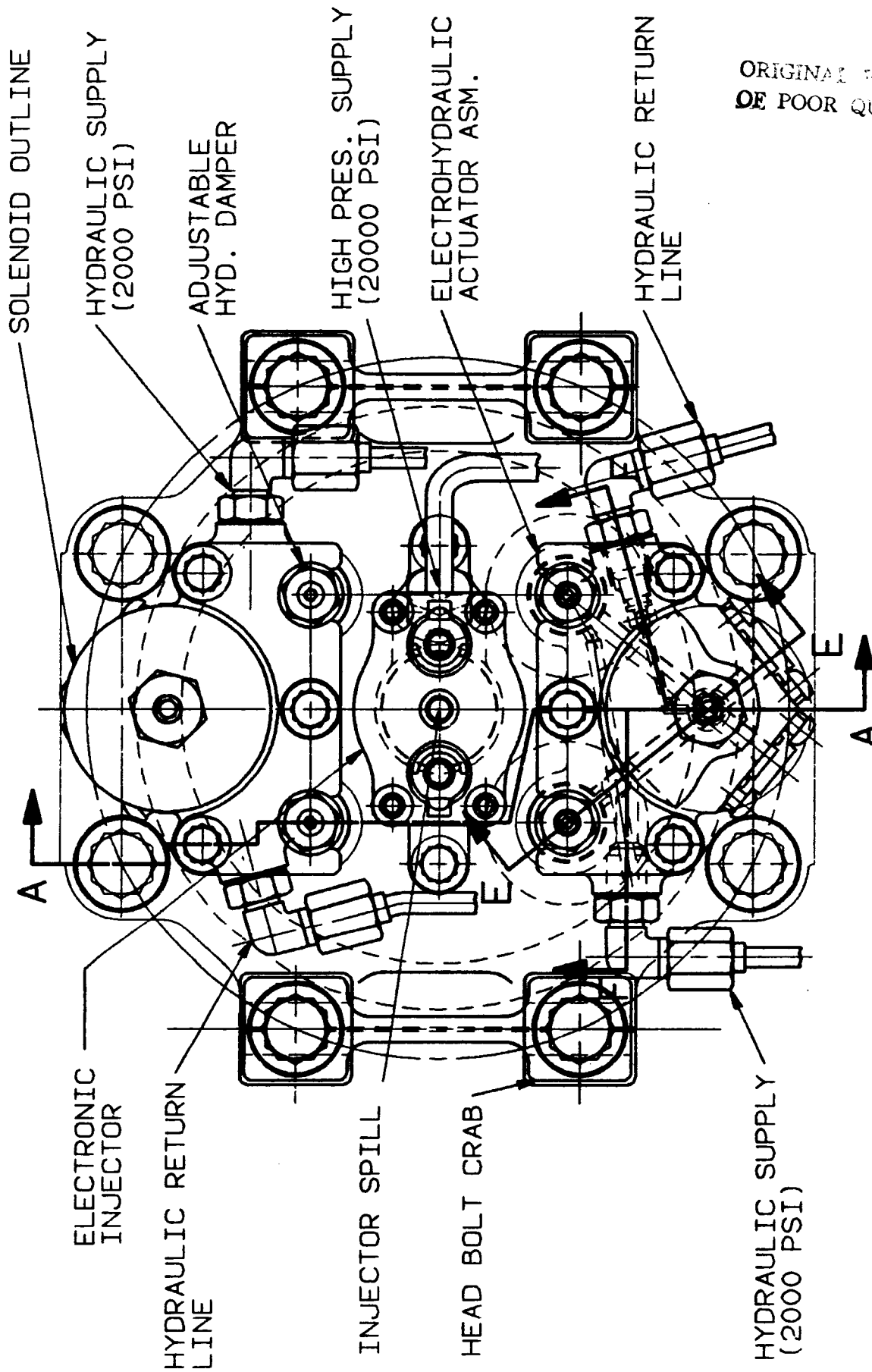


Figure III.1-5: Layout of Overhead Components (Cylinder Head Injector - Valve Actuator Arrangement)

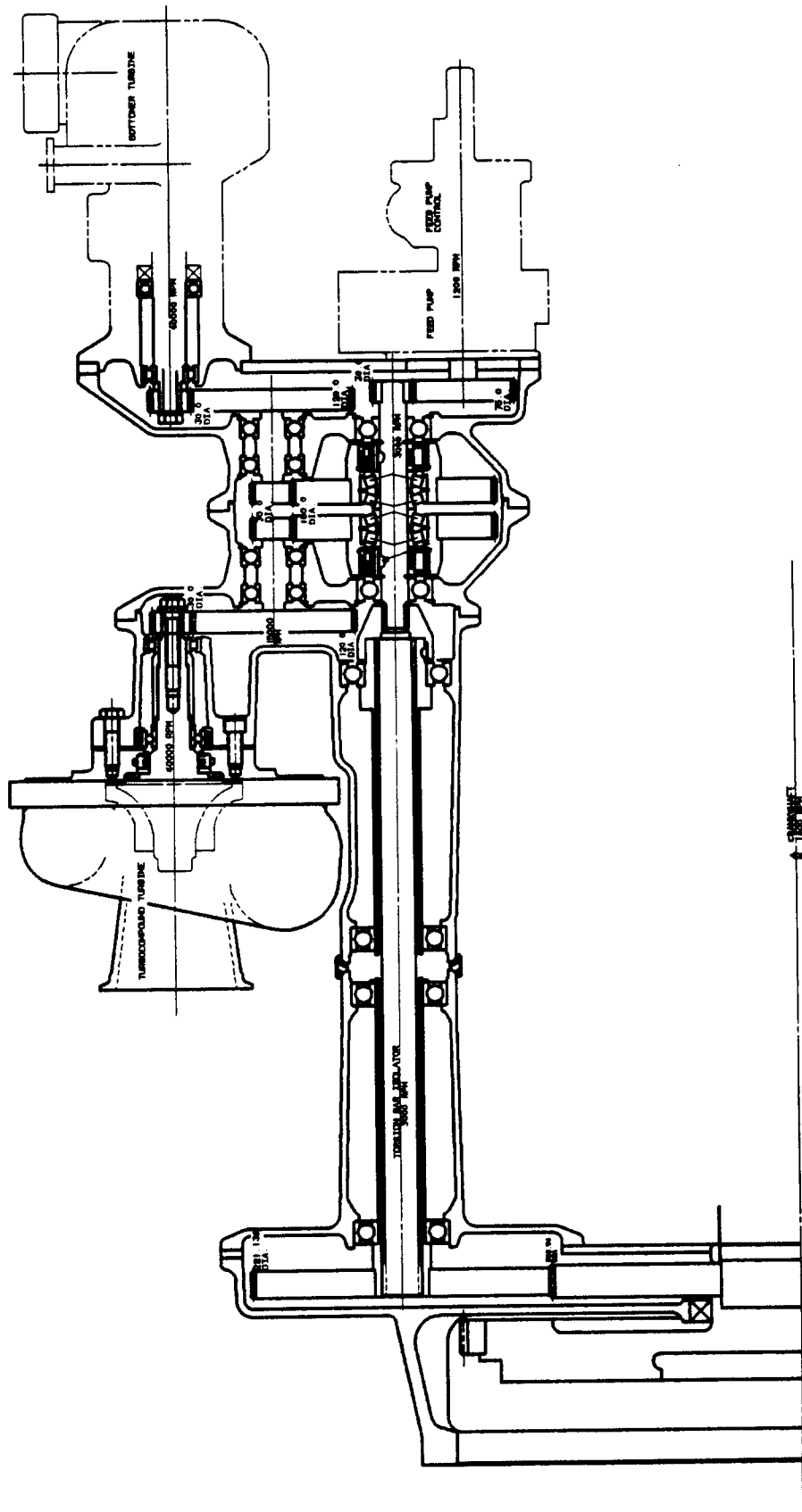


Figure III.1.1-6: Exhaust Energy Recovery Power Transfer System

Figure III.1-7: Accessory Drives

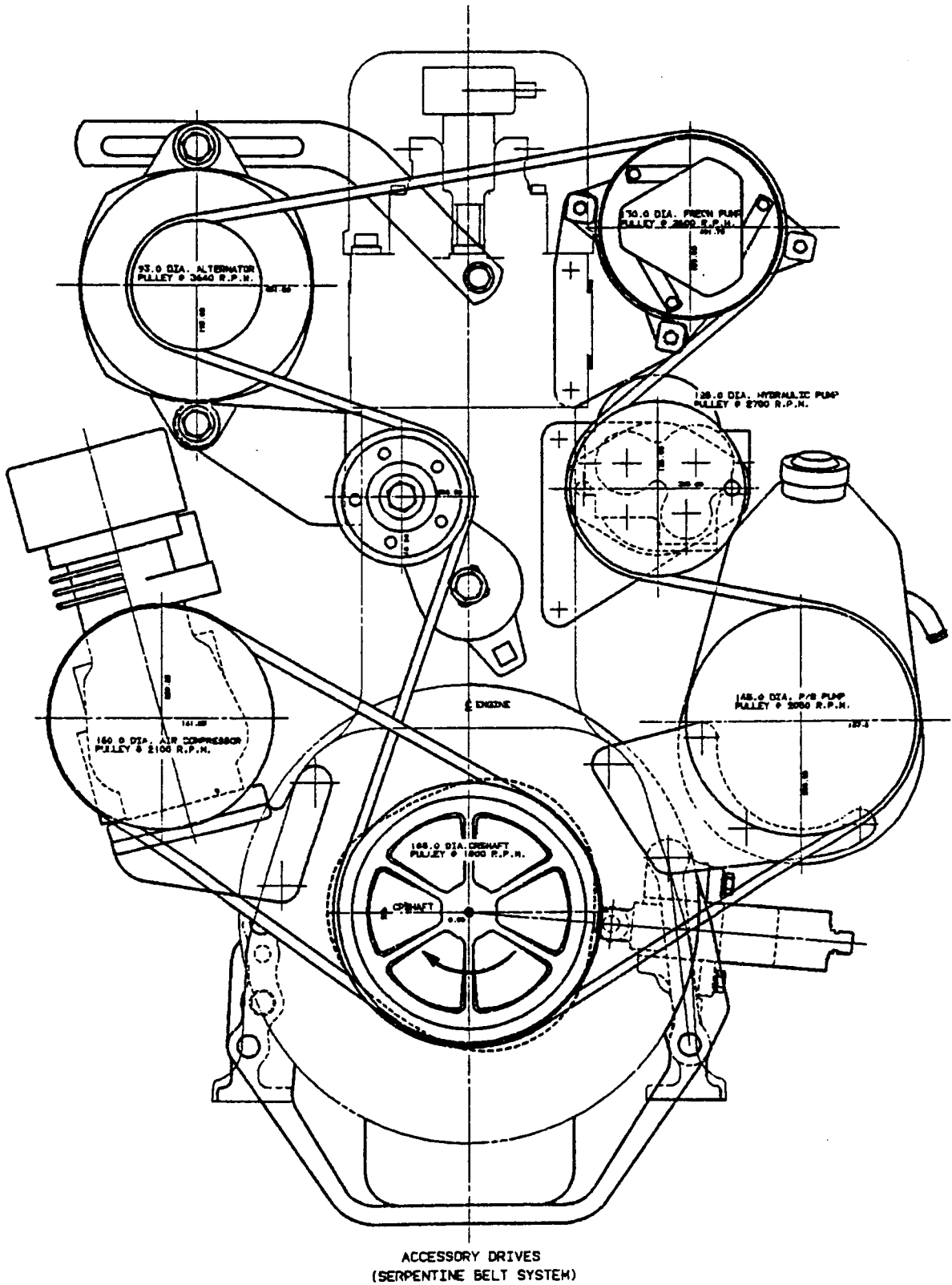


Figure III.1-8: ADRE Package Size Comparison - Front View

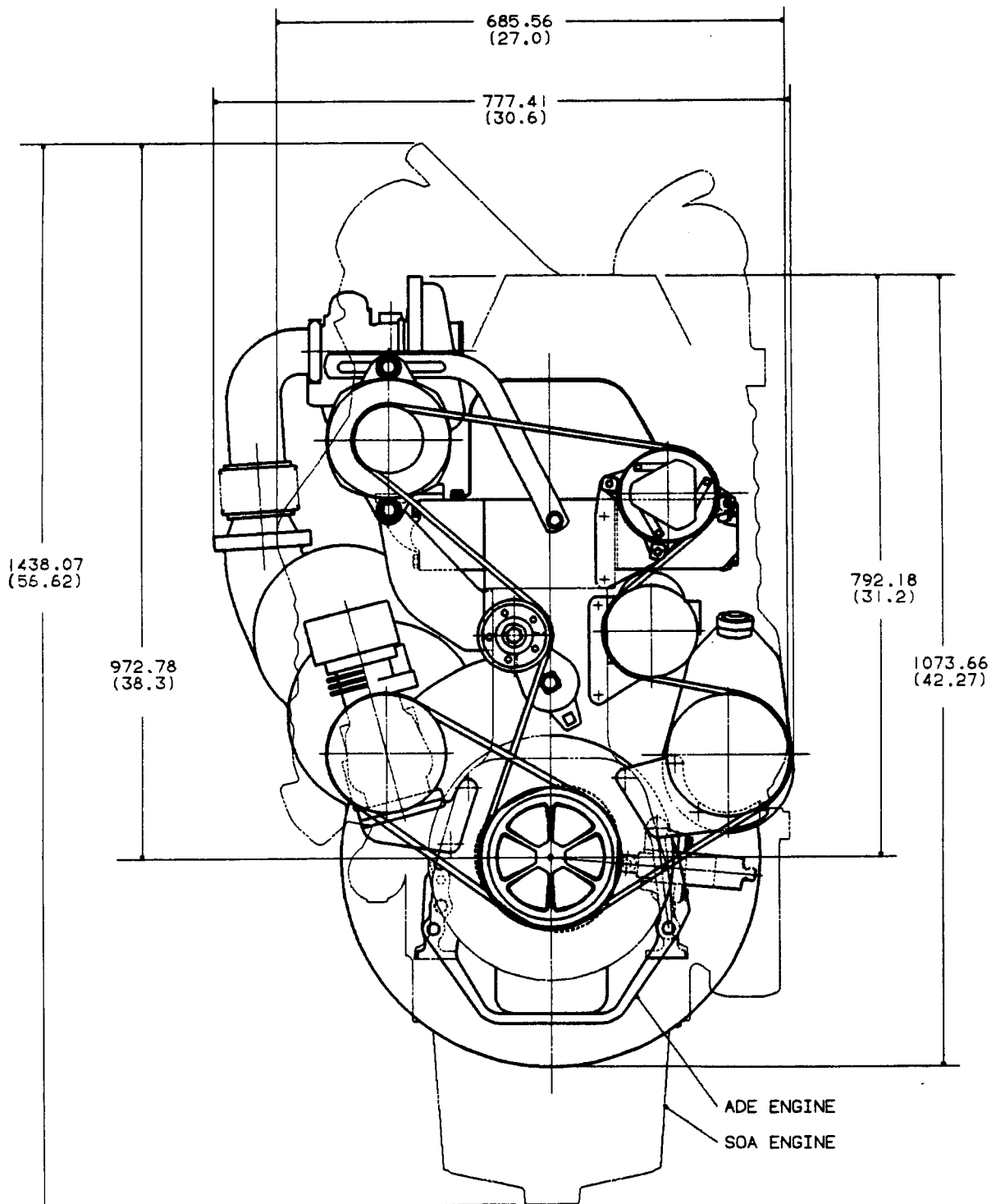


Figure III.1-9: ADRE Package Size Comparison - Side View

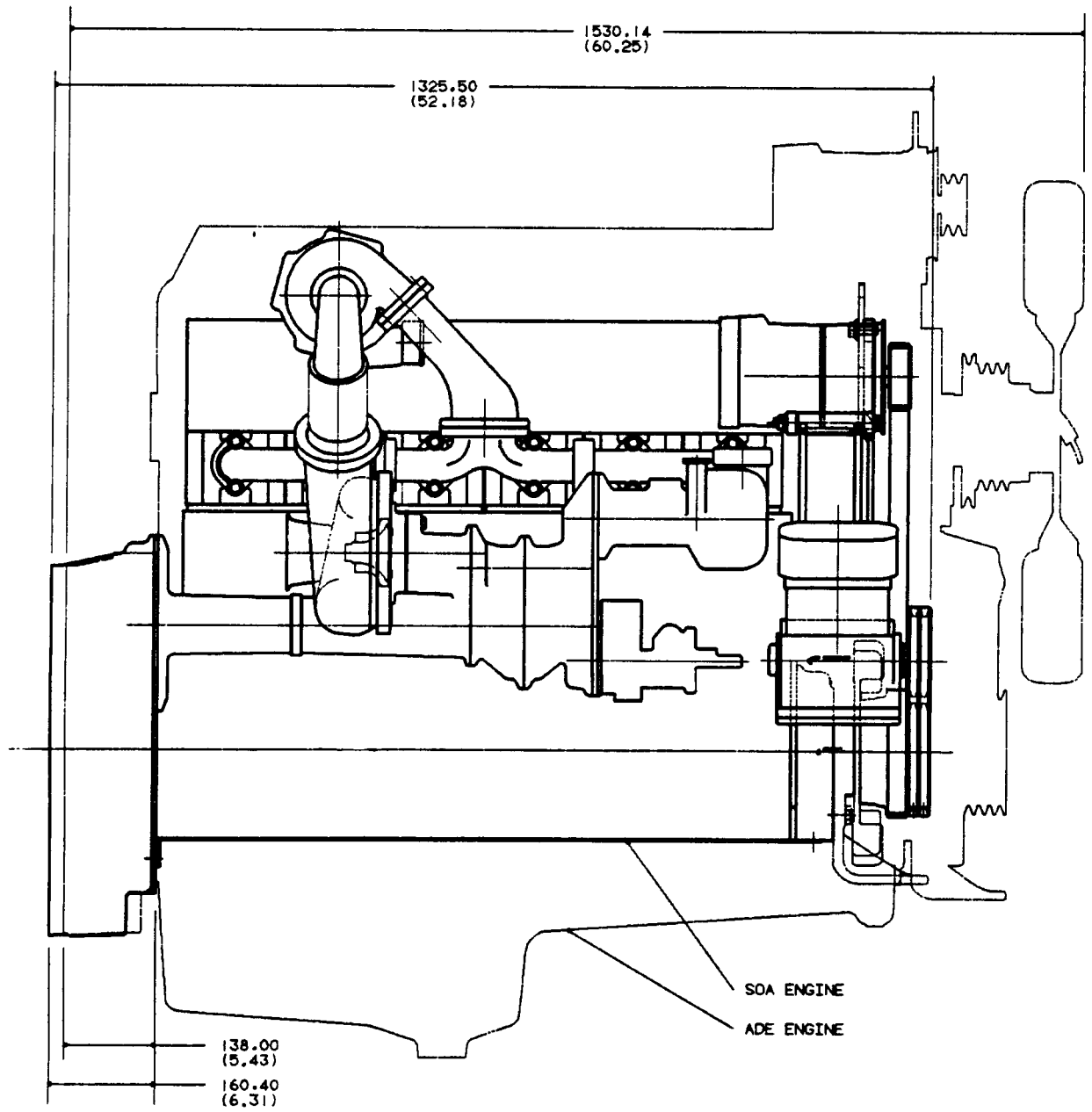


Figure III.1-10: Truck Installation - Side View

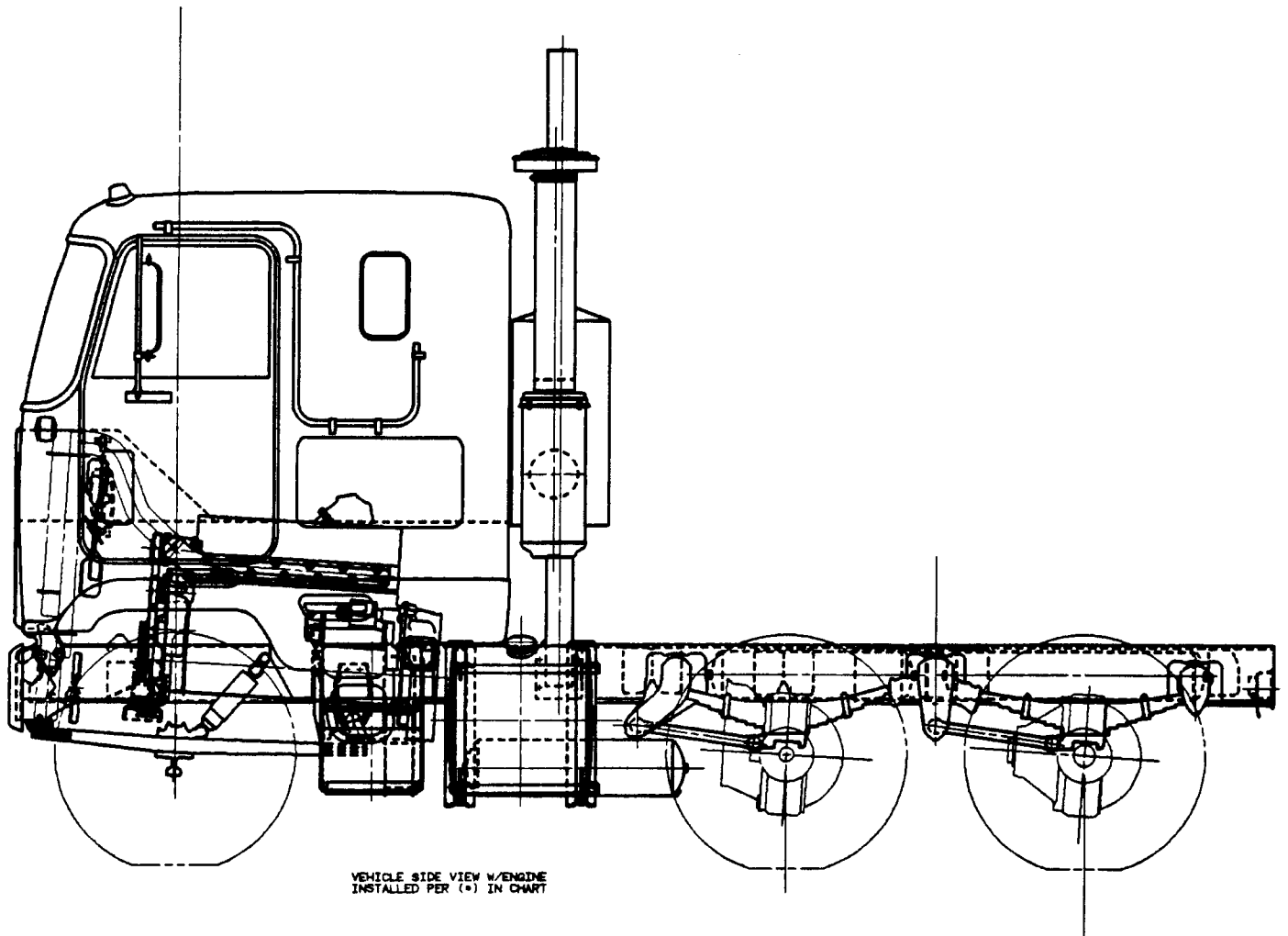


Figure III.1-11: Truck Installation - Front View
(Isotherms and Thermal Stress Contours)

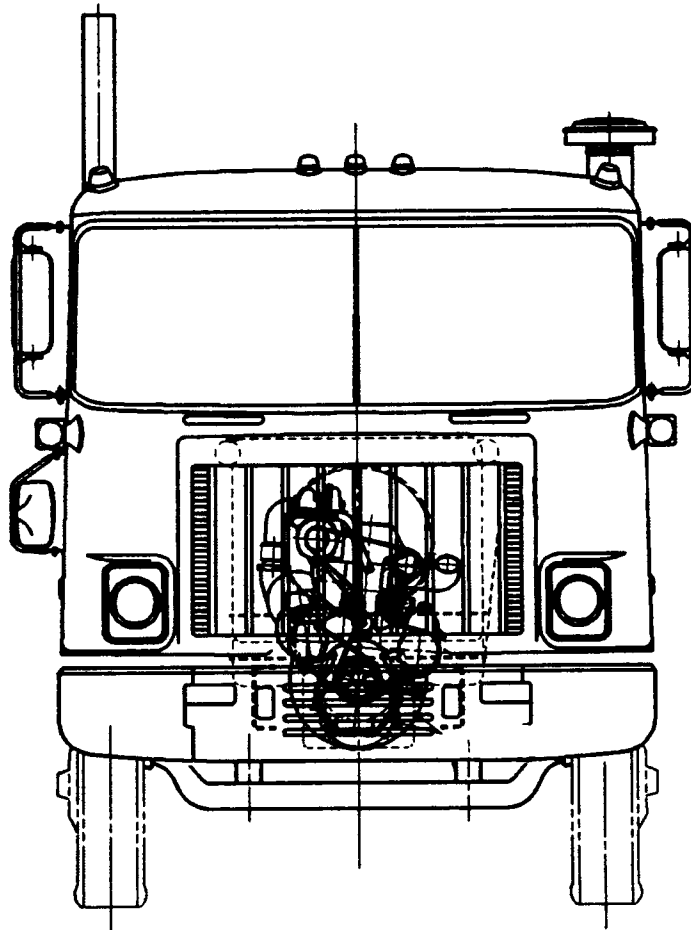


Figure III.1-12: Truck Installation - Top View

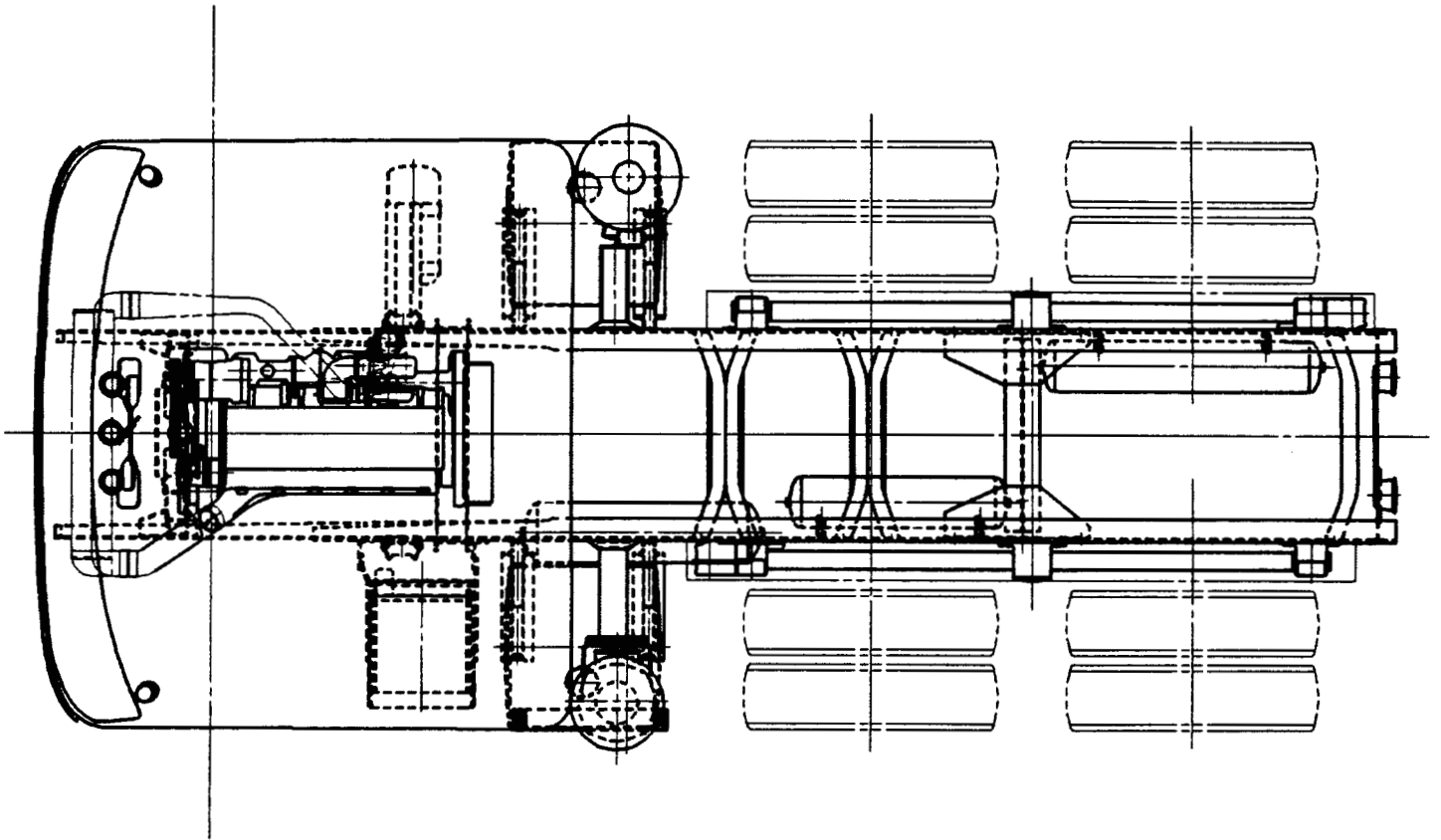
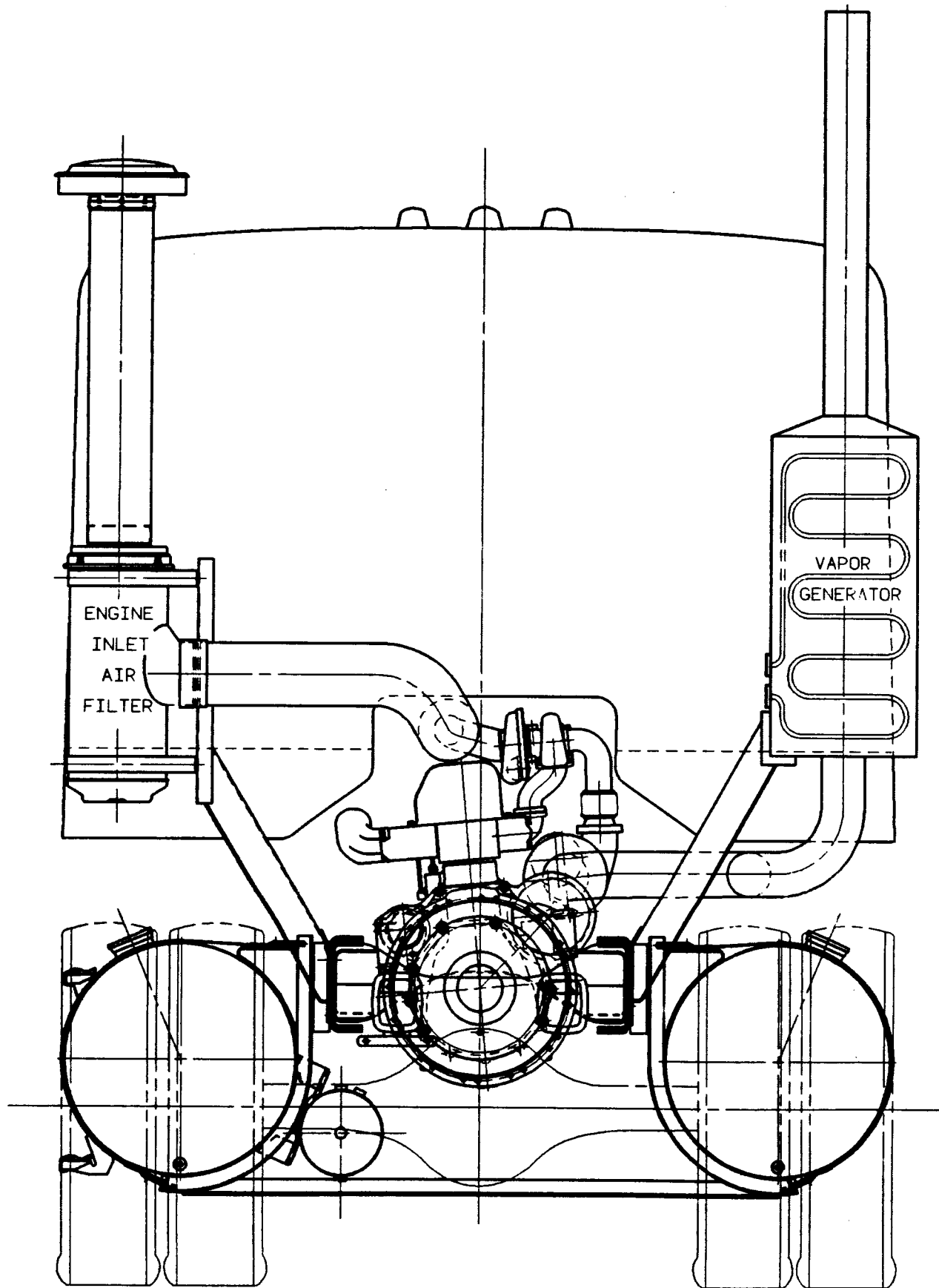


Figure III.1-13: Truck Installation - Rear View



REAR OF VEHICLE W/ENGINE INSTALLED @ 5°

III.2 PERFORMANCE ANALYSIS

The performance analysis effort of the ADRE system aimed at generating the performance maps and generating the boundary conditions required for the structural analysis of various components. In addition, the selection of an electrohydraulic valve actuation system prompted the investigation of the potential effects of flexible valve events on the ADRE system performance. In the context of the latter study, alternate reciprocator-EER combination scenarios were investigated, with the goal of maximizing the bottomer's contribution to the system power.

The performance analyses were carried out jointly at Detroit Diesel Allison in collaboration with Integral Technologies Incorporated (ITI). The ITI subcontract report is provided as Appendix B, and, hence, only highlights of the results will be provided here. The results of in-house analytical work will also be reported.

III.2.1 PERFORMANCE MAPS

In carrying out cycle simulation to generate the performance maps, the following factors were considered:

- The engine was emission limited, per the constraints discussed before in Section II.1
- Exhaust and intake valve timings were optimized at each operating point, to provide the best possible bsfc within the predefined constraints.
- The simulation took into account an assumed 65 percent insulation effectiveness. This means that the heat rejected to the "sink" was 35 percent of a baseline, conventionally cooled engine.

- The friction level of the reciprocator was assumed to be 70 percent of an equivalent state-of-the-art engine providing the same power output. This means that the ADRE system was considered to have 30 percent less friction. This is believed to be a reasonable assumption for the 1995 technology demonstration time frame. The two elements that contribute to friction reduction are the advancement in the engine tribology, and the fact that the ADRE reciprocator is of a smaller size than the conventional engine.

The generated engine performance curve is shown in Figure III.2-1. The ADRE system brake power was the resultant output of the reciprocator, turbocompounding turbine power, and the organic Rankine system bottomer power. Specifically, the following bsfc values are shown on the figure for the specified operating points:

- Rated point bsfc is 153.2 g/kWh (.252 lb/bhp.hr).
- Peak torque bsfc is 150.8 g/kWh (.248 lb/bhp.hr).
- Minimum ADRE system bsfc is 150.2 g/kWh (.247 lb/bhp.hr).

III.2.2 PERFORMANCE ADVANTAGES OF VARIABLE VALVE EVENTS

The investigation of the performance advantages of the variable valve events consisted of four main studies:

- Valve opening and closing rate.
- Pressure compounding.
- Alternate reciprocator-EER power combination scenarios.
- Cylinder cut-off, based on power demand.

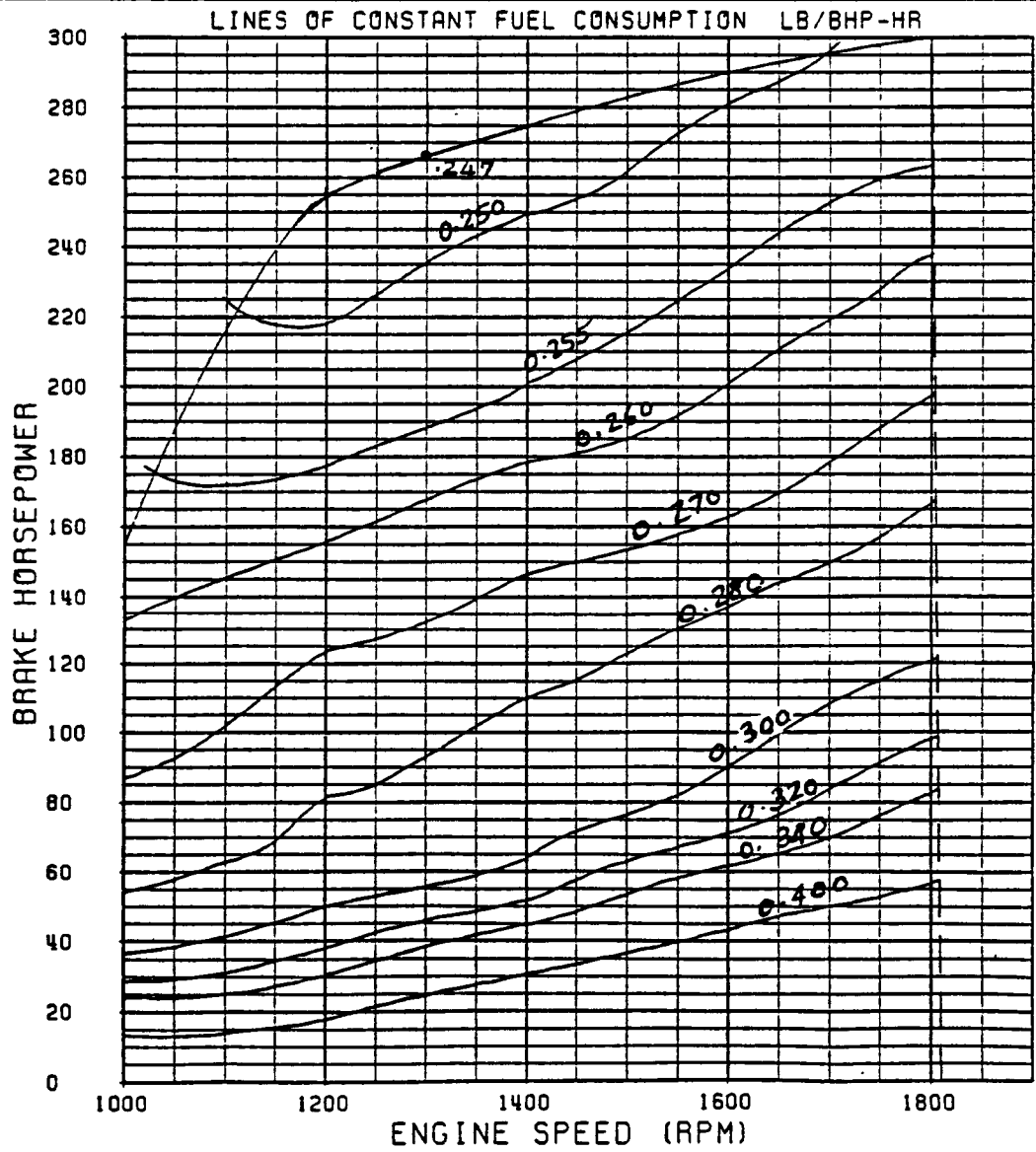
The first three studies were conducted mainly by ITI, and the detailed findings are reported in Appendix B. Essentially, it was concluded that a faster valve event, by itself, does not necessarily result in significant performance improvements. It was noted that the optimum timing for the event is dependent on the specified rates. Hence, best bsfc can be obtained for certain opening and closing rates when the matching optimum timing is utilized. However, it should be noted that the optimum timing changes with speed and load.

The pressure compounding, or early intake valve closure, was investigated next. The merits of this approach were not significant enough to warrant the use of the variable valve events concept. This prompted the investigation of alternatives utilizing the bottomer power. As explained in Appendix B, the most feasible alternative turned out to be in combination with pressure compounding. In this scenario, the bottomer power was used to derive the required pressure compounding compressor. The findings showed that this approach would not offer any performance gain over the baseline ADRE system with turbocompounding and bottomer.

The electrohydraulic valve actuation system can be adopted to provide cylinder cut-off, based on part load demands. In-house investigations revealed that this would offer the most gain. A case study considered a typical road load of 105 kW (141 hp). The conventional engine would have six cylinders, running at 1800 r/min, using the standard turbocharger turbine, and having an air/fuel ratio of 41:1. With cylinder cut-off, on the other hand, the ADRE system would have three firing cylinders, running at 1800 r/min, using a 15 percent reduced turbine, and having the smoke-limited air/fuel ratio of 22:1. The resulting bsfc would be 161.1 g/kWh (.265 lb/bhp.hr), compared to the baseline ADRE system value of 176.3 g/kWh (.290 lb/bhp.hr). This means that, in this case, the bsfc improvement due to cylinder cut-off is 15 points or 8.6 percent improvement in fuel economy.

Figure III.2-1: ADRE Performance Map

DETROIT DIESEL ALLISON	ENGINE PERFORMANCE
	ENGINE DESCRIPTION NASA/DOE ADECO
	APPLICATION AUTOMOTIVE
	INJECTOR ELEC
300BHP • 1800RPM	



III.3 VALVE AND VALVE ACTUATION SYSTEMS

This section reports on the ADRE system studies on valve dynamics, investigations on non-mechanical valve actuation mechanisms, and monolithic ceramic valve structural analysis.

III.3.1 VALVE DYNAMICS

The purpose of this study was to define and analyze the intake and exhaust poppet valves proposed for the ADRE. Valve event definition, kinematic, and power analyses were undertaken. Specific tasks undertaken were geometric definition and limitations of the ADRE valves, valve displacement versus crank angle event definition, kinematic and kinetic analysis, and ideal power required to actuate the valves.

CONCLUSIONS

1. A common monolithic ceramic valve design will be used in the intake and exhaust positions. Estimated valve weight is 0.058 kg.
2. Performance based optimized air flow event was modified for acceptable valve seating velocity, without sacrificing performance. The projected valve seating is 0.25 mm/s max., or .0231 mm per crank degree.
3. The mean 'ideal' power to operate all the 24 ADRE valves, without springs, is 2303 W. This accounts for 746 W for the intake valves, and 1557 W for the exhaust valves.
4. A valve return spring will require additional operational force and can result in more power demands.

5. The results were compared to the case for a Detroit Diesel Allison state-of-the-art engine. It is concluded that the proposed ADRE valve and valve events are significantly different from today's conventional systems, and further proof-of-concept effort should be pursued.

DISCUSSION

Valve Design - The elimination of liquid lubrication from the ADRE, and the selection of the high risk configuration required the use of monolithic ceramic valves. In addition to the tribological benefits, the low mass and inertia of a lighter weight valve is an additional advantage of a ceramic valve. Adopting a common valve design for both intake and exhaust locations is desirable, but imposes certain challenges to maintain optimal features for both events, with minimum trade-off's. The common monolithic valve design adopted for the ADRE is shown in Figure III.3-1. It is noted that the objective of this phase of the ADECD program was to establish the feasibility of a certain design. The valve design in Figure III.3-1 meets this objective. Detailed analysis and design refinements will be carried out during the next phase of the program, for the purpose of hardware procurement and testing.

Valve Event, Kinematic and Power Studies - Extensive testing, within General Motors and by outside suppliers, established desirable limits for safe seating velocities for metallic and monolithic ceramic valves as .5 mm/s and .05 mm/s, respectively. The limit for the ceramic valve is believed conservative, and is being progressively relaxed as better materials and proof-of-concept data become available. At rated engine speed of 1800 r/min, a design seating velocity limit of 0.25 mm/s was adopted for the ADRE monolithic ceramic valves. This translates to 0.0231 mm per crankshaft degree.

The performance-based recommendations of the time dependent exhaust and intake valve opening areas are shown in Figure III.3-2. These minimum gas flow areas were translated into valve displacements, using the valve geometry shown in Figure III.3-1 and a flow coefficient of 0.25. The resulting intake and exhaust valve displacements versus crank angle are shown in Figures III.3-3 and -4, respectively. The figures show a 6.81 mm maximum required displacement, corresponding to the recommended 8 cm² flow area per valve. Differentiation of the shown valve displacements, however, resulted in valve seating velocities that are higher than the target design limit of 0.0231 mm per crank degree.

To simultaneously maintain the desired performance characteristics and allow for reasonable valve durability, a new valve event design was necessary.

The 8° x 42° Exhaust Valve Event - The following valve event characteristics were used to define a new exhaust valve event that maintained the desired performance characteristics and a reasonable seating velocity:

- . 250° event duration
- . maintain or exceed the 130° dwell at 6.81 mm displacement
- . add a 22° 0.0231 mm/crank degree constant velocity section to the event for seating

An exhaust valve event that meets these criteria has been developed, and is shown in Figure III.3-5. The designation for this event, 8° x 42°, identifies the 8° duration to maximum acceleration and the 42° duration to 6.81 mm displacement or 6.0 cm² flow area per valve. The maximum valve displacement, shown in Figure III.3-5, is 9.0 mm. This allows up to 0.45 mm of relative expansion between the cylinder head and the exhaust valve actuation mechanism, while maintaining the 0.0231 mm/crank degree seating velocity limit.

The flow area per exhaust valve, flow area per cylinder, velocity and acceleration versus crank angle are shown in Figures III.3-6 to -9. The inertia, gas pressure, and resultant forces acting on the exhaust valve are shown in Figures III.3-10 to -12, respectively. Figure III.3-12 shows that the maximum force required to actuate each $8^\circ \times 42^\circ$ exhaust valve is 1181 N. The ideal power required to actuate each $8^\circ \times 42^\circ$ exhaust valve per crank angle is shown in Figure III.3-13. It is noted that no power is required to hold the valve open during the dwell portion of the event. The maximum instantaneous ideal power required is 2031 W. The total power required to actuate the exhaust valves of the six cylinder ADRE is the sum of the required instantaneous power per each cylinder over a full four-stroke cycle. This resultant power requirement is shown in Figure III.3-14. The calculated mean power requirement is 1594 W. However, the figure shows that the maximum instantaneous power required from a valve actuation system will be in excess of 4000 W. This value will be critical in sizing the valve actuation system according to the required time-dependent power capacity.

It is interesting to note that the inertial load spike associated with maximum acceleration occurs when the pressure loading is also very high. This increases the required instantaneous peak and mean power levels. Further analyses were undertaken for the exhaust and intake valves, in order to decrease the cycle peak power requirements without significant sacrifice in the performance constraints.

Design Point Valve Events - Similar analyses were undertaken to determine new valve events that offer the best compromise between the performance requirements and the actuation system power requirements. Using the same terminology as above, a $28^\circ \times 50^\circ$ event was selected for both the exhaust and intake valves.

For the exhaust valve, this new event effectively shifted the peak of the inertia load to a more favorable location, away from

the gas pressure peak. The performance based constraints were all maintained, except that the dwell of 130° shown in Figure III.3-2 was changed to 126° . The maximum instantaneous ideal power required for this event is 1692 W, compared to the 2031 W of the prior $28^\circ \times 42^\circ$ valve event case. This resulted in a saving of 16.7 percent over the original peak demands per valve. The valve actuator would, thus, be reduced in size and power consumption in a proportionate manner.

The modified net ideal actuation power for the entire ADRE exhaust valve train is shown in Figure III.3-15. For this case, the mean power requirement was reduced to 1547 W. The figure also shows that the maximum instantaneous power required from the ADRE exhaust valve actuation system is now less than 3500 W. Compared to the prior case, this would have significant positive impact on the valve actuation system design and feasibility. Further, it would most likely effect reasonable savings on the engine parasitic losses, with respect to the actuation system power consumption.

The intake valve event was designed using the $28^\circ \times 50^\circ$ scenario. The resulting total power requirement was superimposed on the exhaust valves power curve and is shown in Figure III.3-16. The combined ideal power to actuate the twenty-four ADRE intake and exhaust valves is shown in Figure III.3-17.

III.3.2 NON-MECHANICAL VALVE ACTUATION CONCEPTS

An ideal poppet valve actuation system would provide an "infinitely" variable valve timing, duration and lift with minimal input power. Variable valve timing, duration, and lift could provide numerous performance benefits and operational features, including idle control, improved startability and engine braking. This ideal valve actuation system must meet the functional and dynamic requirements, as well as the space limitations of the ADRE.

Several mechanical system concepts and demonstration hardware exist that, in principal, can meet the ADRE valve actuation design goals. All of these systems, however, require well-lubricated infrastructure. The fact that the ADRE does not have liquid lubricant precludes further consideration of any of these mechanical systems.

Four valve actuation systems were conceived for the ADRE. The end objective was to select the most feasible concept for the ADRE reciprocator. The non-mechanical valve actuation systems investigated during this study included:

- A hydraulic actuation system, with electronic controls.
- An electronically controlled, electromagnetic system.
- A pneumatic system, with electronic controls.
- A hybrid hydraulic-pneumatic system with electronic controls.

Each of these systems offers variable timing and duration. They also have common concerns, including difficulty in the control of valve seating velocities and likely require cooling burden. In addition, each system has its unique aspects that will be described below.

CONCLUSIONS

1. The hydraulic system concept is recommended. This system appears to be the most reliable and efficient. It can potentially be developed to have the following features:
 - It appears to have the ability to meet the valve event and kinematic requirements,
 - It will have the ability to vary the valve timing,
 - System power consumption appears reasonable,
 - This concept seems to be simpler and more reliable, relative to the other concepts considered.
2. A non-mechanical valve actuation system appears feasible. This system can meet the design criteria, including variable valve timing and duration, required flow area versus crank angle, capability of engine braking, no lubrication system, and limited cooling.
3. The study of the pneumatic-based actuation concept revealed serious limitations on its technical feasibility. This is due to potential lack of valve control, compressed air seal reliability and durability, lubrication needs, and system cooling requirements.
4. The hydraulic-pneumatic system concept was also eliminated from further consideration, due to the increased complexity of the actuator, and the multi-fluids and electronic circuits required.
5. The electromagnetic concept, which appeared attractive in the initial stages, was also ruled out. Careful assessment of current and projected technologies indicated that the ADRE's

opening duration, required opening force, and maximum valve lift cannot all be met by a solenoid of a reasonable size and capacity.

6. Dynamic engine braking is a desired feature for the ADRE. Conceptually, this feature can be implemented with a hydraulic actuation concept. No further assessment was carried out in this study.
7. The fail-safe aspects of the investigated concepts needs to be resolved. It is planned to handle this issue during the next phase of the ADECD program.

DISCUSSION

The valve events prescribed in Section III.3.1 are beyond the capability of a conventional mechanical valve actuation system. Each of the four different concepts of non-mechanical valve actuation systems studied requires some type of an Electronic Control Module (ECM), along with the associated drivers, sensors, motors, and/or solenoids. Some means of controlling valve seating velocities and dissipation of the friction generated have to be incorporated. The systems are not considered fail safe in their current configurations. In addition to these common features, each system has its unique features.

Pneumatic Concepts - A pneumatic system is theoretically capable of meeting the ADRE design criteria. As the name implies, this system uses air as a working fluid. A problem with using air is that its compressibility can result in a lack of desired accurate valve control.

A pneumatic concept system requires air pressure supply hardware, including compressor, accumulator, regulator, filters, and high pressure gas plumbing. In addition to these components, a means of priming and sequencing the actuators prior to starting the

engine is needed. There are potential concerns in the areas of seals, internal temperature control, internal lubrication, and accurate, repeatable, valve motion control. Hence, the pneumatic concepts were eliminated from further consideration.

Hydraulic-Pneumatic Concepts - Some manufacturers of the large bore, slow speed diesel engines use a hydraulic pneumatic valve actuation system that is controlled by an electromagnetic circuit. In this type of system, the noncompressible hydraulic fluid provides good system control, while the compressible air provides some much needed damping prior to valve seating. Combining the hydraulic and pneumatic systems allows the strong points of each system to overcome the other systems' weak points. The most significant problems with such systems result from the complexity in the actuator design and the numerous sub-systems (air, hydraulic, and electrical) required for the actuator. For a package of the ADRE size, for on-highway applications, these concerns ruled out the hydraulic pneumatic concepts from further consideration.

Electromagnetic Concepts - An electromagnetic system is relatively simple in comparison to the other systems. The most significant problems with the electromagnetic systems considered were achieving enough valve lift in the required time frame and controlling the valve seating velocities. Another concern with these systems was the relatively large amount of power required to generate the forces needed to actuate the ADRE valves.

The electromagnetic valve actuation approach was discussed with Lucas' SGRD Ltd England. Lucas experimented with solenoid valve actuation. A Helenoid actuator opened the valve against a spring, and the spring was used to return the valve. Limited success was reported. This experience appeared to confirm the results of our own studies.

A system concept that is based on linear actuation was conceived. An electric motor with linear actuator could be

incorporated into the ADRE overhead system. However, analysis showed that the required rate and accuracy of the valve events could not be accommodated.

Our in-house research efforts show that an electromagnetic system, capable of moving the valve according to the ADRE valve lift curve, can be designed. However, there are some major problems that must be overcome, such as the insufficient space on the cylinder head, achieving required opening force with reasonable number of electric coils, controlling and changing the rate of acceleration, and providing an acceptable electrical shielding environment.

Based on these studies, a solenoid-based electromagnetic valve actuation system was designed into the ADRE cylinder head, as shown in Figures III.3-18 and -19. As shown in Figure III.3-19, the size constraints were addressed, using a "Y" shaped rocker arm with a bend at the rocker shaft, so that a solenoid could be mounted to the side of the cylinder head. In this arrangement, the rocker arm opens two valves by an actuating solenoid, having its linear motion perpendicular to the valve center line. The use of a rocker arm in the system also provided a significant reduction in the required actuator force, as a result of the rocker ratio. However, such reduction in the solenoid force requires a proportionally longer actuator stroke. Based on our assessment of current and projected technologies, the ADRE valve actuation requirement and objectives cannot likely be met by a solenoid actuation system.

Evaluating the power requirements of an electromagnetic system proved to be quite difficult. The lack of experimental data on a solenoid of this type of application required speculative estimates of the solenoid efficiency. Limited testing and analysis carried out within General Motors shows little difference in power consumption between an electromagnetic system and a conventional mechanical system, at relatively low opening speeds and low force levels. At the valve opening speeds and forces required for the ADRE, analysis indicates that the power consumption can potentially increase by about 3 to 4 times.

The control of the valve seating velocity can conceivably be achieved by reversing the current in the solenoid, just prior to the seating event. This would provide a "damped electronic braking." However, bringing the valve seating velocity characteristics to the required profile requires further investigation. Another approach to control valve seating characteristics is through the use of a hydraulic or pneumatic damper. A simple version of a pneumatic type damper has been used in limited laboratory tests for a passenger car valve actuation system. The preliminary results indicate the feasibility of the concept for that particular application.

For the ADRE, it is estimated that at least 40 A at 100 V, or 4 kW, would be required to open the exhaust valves against the cylinder pressure at rated conditions. This implies a high rate of power consumption and potential concern, with respect to electric shielding and safety. Further, the high level of power consumption would result in significant amount of heat rejection. This would necessarily require some form of forced cooling, since the current state-of-the-art magnet system has an operating temperature limit of about 125°C.

The above described system is believed to be the most viable among the electromagnetic concepts. However, it still does not meet the other ADRE goals. This leaves the hydraulic actuation concept as the remaining approach for a viable ADRE operating system.

Hydraulic Concepts - The hydraulic actuation concepts are, in fact, a hybrid hydraulic-electromagnetic system that uses solenoids to activate moving parts within a fluid network. These systems will have to be electronically controlled via the ADRE computer-based control system. They appear capable of meeting the ADRE actuation specifications.

One form of a hydraulic valve train was reportedly pursued by Lucas (SGRD) of England. A mechanically assisted hydraulic valve

actuator consisted of a high pressure rail supplying fluid to a hydraulic cylinder that opened the valve. The valve closure was by a valve spring. The rate of opening and closing was controlled by two solenoid actuators which "pulsed" on command, controlling the fluid inlet and outlet. Lucas believes this system shows promise over the previously pursued electromagnetic systems.

Within General Motors, the hydraulic valve actuation systems have been investigated. These systems can either use a valve spring or control both the valve opening and closing via the hydraulic system. A double acting hydraulic actuation system is believed viable for the ADRE. The layout drawing of this system concept is shown in Figures III.3-20 and -21. The basic design consists of a hydraulic actuator positioned on top of each valve. Each pair of exhaust or intake actuators are controlled by a signal spool valve and solenoid assembly.

The hydraulic system requires a pump, accumulator, regulator, filters, cooler and other miscellaneous hardware. A means of priming and sequencing the actuators prior to starting the engine needs to be developed. System cooling aspects may require further investigation. The ADRE overhead is designed with a protective cover that can form a tunnel over the solenoids of the valve actuation system. A forced air cooling fan can be incorporated to provide the necessary cooling. The estimated total power required to actuate the ADRE valve system at 1800 r/min is 6043 W (8.1 hp). This figure is competitive when compared to the state-of-the-art conventional camshaft systems. Detailed design and analytical studies are planned for the following phases of the ADECD Program.

The RPD hydraulic electromagnetic system was selected as the most reliable and efficient variable timing/duration system investigated.

III.3.3 CERAMIC VALVE STRUCTURAL ANALYSIS

Finite element and probability of survival analyses were carried out on an exhaust valve. The valve was subjected to both thermal and mechanical loading. This section briefly reports on this study.

CONCLUSIONS

It is concluded that a well-designed valve made of high quality structural ceramic material, such as silicon nitride, will survive the ADRE operating constraints.

DISCUSSION

An axisymmetric finite element mesh of the proposed valve design was developed. The valve was constrained to slide along the ceramic deck along the 45° plane of contact with the seat area. From engine cycle simulation, boundary conditions were generated for thermal finite element analysis, which determined the temperature distribution. To study the effect of the ceramic material thermal conductivity (k) on the temperature distribution and heat rejection through the valve, two values of k were examined. The first value used was a typical state-of-the-art conductivity for a sintered silicon nitride material. The other value was one half of the current k values, which conceivably represents the state of developments of monolithic and composite ceramics in the 1995 time frame. The results of the thermal analysis are shown in Figure III.3-22.

The structural analysis included examination of the thermally and mechanically induced stresses, and superposition of both loads. The results are shown in Figure III.3-23. The probability of survival of the valve under simulated static loads is very close to 1.0. Further investigation on response to dynamic and impact loading is planned for the future ADECD phases.

Figure III.3-1: Monolithic Ceramic Valve

Volume = 18.078 cm³
Density = 3.22 grams/cm³
Mass = 58.20 grams

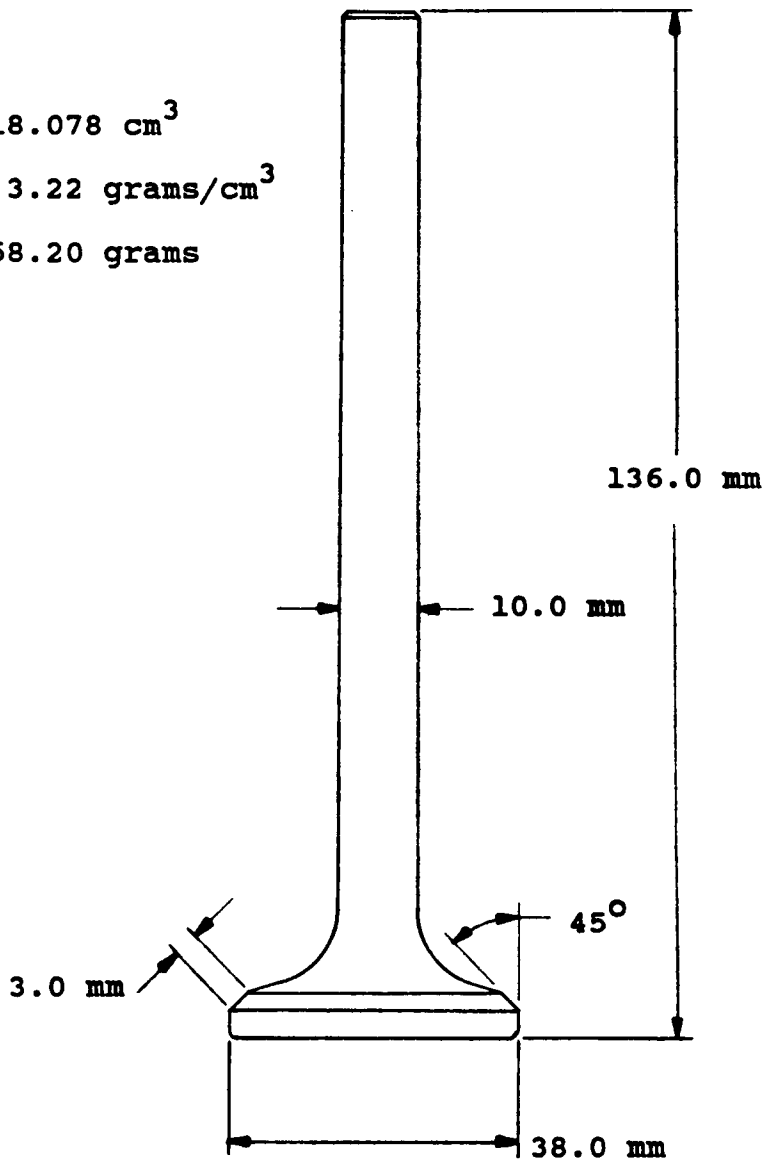


Figure III.3-2: Performance-Based Air Flow Recommendation
(1800 r/min/223.7 kW)

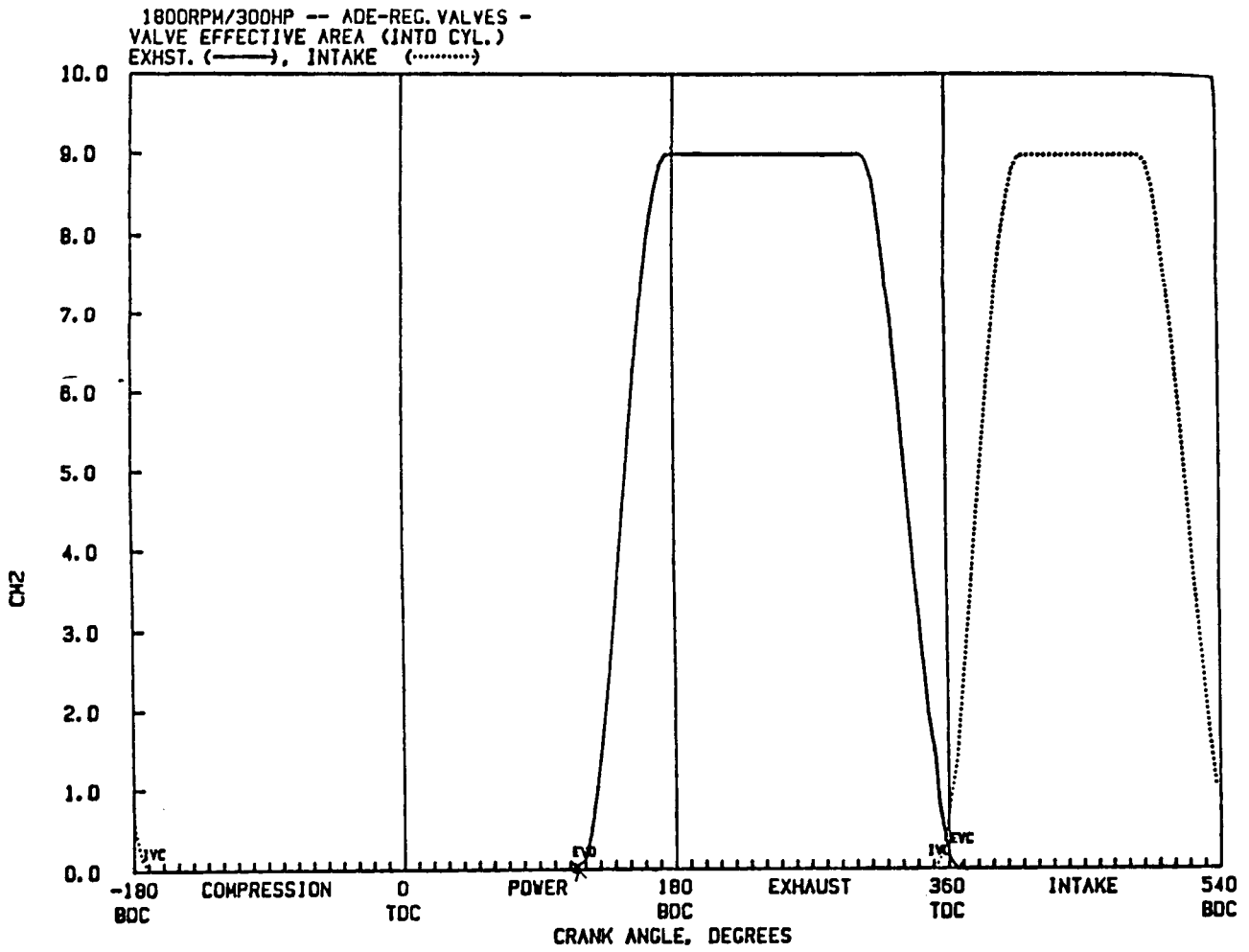


Figure III.3-3: Performance-Based Intake Valve Displacement

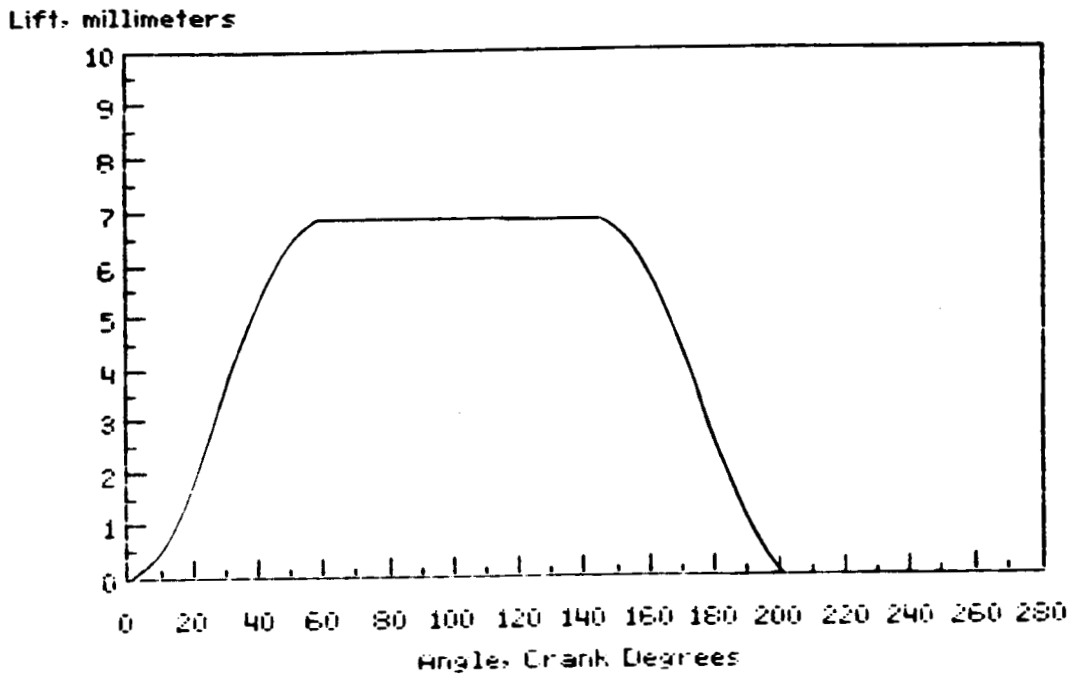


Figure III.3-4: Performance-Based Exhaust Valve Displacement

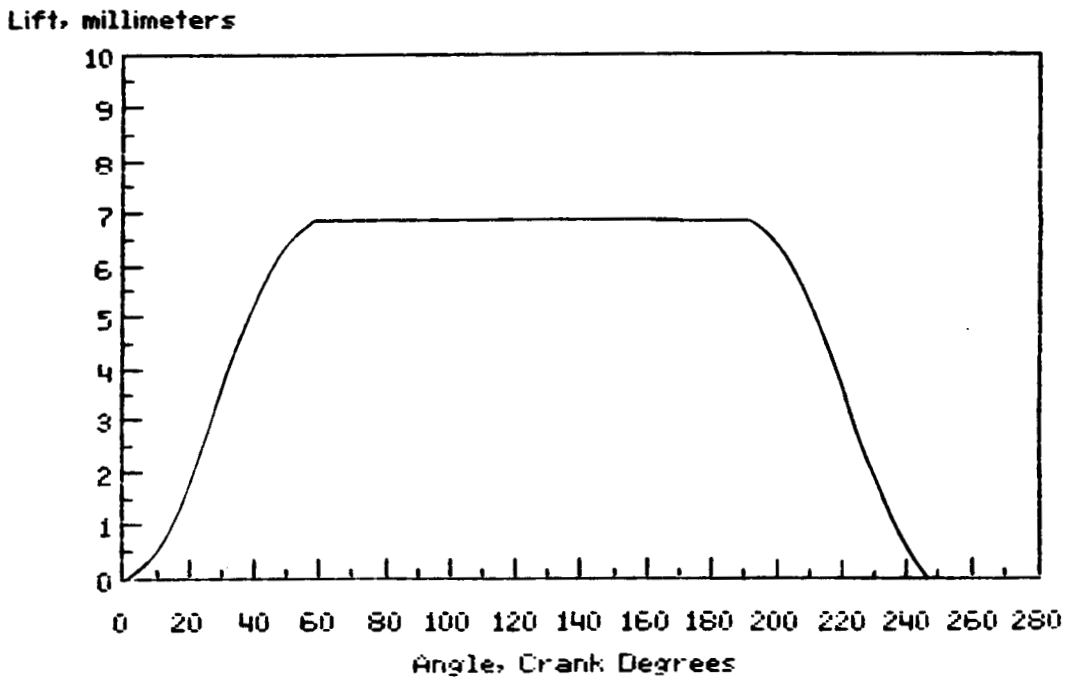
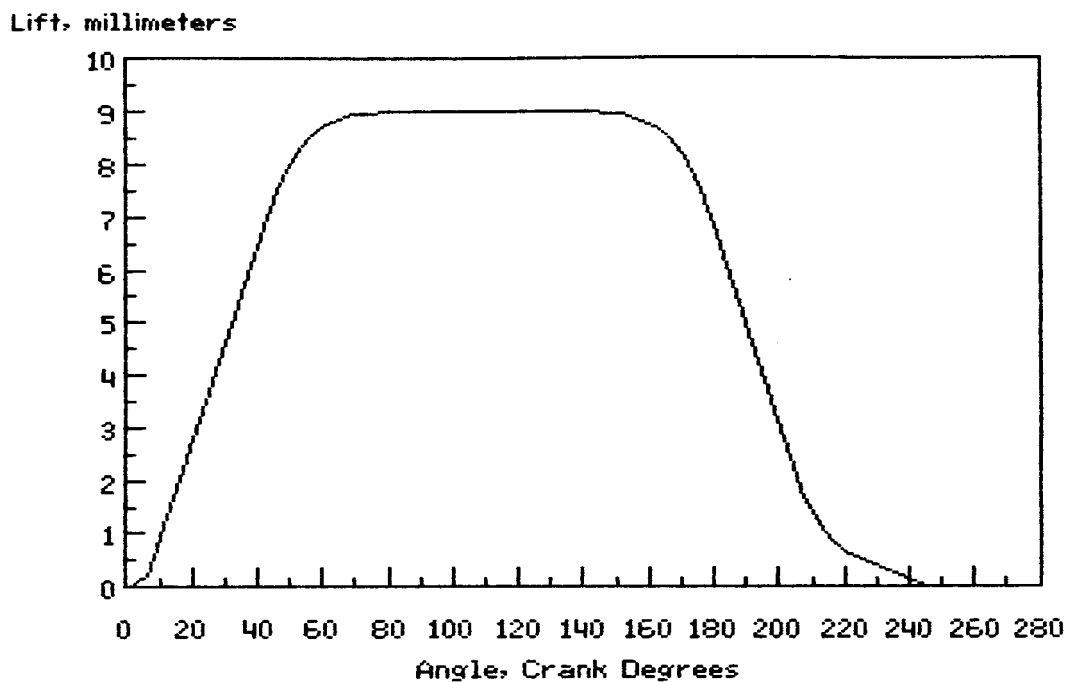
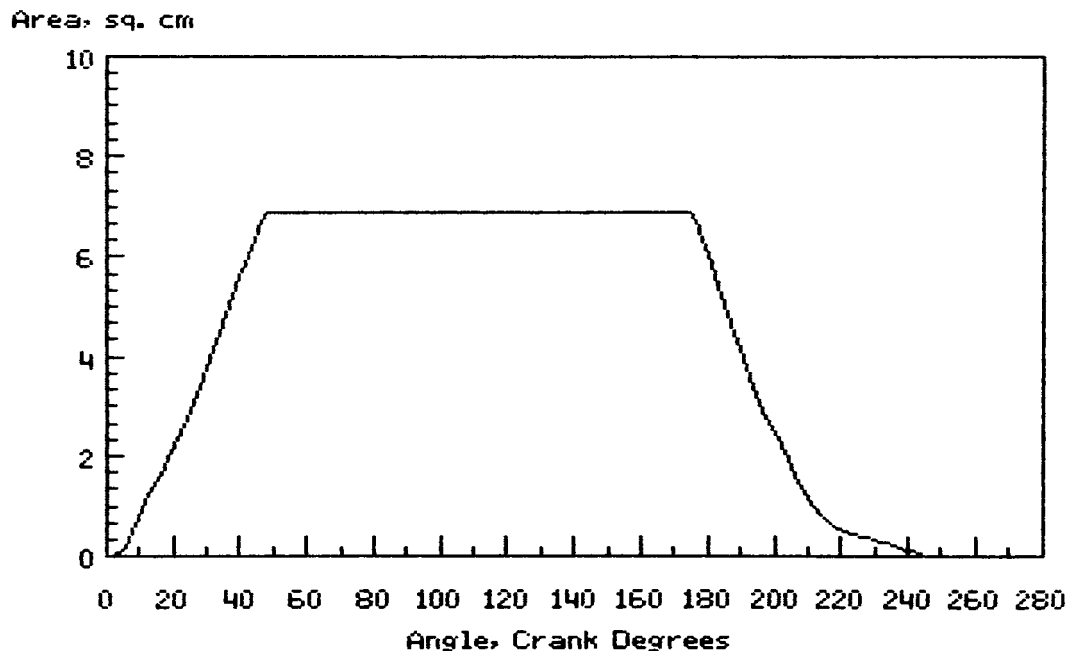


Figure III.3-5: 8° X 42° Exhaust Event



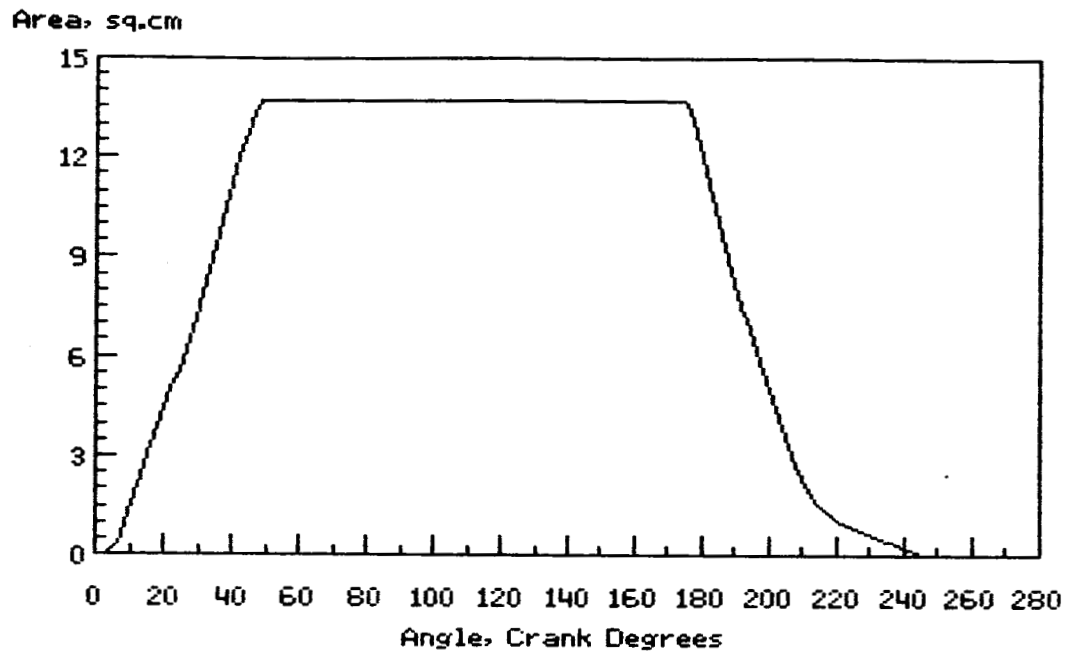
Lift: 8 Deg Max-accel, 42 Deg Ramp

Figure III.3-6: Air Flow per Valve for the 8° X 42° Exhaust Event



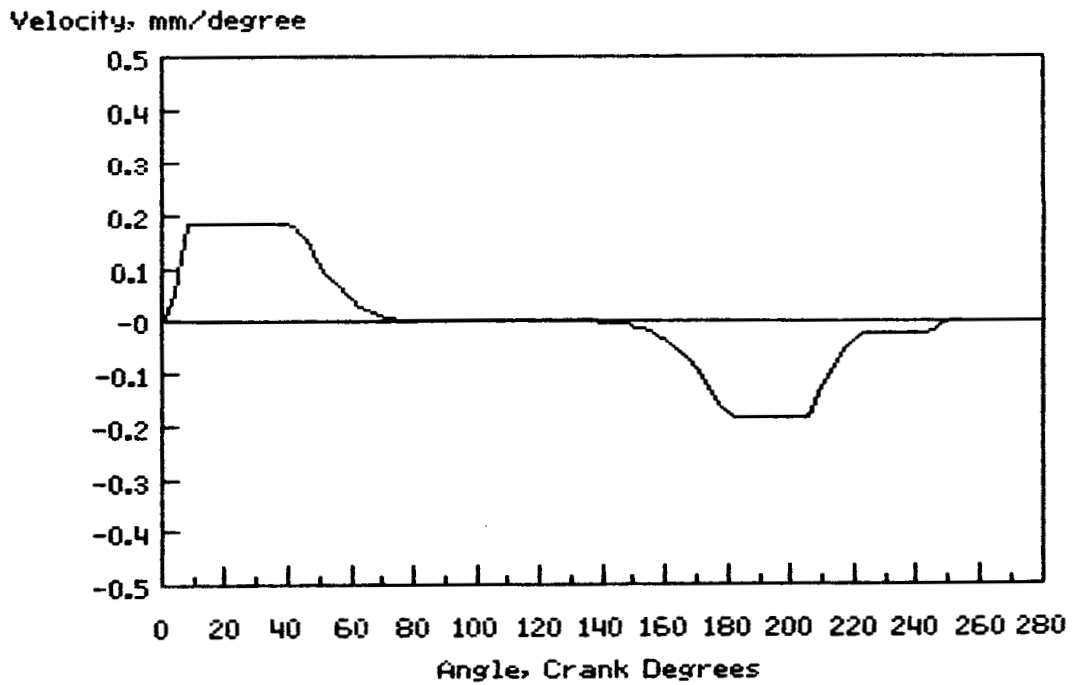
Lift: 8 Deg Max-accel, 42 Deg Ramp

Figure III.3-7: Air Flow per Cylinder for the 8° X 42° Exhaust Event



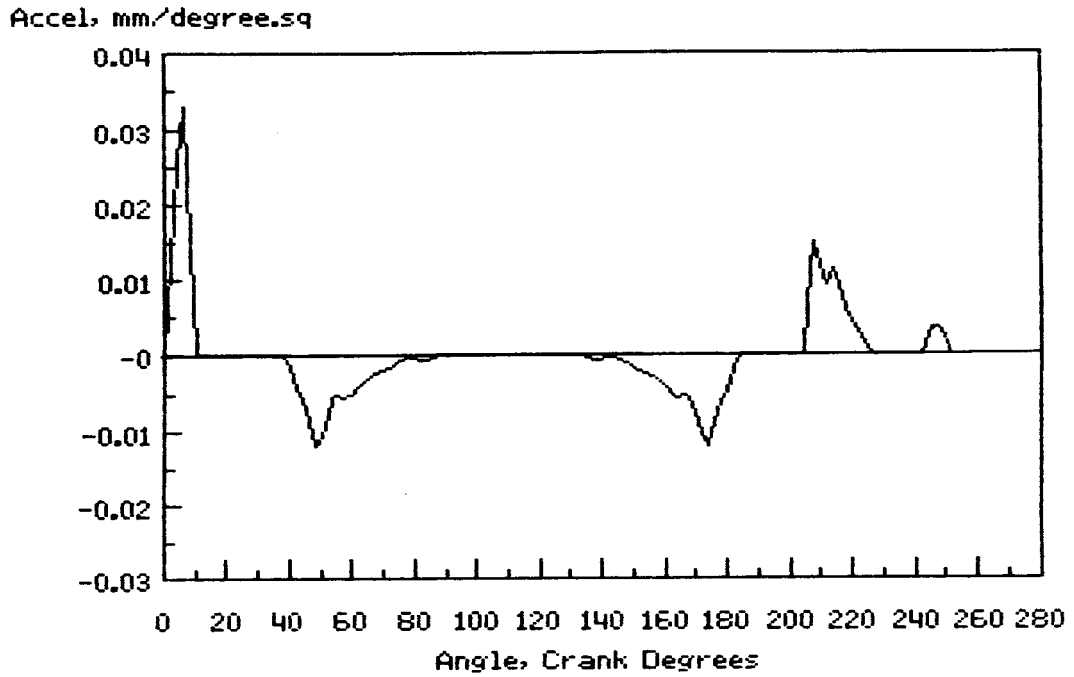
Lift: 8 Deg Max-accel, 42 Deg Ramp

Figure III.3-8: Velocity Profile for the 8° X 42° Exhaust Valve Event



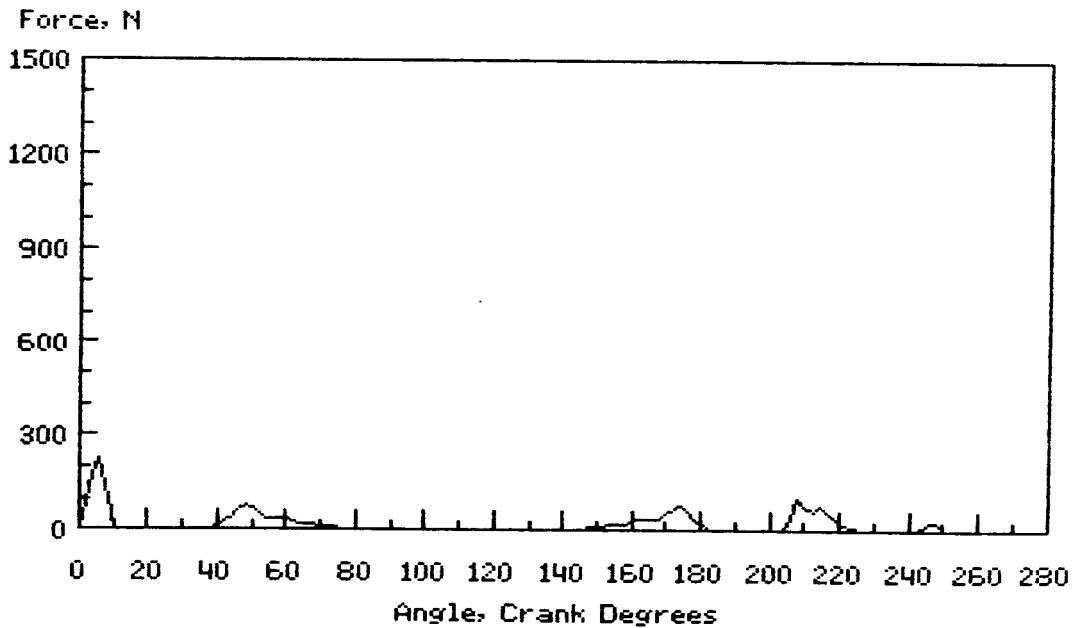
Lift: 8 Deg Max-accel, 42 Deg Ramp

Figure III.3-9: Acceleration Profile for the 8° X 42° Exhaust Valve



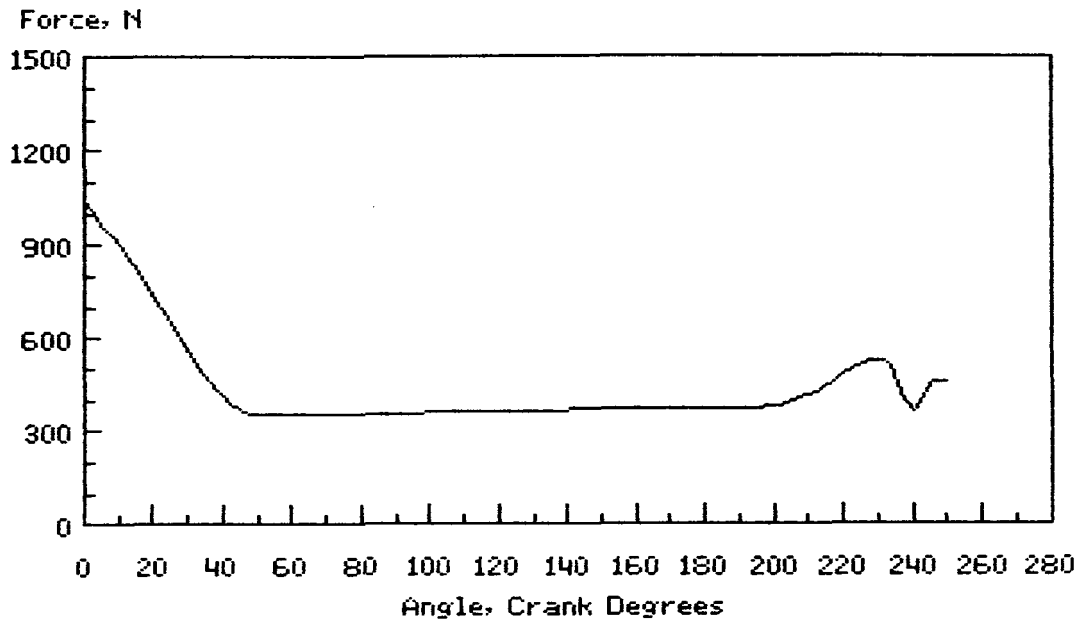
Lift: 8 Deg Max-accel. 42 Deg Ramp

Figure III.3-10: Inertia Force on Each Exhaust Valve



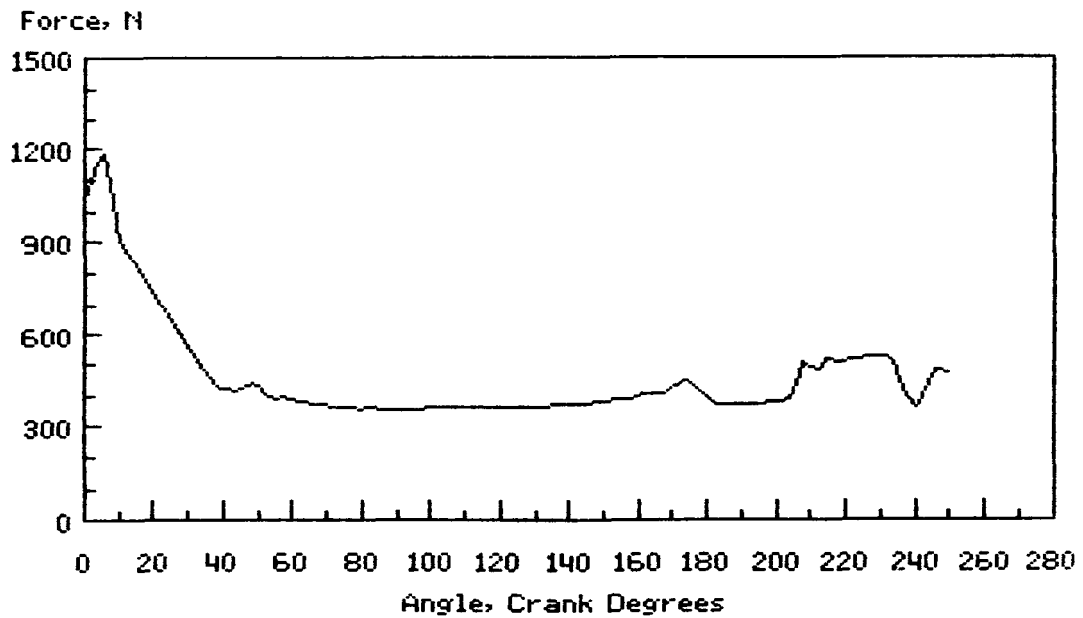
Lift: 8 Deg Max-accel. 42 Deg Ramp

Figure III.3-11: Pressure Force on Each Exhaust Valve



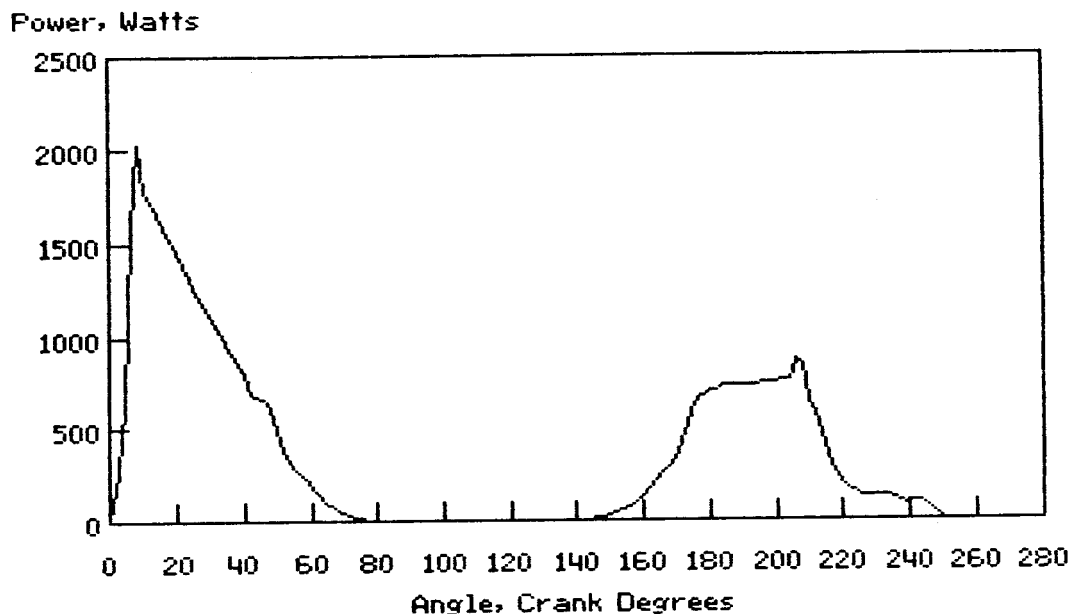
Lift: 8 Deg Max-accel, 42 Deg Ramp

Figure III.3-12: Required Actuation Force Profile for the 8° X 42° Exhaust Valve at 1800 r/min Engine Speed



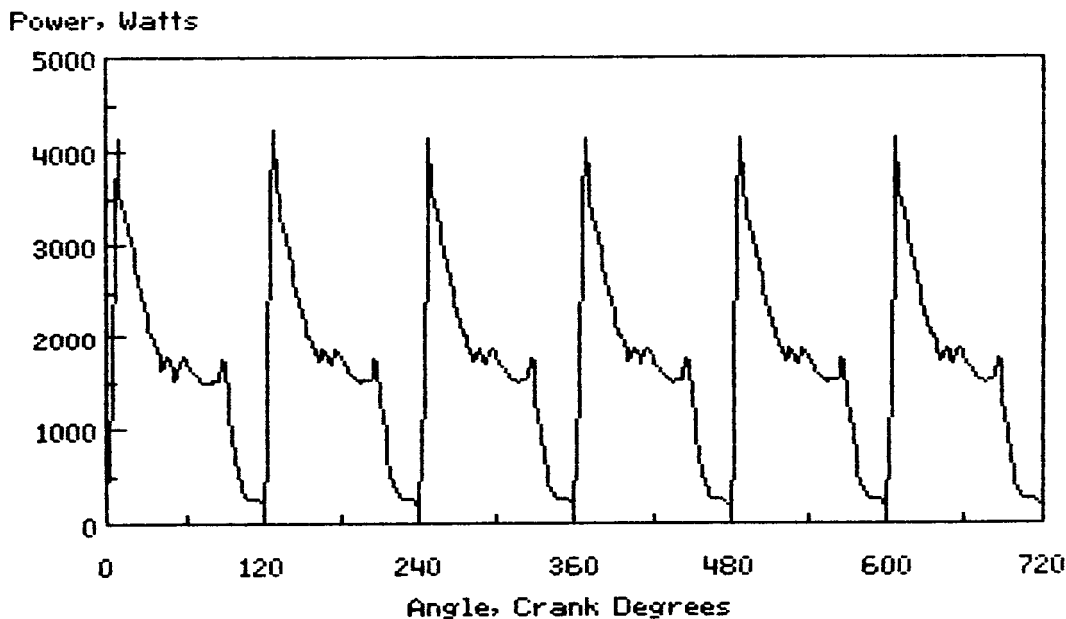
Lift: 8 Deg Max-accel, 42 Deg Ramp

Figure III.3-13: Power Required to Actuate Each Exhaust Valve for the 8° X 42° Valve Event at 1800 r/min Engine Speed



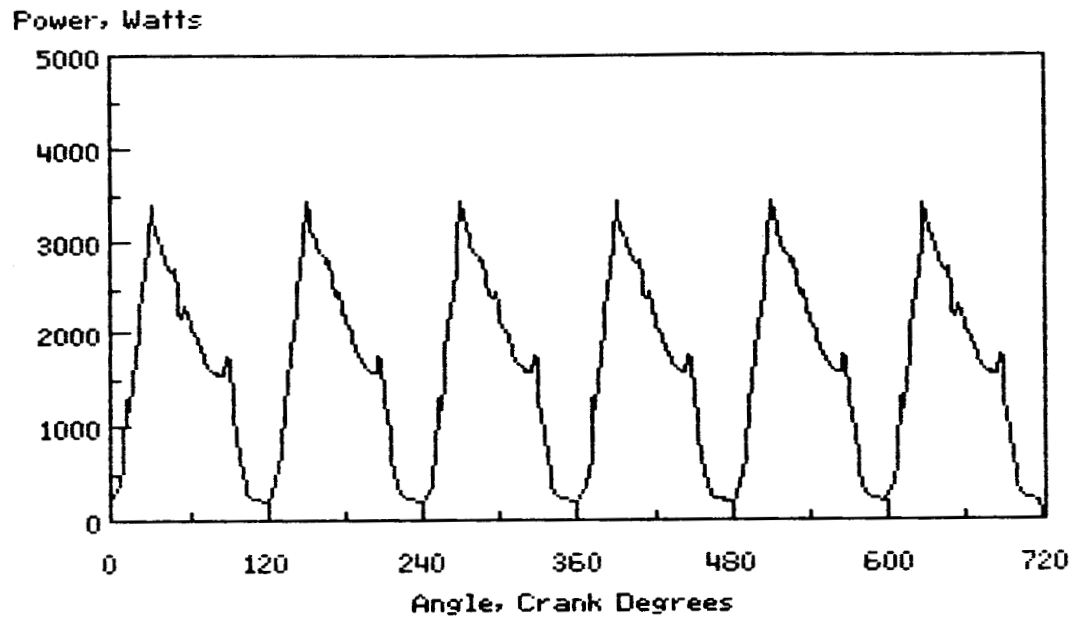
Lift: 8 Deg Max-accel, 42 Deg Ramp

Figure III.3-14: Power Required to Actuate the Exhaust Valves of the ADRE for the 8° X 42° Valve Event at 1800 r/min Engine Speed



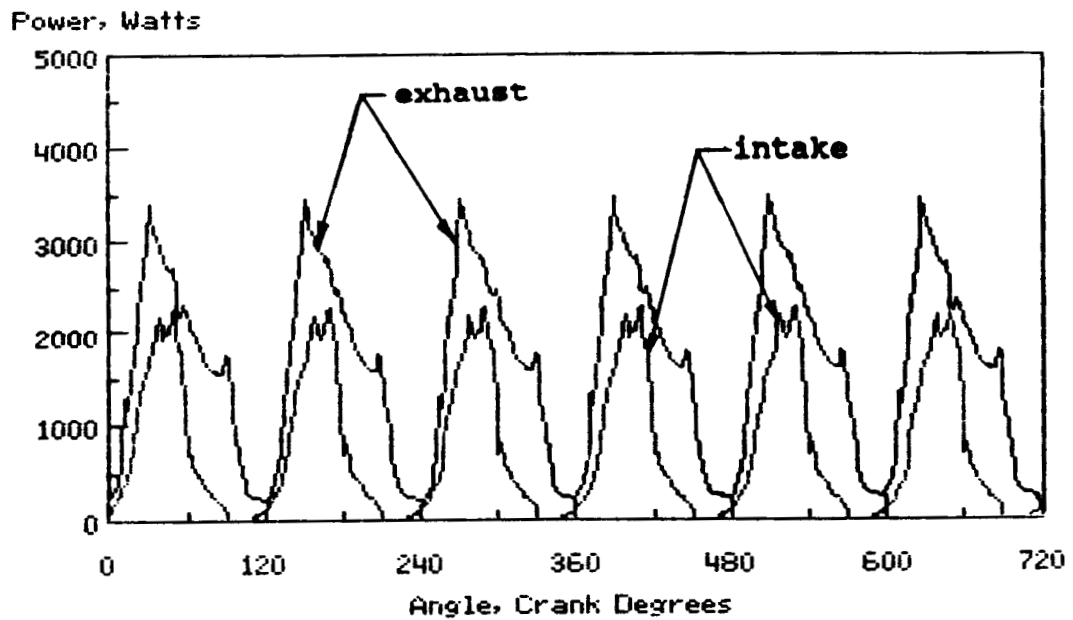
Lift: 8 Deg Max-accel, 4 Deg Ramp

Figure III.3-15: Power Required to Actuate the Exhaust Valves of the ADRE for the 28° X 50° Valve Event at 1800 r/min Engine Speed



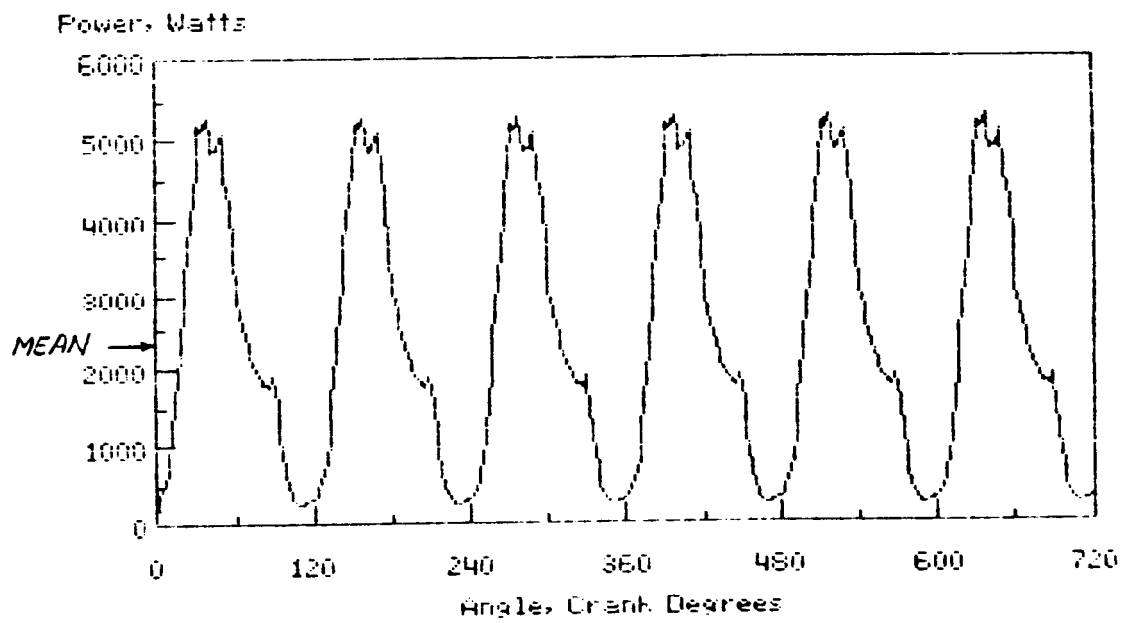
Lift: 28 Deg Max-accel, 50 Deg Ramp

Figure III.3-16: Power Required to Actuate the ADRE Intake and Exhaust Valves for the 28° X 50° Valve Event at 1800 r/min Engine Speed



Intake- 28 Deg Max-accel, 50 Deg Ramp

Figure III.3-17: Total Ideal Power Requirements for the ADRE Valve System



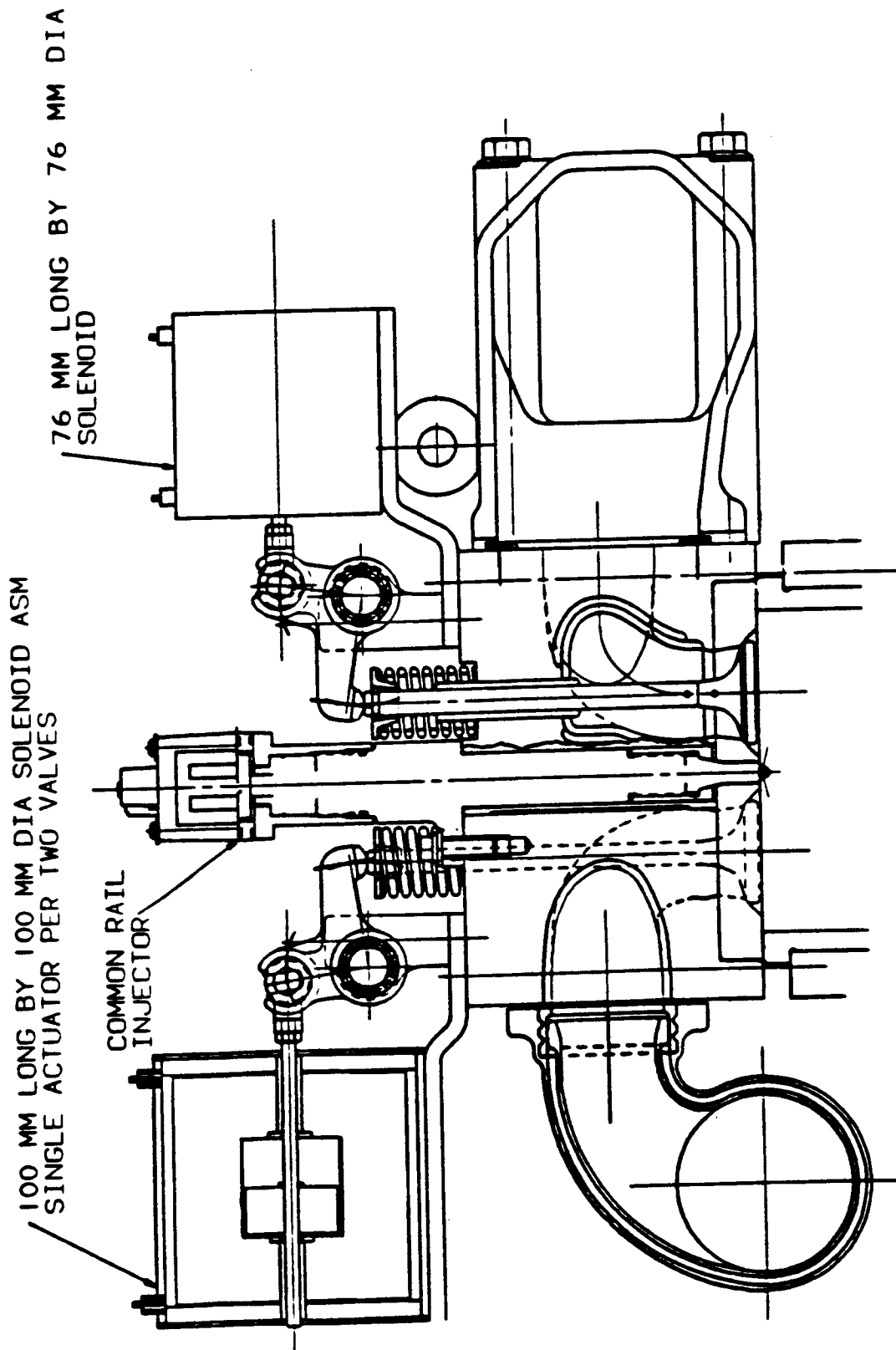


Figure III.3-18: Electromagnetic Valve Actuation System -
Side View

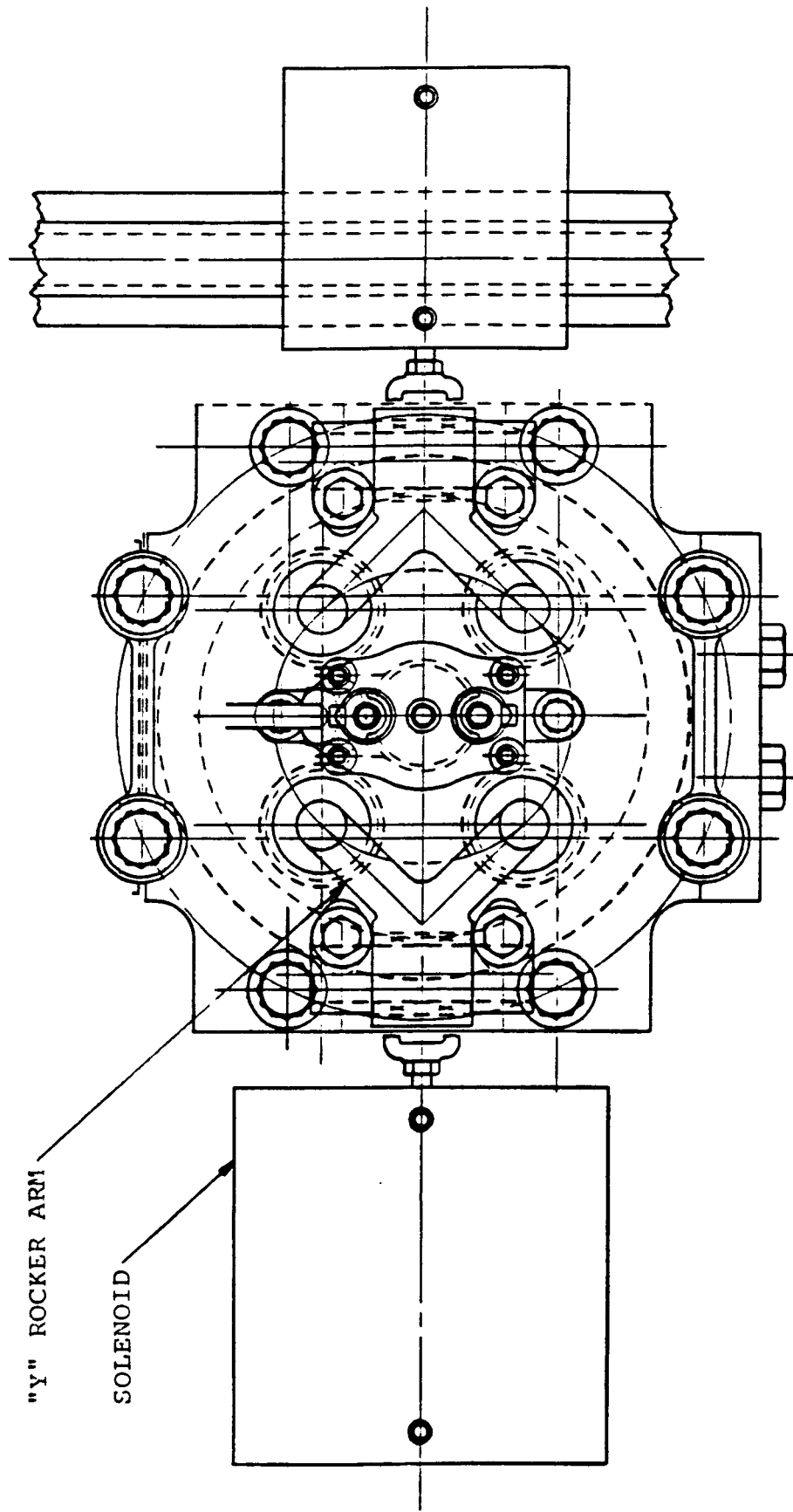


Figure III.3-19: Electromagnetic Valve Actuation System -
Top View

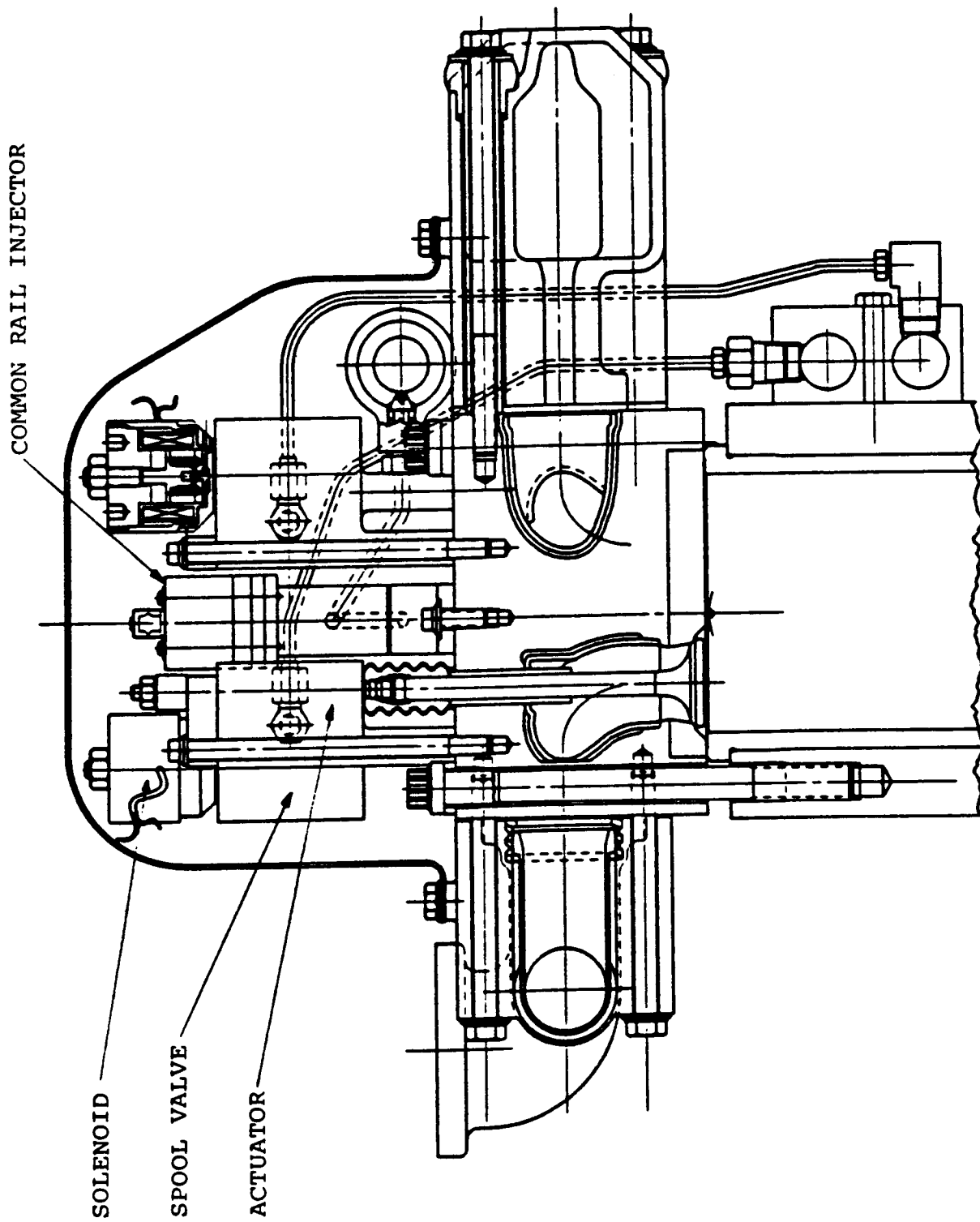


Figure III.3-20: Hydraulic Valve Actuation System - Side View

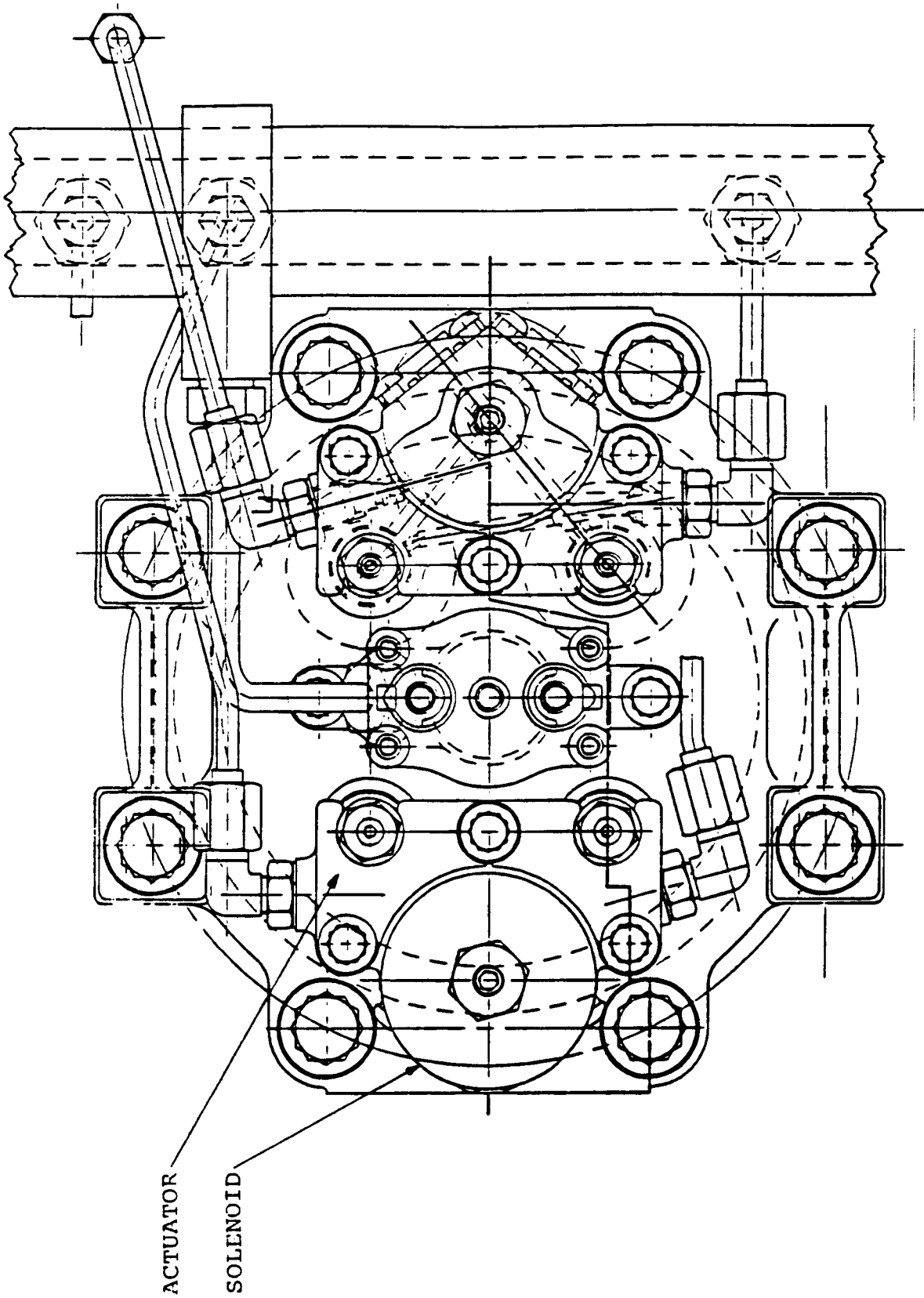
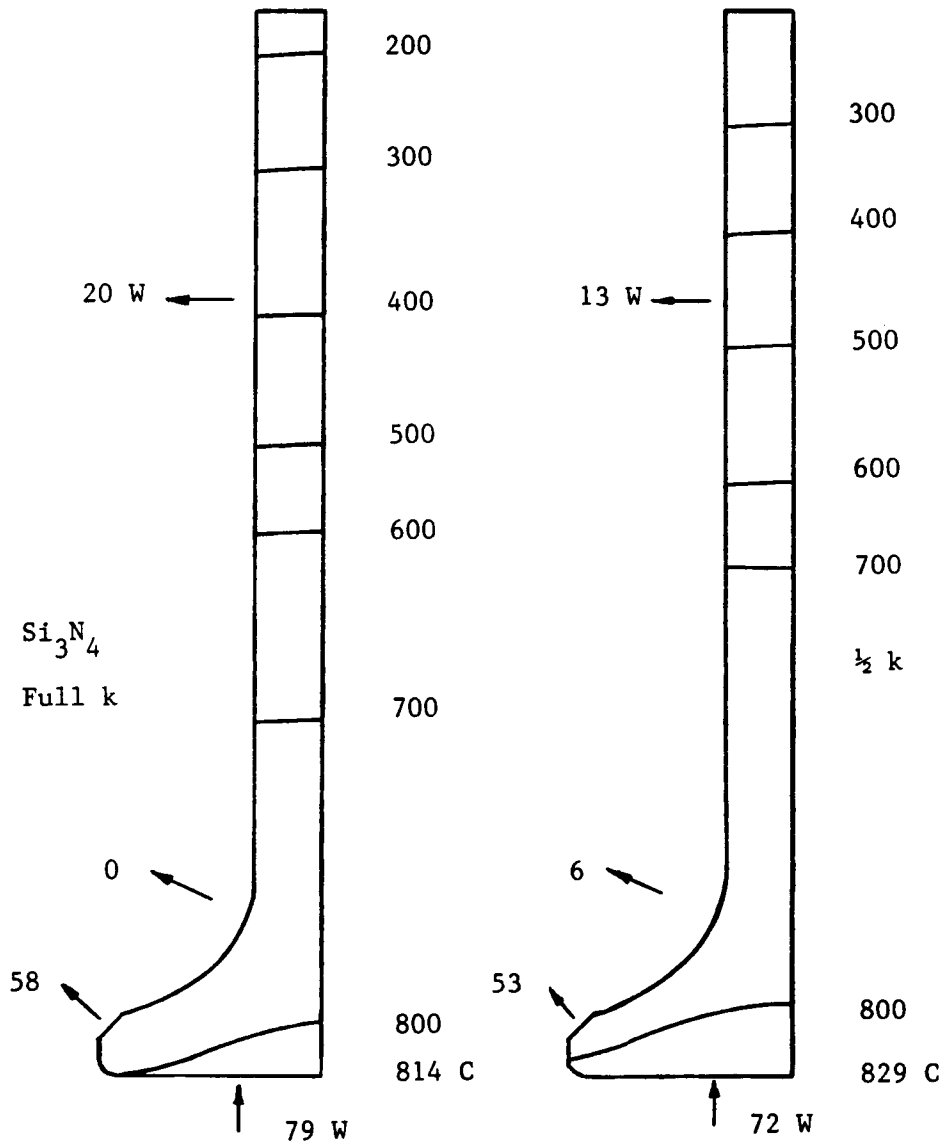


Figure III.3-21: Hydraulic Valve Actuation System -
Top View

Figure III.3-22: Finite Element Heat Transfer Analysis of the ADRE Exhaust Valve
 [Note Effect of Thermal Conductivity on Temperature and Heat Flow]



0 UNDER STATIC LOAD, THE PROBABILITY OF SURVIVAL = 1.00

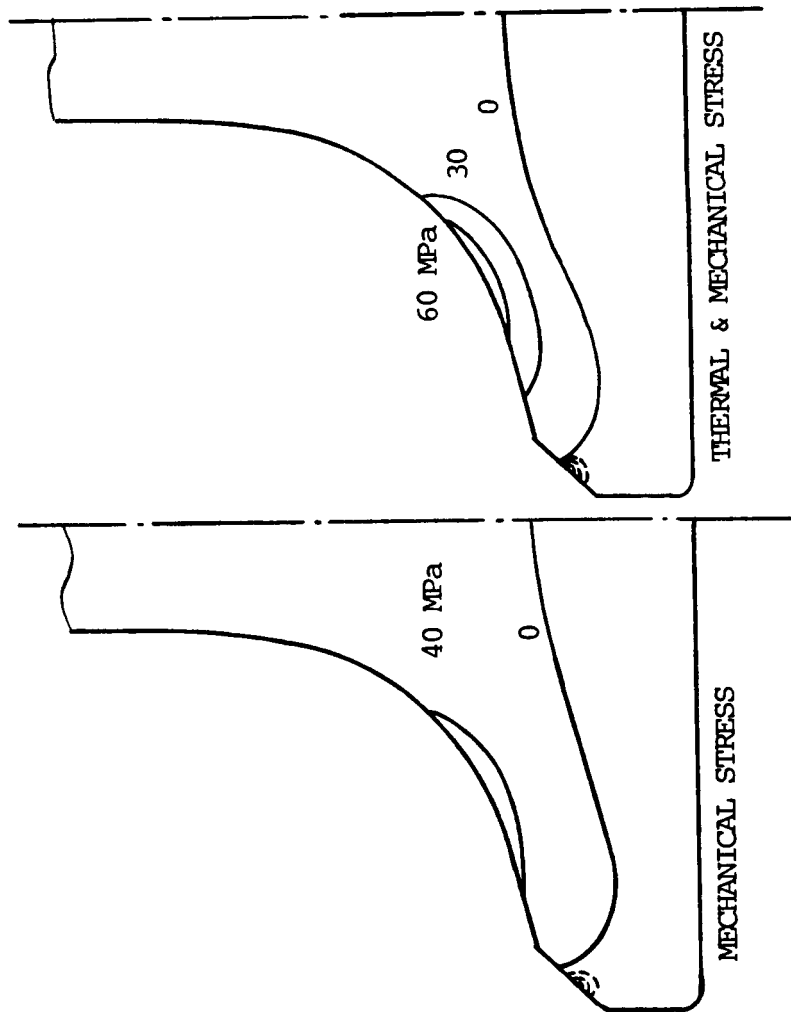


Figure III.3-23: Structural Finite Element Analysis of the ADRE Exhaust Valve

III.4 FUEL INJECTION SYSTEM

This section reports on the ADRE fuel injection system. An advanced technology fuel system was designed that is concurrent with the constraint of a non-mechanically actuated overhead mechanism with no liquid lubrication.

III.4.1 COMMON RAIL FUEL INJECTION CONCEPT

CONCLUSIONS

An electronically controlled common rail injection system is recommended. A high pressure supply pump is required and will offer potential improvements in part load engine combustion characteristics, emissions, and performance. This is plausible because control of injection pressure is possible throughout the load and speed range. Many conceptual design and development problems require further investigation before the proof of concept can be established.

The common rail injection nozzle pressure-time response characteristics, effective needle sealing, structural integrity under high pressure dynamic loading, and electronic control of the mechanical and fluid parameters are among the many challenging problems that will be addressed during the next phase of the ADECD program. Preliminary calculations of system power requirements compare favorably with today's state-of-the-art electronic injection systems.

DISCUSSION

Operating Principle - The common rail injection system consists of an electronically controlled fuel injector (nozzle).

The high pressure fuel is supplied to the nozzle via a remote pump, that is also electronically controlled. Two injector concepts were conceived.

Single Piston Fuel Injector Concept - This design concept is shown in Figure III.4-1. The high pressure fuel is supplied to the injector, all the way to its tip. Control of injection into the combustion chamber is achieved by managing the needle opening event, through a solenoid actuated hydraulic system. Fuel at the common rail pressure level is supplied to the cavity between the control valve and the needle by a 0.12 mm diameter passage. When the solenoid closes the needle, the pressure is equalized, and the needle is in a statically balanced position. Upon opening of the control valve, the pressure above the needle is reduced. This differential pressure across the needle forces its lift off the seat, effecting the start of injection, as shown in Figure III.4-2. When the electromagnet current is turned off, the spring force closes the control valve. This creates pressure build up above the needle, causing it to close and effecting the end of injection, as shown in Figure III.4-3. The equations governing the operation of this injector are provided on the fluid circuit schematic of Figure III.4-4.

Double Piston Fuel Injector Concept - This design of the injector features a low pressure zone between the needle stop and control piston, as shown in Figure III.4-5. This allows larger needle stop seat, without compromising the area of the needle or piston which is exposed to the hydraulic pressure for effective needle closing. The needle and control piston are continually exposed to the high common rail pressure, which may cause higher leakage rates within the injector. The equations governing the operation of this injector are provided on the fluid circuit schematic of Figure III.4-6.

High Pressure Supply Pump Concept - The electromagnetically controlled high pressure fuel pump layout is shown in Figure III.4-7. The pump supplies fuel to the injector at pressures

reaching 138 MPa (20,000 psi). Its output is regulated by the control valve closure, allowing control of the pressure in the common rail as a function of speed and load. This pump is driven by a three lobe cam, located on the crankshaft.

Injection simulation analysis was carried out to size the main components of the high pressure injection pump. It is indicated that an 8 mm plunger and a 7 mm cam lift are adequate for meeting the fuel injection demands of the ADRE.

Injector Cooling Provisions - The fuel temperatures inside the injector should be maintained as low as possible, but not higher than 175 to 200° C range, in order to maintain the diesel fuel integrity. The primary concept for injector and fuel temperature control is shown in Figure III.4-8. It consists of providing a high level of insulation around the injector, such that the normal fuel injection into the combustion chamber provides adequate thermal capacity to maintain the desired temperature. As shown in the figure, this high level of insulation is obtained by pressing a zirconia insert over the spray tip to create a thermal barrier between the tip and firedeck. Additionally, an airgap and a ceramic insulator are designed around the outside of the injector.

Preliminary heat transfer analysis indicates the adequacy of this design approach to prevent fuel degradation. However, should additional injector protection be required, additional internal cooling can be accomplished by flowing low pressure fuel down to the spray tip area.

This high insulation, low pressure cooling flow concept approach minimizes the need for an external fuel cooling system. It also alleviates the concern of high localized thermal stresses that would be generated by other approaches of external cooling of the injector.

Figure III.4-1: Single Piston Fuel Injector Concept

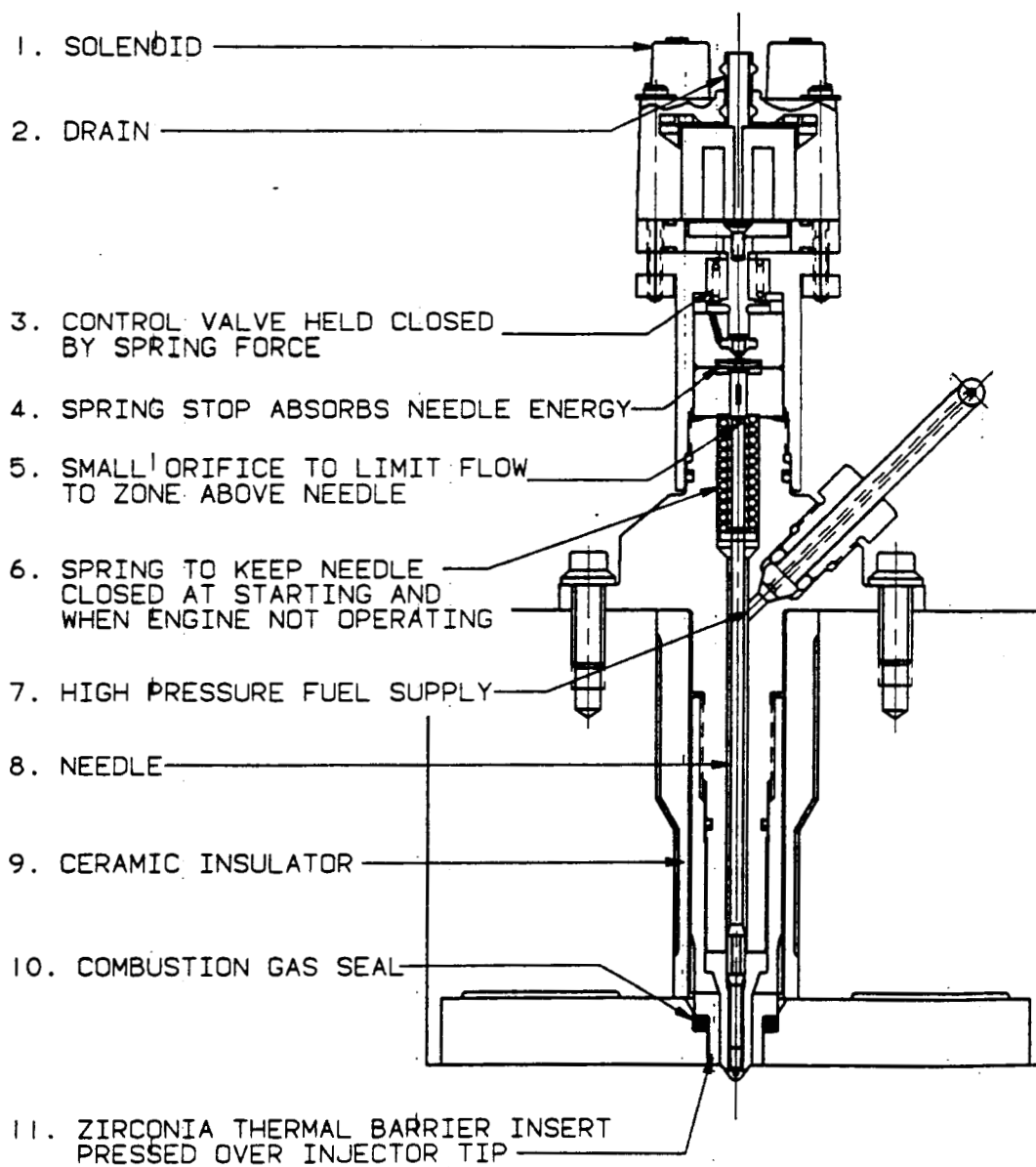


Figure III.4-2: Start of Injection Event for Single Piston Injector

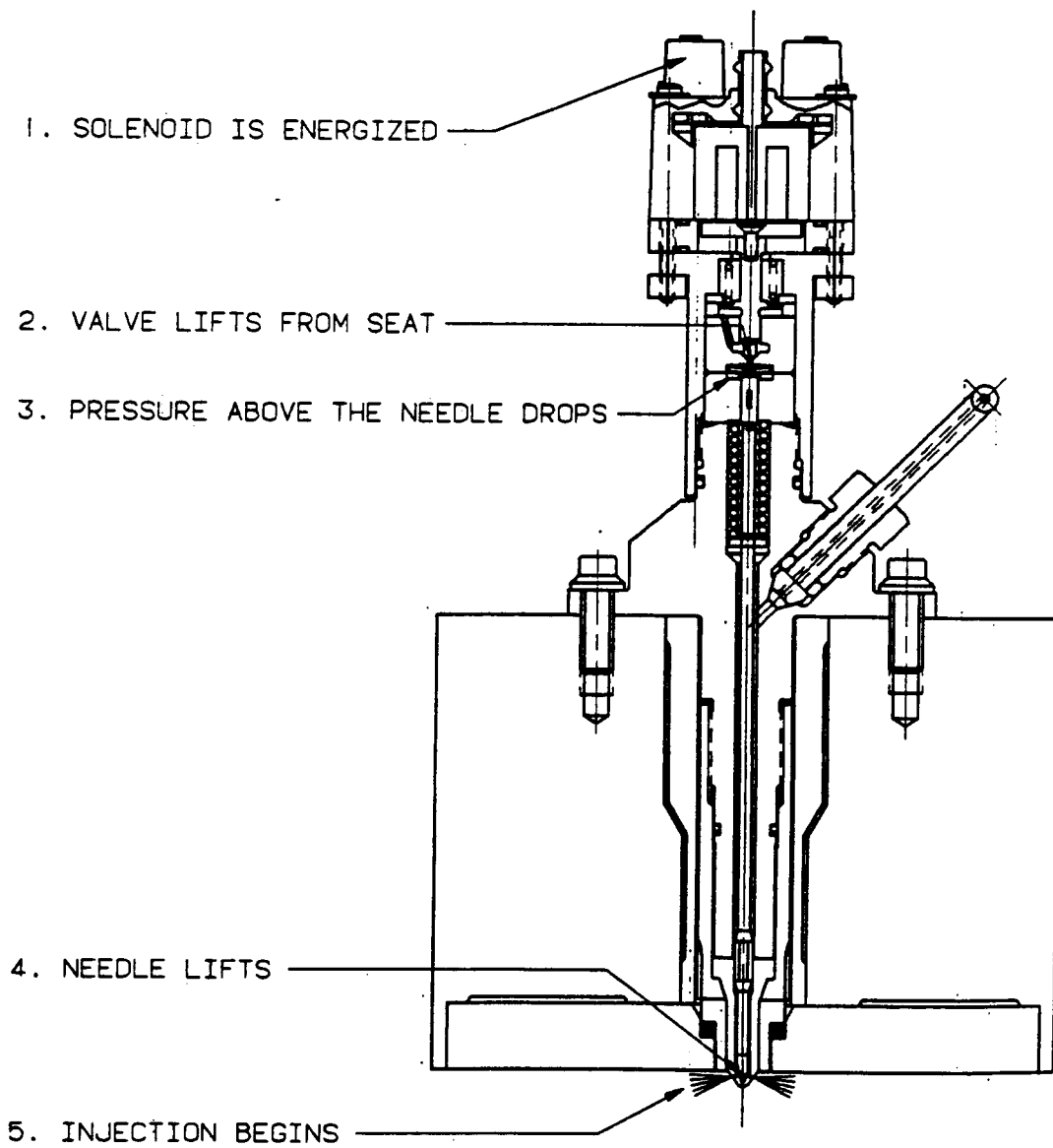


Figure III.4-3: End of Injection Event for Single Piston Injector

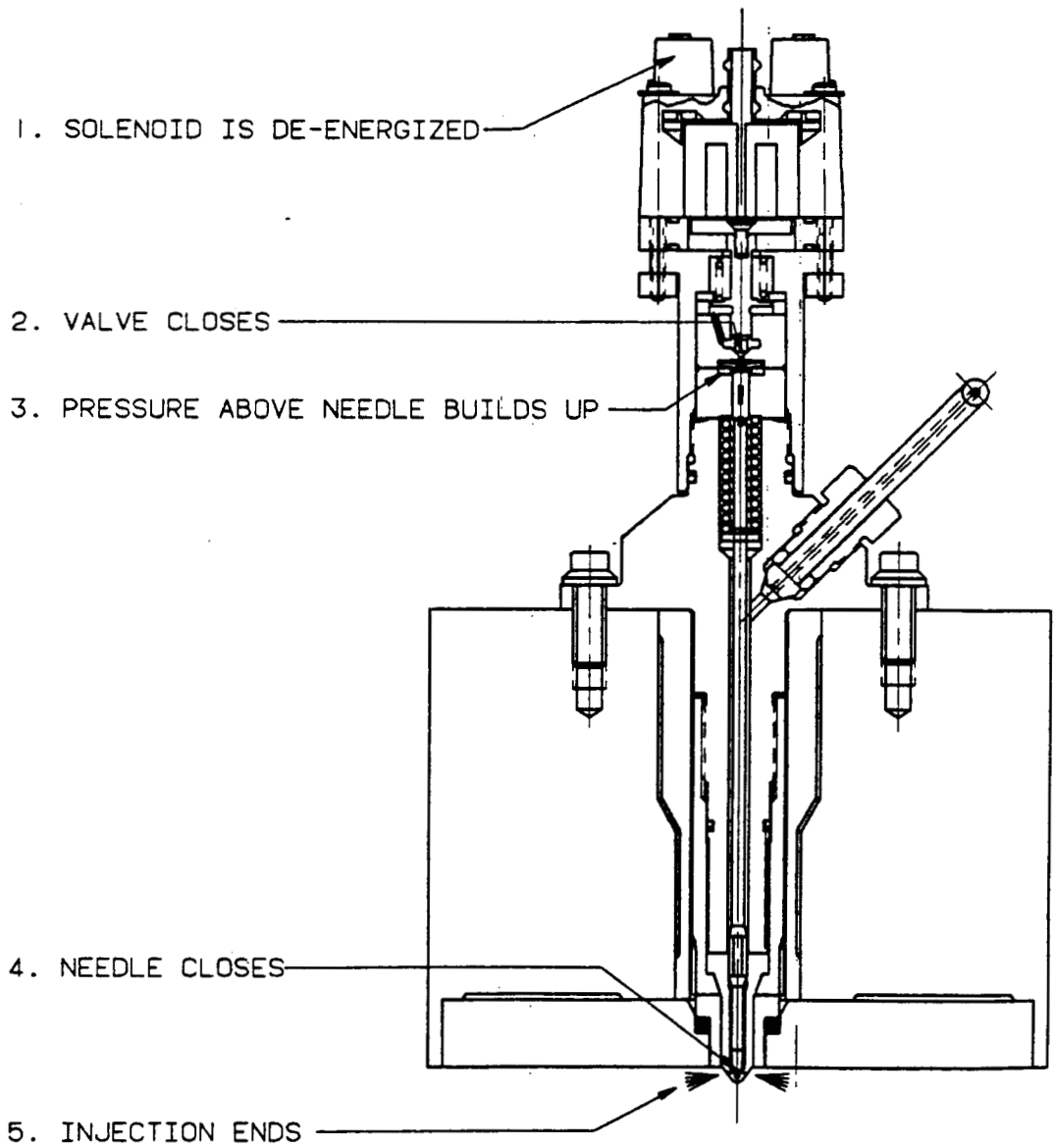


Figure III.4-4: Kinetics of the Fuel Injection Events for the Single Piston Injector

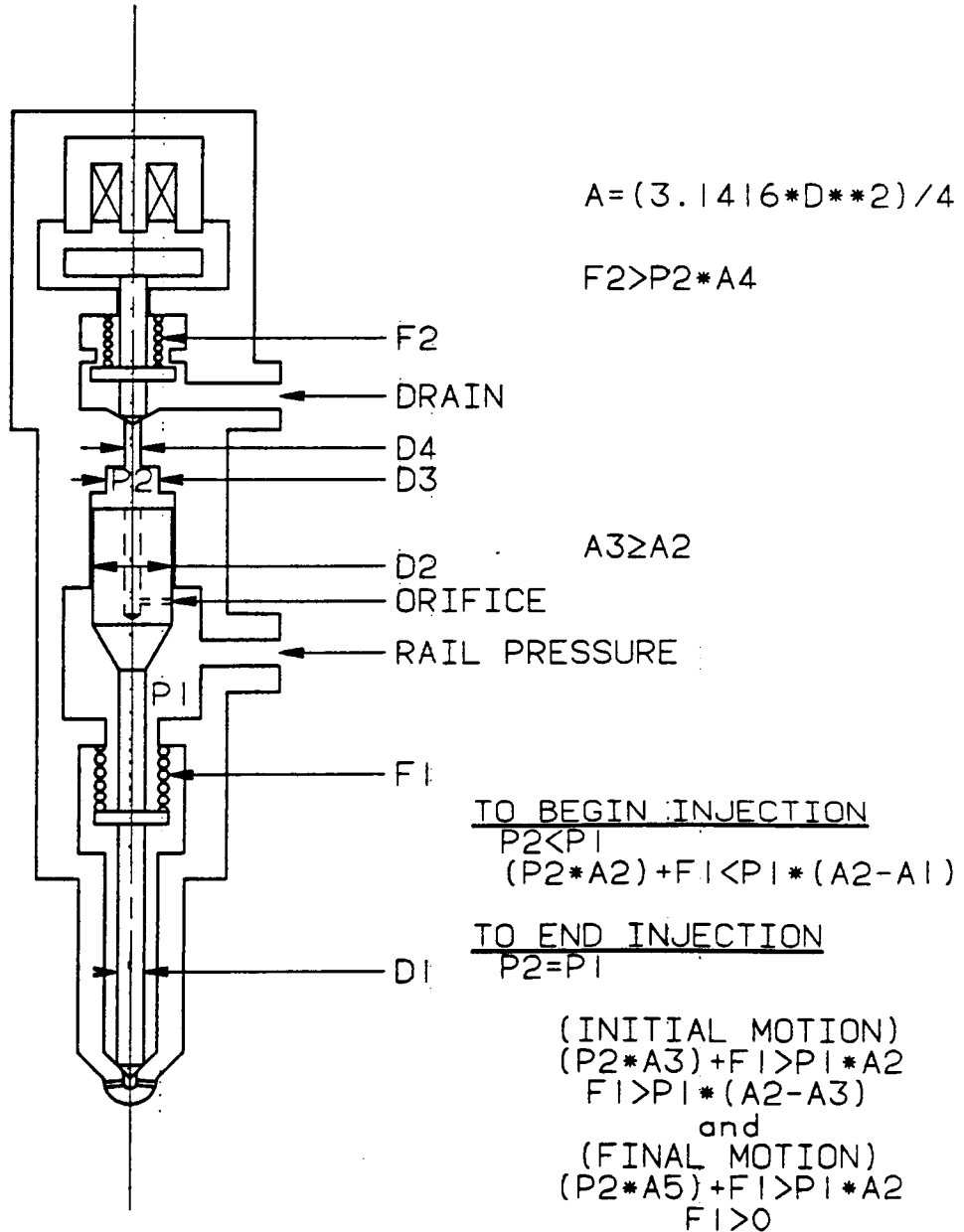


Figure III.4-5: Double Piston Fuel Injector Concept

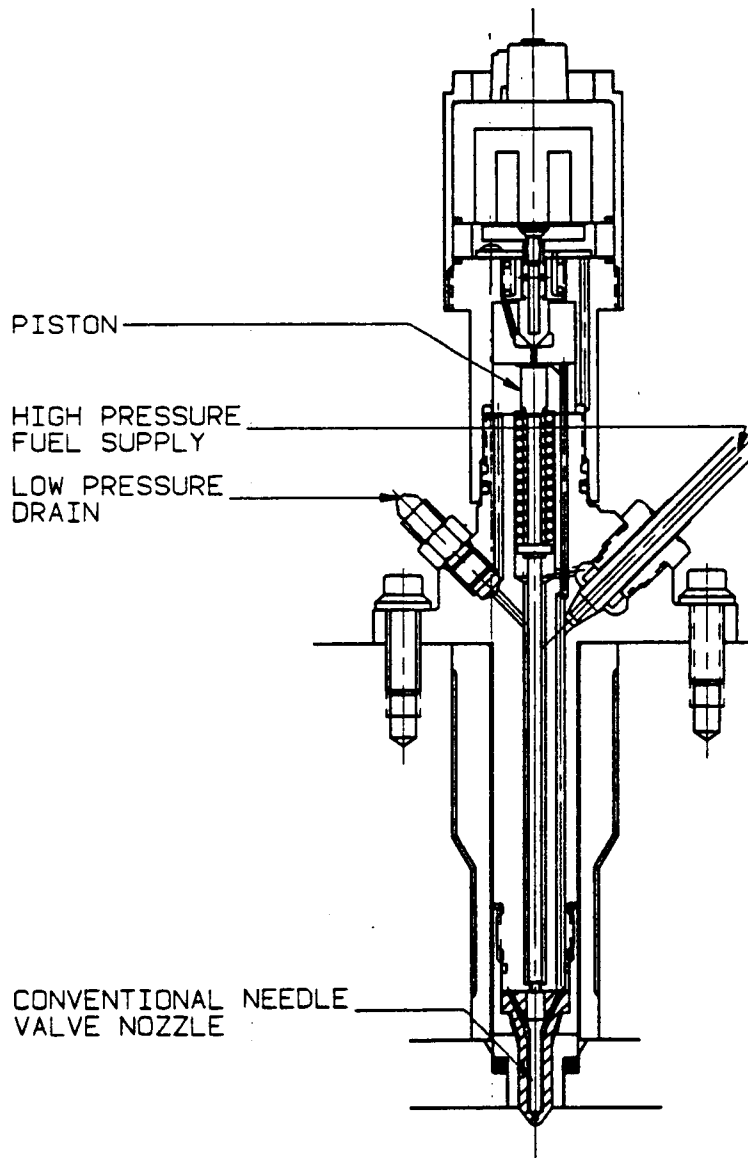


Figure III.4-6: Kinetics of the Fuel Injection Events for the Double Piston Injectors

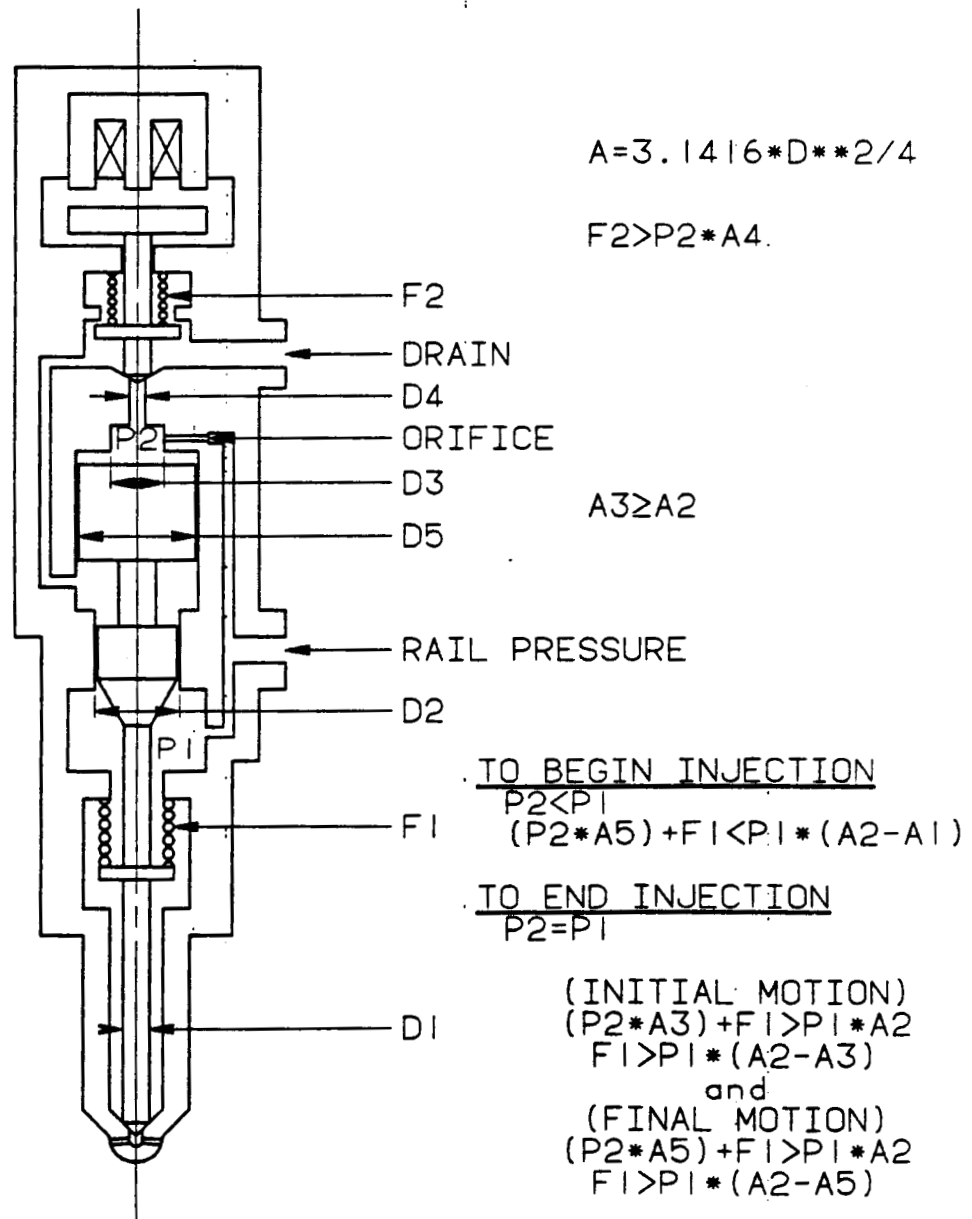


Figure III.4-7: High Pressure Fuel Pump

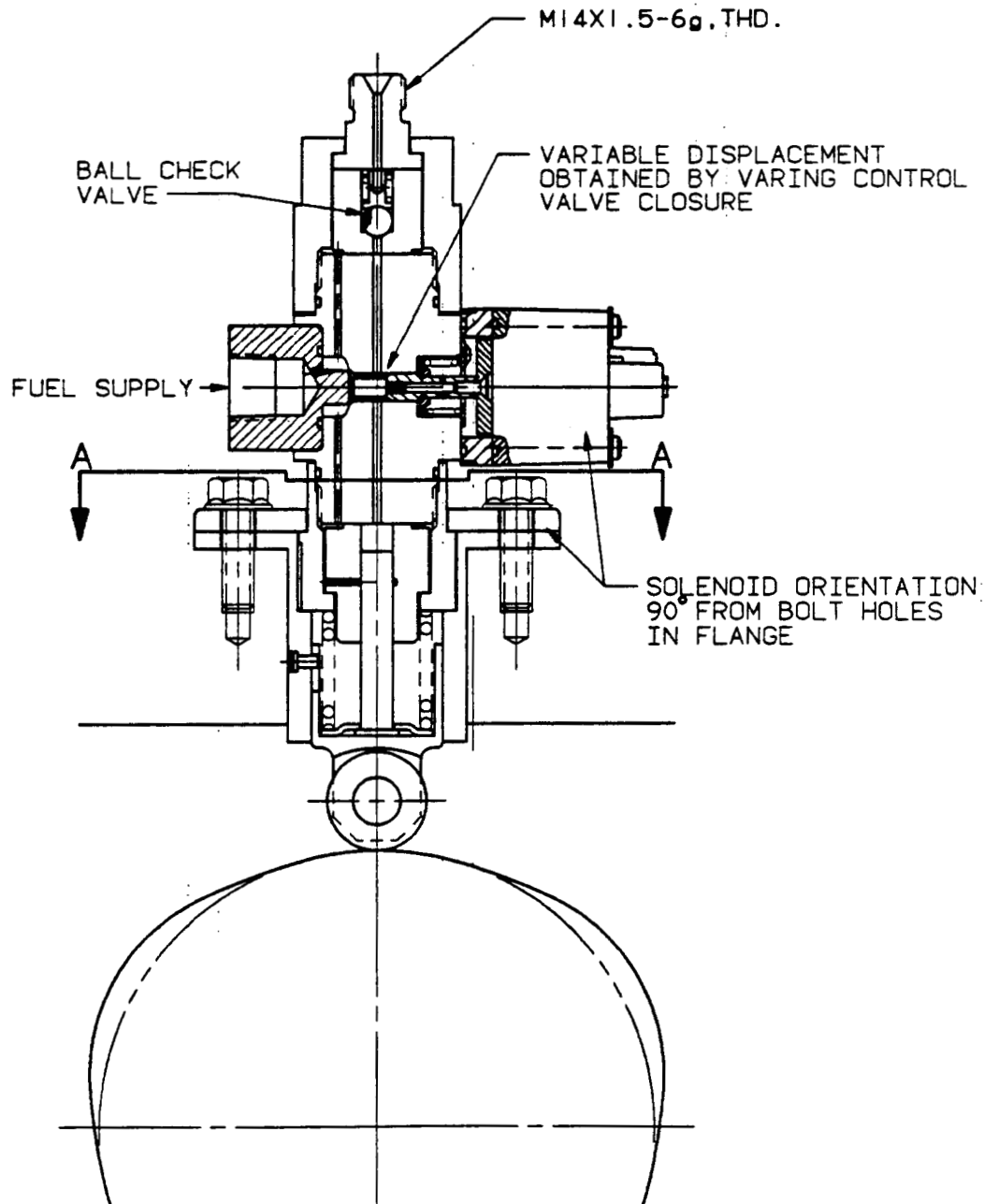
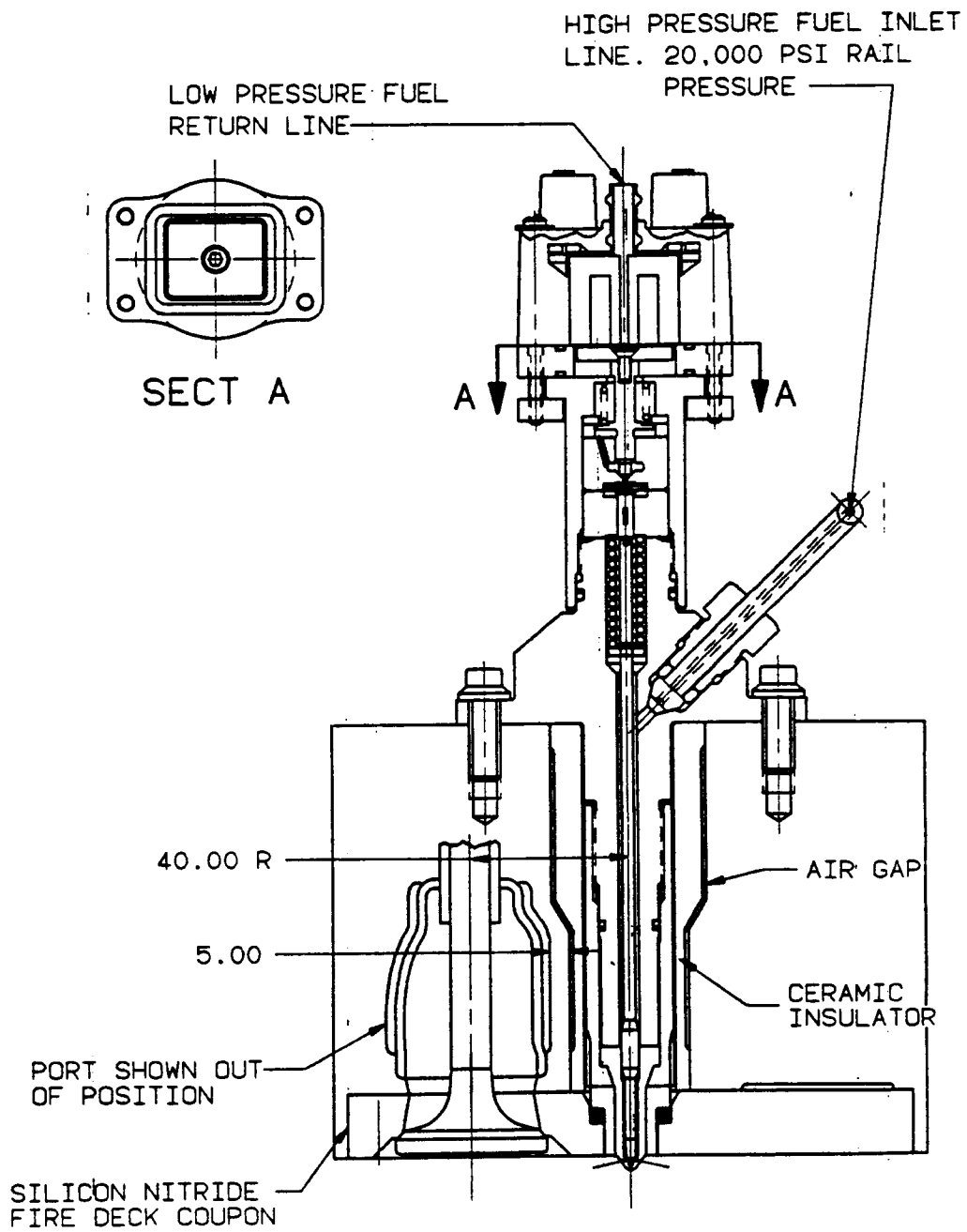


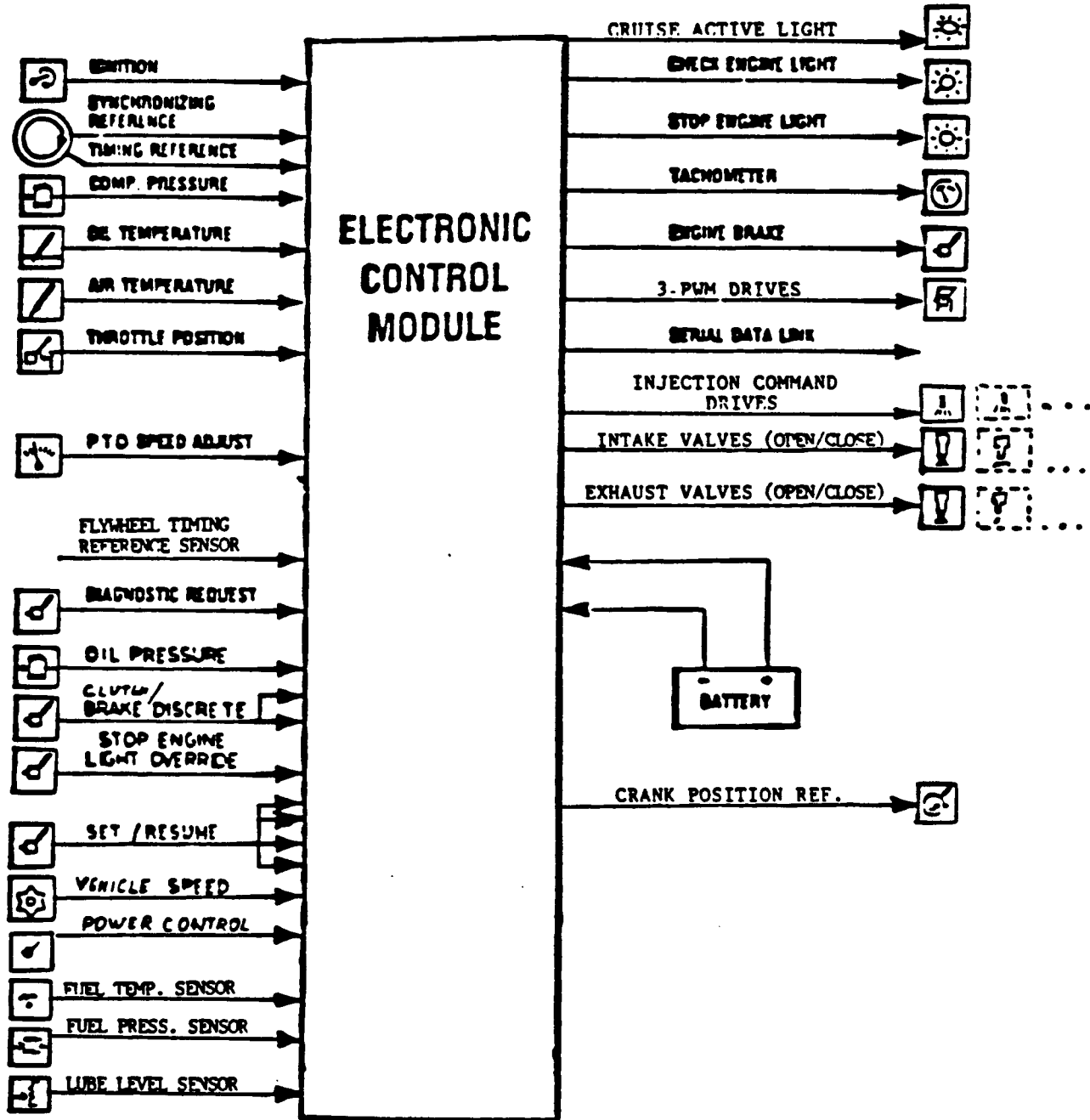
Figure III.4-8: Insulation Provisions for the Injector



III.5 ELECTRONIC CONTROL SYSTEM

A specification manual was established for the ADRE electronic control system. This manual is based on Detroit Diesel Electronic Control [DDEC] system specifications, which is commercially available. Performance and interface requirements are specified. The proposed system provides fuel, valve, and lubrication management for the 6 cylinder, 4 stroke advanced engine. A schematic of the ADRE engine control system is shown in Figure III.5-1.

Figure III.5-1: ADRE Electronic Control System



III.6 POWER TRANSFER SYSTEMS

Two power transfer systems have been designed for the ADRE. The first system is required to transfer power extracted from the exhaust energy recovery systems. As stated in Section II, the selected ADRE has both turbocompounding and organic Rankine bottomer. Thermo Electron Corporation was subcontracted for the bottomer system studies and was consulted on the power transfer system. The subcontract report is attached here as Appendix C. A single mechanical gear system was designed for the power transfer from both the turbocompound and bottomer turbines to the reciprocator flywheel. The following constraints were considered in this design:

- High mechanical efficiency
- Minimal space requirements
- Isolation from engine torsional activity
- Reduced costs

The second system is to provide a means of driving the necessary accessory components for normal vehicle operation. The same design constraints were used in this system.

CONCLUSIONS

1. The recommended exhaust energy recovery drive train design is shown in Figure III.6-1. It utilizes a single gearbox, with a simple three-step gear reduction from the energy recovery turbines to a crankshaft gear located in front of the flywheel. The following features describe the drive train:

- The mechanical drive train gears are helical, and have crowned surfaces. The system mechanical efficiency approaches 96 percent.
 - Overrunning clutches are designed to disengage the individual energy recovery system when necessary.
 - A torsion shaft is utilized to isolate the energy recovery systems from normal engine torsional vibration modes. This design approach has been successfully demonstrated by Thermo Electron.
 - The gear mesh frequencies are above 3000 Hz during normal operating conditions.
 - The gearbox and associated components are sealed and lubricated with conventional oil, e.g., current engine crankcase oil.
2. A serpentine belt system, incorporating a belt tensioner, has been designed for the accessory drives. As shown in Figure III.6-2, this belt drives the alternator, freon pump, overhead hydraulic pump, and power steering pump. A separate vee belt design drives the air compressor. Two electric fan systems will likely be needed to provide the necessary cooling for the charge air radiator, bottomer condenser, overhead fluid radiator, and air conditioner coils.

DISCUSSION

Exhaust Energy Drive Train - A means of transferring the power extracted from both the exhaust energy recovery systems was developed with the constraints of high mechanical efficiency, minimal engine space availability, isolation from engine torsional activity, and reduced costs. Initial energy recovery system power estimates, turbine speeds, and engine speed were used to establish

a design concept. This concept was later modified to incorporate improvements, including updated energy recovery system information which became available from Thermo Electron. The finalized drive system is described below.

Initially, a concept of a separate gear system for each exhaust energy recovery unit was considered. Eventually, this concept was eliminated, based on considerations of cost and space availability. A single gearbox was designed, which mounts on the right side of the engine. The single gearbox design, in combination with a 5 degree engine tilt, provides an acceptable vehicle installation, as shown earlier in Figure III.1-13.

The energy recovery system has a rated turbine speed of 60,000 r/min, while the rated engine speed is 1800 r/min. The required gear reduction ratio is 100:3. A simple, three step gear reduction having the ratios of 4:1, 5:1, and 5:3 is recommended. This gear system, shown in Figure III.6-3, provides for minimum mechanical energy losses, a compact gearbox, the necessary design limitations on gear speeds that are imposed by the overrunning clutch, and the desired torsional isolation.

The gears utilized have a 20 degree helix angle and crowned surfaces. A diametral pitch of 12 has been chosen for the crankshaft gear and the rear torsion shaft gear. The other drive gears have a diametral pitch of 18, which ensures that the gear mesh frequency will be well above 3000 Hz during normal operating conditions. Standardization of these gear sizes will allow for reduced cost and a compact gearbox assembly. Ball and roller type bearings are recommended.

Clutching mechanisms were deemed necessary for the bottomer and turbocompound turbines for the following reasons:

- Engine operating conditions where the exhaust energy recovery unit may provide marginal increases in performance, e.g., at idle or during downhill operations.

- Additional system overspeed protection during engine motoring conditions.
- Engine gear system protection in case of pinion gear, turbine or any other exhaust energy related failures.
- Likely additional torsional isolation in extreme conditions.
- Reduced overall costs due to the use of an inexpensive clutch mechanism and standard parts.

Commercially available roller-ramp type clutch, e.g., Morse Model #NFS-20, is selected for this application. The cited clutch provides a torque capability of 107 J (79 ft.lb), compared to the design torque value of 72 J (53 ft.lb) that corresponds to 22.4 kW (30 HP) turbine output at 1800 r/min. The clutch rated overrunning speed is 3000 r/min on the inner race, and 3600 r/min on the outer race.

Isolating the exhaust energy recovery units from normal engine torsional vibration is an important factor for long term system reliability. A fluid coupling was initially considered for isolation. However, based on the past experience of Thermo Electron, a torsion shaft isolator was considered more advantageous. This provides cost and space availability advantages over a fluid coupling. The designed torsion shaft has sufficient strength to transmit the maximum horsepower output of the two energy recovery systems and has a stiffness such that the natural frequency of the gear system is lower than the lowest engine forced frequency.

Accessory Drives - A 14 rib serpentine belt arrangement has been developed to drive the alternator, freon pump, overhead hydraulic pump, and power steering pump. A tensioner was incorporated in this system to provide a near optimum belt load of 623 N (140 pounds), providing extended belt life. The drive

requirements are based on the following projected accessory drive power demands, as well as typical on highway duty cycle performance expectations:

- Alternator	6. to 7.5 kW (8-10 HP)
- Freon Pump	3.7 to 7.5 kW (5-10 HP)
- Hydraulic Pump	3.7 to 6. kW (5-8 HP)
- Power Steering Pump	11.2 kW (15 HP)

The limiting factor in the belt life calculation is the power required to drive the power steering pump during low speed idle conditions. Advancements in the area of electro-hydraulic pumps and electronic steering in the 1995 time frame will likely result in a substantial reduction in associated parasitic power loss, and this would subsequently reduce the belt width and tension requirements. A separate vee belt design is recommended to drive the air compressor directly from the crankshaft pulley.

Although the ADRE has no water system and, thus, requires no cooling system radiator, other engine systems require provision for forced cooling. An electric fan system is expected to provide cooling for the bottomer condenser, charge air radiator, overhead fluid radiator, and air conditioner coils, when necessary. This "on-demand" method of cooling has distinct efficiency advantages over the typical mechanical drive approach. It also reduces the mechanical component drive requirements, allowing extended belt life. The electric fan system is widely used in today's small passenger car engines.

The bottomer condenser and charge air radiator have been stacked in front of the engine installation, as shown earlier in Figure III.1-10, to take advantage of normal "ram air" conditions. The bottomer condenser is sized as 610 X 914 X 76 mm (24 X 36 X 3 inch), based on the expected power recovery efficiency of the bottomer cycle. This information is contained in Appendix C. The charge air radiator size of 762 X 1016 X 63.5 mm (30 X 40 X 2.5 inch) is comparable to the present 223.7 kW [300 HP] engine requirements.

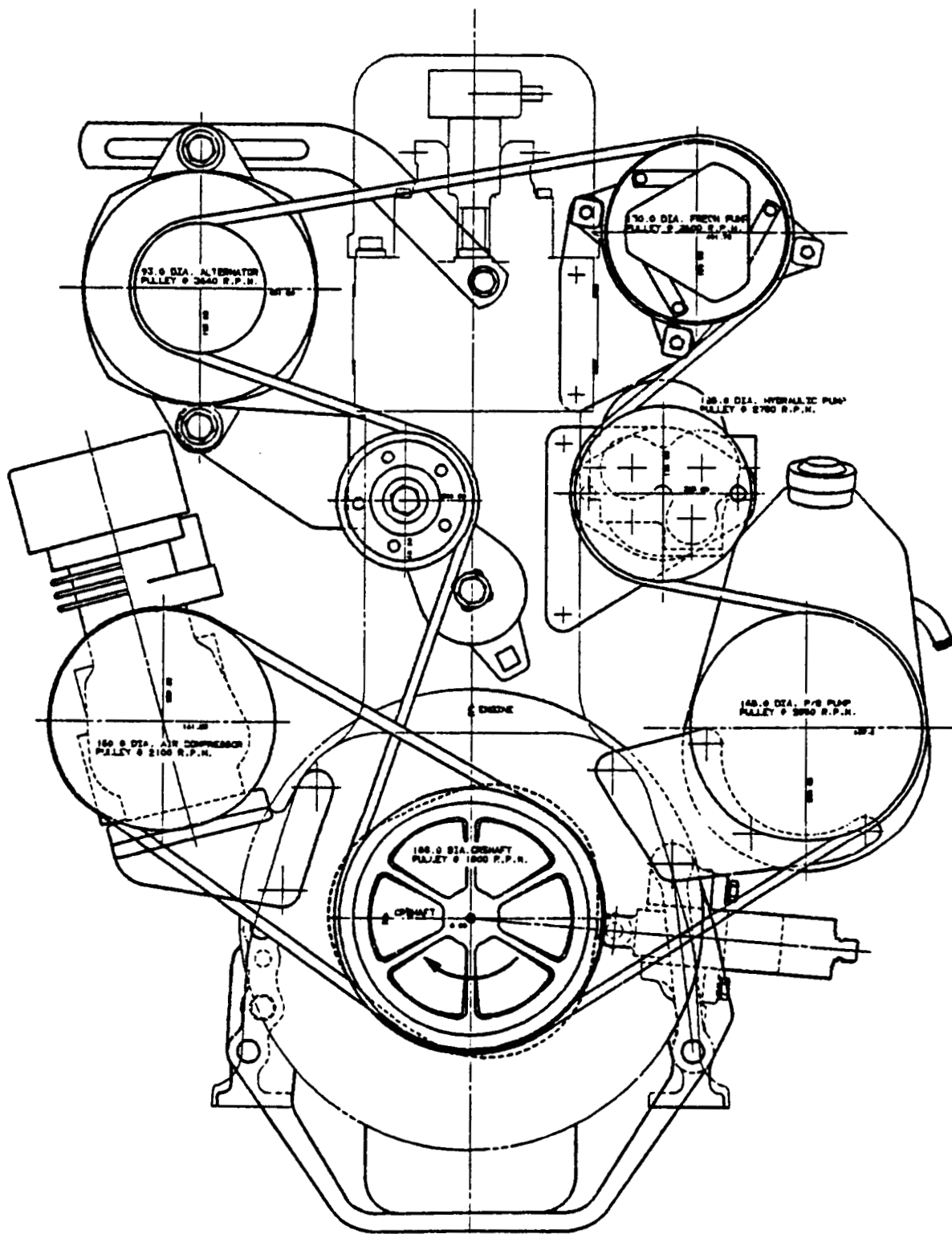
Further iterations of the bottomer system can provide a larger condenser frontal area, which would be equivalent to that of the charge air radiator.

An air flow of approximately $4.2 \text{ m}^3/\text{min}$ at 7.6 m/s (9000 CFM at 17 MPH) is required to provide the necessary bottomer condenser cooling during extreme operating conditions, such as limited ram air while driving on a steep grade. The electric motor power and size to satisfy this requirement are prohibitive and, hence, a much smaller fan motor has been recommended. This will necessitate the use of a by-pass valve in the vapor generator to allow the exhaust heat energy to be expended under such extreme conditions. Use of this valve would guarantee that the bottomer fluid would not overheat when the condenser cooling capacity is insufficient for condensation.

The overhead fuel cooler and the air conditioner coils are also stacked in front of the engine installation, as shown in Figure III.1-10, to take advantage of the effect of the ram air. The power requirements for this fan system are dependent on the heat transfer requirement for cooling the proposed overhead mechanism. During normal operation, a 305 mm high efficiency shrouded fan, in combination with a .37 kW fan motor, is expected to be sufficient to cool the air conditioner condenser coils.

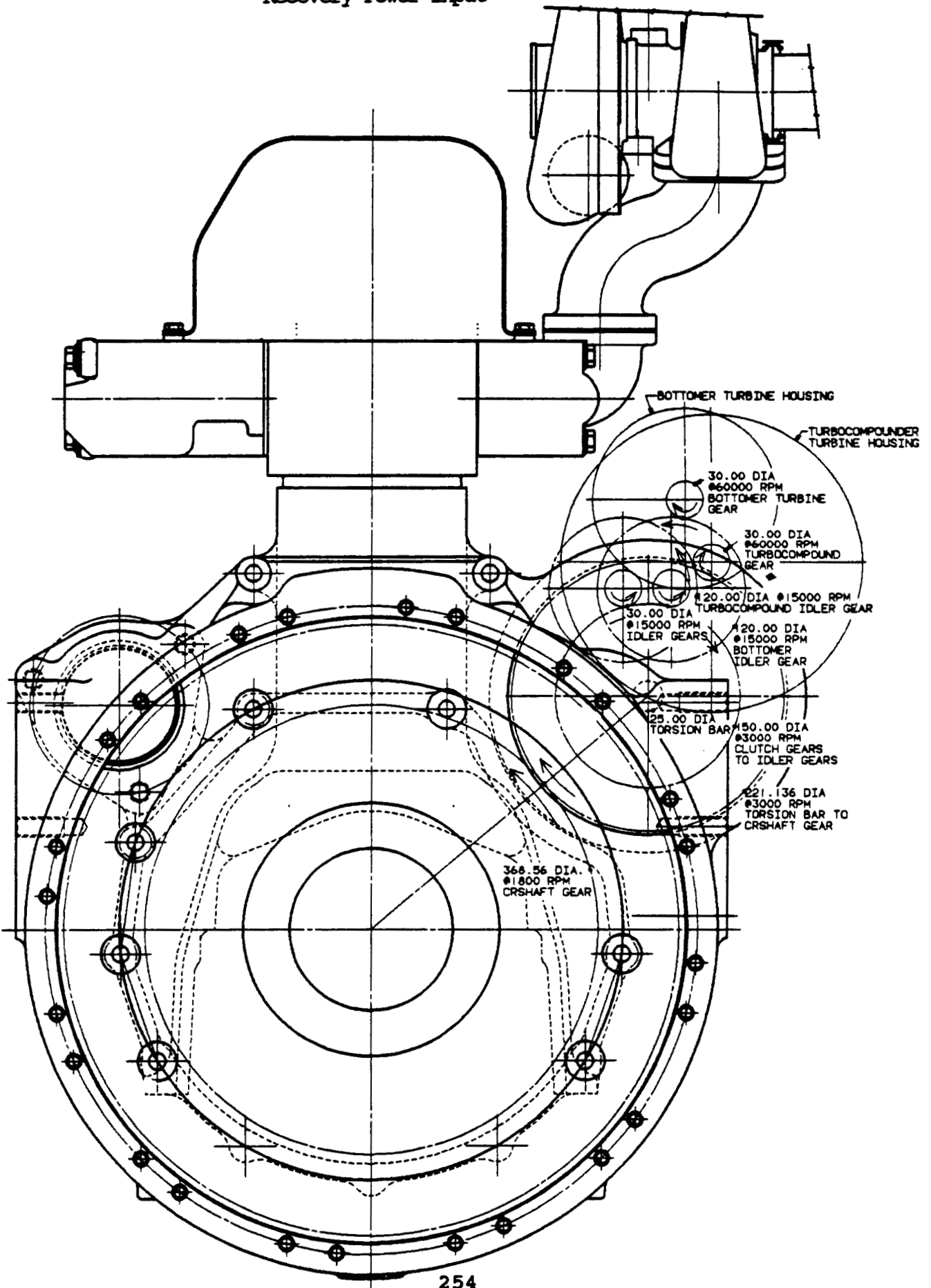
It should be pointed out that overall truck aerodynamic considerations may warrant the consideration of alternate design concepts and/or new approaches to accommodate the cooling requirements of various systems. Such an activity is beyond the scope of the current program.

Figure III.6-2: Accessory Drive System



ACCESSORY DRIVES
(SERPENTINE BELT SYSTEM)

Figure III.6-3: Three-reduction Gear System for Exhaust Energy Recovery Power Input



III.7 ROLLER BEARING DESIGN

A minimum friction crankshaft bearing system is desired for the ADRE to promote fuel economy. The scope of the bearing design work included detailed studies of the main bearing and detailed conceptual evaluation of connecting rod, thrust, and piston pin bearings. Rolling element bearings were selected early on after brief consideration of unconventional journal bearing concepts.

After several months of relatively independent study by SKF Industries on a rolling bearing subcontract, a collaborative development effort was initiated. The subcontractor final report has been provided as Appendix A of this document. This section reports on the basic design methodology that was developed by DDA. This methodology is based on published correlations, past product experience, and generic findings from the SKF subcontract effort. This methodology allows the design of minimum friction roller bearings at targeted levels of technical risk. The detail design work, lubrication studies, and application of advanced technology were performed by SKF and are found in Appendix A.

CONCLUSIONS

The resulting bearing designs offer a substantial fifty percent reduction in friction over the journal bearings found in a current state-of-the-art, 223.7 kW heavy-duty diesel engine. In addition, since the roller bearings are grease-lubricated and the cylinder kit utilizes non-liquid lubrication, the normal oil circulation and cooling system, with their associated design complexities, are not necessary. The areas of technical risk in the bearing designs were identified, and SKF recommended approaches for their resolution.

DISCUSSION

The crankshaft and piston pin bearings are part of this phase of the program because of associated friction losses and their impact on the engine lubrication and cooling systems, which in turn are affected by cylinder component design. The conventional journal bearing systems feature simplicity of assembly and service, low replacement cost, and high durability. Friction loss is typically an area of concern in the design of journal bearings, since their ability to separate loaded members depends solely on subjecting large quantities of lubricant to high shear rates. In a state-of-the-art 223.7 kW, inline six cylinder heavy-duty diesel engine that is designed for maximum durability, about 8 - 9 kW is dissipated by shearing of the lubricating oil. To this must be added approximately .7 kW consumed in driving a pump for supplying oil to the bearings, most of which is for cooling. The power consumed by operation of a cooling fan and water pump, as well as aerodynamic drag associated with a cooling radiator, are other sources of power loss that are harder to quantitatively allocate to the bearings.

Rolling element bearings were considered the leading alternative for several reasons. First, there was a high level of confidence that roller bearings would offer substantial friction reductions over journal bearings of similar durability. Second, roller bearings have been and continue to be used in various reciprocating engine applications. Further, roller bearings are adaptable to a variety of lubrication schemes, thereby facilitating the elimination of the liquid lubricant circulation and cooling systems.

Based on rough assessments of potential, the following goals were set for roller bearing design:

- Elimination of all engine power loss associated with bearing lubricant circulation and cooling.

- Reduction of bearing friction by 50 percent compared to that of a state-of-the-art heavy-duty 223.7 kW diesel engine.
- Overall engine weight reduction and/or design simplification resulting from elimination of galleries, pumps, filters, pickup and fill tubes, and other oil-system related hardware.
- Life cycle costs competitive with conventional journal bearing systems.

Preliminary design studies were conducted by SKF during ADRE selection (Task 1), and followed by highly collaborative redesign and optimization during ADRE Design and Analysis (Tasks 2 and 3). The sections that follow give a quick overview of the ADECD bearing development work, then focus on the work and findings of Tasks 2 and 3.

ADRE Bearing Selection Overview - For ADRE selection, SKF Industries conducted a relatively independent design study based on representative journal sizes and loads for main and connecting rod bearings of a state-of-the-art diesel. The guideline was that the bearings be "low risk," i.e., of conventional materials and lubrication, since it was desired to place the development emphasis on the cylinder components.

DDA selected the designs shown in Table III.7-1 from several SKF proposals provided in Appendix A. This was based on compatibility with the rest of the engine. Grease lubrication was selected based on predicted performance and durability, and because solid lubrication was chosen for the cylinder kit tribology. Thus, grease lubrication of the bearings allowed complete elimination of the oil system from the engine. By the conclusion of the ADRE selection effort, it had been found that friction reductions were precluded by durability limitations under the assumptions of "low risk" design and loading corresponding to the 223.7 kW reciprocator output.

Tasks 2 and 3 began with a review of the key elements of SKF's analysis and recommendations during Task 1. Two additional circumstances developed with implications for the potential of bearing design. The first of these was that a life cycle cost study had shown that a high risk design for the reciprocator was favorable over lower risk designs offering less benefit. The second was the decision, also based on life cycle cost, to compound the engine's output with exhaust energy recovery systems [EERS], thus reducing the reciprocator requirement to 179 kW. Reductions in bore and stroke accompanied the incorporation of EERS.

Based on this review, it was decided that a highly collaborative effort was not only possible, but necessary, in order to ensure good design integration and satisfaction of the friction goals. DDA thus undertook the basic design work of sizing the rollers and races, and SKF provided technological guidance. The philosophy adopted was that the bearing designs should minimize friction, even at the expense of durability, to the extent that they may be considered high risk. The major role of SKF during this period was to identify the development paths required to achieve the required durability.

It was decided to give greatest attention to detail in the design of the main bearings and address the rod, piston pin, and thrust bearings at a somewhat more abstract level.

Main and Connecting Rod Bearings - The main and connecting rod bearings have split outer races to facilitate installation over the crankshaft and use the crank journal surfaces as inner races. This approach requires that attention be given to the specification of crankshaft material and processing but allows rather large diameter rollers to be used. While there is flexibility in the packagable sizes of these bearings, there are geometric and design constraints, such as the cylinder bore size and crankshaft torsional and fatigue limits.

Basic Design - SKF Industries' Task 1 findings on the main and rod bearings are summarized in Table 1 and detailed in Appendix A. With these as a starting point, DDA lead the effort to achieve friction reductions, beginning with a study of inherent relationships between roller bearing size, friction, and durability. This was undertaken to assess the impact of friction minimizing design changes on bearing and crankshaft durability. This study was based on information commonly available in bearing supplier literature.

The bearing friction is related to pitch diameter, applied load, and speed as follows:

$$P_f = C_f (\pi/30) (\text{rpm}) (D_p/2) (4.48P) * \quad (1a)$$

*These imperical formulas are developed using mixed SI and U.S. units.

where P_f is the friction power in Watts, rpm is the shaft speed in revolutions per minute, D_p is the pitch diameter of the bearing in meters, and P the "RDS" average load (root mean load to the 10/3 power) in pounds.

The friction coefficient (C_f) can vary with the construction of the bearing, e.g., caged vs. full complement, and may also depend on lubricant effects. Hence, its value in the reference engine context is not known. Effects of the various available lubricants on bearing life and load carrying capacity are also unknown. Therefore, a similarity approach was used for making new friction estimates. The friction power loss of the main bearing design from the ADRE selection task is 918 W, with Texaco MARFAC #2 grease. Thus, for a new main bearing design, the friction power would be estimated by:

$$P_f/918W = (D_p/136\text{mm}) (P/8000\text{lb}) \quad (2a)$$

Likewise, friction power losses for a new rod bearing design would be estimated by:

$$P_f/576W = (D_p/96\text{mm})(P/10,990\text{lb}) \quad (2b)$$

Bearing life is related to applied load through the relation:

$$L_{10} = (C/P)^{10/3} \quad (3)$$

where L_{10} is the number of millions of revolutions at which 10 per cent of the bearings will have failed, and C is the "load rating" of the bearing, which is a characteristic of the bearing design. Efforts to reduce the friction power loss of a bearing may require design changes which reduce the load rating of the bearing from its base value, which will be designated " C_{base} ." A life factor can be defined as a required characteristic of bearing materials, surfaces, etc., to maintain a given L_{10} :

$$F_L = (C_{\text{base}} * P / C * P_{\text{base}})^{10/3} \quad (4a)$$

or

$$F_L^* = (C_{\text{base}}/C)^{10/3} = F_L (P_{\text{base}}/P)^{10/3} \quad (4b)$$

The load rating of a rolling element bearing is given in pounds by:

$$C = 4976.6Z^{.7834} (1-d/5)^{7/9} d^{9/27} \quad (5)$$

where Z is the number of rollers, and l and d are the roller length and diameter in inches.

Pitch and inner race diameter play important roles in bearing friction and crankshaft durability. The pitch diameter of a bearing with Z rollers of diameter d is given by:

$$D_p = d/\sin(\pi/Z) \quad (6a)$$

and the inner race diameter by:

$$D_{ir} = D_p - d \quad (6b)$$

Finally, a base load rating can be defined from Equation (3) in terms of desired life:

$$C_{base} = P_{base} L_{10}^{3/10} \quad (7)$$

The foregoing relations were used as the basis of the parametric study to establish both the friction and the life factor (an indicator of technical risk) for a wide variety of bearing designs. Crankshaft durability was also indicated, since it is strongly related to journal or inner race diameter.

The analysis was carried out through the following sequence of steps:

- Establish a proposed bearing design by specifying roller diameter, length, and quantity.
- Calculate C_{base} by Equation (7), divide by C (Equation (5)), and substitute into Equation (4) to obtain the life factor required for the given design.
- Obtain the bearing pitch diameter from Equation (6a). Calculate the ratio of pitch diameter to 136 mm for main bearings, 96 mm for rod bearings.
- Obtain inner race diameter from Equation (6b).
- Repeat above steps for all proposed bearing designs.
- Sort designs by life factor.

- For each life factor, plot inner race diameter vs. pitch diameter ratio.
- Based on the plot, one can determine both the crankshaft safety factor and the bearing technical risk implied by a given friction target by properly scaling for loads.

The plots corresponding to this analysis for the main and connecting rod bearings are shown in Figures III.7-1 and -2. The absolute friction scale reflects the incorporation of an exhaust energy recovery system to reduce the reciprocator output for a system power rating of 223.7 kW. In other words, without changing the bearing designs, a reduction in friction loss is expected because of the reduced RDS loads brought about by derating the reciprocator to 172 - 179 kW. The information in these figures bracket what is expected to constitute good design practice.

RDS loads for the main and rod bearings were calculated to be 27 and 39 kN (6082 and 8783 lbf), respectively. This is based on 240 BHP reciprocator output and estimated rotating and reciprocating weights. For conversion of durability to hours and for subsequent lubrication studies, engine speed was assumed to be 1800 r/min.

Stress analysis of the crankshaft confirmed that satisfactory durability would still be achievable with main and pin journals diameter reduction to 100 mm and 65 mm, respectively. This suggests that roller diameters of 9 mm for the main bearings and 12 mm for the rod bearings be selected. In caged (less than full complement) form, these bearing designs can be expected to require life factors of about 6 to 8. That is why they are considered high risk designs. These final bearing designs are illustrated in Figure III.7-3.

Life factors can be realized through combinations of three design factors: material strength, surface finishes, and lubricant viscosities. The latter two actually combine to form the ratio of

lubricant film thickness to composite surface roughness, which in turn correlates to a life multiplication factor. This lubrication-life factor ranges from 0 - 3.5. Life multiplying factors accounting for material strength can apparently be in the range 5-7, per Appendix A.

Detailed Analysis and Technological Requirements - SKF's review of material and lubrication considerations for the ADRE main and rod bearings presented several recommendations, which are summarized as follows:

1. The crankshaft can be made from standard materials (SAE 1548 or 1046 steel), provided that the stock is vacuum or consumable electrode melted.
2. The crankshaft journal surfaces should be induction hardened to at least 58 R_c and coated by the Armoloy hard coat chrome process. The induction hardened zone should be at least .46 mm deep.
3. The crankshaft journal surfaces should be finished to .23 micrometer RMS for the mains, and .16 micrometer RMS for the crankpins.
4. All rollers, cages, and outer rings, should be made from consumable electrode vacuum melted (CVM) AISI 52100 steel in accordance with ASTM A-535.

DDA's estimates of basic durability were confirmed by SKF's more detailed analyses.

The friction losses calculated by SKF for the bearings designed during ADRE selection task were actually higher than for conventional journal bearings. The reduction of reciprocator power from 223.7 to 179 kW resulted in a large drop in friction. This was further enhanced by reducing the journal diameters to 100 and 65 mm. SKF's lubrication studies and cage design work with the

redesigned, lighter loaded bearings lowered the predicted friction levels essentially to the originally established 50 percent goal. These studies assumed clearances and cage designs according to standard bearing design practice. It is possible that further performance and/or durability improvements would result from optimizing these features.

Seal Configurations - DDA's investigation of seal configurations for the main and rod bearings concluded that a suitable seal could be bonded to the journal fillets and ride on the outer rings, as shown in Figure III.7-3. This method would prevent wear of the crank journals by seal lips. An attractive alternative suggested by SKF is their W64 lubrication system in which lubricant is retained in a polymer matrix and is supplied or soaked up depending on the operational status of the bearing. The polymer matrix is configured to replace the cage and provide adequate sealing.

Thrust Bearing - The thrust bearing was subjected to quantitative attention during ADRE system analysis and design efforts. The thrust bearing is placed at the rear main location for logistical reasons. The rear main diameter could be no less than 120 mm, due to the requirements of interfacing with the flywheel. Placing the thrust bearing there allowed use of conventional, non-split race, off the shelf, tapered roller bearings, as shown in Figure III.7-3. It also obviated the design of a special main bearing. For analytical purposes, it was assumed that the thrust bearing would be a Timken bearing part number L624510 or equivalent.

DDA found its analysis of these bearings to be less conclusive than for the main, rod, and piston pin bearings because the main 6 - main 7 system is statically indeterminate. Maximum thrust loads for the required high risk durability were estimated based on several scenarios of radial load sharing between the two tapered roller bearings. These thrust load capacities seemed acceptable.

SKF's lubrication study of the thrust bearing indicated an L_{10} life of over 4000 hours, without material or surface upgrade, and with a continuous thrust load of 4.4 kN (1000 lbf) and total RDS mean radial load of 19.3 kN (4334 lbf). Friction loss was estimated to be 327 W. The friction loss and durability of this bearing are thus quite satisfactory. The good durability of the thrust bearing relative to the other mains is attributable to its larger inner race diameter that is required for flywheel mounting and its lighter loading since it serves only one cylinder.

Piston Pin Bearing - DDA division and General Motors have had previous experience in the use of rolling element bearings for the piston pins of production heavy-duty diesel engines. Needle bearings were used for piston pins in the Winton, Electro-Motive, and Detroit Diesel two stroke engines between about 1929 and about 1940. While they were apparently replaced in favor of bronze bushings for cost-related reasons, as power ratings increased, the experience indicates a basic cost-competitiveness.

Basic Design - The design of the piston pin bearing is heavily constrained by the size of the cylinder bore and basic piston dimensions. A design proposal was formulated within these constraints in the latter stages of ADRE selection task, and is shown in Figure III.7-4. This initial design was an optimistic proposal which best enabled packaging, sealing, and assembly. Since piston pin bearings are thought to be inherently low-friction, no specific effort was made to minimize friction.

A subsequent quantitative analysis showed that the L_{10} life of this design was 200-250 hours, rather than the 625-833 hours desired to fall into the high risk category. Analysis work was undertaken to evaluate proposals to increase durability without expanding the bearing envelope by increasing the number of rollers. Two means were available for this: 1) increasing the inner race diameter without changing the outer race diameter, and 2) decreasing the outer race diameter without changing the inner race diameter.

The analysis was based on straightforward rearrangement and combination of the load capacity - bearing geometry equation (Equation (5)), the pitch diameter - number of rollers equation (Equation (6a)), and the outer and inner race diameter relations presented in the discussion of the main and rod bearings. The result is a function defined for the case of fixed outer race diameter and variable inner race diameter or fixed inner/variable outer as:

$$f(d/D) = (3.1416/\sin^{-1}(x))^{.7834} x^{1.07} \quad (8)$$

where d is the roller diameter, and D is the outer race diameter in the former case and the inner race diameter in the latter. The variable x is defined as:

$$x = \frac{d/D}{1 \pm d/D} \quad (9)$$

where the positive sign is taken for the case of constant inner race diameter and D is defined as in Equation (8). The function $f(d/D)$ is related to load capacity by:

$$C = kf(d/D)D^{1.07} \quad (10)$$

where C is the load capacity, k is taken to be a constant of proportionality (cf Equation (5)), and D is defined as in Equation (8).

Equation (8) is graphed in Figure III.7-5 for the two named cases. The least promising proposal being evaluated was to decrease the outer race diameter, leaving the inner race unchanged. This would cause a decrease in d/D and a decrease in load capacity, as shown. Also of interest is that, for the particular baseline bearing geometry, increasing the inner race diameter without changing the outer race diameter would also cause the load capacity to diminish.

This analysis showed that simultaneously increasing the outer race and roller diameters was necessary to significantly improve durability. The final design, shown in Figure III.7-6, has the largest conceivable outer envelope, with rollers sized so as to leave the piston pin diameter unchanged. Analyses of this design by both DDA and SKF indicated that its durability would be commensurate with that of the main and rod bearings.

Detailed Analysis and Technological Requirements - Specification of piston pin bearing outer raceway design and treatment will depend on final connecting rod material selection. The standard material, SAE 1141 steel, would probably be satisfactory if hardened. Some testing would be required for validation, since there is a lack of experience with this material in roller bearings. An alternative would be to use a raceway insert of high quality bearing steel, as illustrated in Figure III.7-6. Such an insert could be cast or brazed in place, depending on the construction of the rod. Standard piston pin materials and heat treating practices will be satisfactory.

The leading proposal for sealing of the piston pin bearing consists of a conical section seal seated in a counterbore on each side of the connecting rod eye and bearing against the "ears" of the piston dome. An alternative would be to use a W64-type system, as proposed in Appendix A.

Although the lubrication analysis of the piston pin bearing was performed using the Texaco Marfac #2 grease, as for the main and rod bearings, it is likely that the piston pin bearing temperature will exceed the useful range of this grease. A viable alternative would be a fluorinated or perfluorinated grease, as recommended by SKF.

Assembly would be somewhat complicated. It would likely require that the rollers be assembled into the rod and held in place with a mandrel. After installing the seals in the rod, the rod-bearing-seal assembly would be set in place between the

pre-heated ears of the dome. The piston pin would then be inserted displacing the mandrel. The bearing could be greased either before or after assembly, depending on the temperature limitations of the grease.

Table III.7-1: Task 1 Selected ADRE Bearing

	<u>MAIN</u>	<u>CONNECTING ROD</u>
Roller Length, mm	22	17
Roller Diameter, mm	11	11
Number of Rollers per Row	30	21
Number of Rows	1	2
Journal Diameter, mm	125	85
Heat Generation* (Watts)	918	576
L10 Fatigue Life*	1949	1377

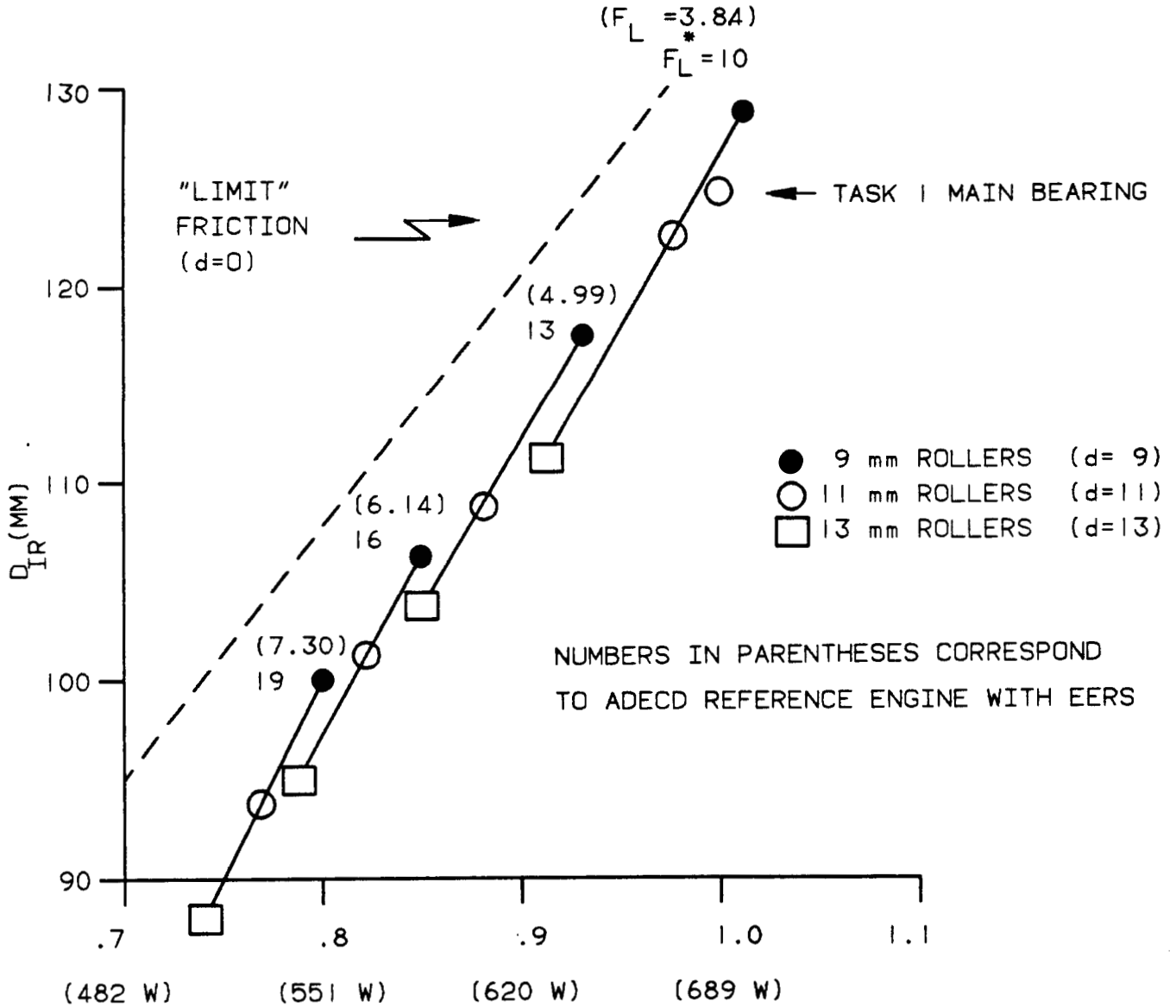
* Lubricant: Texaco Marfac #2 Grease

Figure III.7-1: Main Bearing Design Chart.
 [Inner Race Diameter is Plotted as a Function of Pitch Diameter for Various Levels of Durability.]

MAIN BEARING: 20 mm ROLLER LENGTH
 TEXACO MARFAC #2

LIFE FACTOR =
 FOR 540×10^6 REV.

$$F_L^* \times \left(\frac{P}{8000 \text{ lb}} \right)^{10/3}$$



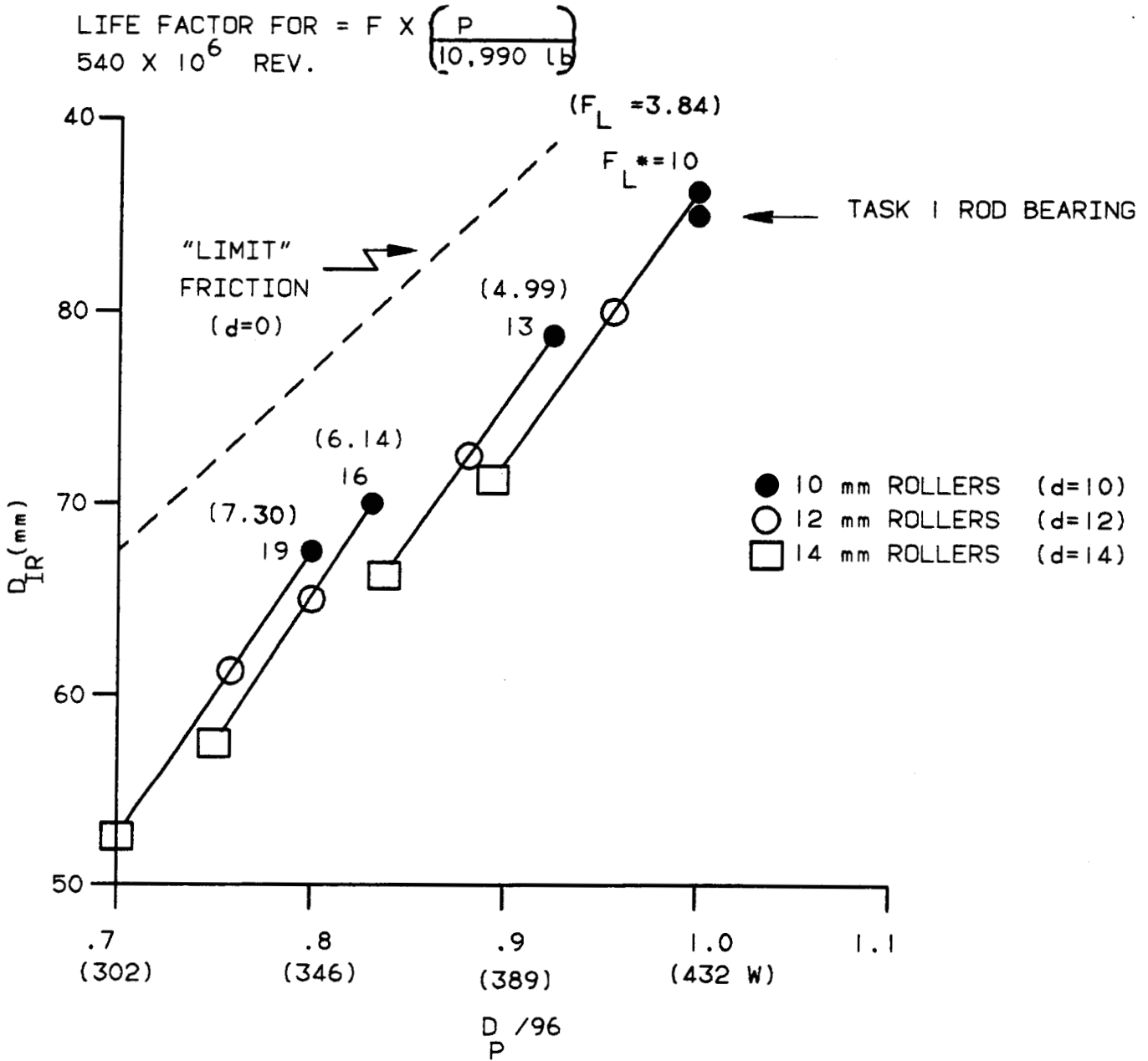
$$D_P / 136$$

$$\frac{\text{FRICTION (W)}}{918} = \frac{D_P}{136} \times \frac{P}{8000}$$

Figure III.7-2: Rod Bearing Design Chart.
 [Inner Race Diameter is Plotted as a Function of Pitch Diameter for Various Levels of Durability.]

ROD BEARINGS (40 mm ROLLER LENGTH) TEXACO MARFAC #2

NUMBERS IN PARENTHESES REFER TO ADECD REFERENCE ENGINE WITH EERS



$$\frac{\text{FRICTION (W)}}{576} = \frac{D_P}{96} \frac{P}{10,990}$$

Figure III.7-3: Cross-Section Illustrating Main, Rod, and Thrust Bearings

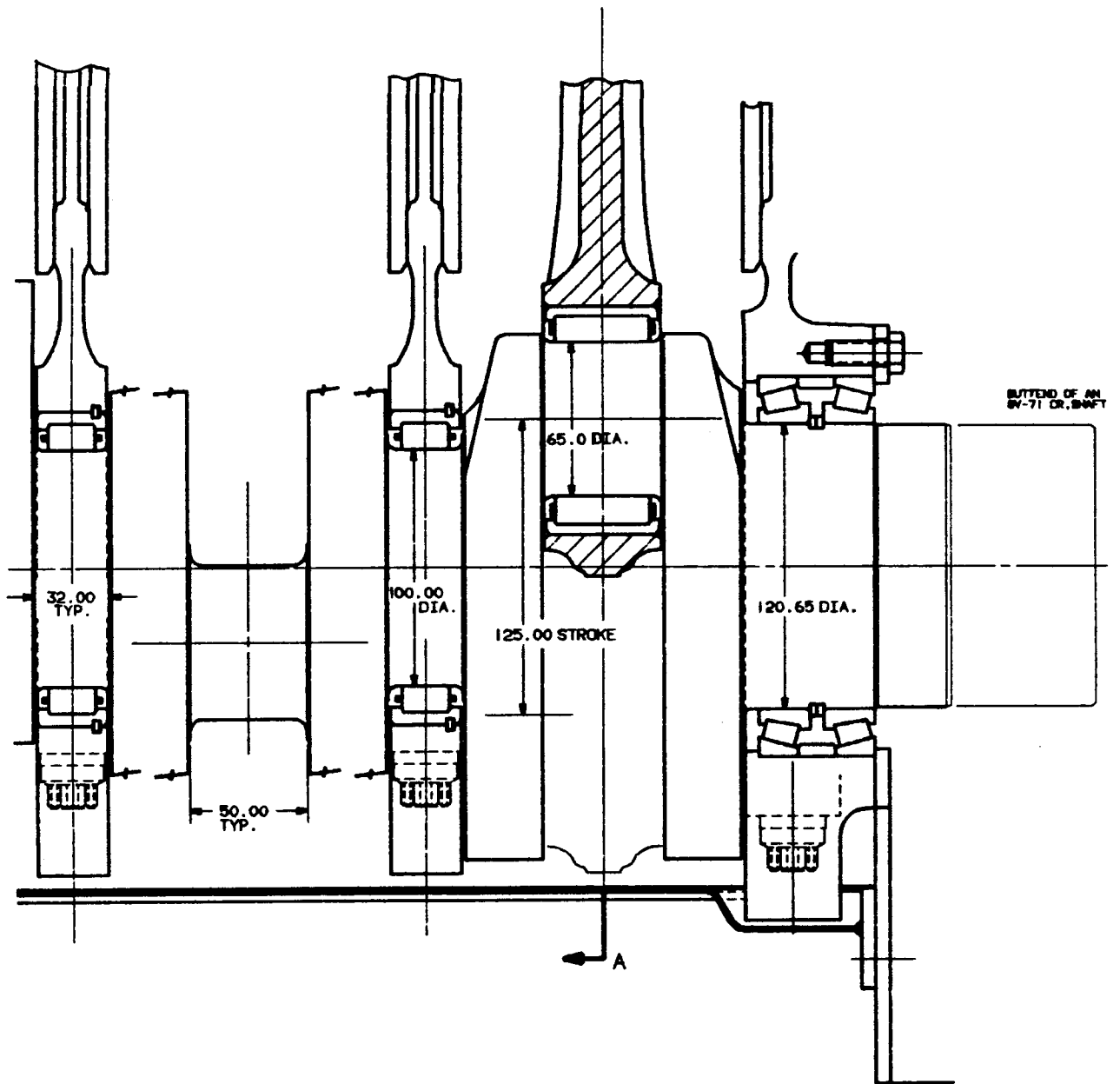


Figure III.7-4: Preliminary ADRE Piston Bearing Design Concept

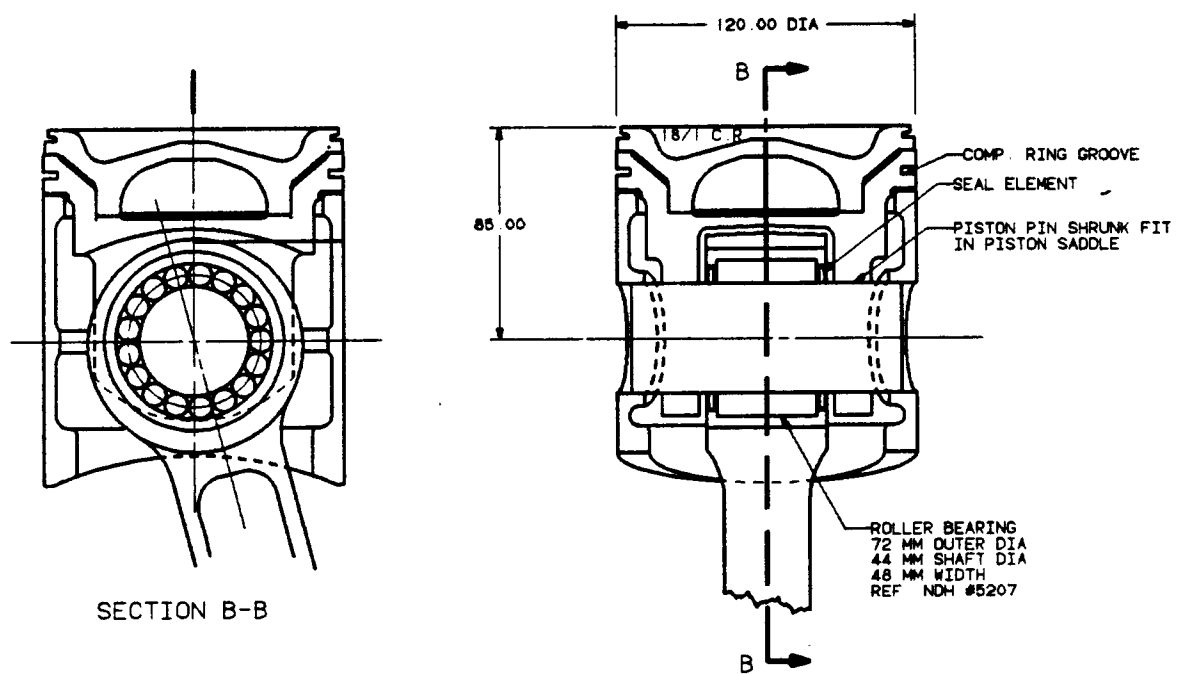
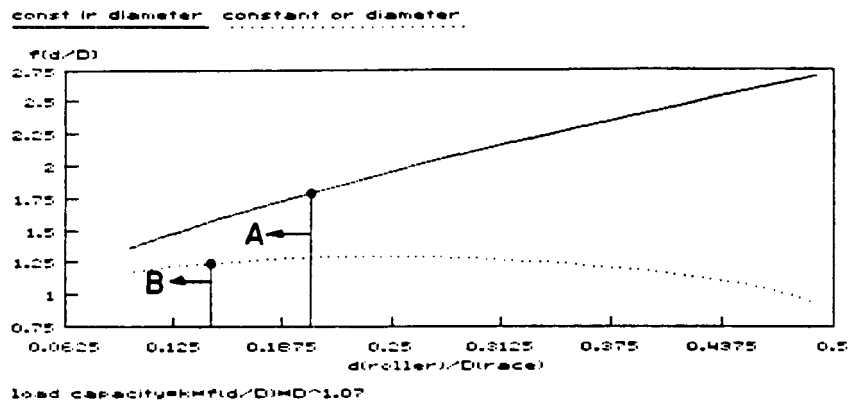


Figure III.7-5: Relative Piston Pin Bearing Load Capacity as a Function of Roller Size



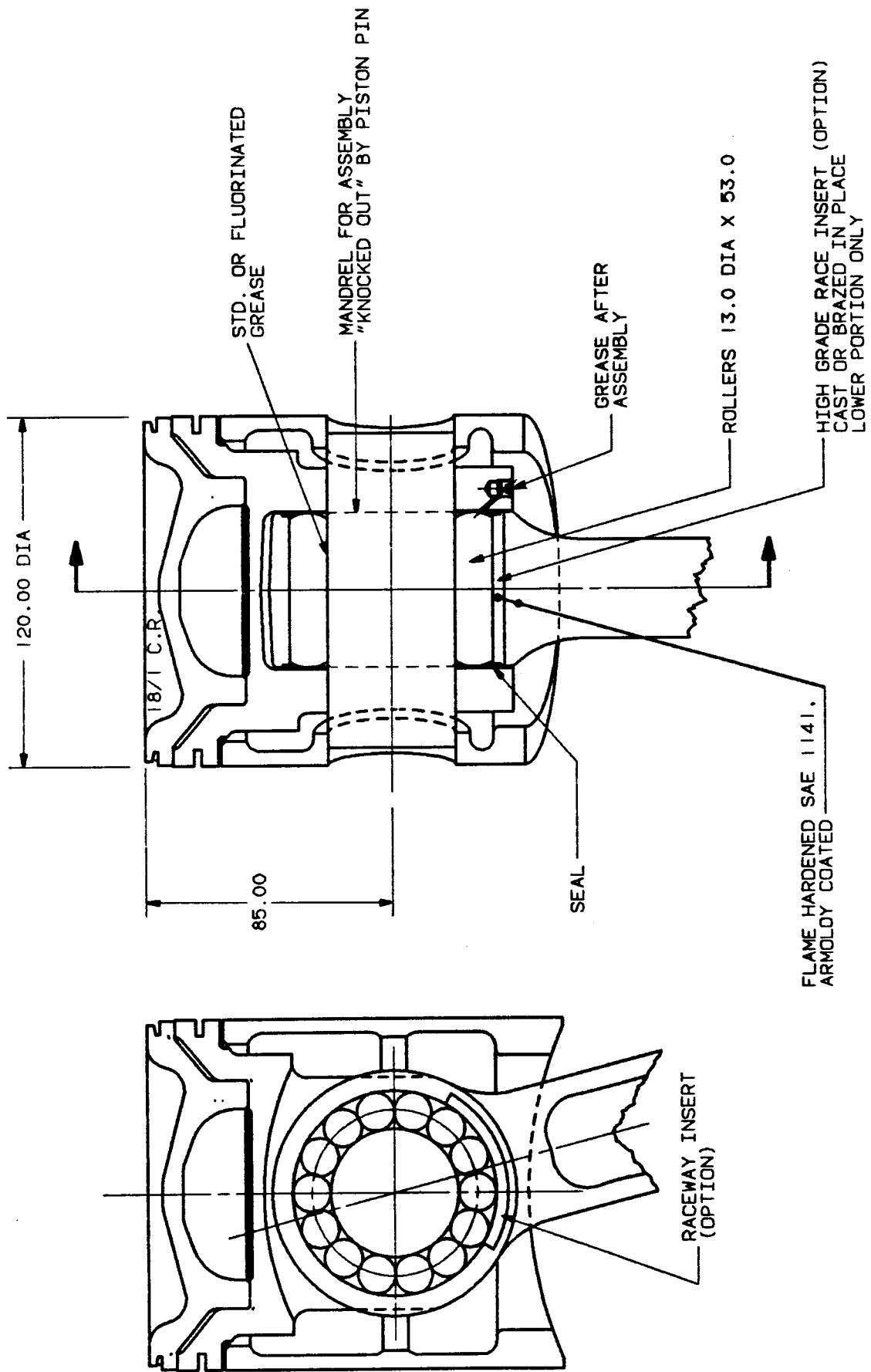


Figure III.7-6: Final ADRE Piston Pin Bearing Design

III.8. SOLID LUBRICATION TRIBOLOGY

Solid lubrication was the selected approach for the ADRE tribology. During the ADRE System Analysis and Design activity, review of the state-of-the-art of solid lubrication was undertaken. Further, design concepts were generated to enable the utilization of various forms of solid lubrication for the ADRE reciprocator. The choice of camless valve and injector actuation systems was made, in part, so that the pursued tribology treatments concentrate on solving the challenge of the in-cylinder high temperature components.

CONCLUSIONS

The following conclusions are based on careful assessment of applicable solid lubrication science and technology to the ADRE. Recommendations are also included:

1. The solid lubrication tribology for application in severe environment is an emerging technology. Basic generic scientific research is needed in the areas of lubricants, surface treatments, and in the understanding of the tribological interactions at the solid lubricated interfaces.
2. Current solid lubrication science and knowledge indicate that the friction and wear characteristics will be unacceptable for applications of the ADRE type. It is uncertain whether this technical barrier will be overcome in the 1995 time frame.
3. Liquid lubrication should be used in a heavy-duty diesel engine, at least for the crankcase region.

4. It is recommended that high temperature tribology investigations for hot section components consider both non-liquid and high temperature liquid lubrication approaches.

DISCUSSION

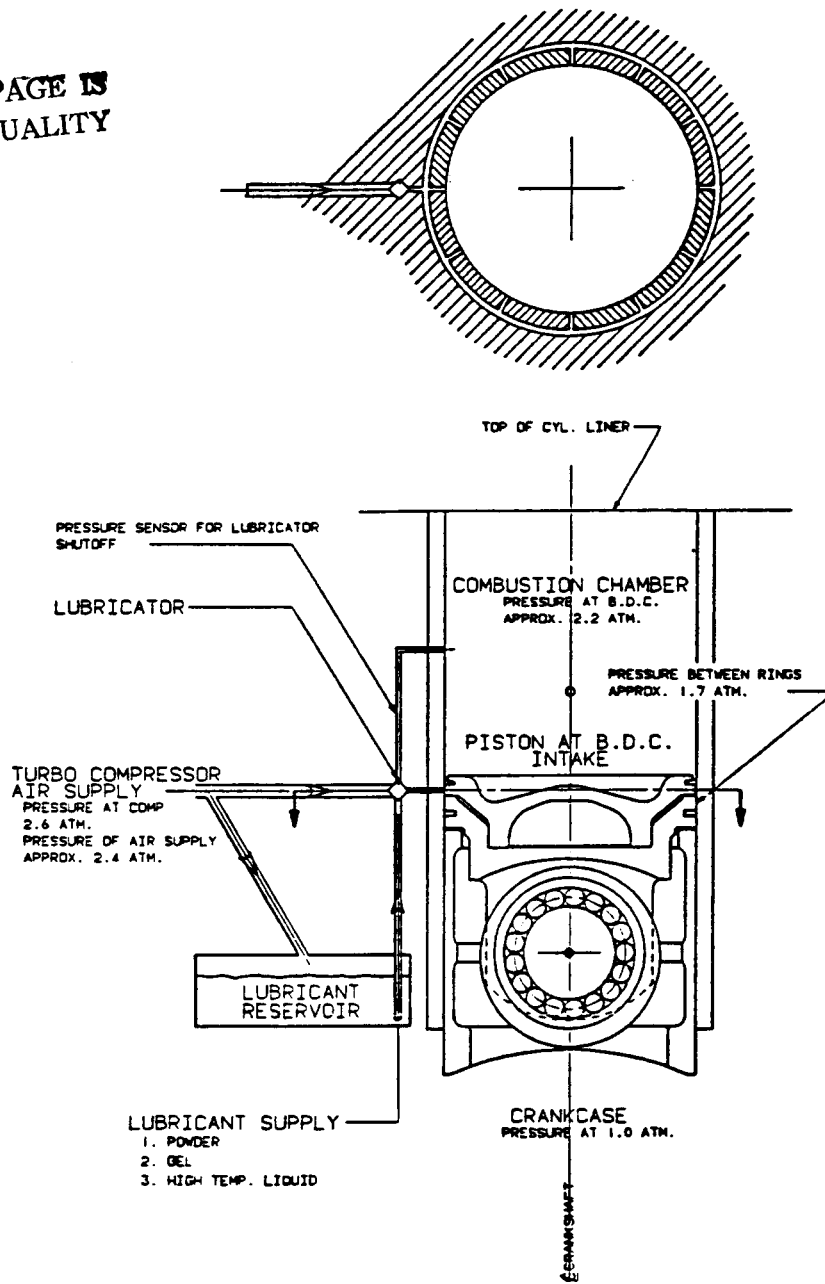
The Survey of the state-of-the-art of reciprocating motion solid lubrication has not revealed any encouragement as to the potential of a solid lubricated cylinder kit. The majority of solid lubrication work has been directed at roller element bearings, which require a rather limited component life when compared with the ADRE goals. Several leading consultants in solid lubrication tribology were identified and asked to provide their expert opinion. The solid lubrication tribology pursuit will continue during the following phases of the program.

Many proposals for a cylinder kit solid lubricant injection system were completed, for both in situ as well as continuously replenishing systems. It is emphasized that these systems are just conceptual proposals and do not represent a recommendation for a prime path approach at this time. Representative examples of these concepts are shown in Figures III.8-1 through III.8-8. For example, the concept shown in Figure III.8-1 represents a replenishing solid lubrication system concept that utilizes the turbocharger compressor air for lubricant atomization and delivery. It would have electronic timing and would be actuated via a solenoid. The concept in Figure III.8-2 also uses a mixture of turbocharger compressor air and lubricant injected into the cylinder. However, it is timed and actuated by a cylinder pressure sensing device. Other figures should be self-explanatory.

FIGURE III.8-1

SOLID LUBRICANT SUPPLYING SYSTEM PROPOSAL

ORIGINAL PAGE IS
OF POOR QUALITY



c-4

FIGURE III.8-2

SOLID LUBRICANT SUPPLYING SYSTEM PROPOSAL

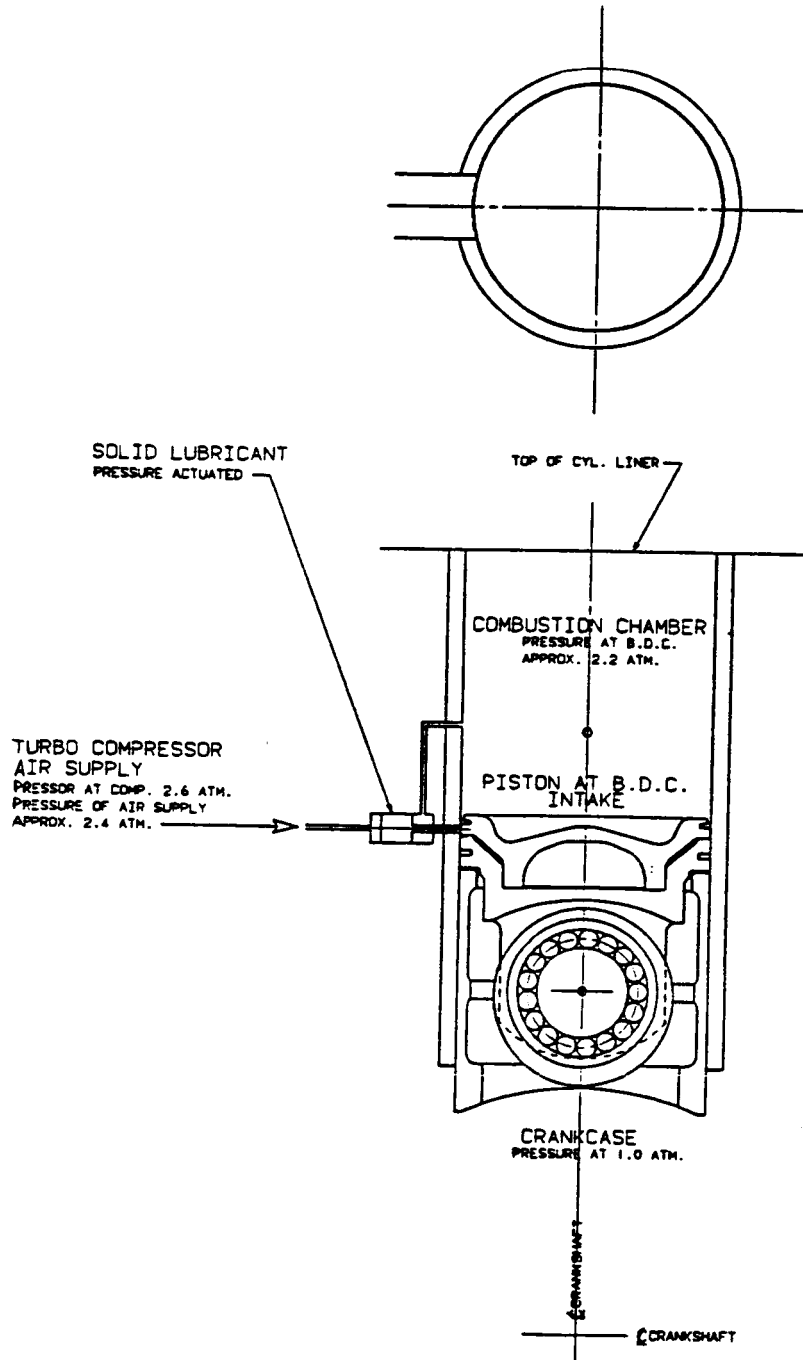
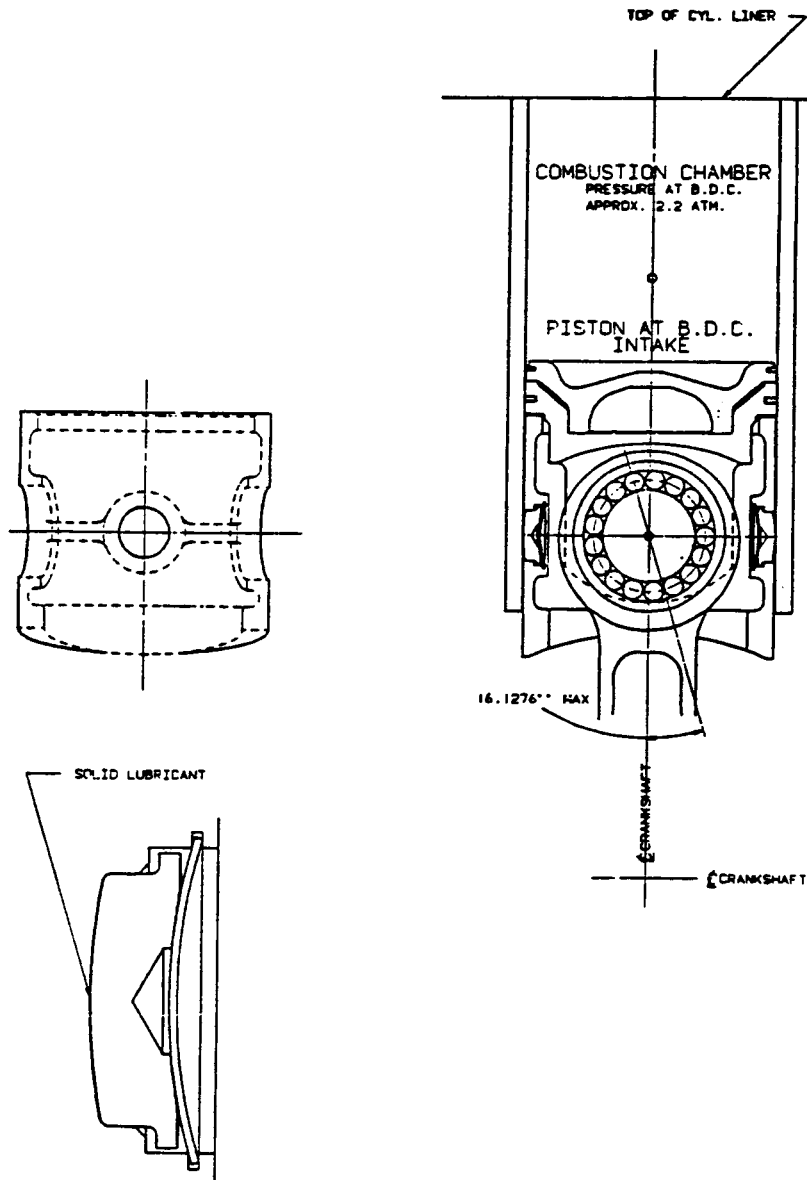


FIGURE III.8-3

SOLID LUBRICANT SUPPLYING SYSTEM PROPOSAL



SOLID LUBRICANT SUPPLYING SYSTEM PROPOSAL

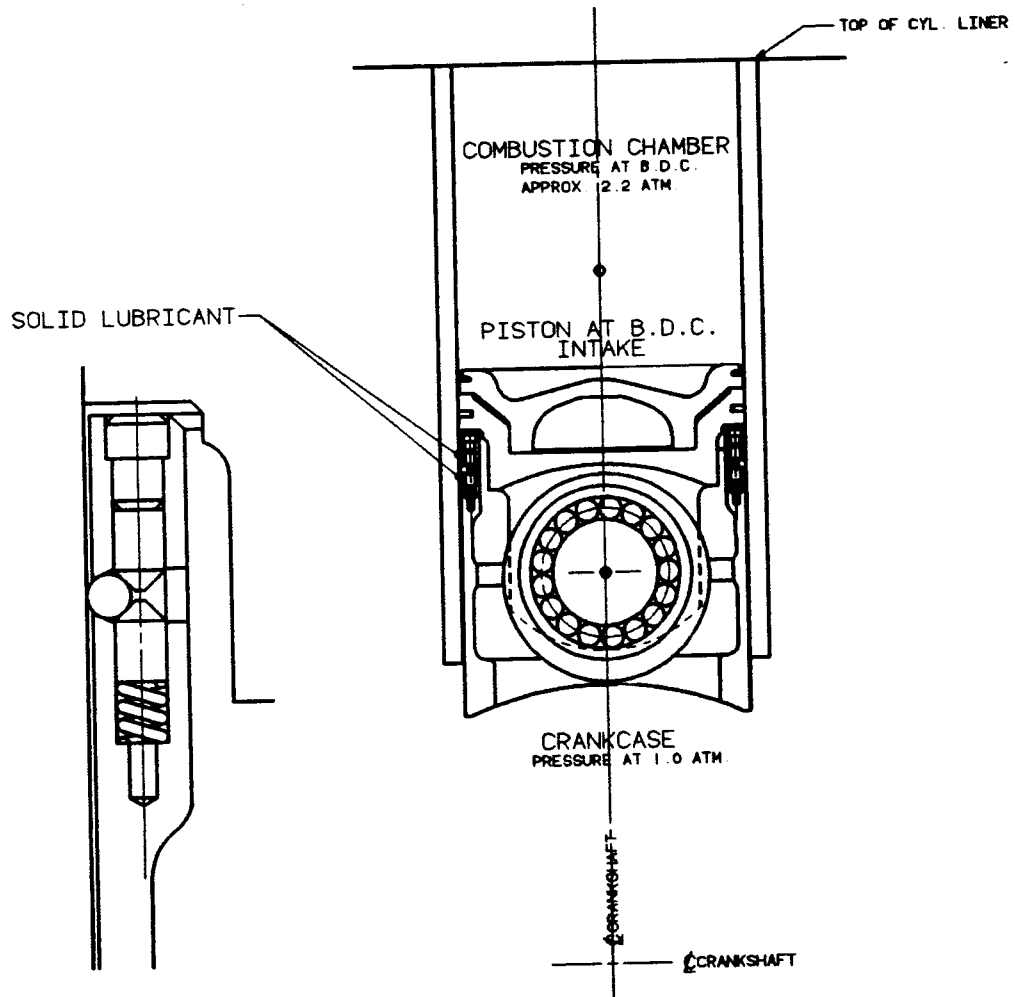


FIGURE III.8-5

SOLID LUBRICANT SUPPLYING SYSTEM PROPOSAL

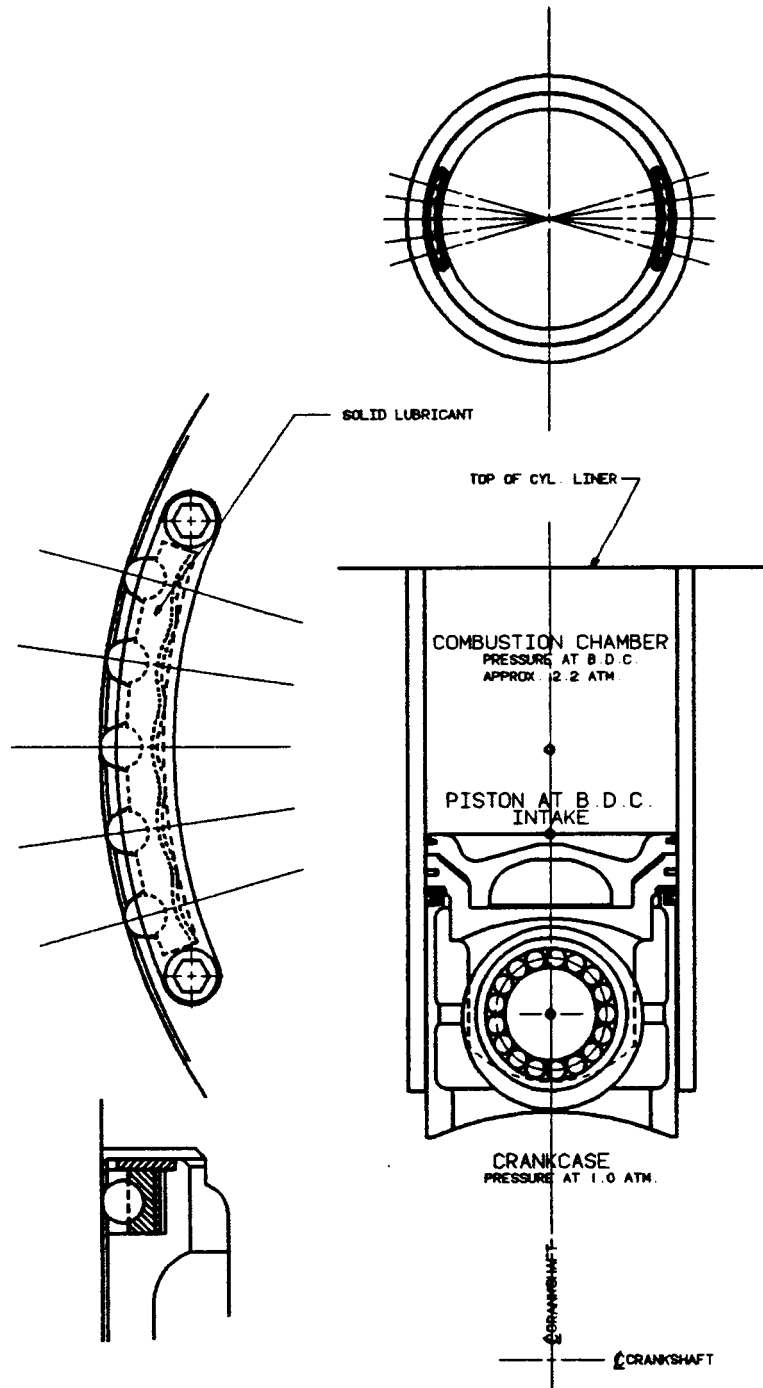


FIGURE III.8-6

SOLID LUBRICANT SUPPLYING SYSTEM PROPOSAL

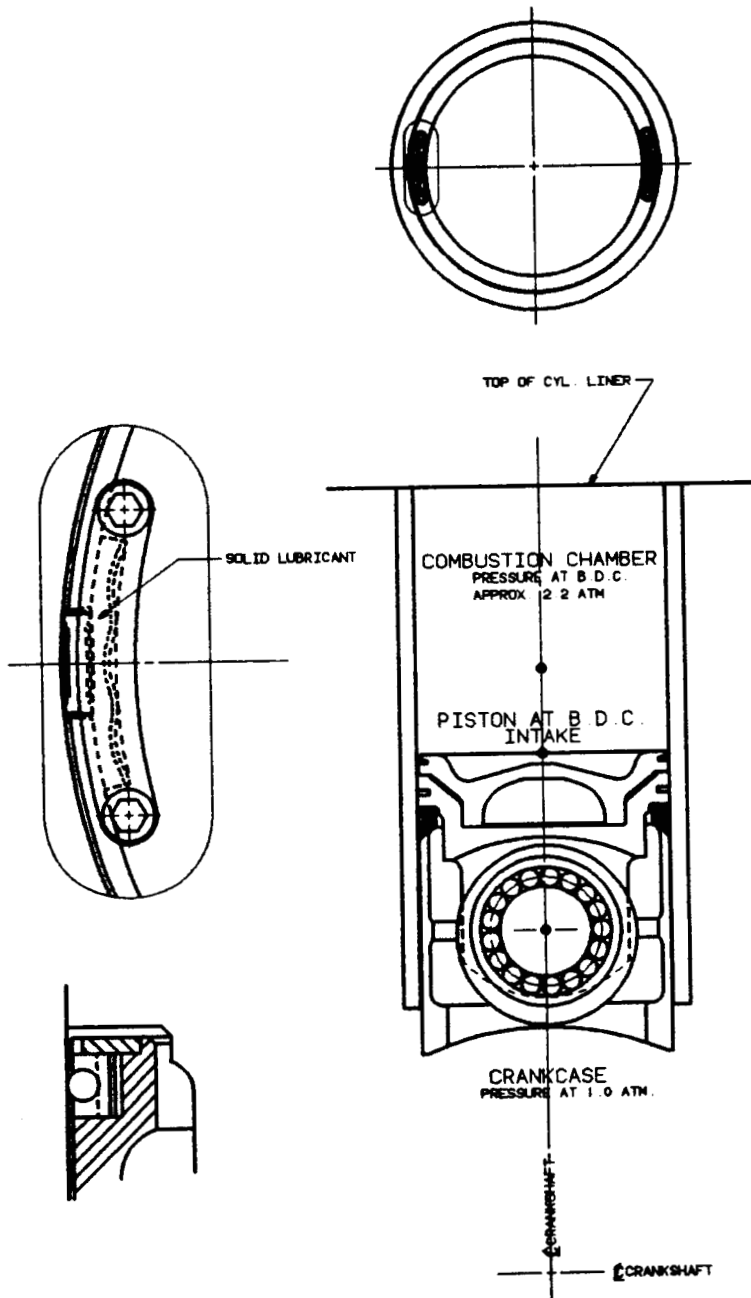


FIGURE III.8-7

SOLID LUBRICANT SUPPLYING SYSTEM PROPOSAL

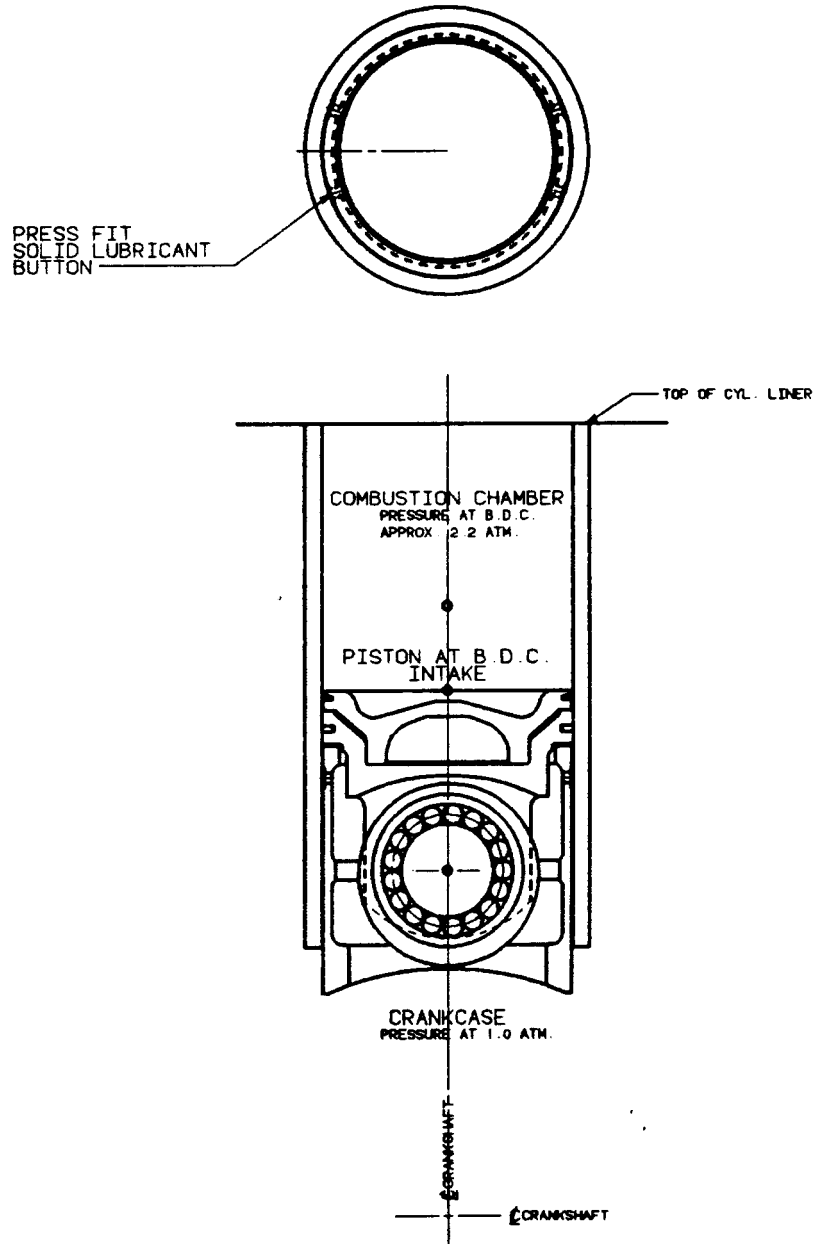
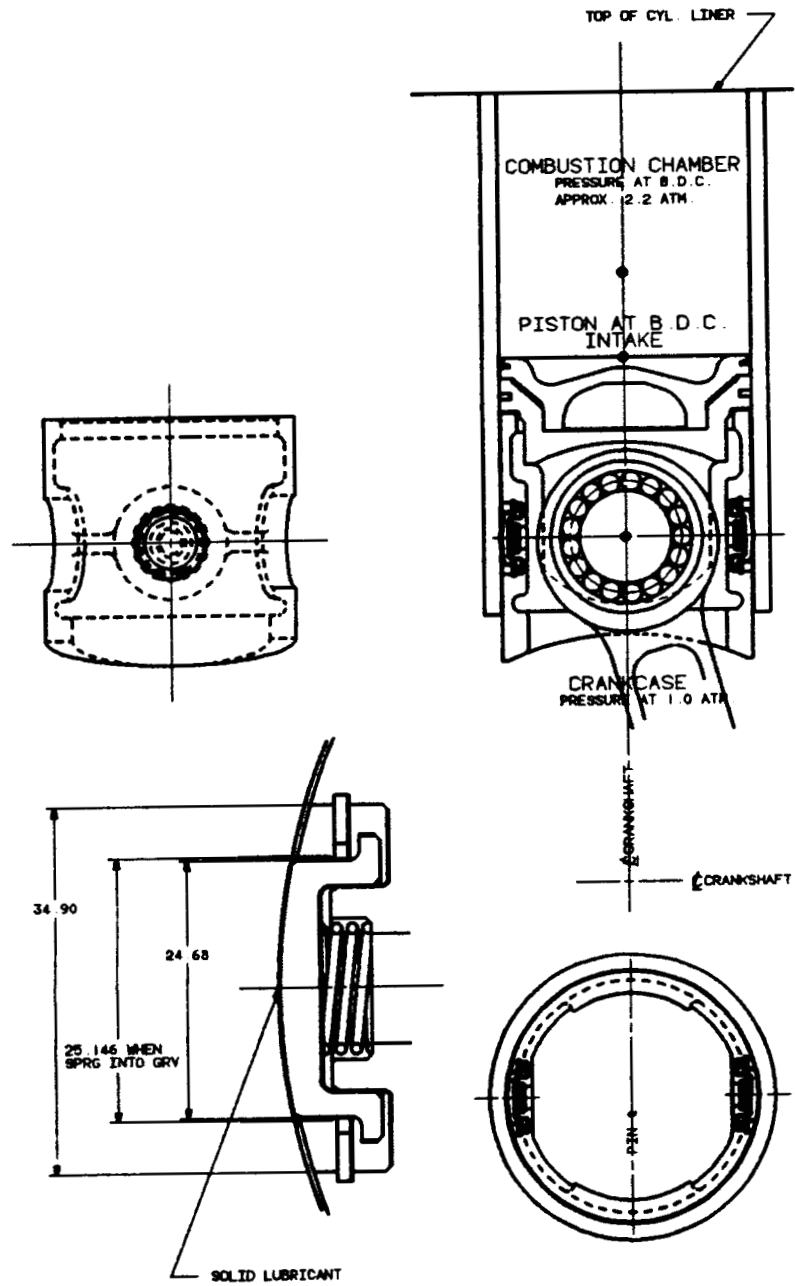


FIGURE III.8-8

SOLID LUBRICANT SUPPLYING SYSTEM PROPOSAL



III.9 ADDITIONAL COMPONENT AND CONCEPT ANALYSES

To ensure a sound ADRE system, many support analyses were undertaken. This section reports on the following additional studies:

1. Piston Assembly
2. Firedeck and Cylinder Head
3. Gasketless Combustion Seal
4. Crankshaft

III.9.1 PISTON ASSEMBLY

PISTON DESIGN EVALUATION

This analytical study was undertaken to evaluate the ADRE piston and to analyze the total and side forces applied to this piston during operation at the rated condition.

Conclusions - The following conclusions are based on comparisons between the ADRE piston design and production type pistons for both 2-stroke and 4-stroke heavy-duty diesel engines.

1. Comparative evaluation of the normalized values of pertinent piston dimensions indicates that the ADRE piston design is reasonably within the practical limits.
2. Total unit bearing load calculations for the pin boss during the power stroke show the ADRE engine loads to be higher than the conventional piston design by a factor of 2.5.

3. Side forces applied to the ADRE piston, during the power stroke are higher than the conventional piston design by a factor of 1.6.
4. Piston pin unit loading on the skirt boss is reasonable, but could be lower if a longer pin is used.
5. Inertia unit load of the ADRE piston is lower than an equivalent conventional 4-stroke engine by a factor of 1.7.

For the detailed component analysis and design phase of the program, it is recommended that the length of the piston pin be increased to the maximum allowable, in order to further reduce skirt-pin unit loading. A separated upper dome and lower skirt design may be adopted for the ADRE single cylinder test bed. This would allow for conventional liquid lubrication on the skirt and piston pin, while the ring belt would be solid lubricated.

Discussion - The evaluation of the ADRE piston and cylinder kit included a comparative assessment of the piston main dimensions, normalized to the bore size. This comparative evaluation was adopted after Mahle, a German piston supplier. The other area of investigation dealt with kinematics, kinetics, and bearing unit loads due to gas pressures and inertia loads.

Dimensional Assessment - This comparative analysis technique was applied to the ADRE piston, along with two conventional piston designs. The latter are of the cross head design and operate at about the same output power levels. Figure III.9-1 shows the pertinent dimensions that were normalized to the bore size. A brief account of the the results is given below as each of the dimensional comparisons will be discussed, and the rationale for making the comparison will also be explained.

1. Piston Total Height. This dimension offers an indication of the piston tilt tendency. Generally, too short a piston will cock excessively, while a piston that is too long will increase the reciprocating mass and induce excess friction. The practical range (provided by Mahle) is 100-130 percent of the cylinder bore. This range is believed applicable to this design. Using this criteria, the ADRE design is acceptable.
2. Skirt Height. This dimension relates to the skirt to liner bearing area available to transfer the side forces. The practical range may be partially applicable in the ADRE case, since the conventional engine has hydrodynamic lubrication in this contact area. The ADRE, as proposed, will not have liquid lubricant between the liner and the skirt. Nevertheless, the skirt height of the ADRE piston is within the defined practical range.
3. Pin Center Line to Dome Top. This dimension gives an indication of the piston crown tipping tendency under operating clearances and loads. On the other hand, it is also important to keep the operating temperatures of the pin boss bearing area as low as possible. Additionally, it is desired to keep the pin centerline as close as possible to the center of gravity of the piston to minimize the rotational inertia. This ADRE dimensionless number is higher than today's practical range. This should be advantageous to the pin bearing tribology, but may have negative effects on the piston secondary forces.
4. Pin Center Line to Skirt Bottom. The value of this parameter of the ADRE compares favorably with the current practical range.
5. Piston Pin Diameter. The piston pin is an essential load path joint between the piston and the connecting rod. The piston pin deflection should be minimized. Bending

stiffness and pin diameter are the influential factors under load. Little space or weight is saved by having a smaller pin, and the potential for bending is increased. The ADRE pin diameter is appropriate.

6. Connecting Rod Small End Width. This dimension relates to the pin bending versus the availability of enough bearing area for the connecting rod small end. The ADRE value appears acceptable. Further optimization is likely during the component design phase.
7. Under Compression Height. The ADRE dimension is within the current practical ranges.
8. Dome Bowl Thickness. The dimensionless number used here related the dome bowl thickness to the bowl diameter instead of the cylinder bore. This dimension, governed by material properties and operating conditions, reflects the dome's ability to handle the applied forces. A secondary consideration for the ADRE piston is the thermal insulation requirements. In this case, the current practical recommendations will not be applicable. The ADRE piston appears to be adequate.
9. Top Land Height. This dimension is concerned with several important tradeoff considerations: First, the volume known as the "K" factor which, with regard to combustion, the smaller the better. A second factor deals with carbon deposits on the top land of the piston leading to bore polish and eventual loss of oil control for the conventionally lubricated engine. The last consideration is the operating temperatures of the ring belt area and the resulting tribological impacts. The ADRE top land height is acceptable. Moving the top ring location should be considered in the context of the tribology approaches during the following phases.

10. Second Land Height. This dimension relates to the available thrust load bearing area of the piston dome. It is also relevant in the ring pack dynamics and how the two compression rings interact under combustion and blow by gas pressure changes. The ADRE piston second land design is acceptable.

Dynamic Analysis - Axial and side forces, and various unit bearing loads to which the ADRE piston is subjected, were analyzed. A DDA piston dynamics computer program was utilized. Simulation runs were made, and the results were compared to data from production engines. The full cycle analysis resulted in defining cylinder pressure, piston kinematics and kinetics, and unit bearing loads as a function of the crank angle. The results of this comparative study have been briefly reported in the conclusions part of this section. They essentially confirm the viability of the ADRE piston and cylinder concept. Detailed component analysis and design activities (that will be undertaken in the next phase of the program) should result in further refinements and/or changes to the proposed design.

PISTON FINITE ELEMENT ANALYSIS

Material Properties - The challenge of forecasting certain technological achievements for the 1995 proof of concept demonstration was addressed earlier in Section II.2.1. The monolithic ceramic material to be used for the ADRE components is supposedly a 1995 state-of-the-art material. This was translated to certain material property values that were used for the finite element analysis. Typical today's state-of-the-art silicon nitride mechanical properties were utilized without a change. Essentially, this meant an MOR of 800 MPa and a Weibull modulus of 14. However, it was speculated that half of the current thermal conductivity for thermal properties would be achievable in the 1995 time frame. This is conceivably achievable by improving the strength of low

conductivity ceramics or, alternatively, developing new ceramic matrix composite materials that have the above thermal and mechanical property values. The thermal conductivity values used for the analysis are 15 W/m.C at room temperature, and 8 W/m.C at 800°C.

Analysis - Gas side boundary conditions were generated through cycle simulation. Other boundary conditions were implemented to simulate the interaction between contacting components. Thermal, structural, and probability of survival analysis were undertaken for both rated and peak torque operating conditions to assess the soundness of the design and material selection. The axisymmetric finite element model of the piston is shown in Figure III.9-2, and the analytical methodology has recently been described.*

The results show that the ceramic piston cap has a probability of survival in excess of 0.9993, which is acceptable, based on prior experience. An example of the FEA output is shown in Figure III.9-3. Upgrading of the iron piston body to a material with greater high temperature strength is likely. It is concluded that this design is feasible for further studies during the next phase of the program.

*Groeneweg, M., et al, "Current Applications of Finite Element Analysis to Diesel Engine Component Design," SAE Paper No. 870813.

Figure III.9-1: ADRE Piston - Pertinent Dimensions

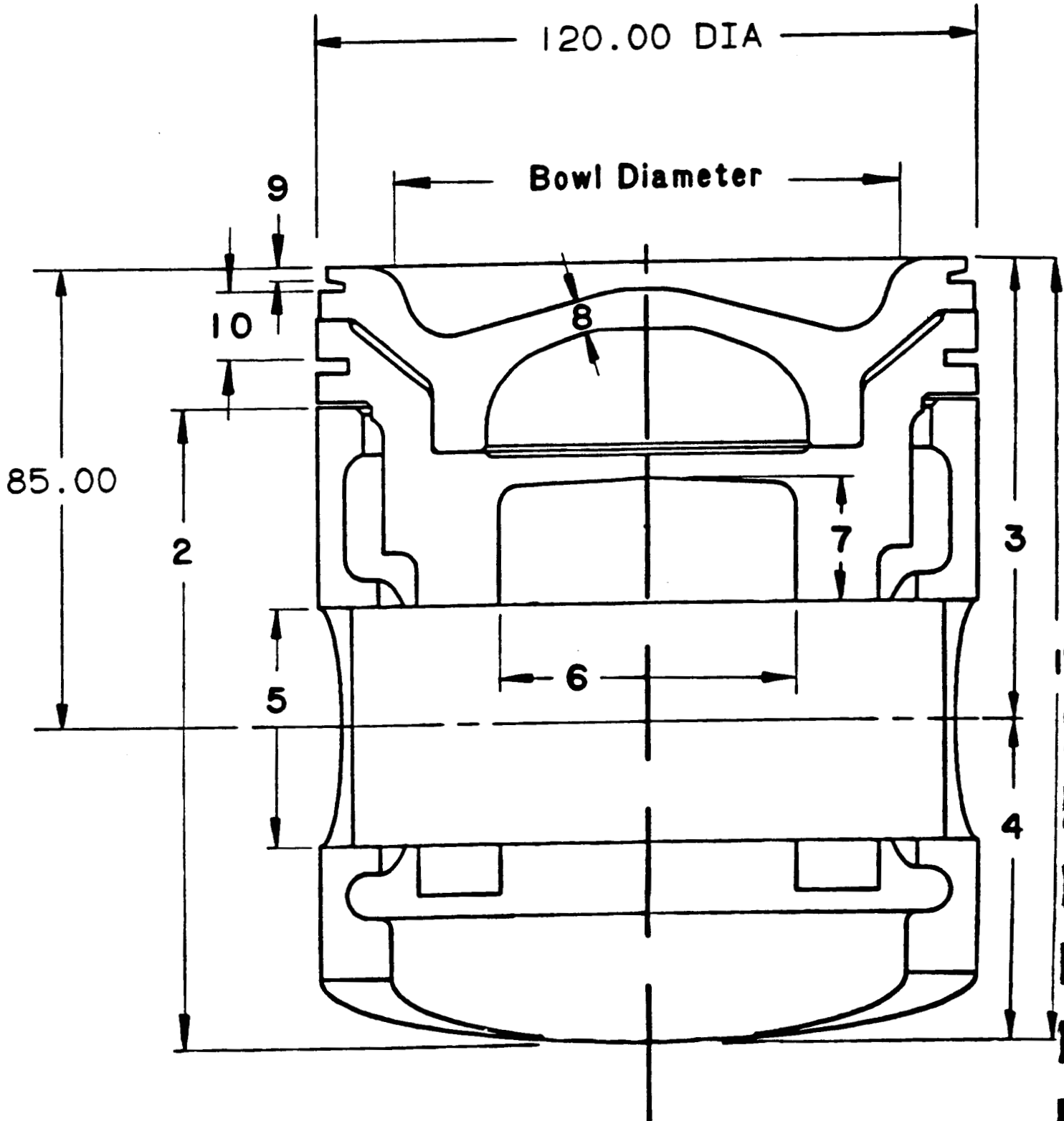


Figure III.9-2: Axisymmetric FEM of ADRE Piston

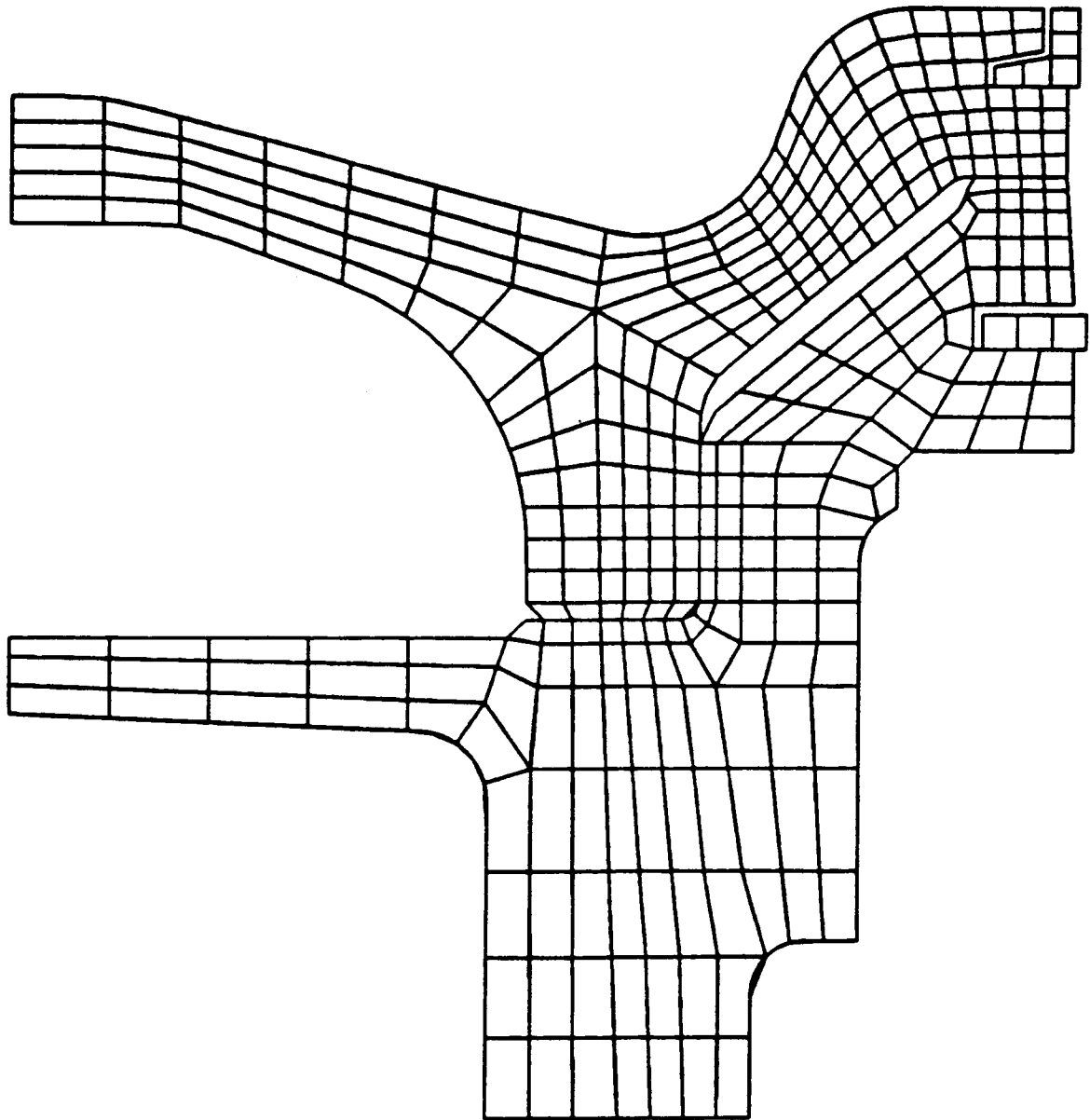
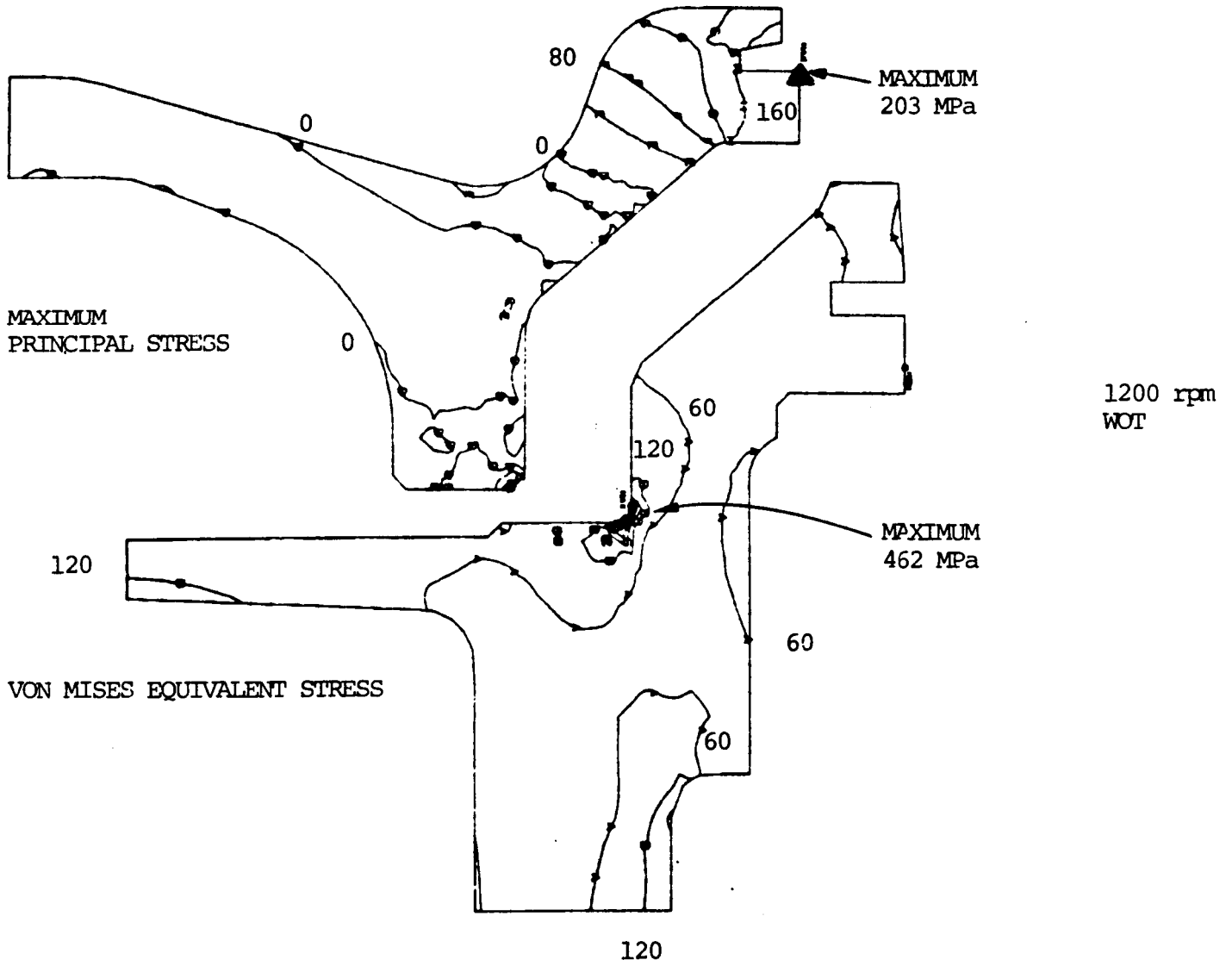


Figure III.9-3: Typical Piston FEA Output



III.9.2 FIREDECK AND CYLINDER HEAD

CYLINDER HEAD AND FIREDECK FINITE ELEMENT ANALYSIS

The objective of this analysis was to determine the temperature distribution within the structure, to calculate the heat flux through the firedeck face, to determine the stress levels and probability of survival for the ceramic component, assess the press fit approach for the firedeck insert, and evaluate the general design concept.

Conclusions - The following are the conclusions, based on the results of the FEA analysis:

1. An O.D. air gap should be used to reduce cylinder head temperatures. With the O.D. air gap, a maximum temperature of 440°C (824°F) is predicted.
2. Heat rejection through the firedeck was 1.0 kW, compared to an estimated baseline rate of 2.0 kW.
3. Stress levels are acceptable:
 Signal firedeck - 330 MPa (48 KSI)
 Von Mises head - 110 MPa (16 KSI) hot
 174 MPa (25 KSI) cold
4. The firedeck OD press fit should be minimized in order to reduce assembly stresses.
5. High strength alloyed gray iron is a viable material for the cylinder head.

Discussions - Thermal, structural, and probability of survival analyses were carried out.

Thermal Analysis - Iterative thermal analysis was performed. In order to reduce the head temperatures, an air gap was added to the O.D. of the ceramic firedeck insert, the ceramic thermal conductivity was cut in half, and the contact thermal resistance between the ceramic insert and the cylinder head was added to the model. This resulted in lowering the cylinder head temperature from the original 535°C to 440°C. This temperature is high enough to cause some concern if the conventional cylinder head cast iron material is used. If detailed Phase II analysis shows high temperature growth or creep as a problem, various alloying elements, such as molybdenum can be added to improve the high temperature properties of the iron.

Justification for the reduction in thermal conductivity was explained earlier in Section III.9.1. The maximum temperature in the ceramic insert is 860°C, which is judged to be acceptable. Peak temperatures occurred between the exhaust valves, as would be expected. The heat flux was summed over several surfaces of the fire deck insert. The total net heat flux for the firedeck face is approximately one half that of the 2000 W estimated heat flux for the baseline water cooled engine. Reductions in the contact area between the cylinder head and firedeck should make it possible to further reduce the heat flux through the firedeck. However, such a reduction in area may make sealing of the firedeck to head interface more difficult.

Structural Analysis - For the analyzed thermal load cases, structural runs were first made to evaluate the thermal expansion of the firedeck insert, relative to that of the cylinder head. Radial displacements corresponding to the above reported thermal results show that the cylinder head expands 0.185 mm more than the deck insert. In order to provide a positive means of controlling the position of the firedeck insert, relative to the head, consideration was given to choosing a press-fit that would maintain contact between the firedeck insert and the cylinder head under all load cases. A press fit of 0.185 mm magnitude would lead to unacceptable assembly stresses at room temperature. Hence, it

is recommended to use a light press-fit; nominally, 0.0762 mm radial interference, for positional control at assembly. Under operating conditions, the head bolt clamp load would prevent radial displacement of the firedeck relative to the cylinder head.

Stress and probability of survival results were also calculated. The results predict moderate stress levels for both the head and the firedeck insert. The lowest probability of survival for the firedeck insert was 0.9999, under all load cases considered in this analysis. The most critical stress conditions occurred within the cylinder head near the press fit interface. Further refinement of the press fit interface and in the FE model should significantly reduce the stress in this region.

The cylinder head has a Von Mises stress of 174 MPa at cold assembly conditions. Thermal loading reduces this stress to 110 MPa. When a cylinder pressure of 16.2 MPa is further imposed, the cylinder head maximum stress becomes 202 MPa. This occurred in a very localized region and, with further refinement, the maximum stress should be reduced. Sample FEA results are shown in Figure III.9-4.

Gasketless Combustion Seal Study

This study was conducted to evaluate and maximize the combustion sealing capability of a gasketless cylinder liner-to-firedeck joint. It was decided to use FEA to determine whether a four (4) cylinder head bolts per cylinder configuration provides adequate joint sealing capability, or if it is necessary to use more head bolts, e.g., an eight (8) bolt configuration. Further, the required cylinder head bolt diameter for gasketless combustion sealing and adequate fatigue safety factor were determined.

Conclusions - The following conclusions are based on the study undertaken, which essentially compared a four-bolt design configuration with an eight-bolt alternative. The latter has two shared bolts between neighboring cylinders, which reduces the effective number to six bolts per cylinder.

1. The eight (8) bolt per cylinder bore (six effective bolts per bore) is the recommended configuration, to be developed further for the ADRE during Phase II.
2. The recommended cylinder head bolts are 14 mm diameter Grade 10.9 bolts, which will have a fatigue safety factor of 4.6 for the worst cyclic load condition.
3. For the eight bolt configuration, the compressive sealing stress, which is the gasketless joint holding pressure, varies from a maximum of 306 MPa to a minimum of 67 MPa, at a design combustion pressure of 16.2 MPa.
4. An intake and exhaust port contour should be developed further to maximize the bending stiffness of the cylinder head firedeck at the port centerline.

Discussion - At the onset of the program, the cylinder head configuration was not fully defined, so a finite element model of the cylinder head was generated that would allow some flexibility in modifying the basic structure. A simplified three-dimensional model of the cylinder head was generated, which was basically a "cube" that could be modified by removing elements. Figure III.9-5 shows an example of the three components modeled for this study. The cylinder head and liner material is gray cast iron, and the firedeck is monolithic ceramic. Cylinder head bolt loads were applied to the components at positions that simulated either a four (4) bolt or eight (8) bolt cylinder head configuration. Also, the magnitudes of the bolt loads were varied to study the effects of higher grade or larger diameter cylinder head bolts.

A typical sealing pressure distribution along the liner/firedeck sealing interface is shown in Figure III.9-6, in a polar plot format. The curves plotted represent the compressive stresses at the outside diameter and inside diameter of the interface between the liner and the firedeck. This Figure shows the large variation in sealing pressure obtained with the four (4) bolt cylinder head configuration. In some cases, when the combustion pressure is applied, the inside diameter of the sealing surface is no longer in contact. This can result in the potential loss of the sealing function of the joint. This Figure also indicates that, with better distributed load of the eight (8) bolt pattern, the joint sealing stresses are less cyclic. The sealing surface remained in contact under combustion gas pressures, with a minimum sealing unit load of 67 MPa.

Increasing the bolt clamp loads resulted in no significant change in the sealing pressure or its distribution pattern. This indicates that the limiting factor to increased joint sealing pressure is the bending stiffness of the cylinder head.

The cylinder head bolt was sized, based on the desire for a compact engine design and to provide adequate gasketless sealing pressure and fatigue resistance. The 14 mm bolts provide a clamping force per cylinder exceeding 3.7 times the combustion force, and their estimated fatigue life is acceptable.

- P.O.S. > 0.9995 at full load
- 70% INSULATION
- DESIGN IS FEASIBLE

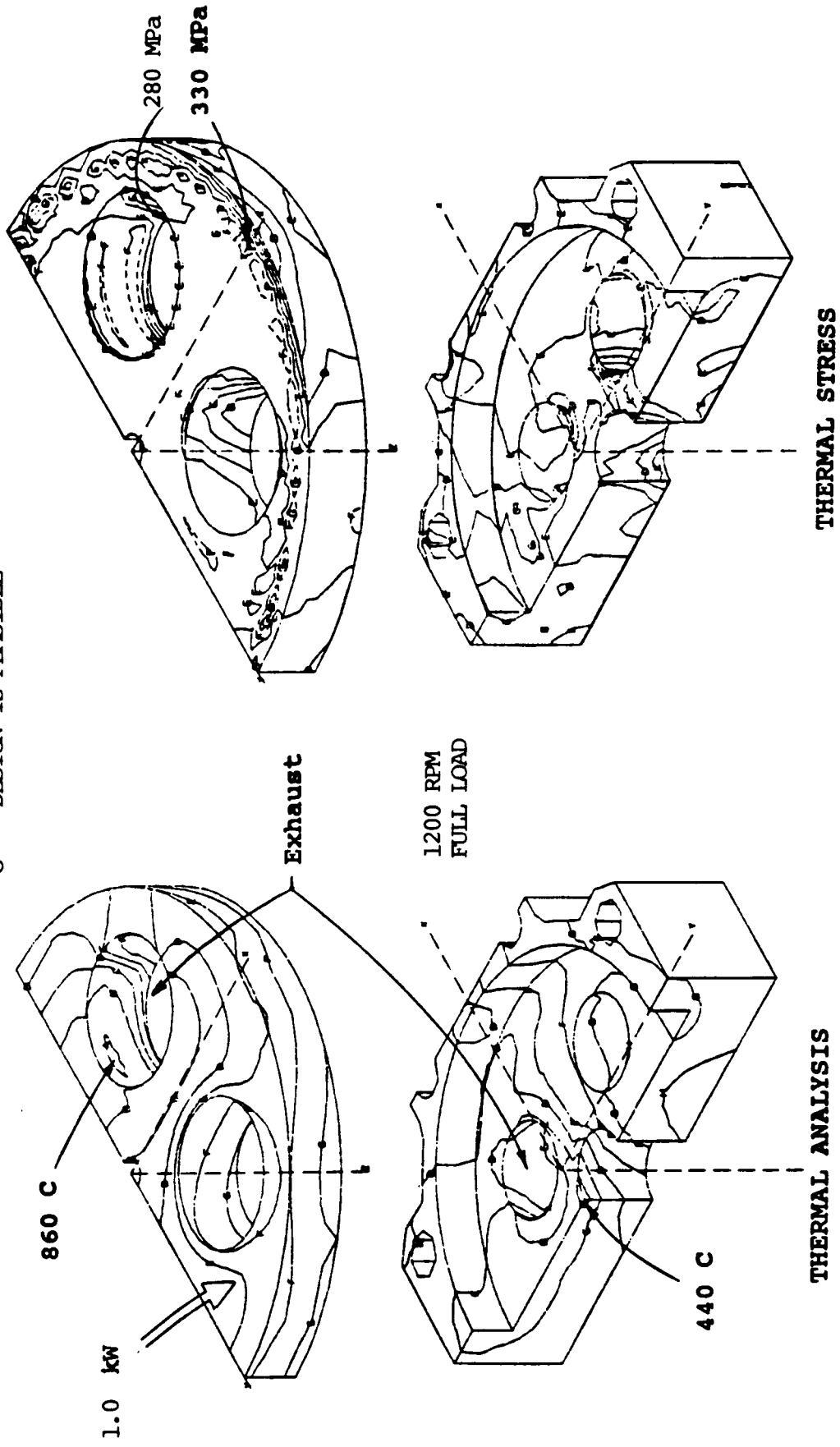


Figure III.9-4: Sample Cylinder Head and Firedeck Analysis

Figure III.9-5: Finite Element Model for the Gasketless Seal Study

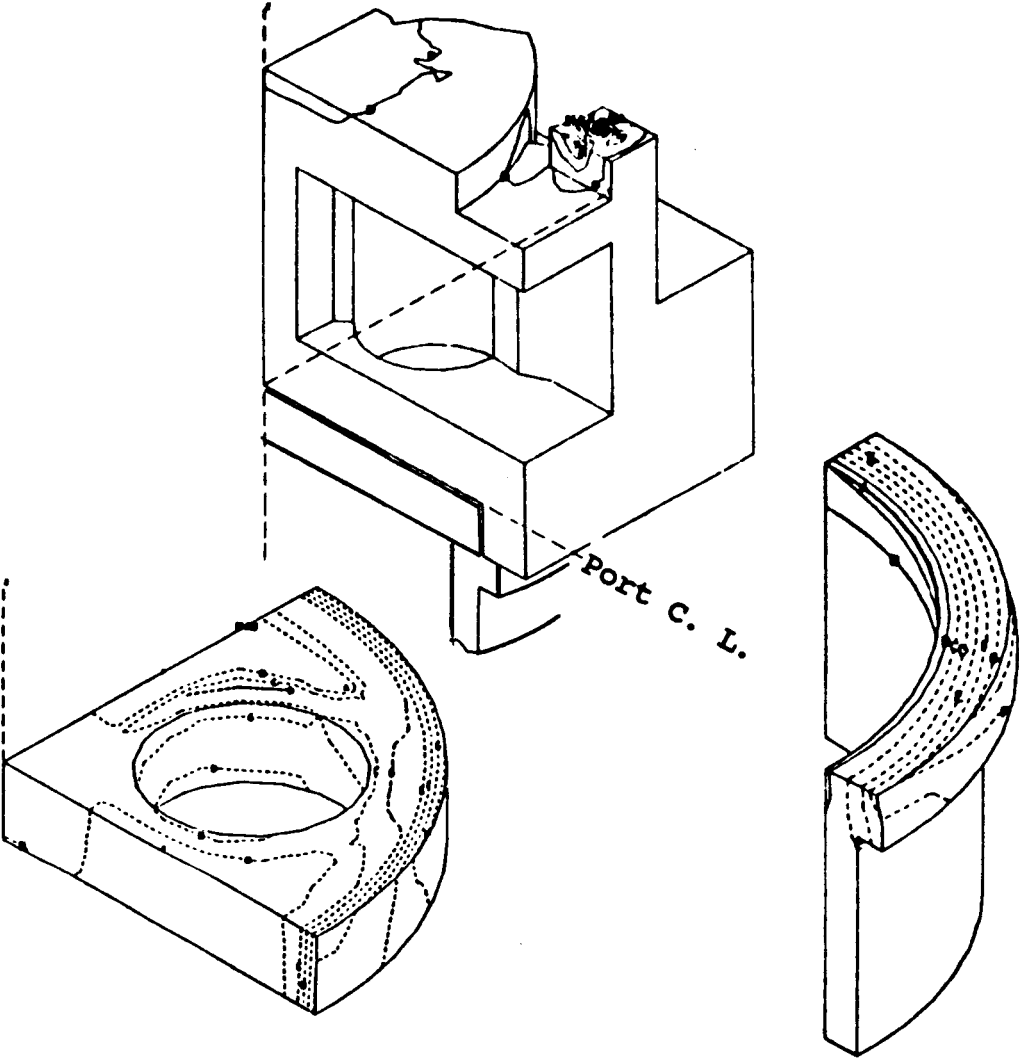
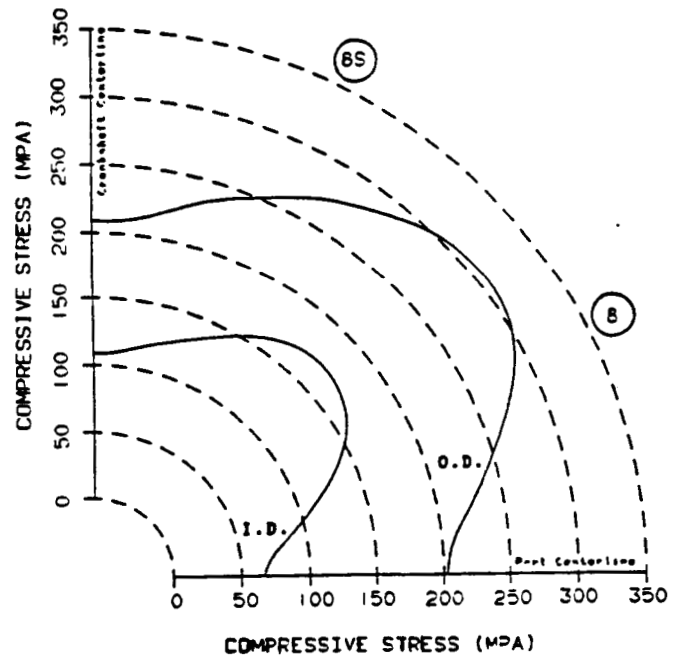
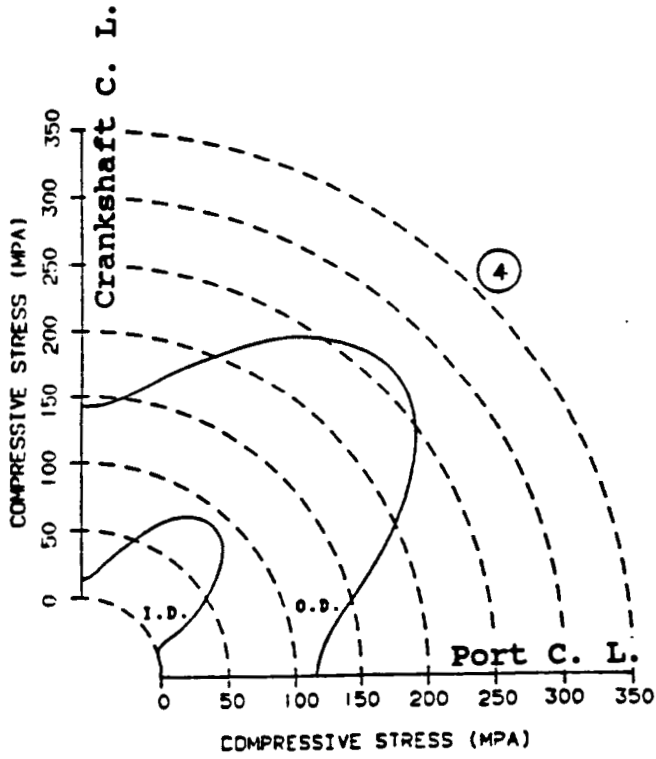


Figure III.9-6: Typical Gasketless Seal Joint Pressure Distribution, for Both the 4-Bolt and the 8-Bolt Patterns



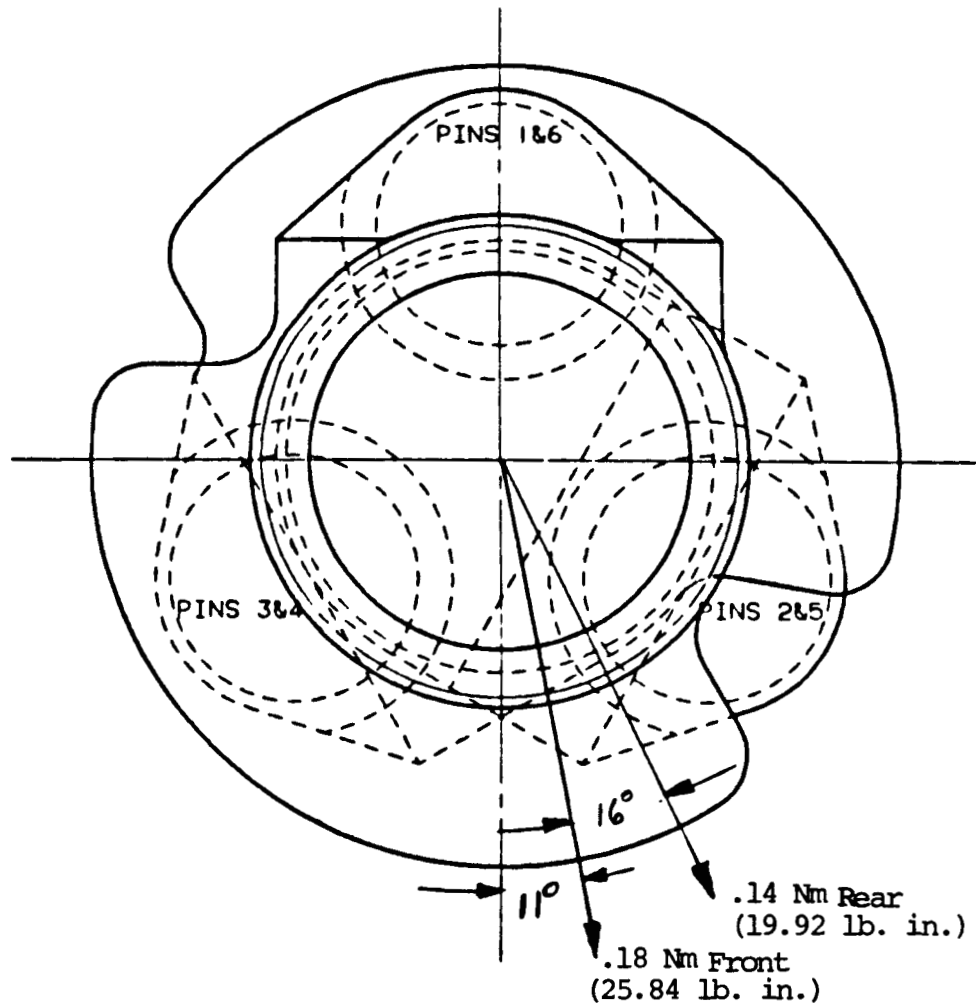
III.9.3 CRANKSHAFT RELATED ANALYSIS

Classical crankshaft analyses were performed, including crankshaft bending stress, crankshaft balance, and torsional vibration. Further, finite element analysis of the main bearing cap and joint was undertaken. The methodology used is a standard procedure and, hence, no discussion will be presented for this section.

CONCLUSIONS

1. A crankshaft bending stress safety factor of 2.30 was computed at the rated speed. Also, a safety factor of 2.08 was computed at the peak torque point. These values are within the acceptable practical range, although efforts to increase them are warranted for a production feasible engine.
2. Studies of balancing requirements at rated speed determined the backbreaking and the counteracting moment resulting from the counterweights. The balancing recommendations will result in a sound design, with the remaining unbalance shown in Figure III.9-7.
3. The torsional vibration analysis determined the critical speeds, stresses, and amplitudes. The inclusion of a commercial engine (12.34 inch) viscous vibration damper is sufficient to bring the vibratory stresses below the acceptable practical limits. The need for a damper could possibly be eliminated if the stiffness of the crankshaft is increased to allow the first mode natural frequency to be above the critical limit.
4. The main bearing cap structural integrity and joint deflection are acceptable.

Figure III.9-7: Remaining Unbalance of the ADRE Crankshaft



REAR END VIEW

IV

PLANNED FUTURE WORK

With the selection, analysis and design of the Reference Engine, the Program moves on to the next Phase. The objectives of this next phase are to examine the proof of concept of the advanced reciprocator components and systems through bench type tests and SCE tests. In this section, an overview of the technical strategy and a brief description of the intended work are offered.

The specific technical approaches and salient features of various activities will be defined early on during the follow-up phase. Because this is a research program, the results of a systematic investigation of an advanced concept can be successful demonstrations of advanced hardware and systems; or the effort can end by identifying the problem areas and where follow-up activities should be directed to enable future demonstration of the feasibility of concept.

If achievable, and within the available program resources, the end product aims at:

- a) Characterization of the proposed advanced concepts, with examination of their feasibility as a minimum. Currently, these concepts include:
 - 1) High Temperature Lubricants
 - 2) Lubricant Delivery Systems
 - 3) Flexible (Variable) Valve Timing
 - 4) Monolithic Ceramic LHR Components
 - 5) Gasketless Seal

- 6) Cast in Place (Ceramic) Ports
- b) Running integrated hardware in an uncooled single-cylinder engine to:
 - 1) Demonstrate the feasibility of the ADRE reciprocator concepts.
 - 2) Run performance/emission hooks.
 - 3) Generate limited pertinent boundary data and integrated systems' interactions in LHR real life environments.

Eight major activities in the areas of low heat rejection and synergistic technologies have been identified to address the next phase objectives of the Program:

- 1) Tribology
- 2) Power Assembly Components
- 3) Cylinder Head
- 4) Valve Components
- 5) Valve Actuation
- 6) Injection System
- 7) Single-Cylinder Test Bed
- 8) Performance Analysis

Tribology activities will include investigation of lubricants and lubrication systems. Both solid film and vapor phase lubrication concepts will be pursued. Cylinder kit is the major area of concern relative to tribology issues.

Power Assembly Components will feature a new piston concept that separates the hot section from the cooler engine crankcase area. This design allows demonstration of the advanced hot section tribology concepts (upper cylinder only) in a single-cylinder engine with a conventionally lubricated lower block.

Cylinder Head will have a ceramic firedeck, with gasketless combustion gas seal. Cast in place ceramic port shields will be pursued, with metal shields as a fallback option. The head will be designed for nonmechanical overhead including electronically controlled common rail injection and hydraulic valve actuation.

Valve Components will consist of ceramic valves and guides. Other valve components include conventional valve spring, spring cap, lock and seat, and a specially designed valve bridge.

Injector and Valve Actuation will utilize the fuel as the working fluid. Injection system will be a common rail type, requiring a new injector and a new remote injection pump delivering 138 MPa rail pressure. This injection pump can be driven directly by the single-cylinder test bed crankshaft, or motor driven on an independent stand. The valve actuation system will most likely be separate from the injection system, requiring 13.8 MPa nominal pressure.

Single-Cylinder Test Engine will have a conventional liquid sump, will be uncooled, and features the following: monolithic ceramic insulation, electronic controls and a hydraulically actuated overhead. Fallback scenarios to this extremely advanced package will be proposed, if necessary. Test bed electronic control will manage the injection and valve actuation systems. It

is not intended to design and deliver a package for multi-cylinder control, but rather to control the single-cylinder demonstration test bed in the most feasible and economic way.

Performance Analysis support will include prediction and limited experimental validation of the optimized, emission limited engine map. Additional mechanical analysis support will include thermal, structural, probability of survival, fluid network, systems dynamics and other simulations, as necessary.

APPENDIX A: SKF SUBCONTRACT FINAL REPORT

SKF TRIBONETICS

ADIABATIC DIESEL ENGINE COMPONENT
DEVELOPMENT PROGRAM

PHASE I - FINAL REPORT

R. A. PALLINI

AUGUST 1986

SKF REPORT NO. AT86D008

PREPARED FOR:

DETROIT DIESEL ALLISON
DIVISION OF GENERAL MOTORS
36880 ECORSE ROAD
ROMULUS, MI 48174

TABLE OF CONTENTS

	<u>PAGE</u>
1.0 INTRODUCTION.....	1
2.0 SUMMARY AND RECOMMENDATIONS.....	3
3.0 INITIAL BEARING DESIGN STUDIES.....	4
3.1 Initial Reference Engine Operating Environment..	4
3.2 Bearing Concept Designs.....	6
3.3 Preliminary Lubrication Analysis.....	14
3.4 Life Cycle Cost Elements.....	22
4.0 REFERENCE ENGINE BEARING BASELINE DESIGN ANALYSIS....	25
4.1 Bearing Design Sizing and Load.....	25
4.2 Baseline Design Analyses.....	25
4.3 Material Design Considerations.....	27
4.4 Solid Lubrication Design Considerations.....	34
4.5 Misalignment Effects.....	37
5.0 REFERENCE ENGINE BEARING DRAWINGS.....	38
5.1 Crankshaft Main Bearing.....	38
5.2 Connecting Rod, Wristpin and Thrust Bearings....	38
5.3 Sealing Concepts.....	38
6.0 REFERENCES.....	49

LIST OF FIGURES

<u>FIGURE NO.</u>		<u>PAGE</u>
3-1	ADE BEARING LOADS AS A FUNCTION OF CRANK ANGLE	5
3-2	CONNECTING ROD BEARING CAPACITY OPTIMIZATION CURVES (NO INNER RING)	8
3-3	CONNECTING ROD BEARING CAPACITY OPTIMIZATION CURVES (WITH INNER RING)	9
3-4	MAIN BEARING CAPACITY OPTIMIZATION CURVES (NO INNER RING)	10
3-5	MAIN BEARING CAPACITY OPTIMIZATION CURVES (WITH INNER RING)	11
3-6	SELECTED LUBRICANT VISCOSITY DATA	18
3-7	LIFE CORRECTION FACTOR FOR LUBRICANT FILM EFFECTS	21
3-8	MAIN BEARING OUTLINE DRAWING FOR LIFE CYCLE COST ANALYSIS	23
3-9	CONNECTING ROD BEARING OUTLINE DRAWING FOR LIFE CYCLE COST ANALYSIS	24
4-1	ROLLER STRESS PROFILE FOR MAIN BEARING ROLLER (CYLINDRICAL LENGTH = 12mm)	28
4-2	ROLLER STRESS PROFILE FOR MAIN BEARING ROLLER (CYLINDRICAL LENGTH = 14mm)	29
4-3	ROLLER STRESS PROFILE FOR MAIN BEARING ROLLER (CYLINDRICAL LENGTH = 16mm)	30
5-1	DRAWING LC320-01 MAIN BEARING CUSTOMER DRAWING	40
5-2	DRAWING LC320-01 MAIN BEARING ASSEMBLY DRAWING	41
5-3	DRAWING LC320-01 MAIN BEARING OUTER RING	42
5-4	DRAWING LC320-01 MAIN BEARING ROLLER	43
5-5	DRAWING LC320-01 MAIN BEARING CAGE	44

LIST OF FIGURES (CONTD)

<u>FIGURE NO.</u>		<u>PAGE</u>
5-6	DRAWING LC320-02 CONNECTING ROD BEARING CUSTOMER DRAWING	45
5-7	DRAWING LC320-02 CONNECTING ROD BEARING ROLLER	46
5-8	DRAWING LC320-03 WRISTPIN BEARING CUSTOMER DRAWING	47
5-9	DRAWING LC320-03 WRISTPIN BEARING ROLLER	48

LIST OF TABLES

<u>TABLE NO.</u>		<u>PAGE</u>
3-1	PRELIMINARY ROLLER BEARING GEOMETRIES	12
3-2	SUMMARY OF INITIAL COMPUTER ANALYSES	13
3-3	PRELIMINARY HEAT GENERATION AND LUBRICANT FILM RESULTS	15
3-4	SELECTED LUBRICANTS AND THEIR PROPERTIES	17
3-5	CONNECTING ROD BEARING CONCEPT DESIGN - LUBRICATION STUDY RESULTS	19
3-6	MAIN BEARING CONCEPT DESIGN - LUBRICATION STUDY RESULTS	20
4-1	ADRE BASELINE BEARING DESIGNS ANALYSIS RESULTS	26

1.0 INTRODUCTION

In the recent past, a number of industry and government programs have been sponsored on the development of adiabatic diesel engine (ADE) concepts. These have included paper studies, as well as, the development of prototype engines, both multicylinder and single cylinder. One of the underlying principals on which the concept of the ADE rests, is that of minimum friction components. This requisite, coupled with the severe operating environment created by the ADE, yields performance demands that approach the limitations of conventional bearings, materials, and lubricants. The results of the early research studies bear witness to this fact.

The U.S. Department of Energy (DOE) in conjunction with the National Aeronautical and Space Administration (NASA) initiated a program in 1981 for the development of technologies applicable to advanced low heat rejection or adiabatic diesel engines. The Heavy Duty Transport Technology Program (HDTT) has the following stated goal [1]:

"To provide the necessary technology base for use by industry in developing advanced heavy duty transport engines to permit a significant reduction of petroleum consumption per vehicle ton-mile."

Four key technology sub-categories were formed:

- (1) component development
- (2) emissions and combustion
- (3) exhaust heat utilization
- (4) engine systems

The latter of these is an all encompassing comprehensive program containing all the technologies needed for a complete ADE package. The Adiabatic Diesel Engine Component Development (ADECD) Program is a multiphase effort to develop and demonstrate the critical technology needed to advance the heavy duty adiabatic diesel engine concept for the line-haul truck market [2]. The main objective of Phase I of the ADECD program is to select an advanced low heat rejection, Adiabatic Diesel Reference Engine (ADRE), through the evaluation of the current state-of-the-art [2]. The ADECD program is being conducted by Detroit Diesel Allison (DDA), Division of General Motors under DOE/NASA Contract DEN3-329.

SKF Industries, Inc. (SKF) has been serving as a subcontractor to DDA under DDA Contract DE0786367 for support during Phase I activity. SKF Phase I work efforts consisted of three tasks aimed at lubrication and life prediction studies necessary for the development of:

- (1) Concept-level specifications and performance characteristics for connecting rod lower end, wristpin, and thrust bearings.

- (2) Detailed specifications and performance characteristics for main bearings.

This report presents the work accomplished by SKF during Phase I of the ADECD program. Baseline designs have been achieved for the main, connecting rod, wristpin, and thrust bearings. Material and lubrication guidelines for successful application of these bearings to the ADRE have been established and suitable layout drawings for all four baseline designs have been constructed. Recommendations for future efforts to insure a successful and reliable application are also presented herein.

2.0 SUMMARY AND RECOMMENDATIONS

Roller bearing designs for the main, connecting rod, wristpin and thrust bearing locations of the Adiabatic Diesel Reference Engine (ADRE) have been conceptualized and analyzed. A primary lubrication scheme has also been conceptualized. The designs as presented in this report should be treated as preliminary. The preliminary analysis as presented herein, demonstrates that the conceptual designs and lubrication scheme are capable of achieving satisfactory operation within the ADRE operating environment.

The desired design goal of 5,000 hours fatigue life can be achieved with the proper attention taken in the selection and processing of the materials to be used for these ADRE components. Section 4.3 of this report elaborates upon material design considerations which are imperative to successfully achieving the 5,000 hour goal. The material for the outer rings and rollers of the main and connecting rod bearings, and the rollers of the wristpin bearing is specified as consumable vacuum melted AISI 52100 bearing steel in accordance with ASTM A-535. This will insure that these components will be capable of achieving the necessary life improvements needed to reach 5,000 hours operation.

The anticipated crankshaft material of SAE 1548 or SAE 1046 if ordered/procured from vacuum melted or consumable electrode melted stock should be of bearing quality. If the journal areas are induction hardened to the maximum attainable depths and surface hardness, it is anticipated that the design goals of the ADE bearings will be achievable. To enhance the reliability of these bearings, SKF strongly recommends hard coating of the journal surfaces via the Armoloy hard coat chrome process. Piston pin material (SAE 8620) and heat treatment is in accordance with high quality bearing practice and is satisfactory.

The piston wristpin bearing outer raceway surface presents some concern. There does not appear to be any technical reason why the AISI 1141 material (if processed with standard bearing practice) should not provide the required performance. However, in view of the fact that there is the lack of an experience base on the use of this material in conjunction with roller bearings, some minor testing in future phases of the ADECD program may be warranted.

SKF recommends that Phase II of the program be structured so as to include efforts to further refine the design of roller bearings and to allow for low level proof-of-concept testing. Bench testing with actual crankshaft materials and ADRE radial loadings can provide data that will allow design refinements that will assure long-term reliable performance.

3.0 INITIAL BEARING DESIGN STUDIES

The DDA Series 60 engine was selected as the reference design for ADE initial bearing design studies. Reference engine design parameters were established and bearing loadings were computed by DDA and submitted to SKF for initial bearing sizing. The computed bearing loads (as a function of crank angle) was supplied by DDA.

3.1 Initial Reference Engine Operating Environment

The initial reference engine design parameters were given as follows:

Nominal Rated Output, HP	300
Nominal Rated Speed, RPM	2000
Brake Mean Effective Pressure, PSIA	225-250
Peak Firing Pressure, PSIA	2000-2400
Specific Power, HP/Cu-In	.5 - .55
Engine Thermal Loading, HP/Sq-In	2.5 - 3.3
Likely Wet Sump	

Each of the six (6) cylinders consisted of a 130mm (5.118 in) diameter piston with a peak firing pressure as stated above and a stroke of 139mm (5.472 in). The nominal rated rotational speed was 209 radians/sec (2000 rpm).

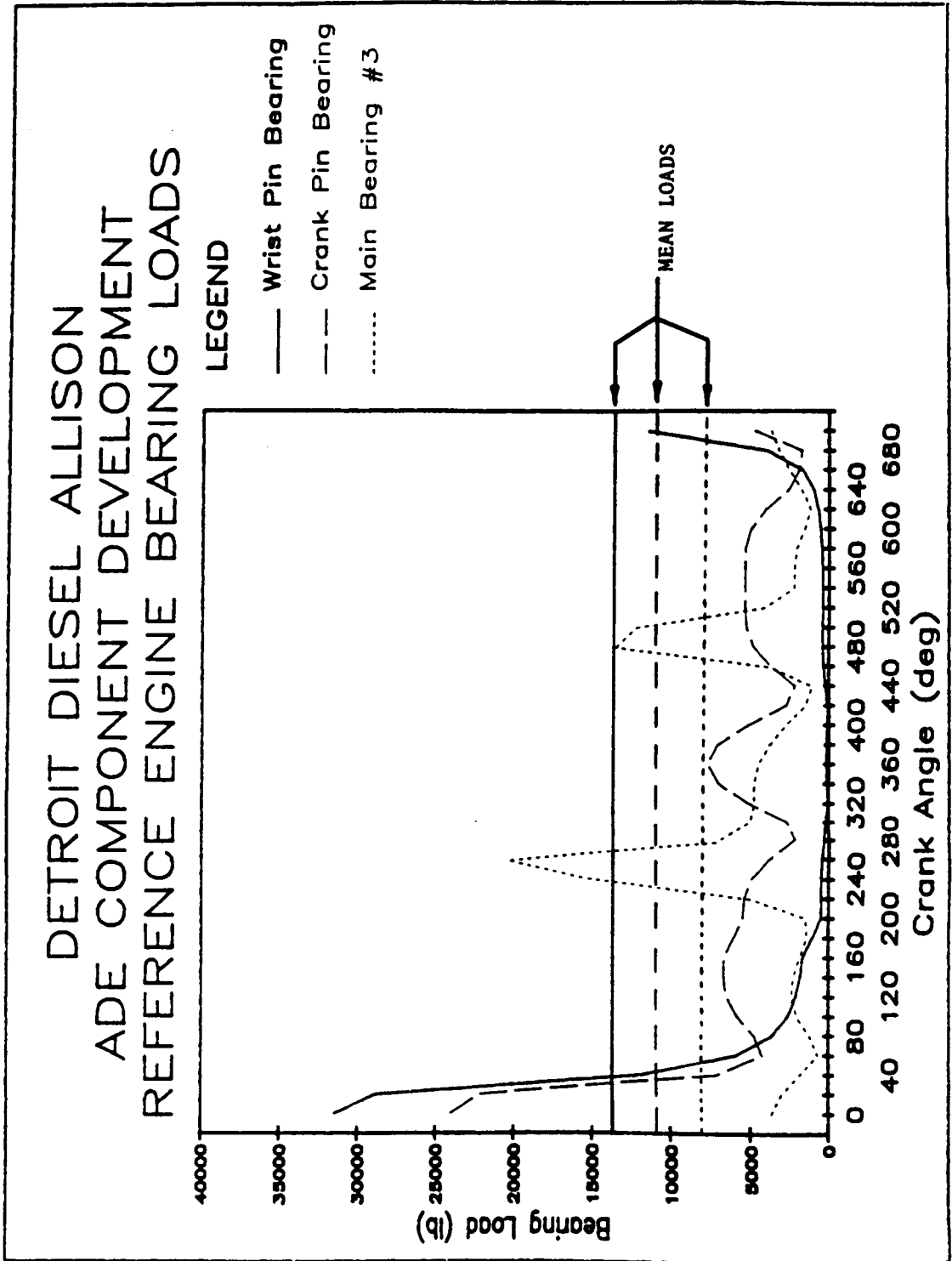
The initial design studies were conducted with the assumption that crankcase temperatures would be in the 93°C to 121°C (200°F to 250°F) range and therefore a conventional wet sump design could be used. The initial design goal for the bearings was 5,000 hours of trouble-free operation at full rated power.

The computer calculated tabulation of expected bearing loads was used to compute a mean load that would be used to select applicable bearing sizes. Fig. 3-1 is a computer generated plot of the load data; plotted as a function of 2 revolutions of the crank are the wristpin bearing load, the connecting rod bearing load, and the most arduous main bearing load (Main Bearing #3). The straight line values represent the computed 10/3 rds power mean effective load. These loads are as follows:

Wristpin Bearing	= 62,272N (14,000 lb)
Connecting Rod Bearing	= 48,888N (10,990 lb)
Main Bearing #3	= 35,584N (8,000 lb)

These loads represent the mean operating loads at full rated power. Bearing sizing was conducted to achieve desired life when operating at these mean load levels.

FIGURE 3-1 ADE BEARING LOADS AS A FUNCTION OF CRANK ANGLE



3.2 Bearing Concept Designs

The expected standard fatigue life of a roller bearing with a 90% chance of survivability is given by

$$B_{10} = L_{10} \bullet 10^6 / 60 \bullet \text{RPM}$$

where

B_{10} = fatigue life in hours
 L_{10} = computed fatigue life in millions of revolutions
RPM = speed of rotation in revolutions per minute

The life of the bearing in revolution, L_{10} , is computed using the Lundberg and Palmgren method [3] and is given by

$$L_{10} = (C/P)^{10/3}$$

where

C = basic dynamic load capacity (N)
 P = dynamic mean effective load (N)

The Lundberg-Palmgren [3] predicted fatigue life of roller bearings is based on theoretical and empirical factors based on 1950's technology. Newer materials and processing techniques now provide the means for improving bearing life. A study conducted by SKF for the U.S. Army [4] showed that life increases of 6 to 10 times were obtained by the use of Vacuum Induction Melted-Vacuum Arc Remelted (VIMVAR) M50 tool steel in well-lubricated bearing tests.

For the purposed of initial design studies, it was assumed that optimum material and lubrication conditions would exist. Therefore, a life multiplier of 5 was assumed for bearing concept design selection. This value is conservative, but was thought sufficient for preliminary design studies.

Using the equations for capacity and life just presented, and substituting in the established life goal (5,000 hours) and multiplier, minimum bearing dynamic capacities were computed for the connecting rod and main bearings as follows:

Connecting Rod Bearing	$C_{\min} = 205,000\text{N}$
Main Bearing	$C_{\min} = 150,000\text{N}$

The dynamic capacity of a roller bearing is computed by:

$$C = f_c (i \ell_{\text{eff}} \cos \alpha)^{7/9} z^{3/4} D^{29/27} \quad [5]$$

where

f_c = a material and rolling element geometry factor
 i = number of element rows
 ℓ_{eff} = effective length of the roller
 α = bearing contact angle
 z = number of rollers
 D = roller diameter

Utilizing this computation capacity, curves were constructed for several design arrangements for the connecting rod and main bearing. The design variations were as follows:

- Design #1 - single row of elements with no inner ring
- Design #2 - single row of elements with inner ring
- Design #3 - double row of elements with no inner ring
- Design #4 - double row of elements with inner ring

These capacity curves are presented in Figs. 3-2 through 3-5. Figs. 3-2 and 3-3 are for the connecting rod bearing. A journal diameter (as supplied by DDA) of 85mm (3.35 in) was assumed. The curves present the capacity for a range of roller diameters for three values of roller length to diameter ratio. A bearing cage web thickness of 3.125mm (.123 in) was assumed. Fig. 3-2 illustrates the results for a bearing design that would operate without an inner ring. That is, the rolling elements would roll directly on the crankshaft surface. Fig. 3-3 illustrates the resulting capacity if an inner ring were present. Figs. 3-4 and 3-5 present the same information for the main bearing location in which case the journal diameter was supplied to be 125mm (4.92 in).

Utilizing the data contained in these curves and the minimum capacities as above roller complement geometries were established for each of the four design variations. These are summarized in Table 3-1.

A preliminary computer analysis was conducted on each selected design to establish roller loading and contact stress levels. These results are presented in Table 3-2.

Each of the four design concepts were further evaluated for frictional losses to aid in the selection of a particular design. For the purpose of formulating preliminary friction losses, an SAE 15W-40 lubricant was selected. This oil represents the DDA standard diesel engine oil. SKF computer code SHABERTH (SHaft BEaring Thermal) was used assuming an ambient bearing and oil temperature of 121°C (250°F). The results are summarized in Table 3-3.

Based on the frictional loss values of Table 3-3 and the life values of Table 3-2, preliminary concept selections were made for the connecting rod and main bearing locations. These are as follows:

FIGURE 3-2 CONNECTING ROD BEARING CAPACITY
OPTIMIZATION CURVES (NO INNER RING)

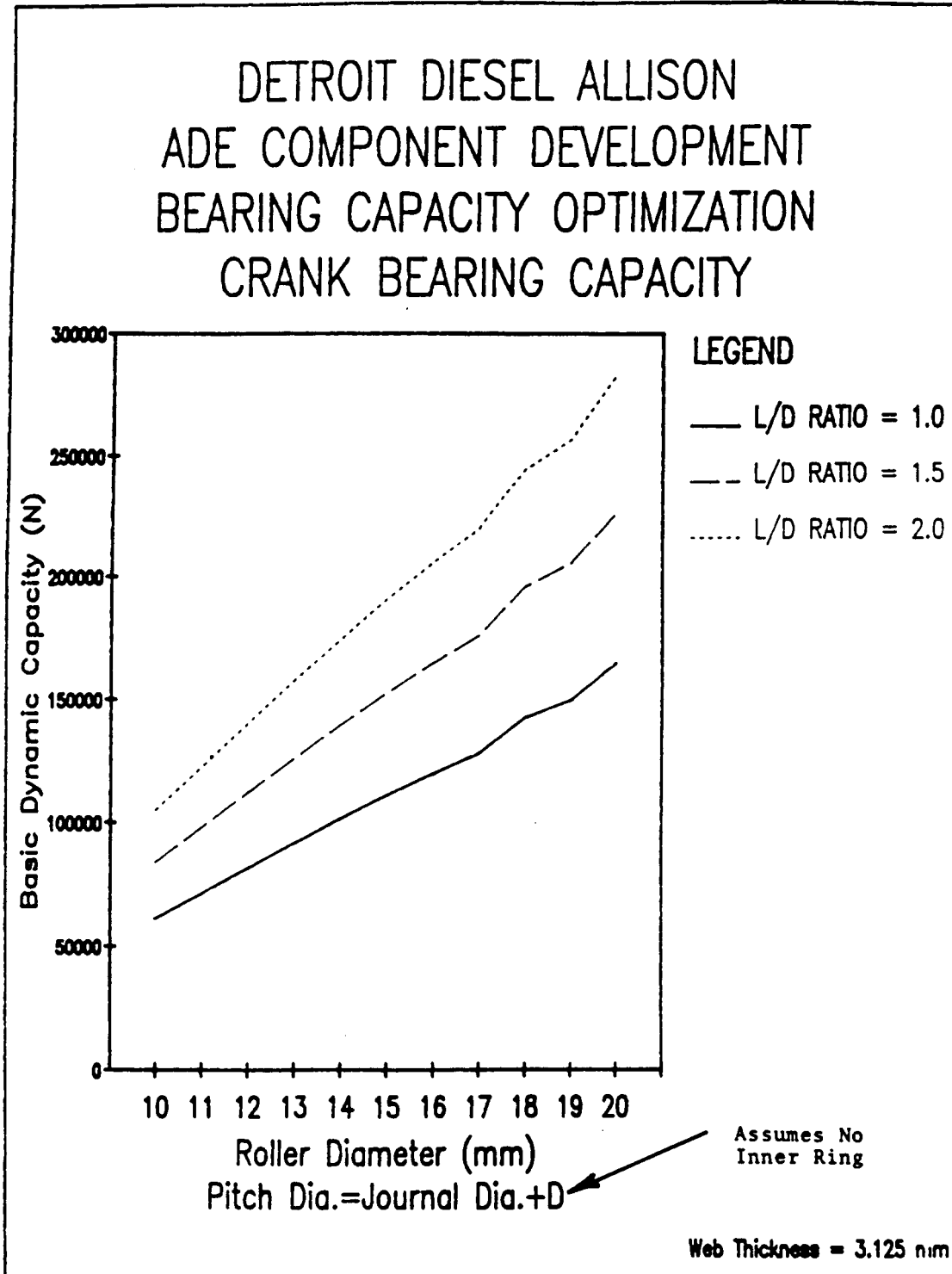


FIGURE 3-3 CONNECTING ROD BEARING CAPACITY OPTIMIZATION CURVES (WITH INNER RING)

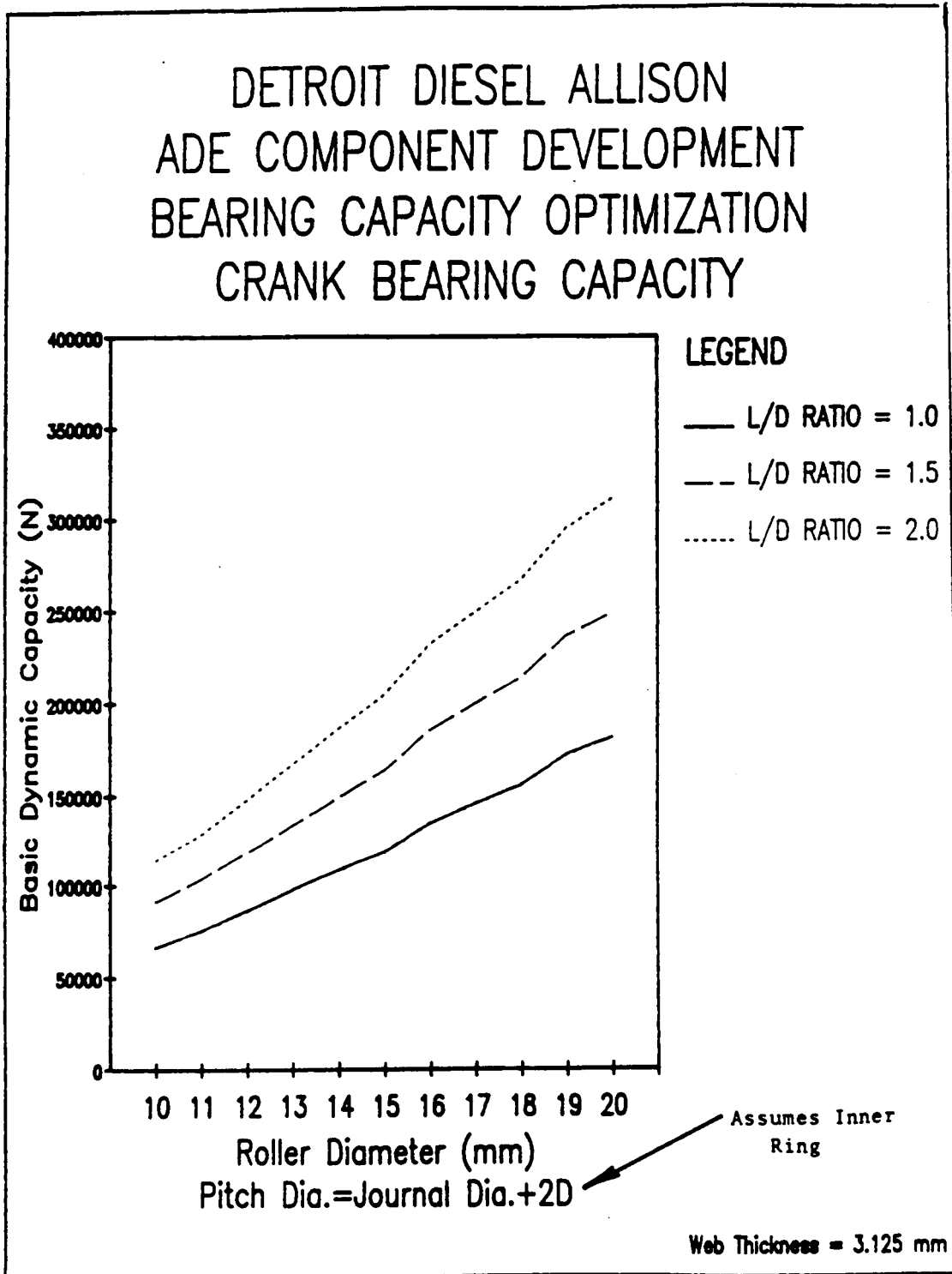


FIGURE 3-4 MAIN BEARING CAPACITY OPTIMIZATION CURVES (NO INNER RING)

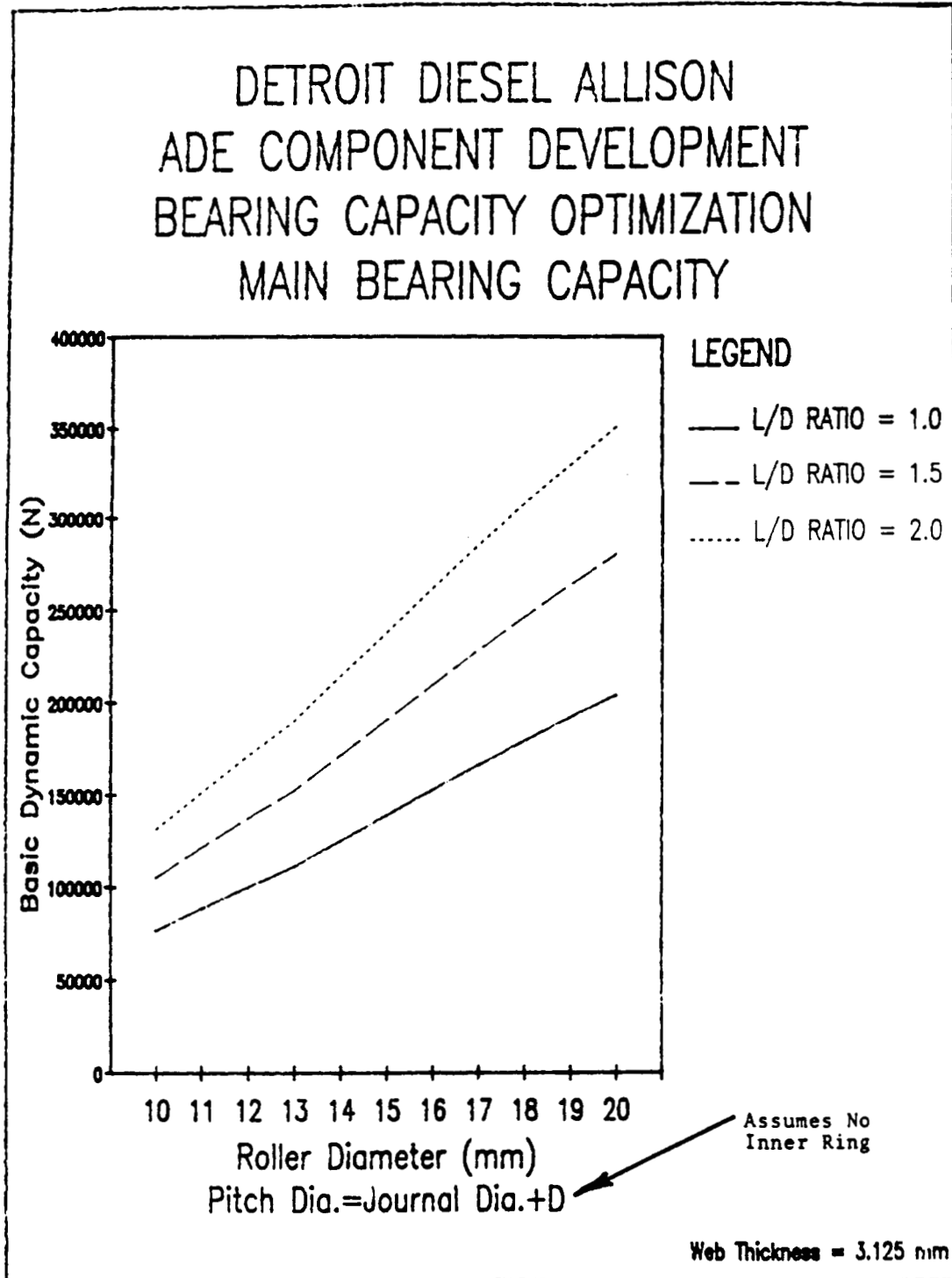


FIGURE 3-5 MAIN BEARING CAPACITY OPTIMIZATION CURVES (WITH INNER RING)

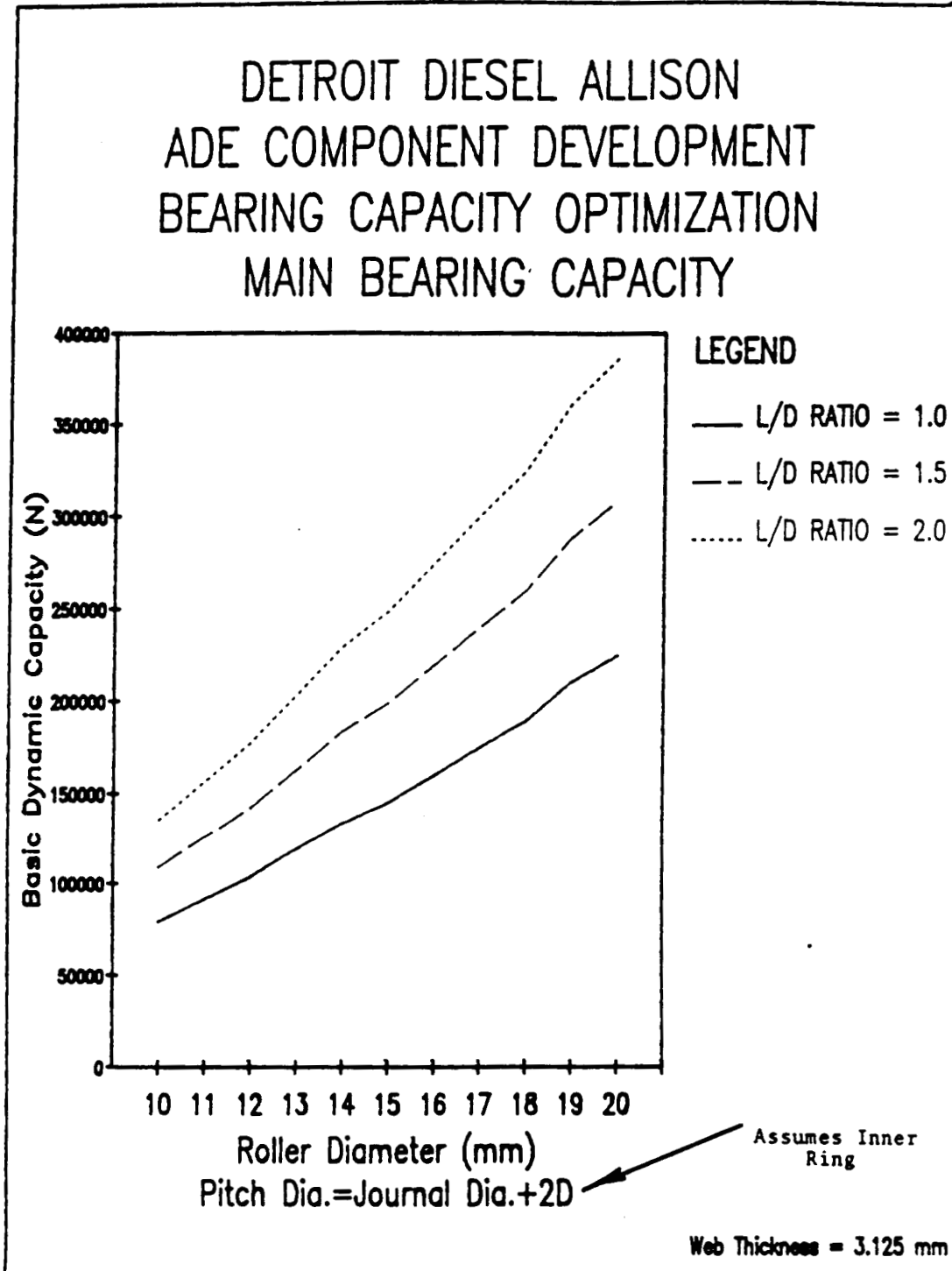


TABLE 3-1

PRELIMINARY ROLLER BEARING GEOMETRIES

	CRANK BEARING	MAIN BEARING
DESIGN #1 No Inner Ring Single Row	Roller Size: 16 x 32 Pitch Dia: 101 No. Rollers: 16 Shaft/Bore: 85 Outside Dia: 133 Width: 44	11 x 22 136 30 125 158 40
DESIGN #2 Inner Ring Single Row	Roller Size: 15 x 30 Pitch Dia: 117 No. Rollers: 19 Shaft/Bore: 85 Outside Dia: 147 Width: 44	11 x 22 147 32 125 169 40
DESIGN #3 No Inner Ring 2-Row	Roller Size: 16 x 16 Pitch Dia: 101 No. Rollers: 16/Row Shaft/Bore: 85 Outside Dia: 133 Width: 44	10 x 15 135 32/Row 125 155 40
DESIGN #4 Inner Ring 2-Row	Roller Size: 16 x 16 Pitch Dia: 117 No. Rollers: 19/Row Shaft/Bore: 85 Outside Dia: 149 Width: 44	9 x 13 143 37/Row 125 161 40

All Dimensions in mm.

TABLE 3-2

SUMMARY OF INITIAL COMPUTER ANALYSES

	CRANK BEARING DESIGNS			
	DESIGN 1	DESIGN 2	DESIGN 3	DESIGN 4
FATIGUE LIFE (HRS)	5,042	4,946	5,167	7,666
MAXIMUM ROLLER LOAD (N)	12,480	10,510	6,241	5,256
MAXIMUM CONTACT STRESS (N/mm ²)	1,446	1,390	1,446	1,310

	MAIN BEARING DESIGNS			
	DESIGN 1	DESIGN 2	DESIGN 3	DESIGN 4
FATIGUE LIFE (HRS)	5,229	5,875	8,750	5,083
MAXIMUM ROLLER LOAD (N)	48,460	45,430	2,271	1,964
MAXIMUM CONTACT STRESS (N/mm ²)	1,254	1,210	1,086	1,137

Design Parameter	Connecting Rod	
	Bearing	Main Bearing
Shaft/Bore Dia. (mm)	85	125
Outside Dia. (mm)	107	158
Width (mm)	44	40
Roller Dia. (mm)	11	11
Roller Length (mm)	17	22
Pitch Dia. (mm)	96	136
No. of Rollers	21/Row	30
Basic Dynamic Capacity (N)	174,044	154,878
Remarks	2 Row/No Inner	Single Row/No Inner

The film thicknesses as reported in Table 3-3 are relatively low and indicated the need for further study of the lubrication type and method. This is the subject of the next section of the report.

3.3 Preliminary Lubrication Analysis

Lubricant films such as recorded in Table 3-3 would place the bearings in an operating regime where penalties on fatigue life would occur. The basic form of the film thickness equation is as follows:

$$h_{\min}/R_x = 3.07 U^{0.71} G^{0.51} W^{-0.11}$$

where $U \equiv$ dimensionless speed parameter = $\mu_0 u/E'R_x$

$G \equiv$ dimensionless materials parameter = $\alpha E'$

$W \equiv$ dimensionless load parameter = F/ER_x^2

$R_x =$ effective radius

with $\mu_0 =$ lubricant viscosity

$u =$ entrainment velocity

$\alpha =$ lubricant pressure-viscosity coefficient

$E' =$ modified elastic modulus

$F =$ roller normal load

Given these components of the film thickness formula, we see that in practical terms, the only parameters at our disposal to change are those dealing with the lubricant properties. That is, the operating viscosity and the pressure-viscosity coefficient, with viscosity providing a more dominant effect.

Based on this fact, seven (7) different lubricants (including 3 greases) were selected for analysis in addition to the 15W-40 engine oil. They were selected on the basis of having the general properties desirable for use in a diesel engine environment while exhibiting high viscosity at the expected bearing operating temperature. The 8 lubricants are as follows:

1. 15W-40 Oil per MIL-L-2104
2. Stauffer Chemical SDL-1 Oil

TABLE 3-3
PRELIMINARY HEAT GENERATION AND LUBRICANT FILM RESULTS

	Connecting Rod Bearing Designs				Main Bearing Designs			
	1	2	3	4	1	2	3	4
Frictional Heat Generation Rates (Watts)	276	413	320	492	583	694	786	864
Friction Torque (N-mm)	1317	1970	1526	2350	2781	3314	3758	4126
Minimum Film Thickness (Microns)	0.14	0.16	0.14	0.16	0.17	0.18	0.17	0.17

3. Mobil Delvac 1340 Oil
4. Mobil SHC629 Oil
5. Texaco Ursa 50 Oil
6. Mobil Grease 28
7. Aeroshell #5 Grease
8. Texaco Marfac #2 Grease

Table 3-4 presents a table of the basic properties for each lubricant. Fig. 3-6 presents the viscosity-temperature curve for each. In the case of the greases, the curve represents the viscosity of the base oil.

A computer analysis using SKF computer code SHABERTH was conducted for the connecting rod bearing concept design and the main bearing concept design. The results of the computer study are summarized in Tables 3-5 and 3-6.

The changes in bearing heat generation are due to the lubricant viscous effects on bearing torque. This effect is independent of load, thus showing an increase in generated heat with an increase in lubricant viscosity.

To gage the effect of lubricant film thickness on bearing performance, i.e. fatigue life, a film parameter, Λ , is utilized.

$$\Lambda = h_{min}/\sigma$$

where σ = composite rms surface roughness

Tables 3-5 and 3-6 list the calculated film parameter assuming standard rolling bearing finishes. In 1971 the ASME published a guideline for formulating a life correction factor as a function of this film parameter. Their curve was based on a compilation of published test results and is included as Fig. 3-7. From the curve it is evident that a film parameter of 1.5 or greater is needed to achieve a life factor greater than 1.0. The fatigue life values of Tables 3-5 and 3-6 have been adjusted to accommodate the factor. However, note that no adjustment has been made to these fatigue lives to account for material improvements. As discussed previously, this factor can be anywhere from 5 to 7, thus giving fatigue lives in line with the 5000 hour design goal.

Also given in the summary tables are the predicted magnitudes of bearing heat generation and bearing operating temperature. For the cases of oil lubrication, a nominal 2 liter/min (0.5 gal/min) flow per bearing was assumed and resulted in a maximum bearing operating temperature of 107°C (224°F). The 3 greases analyzed resulted in a maximum bearing operating temperature of 163°C (325°F). The greases selected are high temperature, high load capacity greases with useful temperature ranges approaching 177°C (350°F).

The bottom two rows of the summary tables predict the bearing fatigue life and heat generation assuming that the rolling elements are manufactured from bearing quality silicon nitride ceramic (Si₃N₄). Owing to its high modulus of elasticity, there is an expected reduction in predicted fatigue life. Predicted heat

TABLE 3-4 SELECTED LUBRICANTS AND THEIR PROPERTIES

LUBRICANT	BASE TYPE	KINEMATIC VISCOSITY		DENSITY @ 15.5°C (gm/cm ³)	PRESSURE VISC. COEFF. (m ² /N)	POUR POINT (°C)	VISCOSITY INDEX
		@ 38°C (cs)	@ 99°C (cs)				
15W-40 Oil	Mineral	103	14.2	0.9	0.013	-29	136
SDL-1	Polyol Ester	69.5	10.1	0.936	0.01	-34	140
Mobil Delvac 1340 Oil	Mineral	154	18.6	0.898	0.015	-15	96
Mobil SHOC 29 Oil	Synthetic Hydrocarbon	158.6	19.8	0.838	0.017	-54	153
Texaco URSA Ex Duty 50 Oil	Mineral	231	19.5	0.898	0.015	-15	96
Mobil Grease 28	Synthetic Hydrocarbon	158.6	19.8	0.838	0.017	-	-
Shell Aeroshell #5 Grease	Mineral	420	32.8	0.89	0.015	-	-
Texaco Marfac Heavy Duty #2 Grease	Mineral	305	18.5	0.9	0.015	-	-

ORIGINAL PAGE IS
OF POOR QUALITY

ASTM Viscosity-Temperature Chart - centistokes

FIGURE 3-6 SELECTED LUBRICANT VISCOSITY DATA

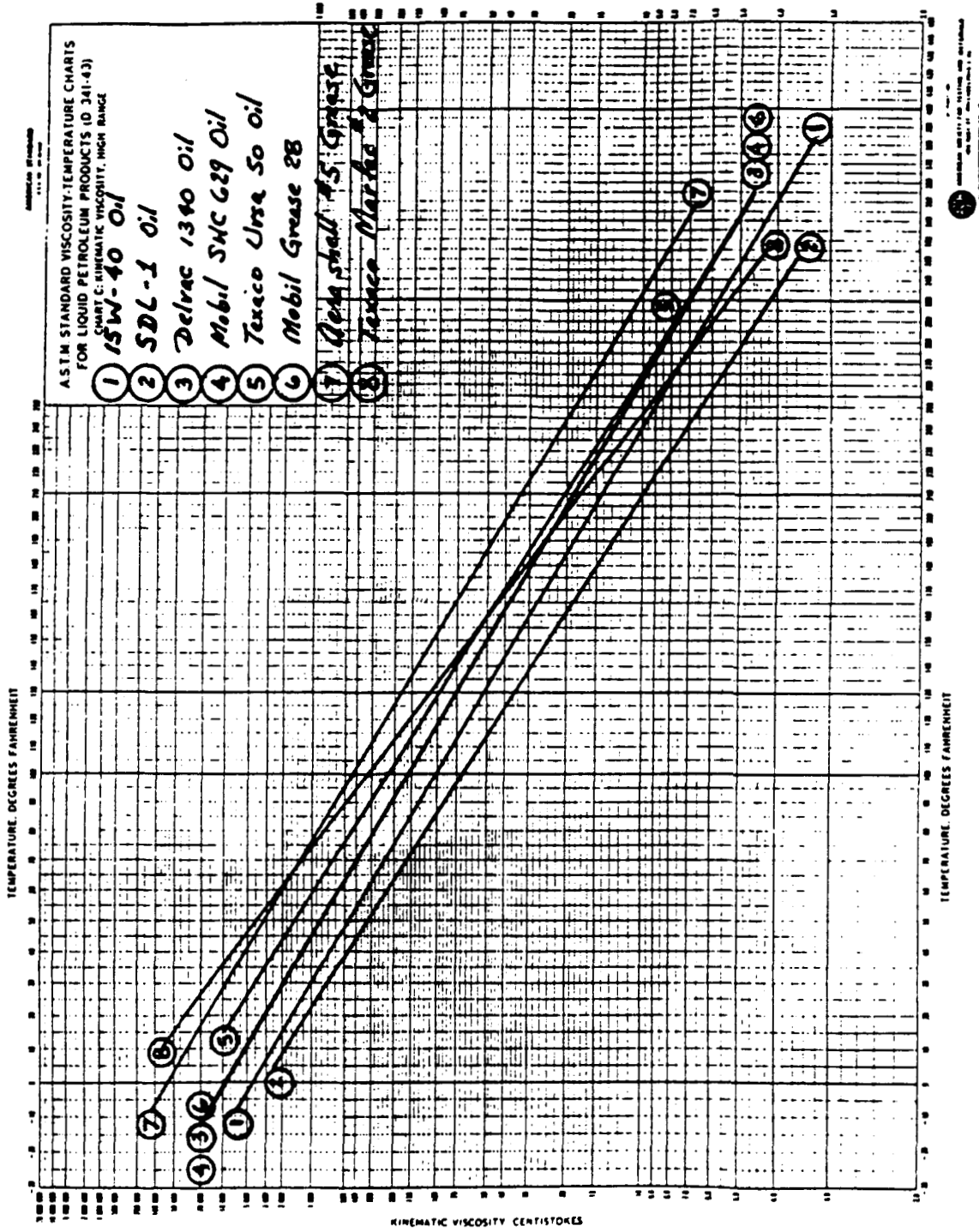


TABLE 3-5

CONNECTING ROD BEARING CONCEPT DESIGN

LUBRICATION STUDY RESULTS

	15W-40	STAUFFER SDL-1	MOBIL DELVAC 1340	MOBIL SHC 629	TEXACO URSA 50	MOBIL GREASE 28	AEROSHELL #5 GREASE	TEXACO MARFAC #2 GREASE
BEARING FATIGUE LIFE (a) (HRS)	547	295	1091	1044	1311	1044	1678	1377
TOTAL HEAT GENERATION (WATTS)	526	420	614	612	616	612	886	576
MINIMUM FILM THICKNESS (μm)	.196	.161	.249	.244	.284	.244	.404	.301
FILM PARAMETER	1.09	0.90	1.39	1.36	1.59	1.36	2.26	1.68
BEARING OPERATING TEMPERATURE (°C) (b)	103	103	103	104	104	161	163	160
BEARING FATIGUE LIFE Si ₃ N ₄ ROLLERS (HRS) (c)	221	119	441	422	530	422	678	556
TOTAL HEAT GENERATION Si ₃ N ₄ ROLLERS (WATTS) (c)	480	383	560	558	562	558	809	526

(a) No material adjustment factor applied.

(b) Assumes 2 l/min flow of oil and/or static grease pack.

(c) Assumes hybrid bearing i.e. silicon nitride Si₃N₄ rollers.

TABLE 3-6

MAIN BEARING CONCEPT DESIGN
LUBRICATION STUDY RESULTS

	154-40	STAUFFER SDL-1	MOBIL DELVAC 1340	MOBIL SHC 629	TEXACO URSA 50	MOBIL GREASE 28	AEROSHELL #5 GREASE	TEXACO MARFAC #2 GREASE
BEARING FATIGUE LIFE (a) (HRS)	1400	882	1748	1723	1892	1723	2156	1949
TOTAL HEAT GENERATION (WATTS)	840	673	981	978	981	978	1406	918
MINIMUM FILM THICKNESS (μm)	.263	.216	.333	.327	.376	.327	.519	.396
FILM PARAMETER	1.47	1.21	1.86	1.83	2.10	1.83	2.90	2.21
BEARING OPERATING TEMPERATURE ($^{\circ}\text{C}$) (b)	106	105	106	107	107	142	145	140
BEARING FATIGUE LIFE Si_3N_4 ROLLERS (HRS) (c)	566	356	706	696	764	696	871	787
TOTAL HEAT GENERATION Si_3N_4 ROLLERS (WATTS) (c)	760	609	888	885	888	885	1272	831

(a) No material adjustment factor applied.

(b) Assumes 2 l/min flow of oil and/or static grease pack.

(c) Assumes hybrid bearing i.e. silicon nitride Si_3N_4 rollers.

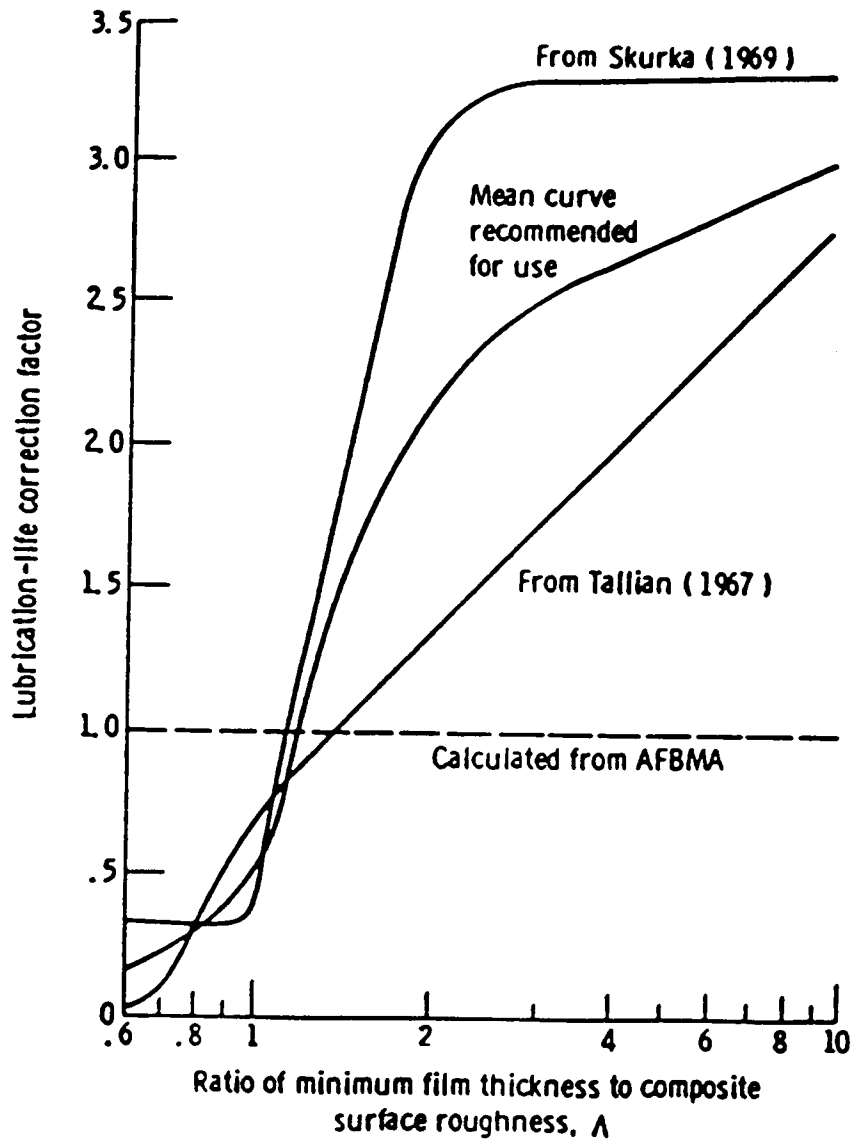


FIGURE 3-7
LIFE CORRECTION FACTOR FOR LUBRICANT FILM EFFECTS

generation should show a decrease owing to the low density of Si₃N₄ causing a reduction in roller centrifugal force and consequential reduction in roller to outer raceway contact loads. The results indicate fatigue lives of only 40% of that of steel; a disadvantage that outweighs the apparent slight (10%) decrease in bearing heat generation. These results tend to indicate that the use of Si₃N₄ rollers would create no distinct advantage.

3.4 Life Cycle Cost Elements

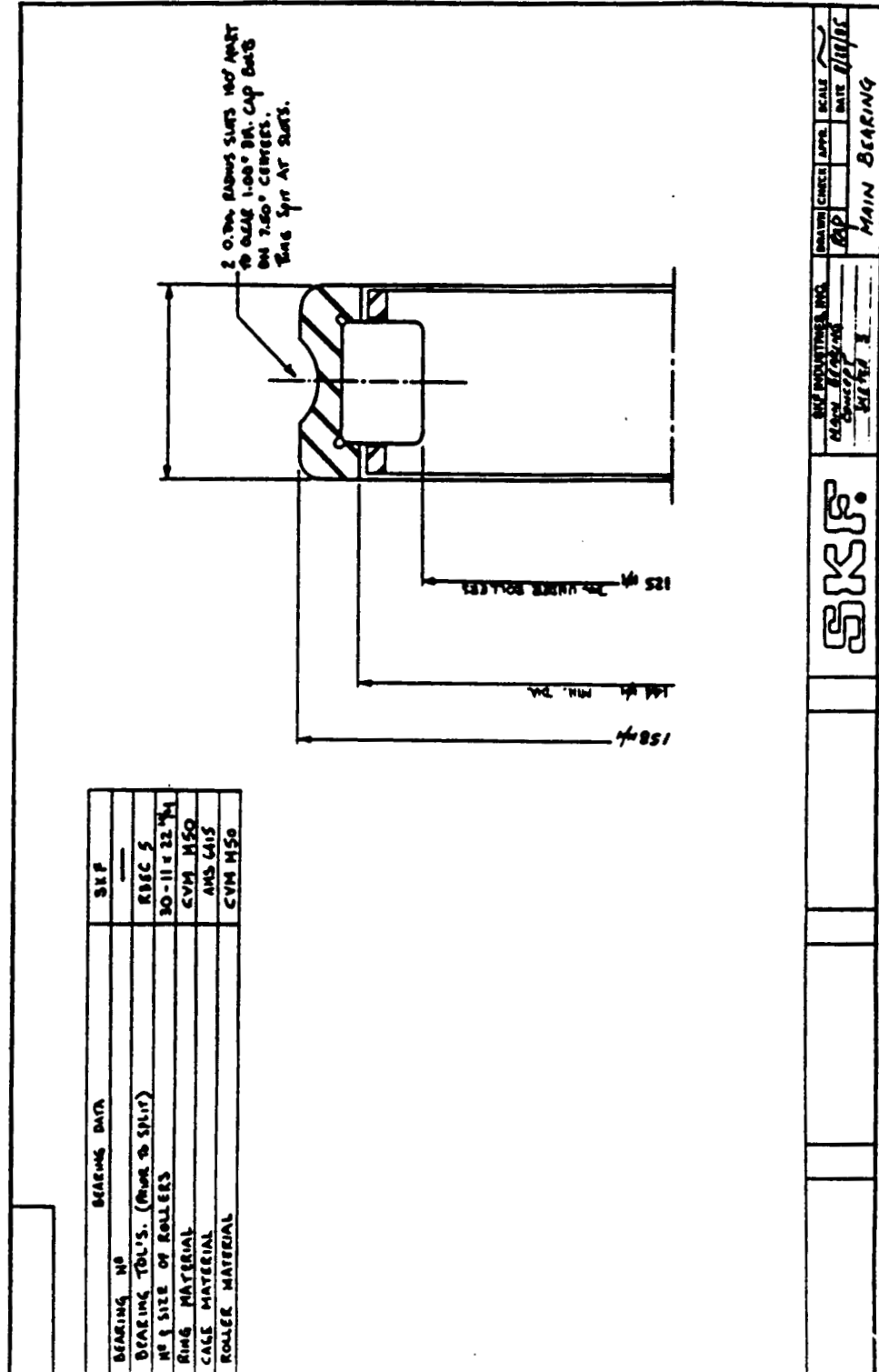
Figs. 3-8 and 3-9 illustrate the conceptual designs in the form of layout drawings. These drawings were used to formulate cost estimates to be considered in the life cycle cost analysis. The cost analysis results were as follows:

Number of Pieces	Approximate Cost (\$)	
	Main Bearing	Connecting Rod Bearing
100	722 ea	920 ea
1000	597 ea	788 ea

The costs are based on the assumption of 1986 labor rates and machining methods.

ORIGINAL PAGE IS
OF POOR QUALITY

FIGURE 3-8 MAIN BEARING OUTLINE DRAWING FOR LIFE CYCLE COST ANALYSIS



4.0 REFERENCE ENGINE BEARING BASELINE DESIGN ANALYSIS

4.1 Baseline Design Sizing and Loading

Following the Task 1 completion there was a redesign (downsizing) of the reference engine crankshaft and cylinder components. The shaft speed was downgraded to 1800 rpm with the bore and stroke finalized at 120mm and 125mm, respectively. Based on these new engine operating parameters, new bearing mean loads were established. These were as follows:

Main Bearing	Load = 27,248N
Connecting Rod Bearing	Load = 39,351N
Wristpin Bearing	Load = 64,576N
Thrust Bearing	Load = 19,415N

Based on these new mean loads new roller compliments were selected by DDA:

	Main Bearing	Connect- ing Rod Bearing	Wristpin Bearing	Thrust Bearing
Roller Dia. (mm)	11	12	13	7
Roller Length (mm)	20	40	53	14
No. of Rollers	24	16	13	32/Row

These basic roller compliments were expanded into full baseline designs with standard roller crowning and internal clearances.

4.2 Baseline Design Analysis

The baseline designs were analyzed via computer code SHABERTH, as before, and the results are shown tabulated in Table 4-1. As a result of the Task 1 lubrication studies, the Texaco Marfac #2 grease was selected as the primary path lubricant.

These results indicate that the baseline designs are acceptable. The low value for lubricant film parameter for the wristpin bearing is not entirely surprising. The lack of appreciable rotational speed is the dominating reason for the low value. This can lead to surface distress and indicates that there may be a need for wear resistant coatings.

All the results presented in Table 4-1 were computed using bearing geometry information that is in accordance with standard SKF design practice. That is, internal geometry features such as radial clearance, cage guiding surface clearances, cage geometry, flange clearances and roller sizing were all assumed to be according to standard SKF design with the exception of roller profile. This design element was investigated for the main bearing.

The design of the ADRE bearings is one that maximizes life. To this end it was deemed necessary to maximize the use of roller

TABLE 4-1
ADRE BASELINE BEARING DESIGNS ANALYSIS RESULTS

	MAIN BEARING	CONNECTING ROD BEARING	WRISTPIN BEARING	THRUST BEARING
ROTATIONAL SPEED (rpm)	1,800	1,800	322	1,800
APPLIED RADIAL LOAD (N)	27,248	39,351	64,576	19,415
FATIGUE LIFE (hrs) (No Factor)	1,130	695	731*	4,380
TOTAL HEAT GENERATION (watts)	294	218	5.66	327
TOTAL FRICTION TORQUE (hp)	0.4	0.3	0.008	0.5
LUBRICANT FILM PARAMETER	1.7	1.3	0.05	>1.0
MAX CONTACT STRESS (N/mm ²)	1,566	1,621	1,869	1,279

* Corrected to account for oscillatory motion.

contact area, i.e., length. SKF computer code HARMONY was used to investigate this for the main bearing roller geometry. Figs. 4-1 through 4-3 illustrate the results. Program HARMONY computes the stress distribution across the length of the roller for a given unit roller load (supplied from SHABERTH) and a given roller profile. Fig. 4-1 presents the distribution that results for the standard profile for a roller of that size. As can be seen, the use of roller length is not optimum. The stress peaks are at the crown blend points and can be avoided by proper manufacture. Figs. 4-2 and 4-3 present what happens as we try to maximize the use of roller length. In these two sets of results we have increased the roller cylindrical length (flat portion) to 14mm and 16mm, respectively. The results of Fig. 4-1 were for a cylindrical length of 12mm.

Clearly, the resultant stress distribution of Fig. 4-2 is optimum. It allows proper maximum use of roller length, as opposed to the profile of Fig. 4-3 which resulted in the dangerous stress peaks at the roller ends.

4.3 Material Design Considerations

As presented in the previous section, the predicted lives of the critical bearing locations of the ADE are as follows:

	Main Bearing	Rod Bearing	Wristpin Bearing	Thrust Bearing
Rotational Speed (rpm)	1,800	1,800	322	1,800
Applied Radial Load (N)	27,248	39,351	64,576	19,415
Predicted Fatigue Life (hrs)	1,130	695	731	4,380

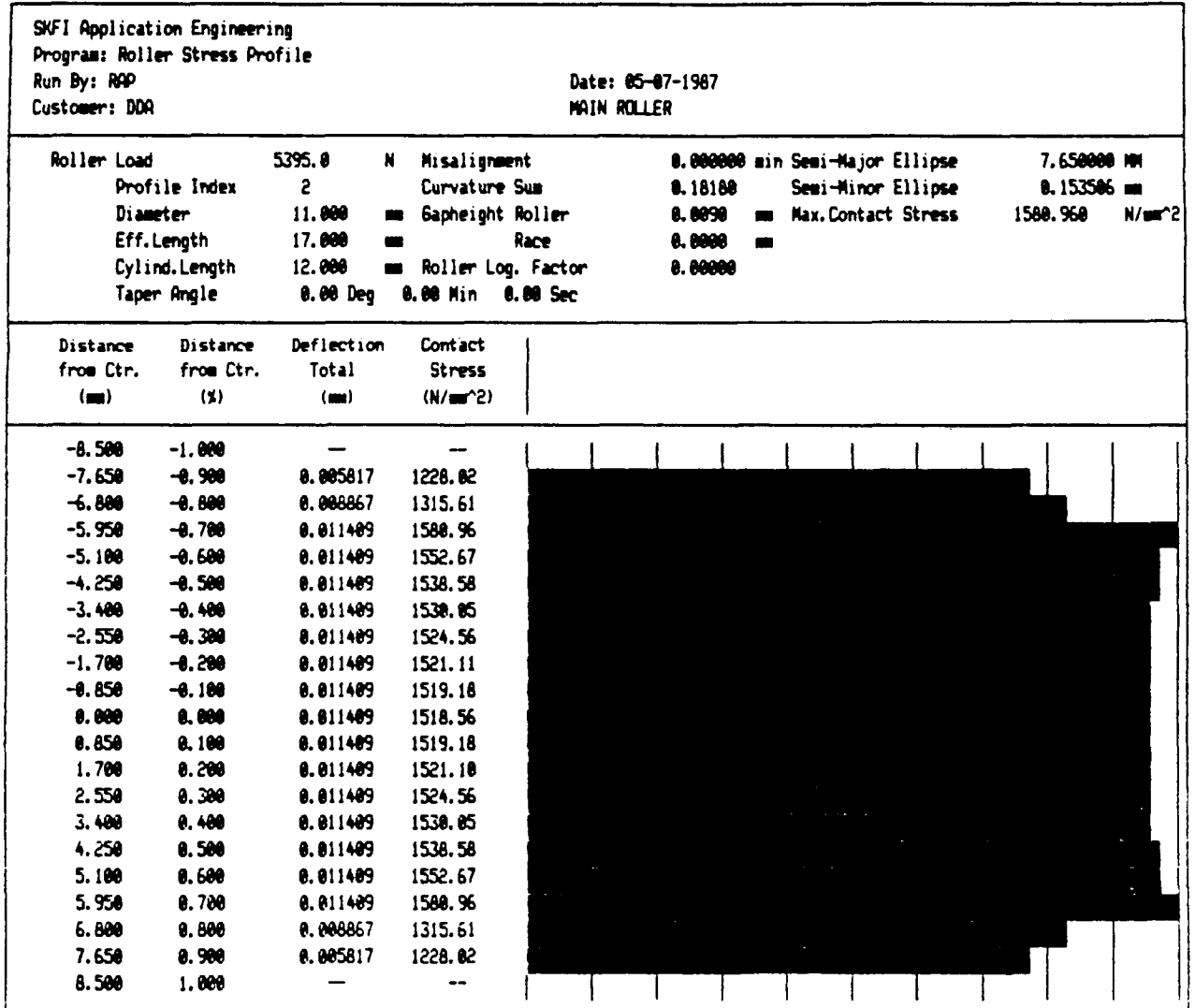
These lives are computed using the methods of Lundberg and Palmgren as published in 1947 and 1952 [3,6] and are based on empirical factors derived from bearing endurance tests. The bearings of these tests were made of 1950's vintage materials. Over the years, newer materials and material processing techniques have been shown to provide greater lives. In 1971 this prompted the publication of an ASME sponsored design guide [7] giving life adjustment factors for materials (type and processing) and operating environment (lubrication and speed).

The ADE overhaul life goal is 5000 hours. This would mean that life adjustment factors are needed for all the ADE concept bearing designs as follows:

	Main Bearing	Rod Bearing	Wristpin Bearing	Thrust Bearing
Life Adjustment Factor	4.4	7.2	6.8	1.14

As reported previously the factor for operating environment is a function of lubricant viscosity, bearing surface speeds, and bearing surface finishes. Since surface speed and lubricant were

FIGURE 4-1 ROLLER STRESS PROFILE FOR MAIN BEARING
ROLLER (CYLINDRICAL LENGTH = 12mm)



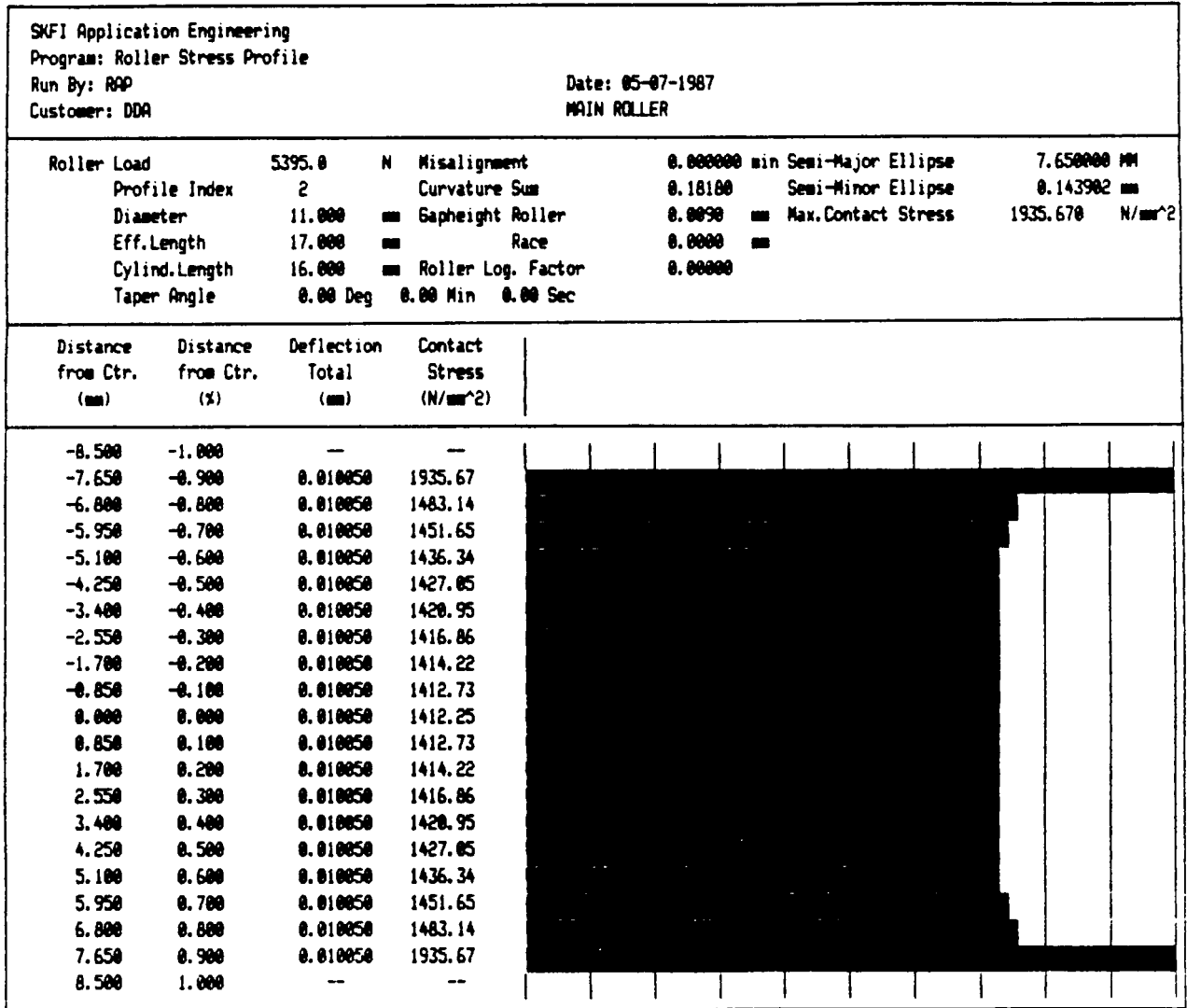
ORIGINAL PAGE IS
OF POOR QUALITY

ORIGINAL PAGE IS
OF POOR QUALITY

FIGURE 4-2 ROLLER STRESS PROFILE FOR MAIN BEARING
ROLLER (CYLINDRICAL LENGTH = 14mm)

SKFI Application Engineering		Date: 05-07-1987				
Program: Roller Stress Profile		MAIN ROLLER				
Run By: RAP						
Customer: DDA						
Roller Load	5395.0	N	Misalignment	0.000000 min	Semi-Major Ellipse	7.650000 mm
Profile Index	2		Curvature Sum	0.18180	Semi-Minor Ellipse	0.150445 mm
Diameter	11.000	mm	Gapheight Roller	0.0090	Max.Contact Stress	1550.870 N/mm ²
Eff.Length	17.000	mm	Race	0.0000		
Cylind.Length	14.000	mm	Roller Log. Factor	0.00000		
Taper Angle	0.00	Deg	0.00 Min	0.00	Sec	
Distance from Ctr. (mm)	Distance from Ctr. (X)	Deflection Total (mm)	Contact Stress (N/mm ²)			
-8.500	-1.000	--	--			
-7.650	-0.900	0.007206	1473.34			
-6.800	-0.800	0.010892	1550.87			
-5.950	-0.700	0.010892	1517.38			
-5.100	-0.600	0.010892	1501.16			
-4.250	-0.500	0.010892	1491.35			
-3.400	-0.400	0.010892	1484.90			
-2.550	-0.300	0.010892	1480.58			
-1.700	-0.200	0.010892	1477.79			
-0.850	-0.100	0.010892	1476.22			
0.000	0.000	0.010892	1475.71			
0.850	0.100	0.010892	1476.22			
1.700	0.200	0.010892	1477.79			
2.550	0.300	0.010892	1480.58			
3.400	0.400	0.010892	1484.90			
4.250	0.500	0.010892	1491.35			
5.100	0.600	0.010892	1501.16			
5.950	0.700	0.010892	1517.38			
6.800	0.800	0.010892	1550.87			
7.650	0.900	0.007206	1473.34			
8.500	1.000	--	--			

FIGURE 4-3 ROLLER STRESS PROFILE FOR MAIN BEARING ROLLER (CYLINDRICAL LENGTH = 16mm)



ORIGINAL PAGE IS
OF POOR QUALITY

optimized we have at our disposal only surface finish to affect a lube-life factor of 1.0 or greater. As reported, to achieve a lube-life factor of greater than 1.0 a lubricant film parameter of 1.5 or greater is needed. The lubricant film parameter is the minimum film thickness divided by the composite surface finish. Given the film thicknesses as optimized and a good quality roller surface finish of 0.1 μm (~4 microinch RMS) the raceway surfaces need to be 0.23 μm (~9 microinch RMS) and 0.16 μm (~6 microinch RMS) for the main and rod bearings, respectively. Finishes of this high quality may be difficult to achieve on crankshaft journal locations.

Assuming that we can achieve a minimum life adjustment factor of 1.0 for operating environment we need to concentrate on a means for achieving the required life factors from materials and processing.

The ASME guide [7] defines the total material factor as the product of two separate factors; one for material type and one for material processing. The predominant material used for rolling bearings is a high carbon, chromium steel, AISI 52100. Rolling bearing basic dynamic capacity (hence endurance life) as defined by the AFBMA (Anti-Friction Bearing Manufacturers Association) is based upon air-melted AISI 52100, fully through-hardened to a minimum of 58 Rockwell C scale hardness. Over the years, improvements in melting practices and the introduction of vacuum remelting have resulted in cleaner and more homogeneous steels. These steels have been shown to have improved life characteristics. Life improvements of 3 to 8 times are not uncommon [7]. Other steels, both through-hardened and case-hardened types have provided increased lives when vacuum melting techniques are used. Even plain carbon steels (such as AISI 1070) have showed comparable fatigue resistance when processed properly [8].

Material factors published in [7] for through-hardened, air-melted AISI 52100 and M50 steels are 2.0. No definitive factors were given for case-hardened materials due to the lack of a substantial database, however, literature was cited that show that lives with case-hardened material are comparable to through-hardened materials.

The cautionary with case-hardened materials is that the depth of hardened zone be sufficient. Common bearing practice is that this depth be a minimum of 3 times the depth of maximum subsurface shear stress. For the ADE main, connecting rod, and wrist pin bearings, this yields the following:

Minimum Depth of Hardness (mm)

Main Bearing	Rod Bearing	Wristpin Bearing
0.46	0.46	0.54

These numbers represent the minimum required depth of hardened zone after grinding. Typical case-hardening materials include, AISI 8620, AISI 3310, AISI 4320 and AISI 4620. These depths do

not appear to be a problem for induction hardened journal areas of the crankshaft, for either the SAE 1548 or SAE 1046 materials. These materials represent the two commonly used crankshaft materials for DDA engines. The piston pins are commonly made from good quality SAE 8620 (SAE and AISI designations are identical) and carburized to a hardness of 58 Rockwell C with depth of 0.5 to 1.2 mm. This is in accordance with good roller bearing design practice. Case crushing under peak firing loads must be guarded against, and should be examined when prototypes are to be fabricated.

The ASME guide [7] recommends that Rockwell C 58 be considered the minimum hardness required for critical bearing applications. Hardness of less than this value can cause reductions in bearing dynamic capacity. Harris [9] gives the following approximation for reduction of dynamic capacity for material hardness less than 58 Rockwell C:

$$C' = C (RC/58)^{3.6}$$

where

C = bearing basic dynamic capacity
RC = material Rockwell C scale hardness

Aside from the standpoint of classical rolling contact fatigue, high hardness is desired to ensure surface integrity. Surface hardnesses of 58 to 62 Rockwell C are commonly specified for roller bearings for the additional reasons of wear resistance and resistance to debris denting. It is unlikely that the surface hardness of the SAE 1548 or 1046 crankshaft material can exceed 55 RC, thus higher surface hardness will have to be achieved by special treatment of the journal locations.

Two hard coating processes that appear most compatible with nominal crankshaft heat treatment are chromium electro-deposition techniques known commercially as Armoloy and Nobilizing. Both these coatings offer corrosion resistance exceeding that of conventional hard chrome plating. Low friction, wear resistant surfaces of up to 75 RC are capable and both processes can be applied to finished components without adversely affecting the heat treated structure or surface finish of the substrate. Both processes have been tested on heavily loaded bearing contact surfaces at SKF and found to exhibit behavior consistent with the rolling contact performance of conventional bearing steels [10]. Both coatings exhibited substantial tolerance to occurrences such as debris denting in rolling contact service. The material, although reportably at a hardness of 70 RC, deforms plastically rather than cracking when intruded by debris [10].

Two additional controllable material characteristics that have been shown to have a decided and direct influence on fatigue life are melting practices and metal working practices. There exists sufficient data and evidence that there is a direct relationship between these practices and the amount, type, and orientation of fatigue life limiting inclusions.

Common steel melting practices include:

- air melting
- vacuum degassing (CVD)
- vacuum induction melting (VIM)
- vacuum arc remelting (VAR)
- consumable electrode vacuum remelt (CVM)

It should be pointed out, that it is possible to achieve very clean (inclusion free) steels with the less sophisticated melting practices. American Society for Testing Materials (ASTM) specification A295-84 [11] which is for high carbon ball and roller bearing steels gives allowable inclusion types and amounts regardless of the melting method. However, ASTM A535 [12] which is used for aircraft quality bearing steels, is a much more stringent specification. ASTM A535 states that the steel be produced by either the CVM or VIM melting processes. Test correlations cited in [7] showed that CVM steels yielded consistently higher (up to 13 times) fatigue lives than conventional air melted steels.

Recently, aircraft bearing research has indicated that large improvements in cleanliness and fatigue life can be gained by double melting. The most popular of these is vacuum induction melted-vacuum arc remelted (VIM-VAR) M50 tool steel. A study for the U.S. Army in 1979 [4] concludes that life multipliers of 3.5 to 5.6 are in order for VIM-VAR material, and the final report states that a multiplier of 5.0 be used for all Army applications using VIM-VAR M50 material.

A compilation of articles in 1974 [13] indicates that fatigue performance of bearing steels is not only influenced by the amount of inclusions, but also by the type of inclusion. Although it is difficult to quantify the relationship between non-metallic inclusions and bearing fatigue life, the work offers some general trends. Oxide inclusions (aluminum and calcium) are for the most part very harmful to fatigue life. Surprisingly, sulfide type inclusions were found to be non-detrimental and in some instances even provided increased lives.

Possibly even more difficult to quantify is the relationship of bearing fatigue life with inclusion orientation/direction. Inclusions, oxides and sulfides, tend to orient themselves ("string-out") in a direction that is parallel to the primary working direction of the material. That is, if the material is bar or tube stock, the inclusions will be "strung-out" in the longitudinal direction. Traditionally, rolling bearing rings are manufactured from "slices" of bar or tube stock. This would mean that the inclusions are running normal to the raceway finish or rolling element rolling direction. Running normal to the finish, inclusions at or near the surface cause stress intensities in the highly stressed region, thereby creating a greater probability to initiate a spall.

Recently, studies have been conducted that indicate that bearings made from pre-rolled rings exhibit longer lives. The reasoning behind this theory is that ring rolling tends to orient the inclusions in a circumferential direction. That is, parallel to the rolling direction, thereby reducing their ability to form spall creating stress intensities.

4.4 Solid Lubrication Design Considerations

A promising alternative to the use of conventional lubricants in LHR (low heat rejection) diesel engines is the use of solid lubricants. Unfortunately, there is very little design data available to aid in the design of solid lubricated rolling and sliding contacts. Testing of solid lubricated concentrated contacts has traditionally been done with pure sliding conditions. Consequently, the data has limited applicability to the technology required for contacts involving rolling or rolling with some sliding. These are the types of contacts that would occur in solid lubricated rolling element bearings for the LHR diesel engine.

SKF recently completed a two phase program for DOE/NASA as part of the Heavy Duty Transport Technology program. The program "Solid Lubrication Design Methodology" was to evaluate solid lubricants and bearing materials in combination under controlled test conditions representative of projected bearing requirements in LHR diesels [14,15]. The aim was to develop quantitative and qualitative guidelines for use in the design of solid lubricated bearings.

Phase II of the program included the performance of analytical studies that demonstrated the promising practical use of the program results.

To demonstrate the practical use of the newly created traction models, a preliminary study of solid lubricated bearing heat generation was conducted. For comparison purposes, preliminary heat generations were computed for oil (SAE 15W-40) and solid lubricated (P3310) M50 steel bearings. A deep groove ball bearing (DGBB) and a cylindrical roller bearing (CRB) were compared under operating conditions typical of diesel engine mainshaft bearing applications. For a deep groove ball bearing where the ball/raceway curvature introduces a significant degree of microslip, the solid lubricated heat generation was found to be about 2.5 times the oil lubricated case. The distribution of heat generated (in watts) at the various contact locations is shown below. The number in parentheses indicate the heat generated with the solid lubricant (P3310).

HEAT GENERATION

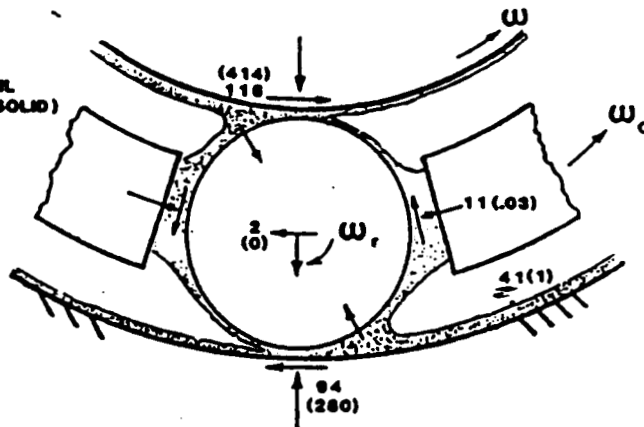
DEEP GROOVE BALL BEARING (6024)

SPEED: 2000 RPM

LOAD: 4000 LBS

TEMP: 200°F

LUBE: 15W40 OIL
(PS310 SOLID)



TOTAL: 266 WATTS
(666)

A cylindrical roller bearing operates with much less microslip in the rolling element to raceway contacts. The preliminary analysis gives a lower heat generation for the solid lubricated CRB as shown here below. The major difference is the heat generated at the raceway contacts. The small amount of microslip in the CRB allows the heat generation to be dominated by viscous inlet pumping of the oil outside the Hertzian contact.

HEAT GENERATION

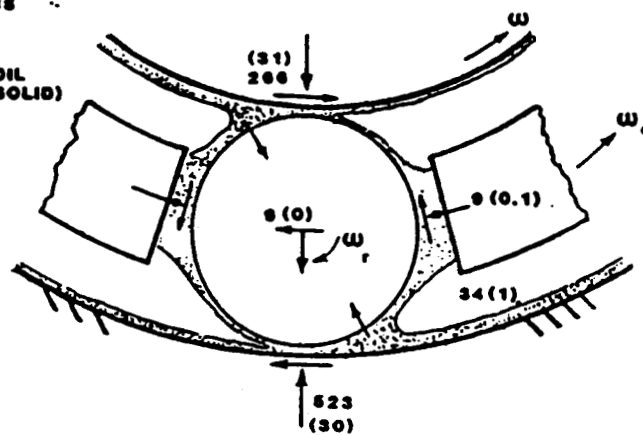
CYLINDRICAL ROLLER BEARING

SPEED: 2000 RPM

LOAD: 8000 LBS

TEMP: 200 °F

LUBE: 15W40 OIL
(PS310 SOLID)



TOTAL: 840 WATTS
(62)

However, the degree to which a similar behavior may exist for solid lubricants is not known. This and other factors, such as

roller/flange heat and cage/rolling element/land heat present unknowns to the study that require that these results be considered tentative at best.

Nevertheless, bearing in mind all the unknowns and assumptions, the possibility of a low friction, solid lubricated, cylindrical roller bearing remains hopeful.

The technical shortcomings in attempting to design solid lubricated rolling bearings revolve around two key issues:

- ° heat dissipation
- ° lubricant replenishment

Several generalized design criteria were formulated:

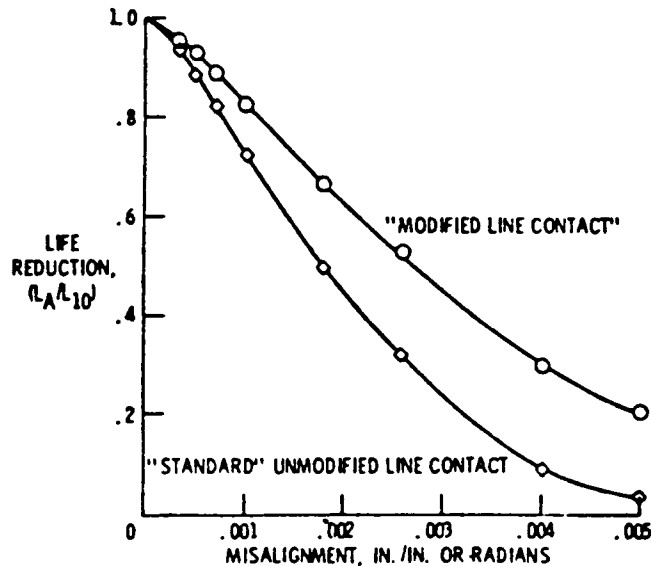
- (1) Reduce Contact Stress - This can be achieved by using a larger number of rolling elements or a larger sized rolling element. This will lower the traction forces at the contact thereby lowering the generated heat. Lower contact stresses will also enhance the maintenance of a solid lubricant film.
- (2) Minimize Sliding in the Contact - Slip within the contacts of rolling bearings is a large contributor to the overall sliding present and hence a contributor to the heat generation. The amount of slip is a function of the conformity of the raceway to the rolling. Reducing the conformity, reduces the slip. A cylindrical roller bearing, therefore, has a decided advantage built into its design. However, where the application warrants a ball bearing be used, a reduced conformity should be considered. Reducing the conformity will, however, increase the contact stress. The design effort should strike a balance between this criterion and criterion 1.
- (3) Heat Dissipation - The bearing and housing design must provide means of dissipating the heat generated at the contacts. Bearing geometry should be constructed in such a manner as to maximize surface area for cooling. The use of cooling air should be considered where possible. Materials with good thermal conductivity should be considered.
- (4) Wear Resistant Coatings and Materials - The use of wear resistant hard coats in selective areas will reduce the wear damage created by the lack of conventional lubrication. One critical area that might benefit from the use of wear resistant hard coats is the cage/land interface.

A recent paper by Christy [16] summarized the state-of-the-art in dry (solid) lubricated rolling bearings. His paper included a survey of some 30 research studies on solid lubrication and showed how replenishment and consistency of performance are still major technical barriers. The conclusions of his paper so well stated the situation. The conclusions read:

"The present state of dry lubrication on rolling elements can best be described as empirical. A large volume of test data on many specific unrelated tests summarizes progress to date. From this past data, it is clear that changing any one of many parameters such as load, speed or temperature, usually results in changes in performance or life. Because of this, extrapolation of data from one system to another is limited, and data from wear test machines can show poor correlation to actual hardware. Previous test data may be used to select candidate dry lubricants for a new application, but life tests on the actual hardware are necessary to assure that performance and life requirements are met."

4.5 Misalignment Effects

A non-material or non-lubricant related design consideration that has fatigue life implications is that of misalignment. Misalignment causes non-uniform loading of the rollers and results in a degradation of the fatigue life of the bearing. Roller crowning is used to combat the ill effects of misalignment, however, over-crowning results in the non-efficient use of roller length and decreases bearing basic capacity. Misalignment is the result of shaft and housing deflections, as well as, machining errors of the bearing seats. Most bearing manufacturers recognize such application loading that can negatively affect internal bearing geometry. As a result, they provide some simple limits beyond which reduction in bearing life may be expected. These limits were reviewed and presented in [7]. For cylindrical and tapered roller bearings this limit is 0.001 radians or 3 to 4 minutes of angular misalignment. The guidelines in [7] went on to present the curve below from [17] which offers an approximate life reduction for misalignment in roller bearings.



5.0 REFERENCE ENGINE BEARING DRAWINGS

5.1 Crankshaft Main Bearing

The main bearing design is presented by means of 5 drawings as follows:

<u>Figure No.</u>	<u>Drawing No.</u>	<u>Title</u>
5-1	LC320-01	Customer or Outline
5-2	LC320-01	Assembly
5-3	LC320-01	Outer Ring
5-4	LC320-01	Roller
5-5	LC320-01	Cage

The outer ring and cage drawings (Figure 5-3 and 5-5) show the details of the split design. Figure 5-4, shows the details of the roller profile. Note that the outer ring is to be located in its housing by means of a snap ring.

5.2 Connecting Rod, Wristpin and Thrust Bearings

The connecting rod and wristpin bearings are included as follows:

<u>Figure No.</u>	<u>Drawing No.</u>	<u>Title</u>
5-6	LC320-02	Con. Rod Customer
5-7	LC320-02	Con. Rod Roller
5-8	LC320-03	Wristpin Customer
5-9	LC320-03	Wristpin Roller

Note that the connecting rod bearing will be located in its housing by two dowel pins as shown on Figure 5-6. Not shown detailed here is the fact that the connecting rod bearing will also be of a split design. Split outer ring and split cage details will be similar to or the same as was shown for the main bearing.

No drawing was supplied for the thrust bearing due to the fact that this bearing is not a standard SKF size but is a competitors standard catalog product.

5.3 Sealing Concepts

The sealing of the ADRE bearing designs was addressed in a conceptual manner. Technically, there are three major barriers or constraints to be satisfied in developing a sealing system for the ADRE bearings:

- (1) Size - the available space at the journal locations of the main and connecting rod bearings will at best be 3mm per side. The ability to design an adequate seal in this small envelope will be greatly diminished.
- (2) Centrifugal Effects - the centrifugal loading (particular on the connecting rod bearing) will be of substantial magnitude to greatly reduce the reliability of any seal.

Grease migration under these forces will be very difficult to prevent.

- (3) Non-Contact with Journal - due to the close proximity to the journal fillet locations, it will be desirable for the seal to be stationary with respect to the journal or be a non-contacting seal. This will prevent the danger of creating a stress riser in the fillet.

In addition to these major constraints there exists the added complexities of assembly and split design.

Given these technical barriers it appears that sealing will be a design point to be addressed with considerable detail in future phases of the ADECD program.

One potential promising solution is the use of a polymeric matrix constrained lubricant system. This is a variation of the presently marketed SKF "Poly-Oil" bearings.

"Poly-Oil" (W64 is the actual SKF product designation), is a mixture of lubricating oil and polymers, thermally cured to a rigid sponge-like gel. This solid but elastic mass completely fills the bearing cavity but permits free rotation of the rolling elements. While the bearing operates, a thin film of oil is continuously released from the polymer "sponge" through light rubbing contact - only as much as is required. When operation is ceased, excess oil is reabsorbed into the polymer "sponge", ready to be released again when needed. Seals to retain lubrication are not required and contamination by abrasive materials is greatly reduced since the entire bearing cavity is filled. With proper blending of a high viscosity oil and a high temperature, 121°C (250°F), polymer, a successful "Poly-Oil" application for the ADRE main and connecting rod bearings seems feasible.

FIGURE 5-1 DRAWING LC320-01 MAIN BEARING CUSTOMER DRAWING

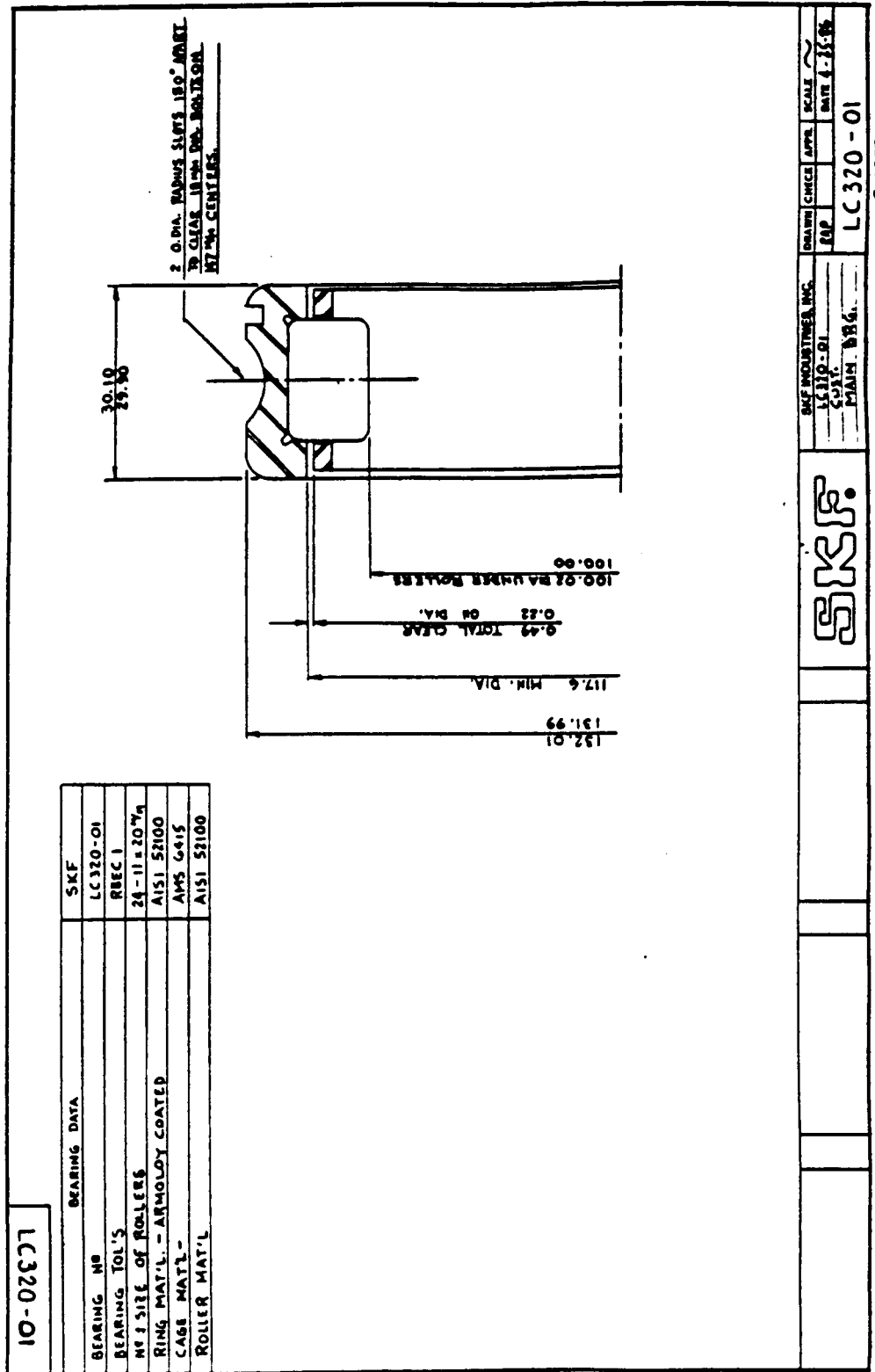


FIGURE 5-3 DRAWING LC320-01 MAIN BEARING OUTER RING

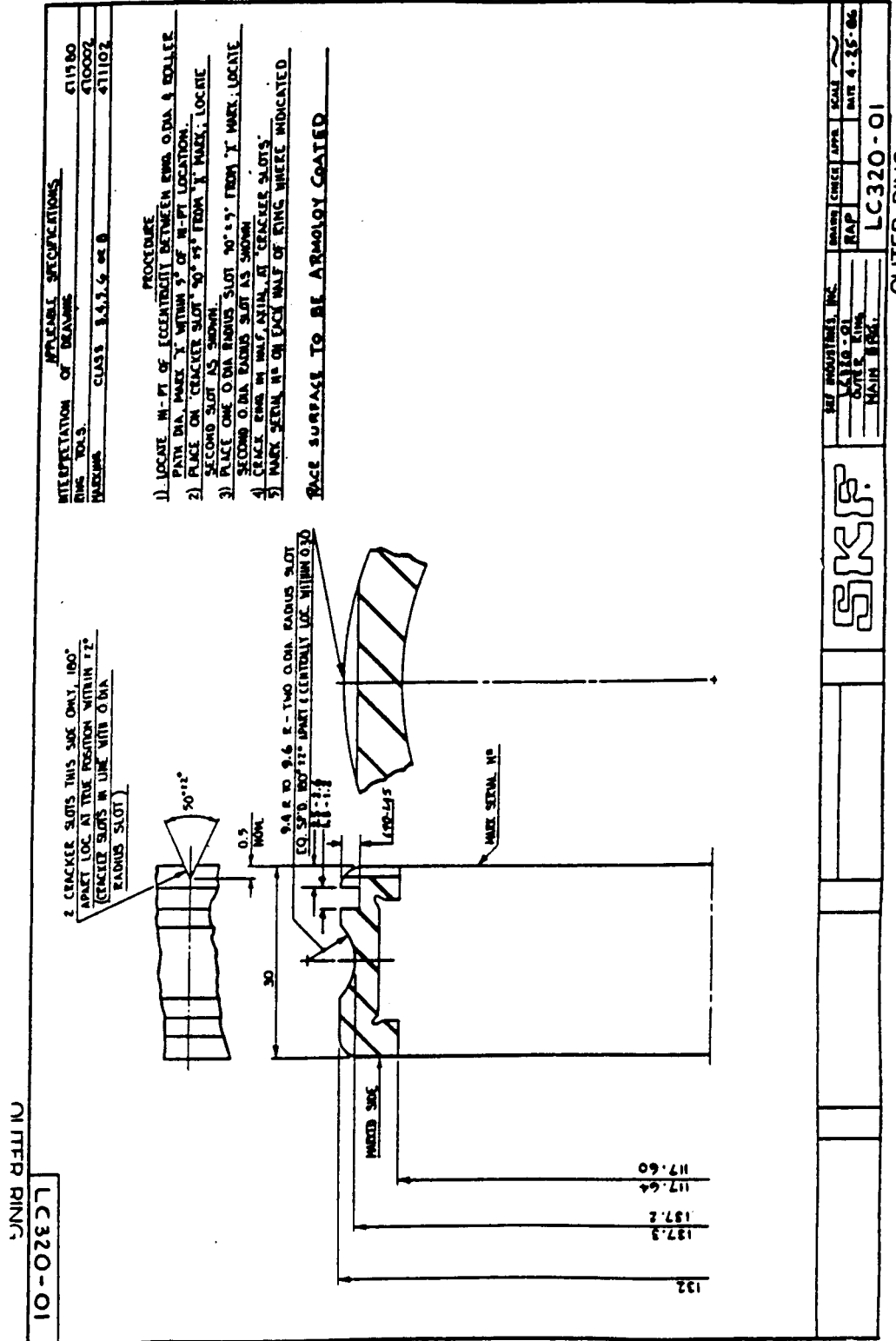
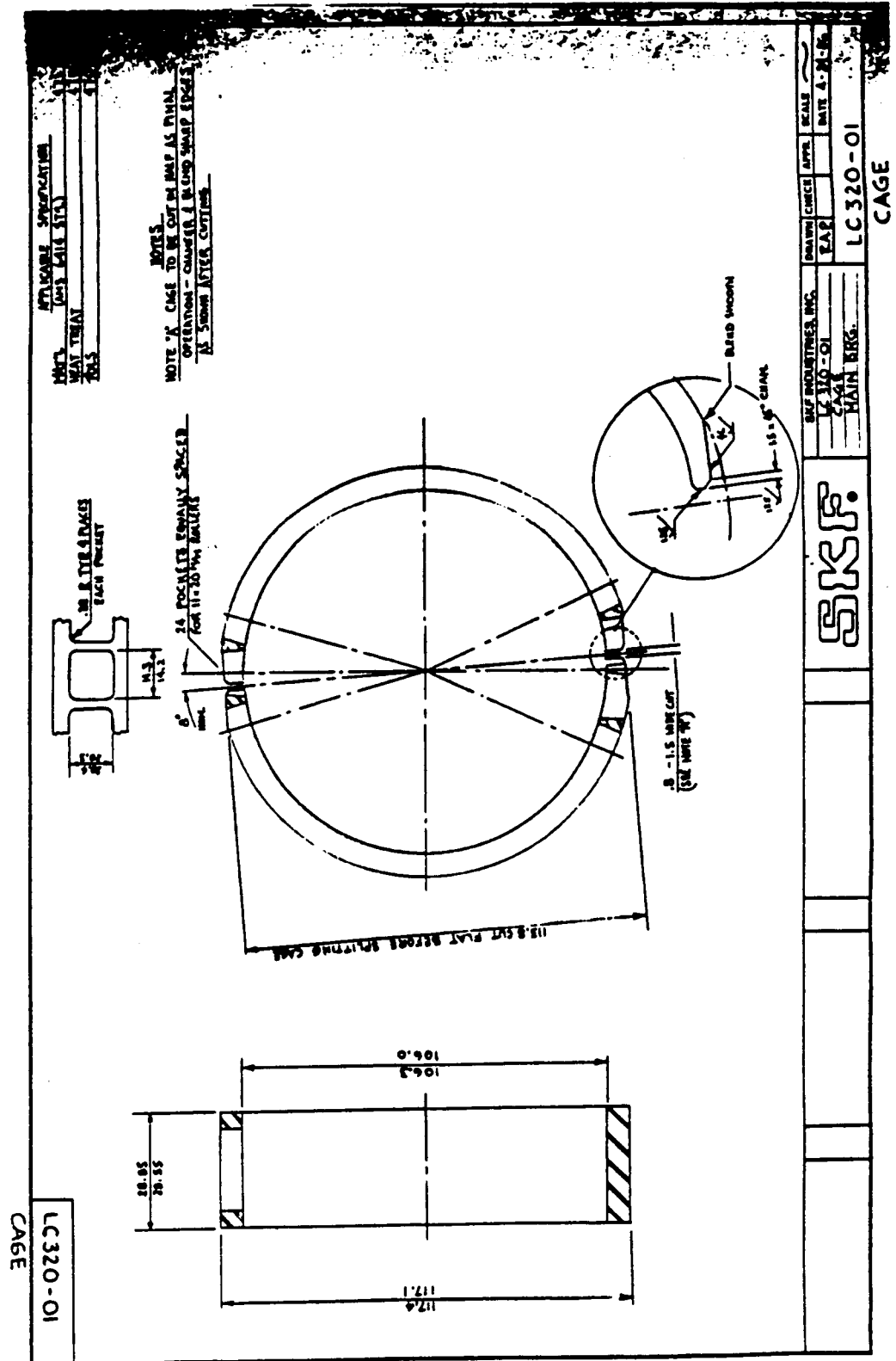


FIGURE 5-5 DRAWING LC320-01 MAIN BEARING CAGE



ORIGINAL PAGE IS
OF POOR QUALITY

FIGURE 5-8 DRAWING LC320-03 WRISTPIN BEARING CUSTOMER DRAWING

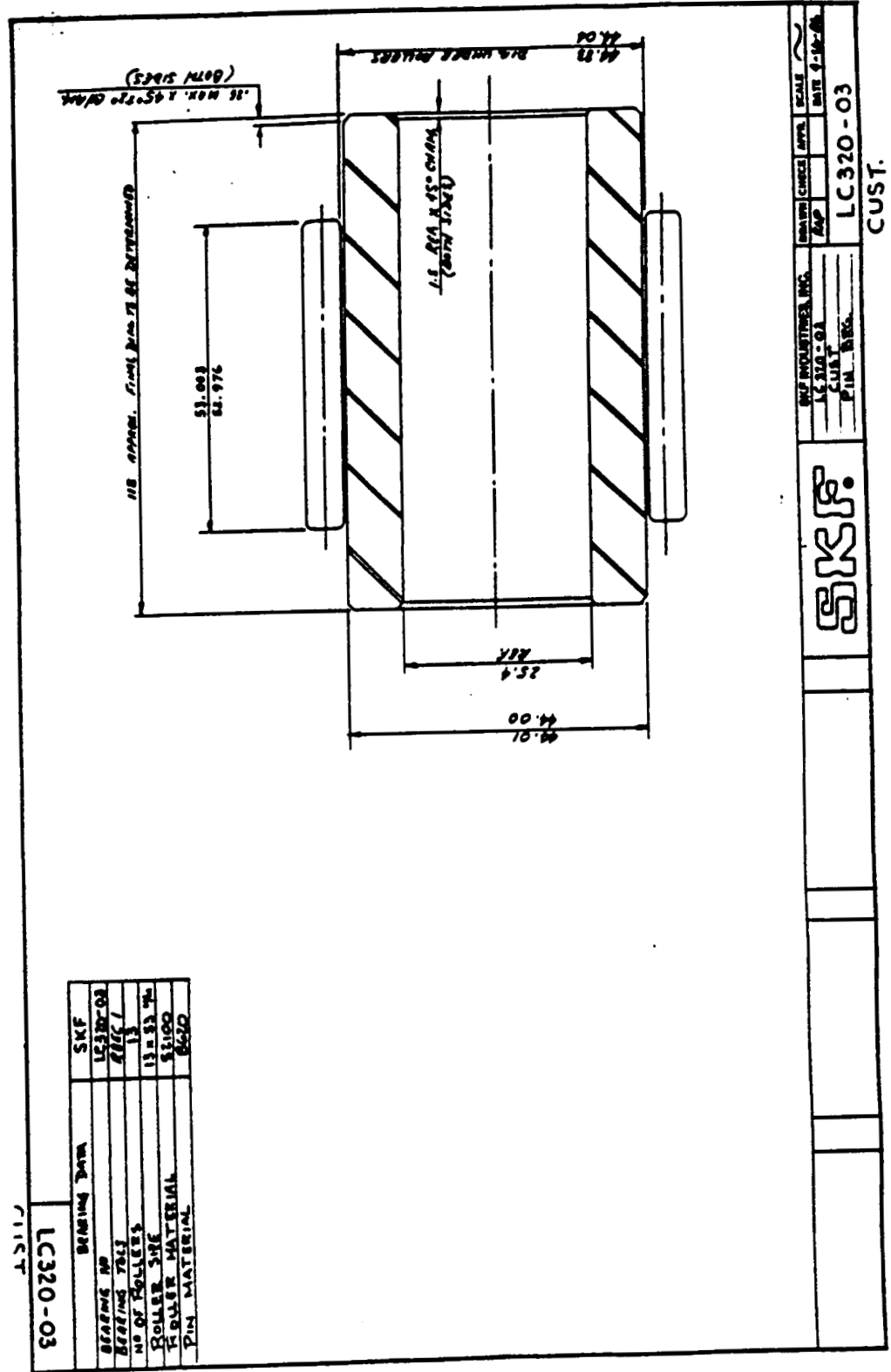
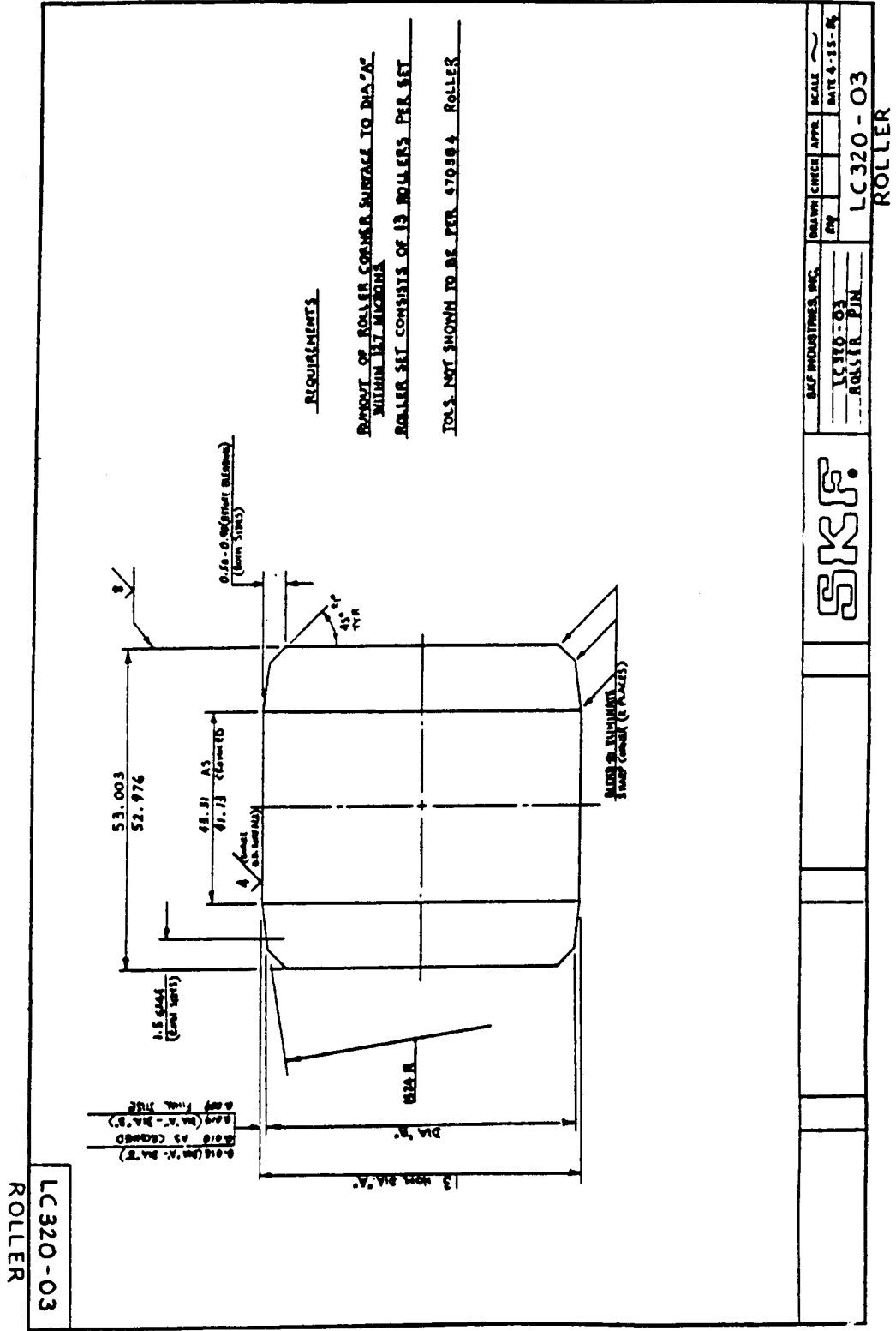


FIGURE 5-9 DRAWING LC320-03 WRISTPIN BEARING ROLLER



6.0 REFERENCES

1. "Heavy Duty Transportation Technology Development Plan," DOE/CE-0130, U.S. Department of Energy, Office of Transportation Systems, June 1985.
2. Bennethum, J. E. and Hakim, N. S., "The Low Heat Rejection (Adiabatic) Reference Engine Design for On-Highway Applications," Proceedings of the 23rd Automotive Technology Development Contractors Coordination Meeting, SAE Publication P-165, March 1986.
3. Lundberg, G. and Palmgren, A., "Dynamic Capacity of Rolling Bearings," Acta Polytechnica, Mechanical Engineering Series, Vol. 1, No. 3, 1947.
4. Morrison, F. R., McCool, J. I. and Ninos, N., "M50 Steel Bearing Material Factors for Rolling Element Life Calculations - Phase II," U.S. Army AVRADCOM Final Technical Report TR79-48, August 1979.
5. Load Ratings and Fatigue Life for Rolling Bearings ANSI/AFBMA Standard II - 1978," Revision of ANSI B3.16 - 1972.
6. Lundberg, G. and Palmgren, A., "Dynamic Capacity of Roller Bearings," Acta Polytechnica, Mechanical Engineering Series, Vol. 2, No. 3, 1952.
7. Bamberger, E. N., Harris, T. A., et al, "Life Adjustment Factors for Ball and Roller Bearings," An Engineering Design Guide, American Society of Lubrication Engineers, New York, 1971.
8. Torrance, A. A., Stokes, R. J. and Howes, T. D., "Steel Composition Effects on Grindability and Rolling Contact Fatigue Resistance of Bearing Steels," Trans of ASME, Journal of Tribology, Vol. 107, No. 4, October 1985.
9. Harris, T. A., Rolling Bearing Analysis, 2nd Ed. Wiley and Sons, New York, 1984.
10. Maurer, R. E., Ninos, N., and Hahn, D., "Functional Testing of Armoloy, Noblizing and Electroless Nickel on Rolling Contact," SKF Industries, Inc. Report No. AL76M001, August 1976.
11. ASTM Specification A295-84, "High Carbon Ball and Roller Bearing Steel," American Society for Testing of Materials, Philadelphia, 1984.
12. ASTM Specification A535-79, "Special-Quality Ball and Roller Bearing Steel," American Society for Testing Materials, Philadelphia, 1979.
13. ASTM STP-575, "Bearing Steels: The Rating of Non-Metallic Inclusions," edited by J.C. Hoo, American Society for Testing Materials, Philadelphia, 1974.

14. Aggarwal, B. B., et al, "Solid Lubrication Design Methodology," DOE/NASA/0323-1, NASA CR-174690, May 1984.
15. Pallini, R. A., et al, "Solid Lubrication Design Methodology - Phase II," DOE/NASA/0323-1, to be published, March 1986.
16. Christy, R. I., "Dry Lubrication for Rolling Element Spacecraft Parts," Tribology International, Vol. 15, No. 5, October 1982.
17. Derner, W. J., "Misalignment Problems in Cylindrical Roller Bearings," Paper 700559, Society of Automotive Engineers, New York, New York, April 1970.

APPENDIX B: INTEGRAL TECHNOLOGIES INC. SUBCONTRACT FINAL REPORT

ITI Reference
ISL-84-114

DDA Subcontract DE-078386

ADIABATIC DIESEL ENGINE COMPONENT DEVELOPMENT -
DESIGN AND PERFORMANCE ANALYSIS SUPPORT

Phase I Summary Report

Prepared for:

Detroit Diesel Allison Division
General Motors Corporation
Romulus Engineering Center
36880 Ecorse Road
Romulus, MI 48174

May 30, 1986

Authors:

Thomas Morel
Rifat Keribar
Edward F. Fort
Paul N. Blumberg
Charles I. Rackmil

Integral Technologies Incorporated
415 East Plaza Drive
Westmont, IL 60559

EXECUTIVE SUMMARY

During Phase I, several studies were carried out by ITI in support of the DDA program. An extensive study was made of advantages of electronically-controlled hydraulically-activated valves (ECV) with variable timings and variable rise times. It was found that the optimum valve ramp duration is about 60 crank angle degrees, since shorter durations bring no additional benefits. For any given valve ramp duration there is an optimum timing crank angle for all four events (IVO, IVC, EVO, EVC), providing the lowest BSFC and/or highest volumetric efficiency. When the conventional valves are well optimized, the introduction of the ECV brings only modest benefits in BSFC. However, once the ECV's are installed on an engine, they permit certain sophisticated valve timing strategies not possible otherwise.

Early valve closing (IVC more than 180 crank angle degrees before firing TDC), coupled with increased boost is a concept that has been suggested in the literature. A study was undertaken to evaluate the concept for a turbocharged engine without exhaust heat recovery, both in insulated and cooled configurations, and for the Adiabatic Diesel Reference Engine (ADRE). It was found that for the turbocharged engine without heat recovery there was up to 3 percent improvement in BSFC (with the same peak pressure and lower NOX), with early valve closing at 255 degrees BTDC and compressor pressure ratio of 4.26. These benefits are substantially lower than those reported previously in the literature. By contrast, when applied to the ADRE, the concept produced no improvement in BSFC. This was the result of reduced work produced by the exhaust heat recovery devices, which cancelled the increased basic engine power output. Thus, the additional complexity of this system produces no advantage for the ADRE, and the approach is not recommended.

The use of organic Rankine cycle bottomer (ORCB) to extract energy from the exhaust stream and to use the output power to drive the engine compressor, was also investigated. For a turbocharged engine with no exhaust energy recovery it was found that this system produced lower power than when the ORCB was used to drive directly the engine shaft. For the ADRE the system output equalled that produced by the directly driven system. This was a result of additional power produced by the exhaust heat recovery devices due to reduced pressure and temperature drops across the turbocharger turbine. Since there was no change in BSFC, the advisability of using the ORCB for driving the engine compressor depends on whether it provides advantages in BSFC at low loads, in mechanical complexity or in engine power control; these aspects have not been addressed at this time.

The insulation package used on the ADRE reduces in-cylinder heat rejection by 65 percent with respect to a cooled configuration. The component temperatures are substantially higher, with the maximum time-average temperature in the piston silicon-nitride cap attaining levels of 1220K at peak torque. Taking into consideration the effects of cyclic temperature swings, the maximum temperature reaches 1260K. The liner temperatures are much higher than in a cooled engine, reaching 640K at the top of the liner, and on the order of 600K at lower locations.

A transient engine response was simulated for a rapidly increasing load/speed trajectory. The response was found to have two time scales, one associated with the turbocharger lag, and one associated with the structure warmup. During the early phases of the transient, steep temperature gradients were observed near the piston surface. The stresses produced during that period (thermal shock) are of great interest in structural analysis of the piston cup, which will be carried out in a follow-on work.

I. INTRODUCTION

The use of high temperature thermal barrier materials and coatings in diesel engines presents major long-term opportunities for improved thermal efficiency, reduced package size and weight, elimination of the cooling system and ultimately longer life and lower cost. Recognizing the benefits of this high-risk technology, the Department of Energy has been funding programs to accelerate its development, thereby supplementing the in-house activities of the diesel engine industry.

In the present DOE/NASA "Adiabatic Diesel Engine Component Development" program, in which DDA is the prime contractor, the objectives are to evaluate and build on the previous work in this area, and to integrate the most promising concepts together with new approaches developed during the program into a "reference engine" design. Integral Technologies Incorporated (ITI) participates in the DOE Heavy Duty Diesel Program by carrying out a three-year NASA program to develop advanced integrated thermal and performance analysis methods for insulated engines. The expertise developed in this work and additional ITI in-house capability were applied to the "Adiabatic Diesel Engine Component Development" program through ITI's participation as a subcontractor to DDA. The primary tool employed in this work was ITI's engine system design and analysis code IRIS, described, for example, in Morel et al (1986).

This report describes the results of various studies carried out by ITI in support of DDA program during its Phase I.

II. OVERVIEW OF SPECIFIC TECHNICAL TASKS

In this program ITI carried out analyses in support of DDA's effort. As a first step, simulations were carried out concerning the performance parameters of a state-of-the-art engine at two operating conditions. This was followed by a performance analysis of the Adiabatic Diesel Reference Engine (ADRE). The objective was to determine heat rejection benefits and projected performance of the concept engine.

An extensive study was made of advantages of electronically controlled valves with variable timings and variable rise times. This was then complemented by a study of early intake valve closing and a concept involving a Rankine cycle driven compressor. In the final investigation, work was carried out on predictions of performance and on characterization of temperature distributions in the piston/liner assembly of the ADRE, utilizing a composite piston with a silicon nitride cap.

The calculations reported in sections III through V below were carried out with plasma-spray coatings on head, valves, piston and top of the liner, providing 62 percent heat rejection reduction. The ports were also insulated. In this configuration, the liner below the top ring reversal point was made of iron, and it was conventionally cooled. This configuration differs from the final design of the ADRE, but for the purposes of the studies reported in sections III through V that difference is not important. The thermal analyses reported in sections VI and VII were carried out with the final ADRE insulation strategy and components.

III. ELECTRONICALLY CONTROLLED VALVE CONCEPT

One of the advanced features of the ADRE is an electronically controlled valve concept, which provides additional engine control flexibility by allowing for a variable valve timing as a function of speed and load, or for a given transient condition. The valves, of unit design, are actuated individually by a camless hydraulic system, which in addition to variable timing, can also produce a faster rate of valve opening and closing than achievable with conventional cam systems.

A study was carried out to assess the benefits that this flexibility can offer in the following areas:

- BSFC
- pumping losses
- volumetric efficiency
- power
- emissions
- cold start
- peak pressure control

The engine analysed in this study was insulated on the piston top, head, valves and top of the liner with plasma sprayed zirconia coating to provide a 62 percent reduction of in-cylinder heat transfer. It differs from the final configuration of the ADRE which uses a monolithic ceramic/air gap approach, but for the purposes of the valve study these differences are unimportant.

The work involved studies of the sensitivity of the engine performance to:

- shape of the opening and closing ramps; these were simulated by sinusoidal curves (Figure 1) with variable durations extending from an abrupt 10° CA ramp to a gradual 115°CA ramp (typical of production cam-driven systems);
- timing of valve opening and closing; searching for the optimum for a particular ramp duration and for a particular engine operating condition.

The engine operating conditions considered were 300 HP and 200 HP power levels at the 1800 RPM rated speed, and 250 HP at the 1200 RPM peak torque speed. The engine was turbocharged with an advanced turbocharger with overall efficiency of 64 percent.

The study was organized in a sequence of steps which constitute analyses of the effects of the individual valve events, and also the interactions between them:

1. intake valve closing, with fixed plenum pressures;
2. exhaust valve opening, both with fixed plenum pressures and with full turbocharger simulation;
3. overlap period, both with fixed plenum pressures and with full turbocharger simulation;
4. interaction of all events at rated conditions, with full turbocharger simulation, and reoptimization of opening and closing timings at off-rated conditions.

Intake Valve Closing. The first evaluation of the intake valve closing event was done with the intake and exhaust plenum conditions and structure temperatures fixed at those levels calculated for the rated conditions with standard valves. The engine was motored, and a search was made for the optimum IVC timing for the maximum volumetric efficiency at three engine speeds 1800, 1400 and 1000 RPM. The results for 1800 RPM are shown in Figure 2. The volumetric efficiency showed a strong sensitivity to timing at any fixed ramp duration. By contrast, the maximum values of volumetric efficiency at the various ramp angles varied much less strongly. In fact, there was almost no loss in going from 10° to 60° . Increasing the ramp angle beyond 60° produced a more substantial loss in η_v , amounting to one percentage point drop at ramp angle of 115° . Plotting the optimum timing angle with respect to ramp duration produces a result shown in Figure 3. The optimum timing for a valve ramp of short duration is just after BDC, which indicates that the intake valve areas are large enough and so the engine is free-breathing even at the rated speed. This timing is retarded roughly linearly with ramp duration, reaching $30\text{-}40^\circ$ CA after BDC (depending on engine speed) at ramp angle of 115 degrees. The figure also shows that the optimum timing depends on engine speed. This means that optimizing the valve timing for rated speed compromises somewhat engine breathing at lower RPM. This is a problem with conventional valves, but it can be eliminated by electronically controlled systems.

IVO/EVC overlap period. The IVO/EVC period was studied first by independent variation of IVO and of EVC. The plenum conditions were fixed, and the IVC and EVO timings and ramps approximated conventional valve practice. The monitored parameters were reciprocator BSFC and η_v . The EVC study was first made with fixed IVO ramp of 60° duration and IVO angle of 8° BTDC. The results for BSFC are shown in Figure 4. They show that best results are obtained with abrupt valve closing at TDC. However, the degradation with increasing ramp angle is again quite small until durations of $60^\circ\text{-}80^\circ$, beyond which it becomes more significant. A similar trend is seen in the volumetric efficiency trends. The IVO study was made with a fixed EVC ramp of 65° duration and EVC angle of 6° ATDC. It showed similar results as for the EVC. Again, only small penalties were accrued by increasing ramp angles up to about 60° , with increasing effects seen afterwards.

Plotting the optimum EVC/IVO timings for minimum BSFC against ramp duration angle, one could observe a large degree of symmetry between EVC and IVO. These results led to a second study, in which a full turbo-charger and exhaust plenum dynamics simulation was used. In this case the EVC and IVO valve schedules were varied symmetrically, i.e., in each run the ramp angles of both were equal and the overlap extent was symmetric with respect to TDC. A series of runs was carried out to determine the optimum overlap for 10 , 60 and 115 degree ramps. (Figure 5a and b). These showed again a relatively small change in BSFC and η_v from 10° to 60° ramps, but a significant rise in BSFC beyond that point. The trends of optimum overlap with ramp duration are shown in Figure 6.

Exhaust valve opening. The study of EVO was first carried out with fixed plenum conditions. Again the ramp duration and timing were varied to determine the optimum points. This had almost no effect on volu-

metric efficiency, and so only BSFC was monitored (Figure 7). The results showed that at the optimum timing, the reciprocator BSFC was quite independent of ramp duration, with only small degradation with increasing duration. As expected, a large sensitivity of BSFC to EVO at a given ramp duration was observed. To confirm this result for a turbocharged engine, the study was rerun with a full turbocharger simulation and exhaust plenum dynamics. The results showed (Figure 8), that when the whole system is considered (with exhaust plenum dynamics, turbocharger, power turbine and Rankine cycle bottoming), the sensitivity to ramp duration is even lower -- the BSFC at best timing for each ramp was essentially independent of the ramp duration. It also indicated that for conventional valve schedules the EVO timing must be well advanced before the BDC, and that even for a sharp 10° ramp it still had to be advanced some 32 degrees. This was an interesting result worth further investigation to identify the processes governing the location of the optimum EVO timing. At first glance it would appear that the optimum EVO event should be a sharp ramp with opening at BDC, allowing the full expansion of the combustion gases and thus producing the maximum piston work. Since the optimum timing is not at BDC, this indicates that there is a counteracting effect during the exhaust period which increases as EVO is delayed, eventually more than offsetting the benefits of the additional piston expansion work.

Examination of the detailed plots of exhaust mass flows versus crank angle for the EVO retarded from optimum shows that some of the blowdown takes place after BDC, implying that the piston moves against an elevated pressure on the exhaust stroke. This generates additional pumping work, which increasingly offsets the rapidly diminishing extra piston work obtained by the late EVO timing. It thus appears that the optimum timing is the one which permits the blowdown to be completed within a few degrees after BDC, before the piston starts moving rapidly upward. Since the intensity of the blowdown decreases with decreasing load, and depends also on engine speed, the optimum timing may be expected to vary with these parameters. This variation could be accounted for in an electronically controlled valve system, resulting in a slightly increased engine efficiency.

Interaction of all Valve Events and Comparison to Conventional Valves.

This part of the study was carried out for the ADRE equipped with power turbine and ORCB machine, both directly coupled to the engine shaft. Comparisons were made of conventional vs. electronically controlled valves. The electronically controlled valves were set to open and close with ramps of 60° in duration. This duration was found to be near optimum in the studies of the individual events discussed above. In this last part of the study we performed the final optimization by simultaneous variation of all four timings for the 60° ramp duration at rated conditions. This optimization resulted in slightly different timings than those detailed in the decoupled studies above, ie. IVC = -168, EVO = 118, IVO = 352 and EVC = 368. The resulting profiles of effective ECV valve areas are shown in Figure 9a, as compared to the standard valve effective areas shown in Figure 9b.

The results are summarized in Table I, which shows comparisons for the three engine operating conditions described above. In all comparisons

at a given engine operating condition the fuel flow rate was kept the same. The turbocharger characteristics were adjusted at the rated conditions to produce a desired air fuel ratio for both the original valves and the electronically controlled valves (ECVs). This required compressor pressure ratios of 2.55 and 2.37, respectively. The ECVs produced a higher volumetric efficiency and lower peak firing pressures, while the BSFC was 1.3% lower and the predicted emissions were unchanged.

The differences produced by the standard and ECV systems were also observed by comparing the valve mass flow profiles, which displayed increased rate of flow through the electronically controlled exhaust valve during the initial blowdown due to the faster rate of valve opening. They also showed a decrease in the extent of backflows across both the intake and exhaust valves in the ECV system.

For peak torque and part load conditions, Table I shows comparisons for three cases: standard valves, ECVs with the same timings as at rated conditions, and ECVs with timing schedule reoptimized (but the same ramp duration) for these two engine operating conditions. The turbocharger maps used were the same as used at the rated conditions for the standard valves and ECVs, respectively. Similar results were found as for the rated conditions: the ECVs produced a higher volumetric efficiency, lower peak firing pressures, slightly lower BSFC and about the same emissions levels.

Summary for Electronically Variable Valves

- 1) It is not necessary to require very fast valve ramps because the point of diminishing return is reached at a ramp angle of about 60° for all three events: IVC, EVO and valve overlap IVO/EVC. This is a significant result from the point of view of the practicality of this concept, as decreasing the valve ramp to very short durations rapidly increases the forces and power required for valve operation beyond those used in present systems.
- 2) For a given EVO ramp duration, the BSFC exhibits a dependence on the EVO timing. Since the timing for best BSFC may be expected to depend on speed and load, there is a loss of efficiency at part load and speed if the timing is optimized at rated conditions. The variable valve concept provides benefits in this area.
- 3) For a given IVC ramp duration, the volumetric efficiency depends on the IVC timing. Since the timing for best volumetric efficiency advances with decreasing speed, if the timing is fixed at a value optimized at a particular speed, there is a loss of volumetric efficiency at other speeds.
- 4) The volumetric efficiency produced with the optimized IVC events was 10 percent higher than that obtained with the conventional valve profiles originally proposed for the ADRE. The maximum valve areas were found to be large enough to allow a relatively free-breathing operation even at the rated speed.

5) Comparison of the optimum ECV's to the original conventional valves showed that the ECVs can provide modest benefits in BSFC and peak firing pressures over the conventional valves, which were quite well optimized to begin with. Thus one concludes that the direct application, in freely breathing engines, of electronically controlled valves with timings similar to those used in conventional systems does not produce sufficiently large benefits in volumetric and thermal efficiency to warrant a serious development program in its own right. However, once ECV's are installed on an engine, they permit certain more sophisticated valve timing strategies not possible otherwise:

- reoptimization of valve events with speed and load,
- early IVC combined with increased boost at high loads to utilize exhaust energy (pressure compounding),
- IVC closing at BDC for cold start and light load operation,
- engine braking by elimination of expansion work, i.e. EVO near TDC.
- selective cylinder cutouts (shutoff valves & injector).

IV. EARLY INTAKE VALVE CLOSING

Early intake valve closing (i.e. IVC more than 180 degrees before firing TDC) has been suggested in the literature by Miller (1946) as a means to accomplish a larger degree of intercooling and higher BMEP. More recently, the idea was proposed by Chute (1985) as a method of producing higher engine thermal efficiency. Chute analysed the concept and concluded that with highly insulated (adiabatic) engines equipped with high efficiency turbochargers (64 percent overall efficiency), early intake valve closing can produce over seven percent improvement in BSFC. The objective of Chute's work was to demonstrate that the energy allowed to be wasted at the exit of turbocharger turbines in today's engines can be used to provide additional compressor boost. This boost would then be used to reduce the engine compression work by early intake valve closing. Since this will lead to a simultaneous increase in engine back pressure which could more than offset any gains, Chute reasoned that the concept can be successful only if used with high efficiency turbochargers (at least 64 percent efficient) and in connection with engine insulation.

The concept was of potential interest to DDA, and ITI was given the task to quantify the benefits achievable. The objective was to first repeat Chute's analysis as closely as possible, to determine whether the reported benefits are confirmed by a simulation which is much more comprehensive and detailed than that used by Chute. This was followed by the specific application to the ADRE.

Turbocharged Engine with no Exhaust Energy Recovery. In this part of the study ITI followed the main assumptions and parameters reported by Chute. The engine was highly insulated, turbocharged, employed no exhaust energy recovery, and had valve ramp durations of 60 degrees except the intake valve closing ramp which was 30 degrees in duration for the early-closing case only. The intake valve closed at 168 degrees before firing TDC for the baseline engine and at 255 degrees for the early-closing case.

The volumetric efficiency declined by almost a factor of two for the early closing case, which required a greatly increased boost so that the fuel air ratio would be unchanged. The air was intercooled to the same level (311°K) for all cases studied.

The early-closing case was run first with injection timing set so that the combustion start would be the same as in the baseline engine (-7.8 BTDC). A parametric study was then run with variable turbocharger efficiency (turbine x compressor peak efficiencies) over a range from 40 to 80 percent. The results are shown in Figure 10, which shows that the early closing produces lower BSFC than the baseline for turbocharger efficiencies greater than about 58 percent. The dependence of the early closing concept on turbocharger efficiency is much stronger than for the baseline case, and the BSFC rises sharply with declining turbo efficiency. At low turbo efficiencies the early closing is clearly inferior. This trend is tied to the sharp variation in engine backpressure illustrated in Figure 11 by the turbine pressure ratio. The compressor pressure ratio was 2.32 for the baseline and 4.26 for the early closing

case, and it was independent of the turbo efficiency. Essentially the same trends were obtained with a cooled version of the engine but at higher overall levels of BSFC, as expected.

The results obtained disagree with the findings of Chute in two areas. First, the benefit in BSFC for 64 percent turbo efficiency (the value used by Chute) was only 1.5 percent compared to 7.5 percent found by Chute. Second, while Chute found that engine insulation increased the viability of the concept, our results showed no such trends. Another way of looking at this is to note that at 64 percent efficiency both the present results and Chute's results show that the early intake valve closing provides almost no improvement in BSFC for the cooled engine. Further, while ITI's calculations show that this result extends to insulated engines, Chute's show a large improvement with insulation. The difference can probably be traced to the heat transfer model which greatly affects the predicted exhaust temperatures. Chute's exhaust temperatures for the adiabatic engines (simulated by setting wall temperatures to unrealistically high values) are sharply higher than for the cooled engine, and this exhaust enthalpy is then available to the turbine for generating the required increased boost. By contrast, the ITI model shows a much smaller temperature increase with insulation than calculated by Chute and this is responsible for the lower observed benefits.

One of the very important effects present in the cases studied is the level of intercooling. As already mentioned, in both cases the air exiting the compressor is intercooled to the same level of 311°K, presumably in an air-to-air intercooler. In the baseline case that requires (at compressor efficiency of 80 percent) a reduction of 86°K, equivalent to a heat removal equal to 6 percent of fuel energy. At the same compressor efficiency, the increased compressor pressure ratio and increased compressor outlet temperature of the early IVC closing case leads to the need to reduce the intake air temperature by 174°K, equivalent to a heat removal equal to 12.2 percent of fuel energy. This would place a severe burden on the air/air intercooling system, requiring perhaps an unrealistically large unit. On the positive side, this means that the intake charge starts with the same temperature at IVC, but since in the early IVC closing case it is expanded inside the engine cylinder after the valve closes, the charge is cooler at the start of compression. As a result the peak pressures are reduced and the lower temperatures lead to lower NOX emissions.

Since the concept shows a measureable predicted benefit in the BSFC, this prompted a more detailed look at the performance at the target level of 64 percent turbo efficiency. The results are shown in Table II. The first two columns refer to the previously discussed two cases, in which combustion begins at the same crankangle. It may be seen that the early closing case provides not only a decrease in BSFC, but also a reduction in peak firing pressure (by 140 psi) and in NOX emissions, and there is a small increase in the soot level. This provides an opportunity to achieve additional decrease in BSFC by injection advance. Advancing by the timing to 19° BTDC increases the peak pressure to about 170 psi above the baseline and the NOX emissions are about the same, while the smoke levels are predicted a little lower than the baseline.

The BSFC has improved, and is in this case 3.7 percent lower than the baseline.

A more detailed look at the differences between the baseline and the early closing cases is provided by Figure 12, comparing the pressure-volume diagrams of the two cases, showing clearly the difference near BDC of the intake stroke, where in the early closing case the trapped air is expanded and then compressed again, and also showing the much higher levels of intake and exhaust pressures.

The study also examined whether the IVC timing used (chosen based on Chute's results) was indeed the optimum for this engine and turbocharger efficiency. A range of IVC timings was scanned, again subject to constant A/F ratio and NO_x levels. The results, displayed in Figure 13, showed that the originally chosen IVC value was very close to the optimum and that no further improvement in BSFC could be obtained at this turbocharger efficiency.

ADRE Engine with Exhaust Heat Recovery Devices. The above study concerning the early IVC timing was carried out at conditions as close as possible to those adopted by Chute in his publication, to allow direct comparison of the two predictions. With that accomplished, the work was extended to the ADRE with a power turbine and with an ORCB bottomer. The turbocharger efficiency was fixed at 64 percent and the power turbine efficiency at 78 percent. In all of the runs the valve ramp durations were fixed at 60° and the timings were fixed at the optimum values. The injection timing was advanced where appropriate, taking advantage of the lower gas temperature, to a point where peak firing pressures matched those of the baseline case and NO_x emissions were lower than for the baseline ADRE. The A/F ratio was maintained at a constant value of 29:1.

A parametric study was carried out over a range of IVC timings seeking the optimum timing for minimum BSFC at rated engine conditions. In contrast to the previous investigation of early IVC for a turbocharged engine, the ADRE results showed a very flat BSFC curve with IVC timing (Figure 14a), maintaining essentially constant values from -168 to -235 degrees before firing TDC. At timings earlier than -235 degrees the BSFC started to sharply increase. The compressor pressures required at early IVC timings for maintenance of constant A/F ratio are shown in Figure 14b.

An analysis of these somewhat surprising results showed that as the IVC timing was advanced, the power produced by the reciprocator kept increasing up to -235 degrees much as it did in the earlier study of a turbocharged engine which had no exhaust energy recovery. However, the power produced by the exhaust energy recovery devices of the ADRE kept decreasing at about the same rate due to the lower energy content of the exhaust downstream of the turbocharger turbine (Table III). As a result, the early IVC produced no efficiency gain for the ADRE engine.

V. ORCB-DRIVEN COMPRESSOR

An idea proposed recently by ThermoElectron Corporation is to use ORCB to recover exhaust energy and to then use the generated work to compress the air ahead of the turbocharger compressor in an extra stage of compression. This would replace the direct use of the ORCB power to augment the mechanical power produced by the engine (i.e. by gearing it to the engine shaft).

An analysis was carried out employing this idea in connection with conventional IVC timing and in connection with the early intake valve closing concept. The objective was to reduce the power requirement on the turbocharger turbine, thus reducing the backpressure and pumping losses. For the purpose of the simulation, a single stage turbocharger compressor was used with a common shaft to the turbocharger turbine and the ORCB. The same boost was generated in each case, but the required turbine pressure ratio was less.

ORCB-driven Compressor with Conventional IVC Timing. At rated conditions, the power available from the ORCB was almost equal to that required by the compressor and so the TC turbine had to produce only a small complementary power. As a result, the engine backpressure was quite low and this provided the opportunity for increasing the power turbine pressure ratio and power. A parametric study was run to determine the optimum power turbine pressure ratio (Figure 15). The optimum was found to be near $PR=2.8$, as a result of opposing trends in reciprocator and power turbine power. However, the total power produced by the engine at the optimum was almost exactly equal to that of the baseline ADRE (Table IV).

Analyzing the results in detail, one observes that using the ORCB to drive the compressor results in the following:

1. A large part of the ORCB power is converted through increased pressure work into increased reciprocator power.
2. This is further compounded by the higher exhaust temperature entering the ORCB (due to small pressure drop across the TC turbine), i.e., by increased ORCB power.
3. When power turbine is used, there are further benefits due to increased power turbine work, produced by higher upstream pressure and temperature.

All of these three elements combine to produce approximately the same amount of power as when the ORCB is used to drive the engine shaft directly. It should be pointed out that this is a more positive result than would be obtained for a turbocharged engine without a power turbine, where it would be more advantageous to drive the engine shaft directly rather than the compressor. The power turbine is capable of taking better advantage of the reduced pressure ratio across the TC turbine and extracts energy from the increased pressure differential.

Combined Early IVC and ORCB-driven Compressor. In this study we combined the two approaches. The calculations were carried out for a single value of IVC timing set at -235 degrees, found earlier to be near-optimum. It was again necessary to reoptimize the power turbine to

take advantage of the reduced TC turbine load (Table V). The optimum power turbine pressure ratio was found to lie near 1.86 (Figure 16). The power produced by the optimum configuration fell slightly short of the power produced by the baseline ADRE.

Summary. The ORCB-driven compressor, investigated in order to improve the efficiency of the baseline ADRE, gave at rated conditions results essentially identical to those attainable with the baseline ADRE with direct coupling of ORCB to the engine shaft. Since there were no advantages in BSFC at steady-state high loads, ORCB-driven compressor would be a favorable alternative only if it could be shown that at low loads or during engine transients there are advantages from BSFC point of view, or for mechanical complexity or for engine power control reasons. These aspects were not addressed in this study.

VI. STEADY-STATE THERMAL ANALYSIS OF THE PISTON/LINER ASSEMBLY

One of the ITI tasks in support of the DDA program involved the analysis of DDA-designed components for the adiabatic diesel reference engine (ADRE). In particular, the work concentrated on the specially designed piston, utilizing a composite silicon nitride cap and air gaps, and the temperature distributions within it.

Piston Assembly Design, Materials and Joining Method. The DDA prototype "adiabatic" engine piston assembly utilizes a silicon nitride ceramic piston crown press-fit into the piston body on a cylindrical surface with a radial mismatch of 0.15 mm, with additional contact on horizontal surfaces (Figure 17). Air gaps between the ceramic crown and body are important inhibitors of heat flow through the structure, since conductivity of silicon nitride, an excellent temperature resistant ceramic, is 16-21 W/m^oK (in the 400-900°C range), i.e. not much less than, for example, that of high alloy steels, although the advanced silicon composites considered by DDA are expected to have conductivity values on the order of 50 percent of the currently quoted values. Calculations were carried out both for the current technology silicon nitride as well as the projected advanced material. However, only the results for the latter are presented here. Cast iron is used for the piston body, skirt and liner. The entire piston-liner assembly has axisymmetric geometry, except bores in the lower part of the piston body and skirt for the wristpin. The wristpin is rigidly attached to the piston body, but the skirt is allowed to rotate around it. There are two rings: an L-ring positioned flush with the ceramic crown surface and a rectangular cross-section ring in a groove in the metal body.

The design is completely uncooled. Since crankshaft, connecting rod and wristpin bearings are grease-lubricated, cooling by crankcase oil splashing is not present. Solid lubrication is contemplated for a liner and skirt-liner contacts. Thus the structure rejects heat only to the vented crankcase air, to the air gap surrounding the liner, and to the ambient air directly or through the engine block.

Finite Element Model of Engine Components. The main objective of the study was the analysis of the piston and liner thermal distributions. Finite element representation of the piston assembly (piston crown, body and rings) was supplied by DDA. In order to represent heat paths to ambient and crankcase air as well as frictional heat generation, the model was augmented by axisymmetric FEM representation of the skirt (crosshead) and liner. The entire assembly is shown in Figure 18. Not shown in Figure 18 is a simplified model of the head which connects to the upper end of the liner. Piston crown and body were assumed to be in perfect thermal contact at the joining surfaces with no additional thermal contact resistance. Connectivities between pairs of piston or ring FEM nodes and nodes on the liner were computed based on the fraction of time during which areas associated with each node in a pair are in contact with each other during the cycle. The wristpin dimensions and thermal properties (low alloy steel) were used to compute the total thermal resistance between piston skirt and body. Since the model is axisymmetric, the connectivity based on this resistance was uniformly distributed in the azimuthal direction. Conductivities for silicon

nitride supplied by DDA were used. Heat capacity (ρc) of sintered silicon nitride was set to $3.35 \times 10^6 \text{ J/m}^3\text{K}$.

The entire finite element heat conduction model including scalar elements representing the engine head and various scalar convectivities, was processed using COSMIC/NASTRAN. Since COSMIC/NASTRAN does not support quadratic axisymmetric 2-D elements, midpoint nodes in the DDA-supplied part of the model were ignored.

Boundary Conditions. Surfaces of the FEM model exposed to combustion chamber and port gases are subject to gas side boundary conditions due to radiation and convection, calculated in a spatially resolved manner by the appropriate IRIS gas-to-wall heat transfer models. Similarly, frictional heat deposition on friction surfaces (ring faces, skirt and liner) is computed by a friction model.¹ The two air gaps incorporated in the piston design are treated by a special transient heat convection submodel, input to which includes a heat transfer coefficient and the thermal inertia (mc_D) of the gap gases. A heat transfer coefficient of $100 \text{ W/m}^2\text{K}$ was chosen for use in both gaps in the ADRE piston design, with values of mc_D , based on gap volumes and specific heat of air, of 0.055 and $0.008 \text{ J/P}^\circ\text{K}$ for the large and small gap, respectively.

The remaining surfaces, which are coolant or oil cooled in conventional engines, are uncooled in this application. Cooling due to crankcase oil splashing, which is the major heat sink in uncooled but oil-lubricated engines, is also absent from the ADRE design, which uses grease-packed bearings. Instead, these surfaces are exposed to vented crankcase air, other air gaps and to ambient air, directly or through the skin of the engine block. There is no dominant heat sink and some heat is transferred to air from large surfaces for which one needs to specify the appropriate air temperatures and heat transfer coefficients. These metal-to-air boundary conditions were estimated based on previous experience, literature on measured temperatures and free or forced convection calculations. The heat transfer coefficients and temperatures used for various "coolant"-side surfaces are shown in Figure 19.

Performance Results for Steady-state Operation. Steady-state performance and heat transfer simulation of the DDA engine concentrated on the rated and peak torque engine conditions. Rated and peak torque speeds were 1800 and 1200 rpm, respectively. Full load fuel injection rates for the two conditions were obtained from full-load horsepower and fuel consumption curves provided by DDA (Figures 20 and 21). Injection quantities (timing, profile, pressure profile) and turbocharger and power turbine maps were those used for the variable valve timing study carried out earlier for the same engine. Valve events were timed at

¹IRIS friction calculations are carried out for hydrodynamic and boundary lubrication with a liquid lubricant. This procedure was retained for the ADRE even though it will be utilizing solid lubricants. This was done on the assumption that the solid lubricants used will have friction no higher than the current state of the art liquid lubricants.

optimum values using results from that study. Valve lift profiles had 60° opening and closing ramps with a prolonged period of dwell at maximum open area.

The performance results for the two engine conditions are summarized in Table VI. They show that the insulation package reduced the in-cylinder heat transfer very substantially, from 13.3 percent down to 4.6 percent of fuel energy at rated conditions. The peak torque value is higher than the rated conditions, and this is mainly due to increased radiation caused by the richer combustion conditions, although convective heat transfer was also higher. The reduced heat transfer level is directly related to increased wall temperatures. The resulting peak time-mean temperatures on the piston and liner were higher at peak torque, reaching 1220K and 638K, respectively, compared to 1090K and 623K at the rated conditions. The heat transfer split between the piston, head and liner showed a ratio 47:28:25.

Power produced by heat recovery devices amounted to 26 and 19 percent of the base reciprocator power, respectively. The relative importance of the power turbine and of the RCB machine was reversed for the two engine conditions. The reduced mass flow at peak torque (compared to the rated conditions) produced a low pressure ratio and as a result the power turbine output was substantially reduced. On the other hand, the inlet temperature to the RCB machine was much higher at peak torque (by 110K) resulting in a large power generation there (13% of base reciprocator power).

The peak pressure constraints of the design (2200 psi or 152 bar) were met at rated conditions, and slightly exceeded at peak torque (157.6 bar). It may be observed that this result is different from that presented earlier, where at peak torque the peak pressure was exceeded by a significant amount. The previous results were generated using provisional turbocharger maps with fixed efficiency of 64 percent at both engine conditions. More realistic maps were used here, with turbocharger efficiency dropping off at the peak torque condition. This resulted in a lower boost and thus lower in-cylinder pressures.

Several of the key engine parameters are shown in the following figures on a crankangle resolved basis. Starting with the rated conditions at 1800 RPM, Figure 22 shows the combustion chamber pressure, which exhibits a higher exhaust backpressure than intake pressure, a characteristic of engines equipped with power turbines. The mass flows through the valves of this engine are on Figure 23, showing a well behaved process with minimum of backflows achieved with the optimized valve schedules and ramps. The heat transfer rates resolved into piston, liner and head are presented in Figure 24, illustrating the dominant heat transfer path to the piston surface.

At 1200 RPM, the cylinder pressure had a higher peak, and the intake and exhaust pressures were about equal. The heat transfer rates were significantly higher than at rated conditions. They also exhibited larger negative lobes due to the higher temperatures of in-cylinder surfaces.

Gas-to-Wall Heat Transfer. The IRIS convective heat transfer model tracks crank-angle by crank-angle variation of combustion chamber fluid motions, turbulence intensities and length scales during the cycle. From these, cyclic histories of local heat transfer coefficients are calculated. Local radiant heat fluxes are computed by a comprehensive radiation model which accounts for soot concentration (via a soot kinetics submodel) burned gas zone volume, instantaneous combustion chamber geometry (view factors), surface to surface reflections and absorption by the soot cloud. An emissivity of 0.85 was used for all combustion chamber surfaces.

Cycle-mean quantities, shown in Table VII, were extracted from the time-dependent parameters, and were used as thermal load for the steady-state conduction model.

The last column for each condition identifies the second order term in steady-state boundary conditions required due to the surface temperature swings. Liner hg's are for gas-to-liner heat transfer only; i.e. they do not include the effect of piston-to-liner heat transfer which is separately computed within the conduction model. Separate boundary conditions are also computed for the firedeck surfaces including valve faces, and all port surfaces.

Structural Heat Conduction and Component Temperatures. IRIS finite element heat conduction calculations are carried out concurrently with, and coupled to the performance simulation, and the gas phase heat transfer computations driven by it. After each cycle the finite element equations are solved, balancing heat transferred from combustion gases to heat conducted through the structure and rejected to coolant or atmosphere, at the same time establishing the structure temperature distribution. As the simulation converges to a steady-state, so do component temperature profiles. Rated and peak torque temperature distributions within the entire piston-liner structure are shown in Figure 25. The ceramic piston crown experiences high temperatures mainly due to the insulating effect of the air pockets and small contact area between the crown and body. Large temperature gradients also prevail for the same reasons. Peak ceramic temperatures are 1084K and 1220K for rated and peak torque conditions respectively. Peak metal temperatures in the piston-liner assembly are 625 and 641K for the same two conditions and they occur near the top of the liner and at the metal-ceramic contact. Detail of the ceramic piston crown and metal piston body temperature profiles are separately illustrated in Figures 26 and 27 respectively, for the two operating conditions considered. Other key results of the steady-state heat conduction calculations are given in Table VIII.

Also of interest are the major heat paths and heat balances on individual components. Figure 28 schematically documents the heat balance on the piston liner assembly for the rated and peak torque conditions. The rate of heat rejection to crankcase and ambient air is approximately equal for the two operating conditions. This is because the higher gas-to-structure heat transfer rates for the peak torque condition is almost exactly offset by a lower frictional heat generation rate due to lower engine rpm. It may be noted that the heat rejection is distributed quite uniformly over all surfaces. This reflects the absence of a major heat sink in this uncooled design.

In thermal analysis of uncooled or insulated engines, results pertaining to heat transfer and temperatures along the liner are of interest for purposes of assessing lubricant and materials behavior/durability, mode and extent of lubrication. A set of results is presented in Figures 29 to 32 which focus on the liner surface. The variation of liner mean surface temperature on the gas side with axial distance from the head, is shown in Figure 29, for the rated and peak torque conditions. Larger gas-side thermal loads for peak torque, offset lower frictional heat generation and cause higher temperatures up to the BDC piston position. Slightly higher temperatures for the rated condition are observed at the lower end of the liner, and these are due to larger skirt-liner frictional heat generation. Axial variation of cycle-mean heat fluxes associated with heat transfer from gas and piston and to crankcase air is plotted in Figures 30, 31, and 32, respectively. Gas-to-liner heat flux is shown to rapidly decay with distance from head due to coverage by the piston (Figure 30). The piston receives heat from the top portion of the liner, while it rejects heat to the lower part (Figure 31), a peak in liner-to-piston heat flux near the TDC ring reversal position. This corresponds to the higher levels of heat transfer at that location, associated with lower piston velocity and thus prolonged contact between rings and liner. The heat fluxes are higher for peak torque, due to higher liner temperatures, and due to lower ring temperatures caused by lower frictional heat generation.

Cyclic Transients in Surface Layers. The highly peaked heat flux into the combustion chamber surfaces produces large temperature swings within the surface layer. These swings are of concern for ceramics because they introduce additional increase in wall temperature and because the stresses they produce may lead to fatigue problems. Cyclic surface temperature transients are calculated in IRIS for all engine surfaces exposed to the combustion gases. The cyclic transient conduction calculations are carried out concurrently with the steady-state calculations. The two are rigorously coupled via the steady-state boundary conditions by a second order correction term, which accounts for their effects on the mean heat flux rate.

The solutions for cyclic surface temperature transients presented here were obtained by numerically integrating the transient one-dimensional heat conduction equation over a 40-node non-uniform grid spanning a penetration depth defined as $(4\pi k/\rho c f)^{1/2}$ where f is the frequency of oscillations (RPM/120). The largest temperature swings occur on the piston cup base.

For the rated engine conditions, piston surface temperature swings of 36.5K occur on the cup base, with the minimum and the maximum occurring at -27 and 24 crank angle degrees, respectively (Figure 33). Temperature profiles within the piston are shown in Figure 34. Although the calculations were carried out with a grid extending up to the depth of 1.6 mm, the temperature oscillations were almost completely damped out at a depth of 1.1 mm. Variations in cyclic temperature transients with respect to position on the cup base were also investigated. It was found that the swing magnitude is the largest at the location where the local time-averaged surface temperature is the lowest. This occurs at the lowest point of the cup, and there the swing reached a value of 38.8K.

For the engine operating at peak torque, piston surface temperatures swings of 50.5K occur on the cup base, with the minimum and the maximum occurring at -21 and 24 crank angle degrees, respectively (Figure 35). This is 38% higher than the swings at the rated conditions, and this is due to the larger effective gas temperature and radiative and convective fluxes at peak torque, and due to their lower frequency. Temperature profiles within the piston at peak torque are shown in Figure 36. At the lowest point of the cup the swing amplitude was again the largest, reaching 54.4K.

Summary. In its insulated configuration, the ADRE was found to have about 65 percent lower in-cylinder heat rejection than in the standard cooled configuration. As a result of the silicon nitride cap/air gap design, the peak time-average temperatures of the piston rose to over 1000K, reaching 1220K at peak torque. Including the effects of cyclic temperature swings, the maximum surface temperature on the piston reached almost 1260K at peak torque. The temperatures were substantially lower towards the edges of the press-fit piston cap. In the area of contact between the cap and the iron substructure, the maximum temperatures were less than 650K. The liner temperatures were on the order of 620-640K at the top of the liner, decreasing gradually by about 120K towards the bottom end. The calculated temperature field is available for thermal stress calculations, but they have been deferred until the next phase of the program.

VII. TRANSIENT THERMAL ANALYSIS OF PISTON/LINER ASSEMBLY (THERMAL SHOCK)

A sudden change in engine speed and load produces a change in the rate of heat flux from in-cylinder gases to the adjacent structural components. As a result, a thermal transient is produced in the components, which is sometimes referred to as thermal shock. This thermal transient generates a moving front of sharp temperature gradients which propagates through the structure and produces high local stresses. An associated effect is the creation of a moving distortion pattern. As a consequence of these effects, severe load/speed transients are considered to be highly adverse engine operating conditions which can lead to early material failures. This is particularly true in low heat rejection engines employing insulating materials. Thus it is important to analyze the temperature distributions in engine components during rapid engine transients, and seek in the solutions the conditions with the steepest temperature gradients. It is these conditions that can be more adverse than the maximum load conditions, and thus must be included in the consideration of the component durability.

Methodology Used in the Calculations. To simulate correctly the variation of gas-to-wall heat transfer during an engine transient, one has to track from a cycle-to-cycle, and on a crankangle resolved basis within a cycle, key charge parameters such as:

- mass trapped
- mean flow velocities
- turbulence level
- air/fuel ratio
- gas temperatures

All of these are required for the calculation of heat loads to the individual surfaces and components in the combustion chamber. These heat loads (their mean values as well as their time-variation) are the inputs, or boundary conditions, to the structure temperature calculations.

The parameters enumerated above are the same that need to be calculated for steady state conditions as well. However, during transients these parameters also depend on engine and turbocharger dynamics, which need to be simulated so that the time-dependent evolution of engine speed, turbocharger speed, intake plenum pressure and temperature, and exhaust plenum pressure can be calculated.

Engine speed dynamics is the result of the balance between brake torque, load torque imposed on the engine, and engine inertia. A sophisticated model of the load system can be constructed to provide dynamic values of T_{load} for particular applications under a variety of operating conditions. For studies of thermal shock, however, these dynamics may be more simply represented by an imposed ramp of engine load and speed, typical of the severe conditions brought about by sudden changes in engine fueling and/or load torque, and this is the approach taken here.

Turbocharger dynamics is the result of the balance between the turbine and compressor torques on one hand, and turbocharger inertia and friction on the other:

$$I_{TC} \frac{d\omega_{TC}}{dt} = T_{Turbine} - T_{Compressor} - T_{Friction} \quad (1)$$

The turbine and compressor torques are calculated using the usual quasi-steady approach, i.e., relying on the steady-state turbine and compressor maps at each instant of time. The friction torque is lumped into the turbine torque through an overall turbine efficiency. On decelerations during rapid load reductions, the compressor operating point may travel beyond the surge line for a brief period of time. The procedure used allows such excursions. A careful treatment of the compressor work during that period is required to obtain a smooth and consistent solution.

The air system consists of turbine, intercooler, intake and exhaust manifolds and compressor. The intercooler and intake plenum are treated in a quasi-steady fashion, but the exhaust manifold dynamics is treated by a filling and emptying dynamic model.

Simulated Engine Transient Event. Information on the simulated transient event was provided by DDA. The event is a segment in the federal smoke cycle for the ADE engine, shown in Figure 37. During the transient, the engine speed is linearly increased from 700 RPM to near-rated speed (1575 RPM) within 5 seconds, segment A'-B-C-D-E' in Figure 37. Steady-state idling at 700 RPM with no load is taken to be the operating condition before and up to the event. At point B where engine RPM starts increasing, a step increase in the requested fuel rate is also applied, which increases up to the full load fuel rate at 1575 RPM.

Simultaneously, a control algorithm is activated that limits actual fuel rate in order to maintain an air-fuel ratio at or above 22 to maintain smoke-free operation. The event lasts until the actual fuel rate reaches the full load rate at the final RPM level. Injection timing is advanced during the event linearly with the fuel rate from 4 degrees BTDC to 10 degrees BTDC. Also, the duration of injection increases depending on instantaneous fuel rate and engine RPM.

Engine and Turbocharger Transient Response. As for steady-state conduction, the transient finite element heat conduction methodology in IRIS is coupled to the transient engine simulation, producing the transient response of the engine and turbocharger simultaneously with transient component temperature distributions. The simulated event in rpm and fuel as well as engine air-fuel ratio and exhaust temperature responses are illustrated in Figure 38a. The event begins at 3 sec. The smoke limitation on air fuel ratio, active between 3.4 and 13 seconds in this case, causes a rather protracted (10 sec) fuel rate increase extending beyond the nominal end of the transient. The exhaust temperature is shown to overshoot during this period, and this is caused by the turbocharger lag. The long-term response of the same quantities (Figure 38b) shows that the air-fuel ratio response ends soon after the end of the fuel event, but exhaust temperature gradually rises by about 25°K to its final steady-state level within the next 4 minutes. This is caused by the slower response of structure temperatures and thus of in-cylinder

heat transfer. Turbocharger lag and structure thermal response are therefore seen to be the two key factors controlling short term (seconds) and long term (minutes) response of the engine. The turbocharger response is more closely examined in Figure 39a (short term) and 39b (long term). In the short term response, the turbocharger is shown to take about 20 seconds to complete the initial acceleration toward its final steady state speed. This long turbocharger response is due to the turbocharger inertia, which was set to 0.0009 kgm^2 . At the start of the event, turbine efficiency drops as the exhaust temperature suddenly increases causing the turbine operating point to move away from the peak efficiency point on turbine map efficiency curves. The initial rise in turbocharger rpm is followed by residual acceleration, caused by the "tail" in the exhaust temperature and turbine intake pressure responses. The responses of engine, turbine and power turbine pressures are shown in Figure 40. In the short term, they exhibit characteristics consistent with response of turbocharger RPM. The long term is governed by the structure thermal response.

In summary, the results indicate the presence of two time scales. The first is the time scale of about 20 seconds is associated with the short-term response (turbo-lag). The second time scale is on the order of minutes and is associated with the structure thermal response. For quantities affected by the structure thermal response, about 90% to 95% of the total transient is achieved relatively quickly during the first time scale, but the rest of the response is complete (99%) only after 5 minutes from the beginning of the event.

Gas-to-Wall Heat Transfer and Structure Thermal Response. During transient simulation, engine quantities affecting gas-to-wall heat transfer are tracked by gas-to-wall heat transfer models, on a crankangle by crank angle basis. Figure 41 shows the transient history of cycle-mean convection heat transfer coefficients on the three piston surfaces (cup base, cup side and crown). During the early response, heat transfer coefficient histories reflect fuel rate variation. In this period when RPM and engine pressure are increasing but are still low, the dominant effect on heat transfer coefficients is fuel injection-related turbulence in this low-swirl engine. The long term history of heat transfer coefficients indicates a decay after an early overshoot; the decay is related to the effect of the increasing wall temperatures on the thermal boundary layer properties.

Radiant heat fluxes and friction heat generation rates are also tracked during the transient, so that correct instantaneous boundary conditions for transient heat conduction calculations can be computed. Similarly the special submodels for air gap heat transfer are integrated in the transient mode. The history of air temperature in the two air gaps is illustrated in Figure 42, which shows the temperature of air in the "dome" remains consistently above that of the air inside the thin gap.

The transient thermal response of the combustion chamber surfaces of the ADE engine may be observed through the histories of temperature on four selected finite element nodes on the piston-liner assembly given in Figure 43.

The predicted history of the entire temperature field for the FEM model is also stored at selected time steps. Contour plots in Figure 44 show temperature distribution in the silicon nitride cap of the ADE engine piston at several instants during the transient simulation. Results indicate the presence of a relatively mild thermal shock (concentration of isotherms in contour plots) compared to those that would be produced by monolithic zirconia which has conductivity up to 10 times lower than silicon nitride. The thermal shock is also somewhat dampened by the relatively long (20 sec) turbocharger lag. However, there is still a discernible increase in surface temperature gradients between cycles 40 and 500, which may be expected to cause compressive thermal stresses exceeding those at the final steady-state.

Summary. A simulation was carried out of a transient engine response along an increasing load/speed trajectory taken from the Federal smoke cycle. The response was found to have two time scales: a short term and a long term. The former is associated with the air system and turbocharger response and is on the order of 5-20 seconds. The latter stems from the much slower structure warmup, and it extends over a period of 10 minutes. During the transient there is temporary steepening of temperature gradients near the piston surface at the bottom corner of the bowl noticeable between 5 and 15 seconds into the transient. The stresses arising during this period (thermal shock) are of great interest, as they may exceed the full load values. The stress analysis of the generated transient temperature fields is planned, and will be carried out in Phase II.

REFERENCES

R. Chute (1985), "Pressure Compounding a Four Cycle Diesel Engine," SAE Paper 851520.

R. H. Miller (1946), "Supercharging and Internal Cooling Cycle for High Output," ASME Paper 46-OGP-4.

T. Morel, R. Keribar, P. N. Blumberg and E. F. Fort (1986), "Examination of Key Issues in Low Heat Rejection Engines," SAE Paper 860316.

	Rated		Peak torque			Part Load		
	Orig	best 60	Orig	best 60	best 60R*	Orig	best 60	best 60R*
Valve timing IVC	standard	-168	standard	-168	-168	standard	-168	-168
EVO	-	118	-	118	130	-	118	126
IVO	-	368	-	368	368	-	368	368
EVC	-	352	-	352	352	-	352	352
BHP	293.7	297.5	247.2	246.9	247.6	187.3	190.3	190.4
Pumping (psi)	16.2	14.8	1.1	0.4	1.8	14.0	13.2	13.7
Friction (psi)	21.3	20.8	20.3	20.3	20.4	17.4	17.1	17.1
BSFC	0.2586	0.2553	0.2561	0.2563	0.2556	0.2706	0.2663	0.2660
Air-fuel ratio	29.0	29.1	24.5	24.1	24.2	35.2	35.7	35.8
η_v	0.807	0.871	0.861	0.893	0.893	0.803	0.869	0.869
Peak pressure (psi)	2220	2151	2412	2396	2404	1704	1658	1660
Ign. delay (CA)	2.3	2.5	1.6	1.6	1.6	3.0	3.2	3.2
Compressor PR	2.55	2.37	2.47	2.34	2.34	2.04	1.91	1.91
Turbine PR	1.76	1.68	1.64	1.56	1.56	1.60	1.53	1.53
Power turbine PR	1.65	1.66	1.34	1.33	1.33	1.49	1.49	1.49
T _{exhaust man.} (K)	913	904	951	959	954	809	799	798
NOX (ppm)	1634	1640	2372	2371	2373	1106	1116	1114
BSNOX (g/hp-hr)	6.0	5.9	7.1	7.0	6.5	5.1	5.1	5.1
Soot (g/m ³)	0.023	0.023	0.013	0.014	0.013	0.019	0.019	0.018
T _{avg} (K)	1735	1732	1901	1911	1909	1592	1583	1582
T _{max} burned (K)	2855	2857	2890	2890	2890	2793	2802	2802

Table I. Engine performance with conventional and electronically controlled valves. Engine equipped with power turbine and Rankine cycle bottom

* Best 60° ramp as determined under peak torque and part load, respectively.

PUB6-H(7/86)

	Baseline	Early IVC Std BOI	Early IVC Advanced BOI
IVC	-168	-255	-255
EVO	126	126	126
BOI	-10.4	-12.0	-19.0
BHP	254.5	258.0	263.9
Pumping (psi)	-1.8	11.4	13.0
Friction (psi)	20.5	19.9	20.2
BSFC	0.2985	0.2945	0.2878
Air-fuel ratio	29.2	29.2	29.1
η_v	0.896	0.482	0.480
Peak pressure (psi)	2135	1993	2302
Ign. delay (CA)	2.6	4.2	6.3
Comb. start (CA)	-7.8	-7.8	-12.7
T _{exhaust}	864	867	856
T _{avg. max.}	1743	1646	1714
T _{burned max.}	2867	2786	2825
Compressor PR	2.32	4.26	4.26
Turbine PR	1.63	2.89	2.94
NOX (ppm)	1776	1208	1706
BSNOX (g/hp-hr)	7.2	4.9	7.0
Soot (g/m ³)	0.025	0.032	0.020

Table II. Comparison of engine performance with conventional valves and early closing EC valves. The latter concept incorporates increased boost, produced by a higher backpressure turbocharger turbine. Engine at rated fuel rate, 1800 RPM, no exhaust heat recovery devices.

	IVC	Comp PR	Turbo PR	TCPD PR	Recip. HP	TCPD HP	ORCB HP	Total HP	BSFC
Baseline	-168	2.37	1.69	1.65	232.1	31.1	27.3	290.5	0.2614
	-180	2.37	1.72	1.66	231.3	31.3	27.6	290.2	0.2617
	-200	2.57	1.78	1.65	232.7	30.5	26.6	289.8	0.2621
	-220	2.96	1.98	1.64	234.1	29.7	25.7	289.5	0.2623
	-235	3.49	2.29	1.64	236.7	28.8	23.8	289.3	0.2625
	-250	4.21	2.67	1.64	232.6	28.4	23.3	284.3	0.2671
	-260	5.03	3.15	1.64	229.5	27.8	22.3	276.1	0.2751

Table III. ADRE with Early IVC -- Optimization of IVC Timing

	IVC	Comp PR	Turbo PR	TCPD PR	Recip. HP	TCPD HP	ORCB HP	Total HP	BSFC
Baseline	-168	2.37	1.69	1.65	232.1	31.1	27.3	290.5	0.2614
no TCPD	-168	2.29	1.0 [*]	1.0	264.4	0.0	-	264.4	0.2872
original TCPD	-168	2.32	1.10	1.65	250.5	31.4	-	281.9	0.2694
	-168	2.32	1.10	1.91	244.8	40.5	-	285.3	0.2662
	-168	2.35	1.12	2.25	237.3	50.8	-	288.1	0.2636
	-168	2.38	1.13	2.50	232.1	57.7	-	289.8	0.2620
optimum	-168	2.40	1.14	2.80	225.3	65.4	-	290.7	0.2612
	-168	2.41	1.15	2.92	222.6	67.9	-	290.5	0.2614
	-168	2.47	1.16	3.78	204.9	83.1	-	288.0	0.2637

* excess ORCB power

Table IV. ADRE Equipped with ORCB-driven Compressor -- Optimization of Power Turbine Pressure Ratio

	IVC	Comp PR	Turbo PR	TCPD PR	Recip. HP	TCPD HP	ORCB HP	Total HP	BSFC
Baseline	-168	2.37	1.69	1.65	232.1	31.1	27.3	290.5	0.2614
original TCPD	-235	3.35	1.48	1.65	259.5	29.6	-	289.1	0.2627
	-235	3.39	1.52	1.86	252.6	37.0	-	289.6	0.2622
	-235	3.41	1.53	2.13	244.4	44.7	-	289.1	0.2627

Table V. ADRE with Early IVC and ORCB-Driven Compressor -- Optimization of Power Turbine Pressure Ratio at IVC = -235°

Table VI. Performance Data for ADRE at Two Operating Conditions

	Rated	Peak Torque
RPM	1800	1200
Fuel rate (kg/hr)	34.46	28.71
BOI (°CA)	-10.	-10.
BHP-rec (HP)	232.7	200.9
BHP-TCPD (HP)	32.0	12.6
BHP-ORCB (HP)	28.3	26.2
BHP-total (HP)	293.0	239.7
BSFC (#/HP-hr)	0.259	0.264
A/F ratio	28.9	22.6
p_{max} (bar)	150.6	157.2
Friction (bar)	1.33	1.27
Friction (HP)	22.7	14.4
Volumetric efficiency	0.856	0.866
Compressor PR	2.38	2.23
Turbine PR	1.67	1.56
Power turbine PR	1.65	1.33
Turbocharger efficiency	0.64	0.56
Power turbine eff.	0.74	0.69
In-cylinder heat transfer (kW)	3.18	3.96
(% fuel energy)	4.64	6.95
piston (%)	48.	47.
head (%)	29.	28.
liner (%)	23.	25.
Structure Temperatures:		
Piston-peak (K)	1084	1220
Liner-peak (K)	625	641
Exhaust Temperatures:		
turbine inlet (K)	913	989
power turbine inlet (K)	826	909
RCB inlet (K)	752	866

	Rated Condition				Peak Torque			
	\bar{h}_g W/m ² K	\bar{T}_g K	\bar{q}_{rad} W	$\frac{\int h_g T_w}{\int h_g}$ K	\bar{h}_g W/m ² K	\bar{T}_g K	\bar{q}_{rad} W	$\frac{\int h_g T_w}{\int h_g}$ K
Cup base	739	1085	291	7.0	647	1219	398	11.2
Cup side	564	1043	100	5.1	483	1181	144	9.0
Piston crown	577	949	52	2.0	467	1048	94	3.2
Liner top 1/6	351	828	57	0.2	273	946	87	0.6
Liner next 1/3	250	663	4	0.0	183	744	9	0.1
Liner next 1/2	209	569	0	0.0	147	615	0	0.1

Table VII. Cycle-averaged heat transfer parameters used as boundary conditions in steady-state heat conduction calculations.

	Rated Condition	Peak Torque
Peak ceramic temperature, °K	1084	1220
Peak metal temperature, °K	625	641
Liner temperature, °K (@ top ring reversal)	625	637
Liner temperature, °K (1/3 of stroke)	586	590
Air temperature, air "dome", °K	718	763
Air temperature, air gap, °K	687	717
Heat transfer rate to piston, W	1530	1860
Heat transfer rate to liner, W	727	986

Table VIII. Summary of key results from steady-state heat conduction calculations.

1800RPM/300HP -- 60 DEG RAMPS
VALVE EFFECTIVE AREA (INTO CYL.)
EXHST. (—), INTAKE (.....)

ITI/IRIS (->)

602

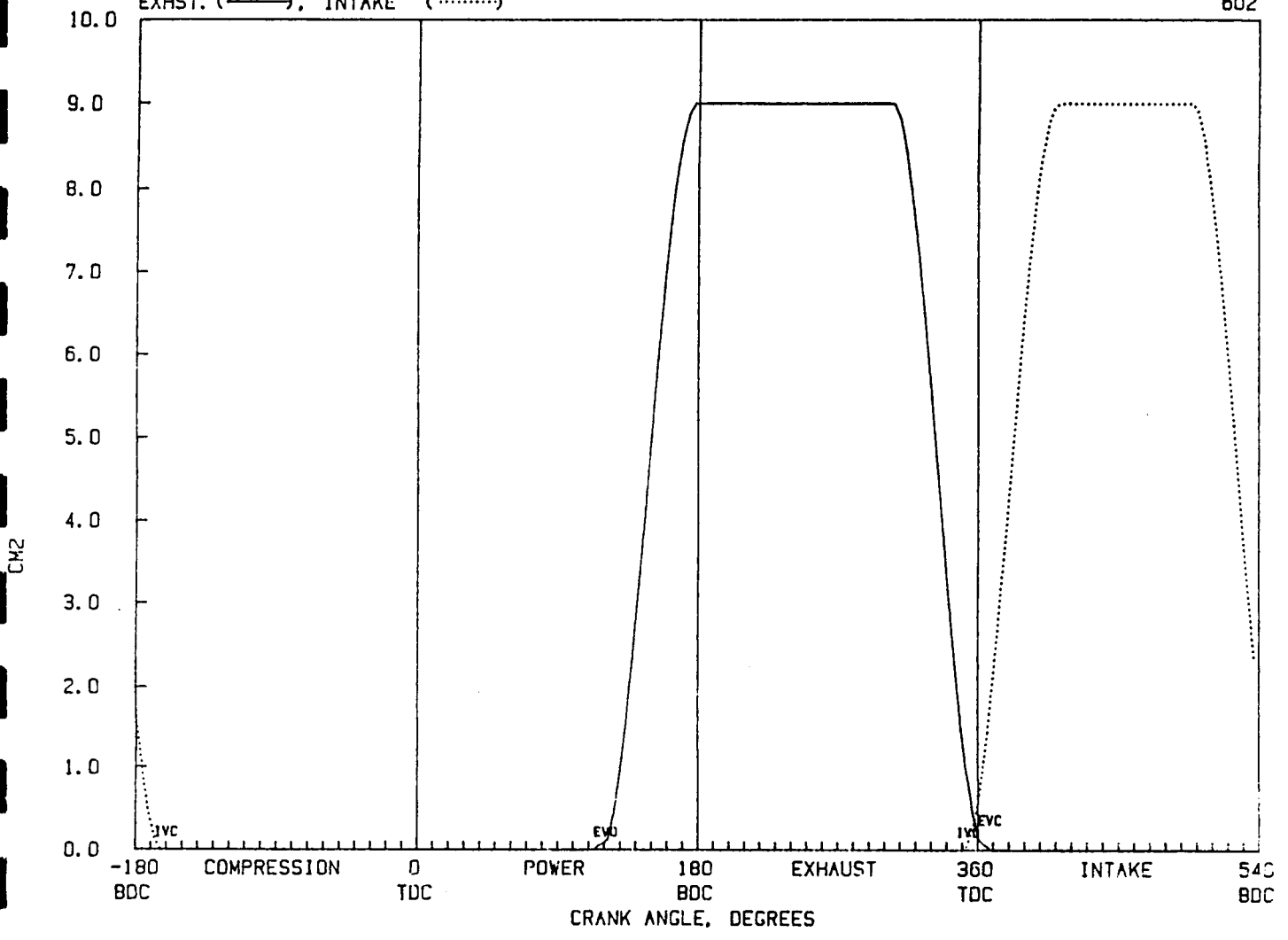


Figure 1. Intake and exhaust events showing 60° sinusoidal valve opening and closing ramps.

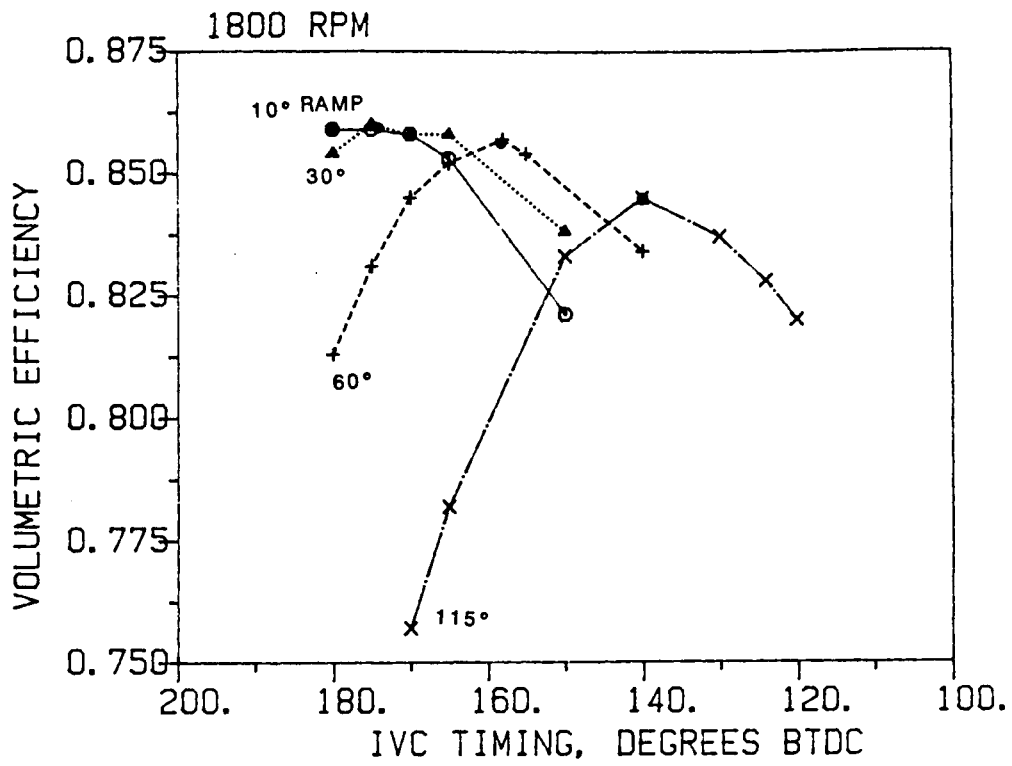


Figure 2 . Variation of volumetric efficiency with intake valve closing angle at various ramp durations - 1800 RPM, fixed plenum conditions.

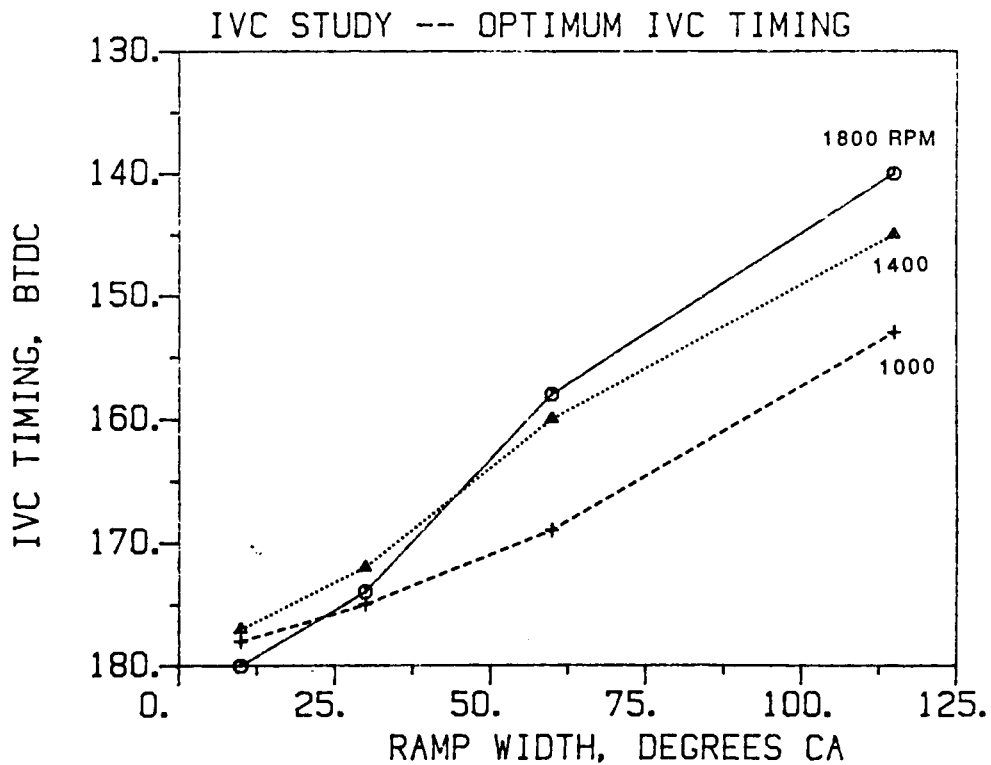


Figure 3. IVC timing for maximum volumetric efficiency as a function of ramp duration and engine speed (data of Figure 2).

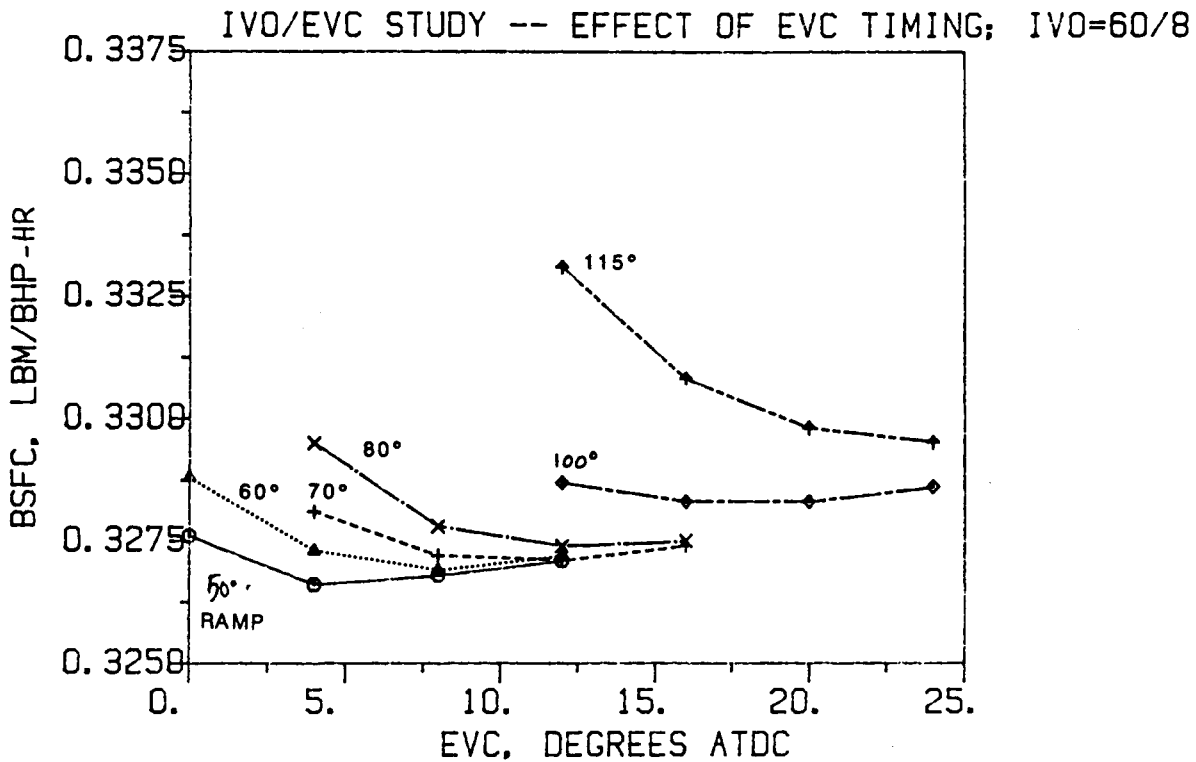


Figure 4 . Variation of reciprocator BSFC with exhaust valve closing angle at various ramp durations (1800 RPM; IVO fixed at 8° BTDC and 60° ramp duration; fixed plenum conditions).

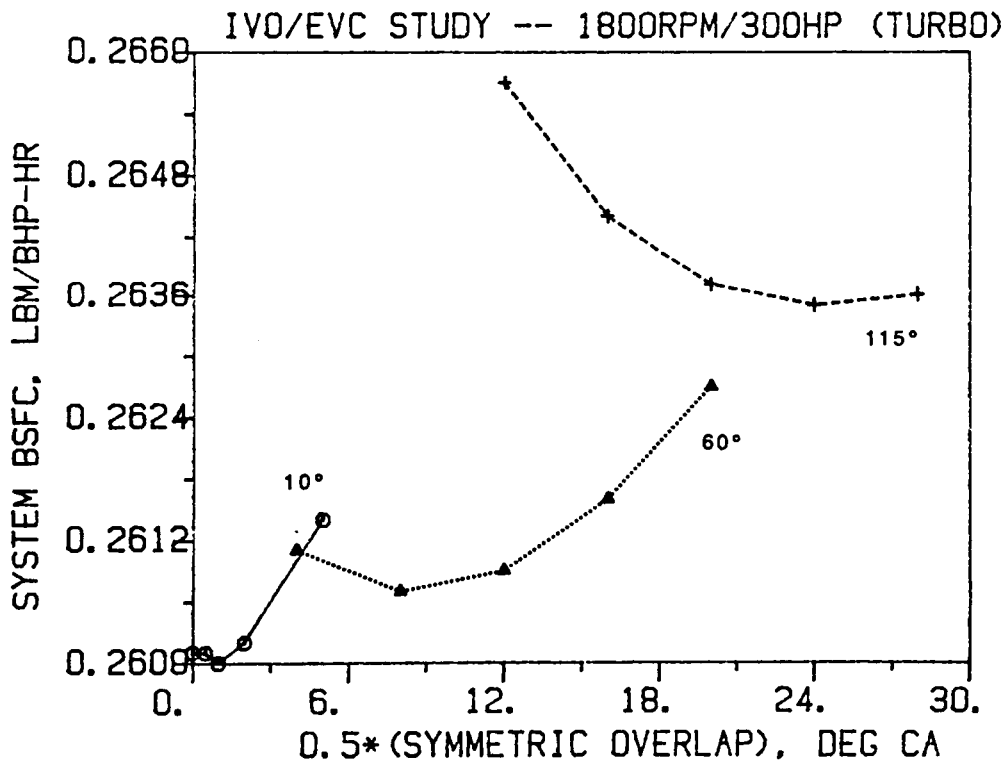


Figure 5a. Variation of system BSFC with valve overlap duration at various ramp durations (1800 RPM; full turbocharger simulation).

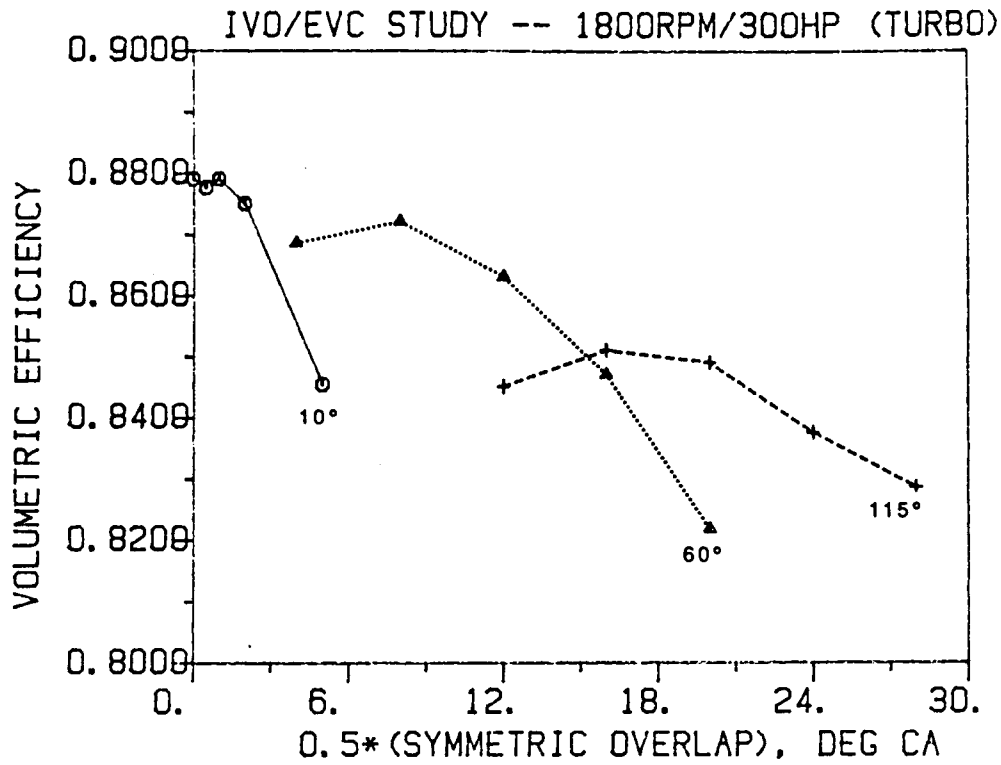


Figure 5b. Variation of volumetric efficiency with valve overlap duration at various ramp durations (1800 RPM; full turbocharger simulation).

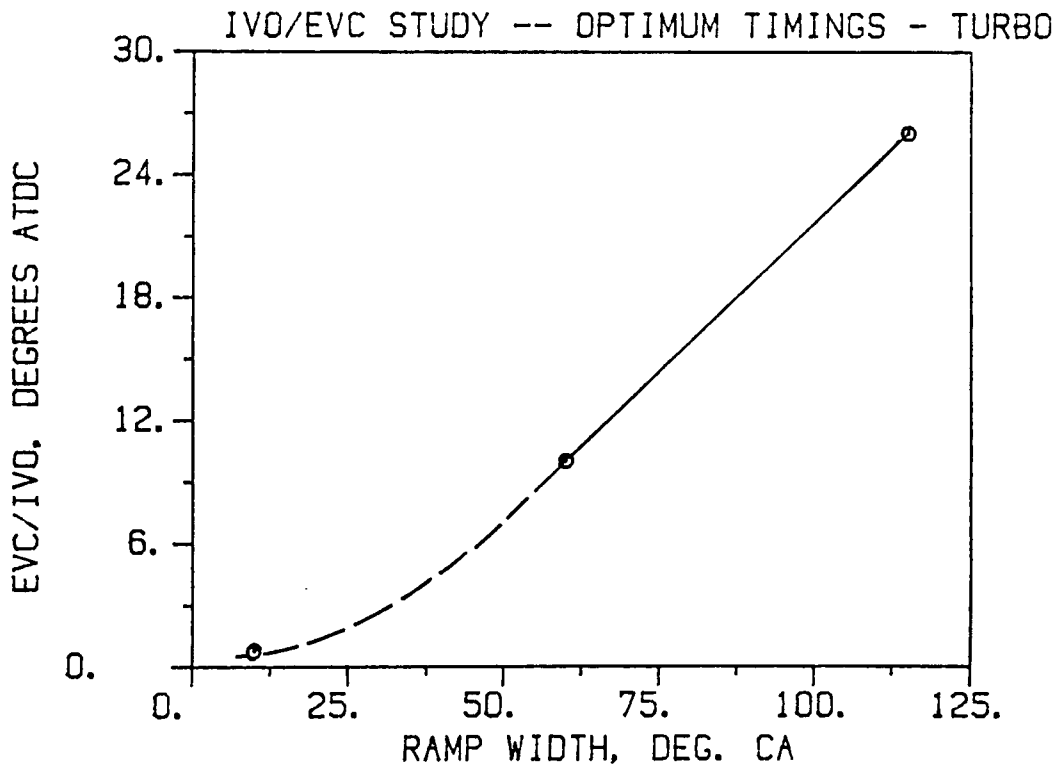


Figure 6 Half overlap duration for best BSFC versus valve event ramp duration (data of Figure 7).

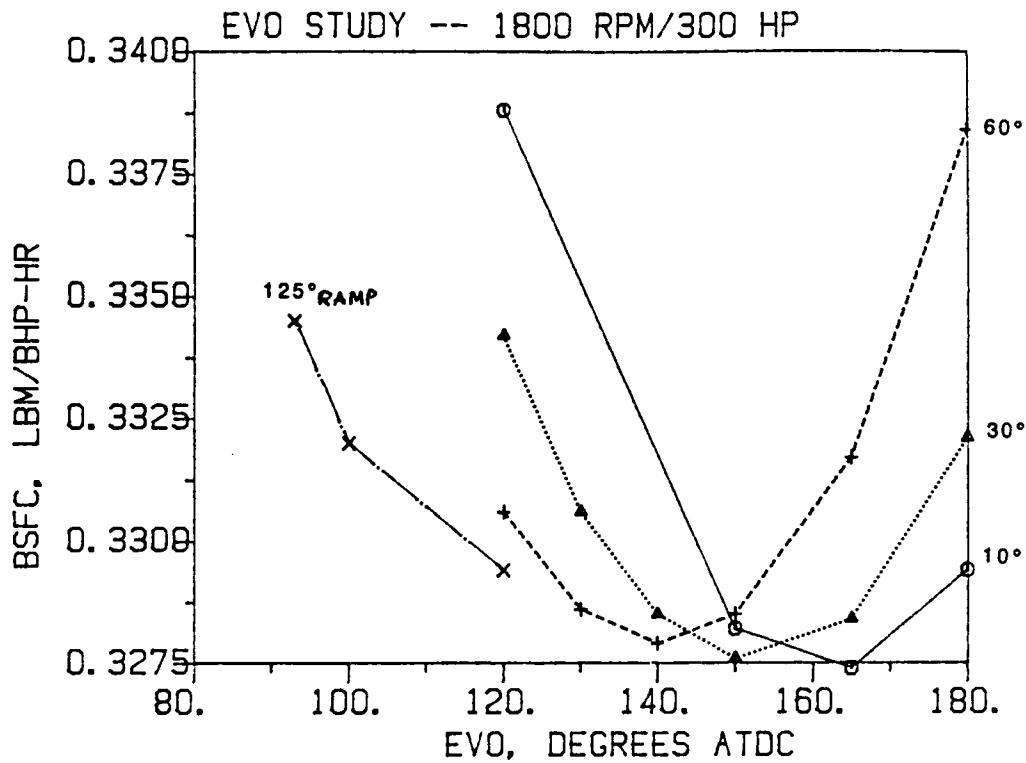


Figure 7. Reciprocator BSFC versus exhaust valve opening angle at various ramp durations (1800 RPM; fixed plenum conditions).

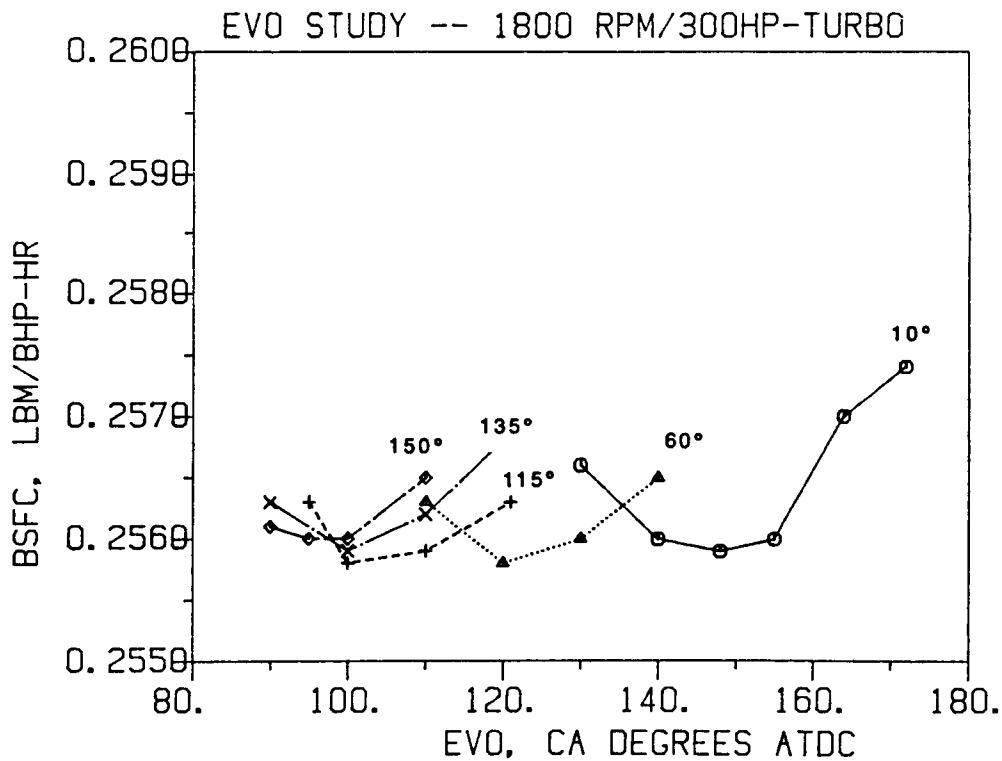


Figure 8. System BSFC versus exhaust valve opening angle at various ramp durations (1800 RPM; full turbocharger simulation).

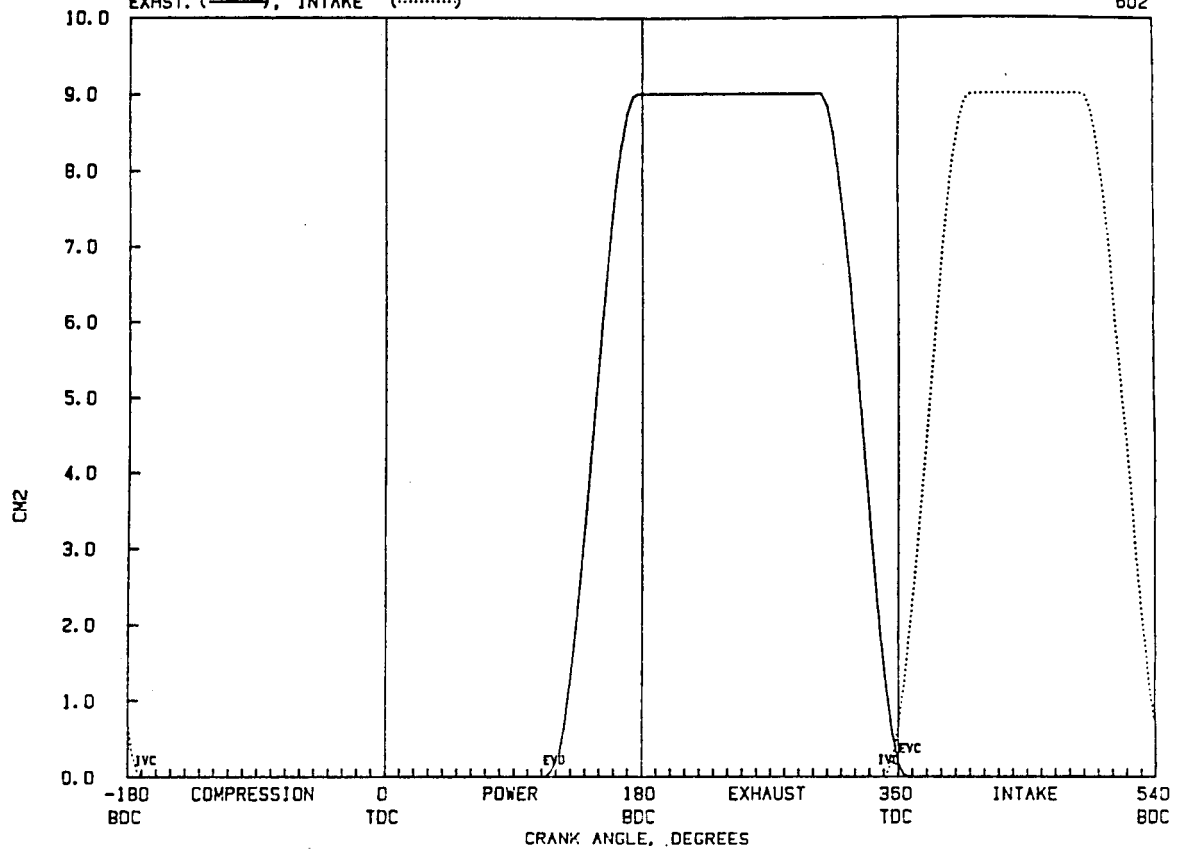


Figure 9a. Effective valve area profiles for ECVs with 60° ramp durations, optimized for operation at rated conditions.

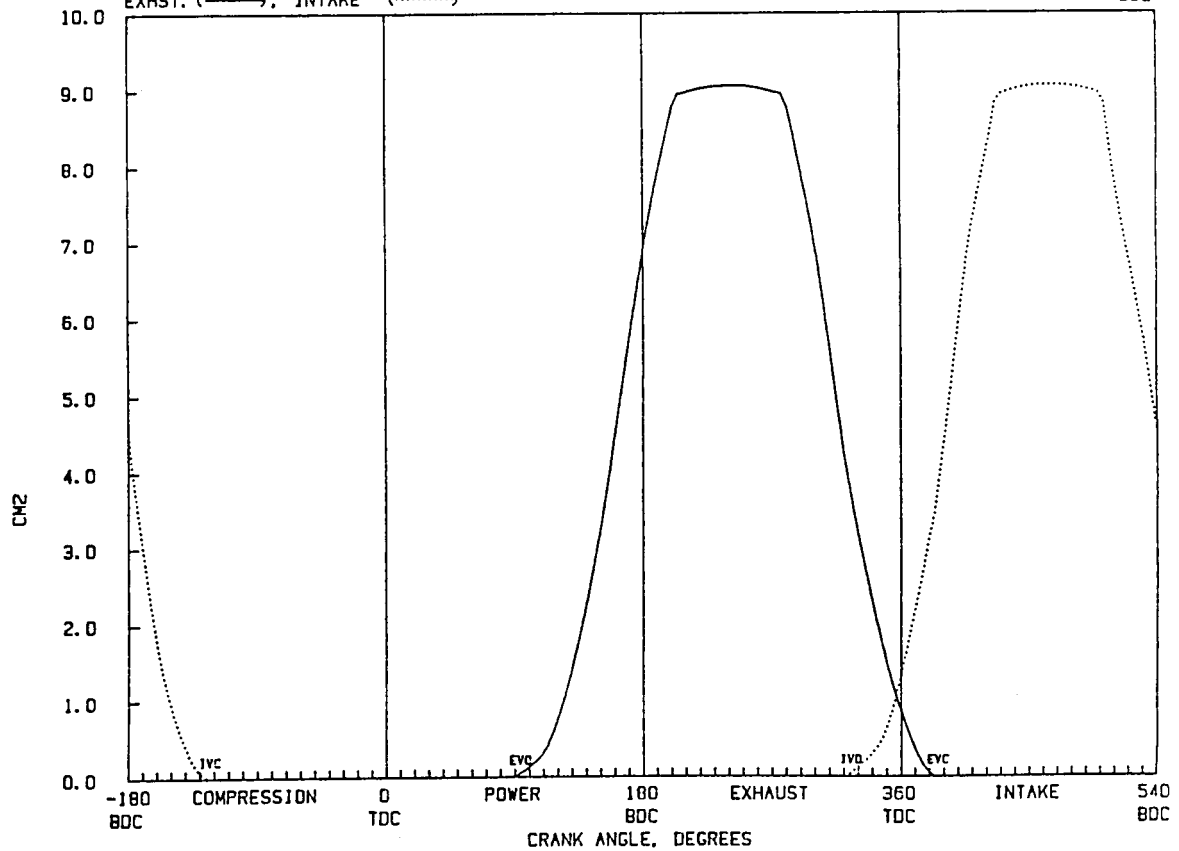


Figure 9b. Effective valve area profiles supplied by DDA.

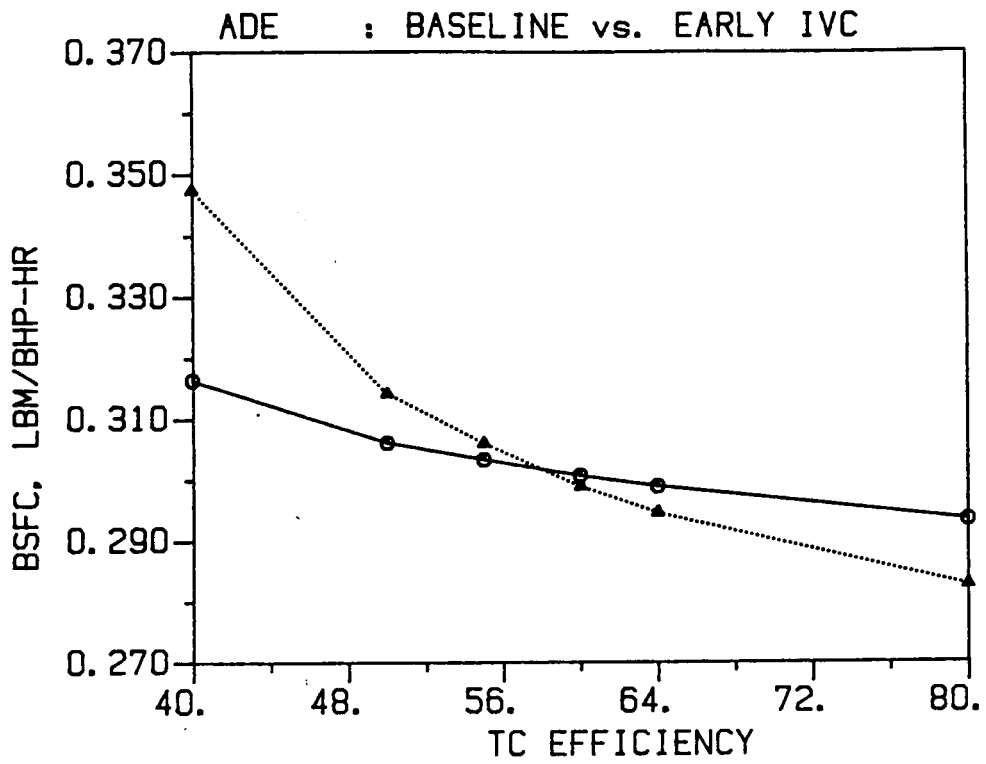


Figure 10 . Fuel consumption as a function of turbocharger efficiency for an ADRE engine: — baseline turbocharged engine, --- same engine with early IVC.

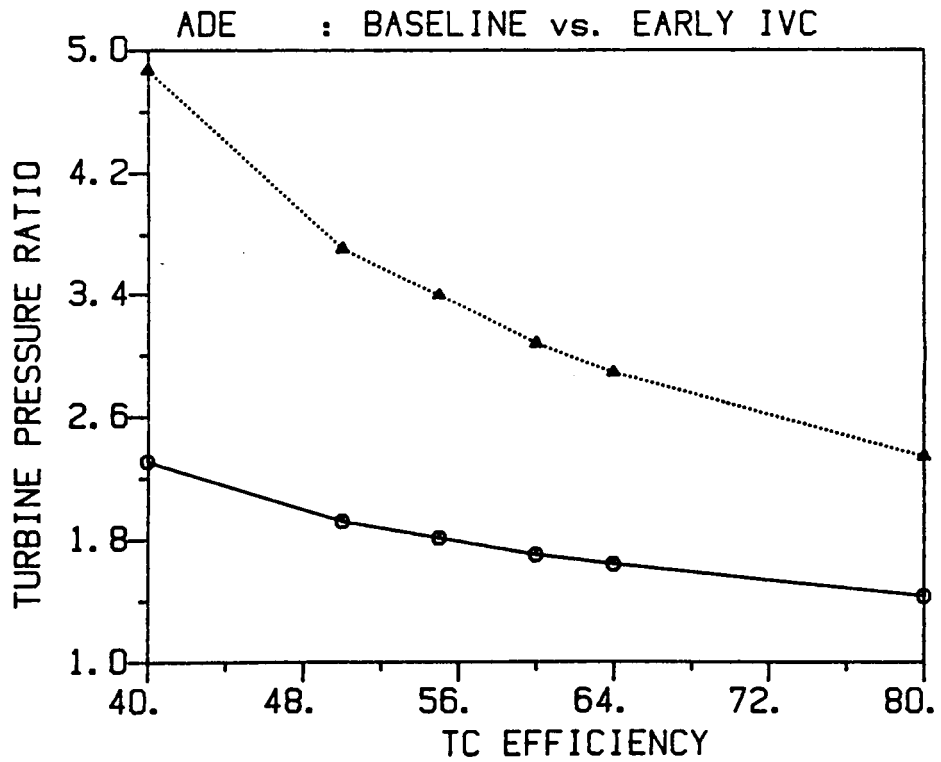


Figure 11. Turbocharger turbine pressure ratio as a function of turbocharger efficiency for an ADRE engine: — baseline turbocharged engine, --- same engine with early IVC.

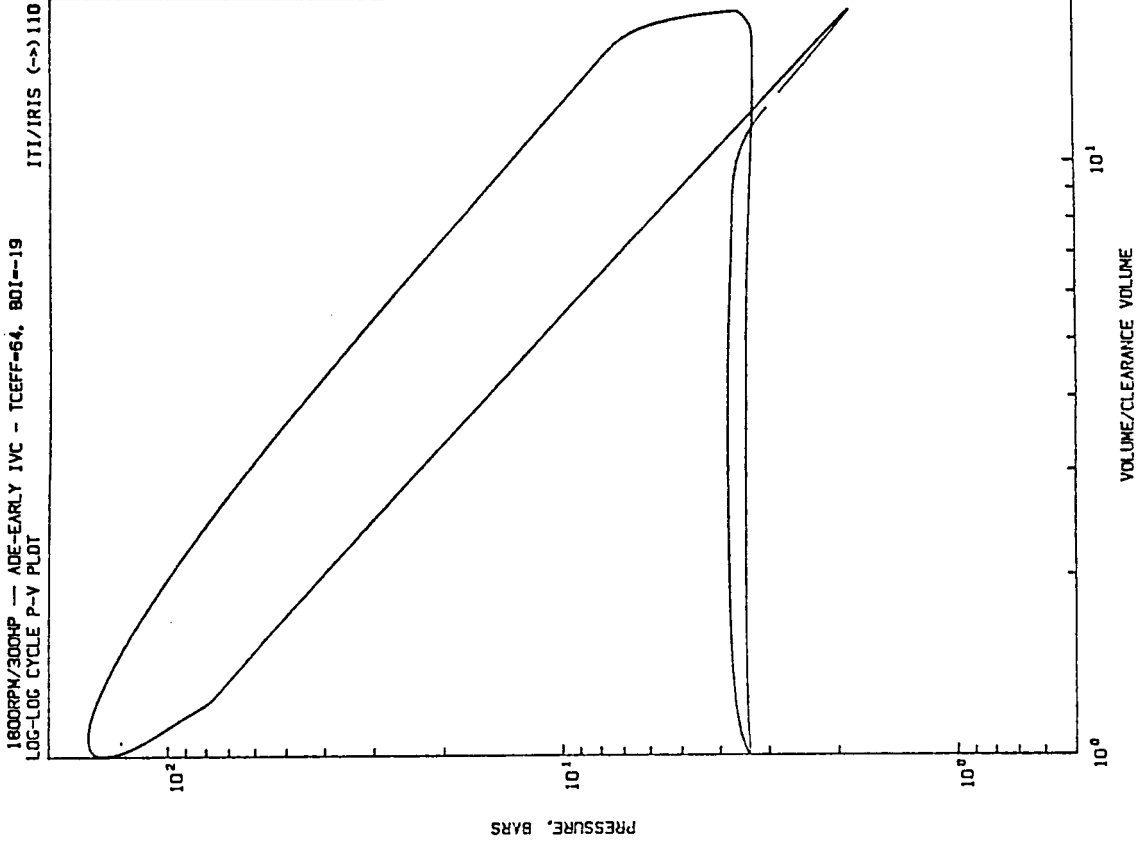


Figure 12b. Pressure-volume diagram, ECVs with early intake valve closing.

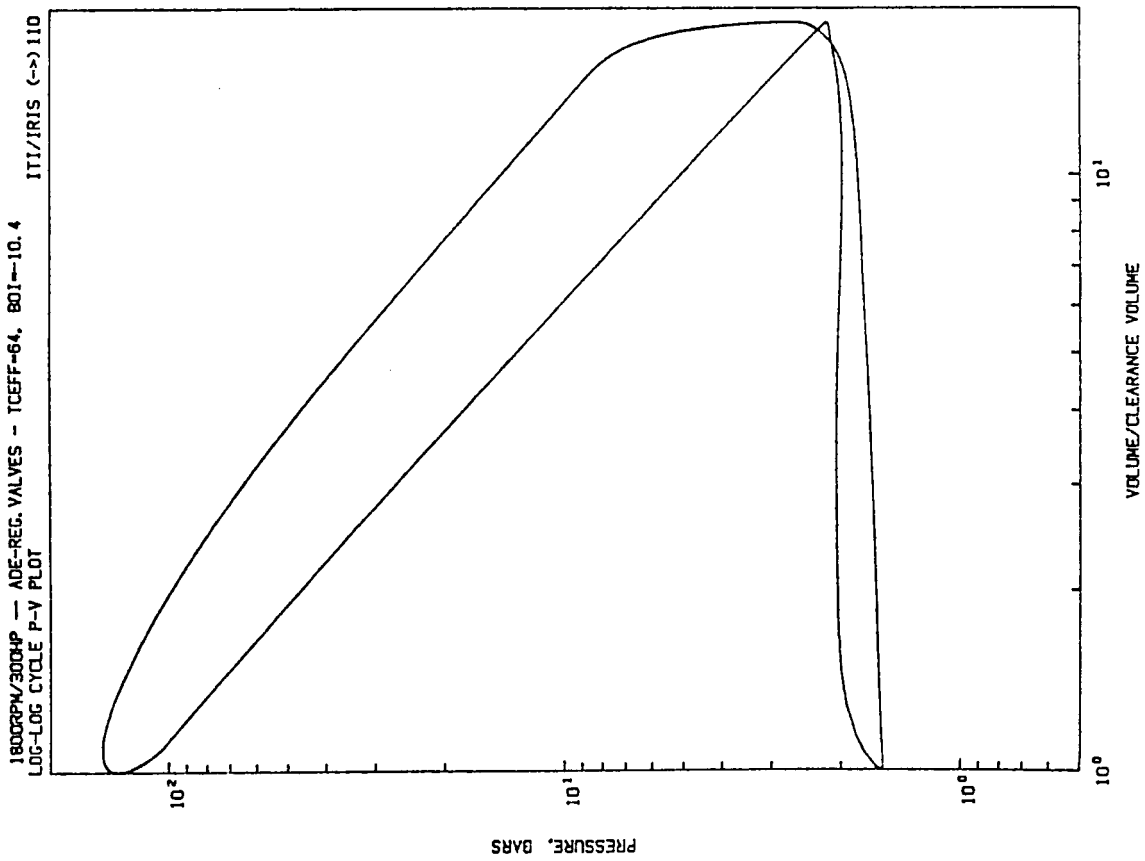


Figure 12a. Pressure-volume diagram, ECVs optimized for conventional valve timing schedules.

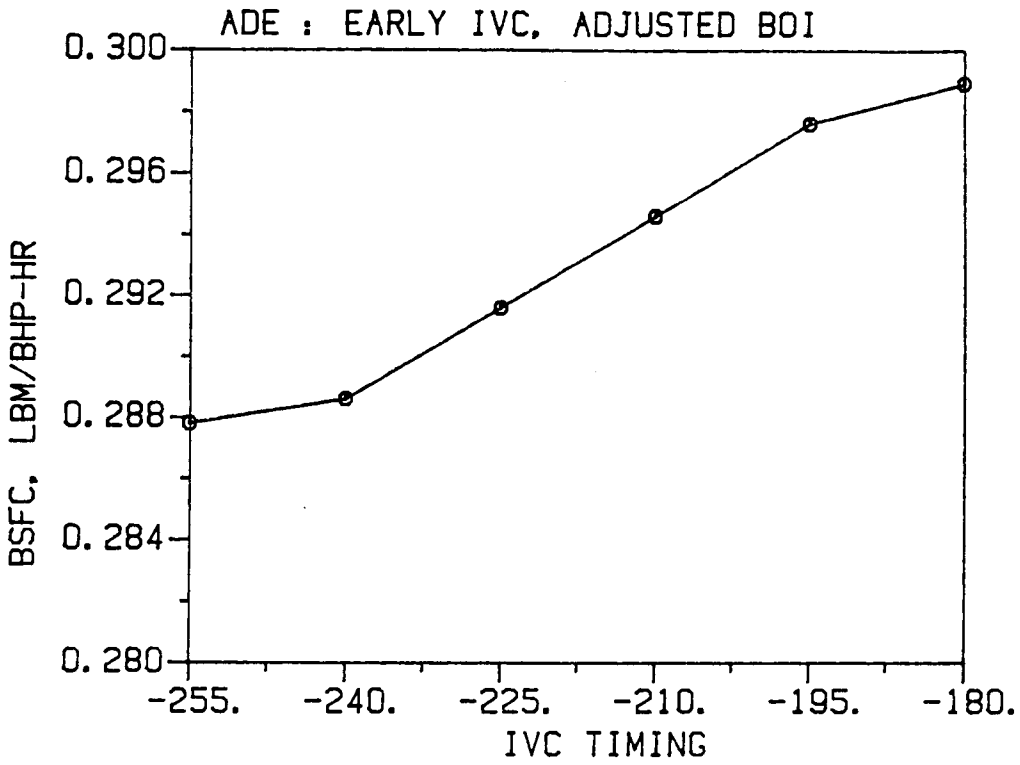


Figure 13 . Fuel consumption for a TC engine with no exhaust heat recovery as a function of IVC timing. Timing of BOI adjusted for constant NO_x emissions; constant A/F ratio.

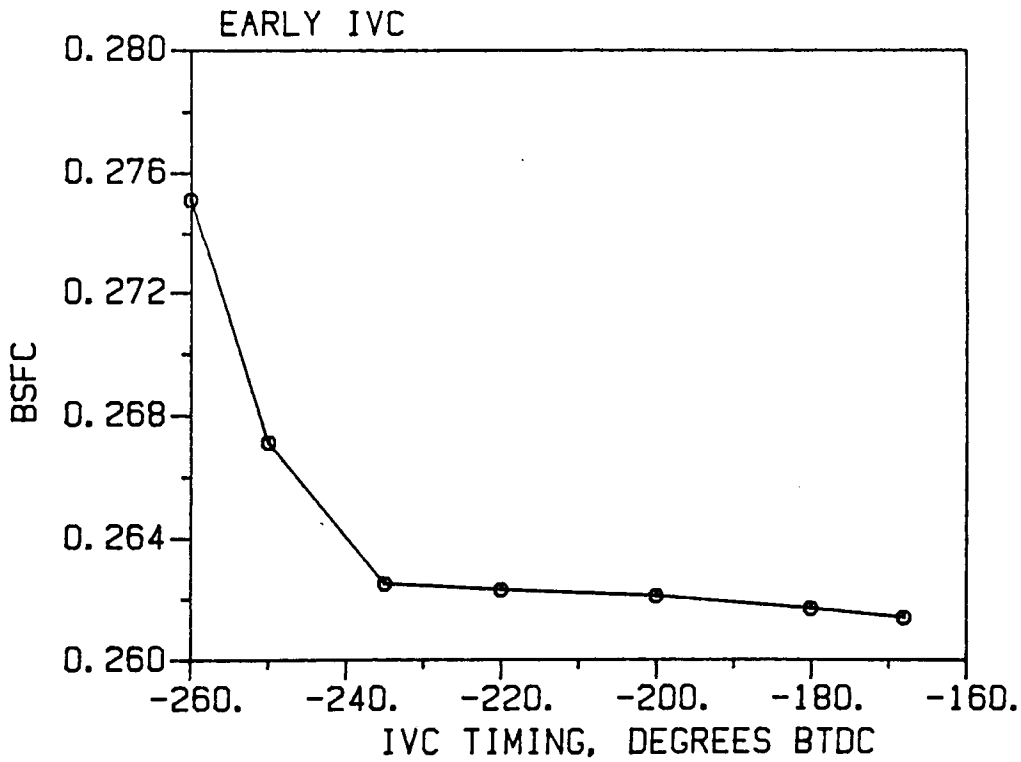


Figure 14a. Fuel consumption of the ADRE engine (with power turbine and RCB bottomer) as a function of IVC timing. Timing of BOI adjusted for constant peak firing pressure; constant A/F ratio.

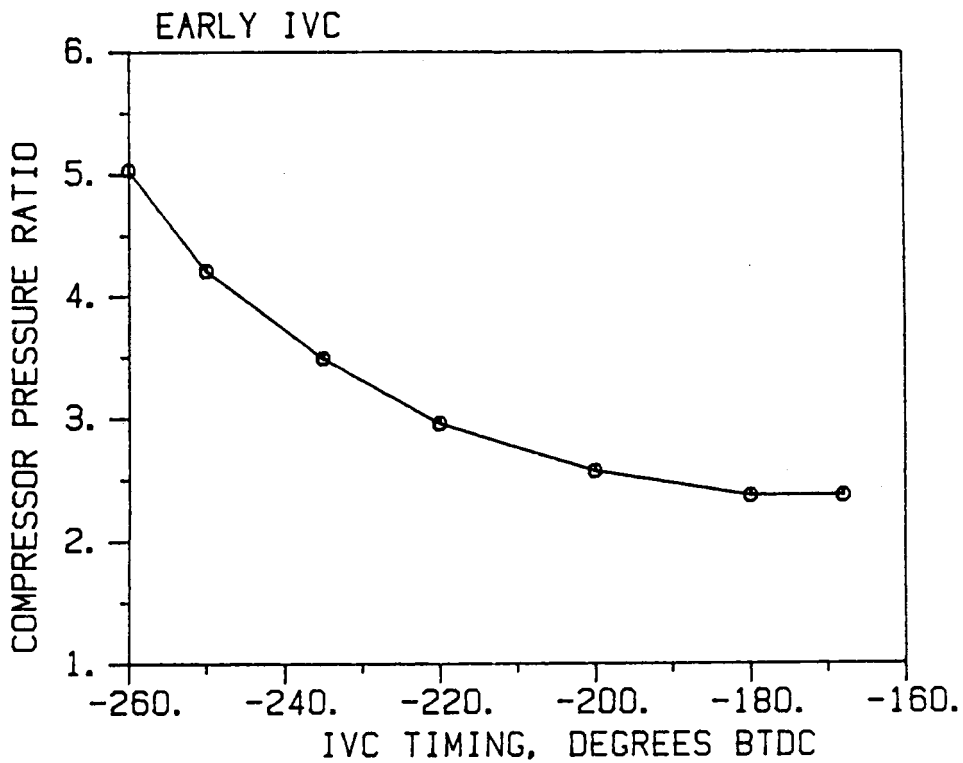


Figure 14b. Compressor pressure ratio of the ADRE engine as a function of IVC timing.

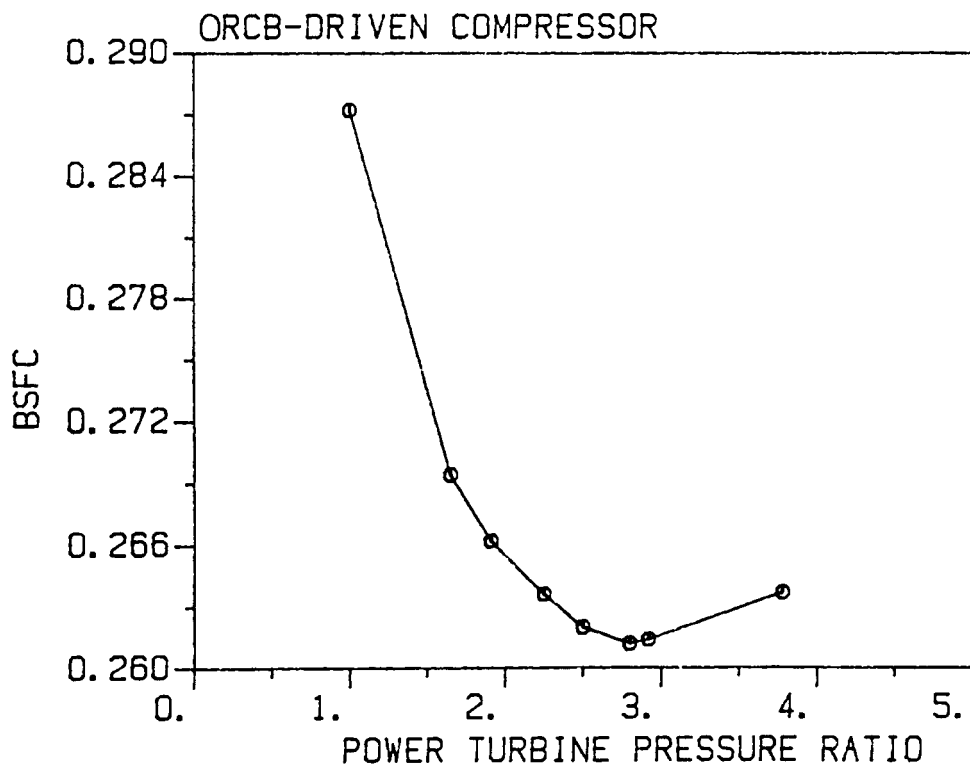


Figure 15. Effect of power turbine pressure ratio on the fuel consumption of the ADE engine, with ORCB power used to drive the compressor rather than the engine shaft.

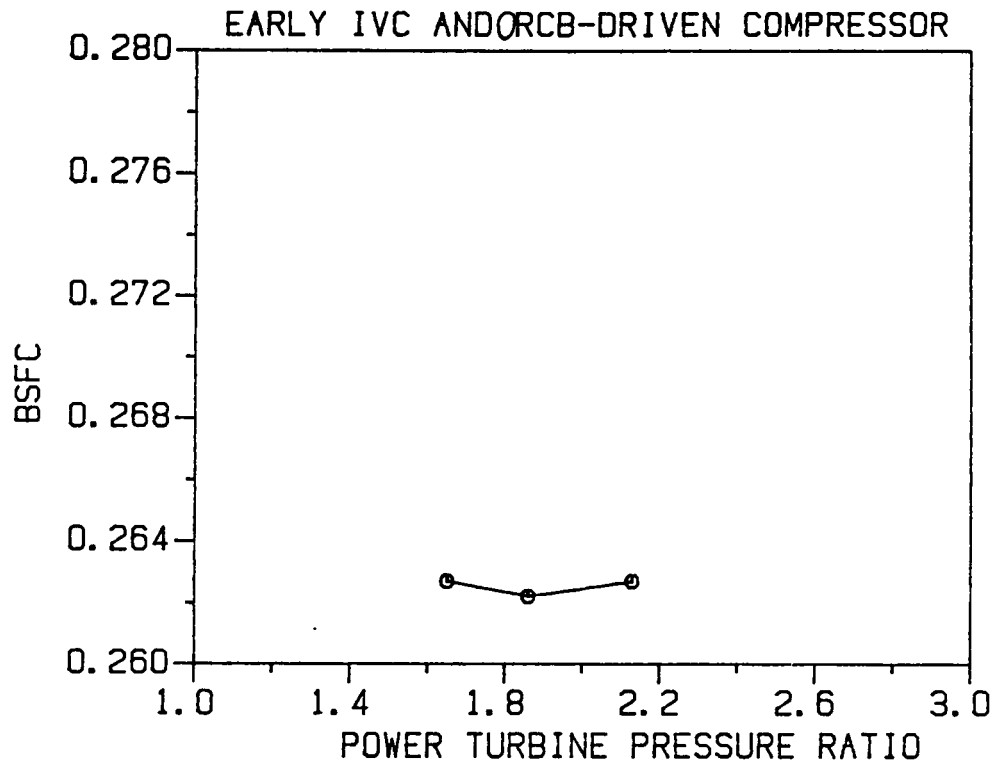


Figure 16. Effect of power turbine pressure ratio on the fuel consumption of the ADRE with early valve closing (IVC = -235°) and ORCB-driven compressor.

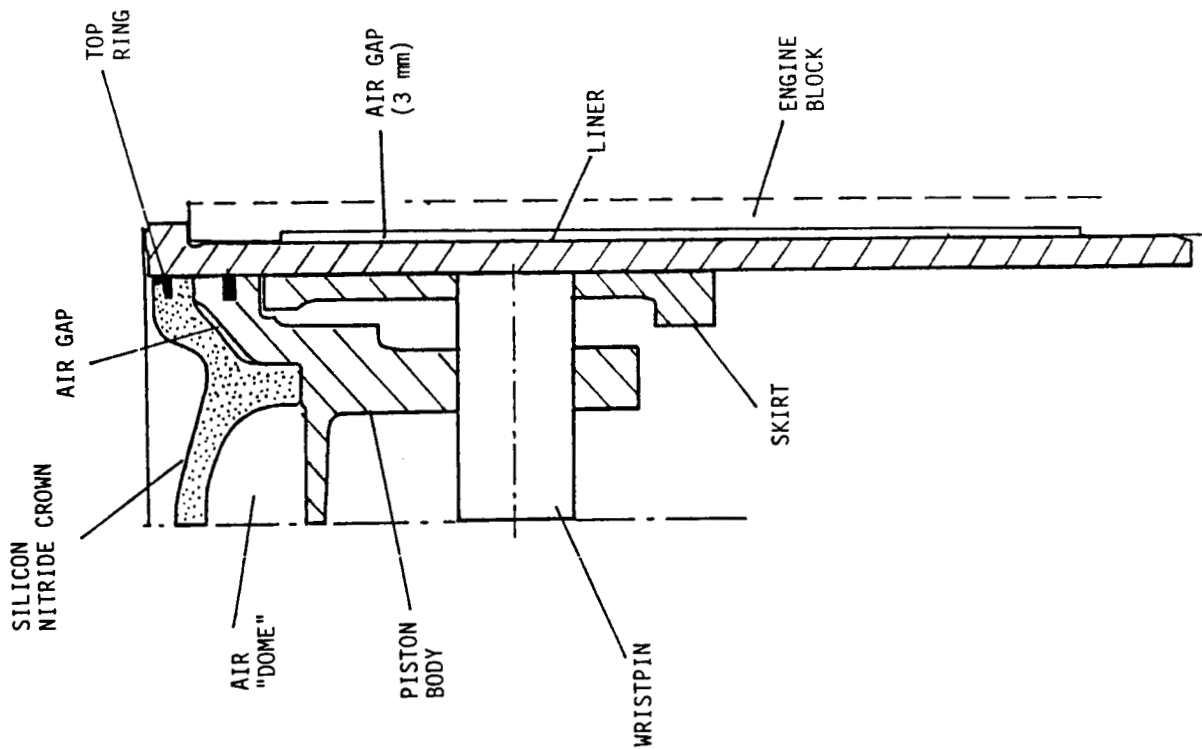


Figure 17. Cross-section of adiabatic diesel engine (ADRE) piston-liner assembly.

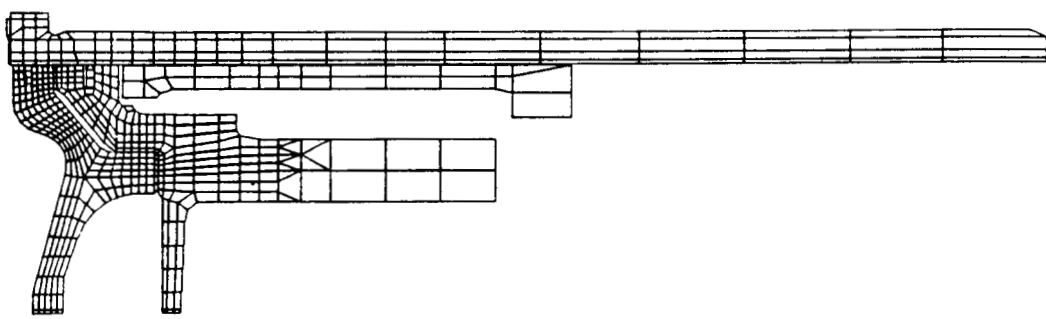


Figure 18. Two-dimensional axisymmetric finite element model of the ADRE engine piston-liner assembly used for IRIS steady-state and transient heat conduction computations.

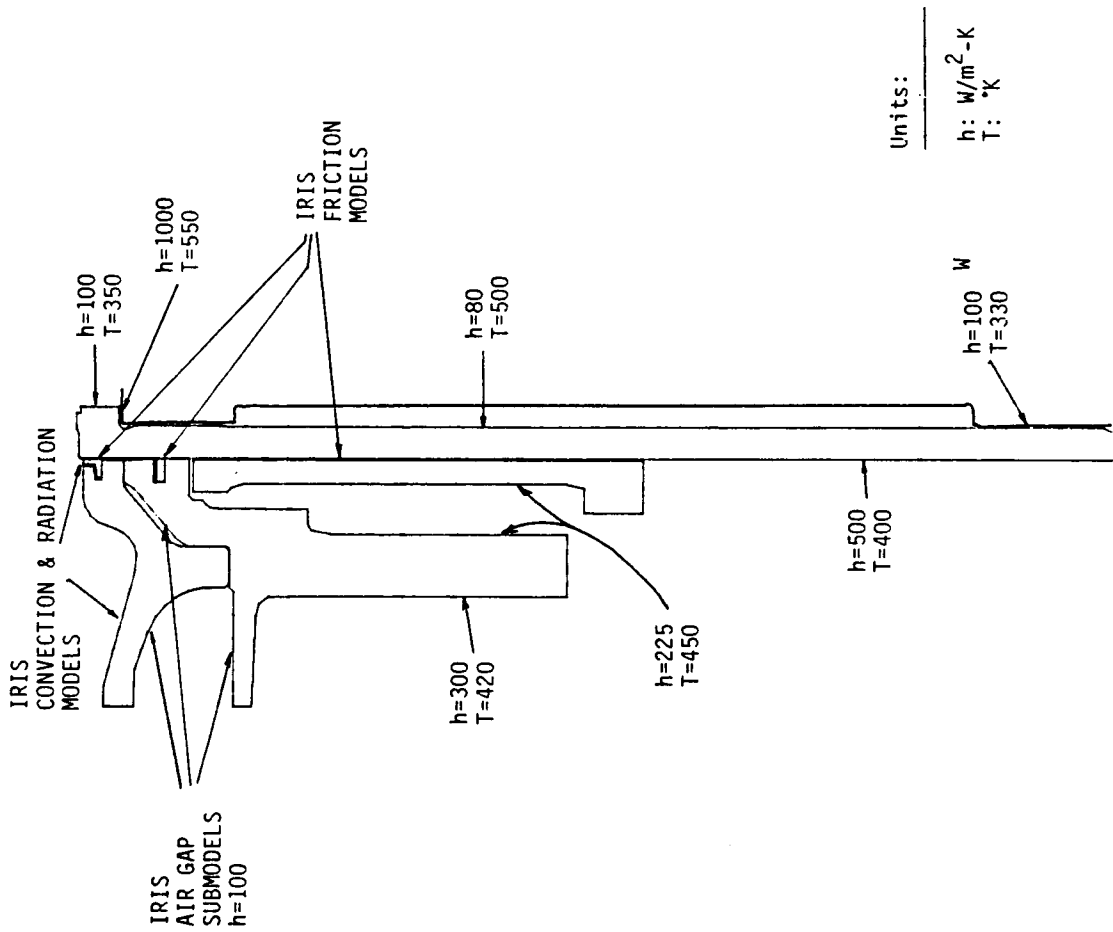


Figure 19 Schematic description of convection, radiation and friction boundary conditions applied to surfaces of the finite element model.

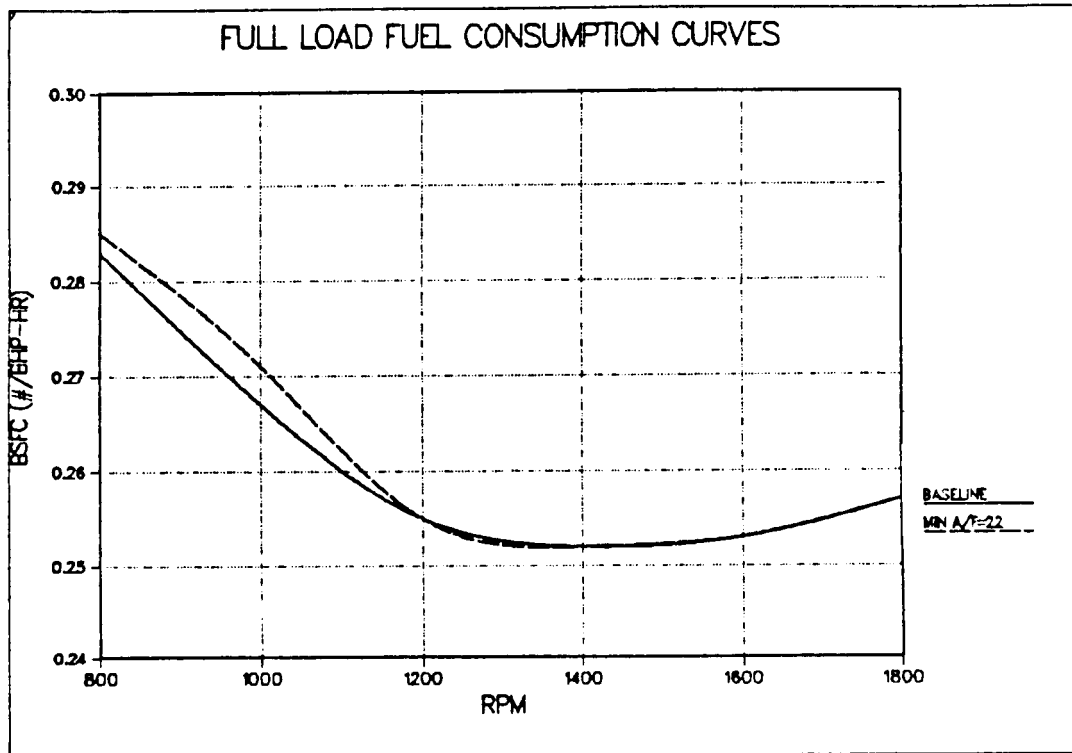


Figure 20 Full load brake-specific fuel consumption curves (supplied by DDA).

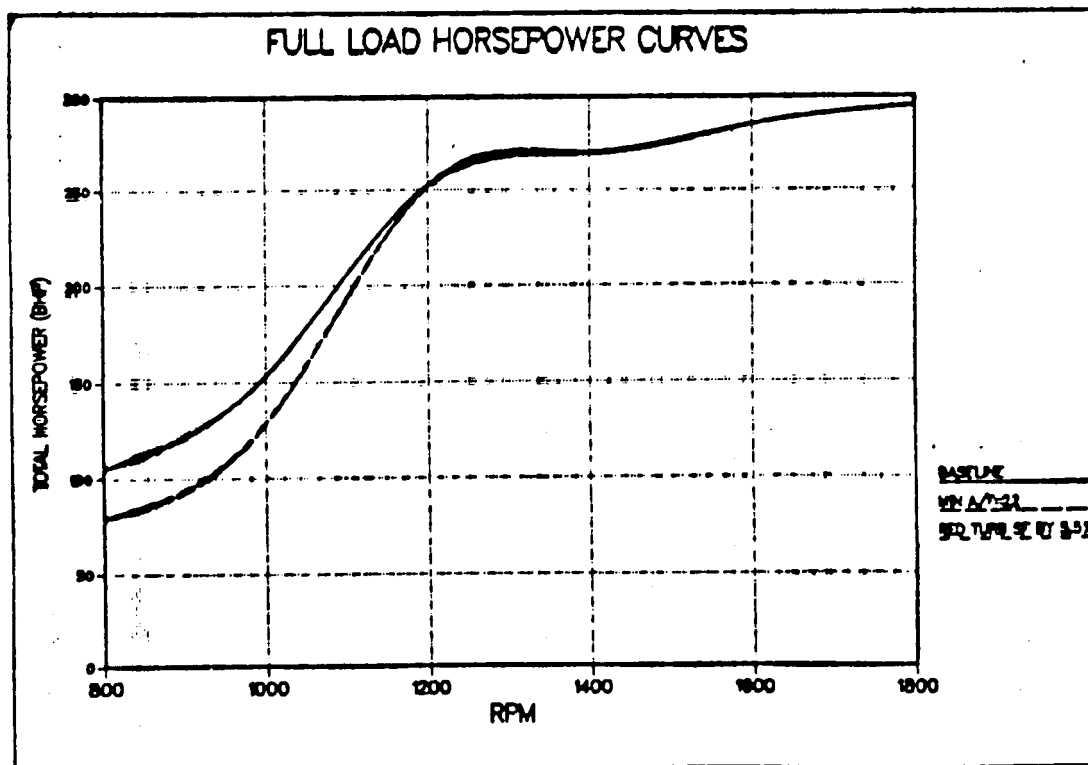


Figure 21 Full load horsepower curves (supplied by DDA).

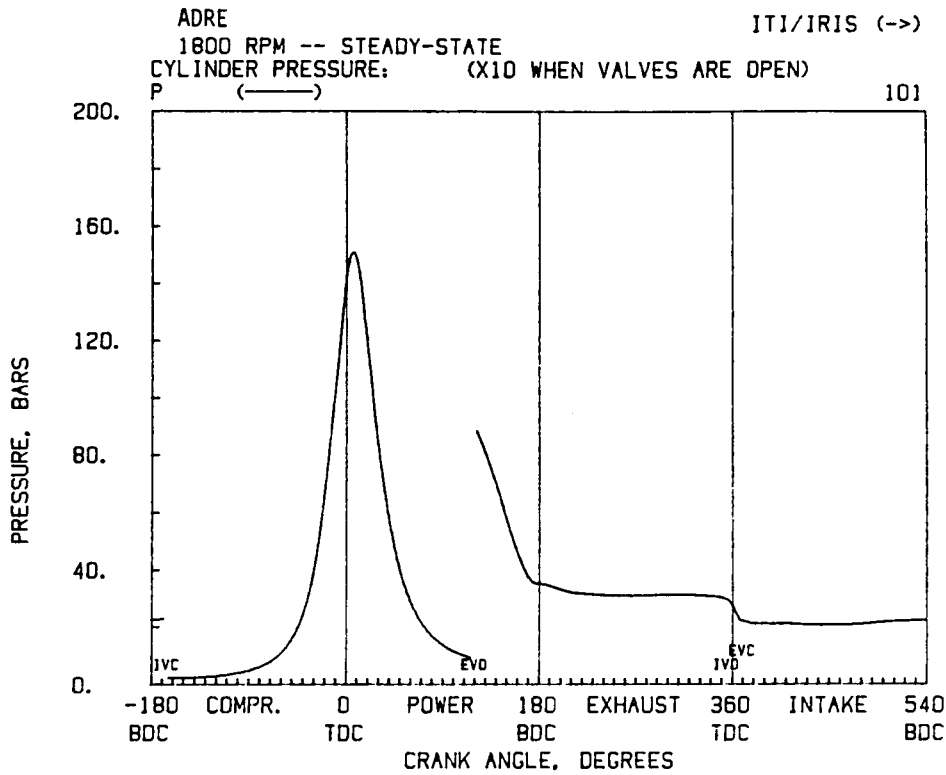


Figure 22 Predicted cyclic variation of cylinder pressure; rated conditions.

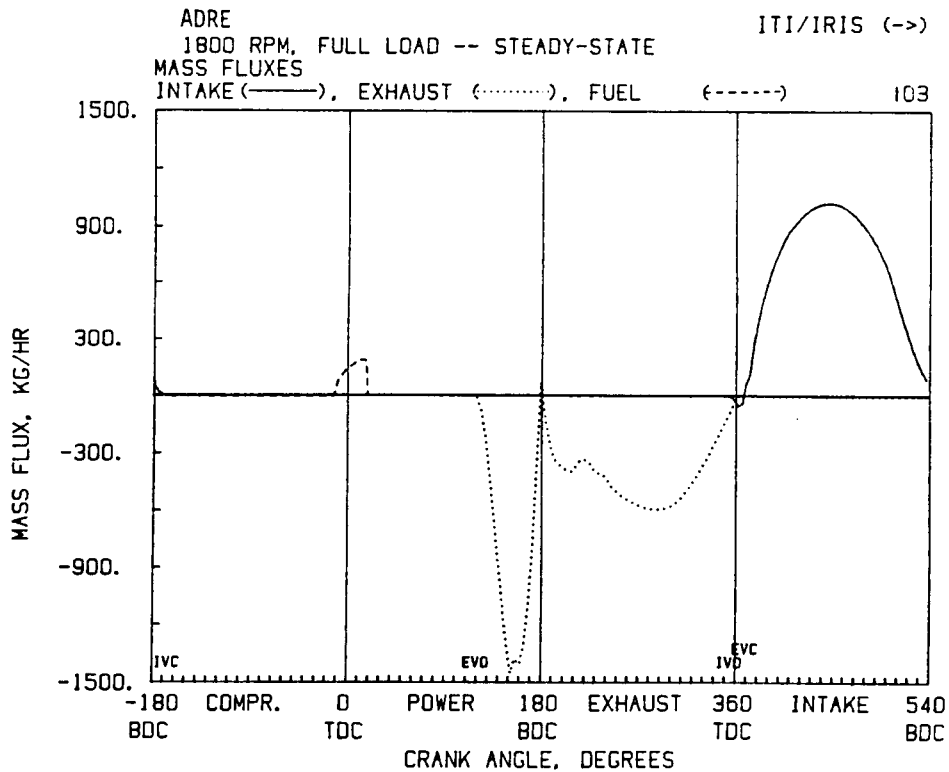


Figure 23 Predicted cyclic history of valve and fuel injection mass fluxes; rated conditions.

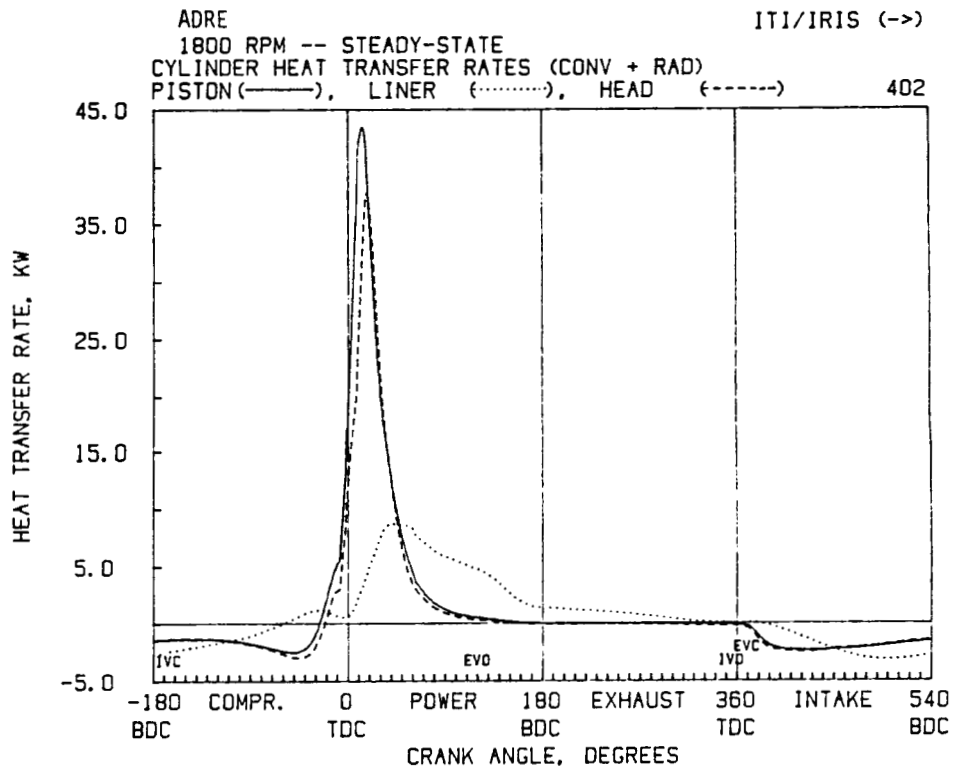


Figure 24 Predicted cyclic variation of heat rejection rates to piston, liner and head; rated conditions.

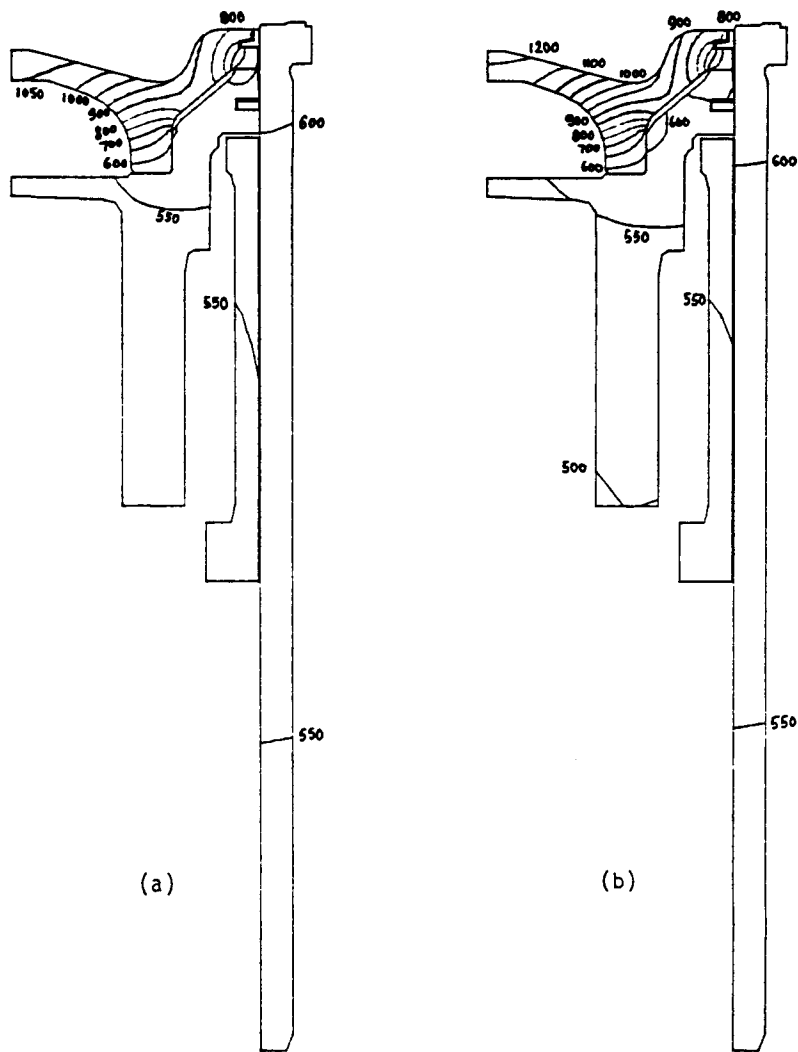


Figure 25 Temperature distribution in piston-liner assembly; a) rated conditions; b) peak torque. ADRE.

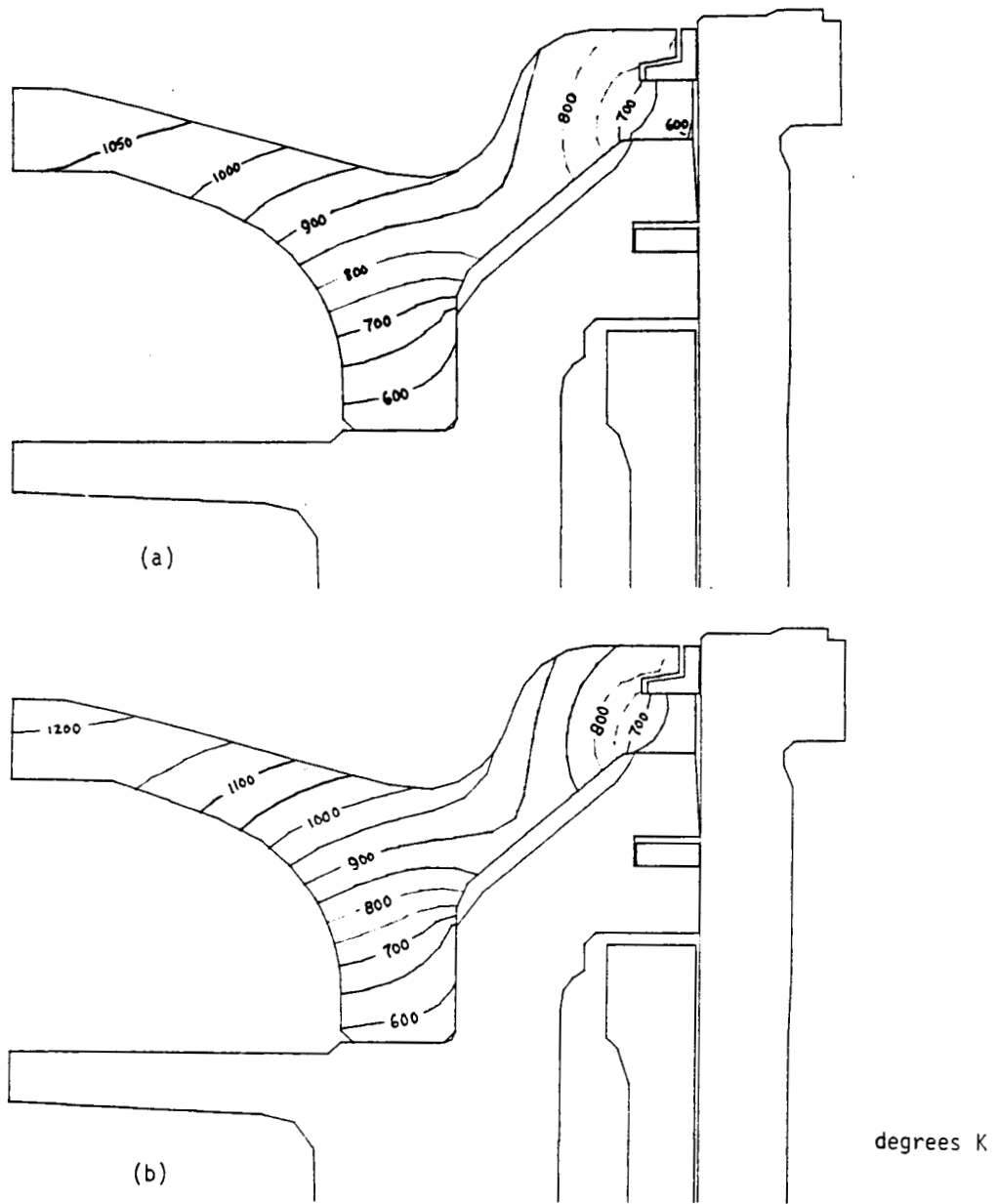


Figure 26 Details of temperature distribution in silicon nitride piston crown: a) rated conditions; b) peak torque. ADRE.

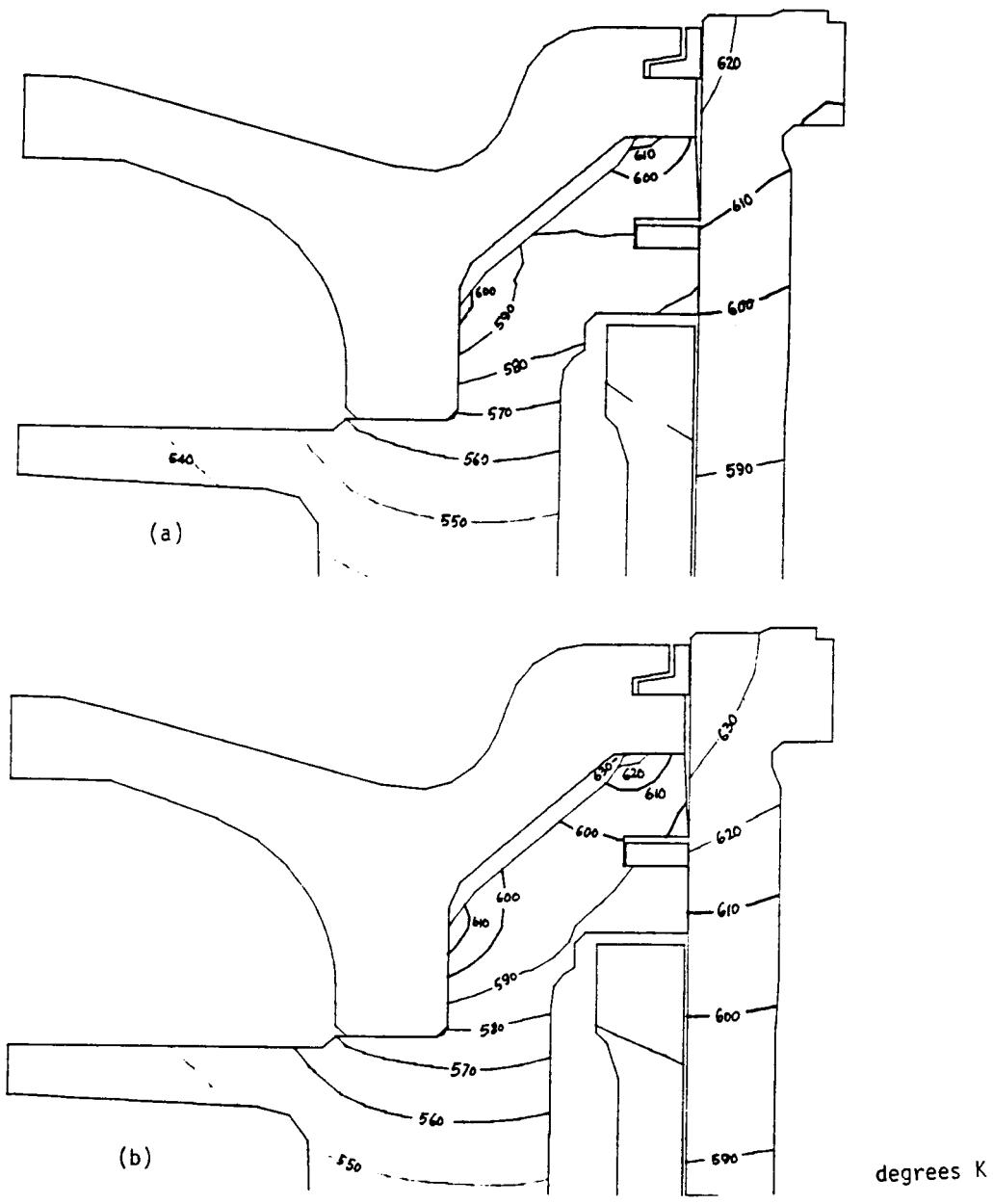


Figure 27 Details of temperature distribution in upper part of metal body and liner: a) rated conditions; b) peak torque. ADRE.

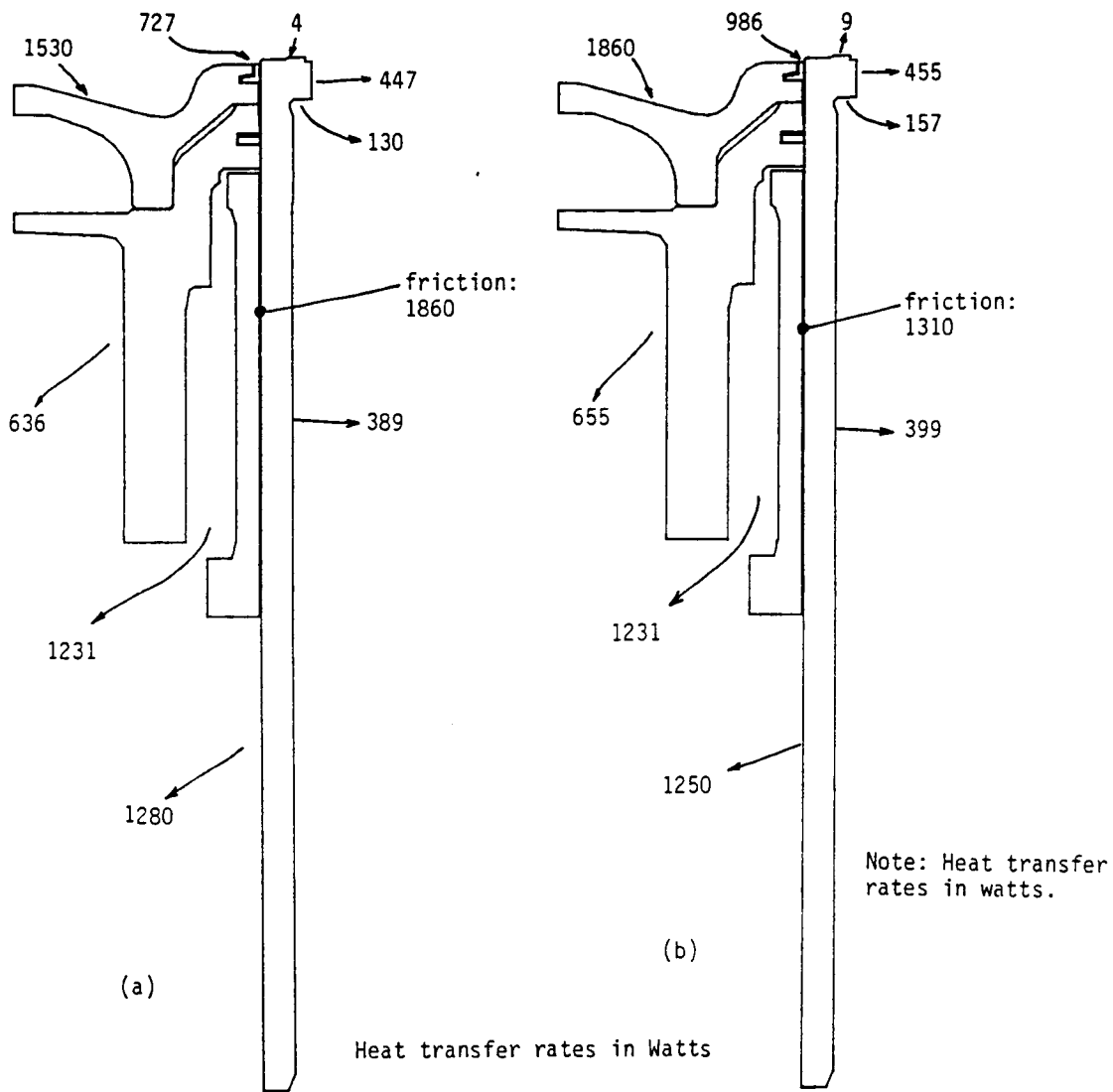


Figure 28 Heat balance on piston-liner assembly showing heat transfer rates on various gas- or air-side surfaces, and frictional heat generation: a) rated conditions; b) peak torque. ADRE.

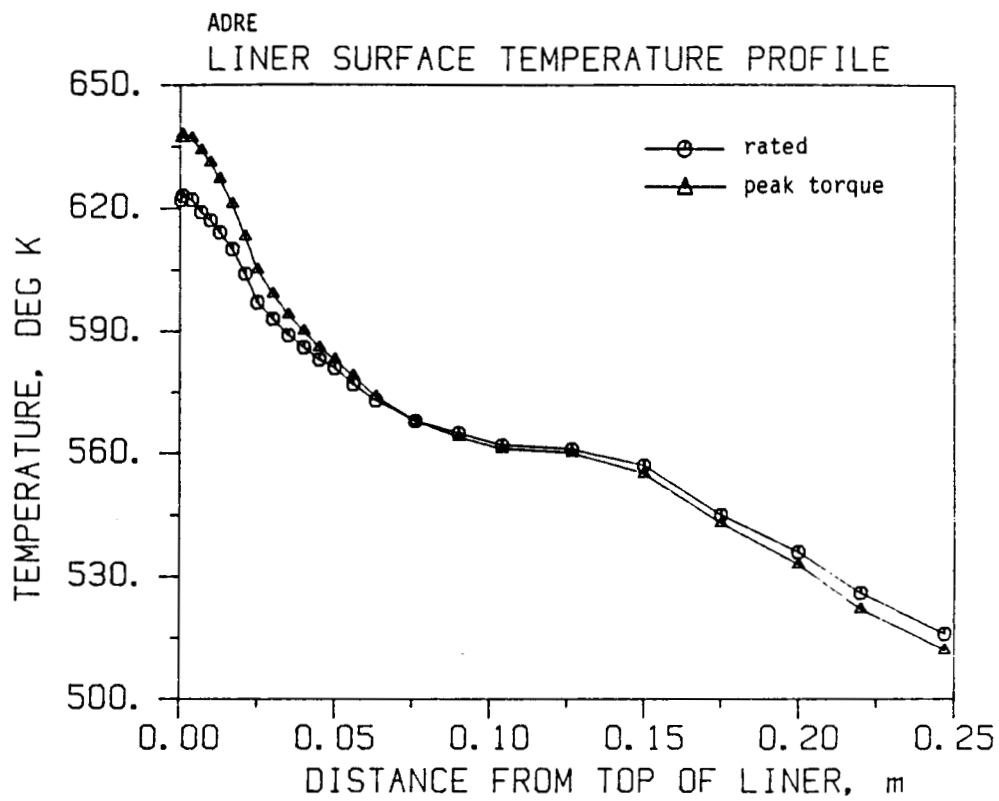


Figure 29 Variation of liner (gas side) surface temperature with axial distance from head.

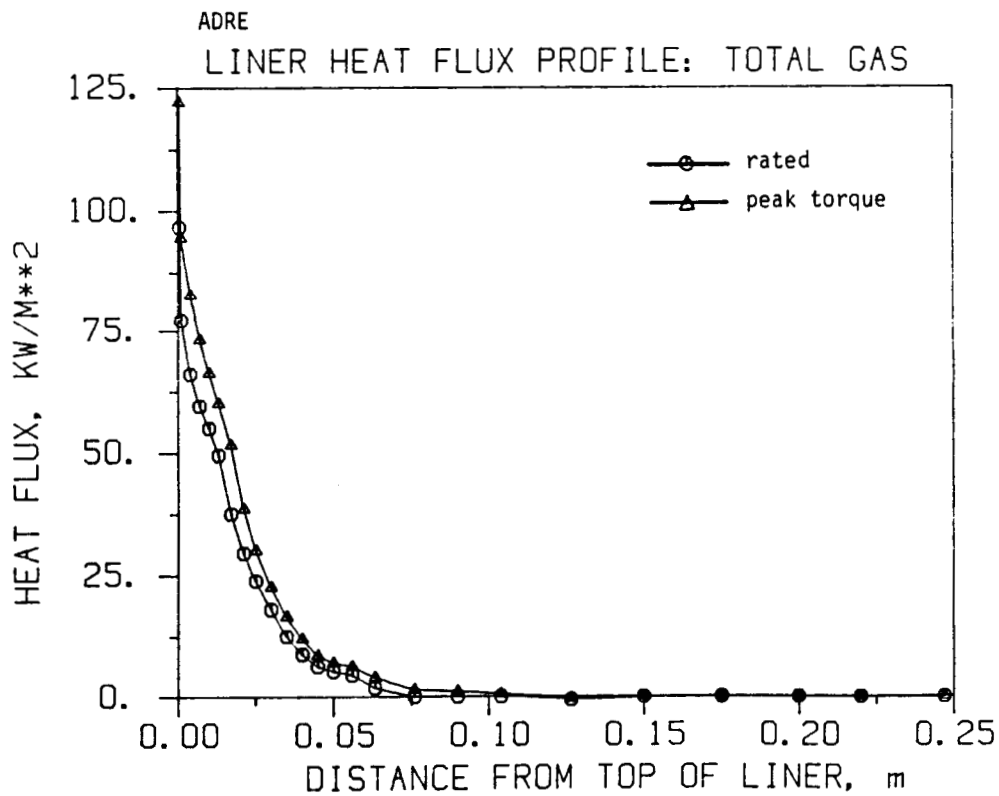


Figure 30 Variation of gas-to-liner heat flux along liner surface with axial distance from head.

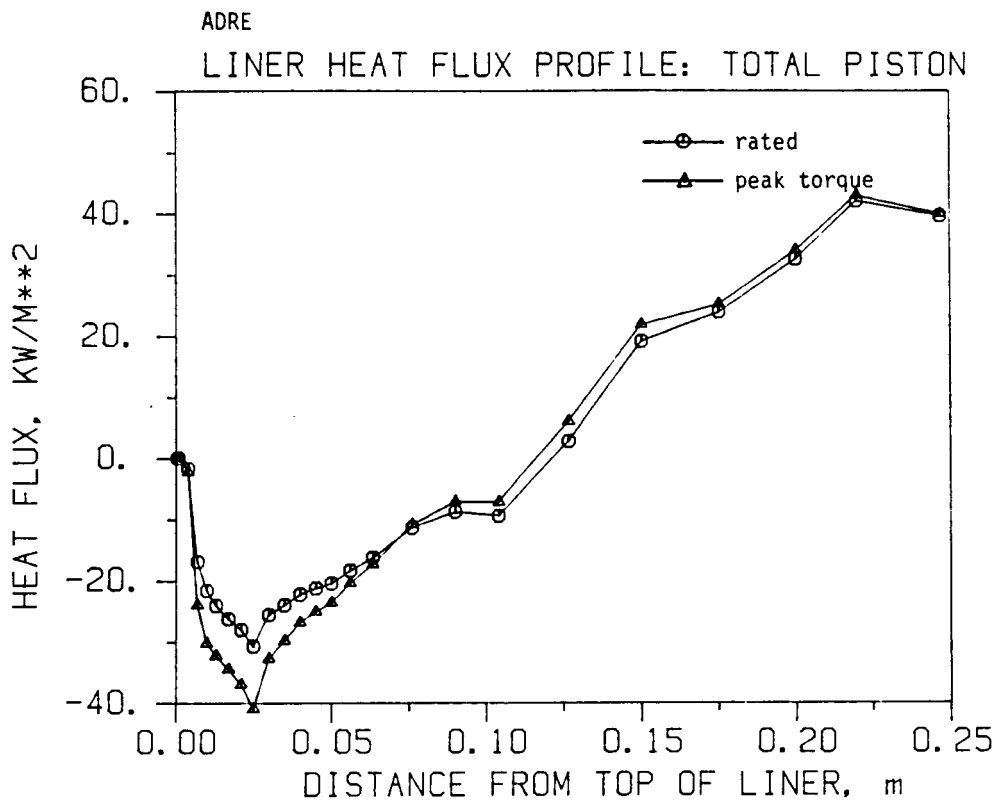


Figure 31 Variation of piston-to-liner heat flux along liner surface with axial distance from head.

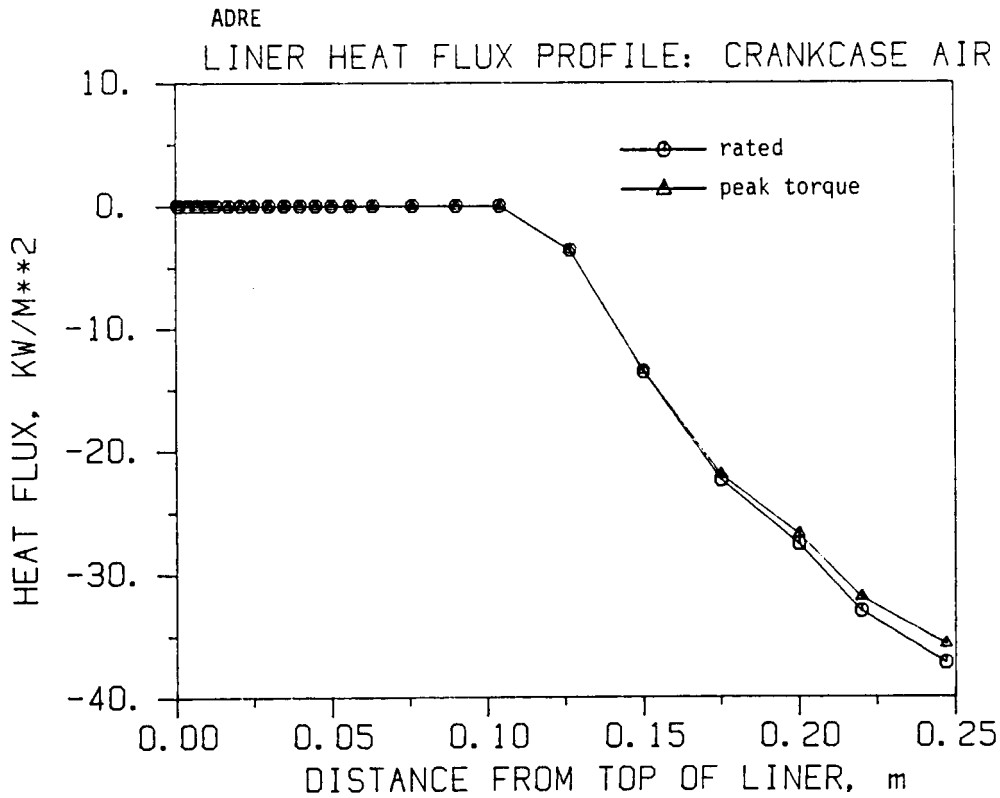


Figure 32 Variation of liner-to-crankcase air heat flux along liner surface with axial distance from head.

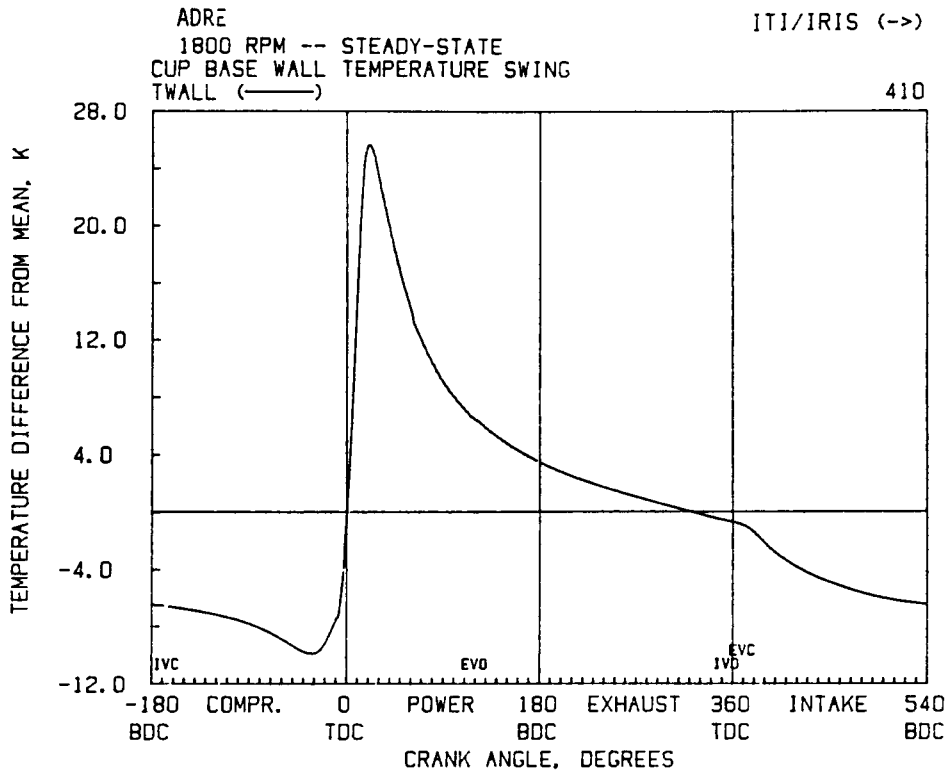


Figure 33 Cyclic piston surface temperatures at rated conditions (cup base average).

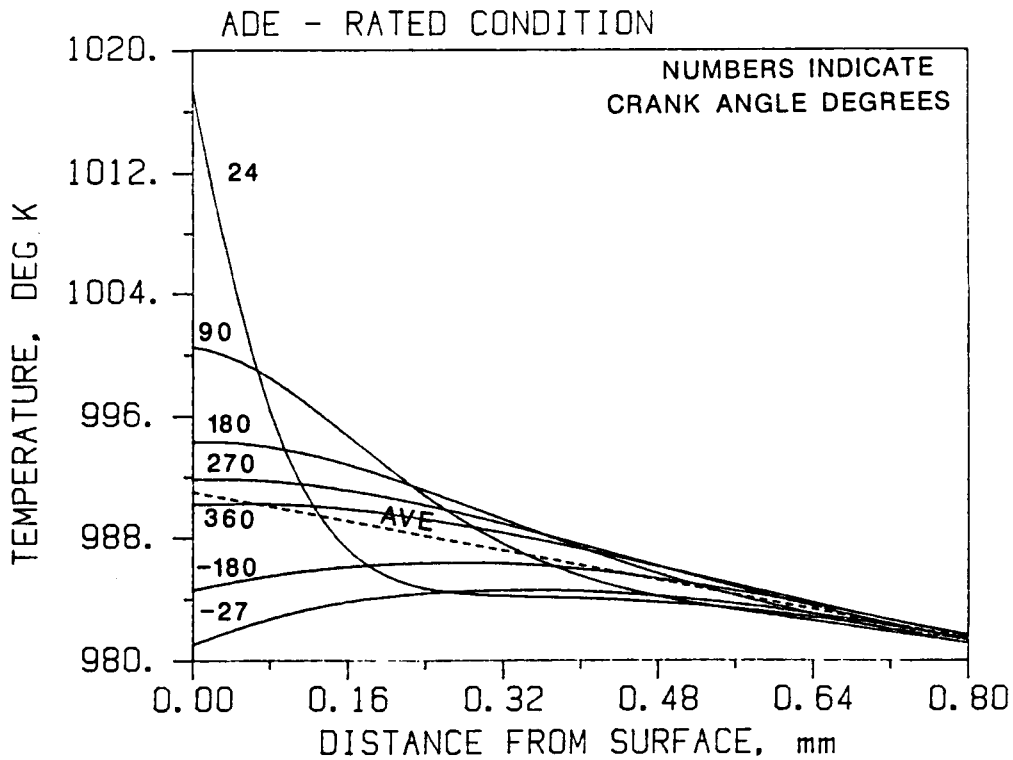


Figure 34 Cyclic in-depth piston temperature profiles at rated condition (cup base average)

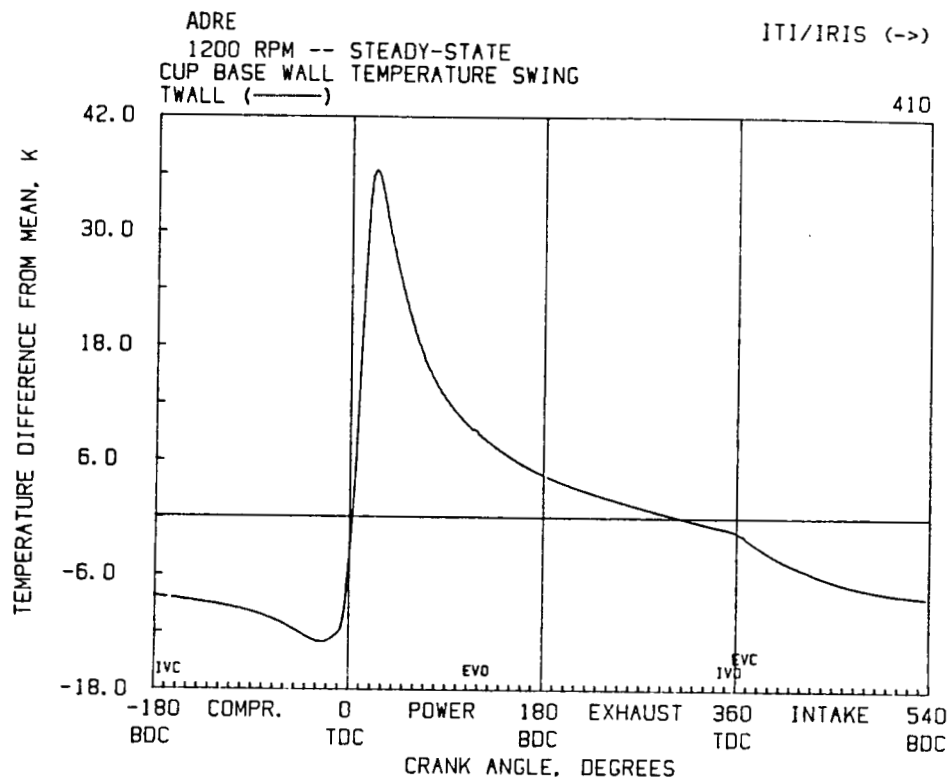


Figure 35 Cyclic piston surface temperatures at peak torque (cup base average).

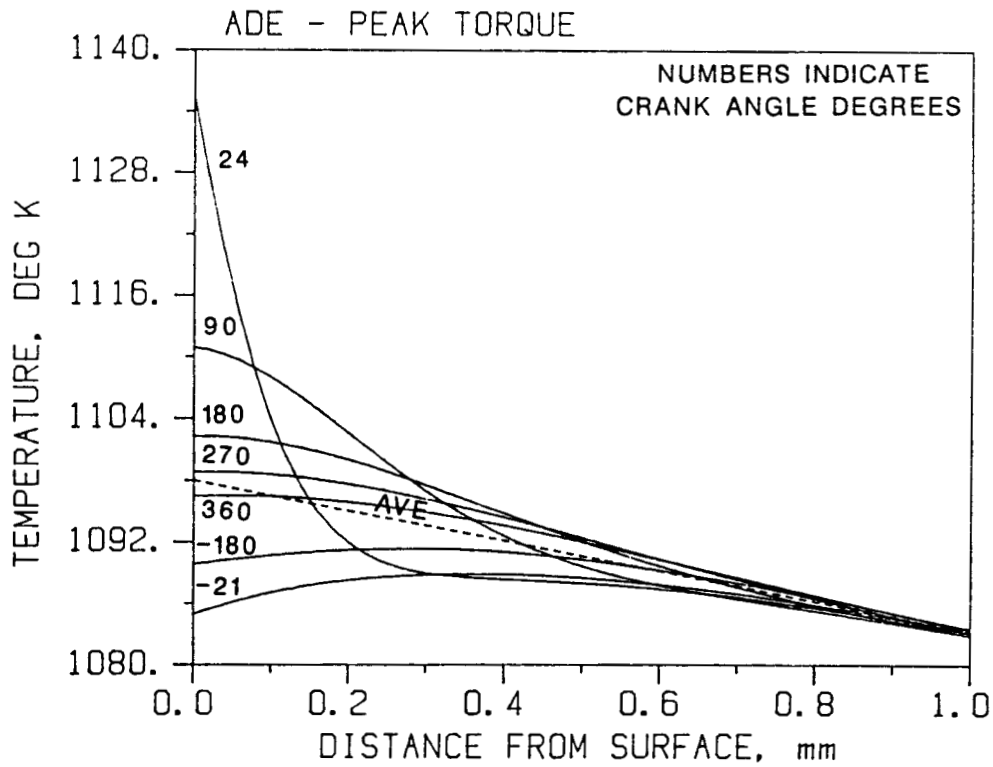
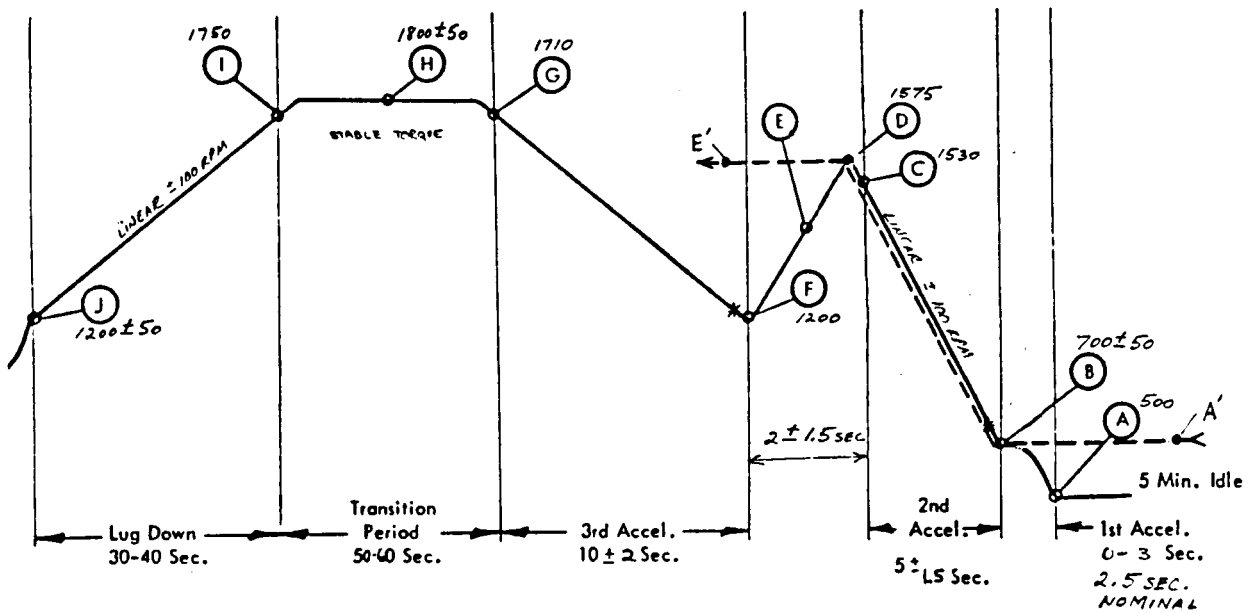


Figure 36 Cyclic in-depth piston temperature profiles at peak torque (cup base average).



- | | | | |
|---|---|---|--|
| A | Idle | G | 95% of Rated Speed |
| B | 200 RPM inc. ± 50 RPM | H | WOT ± 50 RPM |
| C | 85% Rated Speed | I | 50 RPM below rated speed |
| D | 87.5% Rated Speed | J | Peak torque or 60% of rated speed ± 50 RPM |
| E | Vent approx. 150 RPM from F | * | PEN OFFSET FROM OPEN THROTTLE |
| F | Peak torque or 60% of rated speed whichever is higher | | |

Figure 37 RPM history during the federal smoke cycle for the ADRE engine; time scale right to left. The segment A'-B-C-D-E' is the portion simulated in the transient simulation. (Supplied by DDA)

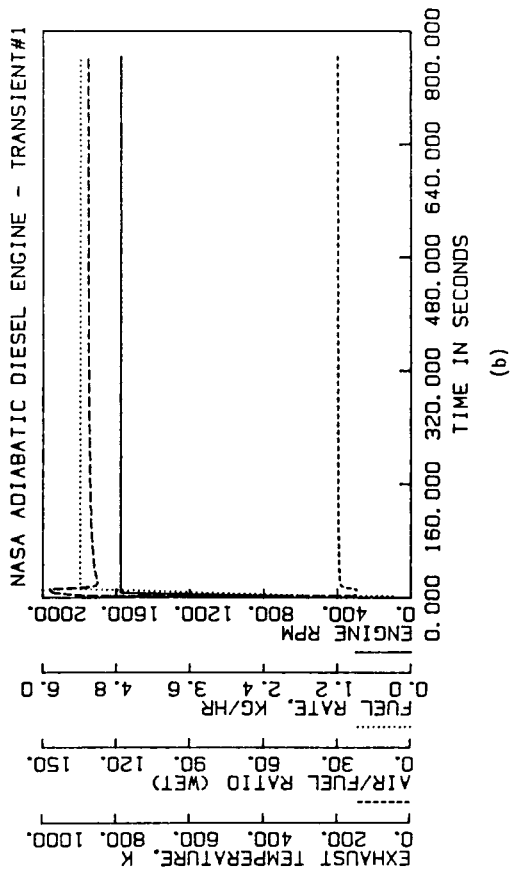
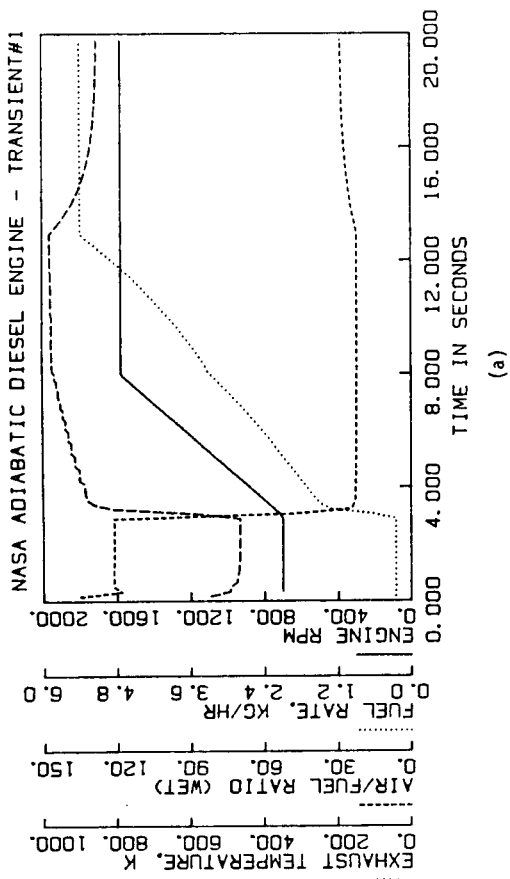


Figure 38 Transient event in RPM/fuel and air-fuel ratio, and the exhaust temperature response: a) short term; b) long term.

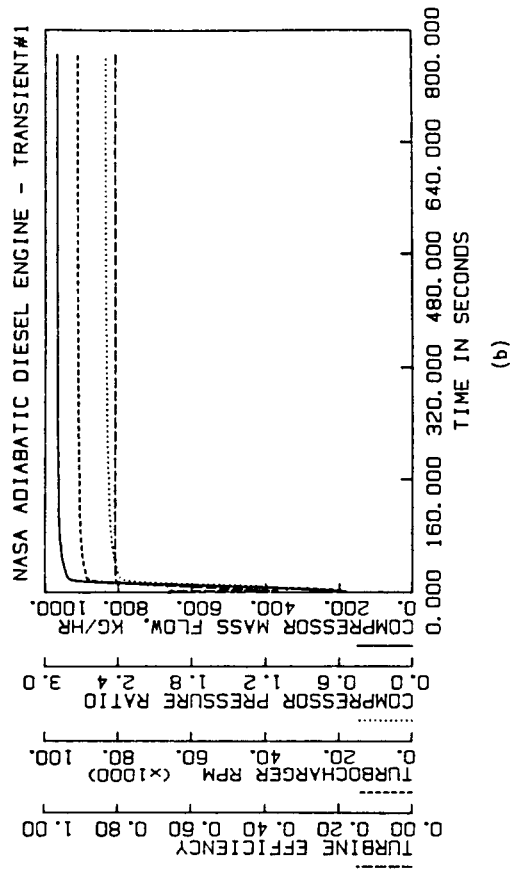
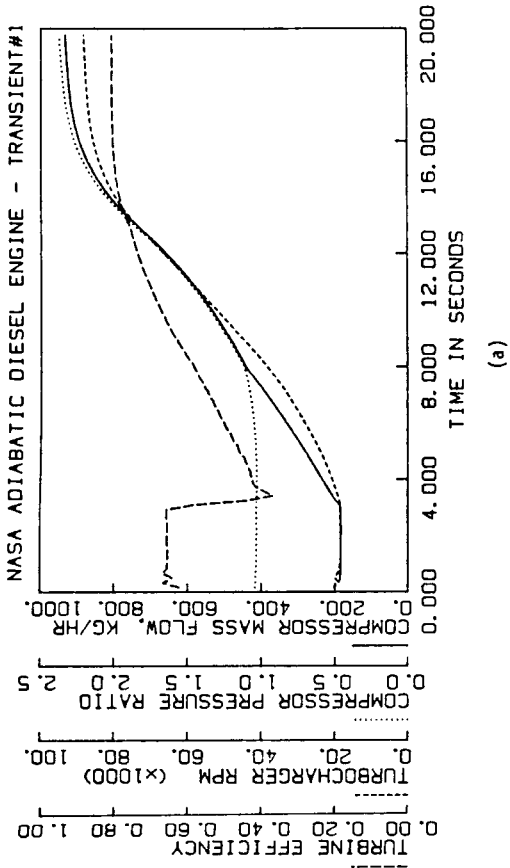


Figure 39 Transient response of selected turbocharger quantities; compressor mass flow, compressor pressure ratio, turbocharger rpm and turbine efficiency: a) short term; b) long term.

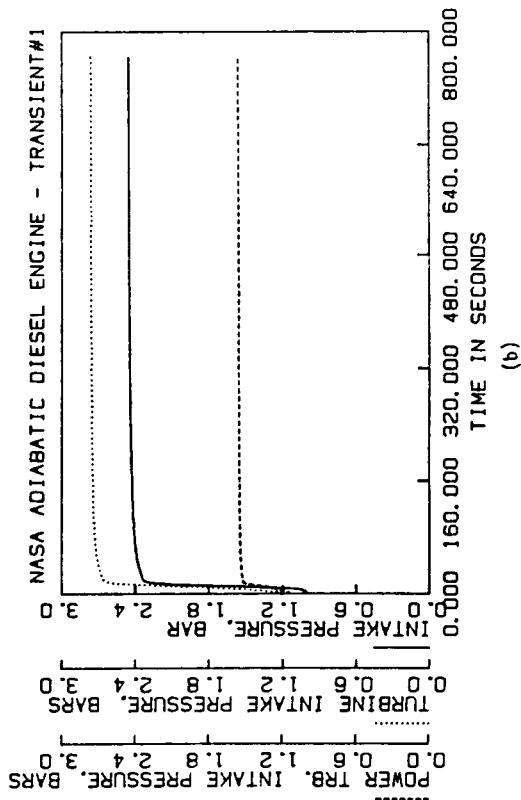
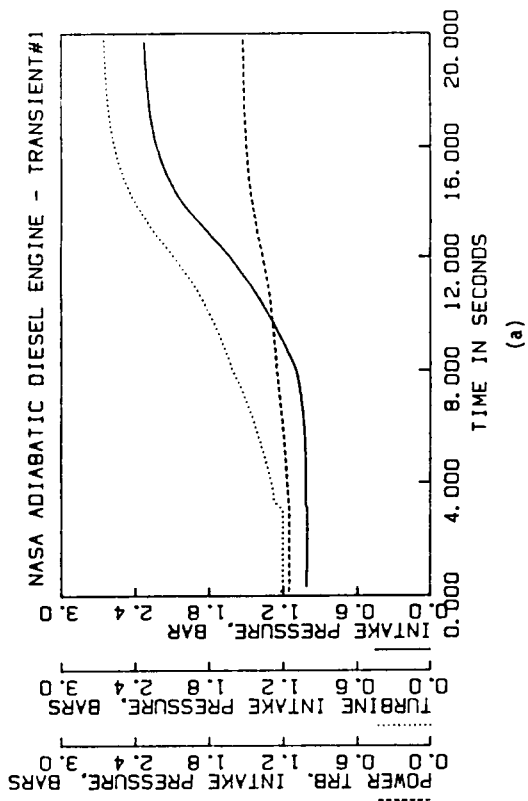


Figure 40 Transient response of engine intake pressure, and of turbo-charger turbine and power turbine inlet pressures: a) short term; b) long term.

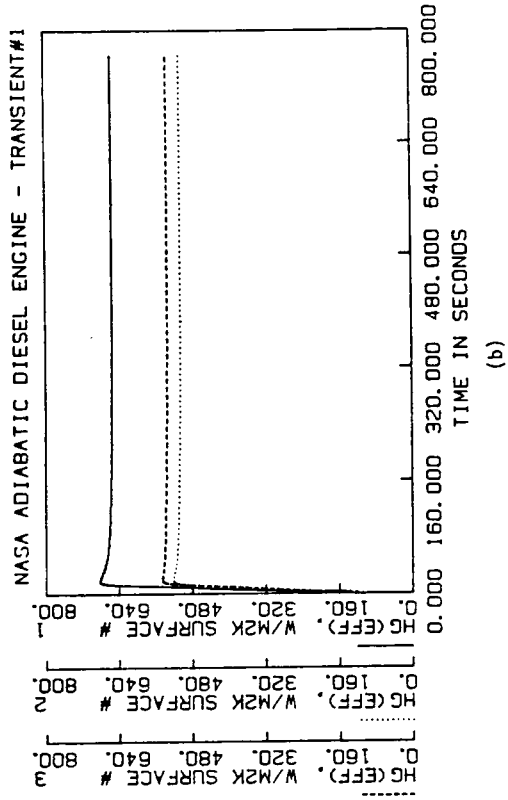
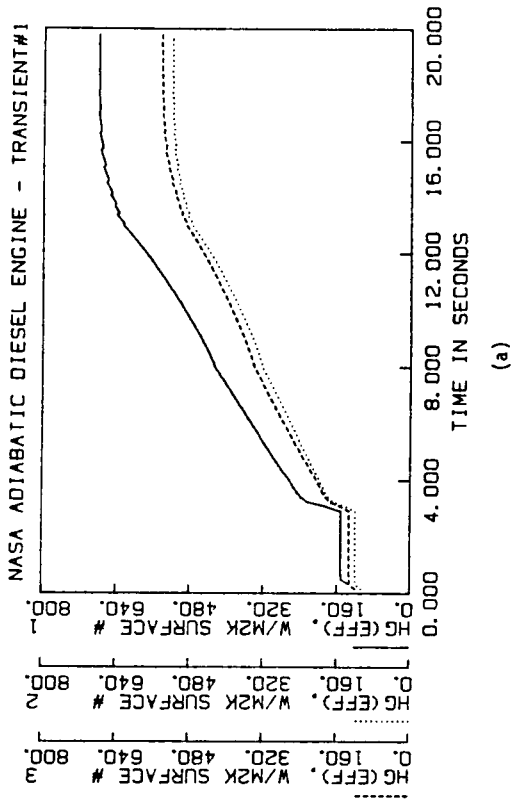


Figure 41 Predicted history of convective heat transfer coefficients on three piston surfaces (cup base, cup side, piston crown): a) short term; b) long term.

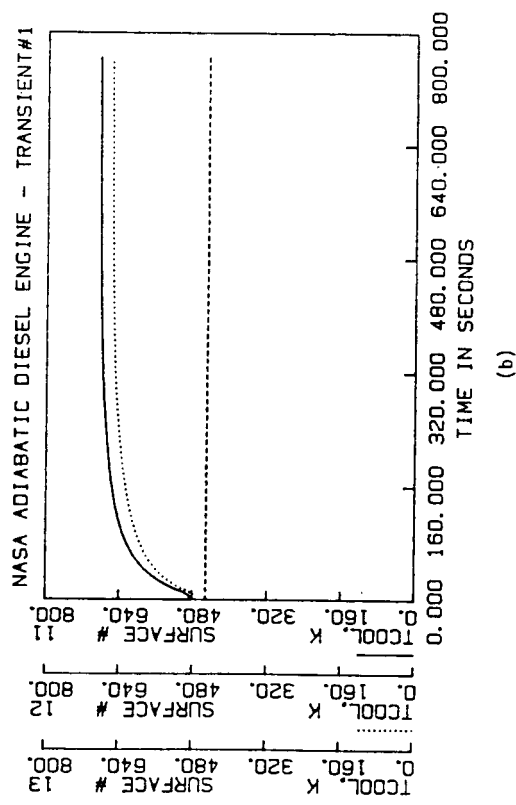
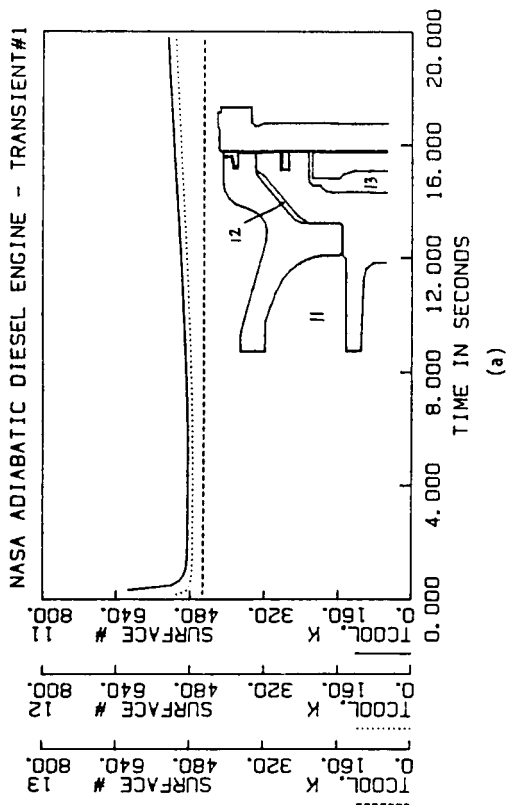


Figure 42 Predicted transient response of air gap temperatures: a) short term; b) long term.

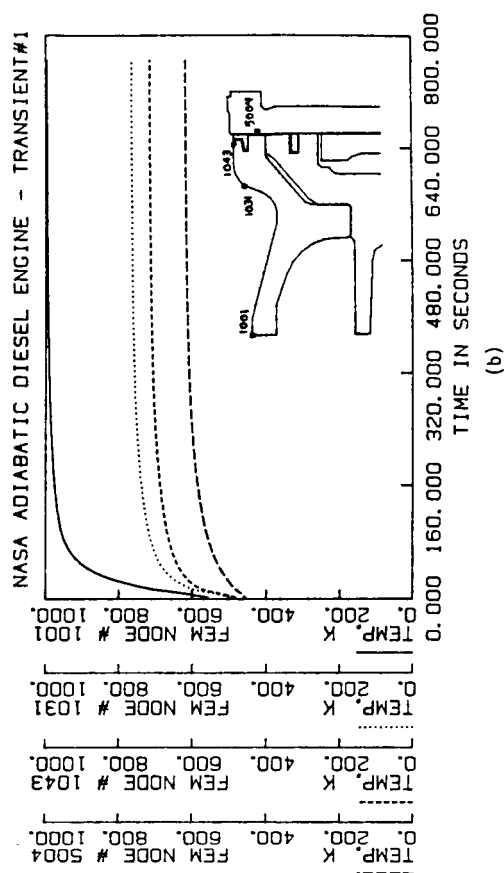
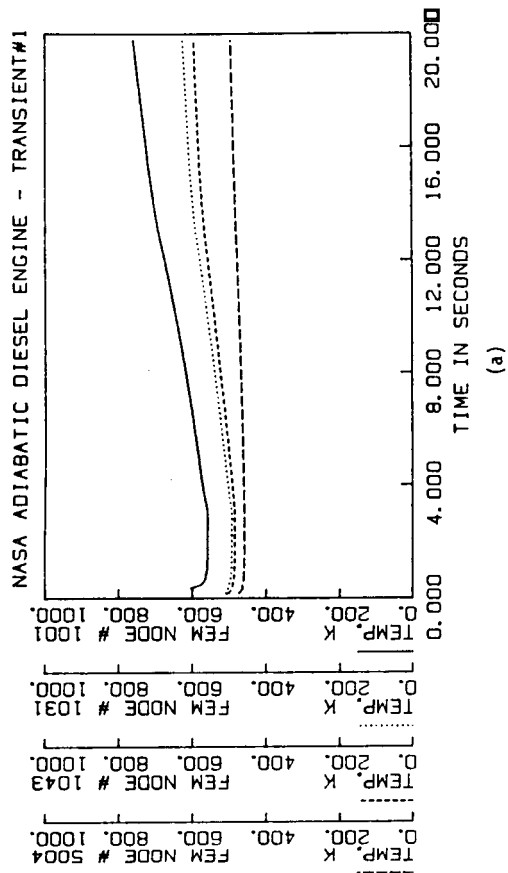


Figure 43 Predicted transient thermal response of structure at selected finite element nodes: a) short term; b) long term.

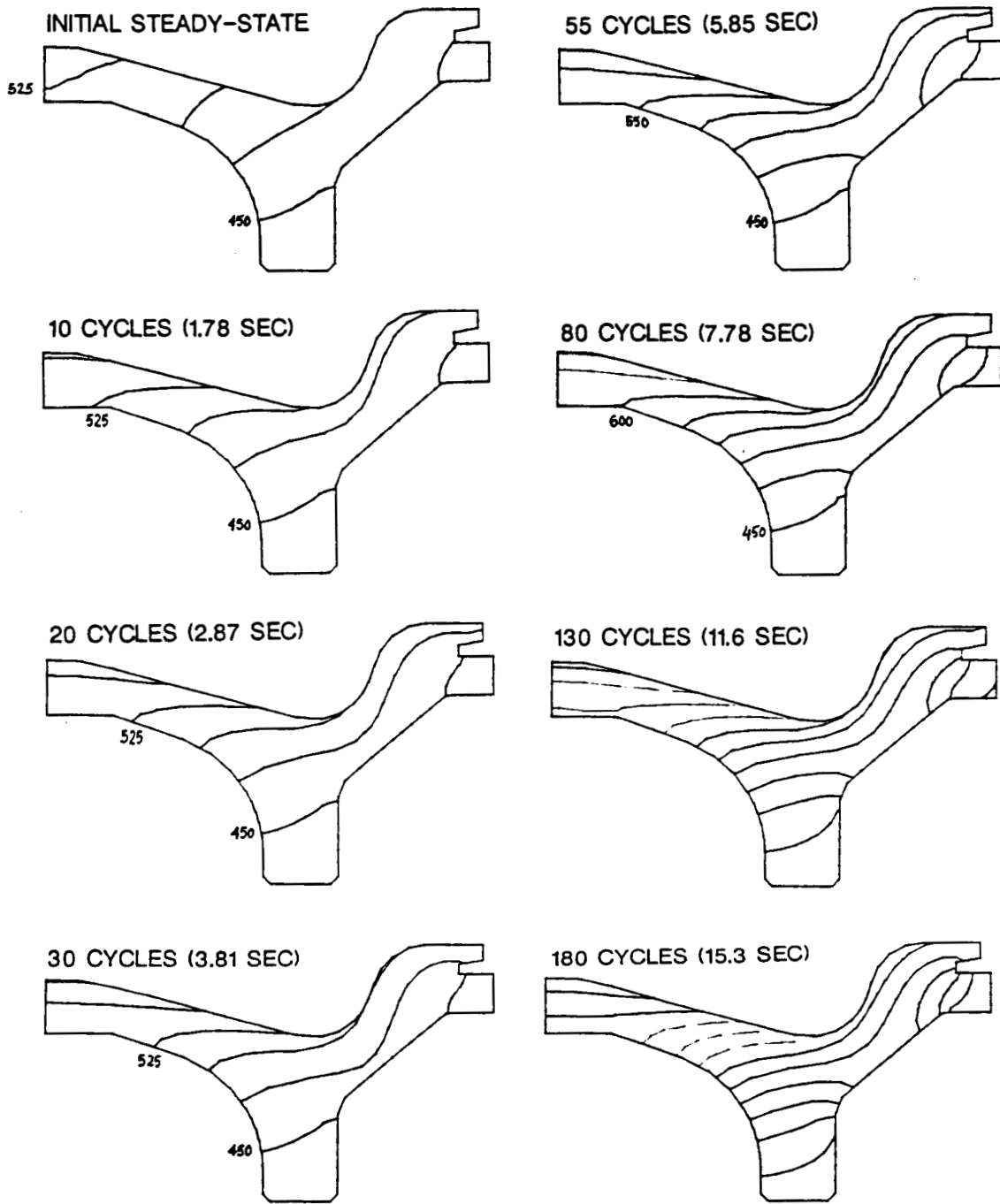


Figure 44 Predicted temperature distributions in ADE engine piston silicon nitride cap, at selected instants during the simulated transient event (nominal cycles, from the beginning of event; contour levels in degrees K and 25K increments).

1	-075.0	12	-700.0
2	-100.0	13	-675.0
3	-125.0	14	-650.0
4	-150.0	15	-625.0
5	-175.0	16	-600.0
6	-200.0	17	-575.0
7	-225.0	18	-550.0
8	-250.0	19	-525.0
9	-275.0	20	-500.0
10	-300.0	21	-475.0
11	-325.0	22	-450.0

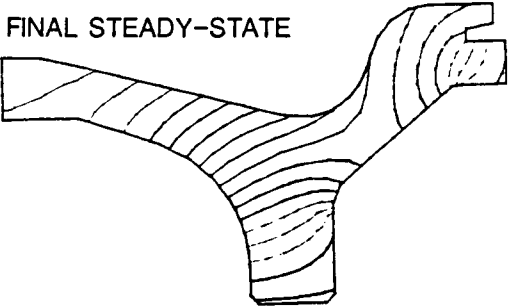
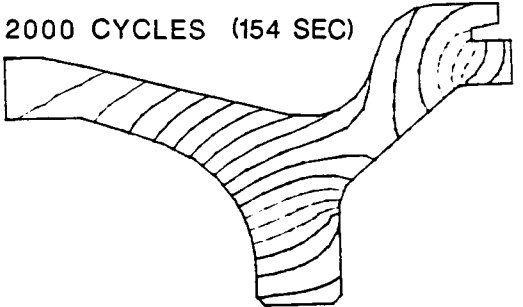
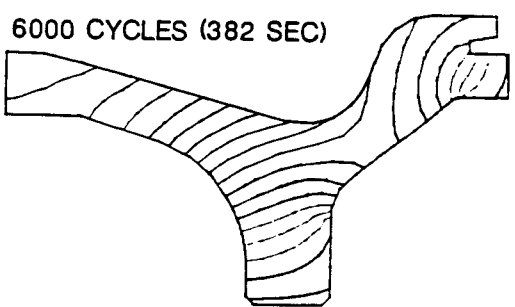
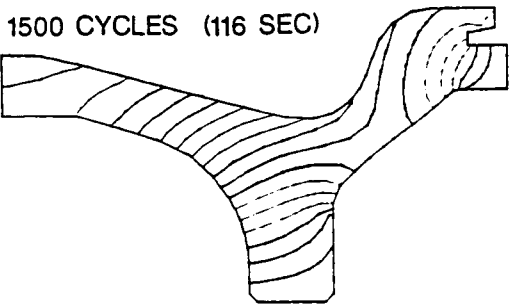
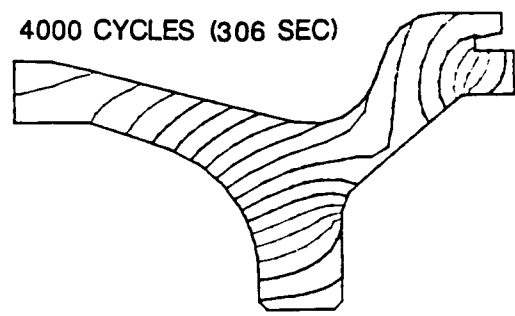
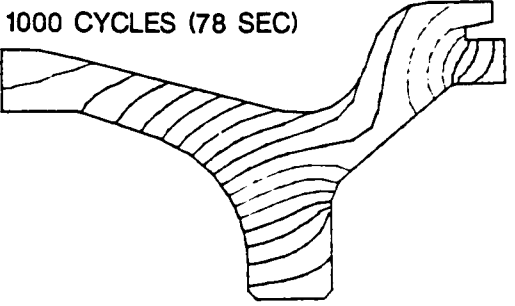
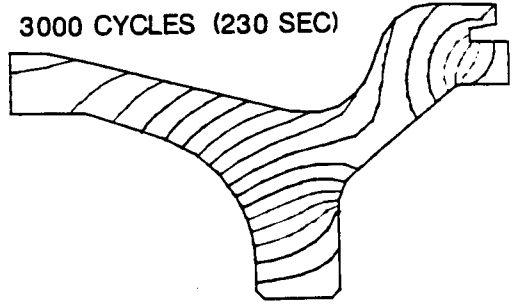
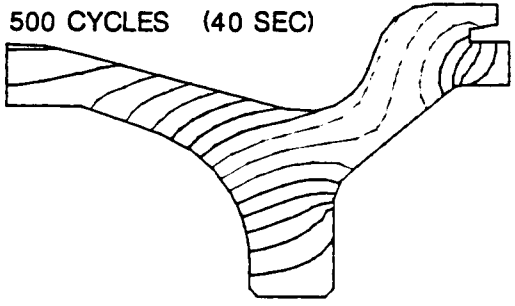


Figure 44 (continued)

1	-975.0	12	-700.0
2	-950.0	13	-700.0
3	-925.0	14	-700.0
4	-900.0	15	-700.0
5	-875.0	16	-700.0
6	-850.0	17	-700.0
7	-825.0	18	-700.0
8	-800.0	19	-700.0
9	-775.0	20	-700.0
10	-750.0	21	-700.0
11	-725.0	22	-700.0

APPENDIX C: THERMO ELECTRON SUBCONTRACT FINAL REPORT

TE 5629-02-86

STUDY OF AN ORGANIC RANKINE
BOTTOMING CYCLE HEAT RECOVERY SYSTEM
FOR THE DDA LOW HEAT REJECTION ENGINE

MAY 1986

PREPARED FOR

DETROIT DIESEL ALLISON
DIVISION OF GENERAL MOTORS CORPORATION
ROMULUS MANUFACTURING OPERATIONS
36880 ENCORSE ROAD
ROMULUS, MICHIGAN 48174

PREPARED BY

THERMO ELECTRON CORPORATION
P. O. BOX 9046
45 FIRST AVENUE
WALTHAM, MA 02254

FL-85 SYSTEM CYCLE ANALYSIS

INTRODUCTION:

An organic Rankine cycle system is composed of five (5) basic elements: the vapor generator (or boiler), regenerator, condenser, turbine and feedpump. Each of these constituents has an efficiency or effectiveness that quantifies its individual performance; which ultimately contributes to the overall performance of the complete system. The proper selection of a system's design point must also consider the temperatures of the heat source and heat sink available to the cycle as well as the packaging of the assembled system. Certainly, the net power output of the system must be weighed with these packaging features in order to achieve an economic as well as power efficient system.

The design point selected for use with the DDA ADRE turbo-compounded diesel engine was determined by first identifying the limitations of the FL-85, organic fluid-based Rankine cycle. For example, restrictions in the minimum exhaust gas stack temperatures between 270 and 300°F are thought to be reasonable considering the products of combustion from No. 2 diesel fuel and the possibility of causing sulfuric acid condensation as a result of lower stack temperatures.

Due to fluid thermal stability requirements, the FL-85 should not be heated to a temperature exceeding 600°F as a result, bulk fluid temperatures leaving the vapor generator were restricted to 550°F. Also to be considered, is the 755 psia critical pressure limit for FL-85. Although, it is technically feasible to operate a "super critical" Rankine cycle system, conventional systems have been sub-critical particularly as a result of the limited availability of organic fluid properties at or near critical pressure and temperature conditions.

The advancement of the adiabatic diesel engine has been primarily fostered by the goal of higher engine efficiencies but also to a lesser extent by the desire to eliminate the water cooling system, specifically the radiator and fan in front of the engine. In order to comply with this secondary intent, we have chosen to use a direct air-cooled condenser located in the rear of the engine. This requires therefore a reasonably sized, integrated regenerator - condenser and induction fan drive system to be packaged into the bottoming cycle system. Certainly, this criteria of using a "reasonably sized" condenser will impact the power recovery efficiency of the bottoming cycle but it is a necessary compromise considering the end use of the product on a transport vehicle.

The Thermo Electron Corp. has had considerable experience in the design of organic fluid, axial flow, impulse turbines. This experience has been used to determine the design point operating conditions for a FL-85 organic fluid turbine. Based on the final design point selection, the organic, axial flow turbine will require an operating speed of 57,500 RPM and will have a rotor diameter of 3.9 inches. This corresponds to a specific speed of 27 and a specific diameter of 2.8 as taken from O.E. Balje's Figure 15 in his: "A Study On Design Criteria and Matching of Turbomachines: Part A: (Journal of Engineering For Power, Jan., 1962, page 83).

Given all of these guidelines a parametric analysis was conducted in order to reveal the best choice for a design point. The results of this parametric study and the final choice of a design point will also be shown.

A summary of the part loading effects of reduced organic fluid flowrate and governed speed will be given in the following section on Parametric Studies.

PARAMETRIC ANALYSIS:

Changes in a particular component's efficiency will affect the effectiveness and hence size requirements of all of the other components. In order to best judge this interdependency, a parametric study was performed around several preliminary system design point selections. These tentative studies led to a final design point selection and a final parametric study; the results of which are shown in Figures 1 through 4.

For example, the effect of increasing or decreasing the vapor generator size on the regenerator and condenser sizes as well as the system power output was determined and is shown in Figure 1. As shown in Figure 1, if the vapor generator size is increased by 25% (compared to the design point vapor generator size) the result is only a 4% increase in net system power with a subsequent 4% increase in the regenerator and condenser sizes. A 25% decrease in the vapor generator's size, results in an 8% reduction in net system power, in addition to an 8% reduction in the required regenerator and condenser sizes.

Similar results on the system performance and component sizes are given as the regenerator efficiency and condenser efficiency and hence sizes change. These results are given in Figures 2 and 3.

In Figure 4, the effect of system pressure on the vapor generator and the system power output is also shown. Although, the system output changes insignificantly with lower operating pressures, the vapor generator size increases by as much as 12% at 500 psia, for example. (This is due to the slight increase in the regenerator liquid outlet (preheated) temperature.

The final design point selection is given in Figure 5 and an illustration of these statepoints on a FL-85 Temperature-Entropy(T-S) diagram is given in Figure 6. Figure 7 is a schematic of the bottoming cycle system showing the design point conditions.

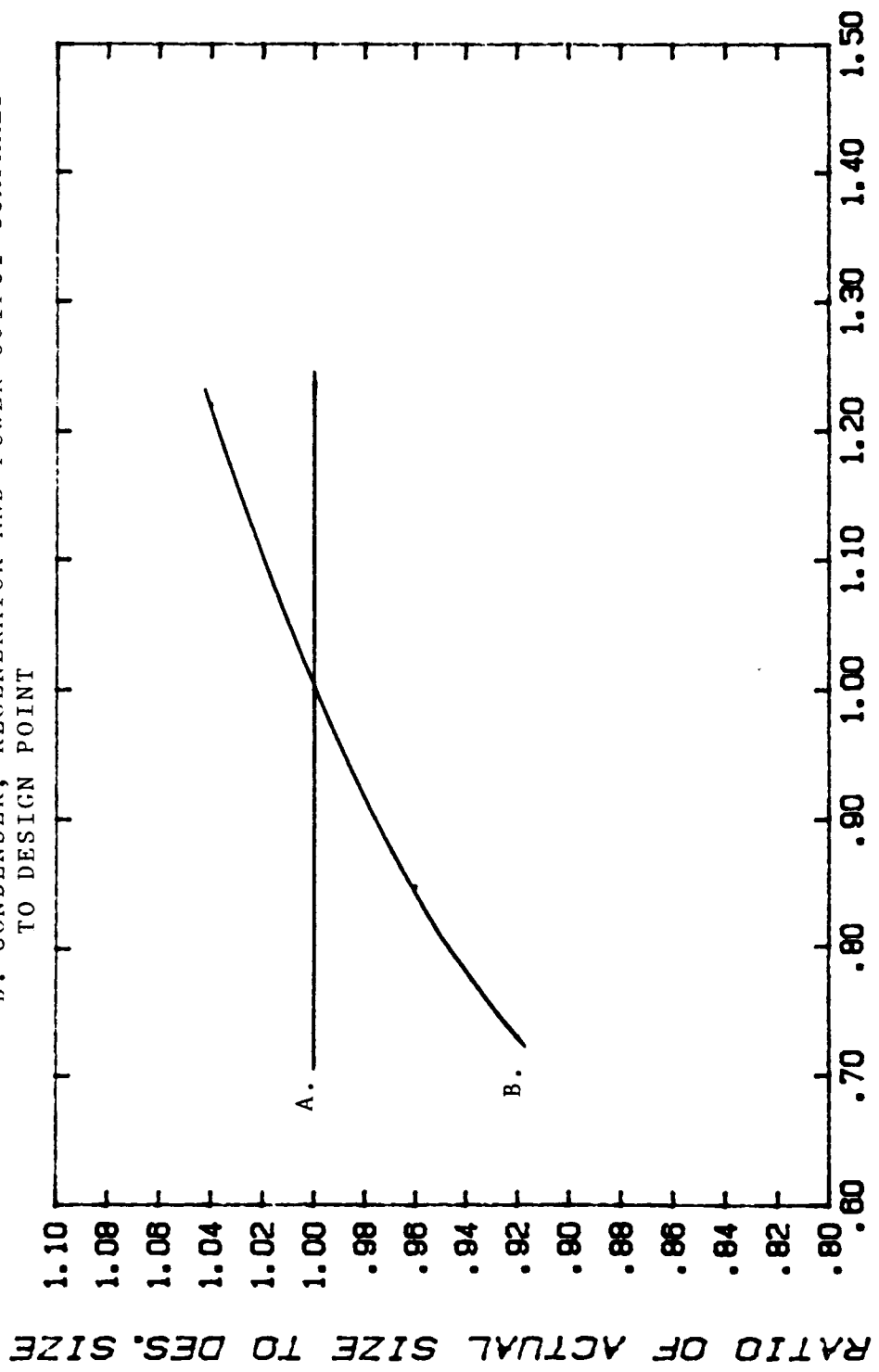
PARTLOAD ANALYSIS:

A partload analysis will be performed using the heat exchanger sizes selected for the design point condition. We have also estimated the effects of changes in the systems mass flow rate and the engine's speed (RPM) on the turbine's thermal efficiency (Figure 8). These effects were determined, in part, from the laboratory testing of a single stage, partial admission turbine that had been used in an earlier bottoming cycle project.

This partload analysis will be performed as soon as engine partload data has been received from DDA.

FIGURE 1 EFFECT OF VAPOR GEN. SIZE ON
SYSTEM COMPONENT PERFORMANCES

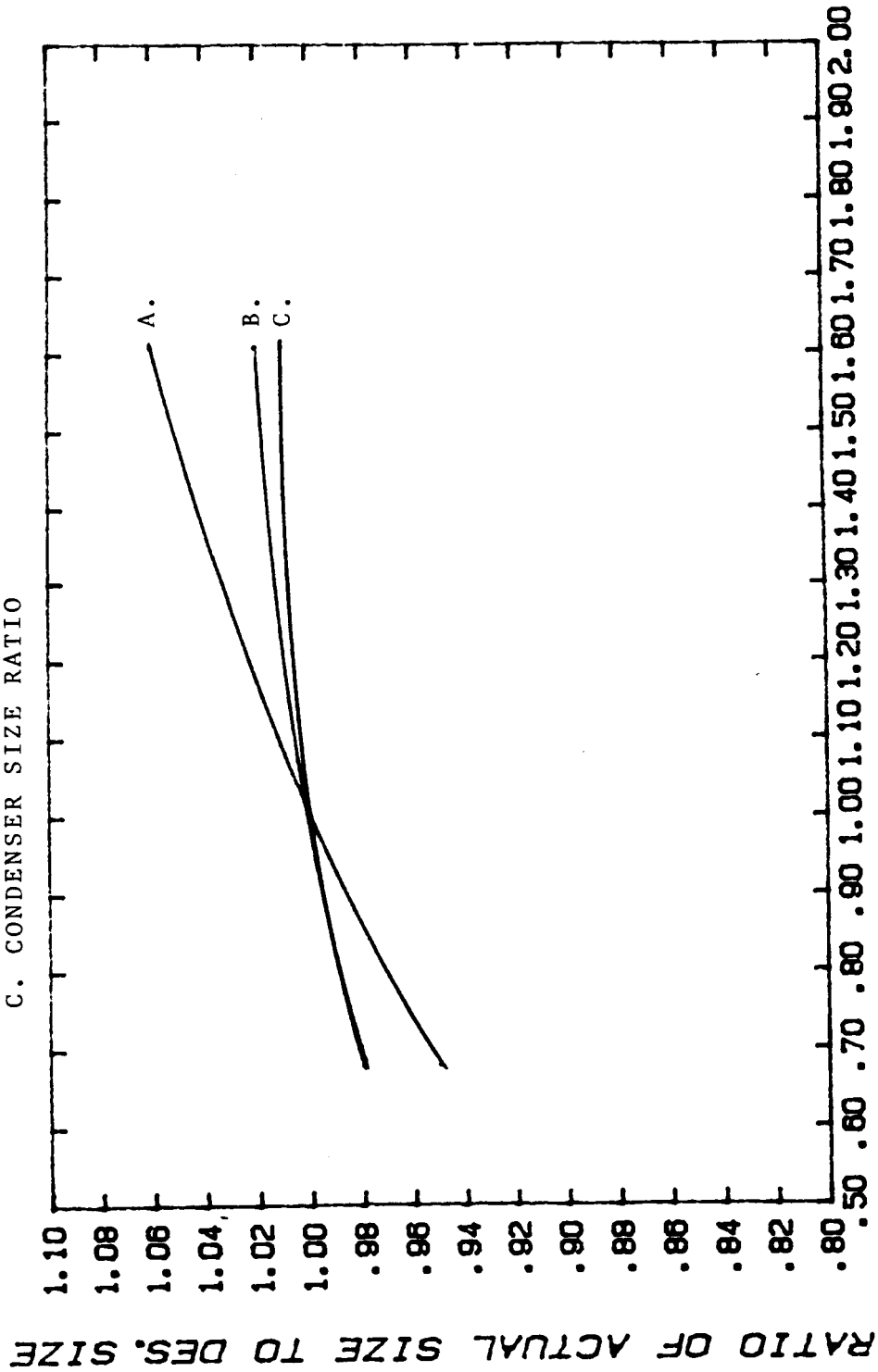
A. CYCLE EFF. COMPARED TO DESIGN POINT
B. CONDENSER, REGENERATOR AND POWER OUTPUT COMPARED TO DESIGN POINT



VAPOR GEN. SIZE RATIO (UA/UA0)

FIGURE 2 EFFECT OF REGENERATOR SIZE ON
SYSTEM COMPONENT PERFORMANCES

- A. VAPOR GENERATOR SIZE RATIO
- B. CYCLE EFF. AND POWER COMPARED TO DESIGN POINT
- C. CONDENSER SIZE RATIO



REGENERATOR SIZE RATIO (UA/UA0)

FIGURE 3 EFFECT OF CONDENSER SIZE ON
SYSTEM COMPONENT PERFORMANCES

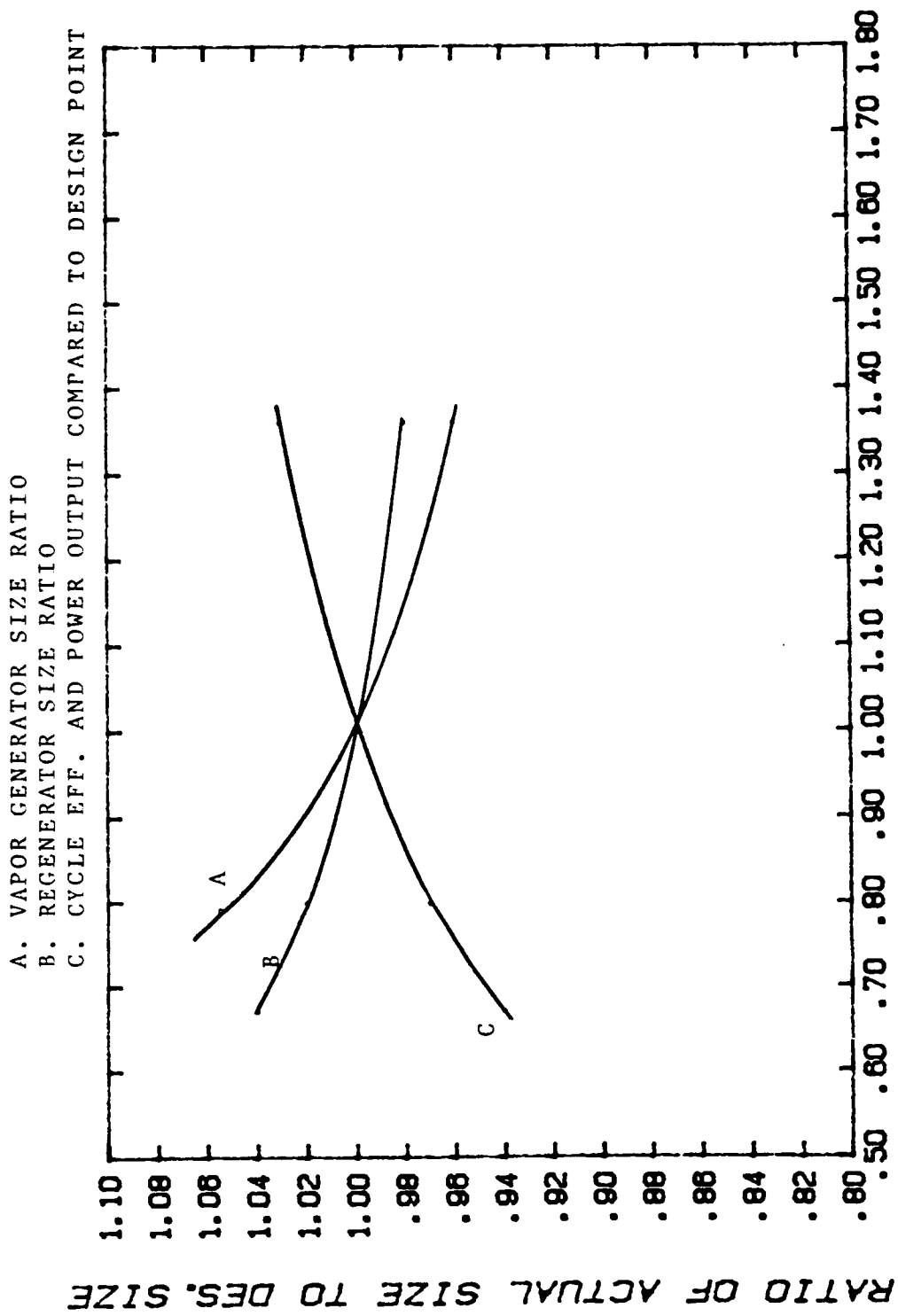
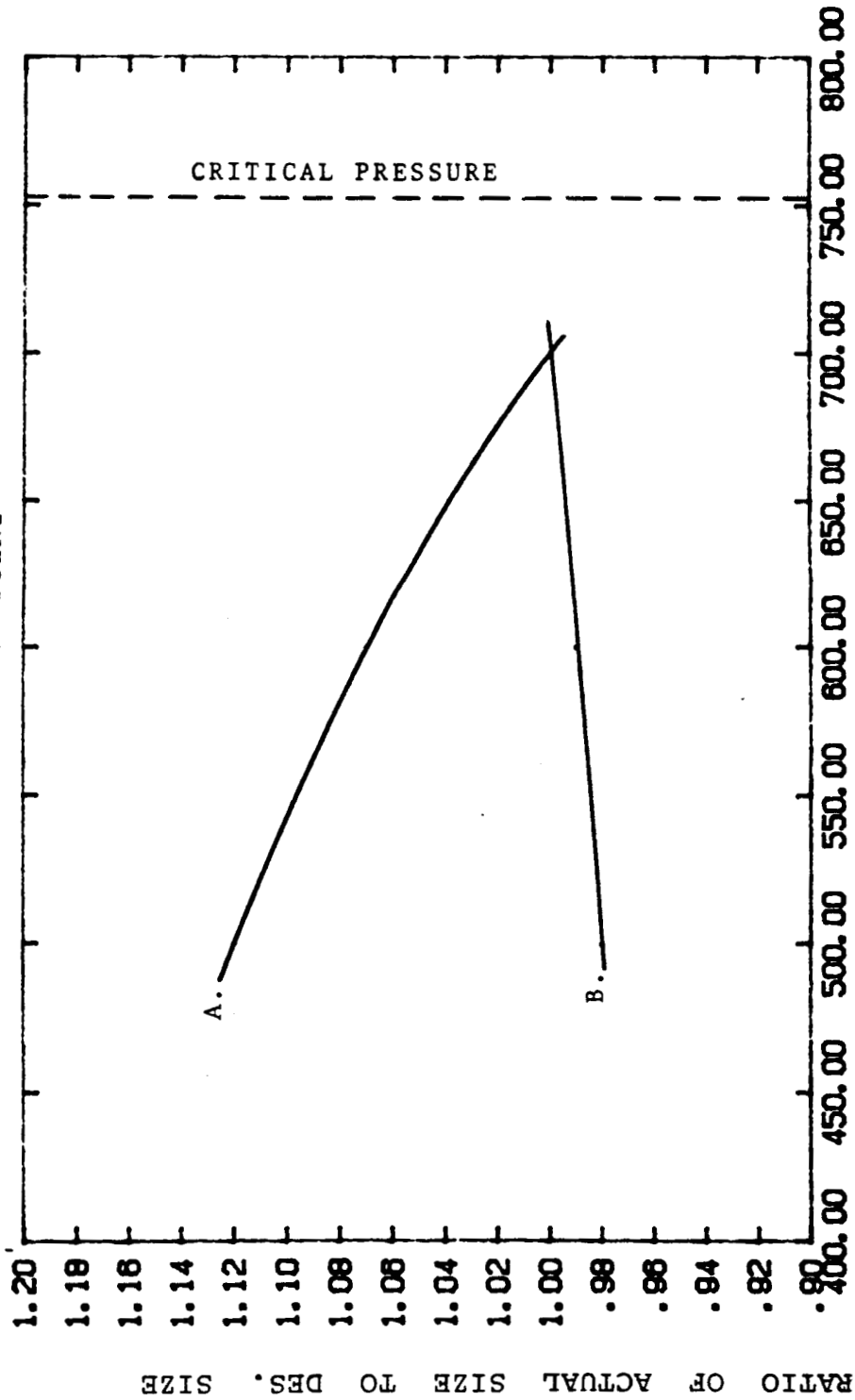


FIGURE 4 EFFECT OF SYSTEM PRESSURE ON
SYSTEM COMPONENT PERFORMANCES

A. VAPOR GENERATOR SIZE RATIO
B. REGENERATOR, CONDENSER, CYCLE EFF. AND POWER
COMPARED TO DESIGN POINT



SYSTEM PRESSURE (PSIA)

	T	P	H		DT	DP	DH
14 BOIL IN	228.95	750.00	89.24	BOIL	321.052	0.000	258.273
1 OUT	550.00	700.00	347.51	LINE	0.000	0.000	0.000
2 ENG IN	550.00	700.00	347.51	ENG	242.329	690.834	61.337
3 OUT	307.67	9.17	286.18	LINE	0.000	0.000	0.000
4 REGV IN	307.67	9.17	286.18	REGV	130.65	0.50	40.28
5 OUT	176.99	8.67	245.90	LINE	0.00	0.00	0.00
6 COND IN	176.99	8.67	245.90	COND	41.99	0.50	199.06
7 OUT	135.00	8.17	46.84	LINE	0.00	0.00	0.00
10 PUMP IN	135.00	8.17	46.84	PUMP	5.49	-746.83	2.12
11 OUT	140.49	755.00	48.97	LINE	0.00	0.00	0.00
12 REGL IN	140.49	755.00	48.97	REGL	88.46	5.00	40.28
13 OUT	228.95	750.00	89.24	LINE	0.00	0.00	0.00

SYSTEM

FLOWRATE = 1136.67 NET POWER(HP)= 25.35 CYCLE EFF= 0.22

EXPANDER

Q= 0.697E+05 GROSS HP= 26.30
 EFFTH= 0.8000 EFFME= 0.9600 EFFALL= 0.7680
 WES= 76.67 WSHAFT= 58.88 WNET= 56.76
 EXPANDER EXH. QUALITY= 1.00

REGENERATOR

EFF=0.8000 Q= 0.46E+05 UA= 833.

CONDENSER

Q= 0.23E+06 UATOTAL= 5768.
 HSUB= 1.93 HLATENT= 186.43 HDSUP= 10.70
 UASUB= 42. UACOND= 5435. UADESUP= 291.
 COOLANT T IN= 85.00 COOLANT T OUT= 115.00 COOLANT FLOW= 31425.79

BOILER

Q= 0.29E+06 UATOTAL= 2533.
 HSENS= 141.07 HLATENT= 55.93 HSUPER= 61.28
 UASENS= 1811. UALAT= 405. UASUPER= 317.

PUMP

EFF=0.8000 GPM= 1.75 HP= 0.95

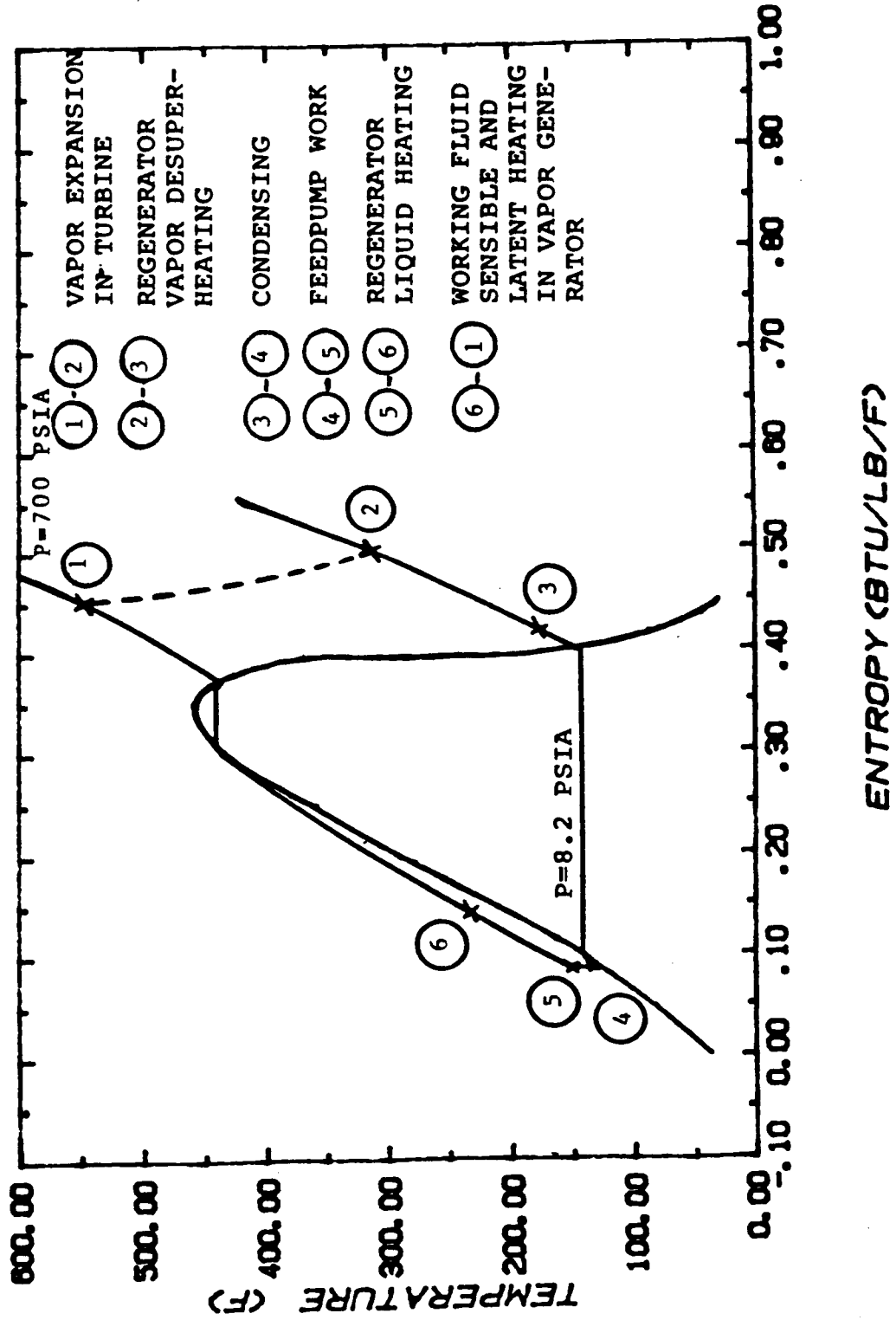
HEAT SOURCE

FLOWRATE= 2392.2 TGAS1= 772.0 TGAS0= 300.0
 T PINCH= 557.8 DT PINCH= 108.6

FIGURE 5 COMPUTER OUTPUT DESIGN POINT FOR AIR-COOLED FL-85 ORCS FOR THE DDA ADRE

ORIGINAL PAGE IS OF POOR QUALITY

FIGURE 6 CYCLE ILLUSTRATED ON FL-85
T-S DIAGRAM.



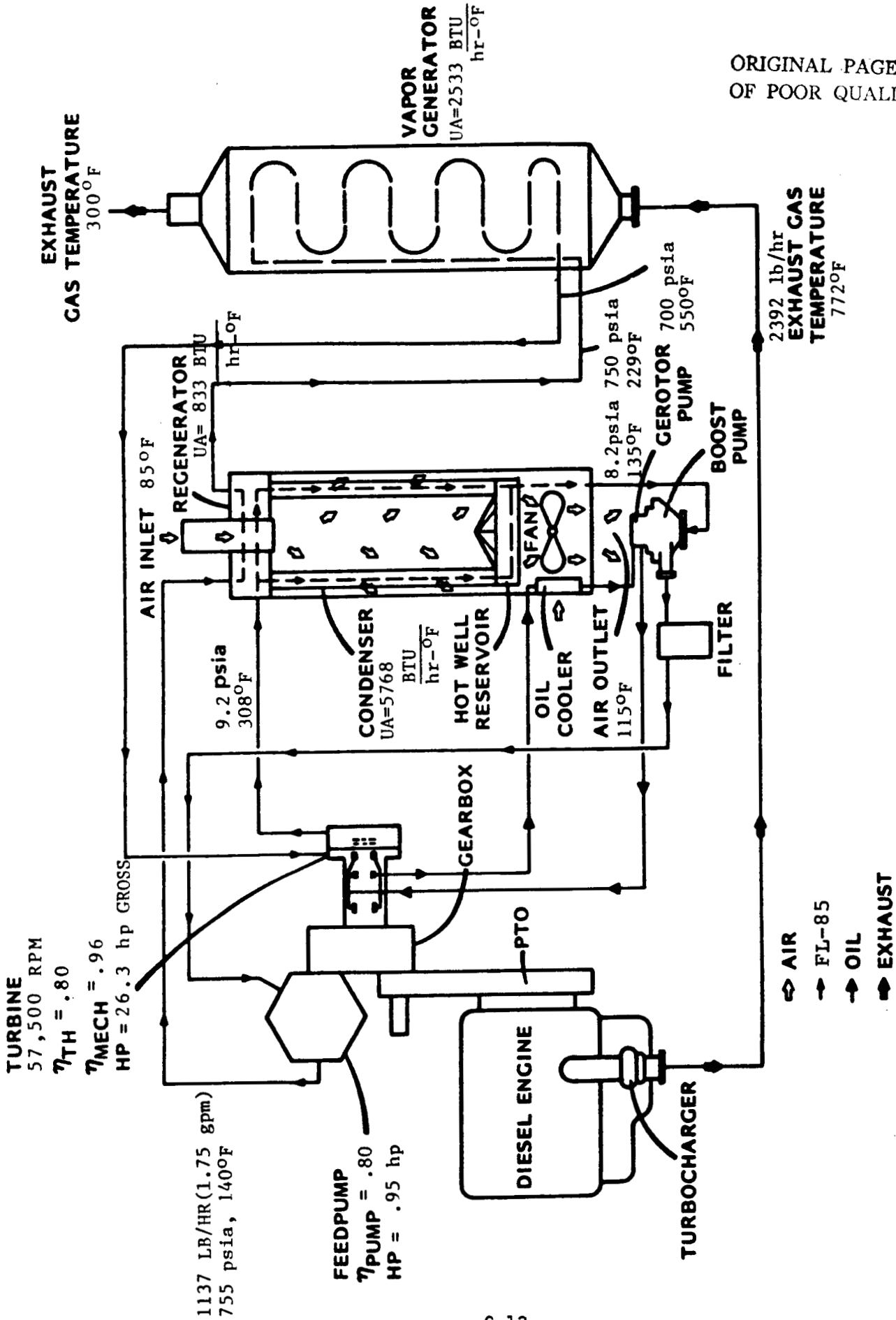
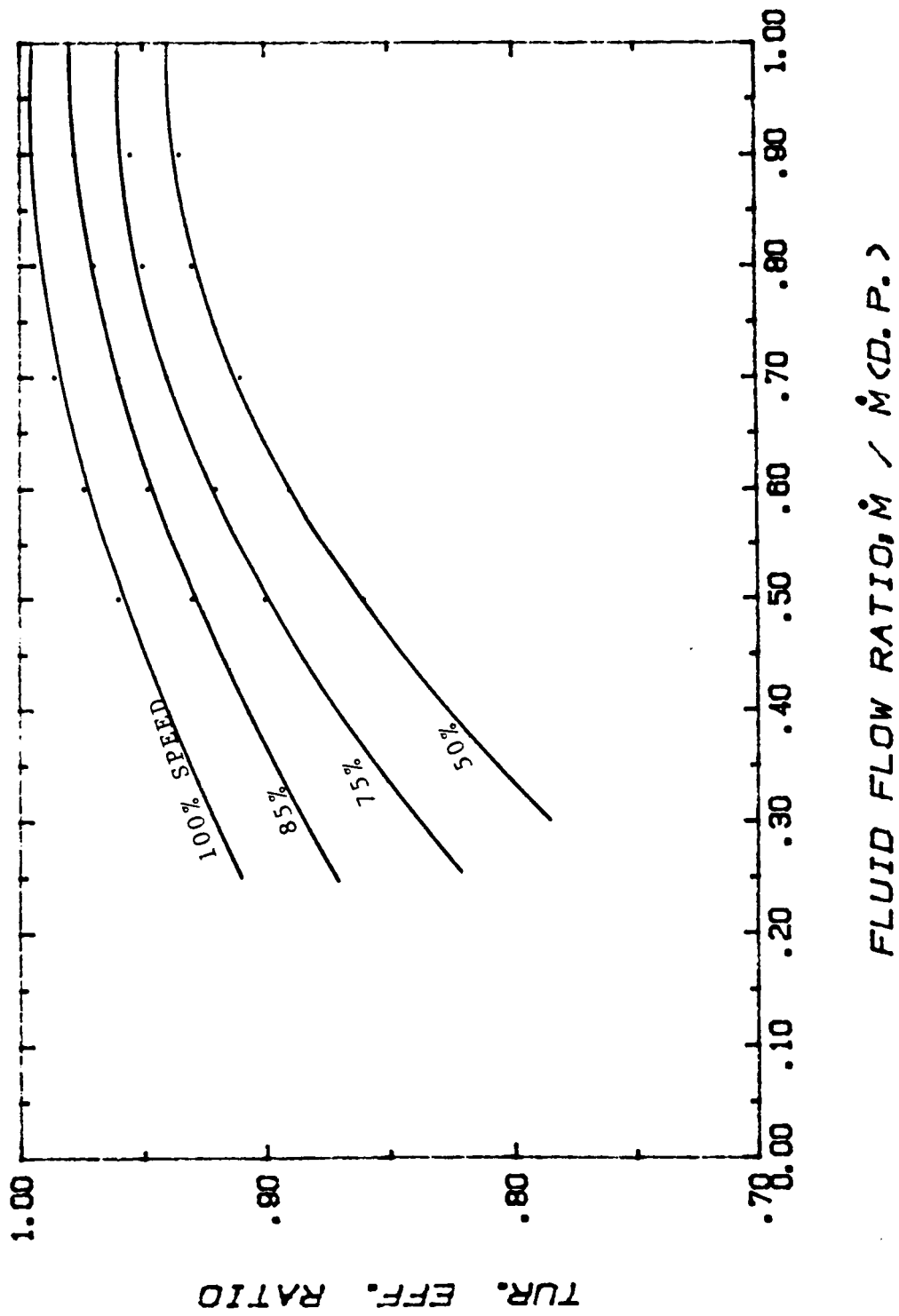


FIGURE 7 BOTTOMING SYSTEM SCHEMATIC WITH DESIGN POINT
CONDITIONS FOR DDA ADRE

FIGURE 8 EFFECTS OF PARTLOAD OPERATION
ON TURBINE EFFICIENCY



POWER CONVERSION UNIT FOR DDA-ADRE

The Organic Rankine Cycle System (ORCS) power conversion unit consists of the following components:

- o Turbine
- o Gearbox
- o Feedpump

These components are arranged around the engine flywheel housing which would have an "ear" at approximately the 10 o'clock position (when viewed from the flywheel end) to accommodate them. The general arrangement is shown in the enclosed drawing.

The turbine is a single stage design with a 3.85 inch diameter wheel operating at 57,500 RPM. The turbine is overhung with a double carbon face shaft seal between the wheel and two journal bearings on the turbine output shaft.

Output of the turbine is through a spline mounted quill shaft which drives the input sun gear in a double planetary gear train followed by one spur gear reduction. The total speed ratio is about 20 to 1. The final output gear has an integrally mounted over-running clutch in its hub which prevents the turbine and gearbox from being driven by the engine at light load conditions and also allows the engine to function normally in the event of an ORCS turbine or gearbox failure.

The gearbox output is connected to a long, flexible shaft which is sized to de-tune the turbine and gearbox from any torsional vibration present at the flywheel gear where the ORCS output flows into the powertrain. This system of over-running clutch and torsion bar coupling system has worked perfectly over many hours of dynamometer and vehicle testing with no failures in past systems. The fluid coupling approach is compact, but more costly and significantly less efficient.

One further gear reduction within the flywheel housing drops the speed from 3000 to 1800 RPM. A second speed reduction gear set on the torsion bar return shaft drives the feedpump at engine speed.

The feedpump is a three cylinder unit with a maximum displacement of 2 GPM at 1200 RPM. The pump is a variable displacement type of our own design. Control of the displacement of the pump is the way in which the power output of the ORCS is controlled. A signal from the engine proportional to total fuel flow is all that is required in the way of controls interface between the Diesel engine and the ORCS. We have found in past applications that the turbocharger boost pressure is a good analog of total fuel flow.

An alternate to the above arrangement would be to have the ORCS turbine and the turbo-compound turbine driving into a single gearbox, since both turbines operate at about the same speed. This arrangement is also shown in an attached drawing. In this arrangement the input sun gear would be driven from each side by each of the turbines. This would require a re-design of one of the two turbine housing castings and modifications of the input sun gear damper, which is now on the opposite side of the gear from the turbine input. The gearbox itself was designed to transmit 60 HP at 60,000 RPM input speed.

An additional advantage to the combined approach, besides the elimination of one entire gear train, would be a reduction in size of the torsion bar isolator due to the much higher effective inertia at the high speed end of the gear train.

The proposed gearbox has been designed, built, and tested as part of previous ORCS programs. It has not been used in vehicular applications to date because its high reduction ratio has not been required.

All of the other power conversion componentry described here has been used in the past, at least in somewhat larger scale configurations.

PARTLOAD ANALYSIS

FOR FL-85 ORGANIC RANKINE CYCLE SYSTEM (ORCS)

A partload analysis has been performed using the design point component sizes and performances previously selected for the D.D.A.-F185 Bottoming Cycle System (See Report TE 5629-01-86). The part load analysis proceeds by determining the performance expected of each system major component: the regenerator, condenser, boiler, turbine-gearbox as a function of working fluid flowrate, exhaustgas flowrate and engine speed. The following relationships were used to model the boiler and regenerator at partload.

UA Boiler = UA Boiler @ Design point

$$\times \left[\frac{\text{Exh. Gas Flow}}{\text{Exh. Gas @ Design Point}} \right] 0.8$$

$$\text{UA REGN.} = \text{UA REGN. @ Design point} \times \left[\frac{\text{Fluid Flow}}{\text{Fluid Flow @ Design Point}} \right]$$

The condenser's performance was assumed not to be significantly affected by the working fluid flow rate. Thus,

UA cond \approx UA cond @ design point for all partload cases.

It should be noted however that it was also assumed that the air flow cooling the condenser was equal to the air flow rate at design point. This assumption is valid if the engine's fan is driven by an electric motor and has only "on" or "off" temperature controls.

The turbine's partload performance is affected by engine speed and the working fluid flow rate. A graph of this dependency was given in the first report that summarized our Part I work (TE 5629-01-86).

The system's pressure was considered to be directly proportional to the working fluid flow rate. The vapor generator's tube side pressure drop was assumed to be proportional to the square of the working fluid flow rate.

The gearbox mechanical power losses (hp) were based on the following equation:

$$\text{HP Gearbox Loss} = \text{HP loss @ design point} \times \left[\frac{\text{ENG. RPM}}{1800} \right] \\ \times \left[\frac{\text{fluid flow rate}}{\text{fluid flow rate @ design point}} \right]$$

The values of exhaust gas temperature and flowrate that were used in this analysis to calculate the ORCS power output are summarized in Table 1 with other engine information submitted by DDA.

The results of this partload analysis are given in Figure 1 and Tables 2 thru 12.

Figure 1

**O. R. C. S. PARTLOAD PERFORMANCE
WITH D. D. A. ENGINE.**

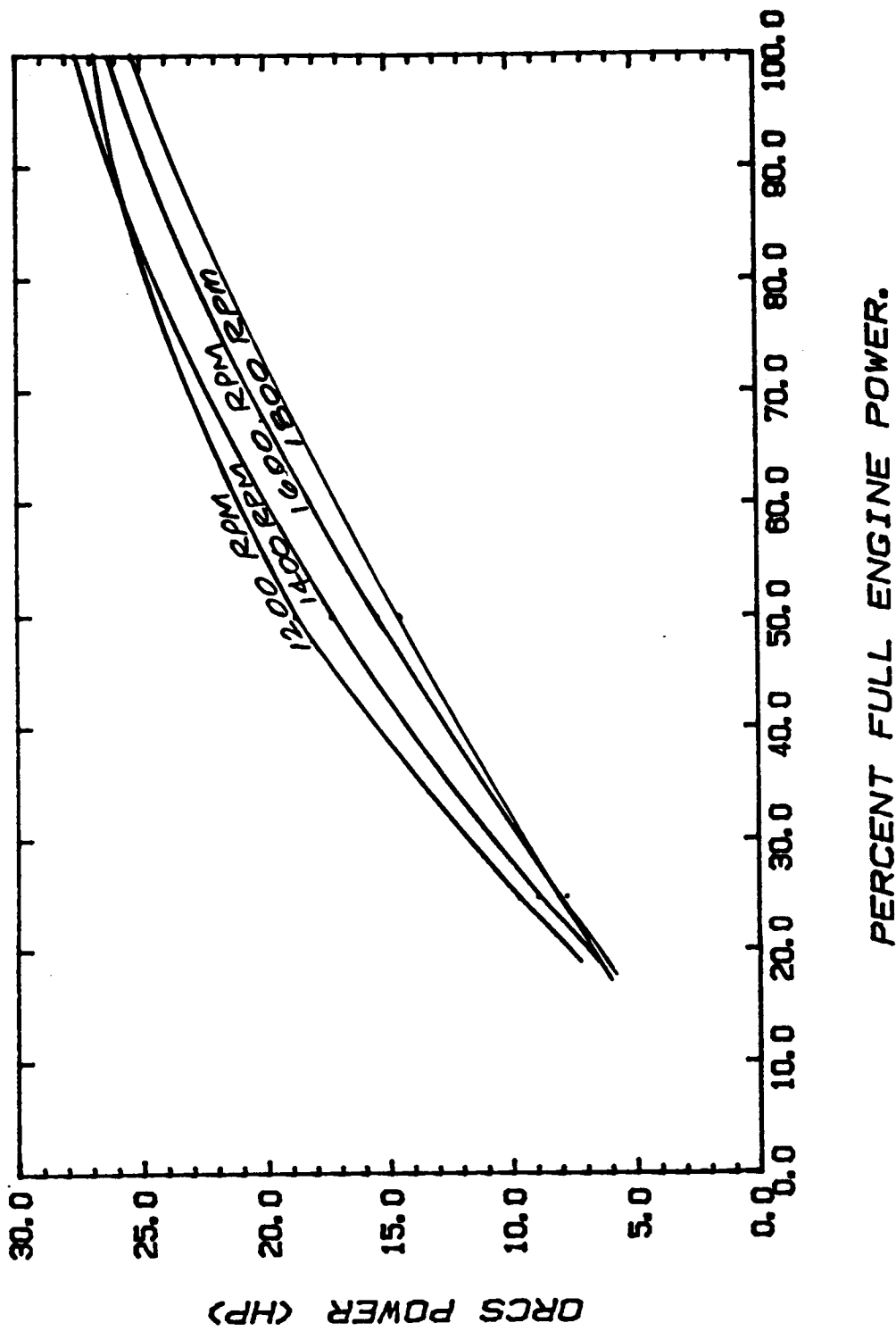


TABLE 1
ORCS POWER OUTPUT
FOR
DDA PARTLOAD ENGINE DATA

Engine Load (%)	Engine Speed (RPM)	Air/Fuel Ratio	Exhaust Temp. (°F)	Exhaust Flowrate (LB/HR)	ORCS Power (HP)
100	1,800	29	780	2,280	25.4*
	1,600	28	870	2,103	26.2
	1,400	25	1,000	1,794	27.5
	1,200	22	1,140	1,461	26.8
50	1,800	41	670	1,785	14.5
	1,600	40	730	1,648	15.4
	1,400	37	850	1,425	17.3
	1,200	35	1,000	1,224	18.8
25	1,800	56	570	1,484	8.1
	1,600	54	610	1,210	7.8
	1,400	53	710	1080	8.9
	1,200	51	840	920	9.7

*This ORCS Power Output is based on previous design point engine conditions specified by DDA (N=1800 RPM, Texh = 772°F and exhaust flowrate = 2392 Lbs/Hr).

TABLE 2
ORCS PERFORMANCE
AT N = 1600 RPM AND 100% ENGINE LOAD

	I	P	H		DT	DP	DH
14 BOIL IN	235.37	750.00	92.63	BOIL	314.629	0.000	254.882
1 OUT	550.00	700.00	347.51	LINE	0.000	0.000	0.000
2 ENG IN	550.00	700.00	347.51	ENG	233.221	689.574	58.473
3 OUT	316.78	10.43	289.04	LINE	0.000	0.000	0.000
4 REGV IN	316.78	10.43	289.04	REGV	133.26	0.50	41.34
5 OUT	183.51	9.93	247.71	LINE	0.00	0.00	0.00
6 COND IN	183.51	9.93	247.71	COND	42.51	0.50	198.54
9 OUT	141.00	9.43	49.17	LINE	0.00	0.00	0.00
10 PUMP IN	141.00	9.43	49.17	PUMP	5.39	-745.57	2.13
11 OUT	146.39	755.00	51.30	LINE	0.00	0.00	0.00
12 REGL IN	146.39	755.00	51.30	REGL	88.98	5.00	41.34
13 OUT	235.37	750.00	92.63	LINE	0.00	0.00	0.00

SYSTEM

FLOWRATE = 1233.50 NET POWER(HP)= 26.20 CYCLE EFF= 0.21

EXPANDER

Q= 0.721E+05 GROSS HP= 27.24
 EFFIH= 0.7840 EFFME= 0.9610 EFFALL= 0.7534
 WES= 74.58 WSHAFT= 56.19 WNET= 54.06
 EXPANDER EXH. QUALITY= 1.00

REGENERATOR EFF=0.8000 Q= 0.51E+05 UA= 904.

CONDENSER Q= 0.24E+06 UATOTAL= 5532.
 HSUB= 1.97 HLATENT= 185.64 HDESUP= 10.93
 UASUB= 42. UACOND= 5199. UADESUP= 291.
 COOLANT T IN= 85.00 COOLANT T OUT= 117.00 COOLANT FLOW= 31887.7

BOILER Q= 0.31E+06 UATOTAL= 2259.
 HSENS= 137.68 HLATENT= 55.93 HSUPER= 61.28
 UASENS= 1692. UALAT= 319. UASUPER= 248.

PUMP
 EFF=0.8000 GPM= 1.90 HP= 1.03

HEAT SOURCE

FLOWRATE= 2103.0 TGASI= 870.0 TGASO= 295.0
 T PINCH= 605.6 DT PINCH= 156.4

TABLE 3
ORCS PERFORMANCE
AT N = 1400 RPM AND 100% ENGINE LOAD

	T	P	H		DI	DP	DH
14 BOIL IN	237.33	750.00	93.66	BOIL	312.666	0.000	253.853
1 OUT	550.00	700.00	347.51	LINE	0.000	0.000	0.000
2 ENG IN	550.00	700.00	347.51	ENG	230.036	689.000	57.477
3 OUT	319.96	11.00	290.04	LINE	0.000	0.000	0.000
4 REGV IN	319.96	11.00	290.04	REGV	132.92	0.50	41.34
5 OUT	187.04	10.50	248.70	LINE	0.00	0.00	0.00
6 COND IN	187.04	10.50	248.70	COND	43.44	0.50	198.51
9 OUT	143.60	10.00	50.19	LINE	0.00	0.00	0.00
10 PUMP IN	143.60	10.00	50.19	PUMP	5.37	-745.00	2.13
11 OUT	148.97	755.00	52.32	LINE	0.00	0.00	0.00
12 REGL IN	148.97	755.00	52.32	REGL	88.36	5.00	41.34
13 OUT	237.33	750.00	93.66	LINE	0.00	0.00	0.00

SYSTEM

FLOWRATE = 1313.77 NET POWER(HP)= 27.53 CYCLE EFF= 0.21

EXPANDER

Q= 0.755E+05 GROSS HP= 28.63
 EFFTH= 0.7800 EFFME= 0.9650 EFFALL= 0.7527
 WES= 73.69 WSHAFT= 55.47 WNET= 53.33
 EXPANDER EXH. QUALITY= 1.00

REGENERATOR EFF=0.7950 Q= 0.54E+05 UA= 945.

CONDENSER Q= 0.26E+06 UATOTAL= 5743.
 HSUP= 1.98 HLATENT= 185.29 HDESUP= 11.24
 UASUB= 43. UACOND= 5386. UADESUP= 315.
 COOLANT T IN= 85.00 COOLANT T OUT= 119.60 COOLANT FLOW= 31405.50

BOILER Q= 0.33E+06 UATOTAL= 2032.
 HSENS= 136.65 HLATENT= 55.93 HSUPER= 61.28
 UASENS= 1590. UALAT= 249. UASUPER= 193.

PUMP

EFF=0.8000 GPM= 2.03 HP= 1.10

HEAT SOURCE

FLOWRATE= 1794.0 TGASI= 1000.0 TGASO= 285.0
 T PINCH= 669.9 DT PINCH= 220.7

TABLE 4
ORCS PERFORMANCE
AT N = 1200 RPM AND 100% ENGINE LOAD

	T	P	H		DT	DP	DH
14 BOIL IN	238.05	750.00	94.03	BOIL	311.954	0.000	253.480
1 OUT	550.00	700.00	347.51	LINE	0.000	0.000	0.000
2 ENG IN	550.00	700.00	347.51	ENG	228.003	689.176	56.804
3 OUT	322.00	10.82	290.71	LINE	0.000	0.000	0.000
4 REGV IN	322.00	10.82	290.71	REGV	135.07	0.50	42.03
5 OUT	186.93	10.32	248.68	LINE	0.00	0.00	0.00
6 COND IN	186.93	10.32	248.68	COND	44.13	0.50	198.81
9 OUT	142.80	9.82	49.88	LINE	0.00	0.00	0.00
10 PUMP IN	142.80	9.82	49.88	PUMP	5.38	-745.18	2.13
11 OUT	148.18	755.00	52.01	LINE	0.00	0.00	0.00
12 REGL IN	148.18	755.00	52.01	REGL	89.87	5.00	42.03
13 OUT	238.05	750.00	94.03	LINE	0.00	0.00	0.00

SYSTEM
FLOWRATE = 1288.78 NET POWER(HP)= 26.82 CYCLE EFF= 0.21

EXPANDER
Q= 0.732E+05 GROSS HP= 27.90
EFFTH= 0.7680 EFFME= 0.9700 EFFALL= 0.7450
WES= 73.96 WSHAFT= 55.10 WNET= 52.97
EXPANDER EXH. QUALITY= 1.00

REGENERATOR EFF=0.7950 Q= 0.54E+05 UA= 926.

CONDENSER Q= 0.26E+06 UATOTAL= 5680.
HSUB= 1.98 HLATENT= 185.39 HDESUP= 11.43
UASUB= 42. UACOND= 5325. UADESUP= 313.
COOLANT I IN= 85.00 COOLANT I OUT= 118.80 COOLANT FLOW= 31584.89

BOILER Q= 0.33E+06 UATOTAL= 1694.
HSENS= 136.28 HLATENT= 55.93 HSUPER= 61.28
UASENS= 1359. UALAT= 188. UASUPER= 147.

PUMP
EFF=0.8000 GPM= 1.99 HP= 1.08

HEAT SOURCE
FLOWRATE= 1461.0 TGASI= 1140.0 TGASO= 280.0
T PINCH= 742.4 DT PINCH= 293.2

TABLE 5
ORCS PERFORMANCE
AT N = 1800 RPM AND 50% ENGINE LOAD

	I	P	H		DT	DP	DH
14 BOIL IN	238.95	430.00	94.51	BOIL	311.048	0.000	263.673
1 OUT	550.00	400.00	358.18	LINE	0.000	0.000	0.000
2 ENG IN	550.00	400.00	358.18	ENG	211.527	394.365	61.830
3 OUT	338.47	5.64	296.35	LINE	0.000	0.000	0.000
4 REGV IN	338.47	5.64	296.35	REGV	179.36	0.50	55.30
5 OUT	159.11	5.14	241.05	LINE	0.00	0.00	0.00
6 COND IN	159.11	5.14	241.05	COND	47.51	0.50	203.05
9 OUT	111.60	4.64	38.01	LINE	0.00	0.00	0.00
10 PUMP IN	111.60	4.64	38.01	PUMP	3.21	-430.36	1.21
11 OUT	114.81	435.00	39.21	LINE	0.00	0.00	0.00
12 REGL IN	114.81	435.00	39.21	REGL	124.14	5.00	55.30
13 OUT	238.95	430.00	94.51	LINE	0.00	0.00	0.00

SYSTEM

FLOWRATE = 633.65 NET POWER(HP)= 14.49 CYCLE EFF= 0.22

EXPANDER

Q= 0.392E+05 GROSS HP= 14.79
 EFFTH= 0.7720 EFFME= 0.9609 EFFALL= 0.7418
 WES= 80.09 WSHAFT= 59.41 WNET= 58.21
 EXPANDER EXH. QUALITY= 1.00

REGENERATOR EFF=0.8350 Q= 0.35E+05 UA= 514.

CONDENSER Q= 0.13E+06 UATOTAL= 5596.
 HSUB= 1.87 HLATENT= 189.16 HDESUP= 12.02
 UASUB= 41. UACOND= 5316. UADESUP= 239.
 COOLANT T IN= 85.00 COOLANT T OUT= 102.10 COOLANT FLOW= 31350.3E

BOILER Q= 0.17E+06 UATOTAL= 2055.
 HSENS= 89.91 HLATENT=106.06 HSUPER= 67.70
 UASENS= 1069. UALAT= 705. UASUPER= 281.

PUMP
 EFF=0.8000 GPM= 0.96 HP= 0.30

HEAT SOURCE

FLOWRATE= 1785.0 IGASI= 670.0 IGASO= 310.0
 I PINCH= 432.8 DT PINCH= 38.8

TABLE 6
ORCS PERFORMANCE
AT N = 1600 RPM AND 50% ENGINE LOAD

	T	P	H		DT	DP	DH
14 BOIL IN	240.71	450.00	95.44	BOIL	309.295	0.000	261.934
1 OUT	550.00	425.00	357.37	LINE	0.000	0.000	0.000
2 ENG IN	550.00	425.00	357.37	ENG	208.619	419.080	60.083
3 OUT	341.38	5.92	297.29	LINE	0.000	0.000	0.000
4 REGV IN	341.38	5.92	297.29	REGV	178.83	0.50	55.27
5 OUT	162.55	5.42	242.02	LINE	0.00	0.00	0.00
6 COND IN	162.55	5.42	242.02	COND	48.55	0.50	203.11
9 OUT	114.00	4.92	38.91	LINE	0.00	0.00	0.00
10 PUMP IN	114.00	4.92	38.91	PUMP	3.38	-450.08	1.26
11 OUT	117.38	455.00	40.17	LINE	0.00	0.00	0.00
12 REGL IN	117.38	455.00	40.17	REGL	123.32	5.00	55.27
13 OUT	240.71	450.00	95.44	LINE	0.00	0.00	0.00

SYSTEM

FLOWRATE = 693.59 NET POWER(HP)= 15.42 CYCLE EFF= 0.22

EXPANDER

Q= 0.417E+05 GROSS HP= 15.77
 EFFTH= 0.7520 EFFME= 0.9630 EFFALL= 0.7242
 WES= 79.90 WSHAFT= 57.86 WNET= 56.60
 EXPANDER EXH. QUALITY= 1.00

REGENERATOR EFF=0.3300 Q= 0.38E+05 UA= 553.

CONDENSER Q= 0.14E+06 UATOTAL= 5707.
 HSUB= 1.87 HLATENT= 188.89 HDESUP= 12.35
 UASUB= 41. UACOND= 5410. UADESUP= 256.
 COOLANT I IN= 85.00 COOLANT I OUT= 103.50 COOLANT FLOW= 31729.5

BOILER Q= 0.18E+06 UATOTAL= 1859.
 HSENS= 91.81 HLATENT=103.58 HSUPER= 66.55
 UASENS= 1049. UALAT= 583. UASUPER= 227.

PUMP
 EFF=0.8000 GPM= 1.05 HP= 0.34

HEAT SOURCE

FLOWRATE= 1648.0 TGASI= 730.0 IGASO= 306.0
 I PINCH= 454.6 DI PINCH= 56.3

TABLE 7
ORCS PERFORMANCE
AT N = 1400 RPM AND 50% ENGINE LOAD

	T	P	H		DT	DP	DH
14 BOIL IN	240.26	500.00	95.20	BOIL	309.742	0.000	260.517
1 OUT	550.00	475.00	355.71	LINE	0.000	0.000	0.000
2 ENG IN	550.00	475.00	355.71	ENG	209.471	468.452	58.738
3 OUT	340.53	6.55	296.98	LINE	0.000	0.000	0.000
4 REGV IN	340.53	6.55	296.98	REGV	171.20	0.50	53.05
5 OUT	169.33	6.05	243.92	LINE	0.00	0.00	0.00
6 COND IN	169.33	6.05	243.92	COND	50.43	0.50	203.19
9 OUT	118.90	5.55	40.74	LINE	0.00	0.00	0.00
10 PUMP IN	118.90	5.55	40.74	PUMP	3.75	-499.45	1.41
11 OUT	122.65	505.00	42.14	LINE	0.00	0.00	0.00
12 REGL IN	122.65	505.00	42.14	REGL	117.61	5.00	53.05
13 OUT	240.26	500.00	95.20	LINE	0.00	0.00	0.00

SYSTEM
FLOWRATE = 792.15 NET POWER(HP)= 17.30 CYCLE EFF= 0.21

EXPANDER
Q= 0.465E+05 GROSS HP= 17.73
EFFTH= 0.7400 EFFME= 0.9700 EFFALL= 0.7178
WES= 79.38 WSHAFT= 56.98 WNET= 55.57
EXPANDER EXH. QUALITY= 1.00

REGENERATOR EFF=0.8150 Q= 0.42E+05 UA= 600.

CONDENSER Q= 0.16E+06 UATOTAL= 5726.
HSUB= 1.88 HLAIENT= 188.35 HDESUP= 12.96
UASUB= 41. UACOND= 5405. UADESUP= 281.
COOLANT T IN= 85.00 COOLANT T OUT= 106.40 COOLANT FLOW= 31338.36

BOILER Q= 0.21E+06 UATOTAL= 1674.
HSENS= 98.90 HLAIENT= 97.17 HSUPER= 64.44
UASENS= 1084. UALAI= 422. UASUPER= 168.

PUMP
EFF=0.8000 GPM= 1.21 HP= 0.44

HEAT SOURCE
FLOWRATE= 1425.0 TGASI= 850.0 TGASO= 293.0
T PINCH= 504.5 DT PINCH= 96.2

TABLE 8
ORCS PERFORMANCE
AT N = 1200 RPM AND 50% ENGINE LOAD

	T	P	H		DT	DP	DH
14 BOIL IN	240.38	570.00	95.26	BOIL	309.624	0.000	258.217
1 OUT	550.00	540.00	353.48	LINE	0.000	0.000	0.000
2 ENG IN	550.00	540.00	353.48	ENG	212.606	532.858	57.555
3 OUT	337.39	7.14	295.92	LINE	0.000	0.000	0.000
4 REGV IN	337.39	7.14	295.92	REGV	165.70	0.50	51.37
5 OUT	171.69	6.64	244.55	LINE	0.00	0.00	0.00
6 COND IN	171.69	6.64	244.55	COND	48.67	0.50	202.27
9 OUT	123.02	6.14	42.28	LINE	0.00	0.00	0.00
10 PUMP IN	123.02	6.14	42.28	PUMP	4.26	-568.86	1.61
11 OUT	127.28	575.00	43.89	LINE	0.00	0.00	0.00
12 REGL IN	127.28	575.00	43.89	REGL	113.10	5.00	51.37
13 OUT	240.38	570.00	95.26	LINE	0.00	0.00	0.00

SYSTEM

FLOWRATE = 881.20 NET POWER(HP)= 18.79 CYCLE EFF= 0.21

EXPANDER

Q= 0.507E+05 GROSS HP= 19.35
 EFFIH= 0.7280 EFFME= 0.9710 EFFALL= 0.7069
 WES= 79.06 WSHAFI= 55.89 WNET= 54.28
 EXPANDER EXH. QUALITY= 1.00

REGENERATOR EFF=0.8150 Q= 0.45E+05 UA= 672.

CONDENSER Q= 0.18E+05 UATOTAL= 5753.
 HSUB= 1.89 HLATENT= 187.87 HDESUP= 12.51
 UASUB= 41. UACOND= 5423. UADESUP= 289.
 COULANT I IN= 85.00 COULANT I OUT= 108.62 COULANT FLOW= 31442.24

BOILER Q= 0.23E+06 UATOTAL= 1458.
 HSENS= 108.15 HLATENT= 87.97 HSUPER= 62.10
 UASENS= 1043. UALAT= 289. UASUPER= 127.

PUMP
 EFF=0.8000 GPM= 1.34 HP= 0.56

HEAT SOURCE

FLWRATE= 1224.0 TGASI= 1000.0 TGASO= 285.0
 T PINCH= 584.5 DT PINCH= 163.1

TABLE 9
ORCS PERFORMANCE
AT N = 1800 RPM AND 25% ENGINE LOAD

	T	P	H		DT	DP	DH
14 BOIL IN	250.97	260.00	100.99	BOIL	299.033	0.000	261.811
1 OUT	350.00	250.00	362.80	LINE	0.000	0.000	0.000
2 ENG IN	550.00	250.00	362.80	ENG	185.530	245.658	57.816
3 OUT	364.47	4.34	304.98	LINE	0.000	0.000	0.000
4 REGV IN	364.47	4.34	304.98	REGV	216.34	0.50	66.94
5 OUT	148.13	3.84	238.04	LINE	0.00	0.00	0.00
6 COND IN	148.13	3.84	238.04	COND	48.93	0.50	204.72
9 OUT	99.20	3.34	33.32	LINE	0.00	0.00	0.00
10 PUMP IN	99.20	3.34	33.32	PUMP	1.91	-261.66	0.73
11 OUT	101.11	265.00	34.05	LINE	0.00	0.00	0.00
12 REGL IN	101.11	265.00	34.05	REGL	149.85	5.00	66.94
13 OUT	250.97	260.00	100.99	LINE	0.00	0.00	0.00

SYSTEM
FLOWRATE = 375.80 NET POWER(HP)= 8.06 CYCLE EFF= 0.21

EXPANDER
Q= 0.217E+05 GROSS HP= 8.17
EFFTH= 0.7360 EFFME= 0.9570 EFFALL= 0.7044
WES= 78.55 WSHAFT= 55.33 WNET= 54.60
EXPANDER EXH. QUALITY= 1.00

REGENERATOR EFF=0.8600 Q= 0.25E+05 UA= 333.

CONDENSER Q= 0.77E+05 UATOTAL= 5407.
HSUR= 1.90 HLATENT= 190.56 HDESUP= 12.26
UASUR= 43. UACOND= 5182. UADESUP= 182.
COOLANT T IN= 85.00 COOLANT T OUT= 95.20 COOLANT FLOW= 31427.98

BOILER Q= 0.98E+05 UATOTAL= 1747.
HSENS= 55.72 HLATENT=127.65 HSUPER= 78.44
UASENS= 546. UALAT= 740. UASUPER= 460.

PUMP
EFF=0.8000 GPM= 0.56 HP= 0.11

HEAT SOURCE
FLOWRATE= 1484.0 TGASI= 570.0 TGASO= 315.0
T PINCH= 369.3 DT PINCH= 20.6

TABLE 10
ORCS PERFORMANCE
AT N = 1600 RPM AND 25% ENGINE LOAD

	T	P	H		DT	DP	DH
14 BOIL IN	252.32	260.00	101.72	BOIL	297.681	0.000	261.079
1 OUT	550.00	250.00	362.80	LINE	0.000	0.000	0.000
2 ENG IN	550.00	250.00	362.80	ENG	182.409	245.735	56.774
3 OUT	367.59	4.26	306.02	LINE	0.000	0.000	0.000
4 REGV IN	367.59	4.26	306.02	REGV	219.61	0.50	68.01
5 OUT	147.98	3.76	238.01	LINE	0.00	0.00	0.00
6 COND IN	147.98	3.76	238.01	COND	49.68	0.50	205.03
9 OUT	98.30	3.26	32.98	LINE	0.00	0.00	0.00
10 PUMP IN	98.30	3.26	32.98	PUMP	1.91	-261.74	0.73
11 OUT	100.21	265.00	33.71	LINE	0.00	0.00	0.00
12 REGL IN	100.21	265.00	33.71	REGL	152.11	5.00	68.01
13 OUT	252.32	260.00	101.72	LINE	0.00	0.00	0.00

SYSTEM
FLOWRATE = 366.32 NET POWER(HP)= 7.76 CYCLE EFF= 0.21

EXPANDER
Q= 0.208E+05 GROSS HP= 7.87
EFFTH= 0.7200 EFFME= 0.9630 EFFALL= 0.6934
WES= 78.85 WSHAFT= 54.67 WNET= 53.94
EXPANDER EXH. QUALITY= 1.00

REGENERATOR EFF=0.8600 Q= 0.25E+05 UA= 325.

CONDENSER Q= 0.75E+05 UATOTAL= 5599.
HSUR= 1.90 HLATENT= 190.66 HDESUP= 12.47
UASUB= 45. UACOND= 5369. UADESUP= 185.
COOLANT T IN= 85.00 COOLANT T OUT= 95.00 COOLANT FLOW= 31294.99

BOILER Q= 0.96E+05 UATOTAL= 1486.
HSENS= 54.99 HLATENT=127.65 HSUPER= 78.44
UASENS= 574. UALAT= 643. UASUPER= 269.

PUMP
EFF=0.8000 GPM= 0.55 HP= 0.10

HEAT SOURCE
FLOWRATE= 1210.0 TGASI= 610.0 IGASO= 306.0
T PINCH= 370.0 DT PINCH= 21.4

TABLE 11
ORCS PERFORMANCE
AT N = 1400 RPM AND 25% ENGINE LOAD

	T	P	H		DT	DP	DH
14 BOIL IN	258.83	260.00	105.33	BOIL	291.171	0.000	257.466
1 OUT	550.00	250.00	362.80	LINE	0.000	0.000	0.000
2 ENG IN	550.00	250.00	362.80	ENG	172.072	245.394	53.349
3 OUT	377.93	4.61	309.45	LINE	0.000	0.000	0.000
4 REGV IN	377.93	4.61	309.45	REGV	225.56	0.50	70.22
5 OUT	152.37	4.11	239.23	LINE	0.00	0.00	0.00
6 COND IN	152.37	4.11	239.23	COND	50.38	0.50	204.85
9 OUT	101.99	3.61	34.38	LINE	0.00	0.00	0.00
10 PUMP IN	101.99	3.61	34.38	PUMP	1.92	-261.39	0.73
11 OUT	103.91	265.00	35.11	LINE	0.00	0.00	0.00
12 REGL IN	103.91	265.00	35.11	REGL	154.92	5.00	70.22
13 OUT	258.83	260.00	105.33	LINE	0.00	0.00	0.00

SYSTEM

FLOWRATE = 447.16 NET POWER(HP)= 8.91 CYCLE EFF= 0.20

EXPANDER

Q= 0.239E+05 GROSS HP= 9.04
 EFFTH= 0.6880 EFFME= 0.9640 EFFALL= 0.6632
 WES= 77.54 WSHAFT= 51.43 WNET= 50.70
 EXPANDER EXH. QUALITY= 1.00

REGENERATOR EFF=0.8600 Q= 0.31E+05 UA= 400.

CONDENSER Q= 0.92E+05 UATOTAL= 5719.
 HSUB= 1.89 HLATENT= 190.24 HDESUP= 12.72
 UASUB= 44. UACOND= 5465. UADESUP= 210.
 COOLANT I IN= 85.00 COOLANT I OUT= 97.14 COOLANT FLOW= 31438.31

BOILER Q= 0.12E+06 UATOTAL= 1344.
 HSENS= 51.37 HLATENT=127.65 HSUPER= 72.44
 UASENS= 620. UALAT= 546. UASUPER= 178.

PUMP
 EFF=0.8000 GPM= 0.67 HP= 0.13

HEAT SOURCE

FLOWRATE= 1080.0 IGASI= 710.0 IGASO= 300.0
 I PINCH= 381.8 DI PINCH= 33.2

TABLE 12
ORCS PERFORMANCE
AT N = 1200 RPM AND 25% ENGINE LOAD

	T	P	H		DT	DP	DH
14 BOIL IN	262.45	260.00	107.34	BOIL	287.553	0.000	255.461
1 OUT	550.00	250.00	362.80	LINE	0.000	0.000	0.000
2 ENG IN	550.00	250.00	362.80	ENG	164.126	245.084	50.695
3 OUT	385.87	4.92	312.10	LINE	0.000	0.000	0.000
4 REGV IN	385.87	4.92	312.10	REGV	226.95	0.50	71.02
5 OUT	158.92	4.42	241.08	LINE	0.00	0.00	0.00
6 COND IN	158.92	4.42	241.08	COND	53.77	0.50	205.49
9 OUT	105.15	3.92	35.59	LINE	0.00	0.00	0.00
10 PUMP IN	105.15	3.92	35.59	PUMP	1.94	-261.08	0.73
11 OUT	107.09	265.00	36.31	LINE	0.00	0.00	0.00
12 REGL IN	107.09	265.00	36.31	REGL	155.35	5.00	71.02
13 OUT	262.45	260.00	107.34	LINE	0.00	0.00	0.00

SYSTEM

FLOWRATE = 510.31 NET POWER(HP)= 9.68 CYCLE EFF= 0.19

EXPANDER

Q= 0.259E+05 GROSS HP= 9.83
 EFFTH= 0.6640 EFFME= 0.9670 EFFALL= 0.6421
 WES= 76.35 WSHAFT= 49.02 WNET= 48.29
 EXPANDER EXH. QUALITY= 1.00

REGENERATOR EFF=0.8500 Q= 0.36E+05 UA= 439.

CONDENSER Q= 0.10E+06 UA TOTAL= 5709.
 HSUB= 1.88 H LATENT= 189.88 H DESUP= 13.74
 UASUB= 43. UACOND= 5432. UADESUP= 234.
 COOLANT T IN= 85.00 COOLANT T OUT= 98.90 COOLANT FLOW= 31434.64

BOILER Q= 0.13E+06 UA TOTAL= 1175.
 HSENS= 49.37 H LATENT= 127.65 H SUPER= 78.44
 UASENS= 609. UALAT= 436. UASUPER= 130.

PUMP
 EFF=0.8000 GPM= 0.77 HP= 0.15

HEAT SOURCE

FLOWRATE= 920.0 TGASI= 840.0 TGASO= 295.0
 T PINCH= 400.3 DT PINCH= 51.7

APPENDIX D: ACRONYM DEFINITIONS

ADE - Adiabatic Diesel Engine
 ADECD - Adiabatic Diesel Engine Component Development
 ADRE - Adiabatic Diesel Reference Engine
 A/F - Air/Fuel Ratio
 BBS - Brayton Bottoming System
 BHP - Brake Horse Power
 BMEP - Reciprocator Brake Mean Effective Pressure
 BOI - Beginning of Injection
 BSFC - Brake Specific Fuel Consumption
 BTDC - Before Top Dead Center
 CFM - Cubic Feet per Minute
 DDA - Detroit Diesel Allison
 DDEC - Detroit Diesel Electronic Control
 ECM - Electronic Control Module
 EER - Exhaust Energy Recovery
 EERS - Exhaust Energy Recovery System
 EHD - Elastohydrodynamic
 FE - Finite Element
 FL-85 - Fluorinol-85
 FMEP - Friction Mean Effective Pressure
 HR - High Risk
 i - Index for Friction Parameter Level in Orthogonal Array
 IR - Intermediate Risk
 ITI - Integral Technologies Incorporated
 K - Kelvin
 LCC - Life Cycle Cost
 LHR - Low Heat Rejection
 LHRE - Low Heat Rejection Engine
 MOR - Modulus of Rupture
 MR - Moderate Risk
 N - Newton
 OA - Orthogonal Array
 ORCS - Organic Rankine Cycle Systems
 PBBS - Pressureized Brayton Bottoming System
 R - Rankine
 RC-1 - Thermo Electron Corp. Trade Name for Organic Working Fluid
 SOA - State of the Art

STEAM - Steam Rankine Cycle Systems
TBC - Thermal Barrier Coating
TC - Turbocharged
TC/A - Turbocharged and Aftercooled
TCPD - Turbocompound
UTRC - United Technologies Research Center
W - Watt